Research Article

1-Nitropyrene Induced Reactive Oxygen Species–Mediated Apoptosis in Macrophages through AIF Nuclear Translocation and AMPK/Nrf-2/HO-1 Pathway Activation

Chun-Hung Su,[1,2,3] **Yung-Chuan Ho,**[4] **Min-Wei Lee,**[5] **Ching-Chi Tseng,**[6] **Shiuan-Shinn Lee,**[7] **Ming Kun Hsieh,**[5] **Hsin-Hung Chen,**[8,9,10] **Chien-Ying Lee,**[11,12] **Sheng-Wen Wu,**[13,14] **and Yu-Hsiang Kuan** [11,12]

[1]*Department of Internal Medicine, Chung Shan Medical University Hospital, Taichung, Taiwan*
[2]*Department of Internal Medicine, School of Medicine, Chung Shan Medical University, Taichung, Taiwan*
[3]*Institute of Medicine, Chung Shan Medical University, Taichung, Taiwan*
[4]*School of Medical Applied Chemistry, Chung Shan Medical University, Taichung, Taiwan*
[5]*A Graduate Institute of Microbiology and Public Health, National Chung Hsing University, Taichung, Taiwan*
[6]*Aerospace Center Hospital, Peking University, Beijing, China*
[7]*School of Public Health, Chung Shan Medical University, Taichung, Taiwan*
[8]*Division of Endocrinology and Metabolism, Department of Internal Medicine, Asia University Hospital, Taichung, Taiwan*
[9]*School of Medicine, Institute of Medicine and Public Health, Chung Shan Medical University, Taichung, Taiwan*
[10]*Chung Sheng Clinic, Nantou, Taiwan*
[11]*Department of Pharmacology, School of Medicine, Chung Shan Medical University, Taichung, Taiwan*
[12]*Department of Pharmacy, Chung Shan Medical University Hospital, Taichung, Taiwan*
[13]*Division of Nephrology, Department of Internal Medicine, Chung Shan Medical University Hospital, Taichung, Taiwan*
[14]*The School of Medicine, Chung Shan Medical University, Taichung, Taiwan*

Correspondence should be addressed to Yu-Hsiang Kuan; kuanyh@csmu.edu.tw

1-Nitropyrene (1-NP), one of the most abundant nitropolycyclic aromatic hydrocarbons (nitro-PAHs), is generated from the incomplete combustion of carbonaceous organic compounds. 1-NP is a specific marker of diesel exhaust and is an environmental pollutant and a probable carcinogen. Macrophages participate in immune defense against the invasive pathogens in heart, lung, and kidney infection diseases. However, no evidence has indicated that 1-NP induces apoptosis in macrophages. In the present study, 1-NP was found to induce concentration-dependent changes in various cellular functions of RAW264.7 macrophages including cell viability reduction; apoptosis generation; mitochondrial dysfunction; apoptosis-inducing factor (AIF) nuclear translocation; intracellular ROS generation; activation of the AMPK/Nrf-2/HO-1 pathway; changes in the expression of BCL-2 family proteins; and depletion of antioxidative enzymes (AOE), such as glutathione peroxidase (GPx), catalase (CAT), and superoxide dismutase (SOD) These results indicate that 1-NP induced apoptosis in macrophages through AIF nuclear translocation and ROS generation due to mitochondrial dysfunction and to the depletion of AOE from the activation of the AMPK/Nrf-2/HO-1 pathway.

1. Introduction

1-Nitropyrene (1-NP) is a nitropolycyclic aromatic hydrocarbon (nitro-PAH), a class of environmental pollutants generated from the incomplete combustion of carbonaceous organic fuels, biomass, and other compounds [1]. 1-NP is a highly specific marker of diesel exhaust. Various studies have detected 1-NP in the environment and in foods, including in

soil, road dust, rice, cabbage, and the atmosphere [2, 3]. The high lipid solubility of 1-NP allows it to permeate the gastro-intestinal system, respiratory system, and skin [4]. 1-NP is one of the most abundant nitro-PAHs in urban ambient air and is a major contributor to mutagenic and carcinogenic effects [5–7]. The International Agency for Research on Cancer (IARC) has classified 1-NP as a group 2A carcinogen, indicating that it is probably carcinogenic to humans [8]. The 1-NP exposures experienced by ambient the concentrations in air ranged from 10 to 1000 pg/m^3 in urban areas. The concentration of 1-NP in the rural and remote areas with low traffic intensity ranges from 1 to 100 pg/m^3 in the whole world. Concentrations of 1-NP tend to be higher in winter than in summer [8]. Up to now, there is no evidence showing the human carcinogen induced by 1-NP [8]. However, several diseases caused by the long-term exposure lead to accumulation of 1-NP in the animal model. The liver, lung, and mammary gland carcinomas are induced by 1-NP at the concentration range from 25 to 100 μM/kg for long-term exposure above 12 weeks in animals [8]. Apoptosis plays a significant role in pathogenesis, metagenesis, and tumorigenesis through mitochondrial dysfunction [9]. 1-NP induces apoptosis in liver epithelial Hepa1c1c7 cells, hepatoma HepG2 cells, bronchial epithelial BEAS-2B cells, and type II pulmonary epithelial A549 cells [6, 10–12].

Macrophages, which differentiate from monocytes, are a group of mononuclear phagocytes that participate in immune defense against invasive pathogens in heart, lung, and kidney infections [13]. Alveolar macrophages are the predominant resident phagocytes in the alveolar air space. When activated, they defend against inhaled pathogens, such as environmental pollutants and invasive bacteria, and lung trauma [13, 14]. The excess activation of macrophages can result in inflammatory responses and lead to cytotoxicity and apoptosis [15, 16]. Mitochondrial disruption plays a key role in macrophage apoptosis [14, 17]. Several molecular mechanisms participate in mitochondrial disruption which include the expression of the Bcl-2 family; translocations of apoptosis-inducing factor (AIF) and cytochrome c; and depletion of antioxidative enzymes (AOEs), such as glutathione peroxidase (GPx), catalase (CAT), superoxide dismutase (SOD), and heme oxygenase-1 (HO-1) [14, 18–20]. Recently, we have reported that cytotoxicity and genotoxicity were induced by 1-NP by poly (ADP-ribose) polymerase-1 (PARP-1) cleavage via caspase-3 and -9 activation through cytochrome c release from mitochondria and its upstream p53-dependent pathway in macrophages [21]. However, no evidence has indicated 1-NP-induced apoptosis in macrophages. Therefore, the current study examined cell viability and apoptosis in macrophages exposed to 1-NP and analyzed the mechanism of action.

2. Materials and Methods

2.1. Materials.
Dulbecco's modified Eagle's medium (DMEM), trypsin, fetal bovine serum (FBS), penicillin, streptomycin, and fungizone were obtained from Hyclone (Logan, UT, USA). 1-Nitropyrene (1-NP), 2′,7′-dichlorodihydrofluorescein diacetate (DCFH-DA), 3-(4,5-dimethylthiazol-

2-yl)-2,5-diphenyl-tetrazolium bromide (MTT), phosphate-buffered saline (PBS), dimethyl sulfoxide (DMSO), and other reagents of analytical grade were obtained from Sigma-Aldrich (St. Louis, MO, USA). Tetraethylbenzimidazolylcarbocyanine iodide (JC-1), catalase (CAT) assay kit, superoxide dismutase (SOD) assay kit, and glutathione peroxidase (GPx) assay kit were obtained from Cayman (Ann Arbor, MI, USA). Mitochondrial permeability transition pore (MPTP) assay kit was obtained from BioVision (Milpitas, CA, USA). Primary antibodies for the detection of AIF, cytochrome c, Bcl-2, Bcl-xL, Bad, Bax, Bid, HO-1, Nrf2, P-AMPK, AMPK, COX-IV, GAPDH, and β-actin were obtained from Santa Cruz (Santa Cruz, CA, USA). Secondary antibodies for horseradish peroxidase- (HRP-) conjugated mouse anti-rabbit IgG or goat anti-mouse IgG were purchased from Jackson ImmunoResearch Laboratories (Baltimore, MD, USA). Dissolve 1-NP in DMSO, in which the final concentration was not higher than 0.05% (v/v).

2.2. Cell Culture.
The murine macrophage-like cell line RAW264.7 (BCRC 6001) was obtained from the Bioresource Collection and Research Centre (Taiwan). All cells were grown as monolayer cultures at 37°C in 5% CO_2 using DMEM supplemented with 1% penicillin, streptomycin, fungizone, and 10% FBS. Cell passaging was conducted using 0.05% trypsin with 0.53 mM EDTA [20]. After seeding, the cells were incubated with 1-NP at the concentrations of 0, 3, 10, 30, and 50 μM for 6, 12, 24, and 48 h for cell viability assay. On the other hand, the cells were incubated with 1-NP at the concentrations of 0, 3, 10, 30, and 50 μM for 24 h used for other experimental assays.

2.3. Cell Viability Assay.
3-(4,5-Dimethylthiazol-2-yl)-2,5-diphenyltetrazolium bromide (MTT) assay was used to evaluate cell viability [22]. The RAW264.7 cells were seeded at a density of 5×10^4 cells/well in 96-well plates for 12 h. After replacing the serum- and phenol red-free medium with culture medium, the cells were exposed to 0, 3, 10, 30, and 50 μM concentrations of 1-NP for 6, 12, 24, and 48 h. After treatment, 5 mg/mL MTT was added into each well. After 4 h at 37°C, the supernatant was carefully removed. DMSO was added into each well. Optical density (OD) was measured on a microplate reader (Synergy HT Multi-Mode Microplate Reader, BioTek, Winooski, VT) at a test wavelength of 550 nm.

2.4. Flow Cytometric Analysis of Necrosis and Apoptosis.
Differentiation of apoptosis and necrosis was performed on a BD Accuri C6 flow cytometer (San Jose, CA, USA) using an FITC-Annexin V/PI apoptosis detection kit. The RAW264.7 cells were seeded at a density of 5×10^5 cells/well in 24-well plates for 12 h. After replacing the serum- and phenol red-free medium with culture medium, the cells were exposed to 0, 3, 10, 30, and 50 μM concentrations of 1-NP for 24 h. After 10^5 cell collection, the apoptosis and necrosis were identified through dual staining with FITC-Annexin V and PI staining solution in the dark at room temperature for 15 min, as described previously [22]. Early apoptotic cells were Annexin V-positive and PI-negative (FITC-Annexin

V+/PI−), late apoptotic cells were Annexin V- and PI-double-positive (FITC-Annexin V+/PI+), necrotic cells were Annexin V-negative and PI-positive (FITC-Annexin V −/PI+), and surviving cells were Annexin V- and PI-double-negative (FITC-Annexin V−/PI−).

2.5. Mitochondrial Membrane Potential (MMP) Assay. Mitochondrial membrane potential (MMP) was assessed using mitochondrial membrane potential assay dye JC-1, according to the manufacturer's protocol, as described previously [22]. After the 5×10^5 cells were treated with 1-NP at various concentrations for 24 h, they were washed twice with PBS and incubated with JC-1 dye in serum-free medium for 30 min at 37°C. After washing, the cells were analyzed using the BD Accuri C6 flow cytometer.

2.6. Mitochondrial Permeability Transition Pore (MPTP) Assay. Mitochondrial permeability transition pore (MPTP) was assessed using the commercial assay kit according to the manufacturer's protocol. After the 5×10^5 cells were treated with 1-NP at various concentrations for 24 h, they were washed and incubated with MPTP staining dye in serum-free medium for 15 min at 37°C. And then, the cells were incubated with 1 mM $CoCl_2$ for 15 min at 37°C. After washing, the cells were analyzed using the BD Accuri C6 flow cytometer.

2.7. Measurement of Intracellular ROS Concentration. Intracellular ROS generation was evaluated using DCFH-DA, per the method of our previous study [14]. After the 5×10^5 cells were treated with 1-NP at various concentrations for 24 h, the cells were incubated with DCFH-DA for 30 min at 37°C. After washing with PBS, the fluorescence was measured in a microplate reader at an excitation wavelength of 488 nm and emission wavelength of 515 nm.

2.8. Cell Fractionation and Western Blot Assay. The levels of protein expression from whole cells and subcellular fractions were measured using western blot assay, per a previously described method [14]. The RAW264.7 cells were seeded at a density of 5×10^6 cells/well in a 10 cm dish for 12 h. After replacing the serum- and phenol red-free medium with culture medium, the cells were exposed to 0, 3, 10, 30, and 50 μM concentrations of 1-NP for 24 h. After cell collection, protein from whole cells was extracted in lysis buffer (25 mM Tris-HCl at pH 7.6, 1 mM phenylmethylsulphonyl fluoride, 150 mM sodium chloride, 1% Nonidet P-40, 1 mM sodium orthovanadate, 10% glycerol, 0.1% SDS, and phosphatase and protease inhibitors). The fraction protein, containing cytosol, mitochondria, and nuclei, was isolated from cells using a cytoplasmic and nuclear protein extraction kit and mitochondria extraction kit. The protein content of the supernatant was determined using Bradford assay. Equal amounts of proteins were incubated with 5X sample buffer, separated by 7.5%–12.5% SDS-PAGE, and electrophoretically transferred onto polyvinylidene difluoride membranes. The membranes were blocked with 5% skimmed milk for 1 h at room temperature. They were then incubated with the indicated primary antibodies (AIF, Bcl-2, Bcl-xL, Bad, Bax, Bid, HO-1, Nrf2, P-AMPK, AMPK, and β-actin) with
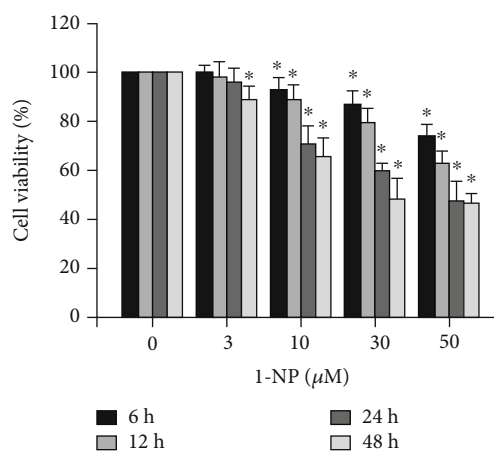
FIGURE 1: 1-Nitropoyrene (1-NP) reduced cell viability in RAW264.7 macrophages. The cells were incubated with 1-NP at concentrations of 0, 3, 10, 30, and 50 μM for 6, 12, 24, and 48 h at 37°C. Cell viability was measured using the MTT assay. Data are expressed as mean ± SD ($n = 5$). $^*P < 0.05$ was considered significant compared with the control group.

0.5% skim milk overnight at 4°C and then with the secondary antibody for 1 h at room temperature. Finally, the membranes were visualized with protein densitometry analysis using the electrochemiluminescence (ECL) detection system.

2.9. Measurement of AOE Activities. The RAW264.7 cells were seeded at a density of 10^6 cells/well in 6-well plates for 12 h. After replacing the serum- and phenol red-free medium with culture medium, the cells were exposed to 0, 3, 10, 30, and 50 μM concentrations of 1-NP for 24 h. After cell collection, the AOE activities which include GPx, CAT, and SOD were assayed with the respective detection kits according to the manufacturer's instructions [14].

2.10. Statistical Analysis. Data of the results were representative of three independent experiments in western blot assay, fourth independent experiments in measurement of AOE activities, fifth independent experiments in cell viability assay, necrosis and apoptosis analysis, MMP assay, and measurement of intracellular ROS concentration. The values of the results were representative in terms of the mean ± standard deviation (SD). All data were analyzed in SPSS software. Multiple group comparisons were performed using one-way ANOVA followed by Bonferroni's post hoc test. $P < 0.05$ indicated statistical significance for all tests.

3. Results

3.1. Effects of 1-NP on Cell Viability in RAW264.7 Macrophages. The cell viabilities of RAW264.7 macrophages incubated with 0, 3, 10, 30, or 50 μM concentrations of 1-NP for 6, 12, 24, and 48 h were monitored using MTT colorimetric assay (Figure 1). 1-NP reduced cell viability in a concentration- and time-dependent manner. The survival rate was significantly lower in RAW264.7 cells incubated with 3 μM
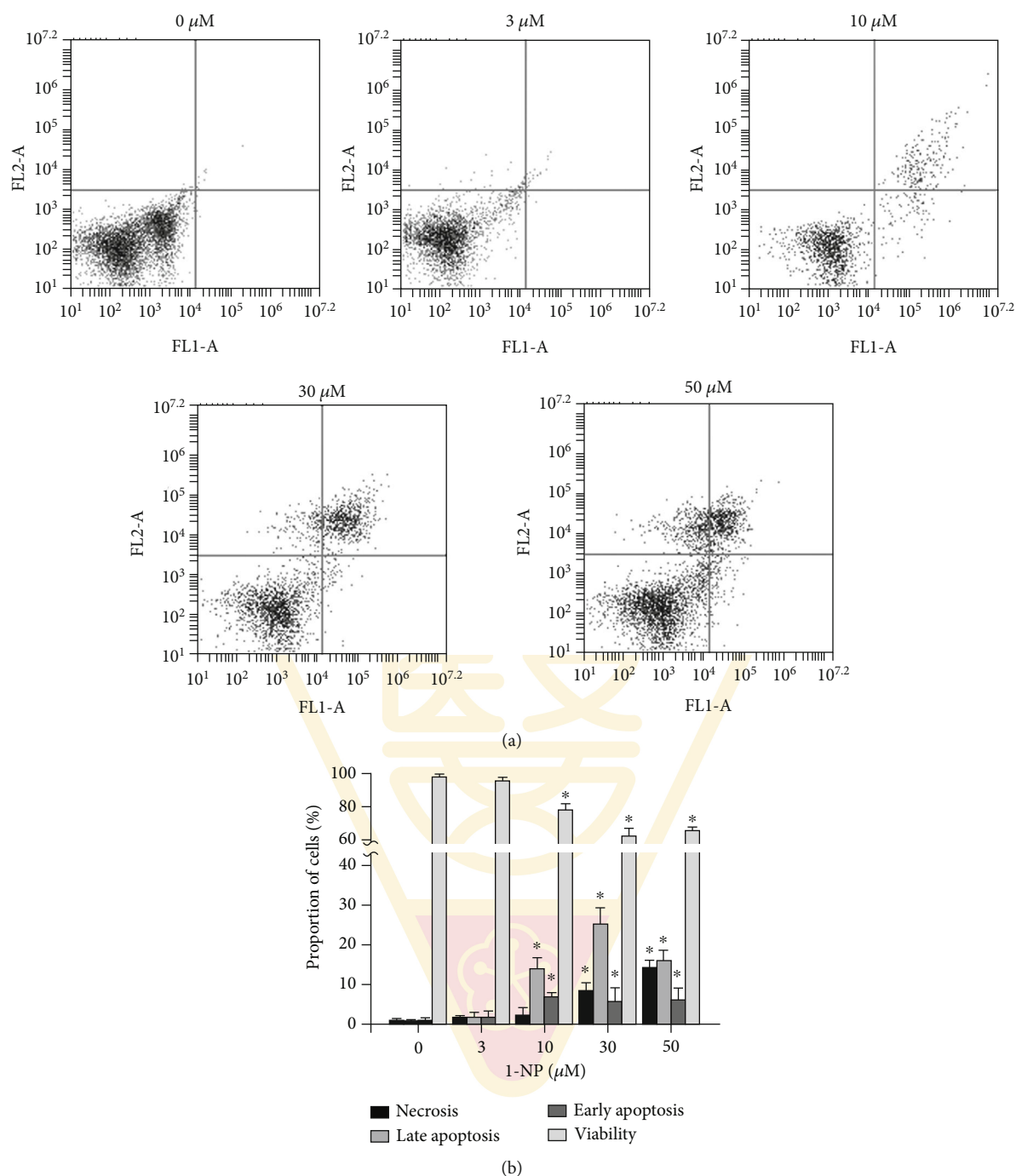
(a)

(b)

Figure 2: 1-NP induced apoptosis and necrosis in RAW264.7 macrophages. The portion of apoptosis and necrosis was measured by Annexin V-FITC and PI assays using flow cytometry. (a) Cells were incubated with 1-NP at concentrations of 0, 3, 10, 30, and 50 μM for 24 h at 37°C. The upper left quadrant (Annexin V−/+) is representative of necrosis; the upper right and lower right quadrants (Annexin V+/PI+ and Annexin V+/PI−) are representatives of apoptosis; and the lower left quadrant (Annexin V−/PI−) is representative of living cells. (b) Quantitatively, the percentage of necrotic cells, viable cells, and apoptotic cells was calculated and analyzed. Data are expressed as mean ± SD ($n = 5$). $^{*}P < 0.05$ was considered significant compared with the control group.

of 1-NP for 48 h and in cells incubated with 10 μM of 1-NP for 12 h ($P < 0.05$).

3.2. Effects of 1-NP on Apoptosis and Necrosis in RAW264.7 Macrophages. The effects of 1-NP-induced apoptosis and necrosis in RAW264.7 cells were assessed using FITC-

Annexin V and PI double staining. Annexin V detects phosphatidylserine externalization during apoptosis, and PI stains detect necrotic and dead cells. 1-NP induced apoptosis and necrosis in a concentration-dependent manner (Figures 2(a) and 2(b)). After 24 h, a concentration of 10 μM of 1-NP significantly increased early and late
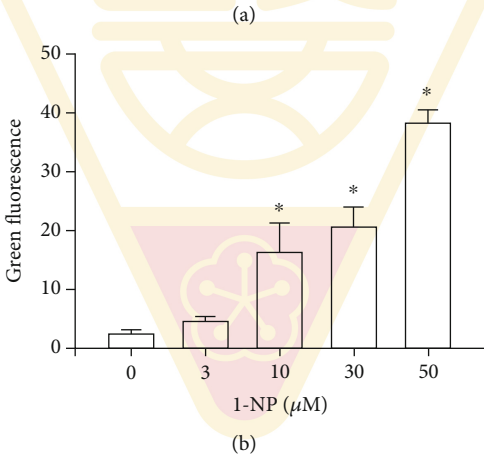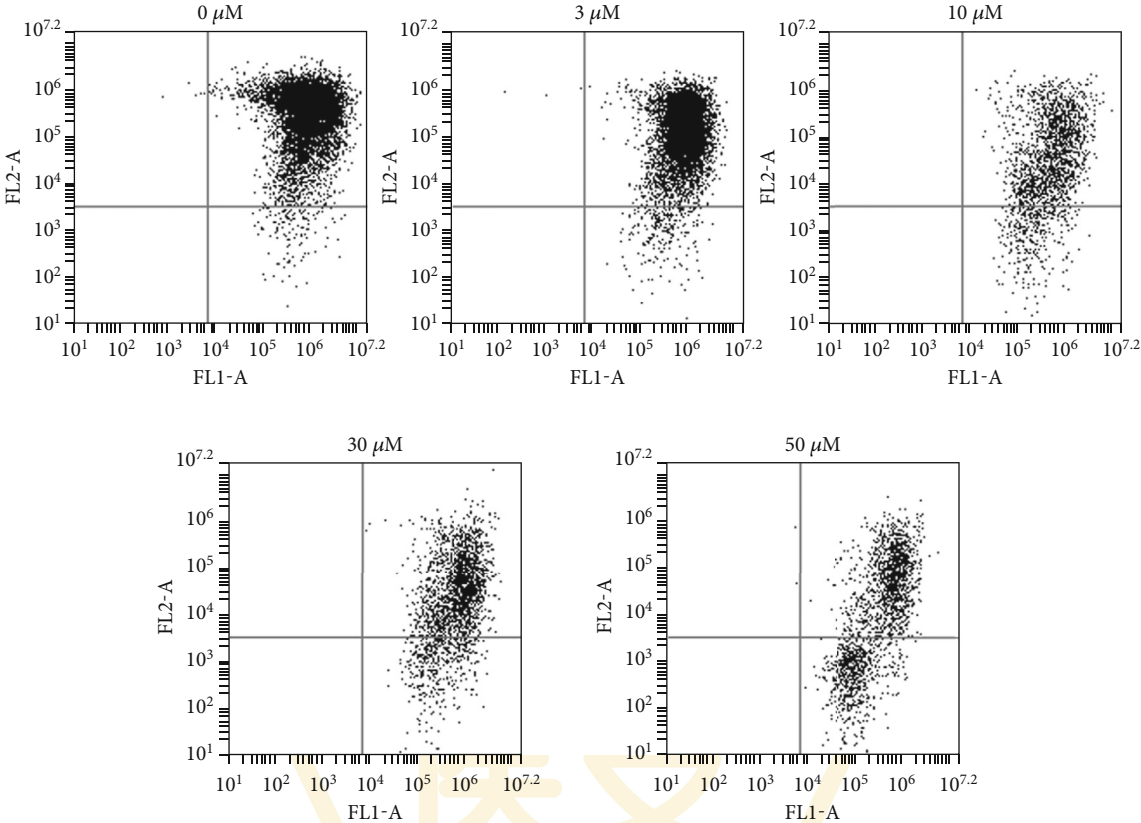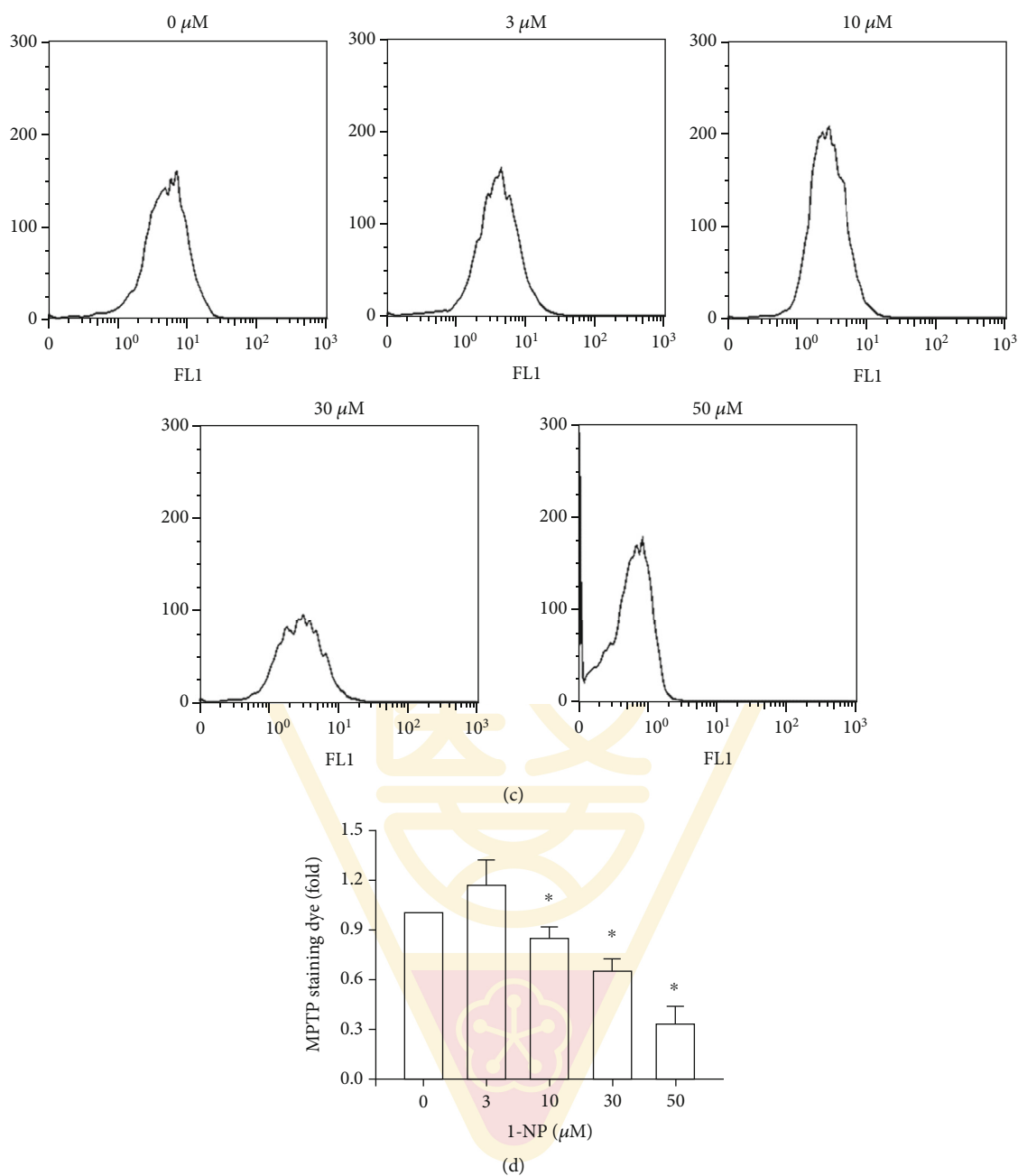
(a)

(b)

Figure 3: Continued.

(c)

(d)

FIGURE 3: 1-NP induced mitochondria dysfunction in RAW264.7 macrophages. The portion of mitochondria dysfunction was measured by JC-1 assays using flow cytometry. (a) After cell treatment, the portion of MMP was measured using the JC-1 assay. (b) Quantitatively, the percentage of MMP downregulation cells was calculated and analyzed. The MPTP opening was measured by flow cytometry. (c) After cell treatment, the histogram of MPTP opening was measured using the MPTP assay kit. (d) The change in fold of MPTP opening cells between the treated and control groups was calculated. Data are expressed as mean $\pm$ SD ($n = 5$). $^*P < 0.05$ was considered significant compared with the control group.

apoptosis ($P < 0.05$). A concentration of $30\,\mu$M of 1-NP significantly increased necrosis ($P < 0.05$).

3.3. Effects of 1-NP on Mitochondrial Dysfunction in RAW264.7 Macrophages. Mitochondrial dysfunction is assessed by MMP and MPTP assays. The effects of 1-NP on mitochondrial dysfunction in RAW264.7 macrophages were investigated using JC-1, a mitochondrion-selective aggregate dye. Active mitochondria with a high membrane potential

exhibited red fluorescence, and dysfunctional mitochondria with a low membrane potential exhibited green fluorescence. 1-NP induced downregulration of MMP in a concentration-dependent manner After 24 h, a concentration of $10\,\mu$M of 1-NP significantly decreased the MMP ($P < 0.05$, Figure 3). 1-NP induced upregulation of the MPTP opening in a concentration-dependent manner. After 24 h, a concentration of $10\,\mu$M of 1-NP significantly increased the MPTP opening ($P < 0.05$, Figure 3). These results indicated that 1-
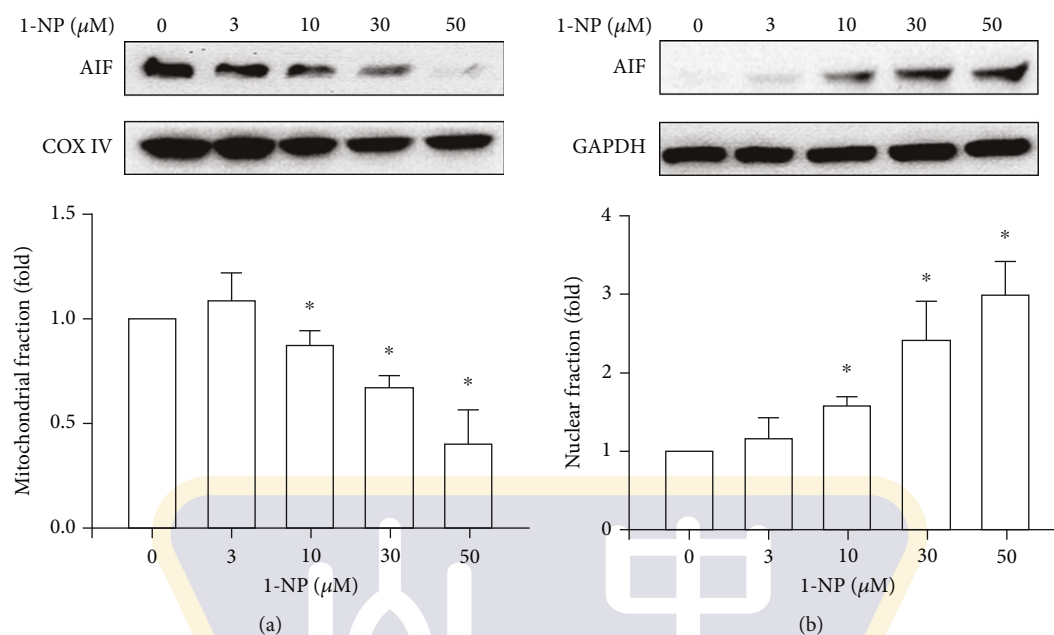
Figure 4: 1-NP-induced nuclear translocation of AIF in RAW264.7 cells. The expression of AIF in mitochondria (a) and nucleus (b) was measured by western blot assay after treated with 1-NP for 24 h. The change in fold of AIF expression between the treated and control groups was calculated. Results are expressed as means ± SD ($n = 3$). $^*P < 0.05$ was considered significant as compared with the control group.

NP induced mitochondrial dysfunction in a concentration-dependent manner. After 24 h, a concentration of 10 μM of 1-NP significantly increased the mitochondrial dysfunction.

3.4. Effects of 1-NP on Subcellular Fraction Translocation of AIF in RAW264.7 Macrophages.

The translocation of AIF from the mitochondria to the nucleus is critical in the caspase-independent mitochondrial apoptosis pathway. The levels of AIF in the mitochondria and nucleus were measured using western blot assay in RAW264.7 cells incubated with 1-NP. Levels of AIF in the mitochondria were reduced by 1-NP in a concentration-dependent manner and significantly increased at 10 μM ($P < 0.05$; Figure 4). The effects of 1-NP on AIF levels in the nucleus were concentration dependent, with AIF significantly increased at 10 μM ($P < 0.05$).

3.5. Effects of 1-NP on Expression Level of Bcl-2 Family Proteins in RAW264.7 Macrophages.

This study examined the regulation of mitochondrial integrity by Bcl-2 family proteins, with particular attention to the controlled release of AIF and ROS involved in caspase-independent cell death [23, 24]. The effects of 1-NP on the expression of Bcl-2 family proteins in RAW264.7 cells are illustrated in Figure 5. The levels of Bcl-2 and Bcl-xL were reduced by 1-NP in a concentration-dependent manner, and a significant effect was indicated at concentrations ≥ 10 μM ($P < 0.05$). By contrast, the levels of Bad, Bax, Bid, and tBid were increased by 1-NP in a concentration-dependent manner and a significant effect was indicated at concentrations ≥ 10 μM ($P < 0.05$). Moreover, the value of Bax/Bcl-2 ratio was increased by 1-NP in a concentration-dependent manner and significant effect indicated at concentration ≥ 10 μM ($P < 0.05$).

3.6. Effects of 1-NP on Intracellular ROS Generation in RAW264.7 Macrophages.

Intracellular ROS generation results in apoptosis through mitochondrial dysfunction [14]. After RAW264.7 cells were treated with 1-NP for 24 h, the intracellular ROS generation increased in a concentration-dependent manner and a significant effect was indicated at concentrations ≥ 10 μM ($P < 0.05$, Figure 6).

3.7. Effects of 1-NP on AOE Activities in RAW264.7 Macrophages.

The activation of AOEs including GPx, SOD, and CAT plays a critical role in the control of intracellular ROS generation [14]. The activation of AOEs in RAW264.7 cells treated with 1-NP at various concentrations for 24 h was monitored using AOE assay kits. GPx, SOD, and CAT activities were induced by 1-NP in a concentration-dependent manner, and a significant effect was noted at concentrations ≥ 10 μM ($P < 0.05$; Figure 7).

3.8. Effects of 1-NP on the AMPK/Nrf-2/HO-1 Pathway in RAW264.7 Macrophages.

HO-1 is an antioxidative protein involved in the resolution of inflammation. Its expression is regulated by the nuclear translocation of Nrf-2. The nuclear accumulation of Nrf-2 is induced by AMPK phosphorylation. After RAW264.7 cells were treated with 1-NP for 24 h, AMPK phosphorylation, Nrf-2 expression, and HO-1 expression were induced by 1-NP in a concentration-dependent manner; a significant effect was noted at concentrations ≥ 10 μM ($P < 0.05$; Figure 8).

4. Discussion

Air pollution can harm the environment in the forms of haze, acid rain, eutrophication, wildlife injury, and global climate

(a)

(b)

(c)
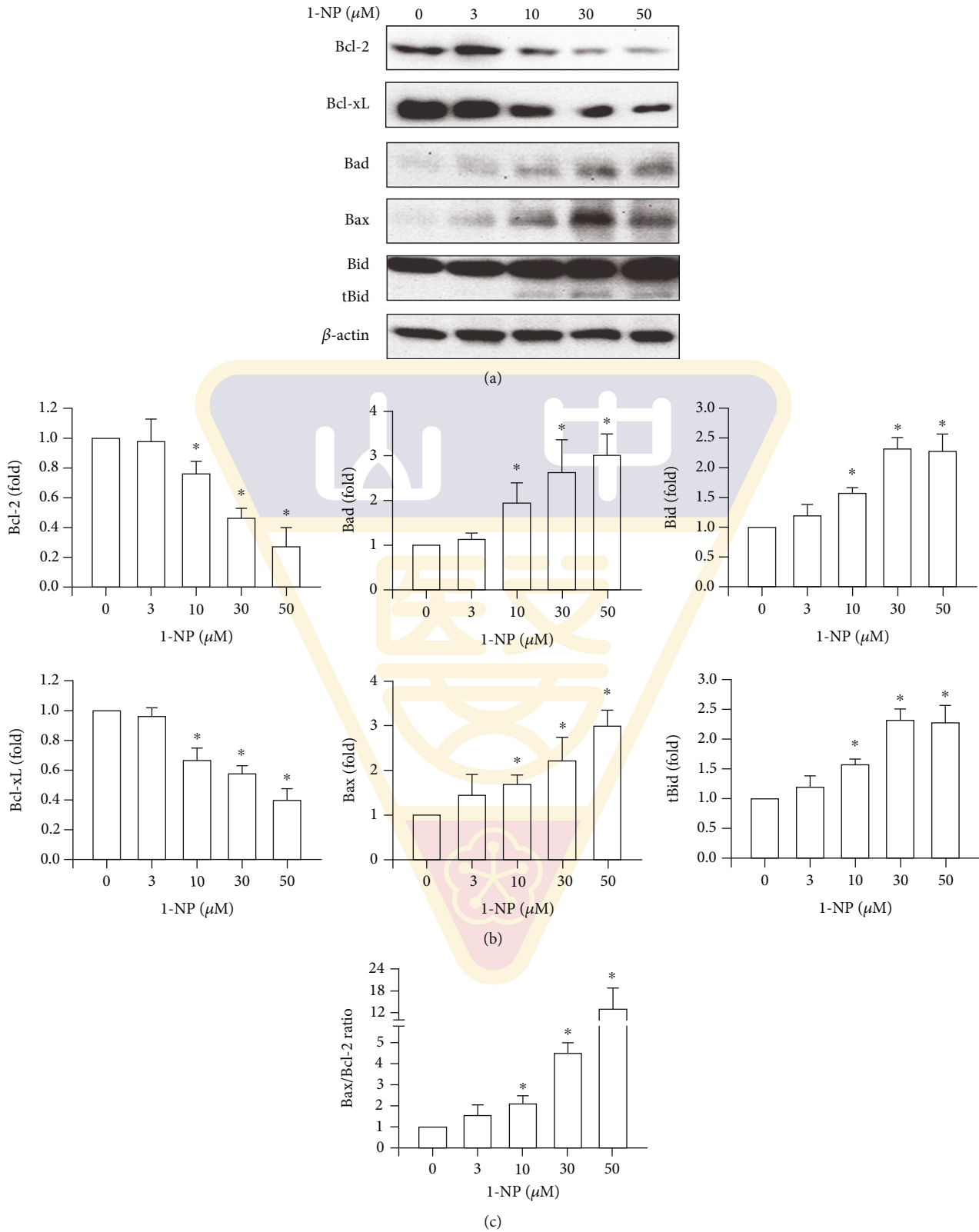
FIGURE 5: 1-NP-induced change in the expression of Bcl-2 family proteins in RAW264.7 cells. (a) The expression of Bcl-2 family proteins was measured by western blot assay after being treated with 1-NP for 24 h. (b) The change in fold of Bcl-2 family expression between the treated and control groups was calculated. (c) The change in the value of Bax/Bcl-2 ratio. Results are expressed as means ± SD ($n = 3$). $^{*}P < 0.05$ was considered significant as compared with the control group.

FIGURE 6: 1-NP induced ROS generation in RAW264.7 macrophages. Data are expressed as mean ± SD ($n = 5$). $^*P < 0.05$ is considered significant compared with the control group.

change. Around the globe, diesel exhaust is a major contributor to air pollution, which can cause health problems, such as al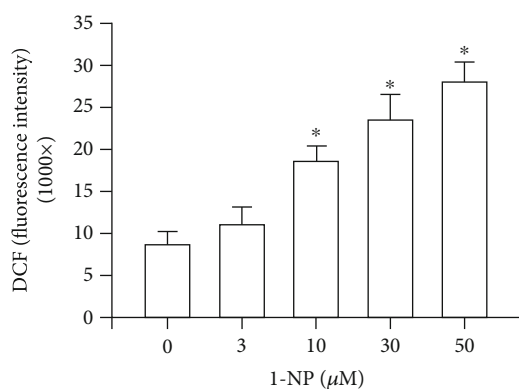lergies, neurodegenerative diseases, and cardiovascular disease [25–27]. 1-NP and its urinary metabolites have been proposed as markers for diesel exhaust from traffic- and factory-related diesel particulate matter [28]. The mutagenic capability of 1-NP is reduced by alveolar macrophages through phagocytosis [29]. A previous study proposed that the cellular viability of RAW264.7 cells was weakly but significantly reduced by 1-NP exposure at 80 nM for 24 h [30]. In our previous study, it was found that cytotoxicity was induced by 1-NP in the concentration- and time-dependent manner. The induction was significant when the cells were treated with 3 μM 1-NP for 48 h or 10 μM 1-NP for 6 h [21]. The results from the present study support existing evidence that 1-NP reduces the viability of RAW264.7 cells. Furthermore, our data suggest that 1-NP reduces the viability of RAW264.7 cells in a concentration- and time-dependent manner.

Apoptosis is a major form of cell death and occurs as a defense mechanism of the immune system when cells are exposed to harmful substances [31, 32]. Previous studies have shown that 1-NP causes apoptosis in human alveolar-basal epithelial A549 cells, human bronchial epithelial BEAS-2B cells, and mouse hepatoma Hepa1c1c7 cells [12, 33, 34]. Necrosis is a type of irreversible cell injury and results in cell death [32]. Previous studies have found that 1-NP causes necrosis in Hepa1c1c7 cells and BEAS-2B cells [33, 34]. Our results also indicate that 1-NP induced apoptosis and necrosis in RAW264.7 cells. Moreover, 1-NP-induced apoptosis was observed in RAW264.7 cells at a lower concentration than 1-NP-induced necrosis. The extent of apoptosis, including early- and late-phase apoptosis, was higher than the extent of necrosis. After RAW264.7 cells were treated with 1-NP at 10 μM for 24 h, cell viability decreased and apoptosis increased significantly. These results suggest that apoptosis is the major form of cell death in 1-NP-treated RAW264.7 cells.

Mitochondrial dysfunction is a critical factor in macrophage apoptosis [20, 35]. During mitochondrial dysfunction, the dissipation of mitochondrial membrane potential and
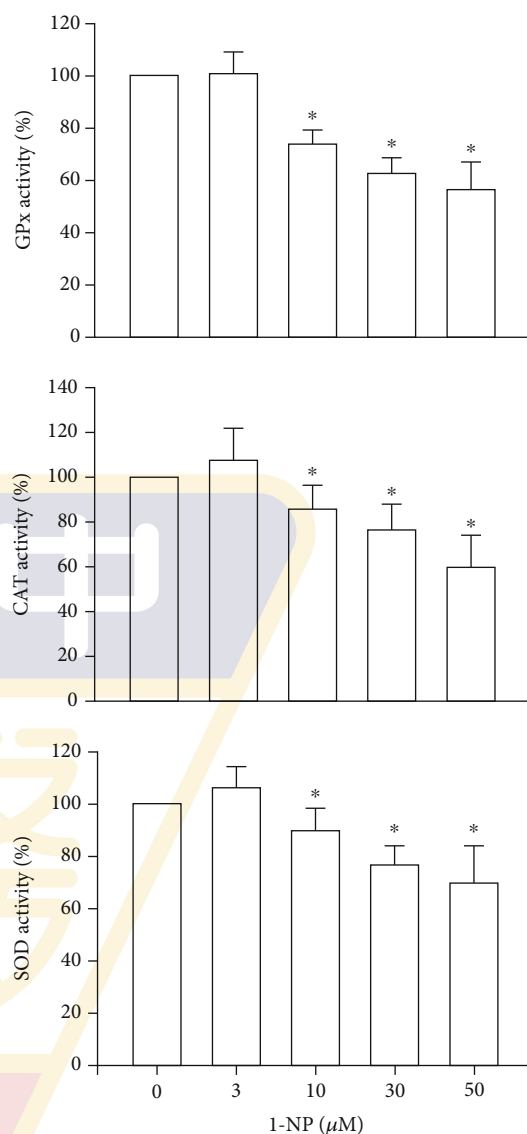

FIGURE 7: 1-NP inhibited the activities of AOEs, including GPx, SOD, and GPx, in RAW264.7 macrophages. The AOE activities were measured by colorimetric assay kit after cells were treated with 1-NP. Results are expressed as means ± SD ($n = 4$). $^*P < 0.05$ was considered significant compared with controls.

loss of mitochondrial membrane integrity were observed in macrophages after exposure to apoptotic stimuli [20, 35]. AIF, a mammalian-soluble protein containing flavin adenine dinucleotide, is a nicotinamide adenine dinucleotide-dependent oxidoreductase located in the mitochondrial intermembrane space [36]. In physiological conditions, AIF plays a crucial role in mitochondrial bioenergetics. During apoptosis, loss of mitochondrial membrane integrity results in the translocation of AIF from the mitochondria to the nucleus [37]. The degradation complex formed by AIF and related proteins promotes apoptotic DNA damage [36, 37]. To the best of our knowledge, no previous studies have proposed that 1-NP decreases the mitochondrial membrane potential in macrophages. However, a previous study reported that the nuclear translocation of AIF from the
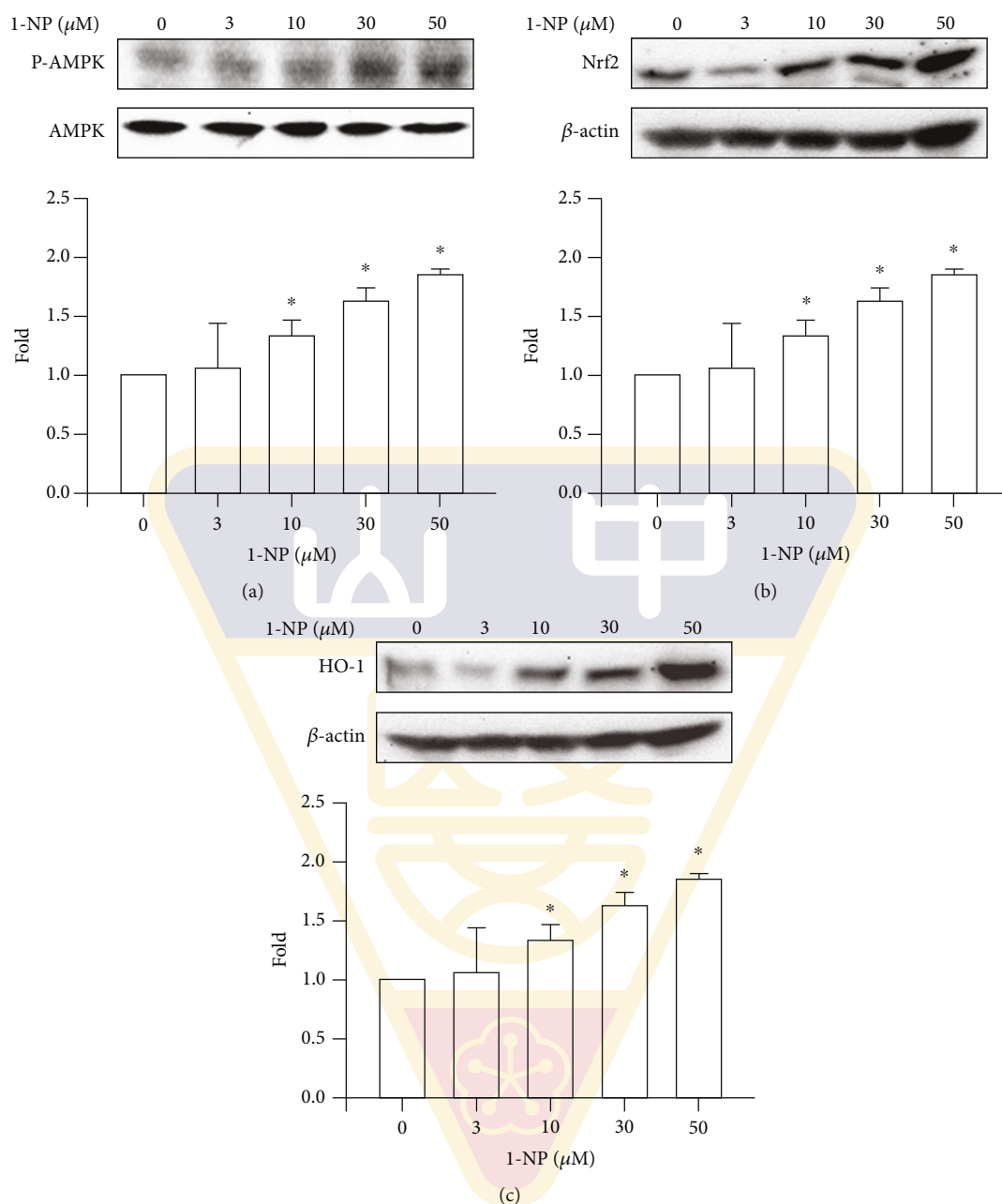
(a)

(b)

(c)

FIGURE 8: 1-NP induced the activation of AMPK/Nrf-2/HO-1 pathway in RAW264.7 macrophages. AMPK phosphorylation (a), Nrf-2 expression (b), and HO-1 expression (c) were measured by colormetric assay kit after cells were treated with 1-NP. The change in fold of AMPK phosphorylation, Nrf-2 expression, and HO-1 expression between the treated and control groups was calculated. Results are expressed as means ± SD ($n = 3$). *$P < 0.05$ was considered significant as compared with the control group.

cytosol to the nucleus occurred after exposure to 1-NP in Hepa1c1c7 cells, as indicated in immunocytochemical analysis [38]. The nuclear translocation of AIF pertains mainly to the elucidation of 1-NP-treated RAW264.7 cells. The present study demonstrated that the nuclear translocation of AIF was induced by 1-NP in a concentration-dependent manner in RAW264.7 cells. These results indicate that 1-NP induces apoptosis through the dissipation of mitochondrial membrane potential and the nuclear translocation of AIF due to the disruption of mitochondrial membrane.

The permeabilization of the mitochondrial membrane and the release of intermembrane space proteins (including AIF) are mediated by Bcl-2 family proteins [39, 40]. The Bcl-2 family proteins can generally be divided into three groups based on their primary function: antiapoptotic proteins, which include Bcl-2 and Bcl-xL; proapoptotic pore-formers, including Bax; and proapoptotic BH3-only proteins, which include a sensitizer protein (Bad) and activator proteins (Bid and tBid) [41]. After cells are incubated with apoptosis inducers, the activator BH3-only proteins (Bid and

tBid) translocate to the mitochondrial membrane and increase their affinity for the pore former, Bax. Bax causes pore formation on the mitochondrial membrane and the leakage of AIF and other soluble proteins from the inter-membrane space [39, 41]. The interaction between the activator BH3-only proteins and the pore-former protein is suppressed by antiapoptotic proteins (Bcl-2 and Bcl-xL). The sensitizer BH3-only protein, Bad, binds to and inhibits the activities of Bcl-2 and Bcl-xL [39, 41]. A previous study proposed that 1-NP induces the mRNA expression of Bax in a concentration-dependent manner in A549 cells [42]. The present study examined the expression of the Bcl2 family in 1-NP-treated RAW264.7 macrophages. We found that 1-NP induced expressions of Bid, tBid, Bax, and Bad in a concentration-dependent manner. By contrast, 1-NP reduced expressions of the antiapoptotic proteins, Bcl-2 and Bcl-xL, in a concentration-dependent manner. Crucially, the parallel trends are suitable in mitochondrial dysfunction, in AIF leakage, and in 1-NP-treated RAW264.7 macrophages. These results indicate that 1-NP induced mitochondrial dysfunction and AIF leakage by changing the expression of Bcl-2 family proteins.

Oxidative stress, triggered by mitochondrial dysfunction, has been shown to play a critical role in apoptosis [43, 44]. Overgeneration of ROS leads to high oxidative stress and encourages AOE and HO-1 [45, 46]. HO-1 degrades heme to biliverdin, which is subsequently converted to bilirubin, an antioxidant that scavenges and neutralizes ROS [46]. SOD catalyzes the reduction of superoxide anions to hydrogen peroxide. GPx and CAT catalyze the reduction of hydrogen peroxide to water and oxygen [45]. Nrf-2 is an important transcription factor that regulates the expressions of AOEs, such as HO-1 and GPx [47]. AMPK is an upstream factor for the reduction of oxidative stress in macrophages [48]. Intracellular ROS generation is induced by 1-NP in the extra-villous trophoblast HTR8/SVneo cells, A549 cells, and BEAS-2B cells in *Tigriopus japonicus* [12, 49, 50]. To clarify the ROS generation and regulative mechanism induced by 1-NP in macrophages, we measured the production of intracellular ROS in RAW264.7 cells exposed to 1-NP. We found that 1-NP induced ROS generation; reduced AOE activity; and downregulated AMPK phosphorylation, Nrf-2 expression, and HO-1 expression. Based on these findings, we suggest that 1-NP induces ROS by causing mitochondrial dysfunction and reducing AOE activity. Further, we propose that 1-NP induces the activation of the AMPK/Nrf-2/HO-1 pathway to reduce oxidative damage in macrophages.

However, there are the limitations in the present study. First, RAW264.7 cells are the mouse macrophage cell line not the human macrophage. Undoubtedly, direct measurement of the toxic mechanism of 1-NP in human macrophage would be ideal, but the sampling of human macrophage raises major ethical concerns and therefore is not suitable for performance. And then, we proposed that the toxic effect of 1-NP was via apoptosis. On the other hand, toxic effect induced by 1-NP might be through other toxic pathways such as ferroptosis, necroptosis, and autophagy. Therefore, we will research on toxic pathways and relative mechanisms in our future studies. Finally, there are few studies to support
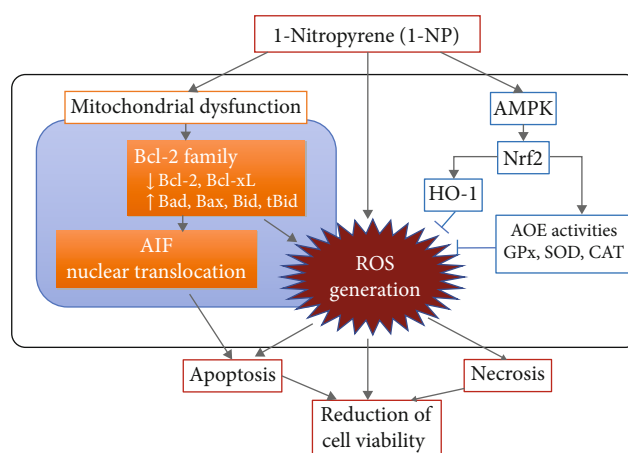

Figure 9: Schemes of the mechanism of the 1-NP-induced apoptosis and cytotoxicity in RAW264.7 cells. After RAW264.7 macrophages were incubated with 1-NP, it caused downregulation of cell viability via upregulation of apoptosis. 1-NP induced apoptosis by inducing AIF nuclear translocation, which was caused by mitochondrial dysfunction. Mitochondrial dysfunction induced by 1-NP occurred due to changes in the expression of BCL-2 family proteins, including downregulation of Bcl-2 and Bcl-xL and upregulation of Bad, Bax, Bid, and tBid. 1-NP induced ROS generation by mitochondrial dysfunction and reducing AOE activity. Additionally, 1-NP treatment led to the activation of the AMPK/Nrf-2/HO-1 pathway due to high levels of oxidative stress. These findings suggested that downregulation of cell viability induced by 1-NP via upregulation of apoptosis was due to mitochondrial dysfunction, AIF nuclear translocation, ROS generation, AOE activity reduction, and AMPK/Nrf-2/HO-1 pathway activation.

that clinical disease associated with macrophage toxicity and activity induced by 1-NP. In the future work, we will research on 1-NP-induced macrophage dysfunction result in diseases, including atherosclerosis, diabetes, and inflammatory bowel disease in the differential animal models.

In conclusion, the present study found that 1-NP treatment led to downregulation of cell viability and upregulation of apoptosis in RAW264.7 macrophages (Figure 9). The findings indicate that 1-NP led to apoptosis by inducing AIF nuclear translocation, which was caused by mitochondrial dysfunction. Our data suggest that mitochondrial dysfunction occurred due to changes in the expression of BCL-2 family proteins. In addition, 1-NP induced ROS generation by reducing AOE activity. Moreover, 1-NP treatment led to the activation of the AMPK/Nrf-2/HO-1 pathway due high levels of oxidative stress. Taken together, these results suggest that 1-NP causes downregulation of cell viability and upregulation of apoptosis due to mitochondrial dysfunction, AIF nuclear translocation, ROS generation, AOE activity reduction, and AMPK/Nrf-2/HO-1 pathway activation.

Data Availability

The data of this manuscript entitled "1-Nitropyrene Induced Reactive Oxygen Species–Mediated Apoptosis in Macrophages through AIF Nuclear Translocation and

AMPK/Nrf-2/HO-1 Pathway Activation" is under license and so cannot be made freely available. Requests for access to these data should be made to Yu-Hsiang Kuan through the following E-mail address: kuanyh@csmu.edu.tw.

Conflicts of Interest

The authors declare that they have no known competing financial interests or personal relationships that could have appeared to influence the work reported in this paper.

Authors' Contributions

Chun-Hung Su was responsible for conceptualization, formal analysis, investigation, data curation, writing original draft, review, editing, supervision, and funding acquisition. Yung-Chuan Ho was responsible for conceptualization, formal analysis, investigation, data curation, writing original draft, review, and editing. Min-Wei Lee was responsible for formal analysis, investigation, data curation, and writing original draft. Ching-Chi Tseng was responsible for formal analysis, data curation, and writing original draft. Shiuan-Shinn Lee was responsible for formal analysis, investigation, data curation, and writing original draft. Ming Kun Hsieh was responsible for investigation and data curation. Hsin-Hung Chen was responsible for investigation and data curation. Chien-Ying Lee was responsible for investigation, data curation, and visualization. Sheng-Wen Wu was responsible for data curation, investigation, writing, review, editing, supervision, and project administration. Yu-Hsiang Kuan was responsible for conceptualization, writing, review, editing, supervision, project administration, and funding acquisition. Sheng-Wen Wu and Yu-Hsiang Kuan contributed equally to this work.

Acknowledgments

References

[1] Y. Gao, L. Yang, J. Chen et al., "Nitro and oxy-PAHs bounded in $PM_{2.5}$ and $PM_{1.0}$ under different weather conditions at Mount Tai in Eastern China: sources, long-distance transport, and cancer risk assessment," *Science of the Total Environment*, vol. 622-623, pp. 1400–1407, 2018.

[2] S. Uno, H. Tanaka, S. Miki et al., "Bioaccumulation of nitroarenes in bivalves at Osaka Bay, Japan," *Marine Pollution Bulletin*, vol. 63, no. 5-12, pp. 477–481, 2011.

[3] K. Deng and W. Chan, "Development of a QuEChERS-based method for determination of carcinogenic 2-nitrofluorene and 1-nitropyrene in rice grains and vegetables: a comparative study with benzo[a]pyrene," *Journal of Agricultural and Food Chemistry*, vol. 65, no. 9, pp. 1992–1999, 2017.

[4] I. C. Yadav, N. L. Devi, V. K. Singh, J. Li, and G. Zhang, "Concentrations, sources and health risk of nitrated- and oxygenated-polycyclic aromatic hydrocarbon in urban indoor air and dust from four cities of Nepal," *Science of The Total Environment*, vol. 643, pp. 1013–1023, 2018.

[5] H. A. Bamford, D. Z. Bezabeh, S. Schantz, S. A. Wise, and J. E. Baker, "Determination and comparison of nitrated-polycyclic aromatic hydrocarbons measured in air and diesel particulate reference materials," *Chemosphere*, vol. 50, no. 5, pp. 575–587, 2003.

[6] N. E. Landvik, M. Gorria, V. M. Arlt et al., "Effects of nitrated-polycyclic aromatic hydrocarbons and diesel exhaust particle extracts on cell signalling related to apoptosis: possible implications for their mutagenic and carcinogenic effects," *Toxicology*, vol. 231, no. 2-3, pp. 159–174, 2007.

[7] K. N. Kirouac, A. K. Basu, and H. Ling, "Replication of a carcinogenic nitropyrene DNA lesion by human Y-family DNA polymerase," *Nucleic Acids Research*, vol. 41, no. 3, pp. 2060–2071, 2013.

[8] IARC, "Diesel and gasoline engine exhausts and some nitroarenes," *IARC monographs on the evaluation of carcinogenic risks to humans*, vol. 105, pp. 9–699, 2014.

[9] J. Lu, L. K. Sharma, and Y. Bai, "Implications of mitochondrial DNA mutations and mitochondrial dysfunction in tumorigenesis," *Cell Research*, vol. 19, no. 7, pp. 802–815, 2009.

[10] J. G. Su, P. J. Liao, M. C. Huang, W. C. Chu, S. C. Lin, and Y. J. Chang, "Aldo-keto reductase 1C2 is essential for 1-nitropyrene's but not for benzo[a]pyrene's induction of p53 phosphorylation and apoptosis," *Toxicology*, vol. 244, no. 2-3, pp. 257–270, 2008.

[11] N. Asare, N. E. Landvik, D. Lagadic-Gossmann et al., "1-Nitropyrene (1-NP) induces apoptosis and apparently a non-apoptotic programmed cell death (paraptosis) in Hepa1c1c7 cells," *Toxicology and Applied Pharmacology*, vol. 230, no. 2, pp. 175–186, 2008.

[12] Y. Shang, Q. Zhou, T. Wang et al., "Airborne nitro-PAHs induce Nrf2/ARE defense system against oxidative stress and promote inflammatory process by activating PI3K/Akt pathway in A549 cells," *Toxicology In Vitro*, vol. 44, pp. 66–73, 2017.

[13] L. C. Davies and P. R. Taylor, "Tissue-resident macrophages: then and now," *Immunology*, vol. 144, no. 4, pp. 541–548, 2015.

[14] F. M. Huang, Y. C. Chang, S. S. Lee et al., "Bisphenol A exhibits cytotoxic or genotoxic potential via oxidative stress- associated mitochondrial apoptotic pathway in murine macrophages," *Food and Chemical Toxicology*, vol. 122, pp. 215–224, 2018.

[15] V. Lakics and S. N. Vogel, "Lipopolysaccharide and ceramide use divergent signaling pathways to induce cell death in murine macrophages," *Journal of Immunology*, vol. 161, pp. 2490–2500, 1998.

[16] J. Xaus, M. Comalada, A. F. Valledor et al., "LPS induces apoptosis in macrophages mostly through the autocrine production of TNF-alpha," *Blood*, vol. 95, no. 12, pp. 3823–3831, 2000.

[17] W. L. Liang, L. Xiao, H. W. Gu et al., "Solid lipid nanoparticle induced apoptosis of macrophages via a mitochondrial-dependent pathway in vitro and in vivo," *International Journal of Nanomedicine*, vol. Volume 14, pp. 3283–3295, 2019.

[18] X. Zhou, K. Zhang, Z. He, Y. Deng, and Y. Gao, "Downregulated miR-150 in bone marrow mesenchymal stem cells

attenuates the apoptosis of LPS-stimulated RAW264.7 via MTCH2-dependent mitochondria transfer," *Biochem. Biophys. Res. Commun*, vol. 526, no. 3, pp. 560–567, 2020.

[19] Y. Wang, R. An, G. K. Umanah et al., "A nuclease that mediates cell death induced by DNA damage and poly(ADP-ribose) polymerase-1," *Science*, vol. 354, no. 6308, article aad6872, 2016.

[20] C. Y. Chang, C. Y. Chiang, Y. W. Chiang et al., "Toxic effects of urethane dimethacrylate on macrophages through caspase activation, mitochondrial dysfunction, and reactive oxygen species generation," *Polymers (Basel)*, vol. 12, no. 6, p. 1398, 2020.

[21] S. W. Wu, C. H. Su, Y. C. Ho et al., "Genotoxic effects of 1-nitropyrene in macrophages are mediated through a p53-dependent pathway involving cytochrome _c_ release, caspase activation, and PARP-1 cleavage," *Ecotoxicology and Environmental Safety*, vol. 213, article 112062, 2021.

[22] F. M. Huang, Y. C. Chang, C. H. Su et al., "Rutin-protected-BisGMA-induced cytotoxicity, genotoxicity, and apoptosis in macrophages through the reduction of the mitochondrial apoptotic pathway and induction of antioxidant enzymes," *Environmental Toxicology*, vol. 36, no. 1, pp. 45–54, 2021.

[23] M. Donovan and T. G. Cotter, "Control of mitochondrial integrity by Bcl-2 family members and caspase-independent cell death," *Biochimica et Biophysica Acta*, vol. 1644, no. 2-3, pp. 133–147, 2004.

[24] N. Susnow, L. Zeng, D. Margineantu, and D. M. Hockenbery, "Bcl-2 family proteins as regulators of oxidative stress," *Seminars in Cancer Biology*, vol. 19, no. 1, pp. 42–49, 2009.

[25] P. Torres, J. Ferreira, A. Monteiro et al., "Air pollution: a public health approach for Portugal," *Science of The Total Environment*, vol. 643, pp. 1041–1053, 2018.

[26] W. Liu, Z. Xu, and T. Yang, "Health effects of air pollution in China," *International Journal of Environmental Research and Public Health*, vol. 15, no. 7, p. 1471, 2018.

[27] R. L. Li, Y. C. Ho, C. W. Luo, S. S. Lee, and Y. H. Kuan, "Influence of PM2.5 exposure level on the association between Alzheimer's disease and allergic rhinitis: a national population-based cohort study," *International Journal of Environmental Research and Public Health*, vol. 16, no. 18, p. 3357, 2019.

[28] J. P. Miller-Schulze, M. Paulsen, T. Kameda et al., "Evaluation of urinary metabolites of 1-nitropyrene as biomarkers for exposure to diesel exhaust in taxi drivers of Shenyang, China," *Journal of Exposure Science & Environmental Epidemiology*, vol. 23, no. 2, pp. 170–175, 2013.

[29] L. C. King, K. Loud, S. B. Tejada, M. J. Kohan, and J. Lewtas, "Evaluation of the release of mutagens and 1-nitropyrene from diesel particles in the presence of lung macrophages in culture," *Environmental Mutagenesis*, vol. 5, no. 4, pp. 577–588, 1983.

[30] C. Wang, J. Yang, L. Zhu et al., "Never deem lightly the "less harmful" low-molecular-weight PAH, NPAH, and OPAH – disturbance of the immune response at real environmental levels," *Chemosphere*, vol. 168, pp. 568–577, 2017.

[31] S. Elmore, "Apoptosis: a review of programmed cell death," *Toxicologic Pathology*, vol. 35, no. 4, pp. 495–516, 2007.

[32] M. S. D'Arcy, "Cell death: a review of the major forms of apoptosis, necrosis and autophagy," *Cell Biology International*, vol. 43, no. 6, pp. 582–592, 2019.

[33] N. Podechard, X. Tekpli, D. Catheline et al., "Mechanisms involved in lipid accumulation and apoptosis induced by 1-nitropyrene in Hepa1c7 cells," *Toxicology Letters*, vol. 206, no. 3, pp. 289–299, 2011.

[34] J. Ovrevik, V. M. Arlt, E. Oya et al., "Differential effects of nitro-PAHs and amino-PAHs on cytokine and chemokine responses in human bronchial epithelial BEAS-2B cells," *Toxicology and Applied Pharmacology*, vol. 242, no. 3, pp. 270–280, 2010.

[35] P. K. Tsai, S. W. Wu, C. Y. Chiang et al., "Evaluation of cytotoxicity, apoptosis, and genotoxicity induced by indium chloride in macrophages through mitochondrial dysfunction and reactive oxygen species generation," *Ecotoxicology and Environmental Safety*, vol. 193, p. 110348, 2020.

[36] I. F. Sevrioukova, "Apoptosis-inducing factor: structure, function, and redox regulation," *Antioxidants & Redox Signaling*, vol. 14, no. 12, pp. 2545–2579, 2011.

[37] D. Bano and J. H. M. Prehn, "Apoptosis-inducing factor (AIF) in physiology and disease: the tale of a repented natural born killer," *eBioMedicine*, vol. 30, pp. 29–37, 2018.

[38] N. Asare, X. Tekpli, M. Rissel et al., "Signalling pathways involved in 1-nitropyrene (1-NP)-induced and 3-nitrofluoranthene (3-NF)-induced cell death in Hepa1c7 cells," *Mutagenesis*, vol. 24, no. 6, pp. 481–493, 2009.

[39] F. Edlich, "BCL-2 proteins and apoptosis: recent insights and unknowns," *Biochemical and Biophysical Research Communications*, vol. 500, no. 1, pp. 26–34, 2018.

[40] T. Kuwana and D. D. Newmeyer, "Bcl-2-family proteins and the role of mitochondria in apoptosis," *Current Opinion in Cell Biology*, vol. 15, no. 6, pp. 691–699, 2003.

[41] J. Kale, E. J. Osterlund, and D. W. Andrews, "BCL-2 family proteins: changing partners in the dance towards death," *Cell Death and Differentiation*, vol. 25, no. 1, pp. 65–80, 2018.

[42] Y. Nakanishi, X. H. Pei, K. Takayama et al., "Polycyclic aromatic hydrocarbon carcinogens increase ubiquitination of p21 protein after the stabilization of p53 and the expression of p21," *American Journal of Respiratory Cell and Molecular Biology*, vol. 22, no. 6, pp. 747–754, 2000.

[43] X. J. Chen, L. Wang, and X. Y. Song, "Mitoquinone alleviates vincristine-induced neuropathic pain through inhibiting oxidative stress and apoptosis via the improvement of mitochondrial dysfunction," *Biomedicine & Pharmacotherapy*, vol. 125, p. 110003, 2020.

[44] K. Sinha, J. Das, P. B. Pal, and P. C. Sil, "Oxidative stress: the mitochondria-dependent and mitochondria-independent pathways of apoptosis," *Archives of Toxicology*, vol. 87, no. 7, pp. 1157–1180, 2013.

[45] N. Hamada, Y. Fujimichi, T. Iwasaki et al., "Emerging issues in radiogenic cataracts and cardiovascular disease," *Journal of Radiation Research*, vol. 55, no. 5, pp. 831–846, 2014.

[46] S. K. Chiang, S. E. Chen, and L. C. Chang, "A dual role of heme oxygenase-1 in cancer cells," *International Journal of Molecular Sciences*, vol. 20, p. 39, 2019.

[47] K. Zimmermann, J. Baldinger, B. Mayerhofer, A. G. Atanasov, V. M. Dirsch, and E. H. Heiss, "Activated AMPK boosts the Nrf2/HO-1 signaling axis–a role for the unfolded protein response," *Free Radical Biology & Medicine*, vol. 88, no. Part B, pp. 417–426, 2015.

[48] C. Mo, L. Wang, J. Zhang et al., "The crosstalk between Nrf2 and AMPK signal pathways is important for the anti-inflammatory effect of berberine in LPS-stimulated macrophages and endotoxin-shocked mice," *Antioxidants & Redox Signaling*, vol. 20, no. 4, pp. 574–588, 2014.

[49] B. Wang, S. Xu, X. Lu et al., "Reactive oxygen species-mediated cellular genotoxic stress is involved in 1-nitropyrene-induced trophoblast cycle arrest and fetal growth restriction," *Environmental Pollution*, vol. 260, p. 113984, 2020.

[50] E. J. Park and K. Park, "Induction of pro-inflammatory signals by 1-nitropyrene in cultured BEAS-2B cells," *Toxicology Letters*, vol. 184, no. 2, pp. 126–133, 2009.

3-Bromofluoranthene-induced cardiotoxicity of zebrafish and apoptosis in the vascular endothelial cells via intrinsic and extrinsic caspase-dependent pathways

Chun-Hung Su [a,b,c], Shih-Pin Chen [b,d], Li-You Chen [e,f], Jiann-Jou Yang [g,h], Yi-Chia Lee [i,j], Shiuan-Shinn Lee [k], Hsin-Hung Chen [l,m,n], Yan-Yan Ng [o], Yu-Hsiang Kuan [i,j,*]

[a] Department of Internal Medicine, Chung Shan Medical University Hospital, Taichung, Taiwan, ROC
[b] Department of Internal Medicine, School of Medicine, Chung Shan Medical University, Taichung, Taiwan, ROC
[c] Institute of Medicine, Chung Shan Medical University, Taichung, Taiwan, ROC
[d] Department of Internal Medicine, Chung Shan Medical University Hospital, Taichung, Taiwan, ROC
[e] Department of Anatomy, School of Medicine, College of Medicine, Chung Shan Medical University, Taichung, Taiwan, ROC
[f] Department of Medical Education, Chung Shan Medical University Hospital, Taichung, Taiwan, ROC
[g] Department of BioMedical Sciences, Chung Shan Medical University, Taichung, Taiwan, ROC
[h] Department of Medical Research, Chung Shan Medical University Hospital, Taichung, Taiwan, ROC
[i] Department of Pharmacology, School of Medicine, Chung Shan Medical University, Taichung, Taiwan, ROC
[j] Department of Pharmacy, Chung Shan Medical University Hospital, Taichung, Taiwan, ROC
[k] School of Public Health, Chung Shan Medical University, Taichung, Taiwan, ROC
[l] Division of Endocrinology and Metabolism, Department of Internal Medicine, Asia University Hospital, Taichung, Taiwan, ROC
[m] School of Medicine, Institute of Medicine and public health, Chung Shan Medical University, Taichung, Taiwan, ROC
[n] Chung Sheng Clinic, Nantou, Taiwan, ROC
[o] Department of Pediatric, Chung Kang branch, Cheng Ching Hospital, Taichung City, Taiwan, ROC

ARTICLE INFO

ABSTRACT

Fluoranthene, a high-molecular-weight polycyclic aromatic hydrocarbon (PAH), is widely present in air pollutants, including fine inhalable particulate matter. 3-Bromofluoranthene (3-BrFlu), which is a brominated fluoranthene and halogenated PAH, is generated from waste combustion, metallurgical processes, cement production, e-waste dismantling, and photoreaction. Vascular endothelial cells have key functions in the homeostasis and the development of the cardiovascular system. The zebrafish model has been widely employed to study cardiotoxicity and embryotoxicity. However, no evidence has indicated that 3-BrFlu induces cytotoxicity in vascular endothelial cells, or cardiotoxicity and embryotoxicity in zebrafish. In this study, 3-BrFlu induced concentration-dependent changes in embryo- and cardiotoxicity. Cytotoxicity was also induced by 3-BrFlu in a concentration-dependent manner through apoptosis and necrosis in vascular endothelial cells, SVEC4-10 cells. The activities of caspase-3, -8, and -9 were induced by 3-BrFlu via an intrinsic pathway constituting Bcl-2 downregulation, Bad upregulation, and mitochondrial dysfunction; the extrinsic pathway included the expression of death receptors, including tumour necrosis factor α and Fas receptors. These results indicated that 3-BrFlu caused cardio- and embryotoxicity in zebrafish through vascular endothelial cells cytotoxicity resulting from caspase-dependent apoptosis through intrinsic and extrinsic pathways.

1. Introduction

The World Health Organization (WHO) reported that approximately 91% of the global population is living in environments where air quality levels are below the acceptable limit; 4.2 and 3.8 million deaths per year are attributed to ambient and household air pollution, respectively (WHO, 2021; Gupta, 2021). The fine inhalable particulate matter PM2.5, which comprises a mixed composition of hazardous adherents

and solid particles, is the major component in air pollutant. Fluoranthene is a 5-membered ring, nonalternant high-molecular-weight polycyclic aromatic hydrocarbon (PAH) and was prevalent in PM2.5 collected from Japan, China, and the Czech Republic (Xing et al., 2020; Zhang et al., 2021; Polachova et al., 2020). 3-Bromofluoranthene (3-BrFlu) is a secondary formation among the adherents of PM2.5 that is formed through the bromination of fluoranthene (Jin et al., 2017; Shi et al., 2020).

Vascular endothelial cells (VECs) have key functions in the homeostasis of the circulatory system. VECs anchor to the subjacent basal lamina and then constitute the intima on the innermost side of blood vessels (Daneman and Prat, 2015). Dangerous air pollutants induce cytotoxicity in VECs as a result of caspase-dependent apoptosis though extrinsic and intrinsic apoptotic signalling pathways (Wang et al., 2020; Tseng et al., 2017). VEC dysfunction plays a role in various cardiovascular diseases (CVDs), including atherosclerosis, stroke, hypertension, coronary artery disease, and heart failure (Yamamoto and Ando, 2011; Xu et al., 2009). After air pollution exposure, VEC dysfunction and related CVDs led to cardiotoxicity (Borlak and Thum, 2002; Gao et al., 2021; Uzoigwe et al., 2013). Zebrafish have been widely employed to the assessment of cardiotoxicity, including heart rate and blood flow, in the zebrafish model (Bowley et al., 2021). To date, the capacity and mechanisms of cytotoxicity in VECs, embryotoxicity and cardiotoxicity in zebrafish induced by 3-BrFlu remain unclear. Therefore, this study examined cytotoxicity and apoptosis in VECs exposed to 3-BrFlu, and we analysed the mechanism of action of and cardiotoxicity induced by 3-BrFlu in zebrafish.

2. Materials and methods

2.1. Materials

Dulbecco's Modified Eagle's Medium (DMEM), antibiotic solution, trypsin- ethylenediaminetetraacetic acid (EDTA) solution, fetal bovine serum (FBS), and other cell culture materials were purchased from Hyclone (Logan, UT, USA). Annexin V-Fluorescein isothiocynate (FITC) Apoptosis Detection Kit I, Tumour Necrosis Factor α Receptor (TNFR)-FITC, and Fas Receptor (FasR)-FITC were supplied by BD Biosciences (San Diego, CA, USA). 1-phenyl 2-thiourea, $CaCl_2$, $MgSO_4$, 3-BrFlu, 3-(4,5-dimethylthiazol-2-yl)-2,5-diphenyl- tetrazolium bromide (MTT), sodium bicarbonate, propidium iodide (PI), tetraethylbenzimidazolylcarbocyanine iodide (JC-1), dimethyl sulfoxide (DMSO), and other reagents of analytical grade were supplied by Sigma-Aldrich (St. Louis, MO, USA). Primary antibodies for the detection of Bcl-2, Bad, and β-actin were obtained from Santa Cruz (Santa Cruz, CA, USA). Secondary antibodies for horseradish peroxidase (HRP)-conjugated mouse anti-rabbit IgG or goat anti-mouse IgG were purchased from Jackson ImmunoResearch Laboratories (Baltimore, MD, USA).

2.2. Zebrafish embryo collection and maintenance

Adult zebrafish aged 4 months, including wild-type (AB strain) and vascular-specific transgenic line (Tg[*fli-1: EGFP*]), were obtained from the Taiwan Zebrafish Core Facility at Academia Sinica. The fish were housed at 28 °C with a 14:10 h light–dark cycle under a recirculation system, as in pervious study (Su et al., 2020). After feeding twice a day, 2 male and 2 female zebrafish were placed into the breeding tank with a clapboard for 16 h. The clapboard acted as elimination to allow the zebrafish to mate. Embryos collected in the embryonic media (containing 5 mM NaCl, 0.17 mM KCl, 0.003% 1-phenyl 2-thiourea, 0.33 mM $CaCl_2$, 0.33 mM $MgSO_4$, pH 7.4) and those that fertilised and developed normally were selected for the further study. All experiments were conducted in accordance with the Institutional Animal Ethics Committee of Chung Shan Medical University (No. 2416).

2.3. Embryonic mortality assessment

After the 24 hpf stage, 10 embryos per quadruplicate were randomly selected and exposed to embryos incubated with 3-BrFlu at concentrations of 0, 3, 10, 50, and 100 μM for 24 and 48 h. The 3-BrFlu-induced mortality of zebrafish embryos was examined daily after 3-BrFlu exposure using an inverted microscope (Olympus, Japan).

2.4. Cardiotoxicity assessment

For cardiotoxicity analysis, the heart rate and blood flow of individual zebrafish was recorded at the lateral dorsal aortae using a microscope at 24 and 48 h. Video was captured using charge-coupled device cameras with a frame rate of approximately 20 fps and 3 megapixels for 60 s. Cardiac function was assessed through heart rate and blood flow measurement using DanioScope software (Noldus, Netherlands).

2.5. Cell culture and treatment

The murine VEC line SVEC4-10 was purchased from the Bioresource Collection Research Center (Shin-chu, Taiwan). All cells were cultured in DMEM supplemented with 1.5 g/L sodium bicarbonate, 4.5 g/L glucose, 10% heat-inactive FBS, and 1% antibiotics, including penicillin, streptomycin, and fungizone. The cells were maintained at 37 °C in humidified 5% CO_2 and incubated with 3-BrFlu at concentrations of 0, 3, 50, and 100 μM for 24 h (Su et al., 2021).

2.6. Cell viability assay

The cell viability was evaluated through MTT assay (Su et al., 2021). After cells were seeded on a plate for 16 h, the SVEC4-10 cells were incubated with 3-BrFlu at the designated concentrations for 24 h. After treatment, 5 mg/mL MTT was added, and the cells were incubated for 2 h at 37 °C. After the supernatant was discarded, dimethyl sulfoxide was added to dissolve the intracellular formazan crystals. The level of formazan solution was determined through the optical density at 570 nm by using a microplate reader (Synergy HT Multi-Mode Microplate Reader, Biotek, Winooski, VT).

2.7. Flow cytometric analysis of necrosis and apoptosis

Annexin-V-FITC and PI staining was used to determine the apoptosis and necrosis of the SVEC4-10 cells through flow cytometry (Huang et al., 2020). After the SVEC4-10 cells were exposed to 3-BrFlu at various concentrations for 24 h, they were resuspended in the annexin-V binding buffer. FITC-annexin-V and PI were added to each well at room temperature for 15 min in the dark. After the cells were incubated with 1-NP at various concentrations for 24 h, apoptosis and necrosis were identified through dual staining with FITC-annexin-V and PI staining solution in the dark at room temperature for 15 min. Finally, the samples were analysed using a BD Accuri C6 flow cytometer (San Jose, CA, USA). FITC-annexin-V-positive and PI-negative, FITC-annexin-V-positive and PI-positive, FITC-annexin-V-negative and PI-positive, and FITC-annexin-V-negative and PI-negative identified early apoptosis, late apoptosis, necrosis, and viability, respectively.

2.8. Cell cycle analysis

The effects of 3-BrFlu on the progression of cell cycle phases were analyzed by flow cytometry using PI staining (Huang et al., 2020). After treatment, cells were harvested by trypsin and fixed by 70% ethanol at − 20 °C for 12 h. After washed, cells were treated with RNase and PI at 37 °C for 30 min samples were examined using a BD Accuri C6 flow cytometer. The relative percentage of cells in the sub-G1, G0/G1, S, and G2/M phases were analysed.

2.9. Caspase activity assay

The activity of caspase-3, − 8, and − 9 was assayed with the fluorogenic substrates DEVD-AFC, IETD-AFC, and LEHD-AFC, respectively. The caspase-3, − 8, and − 9 assay kits were used according to the manufacturer's instructions (Wu et al., 2021).

2.10. Mitochondrial membrane potential assay

The effects of 3-BrFlu on mitochondrial membrane potential was assessed using JC-1 assay dye, as described in a previous study (Chang et al., 2020). Following treatment with 3-BrFlu, the cells were washed and incubated with JC-1 dye in a serum-free medium for 30 min at 37 °C. The cells were then washed and analysed using the flow cytometer. JC-1 aggregates form red fluorescence in healthy mitochondria; by contrast, the JC-1 monomers with green fluorescence indicate mitochondrial depolarisation.

2.11. Western blot assay

Protein expression was detected using Western blot assay in the SVEC4-10 cells, as described in a previous study (Wu et al., 2021). Following treatment with the 3-BrFlu at various concentrations for 24 h, the protein concentration from the whole-cell lysate was measured using a Bradford assay. The proteins were separated into levels using sodium dodecyl sulfate–polyacrylamide gel electrophoresis and then transferred to polyvinylidene difluoride membranes. Nonspecific binding was blocked with 5% skim milk buffer for 1 h. The membranes were incubated with the primary antibodies B-cell lymphoma 2 (Bcl-2), Bad, and β-actin overnight at 4 °C and then with the secondary antibody for 1 h at room temperature. Finally, the protein bands were visualised using an electrochemiluminescence kit and imaged using the Infiniti Vision System (Vilber, Lourmat, Collegien, France).

2.12. Measurement of TNFR and FasR expression

After treatment with 3-BrFlu, the cells were harvested and incubated with TNFR-FITC and FasR-FITC. After the samples were washed, they were analysed through the BD Accuri C6 flow cytometer.

2.13. Statistical analysis

One-way ANOVA analysis followed by a Bonferroni's post-hoc test was performed using a statistical analysis software package (SPSS Statistics version 22). A p value of < 0.05 was considered significant. Data was represented as mean $\pm$ standard deviation (S.D.).

3. Results

3.1. Embryo cytotoxicity and cardiotoxicity of BrFlu in zebrafish

The zebrafish embryos exposed to 3-BrFlu at various concentrations for 24–48 h were used to assess the embryo cytotoxicity in comparison to the untreated embryos taken as a control group. As depicted in Fig. 1A, the embryo cytotoxicity was observed in the 3-BrFlu-treated zebrafish after 24 h at 50 and 100 μM exhibited 85.00% and 82.50% survival rate, respectively, when compared to control group ($P < .05$). However, the embryos exposed to 3-BrFlu for 48 h exhibited toxicity at 10, 50, and 100 μM exhibited 87.50%, 85.00%, and 75.00% survival rate, respectively, when compared to control group ($P < .05$). Cardiotoxicity was assessed through measurement of the heart rate and blood flow in the zebrafish. Increased 3-BrFlu concentrations increased the heart rate of the treated embryos slightly at 24 h when compared to control group. Heart rate was significantly downregulated from 139.60 bpm (control) to 132.11 and 128.88 bpm by the 3-BrFlu at concentrations of 50 and 100 μM for 48 h ($P < .05$, Fig. 1B). Blood flow was
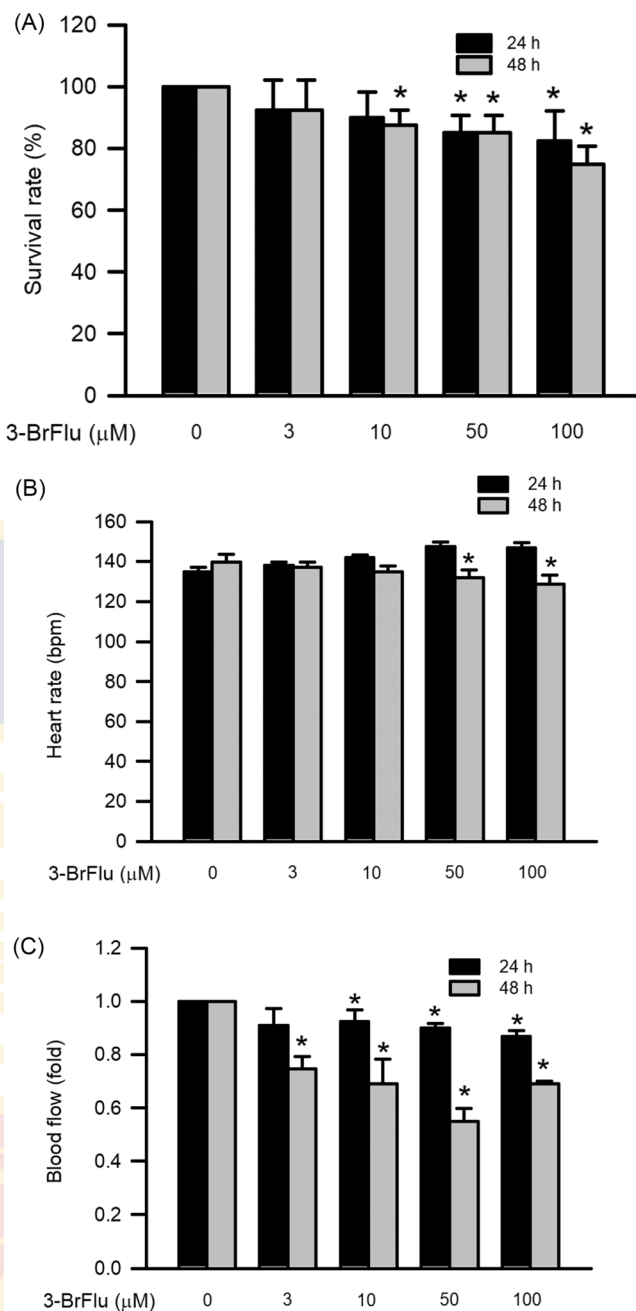
Fig. 1. Embryo Cytotoxicity and Cardiotoxicity of 3-BrFlu in Zebrafish. (A) 3-BrFlu reduced survival rate of zebrafish embryo. Survival rate of zebrafish embryo was incubated with 3-BrFlu at concentration of 0, 3, 10, 50, and 100 μM for 24 h and 48 h. 3-BrFlu reduced heart rate and blood flow in zebrafish. (B) Heart rate (beat per minute, bpm); (C) Blood flow (fold) of zebrafish were incubated with 3-BrFlu at concentration of 0, 3, 10, 50, and 100 μM for 24 h and 48 h. All data are represented as the mean $\pm$ SD. * $P < .05$ was considered significant compared with the control group.

significantly reduced in fold from 1.00 (control) to 0.92–0.87 by 10–100 μM 3-BrFlu for 24 h as compared with control group ($P < .05$, Fig. 1C). Blood flow was significantly reduced in fold from 1.00 (control) to 0.75–0.69 by 3–100 μM 3-BrFlu for 48 h as compared with control group ($P < .05$, Fig. 1C). These results indicated embryo cytotoxicity and cardiotoxicity induced by 3-BrFlu in zebrafish.

3.2. Effects of BrFlu on cytotoxicity, apoptosis, and necrosis in SVEC4-10 endothelial cells

The cytotoxicity of SVEC4-10 endothelial cells incubated with 0, 3, 10, 50, or 100 μM 3-BrFlu for 24 h was monitored through MTT color-imetric assay. We determined that the SVEC4-10 cells incubated with 3-BrFlu exhibited cytotoxicity in a concentration-dependent manner, with significant induction beginning at 3 μM ($P < .05$, Fig. 2A). The survival rate reduced from 100.00% (control) to 88.10–57.86% by 3–100 μM 3-BrFlu. FITC-annexin-V and PI double staining were employed to assess apoptosis and necrosis in the 3-BrFlu-treated SVEC4-10 cells. After the SVEC4-10 cells were incubated with 3-BrFlu for 24 h, the proportion of apoptosis and necrosis was upregulated in a concentration-dependent manner, with significant upregulation beginning at 3 μM ($P < .05$, Fig. 2B). Quantitatively, the population of apoptotic cells elevated from 0.60% (control) to 1.80–3.67% by 3–100 μM 3-BrFlu. The population of necrotic cells elevated from 0.07% (control) to 1.83–4.67% by 3–100 μM 3-BrFlu. In addition, PI staining was employed to measure the sub-G1 cell cycle phase in the cell cycle, which increased in a concentration-dependent manner; with significant induction beginning at 3 μM ($P < .05$, Fig. 2C). Quantitatively, the population of sub-G1 cells elevated from 5.37% (control) to 9.70–12.43% by 3–100 μM 3-BrFlu. These results indicated cytotoxicity, apoptosis, and necrosis induced by 3-BrFlu in SVEC4-10 endothelial cells.

3.3. Effects of BrFlu on Caspase-3, -8, and -9 activity in SVEC4-10 endothelial cells

The activation of caspase-3, -8, and -9 in the SVEC4-10 cells treated with 3-BrFlu at various concentrations for 24 h was monitored using caspase-3, -8, and -9 assay kits. The 3-BrFlu-induced activation of these caspases occurred in a concentration-dependent manner, with significant effects observable beginning at 3 μM ($P < .05$, Fig. 3). The activation of caspase -8 and -9 was significantly increased in fold from 1.00 (control) to 1.53–2.05 and 1.58–2.31, respectively, by 3–100 μM 3-BrFlu. The caspase-3 activity was significantly increased in fold from 1.00 (control) to 1.55–2.95 by 3–100 μM 3-BrFlu. These results indicated that the activation of caspase-3 was induced by 3-BrFlu at a lower concentration than caspase-8 and -9.

3.4. Effects of BrFlu on mitochondrial dysfunction in SVEC4-10 endothelial cells

The effects of 3-BrFlu on mitochondrial dysfunction in the SVEC4-10 endothelial cells was investigated through JC-1 stain assay. Dysfunction of the mitochondria was induced by 3-BrFlu in a concentration-dependent manner, with significant effects noted at 50 and 100 μM ($P < .05$, Fig. 4). Quantitatively, the population of mitochondrial dysfunction elevated in fold from 1.00 (control) to 1.26–2.00 by 3–100 μM 3-BrFlu. These results indicated mitochondrial dysfunction induced by 3-BrFlu in SVEC4-10 endothelial cells.

3.5. Effects of BrFlu on the expression level of Bcl-2 and bad in SVEC4-10 endothelial cells

To examine the regulation of mitochondrial integrity by Bcl-2 and Bad in the SVEC4-10 endothelial cells, a Western blot assay was employed. 3-BrFlu reduced and increased the levels of Bcl-2 and Bad, respectively, in a concentration-dependent manner, with significant effects at concentrations higher than 3 μM and 10 μM (both $P < .05$, Fig. 5). Quantitatively, the Bcl-2 expression reduced in fold from 1.00 (control) to 0.73–0.70 by 3–100 μM 3-BrFlu. The Bad expression increased in fold from 1.00 (control) to 1.17–1.43 by 10–100 μM 3-BrFlu.These results indicated 3-BrFlu-induced upregulation of Bcl-2 expression and downregulation of Bad expression in SVEC4-10 endothelial cells.

3.6. Effects of BrFlu on the expression level of TNFR and FasR in SVEC4-10 endothelial cells
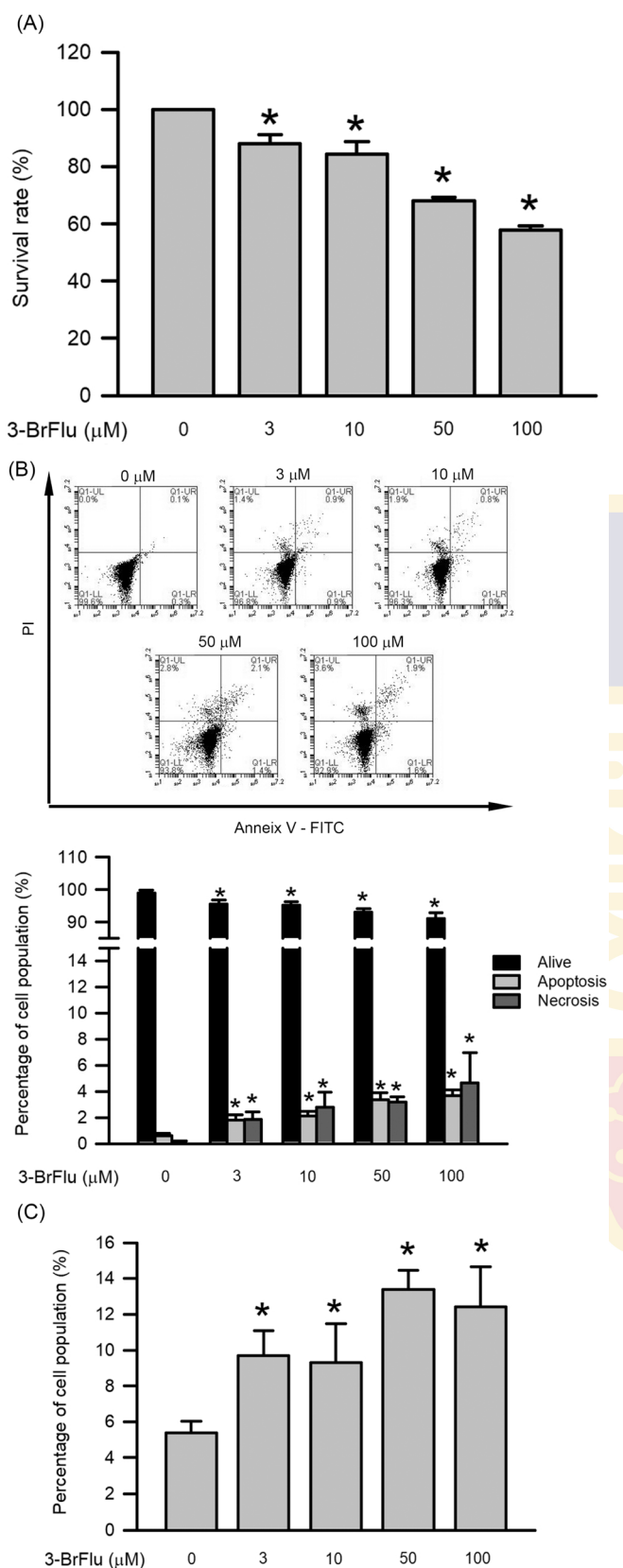
We examined the expressions of the death receptors TNFR and FasR in the SVEC4-10 endothelial cells by using a flow cytometry assay. The expressions of TNFR and FasR increased under 3-BrFlu treatment in a concentration-dependent manner, with a significant effect exhibited at concentrations higher than 3 and 50 μM, respectively ($P < .05$, Fig. 6). Quantitatively, the TNFR expression increased in fold from 1.00 (control) to 1.31–1.68 by 3–100 μM 3-BrFlu. The FasR expression increased in fold from 1.00 (control) to 1.18–1.52 by 10–100 μM 3-BrFlu. These results indicated 3-BrFlu-induced expression of TNFR and FasR in SVEC4-10 endothelial cells.

4. Discussion

Fluoranthene, a toxic and prominent PAH, is present in air pollutants such as PM2.5 (Xing et al., 2020; Zhang et al., 2021; Polachova et al., 2020). 3-BrFlu is a halogenated derivative of PAHs generated through waste combustion, metallurgical processes, cement production, e-waste dismantling, and photoreaction (Jin et al., 2020, 2018). The toxic capacity of halogen-based PAHs is higher than that of their corresponding parent PAHs (Vuong et al., 2020). Fluoranthene can also induce cytotoxicity in Chinese hamster lung fibroblast (V79) cells, colon (HT-29) cells, and haematopoietic and mesenchymal stem cells (Zhou et al., 2021; Harris et al., 2013; Hoque et al., 2019; Yang et al., 2019). The endothelial cell models such as human umbilical vein endothelial cells and SVEC4-10 cells have been widely used to study toxicant-induced physiological responses in in vitro systems (Kadam et al., 2009; Weng et al., 2014). The endothelial cell model, human umbilical vein endothelial cells and SVEC4-10 cells, has been widely applicable to physiological function and toxic response for in vitro studies (Kadam et al., 2009; Weng et al., 2014). In human umbilical vein endothelial cells, cytotoxicity can be induced through a mixture of fluoranthene with phenanthrene and pyrene (Herrera-Bravo et al., 2021). Cardiotoxicity caused by endothelial dysfunction is one of the mechanisms that underlie CVD (Borlak and Thum, 2002; Gao et al., 2021; Uzoigwe et al., 2013). The embryonic zebrafish is an ideal model for a rapid prediction of adverse effects caused by a wide array of air pollutants, environmental toxicants and drugs (Chen et al., 2017; Planchart et al., 2016; Lantz-McPeak et al., 2015; Sarmah and Marrs, 2016). In addition, the zebrafish embryos are transparent and they develop rapidly and outside of the uterus (Teame et al., 2019). The heart is the first well developed and functional organ in the vertebrate model zebrafish embryos (Brown et al., 2016). Therefore, zebrafish model is particularly suitable in embryotoxicity and cardiotoxicity (Lantz-McPeak et al., 2015; Sarmah and Marrs, 2016). In the present study, we assessed the hazardous effects of 3-BrFlu by evaluating the embryo-, cyto- and cardiotoxicity in zebrafish SVEC4-10 cells.

During frequent and low haze periods in Beijing, the concentration of 3-BrFlu in atmospheric particulate matter is 0.58 and 0.17 pg/m^3, respectively (Shi et al., 2020). There is currently no evidence that acute toxic effects of 3-BrFlu. Acute systemic toxicity categories are classified by LC50 via differential routes of administration according to the United Nations global harmonisation system in mammal and aquatic animals (Seidle et al., 2010, 2011). Under acute systemic toxicity categories I to III, the LC50 of 3-BrFlu is 0.17 μM to 3.56 mM and 3.56–355.68 μM in mammal and aquatic animals, respectively. Therefore, the acute toxic effects were assessed by 3-BrFlu at the concentration of 3–100 μM at the present study. Based on our results, we proposed that 3-BrFlu induced cytotoxicity at 24 h in a concentration-dependent manner in VECs.

The normal physiological functions of VECs lead to embryo development and cardiovascular circulation in animals, and zebrafish serve as powerful animal models for the assessment of embryonic development and cardiovascular circulation (Hogan and Schulte-Merker, 2017; Zhong et al., 2019). The zebrafish model is a reliable model through which to

(A)

3-BrFlu (μM)

(B)

(C)

(caption on next column)

study the toxicity of environmental pollutants (Padilla et al., 2012). Downregulation of the heart rate in zebrafish was observed after exposure to fluoranthene, which reduced the survival rate of the embryos (Raftery et al., 2017; Jayasundara et al., 2015; Perrichon et al., 2014). We determined that 3-BrFlu induced a reduction of the heart rate, blood flow, and embryonic survival rate in the zebrafish. Based on these findings, we proposed that 3-BrFlu induced cardiotoxicity and embryotoxicity in zebrafish through the VEC cytotoxicity.

The apoptosis of the VECs participate in the pathogenesis of CVDs, including atherosclerosis, coronary artery disease, atrial fibrillation, and thromboembolism (Zeng et al., 2020; Li et al., 2020; Shan et al., 2019). Cardiotoxicity is caused by VEC dysfunction and related CVDs (Borlak and Thum, 2002; Gao et al., 2021; Uzoigwe et al., 2013). Apoptosis is induced by fluoranthene in Sertoli cells, liver HepG2 cells, T cell hybridomas, and bone marrow-derived mesenchymal stem cells (BM-MSCs) (Raychoudhury and Kubinski, 2003; Yamaguchi et al., 1996; Hoque et al., 2019). We provided evidence that apoptosis and necrosis were induced by 3-BrFlu in a concentration-dependent manner in VECs. Furthermore, we determined that 3-BrFlu induced sub-G1 phase formation as a result of DNA damage in the VECs. These results demonstrate that apoptosis is the main type of cell death in 3-BrFlu-treated VECs.

Following air pollutant exposure, the activation of caspases is a vital signal pathway mediated in endothelial cell apoptosis (Wang et al., 2020; Tseng et al., 2017). Caspase-3 is the executioner caspase and pivotal mediator in the progress of apoptosis in VECs (Oh et al., 2019; Ismail et al., 2021). The mechanism of caspase-3 activation is divided into 2 major pathways, the intrinsic and extrinsic signalling pathway. The intrinsic signalling pathway, also named the mitochondria-dependent pathway, is triggered by caspase-9 activation through mitochondrial dysfunction. The extrinsic signalling pathway, also named the death receptor pathway, is triggered by caspase-8 activation through death receptor activation (Jin and El-Deiry, 2005; D'Arcy, 2019). The expression and activation of caspase-3 and -9 is induced by fluoranthene in the BM-MSC and HT-29 cells (Hoque et al., 2019; Harris et al., 2013). In this study, we determined that caspase-3, -8, and -9 activity was induced by 3-BrFlu in a concentration-dependent manner in the VECs, demonstrating that 3-BrFlu-induced apoptosis occurred through caspase-3 and its upstream factors, caspase-8 and -9.

The Bcl-2 family contains the main proteins involved in the regulation of mitochondrial integrity. Disruption of the mitochondrial integrity causes dissipation of mitochondrial membrane potential through the intrinsic apoptosis pathway. The Bcl-2 protein family contains Bcl-2 and Bad, pro- and anti-apoptosis proteins, respectively (Voss and Strasser, 2020; Dadsena et al., 2021). In addition, the extrinsic apoptosis pathway is primarily triggered by hazardous substances that stimulate death receptors such as TNFR and FasR through the cleavage of caspase-8 into its active fragment (Mandal et al., 2020). Bcl-2 expression and mitochondrial membrane potential are downregulated by fluoranthene in
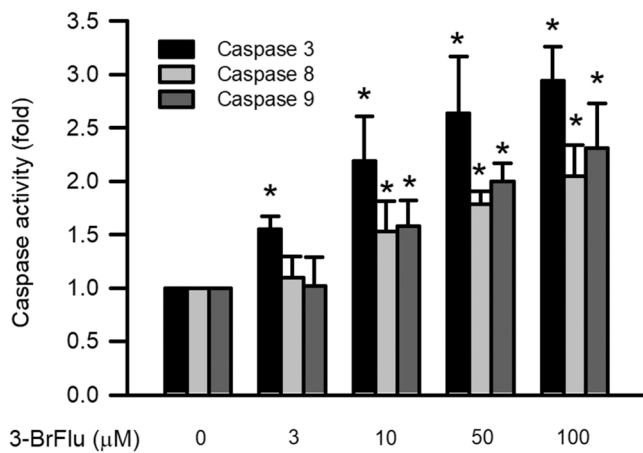
Fig. 3. 3-BrFlu-induced caspase-3, -8, and -9 activity in SVEC4-10 endothelial cells. The activity of caspase-3, -8, and -9 was measured by western blot assay after treated with 3-BrFlu for 24 h. The change in fold of caspase-3, -8, and -9 activity between the treated and control groups were calculated. Results are expressed as means ± SD (n = 3). * $P < .05$ was considers significant as compare with control group.

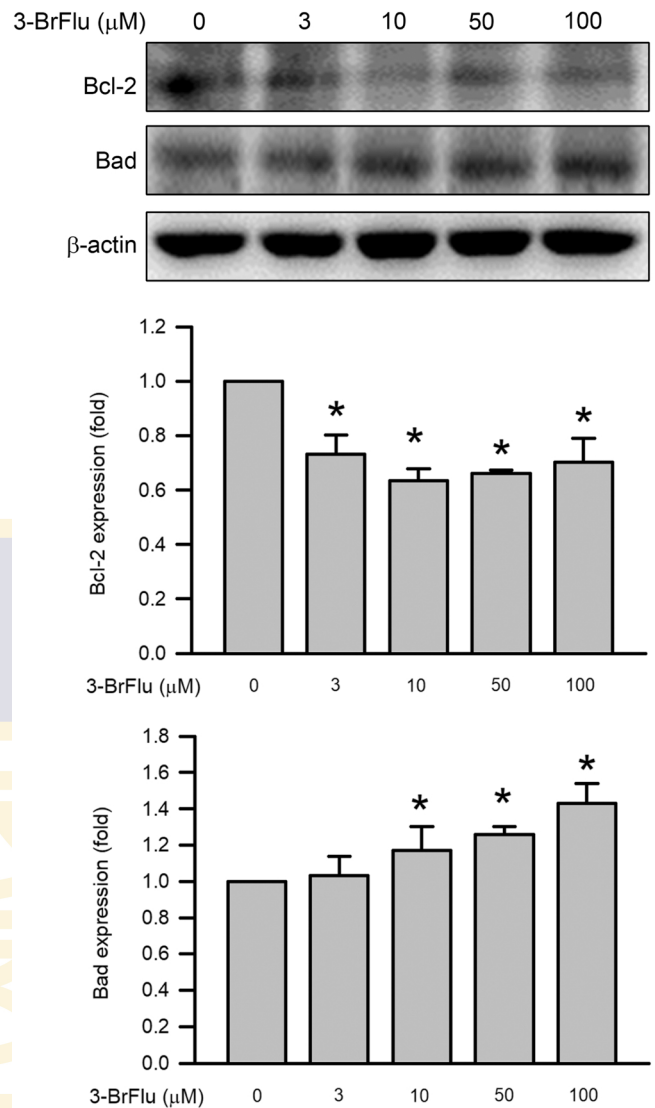**Fig. 5.** 3-BrFlu-induced expression of Bcl-2 and Bad in SVEC4-10 endothelial cells. The expression of Bcl-2 and Bad was measured by western blot assay after treated with 3-BrFlu for 24 h. The change in fold of Bcl-2 and Bad expression between the treated and control groups were calculated. Data are expressed as mean ± SD (n = 3). * $P < .05$ was considered significant compared with the control group.

BM-MSCs (Hoque et al., 2019). In our study, 3-BrFlu treatment induced mitochondrial dysfunction, increased Bcl-2, and decreased Bad in a concentration-dependent manner. The expression of the death receptors TNFR and FasR was also induced by 3-BrFlu in a concentration-dependent manner. In brief, 3-BrFlu induced the activation of caspase-dependent apoptosis through intrinsic and extrinsic pathways in VECs.

5. Conclusion

In conclusion, we demonstrated that zebrafish treated with 3-BrFlu exhibited embryotoxicity and cardiotoxicity and that the incubation with 3-BrFlu for 24 h induced cytotoxicity in VECs, SVEC4-10 cells (Fig. 7). VECs compromised by 3-BrFlu activated the apoptosis pathway; the mechanism of this apoptosis comprises caspase-3 activation through the intrinsic and extrinsic pathways. VEC incubation with 3-BrFlu caused caspase-9 activation in the intrinsic apoptosis pathway through Bcl-2 upregulation, Bad downregulation, and mitochondrial dysfunction. 3-BrFlu treatment induced caspase-8 activation in the extrinsic

Fig. 4. 3-BrFlu-induced mitochondria dysfunction in SVEC4-10 endothelial cells. The portion of mitochondria dysfunction was measured by JC-1 assays using flowcytometry. After cell treatment, the portion of MMP was measured using the JC-1 assay. Quantitatively, the percentage of MMP downregulation cells was calculated and analyzed. The MPTP opening was measured by flowcytometry. The change in fold of MMP dysfunction cells between the treated and control groups were calculated. Data are expressed as mean ± SD (n = 5). * $P < .05$ was considered significant compared with the control group.

Fig. 6. 3-BrFlu-induced expression of TNFR and FasR in SVEC4-10 endothelial cells. The change in fold of Bcl-2 and Bad expression between the treated and control groups were calculated. Data are expressed as mean ± SD (n = 3). * $P < .05$ was considered significant compared with the control group.
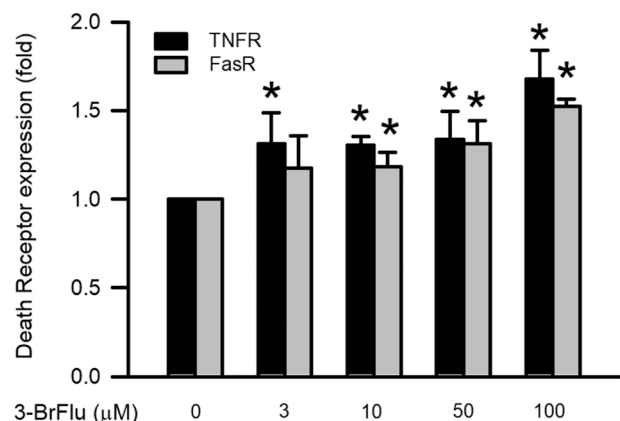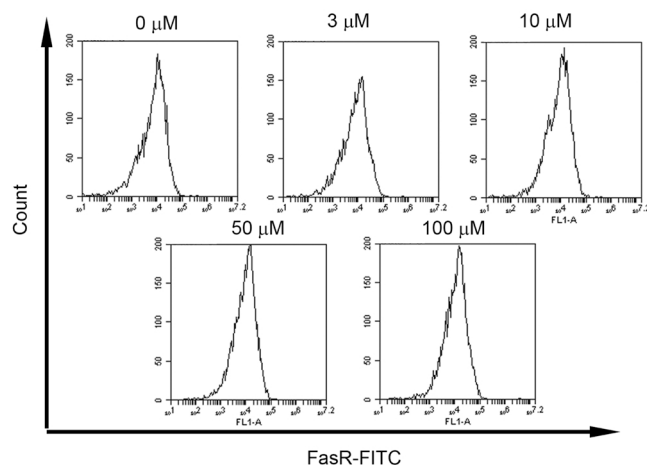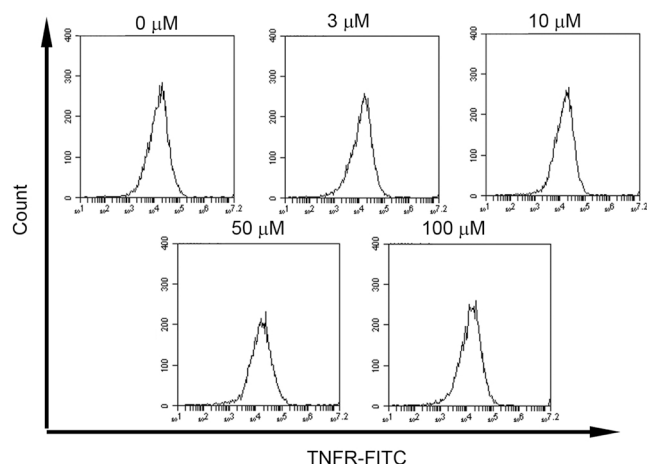
apoptosis pathway through the upregulation of death receptors, including TNFR and FasR. Overall, these results indicated that 3-BrFlu caused cardiotoxicity and embryotoxicity in zebrafish as a result of VEC cytotoxicity through caspase-dependent apoptosis. Moreover, 3-BrFlu induced caspase-dependent apoptosis through intrinsic and extrinsic pathways in the VECs.
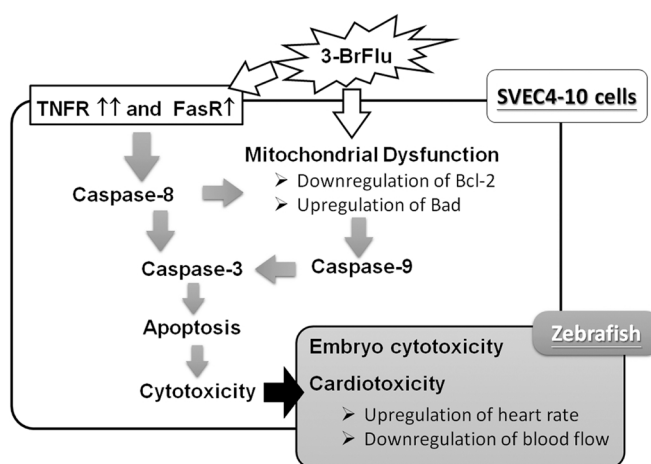
Fig. 7. Schemes of the mechanism of the 3-BrFlu-induced apoptosis and cytotoxicity in SVEC4-10 endothelial cells and Cardiotoxicity of zebrafish.

CRediT authorship contribution statement

Chun-Hung Su: Conceptualization, Writing – original draft, Methodology, Visualization, Investigation, Funding acquisition. **Shih-Pin Chen**: Conceptualization, Writing – original draft, Methodology, Investigation. **Li-You Chen**: Methodology, Validation, Investigation. **Jiann-Jou Yang**: Conceptualization, Methodology, Validation. **Yi-Chia Lee**: Methodology, Validation, Investigation, Writing – review & editing. **Shiuan-Shinn Lee**: Validation, Investigation, Writing – review & editing. **Hsin-Hung Chen**: Writing – review & editing, Visualization. **Yan-Yan Ng**: Conceptualization, Validation, Investigation, Data curation, Writing – review & editing. **Yu-Hsiang Kuan**: Conceptualization, Data curation, Supervision, Writing – review & editing, Funding acquisitionn.

Declaration of Competing Interest

The authors declare that they have no known competing financial interests or personal relationships that could have appeared to influence the work reported in this paper.

Acknowledgements

References

Borlak, J., Thum, T., 2002. PCBs alter gene expression of nuclear transcription factors and other heart-specific genes in cultures of primary cardiomyocytes: possible implications for cardiotoxicity. Xenobiotica 32 (12), 1173–1183.

Bowley, G., Kugler, E., Wilkinson, R., Lawrie, A., van Eeden, F., Chico, T.J.A., Evans, P. C., Noël, E.S., Serbanovic-Canic, J., 2021. Zebrafish as a tractable model of human cardiovascular disease. Br. J. Pharmacol. https://doi.org/10.1111/bph.15473.

Brown, D.R., Samsa, L.A., Qian, L., Liu, J., 2016. Advances in the study of heart development and disease using zebrafish. J. Cardiovasc. Dev. Dis. 3 (2), 13.

Chang, C.Y., Chiang, C.Y., Chiang, Y.W., Lee, M.W., Lee, C.Y., Chen, H.Y., Lin, H.W., Kuan, Y.H., 2020. Toxic effects of urethane dimethacrylate on macrophages through caspase activation, mitochondrial dysfunction, and reactive oxygen species generation. Polymers 12 (6), 1398.

Chen, B., Gao, Z.Q., Liu, Y., Zheng, Y.M., Han, Y., Zhang, J.P., Hu, C.Q., 2017. Embryo and developmental toxicity of cefazolin sodium impurities in zebrafish. Front. Pharmacol. 8, 403.

Dadsena, S., Jenner, A., García-Sáez, A.J., 2021. Mitochondrial outer membrane permeabilization at the single molecule level. Cell. Mol. Life Sci. 78 (8), 3777–3790.

Daneman, R., Prat, A., 2015. The blood-brain barrier. Cold Spring Harb. Perspect. Biol. 7 (1), a020412.

D'Arcy, M.S., 2019. Cell death: a review of the major forms of apoptosis, necrosis and autophagy. Cell. Biol. Int. 43 (6), 582–592.

Gao, J., Pan, X., Li, G., Chatterjee, E., Xiao, J., 2021. Physical exercise protects against endothelial dysfunction in cardiovascular and metabolic diseases. J. Cardiovasc. Transl. Res. https://doi.org/10.1007/s12265-021-10171-3.

Gupta, A.K., 2021. JAHA spotlight on air pollution and cardiovascular disease: a call for urgent action. J. Am. Heart Assoc. 10 (10), e022209.

Harris, K.L., Myers, J.N., Ramesh, A., 2013. Benzo(a)pyrene modulates fluoranthene-induced cellular responses in HT-29 colon cells in a dual exposure system. Environ. Toxicol. Pharmacol. 36 (2), 358–367.

Herrera-Bravo, J., Beltrán-Lissabet, J.F., Saavedra, K., Saavedra, N., Hevia, M., Alvear, M., Lanas, F., Salazar, L.A., 2021. Protective effect of Pinot noir pomace extract against the cytotoxicity induced by polycyclic aromatic hydrocarbons on endothelial cells. Food Chem. Toxicol. 148, 111947.

Hogan, B.M., Schulte-Merker, S., 2017. How to plumb a pisces: understanding vascular development and disease using zebrafish embryos. Dev. Cell 42 (6), 567–583.

Hoque, M.M., Lee, Y.E., Kim, H.R., Shin, M.G., 2019. Potential biomarkers and antagonists for fluoranthene-induced cellular toxicity of bone marrow derived mesenchymal stem cells. Blood Res. 54 (4), 253–261.

Huang, F.M., Chang, Y.C., Su, C.H., Wu, S.W., Lee, S.S., Lee, M.W., Yeh, K.L., Chiang, C.Y., Tu, D.G., Lu, Y.C., Kuan, Y.H., 2020. Rutin-protected BisGMA-induced cytotoxicity, genotoxicity, and apoptosis in macrophages through the reduction of the mitochondrial apoptotic pathway and induction of antioxidant enzymes. Environ. Toxicol. 36 (1), 45–54.

Ismail, M.B., Rajendran, P., AbuZahra, H.M., Veeraraghavan, V.P., 2021. Mangiferin inhibits apoptosis in doxorubicin-induced vascular endothelial cells via the Nrf2 signaling pathway. Int. J. Mol. Sci. 22 (8), 4259.

Jayasundara, N., Van Tiem Garner, L., Meyer, J.N., Erwin, K.N., Di Giulio, R.T., 2015. AHR2-Mediated transcriptomic responses underlying the synergistic cardiac developmental toxicity of PAHs. Toxicol. Sci. 143 (2), 469–481.

Jin, R., Liu, G., Jiang, X., Liang, Y., Fiedler, H., Yang, L., Zhu, Q., Xu, Y., Gao, L., Su, G., Xiao, K., Zheng, M., 2017. Profiles, sources and potential exposures of parent, chlorinated and brominated polycyclic aromatic hydrocarbons in haze associated atmosphere. Sci. Total Environ. 593–594, 390–398.

Jin, R., Yang, L., Zheng, M., Xu, Y., Li, C., Liu, G., 2018. Source identification and quantification of chlorinated and brominated polycyclic aromatic hydrocarbons from cement kilns co-processing solid wastes. Environ. Pollut. 242 (Pt B), 1346–1352.

Jin, R., Zheng, M., Lammel, G., Musa Bandowe, B.A., Liu, G., 2020. Chlorinated and brominated polycyclic aromatic hydrocarbons: sources, formation mechanisms, and occurrence in the environment. Prog. Energy Combust. Sci. 76, 100803.

Jin, Z., El-Deiry, W.S., 2005. Overview of cell death signaling pathways. Cancer Biol. Ther. 4 (2), 139–163.

Kadam, S.S., Tiwari, S., Bhonde, R.R., 2009. Simultaneous isolation of vascular endothelial cells and mesenchymal stem cells from the human umbilical cord. Vitr. Cell. Dev. Biol. Anim. 45 (1–2), 23–27.

Lantz-McPeak, S., Guo, X., Cuevas, E., Dumas, M., Newport, G.D., Ali, S.F., Paule, M.G., Kanungo, J., 2015. Developmental toxicity assay using high content screening of zebrafish embryos. J. Appl. Toxicol. 35 (3), 261–272.

Li, P., Wang, J., Zhao, X., Ru, J., Tian, T., An, Y., Tang, L., Bai, Y., 2020. PTEN inhibition attenuates endothelial cell apoptosis in coronary heart disease via modulating the AMPK-CREB-Mfn2-mitophagy signaling pathway. J. Cell. Physiol. 235 (5), 4878–4889.

Mandal, R., Barrón, J.C., Kostova, I., Becker, S., Strebhardt, K., 2020. Caspase-8: The double-edged sword. Biochim. Biophys. Acta Rev. Cancer 1873 (2), 188357.

Oh, Y., Ahn, C.B., Nam, K.H., Kim, Y.K., Yoon, N.Y., Je, J.Y., 2019. Amino acid composition, antioxidant, and cytoprotective effect of Blue Mussel (Mytilus edulis) hydrolysate through the inhibition of Caspase-3 activation in oxidative stress-mediated endothelial cell injury. Mar. Drugs 17 (2), 135.

Padilla, S., Corum, D., Padnos, B., Hunter, D.L., Beam, A., Houck, K.A., Sipes, N., Kleinstreuer, N., Knudsen, T., Dix, D.J., Reif, D.M., 2012. Zebrafish developmental screening of the ToxCast Phase I chemical library. Reprod. Toxicol. 33 (2), 174–187.

Perrichon, P., Le Bihanic, F., Bustamante, P., Le Menach, K., Budzinski, H., Cachot, J., Cousin, X., 2014. Influence of sediment composition on PAH toxicity using zebrafish (Danio rerio) and Japanese medaka (Oryzias latipes) embryo-larval assays. Environ. Sci. Pollut. Res. Int 21 (24), 13703–13719.

Planchart, A., Mattingly, C.J., Allen, D., Ceger, P., Casey, W., Hinton, D., Kanungo, J., Kullman, S.W., Tal, T., Bondesson, M., Burgess, S.M., Sullivan, C., Kim, C., Behl, M., Padilla, S., Reif, D.M., Tanguay, R.L., Hamm, J., 2016. Advancing toxicology research using in vivo high throughput toxicology with small fish models. ALTEX 33 (4), 435–452.

Polachova, A., Gramblicka, T., Parizek, O., Sram, R.J., Stupak, M., Hajslova, J., Pulkrabova, J., 2020. Estimation of human exposure to polycyclic aromatic hydrocarbons (PAHs) based on the dietary and outdoor atmospheric monitoring in the Czech Republic. Environ. Res. 182, 108977.

Raftery, T.D., Jayasundara, N., Di Giulio, R.T., 2017. A bioenergetics assay for studying the effects of environmental stressors on mitochondrial function in vivo in zebrafish larvae. Comp. Biochem. Physiol. C Toxicol. Pharmacol. 192, 23–32.

Raychoudhury, S.S., Kubinski, D., 2003. Polycyclic aromatic hydrocarbon-induced cytotoxicity in cultured rat Sertoli cells involves differential apoptotic response. Environ. Health Perspect. 111 (1), 33–38.

Sarmah, S., Marrs, J.A., 2016. Zebrafish as a vertebrate model system to evaluate effects of environmental toxicants on cardiac development and function. Int. J. Mol. Sci. 17 (12), 2123.

Seidle, T., Prieto, P., Bulgheroni, A., 2011. Examining the regulatory value of multi-route mammalian acute systemic toxicity studies. ALTEX Altern. Anim. Exp. 28 (2), 95–102.

Seidle, T., Robinson, S., Holmes, T., Creton, S., Prieto, P., Scheel, J., Chlebus, M., 2010. Cross-sector review of drivers and available 3Rs approaches for acute systemic toxicity testing. Toxicol. Sci. 116 (2), 382–396.

Shan, X., Liu, Z., Wulasihan, M., Ma, S., 2019. Edoxaban improves atrial fibrillation and thromboembolism through regulation of the Wnt-β-induced PI3K/ATK-activated protein C system. Exp. Ther. Med. 17 (5), 3509–3517.

Shi, M., Zhang, R., Wang, Y., Zhang, Y., Zhang, Y., Zhang, Y., Zhang, Y., 2020. Health risk assessments of polycyclic aromatic hydrocarbons and chlorinated/brominated polycyclic aromatic hydrocarbons in urban air particles in a haze frequent area in China. Emerg. Contam. 6, 172–178.

Su, C.H., Ho, Y.C., Lee, M.W., Tseng, C.C., Lee, S.S., Hsieh, M.K., Chen, H.H., Lee, C.Y., Wu, S.W., Kuan, Y.H., 2021. 1-Nitropyrene induced reactive oxygen species-mediated apoptosis in macrophages through AIF nuclear translocation and AMPK/Nrf-2/HO-1 pathway activation. Oxid. Med. Cell. Longev. 2021, 9314342.

Su, H.A., Lai, T.W., Li, S.Y., Su, T.R., Yang, J.J., Su, C.C., 2020. The functional role of CONNEXIN 26 mutation in nonsyndromic hearing loss, demonstrated by zebrafish Connexin 30.3 homologue model. Cells 9 (5), 1291.

Teame, T., Zhang, Z., Ran, C., Zhang, H., Yang, Y., Ding, Q., Xie, M., Gao, C., Ye, Y., Duan, M., Zhou, Z., 2019. The use of zebrafish (Danio rerio) as biomedical models. Anim. Front. 9 (3), 68–77.

Tseng, C.Y., Wang, J.S., Chao, M.W., 2017. Causation by diesel exhaust particles of endothelial dysfunctions in cytotoxicity, pro-inflammation, permeability, and apoptosis induced by ROS generation. Cardiovasc. Toxicol. 17 (4), 384–392.

Uzoigwe, J.C., Prum, T., Bresnahan, E., Garelnabi, M., 2013. The emerging role of outdoor and indoor air pollution in cardiovascular disease. N. Am. J. Med. Sci. 5 (8), 445–453.

Voss, A.K., Strasser, A., 2020. The essentials of developmental apoptosis. F1000Research 9 (F1000 Faculty Rev), 148.

Vuong, Q.T., Kim, S.J., Nguyen, T.N.T., Thang, P.Q., Lee, S.J., Ohura, T., Choi, S.D., 2020. Passive air sampling of halogenated polycyclic aromatic hydrocarbons in the largest industrial city in Korea: Spatial distributions and source identification. J. Hazard. Mater. 382, 121238.

WHO , 2021. Global Health Observatory, Air pollution data portal 2021. Available at: ⟨https://www.who.int/airpollution/ambient/about/en/⟩. (Accessed May 7, 2021).

Wang, Y., Wu, T., Tang, M., 2020. Ambient particulate matter triggers dysfunction of subcellular structures and endothelial cell apoptosis through disruption of redox equilibrium and calcium homeostasis. J. Hazard. Mater. 394, 122439.

Weng, C.Y., Chiou, S.Y., Wang, L., Kou, M.C., Wang, Y.J., Wu, M.J., 2014. Arsenic trioxide induces unfolded protein response in vascular endothelial cells. Arch. Toxicol. 88 (2), 213–226.

Wu, S.W., Su, C.H., Ho, Y.C., Huang-Liu, R., Tseng, C.C., Chiang, Y.W., Yeh, K.L., Lee, S.S., Chen, W.Y., Chen, C.J., Li, Y.C., Lee, C.Y., Kuan, Y.H., 2021. Genotoxic effects of 1-nitropyrene in macrophages are mediated through a p53-dependent pathway involving cytochrome c release, caspase activation, and PARP-1 cleavage. Ecotoxicol. Environ. Saf. 213, 112062.

Xing, W., Zhang, L., Yang, L., Zhou, Q., Zhang, X., Toriba, A., Hayakawa, K., Tang, N., 2020. Characteristics of PM(2.5)-bound polycyclic aromatic hydrocarbons and nitro-polycyclic aromatic hydrocarbons at a roadside air pollution monitoring station in Kanazawa, Japan. Int. J. Environ. Res. Public Health 17 (3), 805.

Xu, F., Sun, Y., Chen, Y., Sun, Y., Li, R., Liu, C., Zhang, C., Wang, R., Zhang, Y., 2009. Endothelial cell apoptosis is responsible for the formation of coronary thrombotic atherosclerotic plaques. Tohoku J. Exp. Med. 218 (1), 25–33.

Yamaguchi, K., Near, R., Shneider, A., Cui, H., Ju, S.T., Sherr, D.H., 1996. Fluoranthene-induced apoptosis in murine T cell hybridomas is independent of the aromatic hydrocarbon receptor. Toxicol. Appl. Pharmacol. 139 (1), 144–152.

Yamamoto, K., Ando, J., 2011. New molecular mechanisms for cardiovascular disease: blood flow sensing mechanism in vascular endothelial cells. J. Pharmacol. Sci. 116 (4), 323–331.

Yang, S.H., Kang, M.G., Kim, H.R., Lee, Y.E., Na, B.R., Lee, J.H., Shin, J.H., Shin, M.G., 2019. Fluoranthene-induced cytotoxicity and direct effect of Aryl hydrocarbon receptor antagonist on hematopoietic stem cell differentiation. Ann. Lab. Med. 39 (6), 580–583.

Zeng, Z., Zheng, Q., Chen, J., Tan, X., Li, Q., Ding, L., Zhang, R., Lin, X., 2020. FGF21 mitigates atherosclerosis via inhibition of NLRP3 inflammasome-mediated vascular endothelial cells pyroptosis. Exp. Cell. Res. 393 (2), 112108.

Zhang, L., Yang, L., Bi, J., Liu, Y., Toriba, A., Hayakawa, K., Nagao, S., Tang, N., 2021. Characteristics and unique sources of polycyclic aromatic hydrocarbons and nitro-polycyclic aromatic hydrocarbons in PM2.5 at a highland background site in northwestern China. Environ. Pollut. 274, 116527.

Zhong, X., Qiu, J., Kang, J., Xing, X., Shi, X., Wei, Y., 2019. Exposure to tris(1,3-dichloro-2-propyl) phosphate (TDCPP) induces vascular toxicity through Nrf2-VEGF pathway in zebrafish and human umbilical vein endothelial cells. Environ. Pollut. 247, 293–301.

Zhou, S., Xing, Y., Yuan, X., Wu, G., Zhu, X., Wu, D., 2021. Cytotoxicity and action mechanisms of polycyclic aromatic hydrocarbons by a miniature electrochemical detection system. Biomed. Microdevices 23 (2), 19.

Impact of the Dual Antiplatelet Therapy Score on Clinical Outcomes in Acute Coronary Syndrome Patients Receiving P2Y12 Inhibitor Monotherapy

Sheng-Wei Huang [1†], Po-Wei Chen [2†], Wen-Han Feng [3], I-Chang Hsieh [4], Ming-Yun Ho [4], Chung-Wei Cheng [5], Hung-I Yeh [5], Ching-Pei Chen [6], Wei-Chun Huang [7], Ching-Chang Fang [8], Hui-Wen Lin [2], Sheng-Hsiang Lin [9,10,11], Chin-Feng Tsai [1], Chun-Hung Su [1*] and Yi-Heng Li [2*]

[1] School of Medicine, Chung Shan Medical University Hospital, Chung Shan Medical University, Taichung, Taiwan, [2] College of Medicine, National Cheng Kung University Hospital, National Cheng Kung University, Tainan, Taiwan, [3] Kaohsiung Municipal Ta-Tung Hospital and Kaohsiung Medical University Hospital, Kaohsiung, Taiwan, [4] Chang Gung Memorial Hospital, Chang Gung University College of Medicine, Taoyuan, Taiwan, [5] Mackay Memorial Hospital, Taipei, Taiwan, [6] Changhua Christian Hospital, Changhua, Taiwan, [7] Kaohsiung Veterans General Hospital, Fooyin University, Kaohsiung and National Yang Ming University, Taipei, Taiwan, [8] Tainan Municipal Hospital, Tainan, Taiwan, [9] College of Medicine, Institute of Clinical Medicine, National Cheng Kung University, Tainan, Taiwan, [10] Department of Public Health, College of Medicine, National Cheng Kung University, Tainan, Taiwan, [11] Biostatistics Consulting Center, College of Medicine, National Cheng Kung University Hospital, National Cheng Kung University, Tainan, Taiwan

Background: Dual antiplatelet therapy (DAPT) score is used to stratify ischemic and bleeding risk for antiplatelet therapy after percutaneous coronary intervention (PCI). This study assessed the association between the DAPT score and clinical outcomes in acute coronary syndrome (ACS) patients who were treated with P2Y12 inhibitor monotherapy.

Methods: A total of 498 ACS patients, with early aspirin discontinuation for various reasons and who received P2Y12 inhibitor monotherapy after PCI, were enrolled during the period from January 1, 2014 to December 31, 2018. The efficacy and safety between those with low (<2) and high (≥2) DAPT scores were compared during a 12-month follow-up after PCI. Inverse probability of treatment weighting was used to balance the covariates between the two groups. The primary endpoint was a composite outcome of all-cause mortality, recurrent ACS or unplanned revascularization, and stroke within 12 months. The safety endpoint was major bleeding, defined as Bleeding Academic Research Consortium (BARC) 3 or 5 bleeding.

Results: The primary composite endpoint occurred in 11.56 and 14.38% of the low and high DAPT score groups, respectively. Although there was no significant difference in the primary composite endpoint between the two groups in the multivariate Cox proportional hazards models, the risk of recurrent ACS or unplanned revascularization was significantly higher in the high DAPT score group (adjusted hazard ratio [HR]: 1.900,

95% confidence interval [CI]: 1.095–3.295). The safety outcome for BARC 3 or 5 bleeding was similar between the two groups.

Conclusions: Our results indicate that ACS patients receiving P2Y12 monotherapy with high DAPT score had an increased risk of recurrent ACS or unplanned revascularization.

Keywords: P2Y12 inhibitor, acute coronary syndrome, DAPT score, P2Y12 inhibitor monotherapy, clinical outcome

INTRODUCTION

Dual antiplatelet therapy (DAPT) with aspirin and P2Y12 inhibitor is the foundation therapy for acute coronary syndrome (ACS). Current guidelines recommend 12-month DAPT for patients with ACS who have received percutaneous coronary intervention (PCI) (1–3). However, DAPT-associated bleeding has raised concerns because bleeding complications increase the risk of morbidity and mortality (4–6). As patient-tailored antiplatelet therapy has become necessary, the DAPT score was developed to help physicians select patients who would benefit the most from longer or shorter DAPT after PCI (7). The DAPT scoring system includes eight positive predictors (smoking, diabetes, myocardial infarction [MI] at presentation, prior PCI or MI, paclitaxel-eluting stent, stent diameter <3 mm, congestive heart failure or left ventricular ejection fraction <30%, and vein graft stent) and one negative predictor (age) (7). For patients with a high DAPT score (≥2), who had an increased ischemic risk, treatment with extended DAPT beyond 1 year resulted in a reduction in ischemic events but without an increase in bleeding (7). The DAPT score has been validated as useful for stratifying ischemia and bleeding risk in other patient groups, including Asian patients, outside the derivation cohort of the DAPT trial (8–10). Although there were some controversial results regarding its discriminating ability in one study (11), the DAPT score seems to be a clinically useful tool for determining DAPT duration after PCI.

Recently, several randomized trials evaluated the efficacy and safety of very short duration DAPT (1–3 months) followed by P2Y12 inhibitor monotherapy in patients who underwent PCI for stable coronary artery disease (CAD) and/or ACS (12–16). The rationale for using a very short period of aspirin therapy is that the benefits of intensive antiplatelet therapy with DAPT generally outweigh the risk of bleeding in the first few weeks after ACS or PCI, when the thrombogenic potential is still high. However, this benefit dissipates over time after that period and the antiplatelet potency could be enough with P2Y12 inhibitor monotherapy during later periods (6, 17). Overall, these clinical trials demonstrated a significant reduction in bleeding with P2Y12 inhibitor monotherapy vs. standard 12-month DAPT but no significant difference in terms of major adverse cardiovascular events (MACEs) (18). Among these clinical trials, TICO study was the first performed in Asia, which compared ticagrelor monotherapy after 3 months of DAPT vs. standard 12-month DAPT in ACS patients undergoing PCI (16). The risk of major bleeding was decreased in the ticagrelor monotherapy group but the rate of MACEs was similar to standard DAPT. Since Asian patients carry a higher bleeding risk with DAPT (19), very short

DAPT followed by P2Y12 inhibitor monotherapy may be an alternative choice for Asian ACS patients.

In the TICO study, there was a significant interaction between P2Y12 monotherapy vs. standard DAPT and the presence of multivessel disease for the primary outcome (16). In the *post-hoc* analysis of patients with ST elevation MI in the TICO trial, the incidence of MACEs was slightly higher in the ticagrelor monotherapy group compared with 12-month DAPT in those who underwent complex PCI (4.9 vs. 2.7%) (17). Although P2Y12 inhibitor monotherapy was recommended as an optional antiplatelet strategy with standard DAPT in the 2020 European Society of Cardiology Guidelines for the management of ACS (1), there is no useful clinical outcome-predictive tool for choosing between different strategies. The efficacy of P2Y12 inhibitor monotherapy in high risk ischemic patients is also unknown. The aim of this study was to evaluate the association between DAPT score and clinical outcomes in a cohort of ACS patients undergoing PCI and who received P2Y12 inhibitor monotherapy.

METHODS
Study Population

This was a multicenter, retrospective, registration study and the detailed study design was published previously (20). In brief, we retrospectively recruited ACS patients who were admitted to the 8 major teaching hospitals in Taiwan from January 2014 to December 2018. Patients were eligible if they were ≥18 years old, were admitted with a major diagnosis of ACS, including ST elevation MI, non-ST elevation MI or unstable angina, received PCI with a bare metal stent (BMS) and/or contemporary drug-eluting stent (DES) implantation during hospitalization, survived to discharge, regularly followed up in an outpatient clinic for at least 1 year after discharge, and aspirin discontinuation within 6 months. We only studied a subset of ACS patients in whom aspirin was discontinued prematurely. In all enrolled patients, aspirin was prematurely discontinued within 6 months after PCI at the physician's discretion for different reasons. P2Y12 inhibitor monotherapy was used thereafter in all patients with either clopidogrel 75 mg daily or ticagrelor 90 mg twice daily. Prasugrel was not available during the study period in Taiwan. The exclusion criteria were patients with (1) a life-threatening malignancy with a life expectancy of <1 year, (2) hematological disease with bleeding tendency, (3) treatment with immunosuppressive agents, and (4) concomitant use of oral anticoagulation therapy.

All the clinical data, including coronary risk factors, major disease history, PCI procedures, and medications were collected

from the patients' electrical medical records according to a pre-determined study protocol. The timing of aspirin discontinuation was obtained from the records of medications and the aspirin treatment duration was calculated accordingly. If possible, the reasons for aspirin discontinuation were also collected from the electronic medical records. For all included patients, the DAPT scores were calculated as previously reported (7). The DAPT score was calculated by assigning points according to the patients' characteristics, including age (0 for age <65 years, −1 for age 65–74 years, and −2 for age ≥75 years), smoking habit (1 for yes and 0 for no), diabetes mellitus (1 for yes and 0 for no), MI at presentation (1 for yes and 0 for no), prior PCI or MI (1 for yes and 0 for no), paclitaxel-eluting stent (1 for yes and 0 for no), stent diameter <3 mm (1 for yes and 0 for no), congestive heart failure or left ventricular ejection fraction <30% (2 for yes and 0 for no), and vein graft stent (2 for yes and 0 for no) (7). All the enrolled patients were divided into 2 groups according to their DAPT score: low (<2) or high (≥2) DAPT score. A high DAPT score (≥2) indicated that patients are at high ischemic risk and the ischemic benefits of prolonged DAPT therapy outweigh the bleeding risks. This study was conducted according to the principles expressed in the Declaration of Helsinki and was approved by the Institutional Medical Ethics Committee of National Cheng Kung University Hospital (IRB: A-ER-107-375). The principal investigators in all participating hospitals followed the study protocol strictly and the patients who did not meet the inclusion criteria were not included in this study.

Follow-Up

The follow-up information was mainly obtained from the electronic medical records of the participating hospitals. The two major clinical outcomes of ischemic and bleeding endpoints were defined. The ischemic outcome is a composite endpoint of all-cause mortality, recurrent ACS or unplanned revascularization, and stroke within 12 months after the index PCI. All components of the composite endpoint were separately defined as secondary endpoints. All patients were followed up for at least 12 months after discharge or until one of the composite endpoints occurred. All these endpoint ischemic events were documented in the medical records of the patients and reported by the physicians who were responsible for patient follow-up. Recurrent ACS was defined as readmission to a hospital for management of new onset ST elevation MI, non-ST elevation MI, or unstable angina. Unplanned revascularization was defined as the first unexpected revascularization after discharge, including re-do PCI or a coronary artery bypass graft (CABG) after the index PCI due to new onset ischemic symptoms. Stroke, including ischemic or hemorrhagic stroke, was diagnosed by the occurrence of new-onset neurological symptoms and signs from neuroimaging studies. The bleeding outcome was defined as the occurrence of major bleeding as specified by the Bleeding Academic Research Consortium (BARC) type 3 and 5 bleedings (21).

Statistical Analysis

Continuous variables were expressed as mean ± standard deviation and categorical variables were expressed as numbers and percentages. We used an unpaired Student's t-test for continuous variables and a chi-squared test for categorical variables to make comparisons between groups. The inverse probability of treatment weights (IPTW) method based on propensity scores was used to adjust for the imbalances in clinical characteristics between the groups, while preserving the sample size (22, 23). The propensity score was calculated according to the probability conditional at baseline characteristics, including age, sex, ST elevation MI status, diabetes mellitus, hypertension, hyperlipidemia, smoker, previous MI, previous PCI, previous CABG, previous ischemic stroke, previous hemorrhagic stroke, chronic kidney disease without dialysis, end stage renal disease with dialysis, heart failure, atrial fibrillation, peripheral artery disease, left ventricular ejection fraction, coronary angiography (CAG) finding, PCI procedure, location of treated lesion, stent, and medications.

In the IPTW model, we used the propensity score to generate patient-specific stabilized weights and to control for covariate imbalances. The propensity-score weight was calculated as the inverse of the propensity score for each patient. Comparisons of the clinical characteristics, CAG findings and PCI procedures, and medications between the groups were evaluated *via* absolute standardized mean difference (ASMD), which was calculated as the mean or proportion of a variable divided by the pooled estimate of the standard deviation of that variable. An ASMD >0.1 indicated a significant difference between the two groups. Cox proportional-hazard models were then adjusted for differences in the treatment groups using IPTWs derived from the propensity score, which was designated as the IPTW model. In the IPTW model after matching, the clinical characteristics with an ASMD >0.1 were put into the multivariate Cox proportional-hazards model for further adjustment. Because we already divided the groups by low and high DAPT scores, the criteria for the DAPT score were not in the multivariate model. Adjusted variables included body mass index >30, previous ischemic stroke, end-stage renal disease with dialysis, atrial fibrillation, CAG finding, PCI procedure, location of treated lesion, BMS, and statin use. Adjusted hazard ratios (HRs) and 95% CIs were calculated. We used the same Cox proportional hazards model to estimate the p values for interactions in the subgroup analysis. The SAS statistical package (version 9.4 for Windows; SAS Institute, Cary, NC, USA) was used for all analyses.

RESULTS

A total of 498 ACS patients (mean age 70.18 ± 12.84 years, men: 71.3%), who received PCI with stent implantation during hospitalization and survived to discharge, were included during the study period. There were 199 patients (40%) with low (<2) DAPT scores and 299 patients (60%) with high (≥2) DAPT scores. The mean time for aspirin treatment duration was similar between the low and high DAPT score groups (37.76 ± 52.67 vs. 41.90 ± 57.54 days, p = 0.471). **Table 1** illustrates the reasons for premature discontinuation of aspirin. The most common reason for stopping aspirin was gastrointestinal bleeding (46.59%) with a similar percentage in both groups. Aspirin allergy and

TABLE 1 | Reasons for premature discontinuation of aspirin.

Reason	All	Low DAPT score	High DAPT score	p value
	N = 498 (%)	N = 199 (%)	N = 299 (%)	
Gastrointestinal bleeding	232 (46.59)	95 (47.74)	137 (45.82)	0.742
Other sites bleeding	35 (7.03)	12 (6.03)	23 (7.69)	0.595
Aspirin allergy	53 (10.64)	14 (7.04)	39 (13.04)	0.048
Gastrointestinal upset or discomfort	48 (9.64)	18 (9.05)	30 (10.03)	0.833
Need surgery or thrombocytopenia	13 (2.61)	6 (3.02)	7 (2.34)	0.861
Other or unknown causes	117 (23.49)	54 (27.14)	63 (21.07)	0.145

DAPT, dual antiplatelet therapy.

gastrointestinal upset were also common reasons for stopping aspirin. Aspirin allergy was significantly more common in the group with high DAPT score ($p = 0.048$), while gastrointestinal upset and discomfort were similar in both groups. Old age, anemia, or chronic use of oral non-steroidal anti-inflammatory drugs or steroids were other reasons for stopping aspirin. Unfortunately, the definite reason for stopping aspirin could not be identified in some patients from their medical records as this was a retrospective study.

Table 2 shows a comparison of baseline characteristics between the low and high DAPT score groups before and after matching. Since age, smoking, diabetes, prior PCI, prior MI, left ventricular ejection fraction <30%, and stent diameter <3 mm are the criteria included in the DAPT scoring system, it is natural to see a younger age and a higher proportion of these clinical characteristics in the high DAPT score group even after matching. The following characteristics, including body mass index, previous ischemic stroke, end stage renal disease with dialysis, atrial fibrillation, CAG finding, PCI procedure, location of treated lesion, use of stent, and use of statins, were also different between the groups and were further adjusted in the multivariate Cox proportional-hazards model for outcome evaluation.

All patients were followed up by the physicians who enrolled the patients. The mean duration of follow-up was 341.68 ± 67.58 and 330.97 ± 86.62 days in the low and high DAPT score groups, respectively ($p = 0.123$). **Table 3** shows the clinical outcomes during the 12-month follow-up after the index PCI. The composite ischemic outcome occurred in 11.56% of the low and 14.38% of the high DAPT score group and there was no significant difference between the groups after multivariate adjustment (adjusted HR: 1.169, 95% CI: 0.832–1.643). For the secondary endpoint, there was also no significant difference in stroke and all-cause death between the two groups. However, the risk of recurrent ACS or unplanned revascularization was significantly higher in the high DAPT score group (adjusted HR: 1.900, 95% CI: 1.095–3.295) compared with the low DAPT score group. BARC 3 and 5 bleeding occurred in 3.02% of the low and 4.01% of the high DAPT score group. There was no significant difference in BARC 3 and 5 bleeding (adjusted HR: 1.206, 95% CI: 0.623–2.335) between the two groups.

Figure 1 shows the subgroup analysis results regarding sex, clopidogrel or ticagrelor, hypertension, chronic kidney disease,

3-vessel disease, single or multiple-lesion intervention, and DES between the two groups. The criteria in the DAPT score, such as age, smoking, diabetes, prior PCI, prior MI, left ventricular ejection fraction <30%, and stent diameter <3 mm, were not used for the subgroup analysis. In the subgroup analysis, patients with high DAPT score had a higher risk of primary composite endpoint in the subgroups of chronic kidney disease, 3-vessel disease, and DES (p for interaction < 0.05). There was a borderline interaction between those treated with ticagrelor or clopidogrel (p for interaction = 0.052).

DISCUSSION

In this study, we assessed the association between the DAPT score and the clinical outcomes in ACS patients receiving P2Y12 inhibitor monotherapy after index PCI. We found that the DAPT score was useful for determining the ischemic risk in these patients. Although previous clinical trials found that the efficacy of P2Y12 inhibitor monotherapy for preventing ischemic events was comparable to standard 12-month DAPT, the present study demonstrated that patients with high DAPT score still had a significantly higher rate of recurrent ACS or unplanned revascularization compared with those with low DAPT score.

After its development in the DAPT trial, the DAPT score has been extensively investigated with regard to its ability to stratify ischemic risk in a wide variety of patient groups who have received PCI (8–11). Most of the studies confirmed that patients with a high DAPT score have a higher incidence of ischemic events when compared with patients with a low DAPT score. For the strategy of very short DAPT (1–3 months) followed by P2Y12 inhibitor monotherapy, the influence of the DAPT score remains unclear. GLOBAL LEADERS trial is a randomized study comparing 1 year of DAPT therapy (aspirin plus clopidogrel or ticagrelor) followed by 1 year of aspirin monotherapy with 1 month of DAPT therapy (aspirin plus ticagrelor) followed by 23 months of ticagrelor, among patients undergoing PCI for stable CAD or ACS (12). A recent study analyzed the clinical outcomes from the second year follow up with aspirin or ticagrelor monotherapy in the GLOBAL LEADERS trial. It demonstrated that patients with high DAPT score had a significantly higher rate of the composites of MI or stent thrombosis (0.70% vs. 1.55%, $p < 0.0001$) and a similar rate of BARC type 3 or 5 bleeding (24).

TABLE 2 | Baseline characteristics of patients with different DAPT scores.

Characteristic			Inverse probability of treatment weighting						
			Before					**After**	
	All		**Low DAPT score**		**High DAPT score**		**ASMD**	**Low DAPT score**	**High DAPT score**	**ASMD**
	N = 498	**(%)**	**N = 199**	**(%)**	**N = 299**	**(%)**		**(N = pseudo data)**	**(N = pseudo data)**	
*Age	70.18 ± 12.84		75.72 ± 10.97		66.50 ± 12.68		0.777	76.86 ± 17.54	66.18 ± 15.44	0.647
Male	355	71.29	118	59.30	237	79.26	0.443	72.08	70.48	0.035
*BMI>30	43	8.63	7	3.52	36	12.04	0.322	3.79	8.49	0.197
STEMI	141	28.31	45	22.61	96	32.11	0.214	29.14	31.04	0.041
*Diabetes mellitus	271	54.42	66	33.17	205	68.56	0.757	24.57	70.30	1.030
Hypertension	376	75.50	149	74.87	227	75.92	0.024	77.98	76.23	0.042
Hyperlipidemia	273	54.82	106	53.27	167	55.85	0.052	54.38	55.35	0.020
*Smoker	146	29.32	17	8.54	129	43.14	0.860	7.48	44.66	0.935
*Previous MI	78	15.66	6	3.02	72	24.08	0.647	2.23	24.81	0.700
*Previous PCI	140	28.11	36	18.09	104	34.78	0.386	13.34	34.30	0.508
Previous CABG	16	3.21	5	2.51	11	3.68	0.067	2.39	3.98	0.090
*Previous ischemic stroke	76	15.26	31	15.58	45	15.05	0.015	9.77	13.01	0.102
Previous hemorrhagic stroke	3	0.60	2	1.01	1	0.33	0.082	0.65	0.48	0.024
CKD without dialysis	180	36.14	67	33.67	113	37.79	0.086	38.88	37.81	0.022
*ESRD with dialysis	68	13.65	24	12.06	44	14.72	0.078	9.38	12.89	0.112
Heart failure	168	33.73	17	8.54	151	50.50	1.036	35.34	34.70	0.013
*Atrial fibrillation	66	13.25	22	11.06	44	14.72	0.109	8.18	15.24	0.221
Peripheral artery disease	32	6.43	15	7.54	17	5.69	0.075	5.77	6.13	0.015
Bleeding history	158	31.73	70	35.18	88	29.43	0.123	28.11	31.15	0.066
*LVEF	57.17 ± 14.53		62.55 ± 12.01		53.59 ± 14.97		0.660	58.49 ± 21.21	55.92 ± 17.98	0.130
Hb (g/dL)	12.14 ± 2.81		11.93 ± 2.47		12.28 ± 3.01		0.126	11.94 ± 4.31	12.06 ± 3.86	0.030
WBC	9,822.24 ± 4,308.33		9,214.77 ± 4,099.82		10,226.54 ± 4,402.09		0.238	9,275.96 ± 6,468.48	9,779.31 ± 5,415.31	0.084
*CAG finding							0.050			0.188
1-vessel disease	123	24.70	48	24.12	75	25.08	0.022	36.99	28.42	0.184
2-vessel disease	141	28.31	59	29.65	82	27.42	0.049	26.67	28.56	0.042
3-vessel disease	234	46.99	92	46.23	142	47.49	0.025	36.35	43.02	0.137
*PCI procedure							0.018			0.152
Single lesion intervention	278	55.82	110	55.28	168	56.19		49.08	58.45	
Multiple lesions intervention	220	44.18	89	44.72	131	43.81		49.08	41.55	

(Continued)

TABLE 2 | Continued

Characteristic			Inverse probability of treatment weighting							
			Before					After		
	All		Low DAPT score		High DAPT score		ASMD	Low DAPT score	High DAPT score	ASMD
	N = 498	(%)	N = 199	(%)	N = 299	(%)		(N = pseudo data)	(N = pseudo data)	
*Location of lesion treated										
LM	38	7.63	17	8.54	21	7.02	0.057	4.83	6.53	0.073
LAD	319	64.06	130	65.33	189	63.21	0.044	55.26	63.18	0.162
LCX	194	38.96	78	39.20	116	38.80	0.008	31.83	38.42	0.138
RCA	234	46.99	94	47.24	140	46.82	0.008	52.45	44.55	0.159
SVG	2	0.40	0	0.00	2	0.67	0.116	-	0.90	
*Stent										
Bare metal stent	214	42.97	80	40.20	134	44.82	0.094	35.84	43.62	0.159
Everolimus-eluting stent	93	18.67	35	17.59	58	19.40	0.047	17.16	19.61	0.063
Zotarolimus-eluting stent	99	19.88	43	21.61	56	18.73	0.072	17.40	19.26	0.048
Biolimus-eluting stent	26	5.22	14	7.04	12	4.01	0.133	7.07	4.75	0.098
Sirolimus-eluting stent	65	13.05	31	15.58	34	11.37	0.123	17.55	12.00	0.157
Stent < 3 mm	200	40.16	60	30.15	140	46.82	0.348	20.12	52.30	0.711
Medications										
Clopidogrel	271	54.42	118	59.30	153	51.17	0.164	51.15	46.26	0.098
Ticagrelor	227	45.58	81	40.70	146	48.83	0.164	48.85	53.74	0.098
Beta blocker	367	73.69	133	66.83	234	78.26	0.258	75.79	73.35	0.056
RAS inhibitor	283	56.83	105	52.76	178	59.53	0.137	57.64	56.88	0.015
*Statin	405	81.33	153	76.88	252	84.28	0.188	75.87	82.19	0.156
PPI use	203	40.76	96	48.24	107	35.79	0.254	39.63	40.53	0.018

BMI, body mass index; CABG, coronary artery bypass graft; CAG, coronary angiography; CKD, chronic kidney disease; DAPT, dual antiplatelet therapy; ESRD, end stage renal disease; LAD, left anterior descending artery, LCX, left circumflex artery; LM, left main artery; LVEF, left ventricular ejection fraction; MI, myocardial infarction; PCI, percutaneous coronary intervention; PPI, proton pump inhibitor; RAS, renin angiotensin system; RCA, right coronary artery; STEMI, ST-segment elevation myocardial infarction; SVG, saphenous vein graft; ASMD, absolute standardized difference.

ASMD >0.1 between the groups.

TABLE 3 | Clinical outcomes at 12-months follow-up.

Outcome	All	Low DAPT score	High DAPT score	Crude HR	p value	Adjusted HR	p value
	N = 498	N = 199 (Ref)	N = 299	(95% CI)		(95% CI)	
Primary composite endpoint	66 (13.25)	23 (11.56)	43 (14.38)	0.792 (0.579–1.082)	0.143	1.169 (0.832–1.643)	0.367
Secondary endpoint							
Recurrent ACS or unplanned revascularization	41 (8.23)	12 (6.03)	29 (9.70)	1.965 (1.145–3.372)	0.014	1.900 (1.095–3.295)	0.022
Stroke	1 (0.20)	0	1 (0.33)	-		-	
All-cause death	24 (4.82)	11 (5.53)	13 (4.35)	0.426 (0.277–0.654)	<0.001	0.758 (0.465–1.237)	0.268
BARC 3 or 5 bleeding	18 (3.61)	6 (3.02)	12 (4.01)	1.341 (0.709–2.539)	0.367	1.206 (0.623–2.335)	0.578

ACS, acute coronary syndrome; BARC, Bleeding Academic Research Consortium; DAPT, dual antiplatelet therapy.
Adjusted variables included body mass index >30, previous ischemic stroke, end stage renal disease with dialysis, atrial fibrillation, coronary angiography finding, percutaneous coronary intervention procedure, location of treated lesion, bare metal stent, and statin.

FIGURE 1 | Subgroup analysis of the effect of different dual antiplatelet therapy scores on primary composite endpoints. CAG, coronary angiography; CKD, chronic kidney disease; DES, drug-eluting stent; PCI, percutaneous coronary intervention.
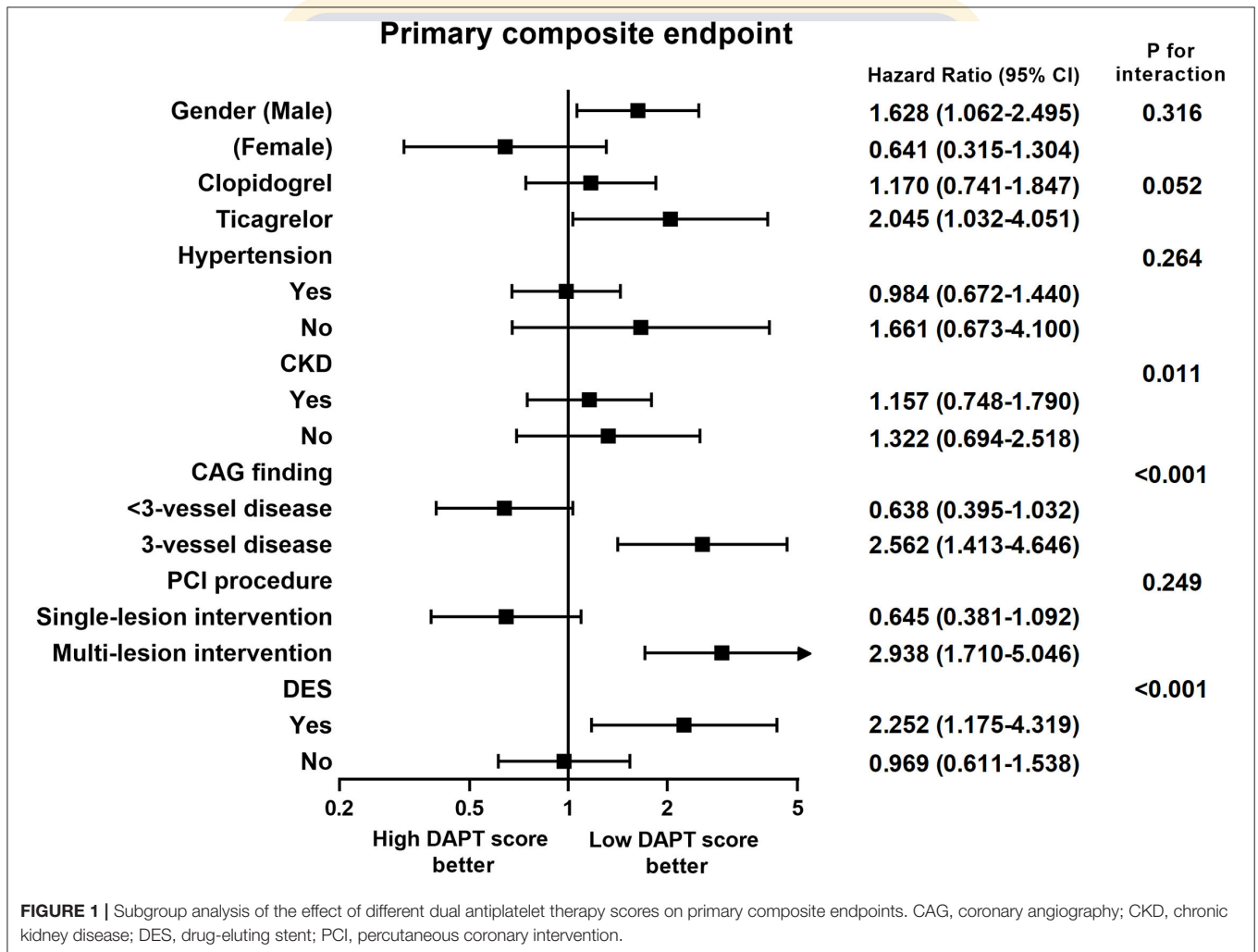
The authors concluded that the DAPT score can stratify ischemic risk but not bleeding risk in a contemporary PCI population during the second year.

Our study only included ACS patients receiving P2Y12 inhibitor monotherapy (ticagrelor or clopidogrel), and we observed the first year outcomes after PCI. We initially hypothesized that a high DAPT score would predict higher composite ischemic events, but the results were not as expected. The potential reasons for this are the limited follow-up time (12 months) and the small case number. However, we did find that

the risk of recurrent ACS or unplanned revascularization was significantly higher in the high DAPT score group. In addition, our study also found that the DAPT score could not stratify bleeding risk in ACS patients undergoing PCI, which was similar to the results of the GLOBAL LEADERS trial (24). Subgroup analysis revealed that there were more ischemic events in the high DAPT score group with 3-vessel disease, and coronary anatomy complexity is a known risk factor for MACEs after PCI (25, 26).

Our study results indicate that early discontinuation of aspirin with P2Y12 inhibitor monotherapy should be the last resort for ACS patients with 3-vessel disease and a high DAPT score because the high ischemic risk is still a major concern. Overall, the patients receiving BMS deployment had higher ischemic events than those receiving DES deployment (recurrent ACS or unplanned revascularization: BMS 11.21 vs. DES 6.72%). However, in the subgroup analysis, we found that patients receiving P2Y12 inhibitor monotherapy with ticagrelor and DES deployment, had higher primary composite endpoints in the high DAPT score group. Probable reasons to explain this result are that the choice of P2Y12 inhibitor and stent in real-world practice are based on the clinician's experience and the local insurance system. Ticagrelor is more expensive than clopidogrel. A previous real-world observation study of ACS in Taiwan demonstrated that ticagrelor offers a better protective effect against ischemic events when compared with clopidogrel (27). However, BMS is still commonly used in Taiwan because the Taiwan National Health Insurance only reimburses the price of BMS. Patients using DES have to pay the price difference, which is around US$1,500 to US$2,000 for one DES (28). Therefore, it is likely that physicians in Taiwan are prone to choosing ticagrelor and DES for ACS patients with a higher ischemic risk and recurrent events.

To the best of our knowledge, this is the first study to assess the ability of the DAPT score to stratify ischemic and bleeding risk in ACS patients with P2Y12 inhibitor monotherapy undergoing PCI in Asia. However, our study did have several limitations. First, our study was a retrospective, nonrandomized, observational study. The unadjusted confounding factors were unavoidable, even though a propensity score-matched analysis was used to compensate for this. Second, the case number was relatively small in our study, which may have caused selection bias of the included patients. Standard 12-month DAPT is still the recommended therapy for ACS patients who undergo PCI in Taiwan (29). Therefore, it is difficult to collect large case numbers of patients with only P2Y12 inhibitor monotherapy from real-world practice. Third, there was only a 12-month follow-up after PCI. A longer follow-up duration may be necessary to determine the definite association of the DAPT score with the clinical outcomes. Fourth, although the guidelines recommend new-generation P2Y12 inhibitors and DES for ACS patients undergoing PCI, BMS and clopidogrel are still commonly used in Taiwan for various reasons. Our study results may be different if all patients were treated with ticagrelor and DES. Fifth, we did not know the exact cause of death in all 24 patients with

mortality. Some patients died from sepsis/pneumonia, cancer, and respiratory failure, but not cardiovascular causes. Finally, our results may not be applicable to non-Asian patients.

In conclusion, ACS patients receiving early P2Y12 monotherapy with high DAPT score had a higher risk of recurrent ACS or unplanned revascularization compared with those with low DAPT score. The risk of major bleeding was similar between those with low and high DAPT scores. This study suggests that the DAPT score is validated for predicting cardiovascular events in ACS patients undergoing PCI with short DAPT treatment followed by P2Y12 inhibitor monotherapy.

DATA AVAILABILITY STATEMENT

The original contributions presented in the study are included in the article/supplementary material, further inquiries can be directed to the corresponding authors.

ETHICS STATEMENT

The studies involving human participants were reviewed and approved by the Institutional Medical Ethics Committee of National Cheng Kung University Hospital (IRB: A-ER-107-375). Written informed consent was not required for this study, in accordance with the local legislation and institutional requirements.

AUTHOR CONTRIBUTIONS

M-YH, W-HF, C-FT, C-HS, S-WH, C-WC, H-IY, C-PC, W-CH, C-CF, I-CH, and Y-HL were responsible for the conceptualization. Data curation was done by M-YH, P-WC, W-HF, C-FT, C-HS, S-WH, C-WC, H-IY, C-PC, W-CH, C-CF, I-CH, and Y-HL. M-YH, P-WC, W-HF, C-HS, S-WH, C-WC, H-IY, C-PC, W-CH, C-CF, I-CH, and Y-HL performed the formal analysis. Funding acquisition was taken care of by W-HF and I-CH. M-YH, P-WC, W-HF, C-HS, H-WL, and Y-HL carried out the investigation. P-WC, W-HF, H-WL, and S-HL took care of the methodology. Project administration was the responsibility of C-HS, P-WC, W-HF, and Y-HL. H-WL and S-HL handled the software. C-HS, C-FT, S-HL, I-CH, and Y-HL supervised the study. C-FT, H-WL, S-HL, and I-CH performed the validation. C-FT, S-HL, and I-CH visualized the study. Writing of the original draft was done by S-WH, P-WC, C-HS, and Y-HL. C-HS, S-WH, Y-HL, and P-WC reviewed and edited the study. All authors contributed to the article and approved the submitted version.

FUNDING

REFERENCES

1. Collet JP, Thiele H, Barbato E, Barthelemy O, Bauersachs J, Bhatt DL, et al. 2020 ESC Guidelines for the management of acute coronary syndromes in patients presenting without persistent ST-segment elevation. *Eur Heart J.* (2021) 42:1289–367. doi: 10.1093/eurheartj/ehaa575

2. Valgimigli M, Bueno H, Byrne RA, Collet JP, Costa F, Jeppsson A, et al. 2017 ESC focused update on dual antiplatelet therapy in coronary artery disease developed in collaboration with EACTS: The Task Force for dual antiplatelet therapy in coronary artery disease of the European Society of Cardiology (ESC) and of the European Association for Cardio-Thoracic Surgery (EACTS). *Eur Heart J.* (2018) 39:213–60. doi: 10.1093/eurheartj/ehx419

3. Levine GN, Bates ER, Bittl JA, Brindis RG, Fihn SD, Fleisher LA, et al. 2016 ACC/AHA guideline focused update on duration of dual antiplatelet therapy in patients with coronary artery disease: a report of the American College of Cardiology/American Heart Association Task Force on Clinical Practice Guidelines. *J Am Coll Cardiol.* (2016) 68:1082–115. doi: 10.1016/j.jacc.2016.03.513

4. Sharma A, Hagstrom E, Wojdyla DM, Neely ML, Harrington RA, Wallentin L, et al. Clinical consequences of bleeding among individuals with a recent acute coronary syndrome: insights from the APPRAISE-2 trial. *Am Heart J.* (2019) 215:106–13. doi: 10.1016/j.ahj.2019.05.004

5. van der Sangen NMR, Rozemeijer R, Chan Pin Yin DRPP, Valgimigli M, Windecker S, James SK, et al. Patient-tailored antithrombotic therapy following percutaneous coronary intervention. *Eur Heart J.* (2021) 42:1038–46. doi: 10.1093/eurheartj/ehaa1097

6. Rodriguez F, Harrington RA. Management of antithrombotic therapy after acute coronary syndromes. *N Engl J Med.* (2021) 384:452–60. doi: 10.1056/NEJMra1607714

7. Yeh RW, Secemsky EA, Kereiakes DJ, Normand SL, Gershlick AH, Cohen DJ, et al. Development and validation of a prediction rule for benefit and harm of dual antiplatelet therapy beyond 1 year after percutaneous coronary intervention. *JAMA.* (2016) 315:1735–49. doi: 10.1001/jama.2016.3775

8. Piccolo R, Gargiulo G, Franzone A, Santucci A, Ariotti S, Baldo A, et al. Use of the dual-antiplatelet therapy score to guide treatment duration after percutaneous coronary intervention. *Ann Intern Med.* (2017) 167:17–25. doi: 10.7326/M16-2389

9. Yoshikawa Y, Shiomi H, Watanabe H, Natsuaki M, Kondo H, Tamura T, et al. Validating utility of dual antiplatelet therapy score in a large pooled cohort from 3 Japanese percutaneous coronary intervention studies. *Circulation.* (2018) 137:551–62. doi: 10.1161/CIRCULATIONAHA.117.028924

10. Montalto C, Ferlini M, Casula M, Mandurino-Mirizzi A, Costa F, Leonardi S, et al. DAPT score to stratify ischemic and bleeding risk after percutaneous coronary intervention: an updated systematic review, meta-analysis, and meta-regression of 100,211 Patients. *Thromb Haemost.* (2021) 121:687–9. doi: 10.1055/s-0040-1721145

11. Ueda P, Jernberg T, James S, Alfredsson J, Erlinge D, Omerovic E, et al. External validation of the DAPT score in a nationwide population. *J Am Coll Cardiol.* (2018) 72:1069–78. doi: 10.1016/j.jacc.2018.06.023

12. Vranckx P, Valgimigli M, Jüni P, Hamm C, Steg PG, Heg D, et al. Ticagrelor plus aspirin for 1 month, followed by ticagrelor monotherapy for 23 months vs aspirin plus clopidogrel or ticagrelor for 12 months, followed by aspirin monotherapy for 12 months after implantation of a drug-eluting stent: a multicentre, open-label, randomised superiority trial. *Lancet.* (2018) 392:940–9. doi: 10.1016/S0140-6736(18)31858-0

13. Mehran R, Baber U, Sharma SK, Cohen DJ, Angiolillo DJ, Briguori C, et al. Ticagrelor with or without aspirin in high-risk patients after PCI. *N Engl J Med.* (2019) 381:2032–42. doi: 10.1056/NEJMoa1908419

14. Watanabe H, Domei T, Morimoto T, Natsuaki M, Shiomi H, Toyota T, et al. Effect of 1-month dual antiplatelet therapy followed by clopidogrel vs 12-month dual antiplatelet therapy on cardiovascular and bleeding events in patients receiving PCI: The STOPDAPT-2 randomized clinical trial. *JAMA.* (2019) 321:2414–27. doi: 10.1001/jama.2019.8145

15. Hahn JY, Song YB, Oh JH, Chun WJ, Park YH, Jang WJ, et al. Effect of P2Y12 inhibitor monotherapy vs dual antiplatelet therapy on cardiovascular events in patients undergoing percutaneous coronary intervention: The SMART-CHOICE randomized clinical trial. *JAMA.* (2019) 321:2428–37. doi: 10.1001/jama.2019.8146

16. Kim BK, Hong SJ, Cho YH, Yun KH, Kim YH, Suh Y, et al. Effect of ticagrelor monotherapy vs ticagrelor with aspirin on major bleeding and cardiovascular events in patients with acute coronary syndrome. *JAMA.* (2020) 323:2407–16. doi: 10.1001/jama.2020.7580

17. Feng WH, Hsieh IC Li YH. P2Y12 inhibitor monotherapy after percutaneous coronary intervention: is it safe to abandon aspirin? *Acta Cardiol Sin.* (2021) 37:1–8. doi: 10.6515/ACS.202101_37(1).20200806A

18. Giacoppo D, Matsuda Y, Fovino LN, D'Amico G, Gargiulo G, Byrne RA, et al. Short dual antiplatelet therapy followed by P2Y12 inhibitor monotherapy vs. prolonged dual antiplatelet therapy after percutaneous coronary intervention with second-generation drug-eluting stents: a systematic review and meta-analysis of randomized clinical trials. *Eur Heart J.* (2021) 42:308–19. doi: 10.1093/eurheartj/ehaa739

19. Kang J, Park KW, Palmerini T, Stone GW, Lee MS, Colombo A, et al. Racial differences in ischaemia/bleeding risk trade-off during anti-platelet therapy: individual patient level landmark meta-analysis from seven RCTs. *Thromb Haemost.* (2019) 119:149–62. doi: 10.1055/s-0038-1676545

20. Chen PW, Feng WH, Ho MY, Su CH, Huang SW, Cheng CW, et al. P2Y12 inhibitor monotherapy with clopidogrel versus ticagrelor in patients with acute coronary syndrome undergoing percutaneous coronary intervention. *J Clin Med.* (2020) 9:1657. doi: 10.3390/jcm9061657

21. Mehran R, Rao SV, Bhatt DL, Gibson CM, Caixeta A, Eikelboom J, et al. Standardized bleeding definitions for cardiovascular clinical trials: a consensus report from the Bleeding Academic Research Consortium. *Circulation.* (2011) 123:2736–47. doi: 10.1161/CIRCULATIONAHA.110.009449

22. Austin PC. An introduction to propensity score methods for reducing the effects of confounding in observational studies. *Multivariate Behav Res.* (2011) 46:399–424. doi: 10.1080/00273171.2011.568786

23. Burden A, Roche N, Miglio C, Hillyer EV, Postma DS, Herings RM, et al. An evaluation of exact matching and propensity score methods as applied in a comparative effectiveness study of inhaled corticosteroids in asthma. *Pragmat Obs Res.* (2017) 8:15–30. doi: 10.2147/POR.S122563

24. Chichareon P, Modolo R, Kawashima H, Takahashi K, Kogame N, Chang CC, et al. DAPT score and the impact of ticagrelor monotherapy during the second year after PCI. *JACC Cardiovasc Interv.* (2020) 13:634–46. doi: 10.1016/j.jcin.2019.12.018

25. Valle JA, Glorioso TJ, Bricker R, Barón AE, Armstrong EJ, Bhatt DL, et al. Association of coronary anatomical complexity with clinical outcomes after percutaneous or surgical revascularization in the veterans affairs clinical assessment reporting and tracking program. *JAMA Cardiol.* (2019) 4:727–35. doi: 10.1001/jamacardio.2019.1923

26. Mohamed MO, Polad J, Hildick-Smith D, Bizeau O, Baisebenov RK, Roffi M, et al. Impact of coronary lesion complexity in percutaneous coronary intervention: one-year outcomes from the large, multicentre e-Ultimaster registry. *EuroIntervention.* (2020) 16:603–12. doi: 10.4244/EIJ-D-20-00361

27. Lee CH, Cheng CL, Kao Yang YH, Chao TH, Chen JY Li YH. Cardiovascular and bleeding risks in acute myocardial infarction newly treated with ticagrelor vs. *clopidogrel in Taiwan Circ J.* (2018) 82:747–56. doi: 10.1253/circj.CJ-17-0632

28. Wu CK, Juang JJ, Chiang JY Li YH, Tsai CT, Chiang FT. The Taiwan Heart Registries: its influence on cardiovascular patient care. *J Am Coll Cardiol.* (2018) 71:1273–83. doi: 10.1016/j.jacc.2018.02.006

29. Li YH, Lee CH, Huang WC, Wang YC, Su CH, Sung PH, et al. 2020 focused update of the 2012 Guidelines of the Taiwan Society of Cardiology for the management of ST-segment elevation myocardial infarction. *Acta Cardiol Sin.* (2020) 36:285–307. doi: 10.6515/ACS.202007_36(4).20200619A

PLOS ONE

CHA2DS2-VASc score as an independent outcome predictor in patients hospitalized with acute ischemic stroke

Chun-Hung Su[1,2], Chien-Hsien Lo[1,2], Hsin-Hung Chen[1,3,4,5], Chin-Feng Tsai[1,2], Hei-Tung Yip[6,7], Kai-Cheng Hsu[7,8,9], Chung Y. Hsu[10], Chia-Hung Kao[10,11,12,13]*, Taiwan Stroke Registry Investigators[¶]

1 Institute of Medicine, School of Medicine, Chung Shan Medical University, Taichung, Taiwan, 2 Division of Cardiology, Department of Internal Medicine, Chung-Shan Medical University Hospital, Taichung, Taiwan, 3 Division of Endocrinology and Metabolism, Department of Internal Medicine, Asia University Hospital, Taichung, Taiwan, 4 Chung Sheng Clinic, Nantou, Taiwan, 5 Department of Law, Providence University, Taichung, Taiwan, 6 Management Office for Health Data, China Medical University Hospital, Taichung, Taiwan, 7 College of Medicine, China Medical University, Taichung, Taiwan, 8 Artificial Intelligence Center for Medical Diagnosis, China Medical University, Taichung, Taiwan, 9 Department of Neurology, China Medical University Hospital, Taichung, Taiwan, 10 Graduate Institute of Biomedical Sciences, College of Medicine, China Medical University, Taichung, Taiwan, 11 Department of Nuclear Medicine and PET Center, China Medical University Hospital, Taichung, Taiwan, 12 Department of Bioinformatics and Medical Engineering, Asia University, Taichung, Taiwan, 13 Center of Augmented Intelligence in Healthcare, China Medical University Hospital, Taichung, Taiwan

¶ Taiwan Stroke Registry Investigators can be found in the S1 Appendix.
* d10040@mail.cmuh.org.tw, dr.kaochiahung@gmail.com

Abstract

Purpose

Atrial fibrillation (AF) is a significant independent risk factor for 1-year mortality in patients with first acute ischemic stroke (AIS). The CHA2DS2-VASc score was initially developed to assess the risk of stroke in patients with AF. Recently, this scoring system has been demonstrated to have clinical value for predicting long-term clinical outcomes in AIS but the evidence is insufficient. This large-scale prospective cohort study investigated the independent predictive value of the score in such patients.

Methods

We included patients with AIS from the Taiwan Stroke Registry (TSR) during 2006–2016 as the present study population. Patients were divided into those with high (≥2) and low (<2) CHA2DS2-VASc scores. We further analyzed and classified patients according to the presence of AF. The clinical endpoint was major adverse cardiac and cerebrovascular events (MACCEs) at 1 year after the index AIS.

Results

A total of 62,227 patients with AIS were enrolled. The median age was 70.3 years, and 59% of the patients were women. After confounding factors were controlled, patients with high CHA2DS2-VASc scores had significantly higher incidence of 1-year MACCEs (adjusted

hazard ratio [HR] = 1.63; 95% confidence interval [CI] = 1.52, 1.76), re-stroke (adjusted HR = 1.28; 95% CI = 1.16, 1.42), and all-cause mortality (adjusted HR = 2.03; 95% CI = 1.83, 2.24) than those with low CHA2DS2-VASc scores did. In the comparison between AF and non-AF groups, the AF group had increased MACCEs (adjusted HR = 1.74; 95% CI = 1.60, 1.89), myocardial infarction (adjusted HR = 4.86; 95% CI = 2.07, 11.4), re-stroke (adjusted HR = 1.47; 95% CI = 1.26, 1.71), and all-cause mortality (adjusted HR = 1.90; 95% CI = 1.72, 2.10). The Kaplan–Meier curve revealed that both CHA2DS2-VASc scores and AF were independent risk predictors for 1-year MACCEs and mortality.

Conclusions

The CHA2DS2-VASc score and AF appeared to consistently predict 1-year MACCEs of AIS patients and provide more accurate risk stratification. Therefore, increased use of the CHA2DS2-VASc score may help improve the holistic clinical assessment of AIS patients with or without AF.

Introduction

Ischemic stroke risk is increased fivefold in patients with atrial fibrillation (AF) [1, 2]. More than half of all cardioembolic strokes are related to AF [3]. In addition, the Framingham study showed that AF is a significant independent risk factor for 1-year mortality in first acute ischemic stroke (AIS) and the elderly are particularly vulnerable to stroke when AF is present [4]. The CHA2DS2-VASc (congestive heart failure, hypertension, age ≥75 years, diabetes mellitus [DM], previous stroke, vascular disease, age 65–74 years, sex category) score is a clinical risk-stratification tool initially used to assess the risk of stroke in patients with non-valvular AF, with a score of ≥2 defined as high risk [5]. The current American Heart Association [6] and European Society of Cardiology guidelines [7] still recommend using this validated scoring system to establish the indication for oral anticoagulation therapy.

However, because all components of the CHA2DS2-VASc score are important cardiovascular risk factors, previous studies have reported the use of this scoring system in predicting clinical prognosis, including the in-hospital mortality of patients with acute coronary syndrome and long-term cardiac outcomes in older patients and those with acute myocardial infarction (AMI) [8–10]. A systematic review demonstrated that the CHA2DS2-VASc score is a useful tool for identifying AF patients at higher risk of 1–5 year all-cause mortality and that the CHA2DS2-VASc score is correlated with the development of AMI, cardiovascular hospitalization, outcome in stroke, and major adverse cardiovascular events (MACEs) [11, 12].

The CHA2DS2-VASc score has been reported to have clinical value for predicting the severity of infarction and short to long-term clinical outcomes after AIS with and without AF in addition to its original purpose of assessing the risk of stroke in patients with AF. However, the evidence is not sufficiently strong due to short-term follow-up and limited studies and the authors suggest that further studies should be conducted to modify the stratification instrument for history of AF and other concomitant risk factors [13, 14].

To date, no consensus has been reached on the usefulness of the CHA2DS2-VASc score to estimate endpoint outcomes in different clinical diseases. In addition, there is still no a clinically useful tool to predict the outcomes after AIS. Thence, this large-scale cohort study using the Taiwan Stroke Registry (TSR), aimed to investigate the independent predictive value of the

CHA2DS2-VASc score in 1-year major adverse cardiac and cerebrovascular events (MACCEs) after AIS.

Materials and methods

Data source

The TSR is a prospective, multicenter registry of patients with acute stroke admitted to 54 major hospitals in Taiwan [15]. The aims of the TSR are to investigate the risk factors and outcomes of stroke in a nationwide registry and to assess the quality of stroke care. It includes the clinical data and outcomes of all patients with stroke. The registry was established in 2006 and involved 65 academic and community hospitals. Data includes demographic profiles, timetables of stroke onset, inpatient records, discharge information, and follow-up information. Informed consent was obtained from all patients before they were included in the registry. The research ethics committee of China Medical University Hospital in Taiwan approved the present study protocol (CMUH102-REC1-086(CR-7)).

Ethics statement

The TSR encrypts personal information of the patients to protect privacy and provides researchers with anonymous identification numbers associated with relevant claims information, including sex, date of birth, medical services received, and prescriptions. Therefore, patient's consent is not required to access the TSR. This study was approved to fulfill the condition for exemption by the Institutional Review Board (IRB) of China Medical University (CMUH102-REC1-086(CR-7)). The IRB also specifically waived the consent requirement. **We confirm that all methods were carried out in accordance with relevant guidelines and regulations.**

Study population and data collection

After patients with hemorrhagic stroke and transient ischemic attack (TIA) were excluded, all patients with AIS were enrolled in our study if the following inclusion criteria were met: (1) aged >18 and <100 years, (2) underwent computed tomography and/or magnetic resonance imaging for the index event, and (3) had complete CHA2DS2-VASc score data at admission. TSR registration data recorded between August 1, 2006, and August 31, 2016, were retrieved and comprised 62,227 patients who met the inclusion criteria (Fig 1). Data were prospectively collected through web-based data entry by TSR-trained study nurses. To assess the impact of CHA2DS2-VASc score and AF on stroke outcome, we collected the following data: (1) preadmission demographic profile, previous medical history of heart failure, hypertension, DM, stroke, TIA, and vascular diseases (inclusive of peripheral arterial disease and previous myocardial infarction); (2) previous AF history or new AF recorded on electrocardiography (ECG) or 24-h Holter ECG during admission; and (3) occurrence of myocardial infarction, re-stroke, or all-cause mortality at 1, 3, 6, and 12 months after the index stroke.

Outcome measurement

The clinical endpoint was MACCE (a composite of myocardial infarction, re-stroke, or all-cause mortality) 12 months after the onset of the index AIS. We defined a CHA2DS2-VASc score of ≥2 points as high and 0–1 points as low according to its original score distinction [5]. For the cumulative incidence of endpoints and survival analysis, we divided all patients into four groups according to their CHA2DS2-VASc score and presence of AF into Group I
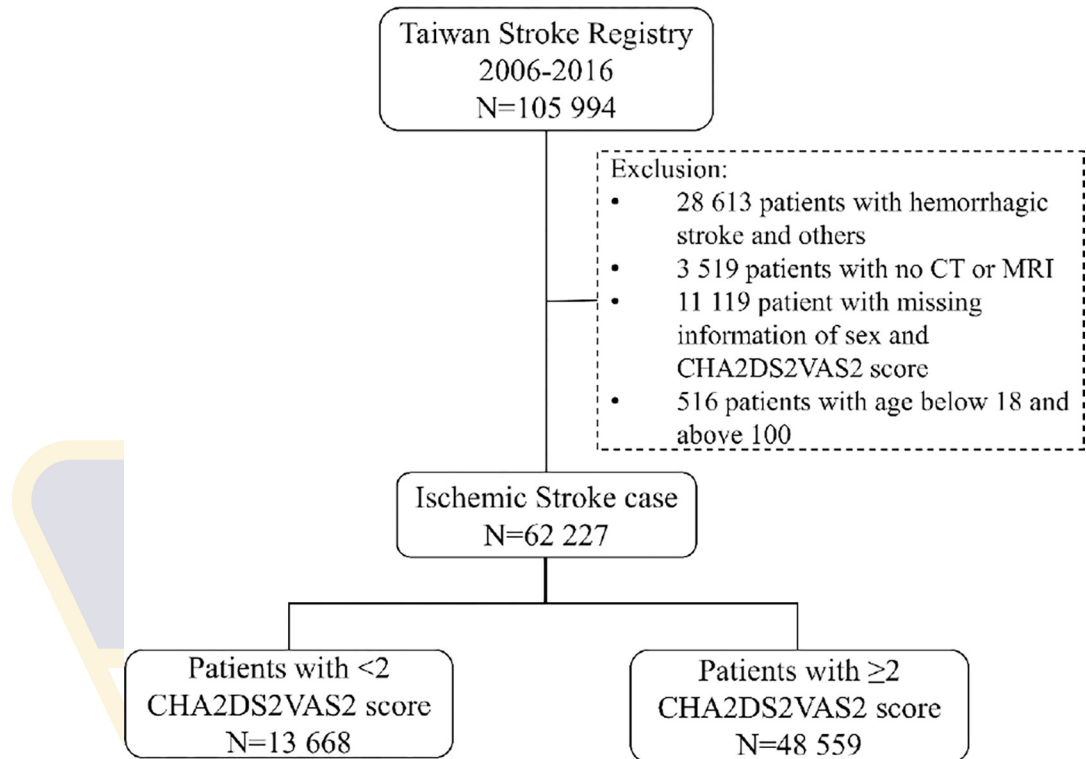
Fig 1. Patient flow in the study comparing high and low CHA2DS2-VASc score.

(reference group; low score without AF), Group II (low score with AF), Group III (high score without AF), and Group IV (high score with AF).

Statistical analysis

The difference in the distribution of continuous variables between the two groups was tested using the standard mean difference (SMD). A SMD less than 0.1 means there was no difference between two groups. Hazard ratios (HRs) were estimated using the Cox proportional model. We made two adjustments for HR: one with AF and body mass index (BMI) and the other with BMI, sex, age, heart failure, hypertension, diabetes, previous stroke, and vascular disease. A survival curve was plotted using the Kaplan–Meier method and assessed with a log-rank test. The risk ratio of each risk factor of the CHA2DS2-VASc score was calculated and visualized on a forest plot. The performance of the predictive model was evaluated by the area under the curve (AUC) of the receiver operating characteristic curve (ROC). All statistical analyses were performed using SAS version 9.4 (SAS Institute, Inc., Cary, NC, USA). A p value of <0.05 was considered significant for all analyses.

Results

Patient characteristics

A total of 62,227 patients (25,497 males and 36,730 females) with AIS who met the inclusion criteria were enrolled. Their median age was 70.3 years, and 59.0% of the patients were women. A total of 48,559 patients (78.0%) had high CHA2DS2-VASc scores and 4,627 patients (7.44%) had AF. In the 1-year cohort, we identified 7105 patients (11.4%) with MACCEs and

Table 1. Characteristics and comorbidities of patients at baseline.

	CHA2DS2-VASc scores <2			CHA2DS2-VASc scores ≥2			
	N = 13 668			N = 48 559			
Variables	N	n	%	N	n	%	SMD
Gender							0.922
female	13 668	12 168	89.0	48 559	24 562	50.6	
male	13 668	1 500	11.0	48 559	23 997	49.4	
Height(cm)							0.797
mean, (±SD)	12 552	165.4	(±7.09)	43 058	159.4	(±8.39)	
Weight(kg)							0.419
mean, (±SD)	12 841	68.3	(±12.5)	44 470	62.3	(±12.2)	
BMI (kg/m2)							0.118
mean, (±SD)	12 432	24.9	(±3.91)	42 276	24.5	(±4.08)	
Age							1.510
mean, (±SD)	13 668	56.1	(±10.3)	48 559	72.4	(±11.2)	
Atrial fibrillation	13 667	524	3.8	48 553	4103	8.5	0.193
Heart failure	13 668	33	0.2	48 559	1458	3.0	0.220
Hypertension	13 668	6 598	48.3	48 559	42213	86.9	0.907
Diabetes	13 668	1 193	8.73	48 559	24547	50.6	1.303
Vascular diseases	13 668	883	6.46	48 559	6926	14.3	0.274
Previous stroke	13 668	0	-	48 559	661	1.4	0.166
Previous TIA	13 405	0	-	47 355	623	1.3	0.062
Discharge medications							
Anti-platelet agents	13 648	11 032	80.8	48 503	37551	77.4	0.084
Anti-HTN agents	13 564	4 921	36.3	48 385	26083	53.9	0.360
Statin	13 668	2 738	20.0	48 559	9096	18.8	0.005
TOAST category							
Large artery atherosclerosis	13 668	3 156	23.9	48 559	12 809	26.4	0.076
Small vessel occlusion	13 668	5 669	41.5	48 559	17 358	35.8	0.118
Cardioembolism	13 668	578	4.23	48 559	460	0.95	0.208

SD: standard deviation; BMI: body mass index; TIA: Transient ischemic attack; HTN: hypertension; TOAST: trial of ORG 10172 in acute stroke treatment)

SMD: standard mean difference (<0.1 means negligible difference between groups)

55,122 patients without MACCEs, as shown in Table 1. Patients with high CHA2DS2-VASc scores had lower BMIs (24.5 vs. 24.9) and older age (72.4 vs. 56.1) than those with low CHA2DS2-VASc scores did. Patients with high CHA2DS2-VASc scores also had significantly more comorbidities, including AF (8.5% vs. 3.8%), hypertension (86.9% vs. 48.3%), DM (50.6% vs. 8.73%), vascular diseases (6.46% vs. 14.3%) and previous stroke or TIA (1.3% vs. 0%).

CHA2DS2-VASc score and 1-year outcomes

Table 2 presents the association between CHA2DS2-VASc score and 1-year clinical outcomes. Among patients with high and low CHA2DS2-VASc scores, 6,143 of the 48,559 (12.7%) and 984 of the 13,668 (7.2%), respectively, reached the composite endpoints. After the confounding factors of AF and BMI were controlled, patients with high CHA2DS2-VASc scores had significantly higher incidences of 1-year MACCEs (adjusted HR = 1.63; 95% CI = 1.52, 1.76), re-stroke (adjusted HR = 1.28; 95% CI = 1.16, 1.42), and all-cause mortality (adjusted HR = 2.03; 95% CI = 1.83, 2.24) than those with low CHA2DS2-VASc scores did.

Table 2. The association of CHA2DS2-VASc score and 1 year outcomes.

| | CHA2DS2-VASc scores | | | | | | | | | | | |
| | 0–1 | | | ≥2 | | | | | | | | |
Outcome	N	PY	IR	N	PY	IR	Crud HR	(95% CI)	p-value	adjusted HR†	(95% CI)	p-value
MACCE	984	6457	1.52	6143	22022	2.79	1.78	(1.67, 1.91)***	<0.001	1.63	(1.52,1.76)***	<0.001
all-cause mortality	502	6619	0.76	4057	22665	1.79	2.30	(2.10, 2.52)***	<0.001	2.03	(1.83,2.24)***	<0.001
myocardial infarction	2	6618	0.003	34	22656	0.02	4.95	(1.19, 20.6)*	0.03	3.85	(0.92,16.2)	0.07
re-stroke	510	6506	0.78	2272	22254	1.02	1.29	(1.17, 1.42)***	<0.001	1.28	(1.16,1.42)***	<0.001

N: number of event; PY: person-years; IR: incidence rate per 10 person-years; HR: hazard ratio; CI: confidence interval; MACCE: major adverse cardiac and cerebrovascular events

†: adjusted by body mass index and atrial fibrillation

*: p-value < 0.05

***: p-value<0.001

AF and 1-year outcomes

The risk of MACCEs between patients with and without AF is compared in Table 3. In patients with and without AF, 845 of 4,627 (18.2%) and 6,282 of 57,600 (10.9%), respectively, reached the composite endpoints. After adjustment for all risk factors in the CHA2DS2-VASc score (sex, age, heart failure, hypertension, DM, previous stroke, and vascular disease), the AF group was associated with increased MACCEs (adjusted HR = 1.74; 95% CI = 1.60, 1.89), myocardial infarction (adjusted HR = 4.86; 95% CI = 2.07, 11.4), re-stroke (adjusted HR = 1.47; 95% CI = 1.26, 1.71), and all-cause mortality (adjusted HR = 1.90; 95% CI = 1.72, 2.10).

Cumulative incidence of MACCE and survival curve

The Kaplan–Meier curves showed that the cumulative incidence of MACCEs was the highest in Group IV (32.1%) and the lowest in Group I (10.6%; Fig 2A). Similar cumulative incidences were observed in Group II (19.3%) and Group III (18.4%). Among patients with AF, Group IV had a higher incidence of MACCEs than did Group II (crude HR = 1.57; p-value = 0.001). Among patients with high CHA2DS2-VASc scores, Group IV had a higher incidence of MACCEs than did Group III (crude HR = 2.06; p-value < 0.001).

Fig 2B shows that the event-free survival rate for all-cause mortality was the lowest in Group IV (75.3%) and the highest in Group I (95.0%). Similar survival probabilities were

Table 3. The association of atrial fibrillation and 1 year outcomes.

| | Atrial fibrillation | | | | | | | | | | | |
| | No | | | Yes | | | | | | | | |
Outcome	N	PY	IR	N	PY	IR	crude HR	(95% CI)	p-value	adjusted HR†	(95% CI)	p-value
MACCE	6282	27028	2.32	845	1448	5.84	2.17	(2.02,2.33)***	<0.001	1.74	(1.60,1.89)***	<0.001
all-cause mortality	3904	27786	1.41	655	1495	4.38	2.66	(2.44,2.89)***	<0.001	1.90	(1.72,2.10)***	<0.001
myocardial infarction	26	27778	0.01	10	1493	0.07	6.92	(3.33,14.4)***	<0.001	4.86	(2.07,11.4)***	<0.001
re-stroke	2568	27281	0.94	214	1476	1.45	1.49	(1.30,1.71)***	<0.001	1.47	(1.26,1.71)***	<0.001

N: number of event; PY: person-years; IR: incidence rate pre 10 person-years; HR: hazard ratio; CI: confidence interval; MACCE: major adverse cardiac and cerebrovascular events

†: adjusted by body mass index, sex, age, heart failure, hypertension, diabetes, previous stroke and vascular.

***: p-value<0.001
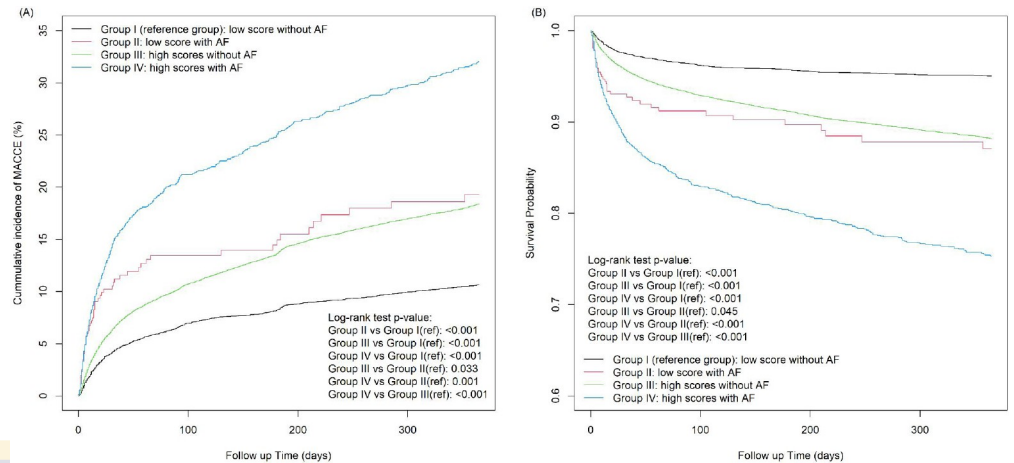
Fig 2. (A) Time-to-Event curves for the major adverse cardiovascular and cerebrovascular events; (B) Kaplan-Meier survival curves for all-cause mortality.

https://doi.org/10.1371/journal.pone.0270823.g002

observed in Group II (87.1%) and Group III (88.1%). Among patients with AF, Group IV had a higher probability of mortality than did Group II (crude HR = 1.81; p-value < 0.001). Among patients with high CHA2DS2-VASc scores, Group IV had a higher incidence of MACCEs than Group III did (crude HR = 2.47; p-value < 0.001).

These results demonstrated that both a high CHA2DS2-VASc score and AF are independent predictors and have an additional effect of unfavorable 1-year outcomes after AIS.

Individual components of the CHA2DS2-VASc score

In the investigation of the effect of individual risk factors in the CHA2DS2-VASc score (Fig 3), age > 65 years, male sex, and a previous history of congestive heart failure, DM, previous stroke/TIA, and vascular disease significantly increased the risk ratio of MACCEs. Patients with a previous history of hypertension had an increasing MACCE trend that did not reach

Risk factors	Risk ratio (95% CI)	p-value
Congestive heart failure	1.86 (1.68,2.06)	<0.001
Hypertension	1.02 (0.97,1.08)	0.452
Age ≥ 65	1.85 (1.75,1.95)	<0.001
Diabetes	1.14 (1.09,1.19)	<0.001
Stroke/TIA	1.37 (1.31,1.44)	<0.001
Vascular disease	1.61 (1.43,1.81)	<0.001
Sex: male	1.19 (1.14,1.24)	<0.001
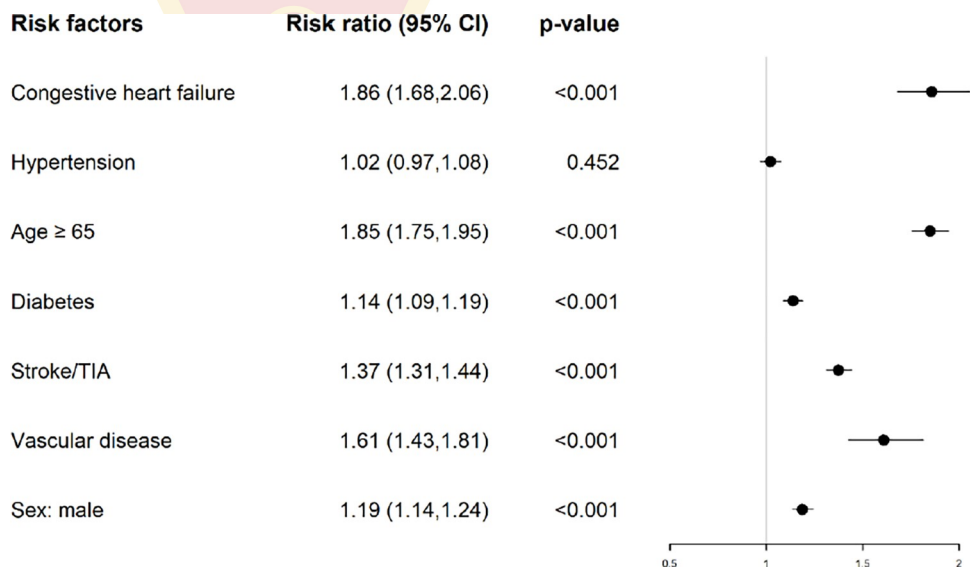
Fig 3. 1 year MACCE associated with individual risk factor of CHA2DS2-VASc score.

https://doi.org/10.1371/journal.pone.0270823.g003

statistical significance, this results may possibly explained by anti-hypertensive agents administration

Discussion

This study was based on the TSR [15], a nationwide, large-scale stroke registry with rigorous control of entry data, to compare 1-year MACCEs after AIS. The data demonstrated that both a high CHA2DS2-VASc score and presence of AF can independently predict unfavorable clinical outcomes. From these results, we can conclude that the CHA2DS2-VASc score at admission is an effective tool for AIS patients with or without AF. Because this scoring system is common and simple, it can be used as a risk-stratification system after AIS that can help physicians identify patients with poor prognoses.

Previous studies have reported AF to be an independent outcome predictor of AIS caused by potential cardiac embolism and large infarct size [3, 16]. Some studies have addressed the effect of the CHA2DS2-VASc score on clinical outcomes after AIS. Tu et al. [13] conducted a study that included 6,612 patients with AIS, of whom 26.5% had AF. The study found that a CHA2DS2-VASc score of ≥2 was associated with higher mortality and more serious adverse cardiac events (acute coronary syndrome, symptomatic heart failure, cardiopulmonary arrest, life-threatening arrhythmia, and cardiac death) 3 months after admission. Ntaios et al. [17] also reported that prestroke CHA2DS2-VASc scores predict long-term stroke outcomes (mortality, stroke recurrence, and cardiovascular events) in 1,756 patients without AF. However, Yang et al. [18] reported that the CHA2DS2-VASc score cannot predict both mortality and re-stroke in patients with lacunar stroke without AF. In summary, whether the CHA2DS2-VASc score and AF are both valuable and independent clinical outcome predictors after AIS remains uncertain.

In 2018, Su et al. [14] studied 1,494 AIS patients (13% AF) and demonstrated that higher CHA2DS2-VASc score was associated with higher re-stroke and mortality rates irrespective of the presence of AF after the mean follow-up time of 37.5 months. In the present study, AF remained a strong outcome predictor, but significantly higher CHA2DS2-VASc scores were detected in patients with AF. The authors considered this to be a possibly major reason for poorer outcomes in ischemic stroke patients with AF. However, the results couldn't clarify the independent predictor value of AF in AIS due to insufficient sample size. In contrast, the patient numbers of our large-scale cohort study allowed us to analyze this issue. After adjustment for BMI and all confounding risk factors in the CHA2DS2-VASc score, patients with AF still had significantly higher odds of 1-year MACCEs and all-cause mortality than those without AF. These results provide stronger evidence of the independent predictive value of the AF in patients with AIS. In addition, inconsistent with previous studies [14, 18], AF was associated with the incidence of 1-year re-stroke despite the common use of anticoagulation agents. More importantly, our results reveal that high CHA2DS2-VASc scores were also significantly associated with higher odds of 1-year MACCEs and all-cause mortality compared with low CHA2DS2-VASc scores.

Our study included a total of 7,127 MACCEs and 4559 mortality events in 62,227 patients with AIS. We separately analyzed the predictive effectiveness of AF and CHA2DS2-VASc scores after adjusting for confounding factors. The results reveal that both had strong, independent predictive value for MACCEs and all-cause mortality. The cumulative 1-year incidence of MACCEs and the survival curve provided clearer evidence that high CHA2DS2-VASc scores and AF have an added effect of unfavorable outcomes after AIS.

The stroke types that divided in TSR include large artery atherosclerosis, small vessel occlusion and cardioembolism. The patient numbers of these three types are not significantly

different between high and low CHA2DS2-VASc score groups. Previous study demonstrated stroke severity measured by the baseline National Institutes of Health Stroke Scale (NIHSS) is also a strong predictor of stroke outcome. Comparing to NIHSS, CHA2DS2-VASc score is well-known and easier to calculate. We compared the prediction model with CHA2DS2-VASc score and NHISS by area under curve (AUC) of receiver operating characteristic curve (ROC). There is no significance difference between two AUC for predicting MACCE (S1 Fig).

Currently, no study has addressed the effect of an individual component of the CHA2DS2-VASc score on clinical outcomes after AIS. In 2010, the INTERSTROKE study [19] reported history of hypertension and DM as significant risk factors in 2,337 patients with AIS. In 2017, Tang et al. [20] reported that low pulse pressure after AIS is associated with unfavorable outcomes based on TSR data. In our large-scale cohort study, the patient number allowed us to evaluate the individual risk factors of the CHA2DS2-VASc score. In addition to age, a history of congestive heart failure, DM, stroke/TIA, and vascular disease were all associated with unfavorable outcomes. Regarding sex, Nielsen et al. [21] reported that female sex is a risk modifier but not a risk factor for stroke in patients with AF. Similarly, our study revealed that female gender was also not a predictor of 1-year MACCEs. According to both the INTERSTROKE study [19] and our results, DM is both a risk factor and an outcome predictor of AIS.

Our study had several potential limitations: (1) Our study design was observational and not a randomized controlled trial. Additional adequately powered prospective clinical trials with larger sample size are necessary to confirm our findings. (2) The registry did not record whether patients performed the 24-h Holter ECG or not. Even for some patients, paroxysmal AF was not detected on ECG or 24-h Holter ECG during admission, and this was a potential reason for the relatively lower incidence of AF in this study compared with that in previous reports. (3) Some patients with AIS were excluded due to loss to follow-up within 1 year after AIS. (4) Patients at higher score group have more comorbidity, that may have impacts on further events.

Conclusion

To the best of our knowledge, this is the first study to demonstrate that both the CHA2DS2-VASc score and AF are strong and independent risk predictors of 1-year MACCEs after AIS. Therefore, wider application of the CHA2DS2-VASc score may help improve the holistic clinical assessment of AIS patients with and without AF.

Supporting information

S1 Fig. AUC of different variables to predict 1 year MACCE and mortality.
(TIF)

S1 Appendix.
(DOCX)

S1 File.
(DOCX)

Author Contributions

Conceptualization: Chun-Hung Su, Hsin-Hung Chen.

Data curation: Chun-Hung Su, Hei-Tung Yip.

Formal analysis: Hei-Tung Yip.

Investigation: Chia-Hung Kao.

Resources: Chung Y. Hsu.

Supervision: Chia-Hung Kao.

Validation: Chun-Hung Su.

Visualization: Chien-Hsien Lo, Hsin-Hung Chen, Chin-Feng Tsai, Kai-Cheng Hsu.

Writing – original draft: Chun-Hung Su, Hei-Tung Yip.

Writing – review & editing: Chun-Hung Su, Chia-Hung Kao.

References

1. Granger CB, Armaganijan LV. Newer oral anticoagulants should be used as first-line agents to prevent thromboembolism in patients with atrial fibrillation and risk factors for stroke or thromboembolism. Circulation. 2012; 125:159–164; discussion 164. https://doi.org/10.1161/CIRCULATIONAHA.111.031146 PMID: 22215890

2. European Heart Rhythm Association; European Association for Cardio-Thoracic Surgery, Camm AJ, Kirchhof P, Lip GY, Schotten U, et al. Guidelines for the management of atrial fibrillation: the Task Force for the Management of Atrial Fibrillation of the European Society of Cardiology (ESC). Eur Heart J. 2010; 31:2369–2429. https://doi.org/10.1093/eurheartj/ehq278 PMID: 20802247

3. Kim YD, Park B, Cha MJ, Nam CM, Nam HS, Ha JW, et al. Stroke severity in concomitant cardiac sources of embolism in patients with atrial fibrillation. J Neurol Sci. 2010; 298:23–27. https://doi.org/10.1016/j.jns.2010.08.011 PMID: 20832823

4. Wolf PA, Abbott RD, Kannel WB. Atrial fibrillation as an independent risk factor for stroke: the Framingham Study. Stroke. 1991; 22:983–8. https://doi.org/10.1161/01.str.22.8.983 PMID: 1866765

5. Mason PK, Lake DE, DiMarco JP, Ferguson JD, Mangrum JM, Bilchick K, et al. Impact of the CHA2DS2-VASc score on anticoagulation recommendations for atrial fibrillation. Am J Med 2012; 125:603.e1–6. https://doi.org/10.1016/j.amjmed.2011.09.030 PMID: 22502952

6. January CT, Wann LS, Calkins H, Chen LY, Cigarroa JE, Cleveland JC Jr, et al. 2019 AHA/ACC/HRS Focused Update of the 2014 AHA/ACC/HRS Guideline for the Management of Patients With Atrial Fibrillation: A Report of the American College of Cardiology/American Heart Association Task Force on Clinical Practice Guidelines and the Heart Rhythm Society in Collaboration With the Society of Thoracic Surgeons. Circulation. 2019; 140:e125–e151. https://doi.org/10.1161/CIR.0000000000000665 PMID: 30686041

7. Hindricks G, Potpara T, Dagres N, Arbelo E, Bax JJ, Blomström-Lundqvist C, et al. 2020 ESC Guidelines for the diagnosis and management of atrial fibrillation developed in collaboration with the European Association for Cardio-Thoracic Surgery (EACTS). Eur Heart J. 2021; 42:373–498. https://doi.org/10.1093/eurheartj/ehaa612 PMID: 32860505

8. Borovac JA, Kwok CS, Mohamed MO, Fischman DL, Savage M, Alraies C, et al. The predictive value of CHA2DS2-VASc score on in-hospital death and adverse periprocedural events among patients with the acute coronary syndrome and atrial fibrillation who undergo percutaneous coronary intervention: a 10-year National Inpatient Sample (NIS) analysis. Cardiovasc Revasc Med. 2021; 29:61–68. https://doi.org/10.1016/j.carrev.2020.08.003 PMID: 32828675

9. Xing Y, Sun Y, Li H, Tang M, Huang W, Zhang K, et al. CHA2DS2-VASc score as a predictor of long-term cardiac outcomes in elderly patients with or without atrial fibrillation. Clin Interv Aging. 2018; 13:497–504. https://doi.org/10.2147/CIA.S147916 PMID: 29636604

10. Kim KH, Kim W, Hwang SH, Kang WY, Cho SC, Kim W, et al. The CHA2DS2VASc score can be used to stratify the prognosis of acute myocardial infarction patients irrespective of presence of atrial fibrillation. J Cardiol. 2015; 65:121–7. https://doi.org/10.1016/j.jjcc.2014.04.011 PMID: 24972564

11. Ivănescu AC, Buzea CA, Delcea C, Dan GA. Stroke Risk Scores as Predictors of Severe Outcomes in Atrial Fibrillation: A Comprehensive Review. Am J Ther. 2021 28:e319–e334. https://doi.org/10.1097/MJT.0000000000001357 PMID: 33852487

12. Proietti M, Farcomeni A, Romiti GF, Di Rocco A, Placentino F, Diemberger I, et al. Association between clinical risk scores and mortality in atrial fibrillation: Systematic review and network meta-regression of 669,000 patients. Eur J Prev Cardiol. 2020; 27:633–644. https://doi.org/10.1177/2047487318817662 PMID: 30861693

13. Tu HT, Campbell BC, Meretoja A, Churilov L, Lees KR, Donnan GA, et al. Pre-stroke CHADS2 and CHA2DS2-VASc scores are useful in stratifying three-month outcomes in patients with and without

atrial fibrillation. Cerebrovasc Dis. 2013; 36:273–80. https://doi.org/10.1159/000353670 PMID: 24135809

14. Su CH, Tsao TF, Chen AC, Chang KW, Yang YS, Ueng KC, et al. CHA2 DS2 -VASc scores for outcome prediction in acute ischaemic stroke. Eur J Clin Invest. 2018; 48(3). https://doi.org/10.1111/eci.12884 Epub 2018 Jan 29. PMID: 29288496

15. Hsieh FI, Lien LM, Chen ST, Bai CH, Sun MC, Tseng HP, et al. Get With the Guidelines-Stroke performance indicators: surveillance of stroke care in the Taiwan Stroke Registry: Get With the Guidelines-Stroke in Taiwan. Circulation. 2010; 122(11):1116–23. https://doi.org/10.1161/CIRCULATIONAHA. 110.936526 PMID: 20805428

16. Tu HT, Campbell BC, Christensen S, Collins M, De Silva DA, Butcher KS, et al. Pathophysiological determinants of worse stroke outcome in atrial fibrillation. Cerebrovasc Dis 2010; 30:389–95. https://doi.org/10.1159/000316886 PMID: 20693794

17. Ntaios G, Lip GY, Makaritsis K. CHADS2, CHA2DS2-VASc, and long-term stroke outcome in patients without atrial fibrillation. Neurology. 2013; 80:1009–1017. https://doi.org/10.1212/WNL. 0b013e318287281b PMID: 23408865

18. Yang HJ, Wang GJ, Shuai W, Shen CJ, Kong B, Huang H. The Value of the CHADS2 and CHA2DS2-VASc Score for Predicting the Prognosis in Lacunar Stroke with or without Atrial Fibrillation Patients. J Stroke Cerebrovasc Dis. 2019; 28:104143. https://doi.org/10.1016/j.jstrokecerebrovasdis.2019.03.027 PMID: 31477449

19. O'Donnell MJ, Xavier D, Liu L, Zhang H, Chin SL, Rao-Melacini P, et al. Risk factors for ischaemic and intracerebral haemorrhagic stroke in 22 countries (the INTERSTROKE study): a case-control study. Lancet. 2010; 376:112–23. https://doi.org/10.1016/S0140-6736(10)60834-3 PMID: 20561675

20. Tang SC, Yin JH, Liu CH, Sun MH, Lee JT, Sun Y, et al. Low Pulse Pressure After Acute Ischemic Stroke is Associated With Unfavorable Outcomes: The Taiwan Stroke Registry. J Am Heart Assoc. 2017; 6:e005113. https://doi.org/10.1161/JAHA.116.005113 PMID: 28642220

21. Nielsen PB, Skjøth F, Overvad TF, Larsen TB, Lip GYH. Female Sex Is a Risk Modifier Rather Than a Risk Factor for Stroke in Atrial Fibrillation: Should We Use a CHA2DS2-VA Score Rather Than CHA2DS2-VASc? Circulation. 2018; 137(8):832–840. https://doi.org/10.1161/CIRCULATIONAHA.117. 029081 PMID: 29459469

Hydroxychloroquine Does Not Increase the Risk of Cardiac Arrhythmia in Common Rheumatic Diseases: A Nationwide Population-Based Cohort Study

Chien-Hsien Lo [1,2†], James Cheng-Chung Wei [3,4,5,6†], Yu-Hsun Wang [7], Chin-Feng Tsai [1,2], Kuei-Chuan Chan [1,2], Li-Ching Li [8], Tse-Hsien Lo [9] and Chun-Hung Su [1,2*]

[1] Institute of Medicine, School of Medicine, Chung Shan Medical University, Taichung, Taiwan, [2] Division of Cardiology, Department of Internal Medicine, Chung-Shan Medical University Hospital, Taichung, Taiwan, [3] Division of Allergy, Immunology and Rheumatology, Chung Shan Medical University Hospital, Taichung, Taiwan, [4] Institute of Medicine, College of Medicine, Chung Shan Medical University, Taichung, Taiwan, [5] Graduate Institute of Integrated Medicine, China Medical University, Taichung, Taiwan, [6] Department of Medical Research, Taichung Veterans General Hospital, Taichung, Taiwan, [7] Department of Medical Research, Chung Shan Medical University Hospital, Taichung, Taiwan, [8] Department of Internal Medicine, Chung-Shan Medical University Hospital, Taichung, Taiwan, [9] Department of Internal Medicine, Da Chien General Hospital, Miaoli, Taiwan

Objectives: Hydroxychloroquine (HCQ) is widely used to treat rheumatic diseases including rheumatoid arthritis (RA), systemic lupus erythematosus (SLE) and Sjögren's syndrome (SS). Cardiac arrhythmia has been concerned as important safety issue for HCQ. The aim of this study was to investigate whether hydroxychloroquine increases new-onset arrhythmia among patients with RA, SLE or SS.

Methods: This was a retrospective cohort study that conducted from the longitudinal health insurance database of Taiwan. Patients with newly diagnosed RA, SLE or SS with age ≥20 years old were selected from 2000 to 2012. Patients who received HCQ and without HCQ treatment groups were matched by propensity score to minimize the effect of selection bias and confounders. The Cox proportional hazard model was used to analyze the risk of arrhythmia between the two groups after controlling for related variables.

Results: A total of 15892 patients were selected to participate and finally 3575 patients were enrolled in each group after matching. There was no different risk of all arrhythmia in patients using HCQ than without HCQ (adjusted hazards ratio 0.81, 95% CI 0.61–1.07) and ventricular arrhythmia as well. The incidence of arrhythmia did not increase when HCQ co-administrated with macrolides. The arrhythmia risk was also not different regardless of daily HCQ dose <400mg or ≥400mg or follow-up duration of ≤4 months or >4 months.

Conclusion: The administration of HCQ did not increase the risk of all cardiac arrhythmia and ventricular arrhythmia regardless of different duration of treatment (≤4 months or >4 months) or cumulative dose (<400mg or ≥400mg) in patients with common autoimmune diseases such as RA, SLE and SS.

Keywords: Hydroxychloroquine, arrhythmia, rheumatoid arthritis, systemic lupus erythematosus, Sjögren's syndrome

INTRODUCTION

Hydroxychloroquine (HCQ) is an antimalarial drug that also has been extensively used in certain rheumatic diseases such as rheumatoid arthritis (RA), systemic lupus erythematosus (SLE) and Sjögren's syndrome (SS) to control disease activity and improve survival for several decades (1–5). HCQ can modulate prothrombotic signaling pathways and protect against systemic inflammation by inhibiting endosomal NADPH oxidase (6). Coronavirus disease 2019 (Covid-19) become pandemic since 2019 December, currently still spreads rapidly, rising number of cases and deaths worldwide (7, 8). Because of Covid-19 pandemic, the efficacy and safety of HCQ has been more concerned and explored recently. Cardiac arrhythmia is one of the safety issues in patients receiving HCQ. Previous studies had been debating on the effect of HCQ and the risk of cardiac arrhythmia (9–11). A recent meta-analysis including 45 articles concluded that HCQ use was not associated with mortality, benefit or harm in Covid-19 patient (12). A prospective trial reported that prolongation of QTc interval was found more frequently in the HCQ group, but there was no increase in arrhythmia (13). Rosenberg et al. reported more patients in the HCQ experienced arrhythmias compared with non-HCQ group (14). McGhie et al. pointed that cumulative antimalarial dose did not significant associate with ECG structural abnormalities, while was protective for ECG conduction abnormalities (15). Recent study for hospitalized patients showed that the risk of supraventricular tachycardia, ventricular arrhythmia and AV block were not increased in HCQ group (16). The data about the treatment of HCQ and clinical outcome are mixing and still inconsistent. Therefore, we designed a retrospective cohort study from large population-based dataset to investigate whether HCQ increase the risk of arrhythmia or not in patients with rheumatic diseases including RA, SLE and SS.

MATERIALS AND METHODS

Data Source

We conducted a retrospective cohort study using data from the Taiwan National Health Insurance Research Database (NHIRD), which contains information on outpatient visits, emergency care, hospitalization, medical procedures, and medications. It contains one million people randomly sampled from the NHIRD with International Classification of Diseases, 9th Revision, Clinical Modification (ICD-9-CM) diagnosis codes (17) and data were collected from 1999 to 2013. This study was approved by the Research Ethics Committee of Chung Shan Medical University and Hospital (CS-17114).

Patient Selection

This data was collected from 1999 to 2013 from the Longitudinal Health Insurance Database. We enrolled all people with age ≥20 years-old, who were newly diagnosed with RA (ICD-9-CM=714.0) (18, 19), SLE (ICD-9-CM=710.0) (6, 20) and SS (ICD-9-CM=710.2) with at least three outpatient clinic visits or one admission from 2000 to 2012. Patients with a diagnosis of arrhythmia (ICD-9-

CM=426–427), before the diagnosis of disease RA, SLE or SS were excluded. The first date of HCQ after a disease diagnosis was set as the index date. The comparison group was non-use of HCQ after disease diagnosis. The comparison group included patients who had not been diagnosed with arrhythmia after the disease diagnosis. The primary outcome was defined as a new diagnosis of all arrhythmias including conduction disorders such as atrioventricular block and bundle branch block (ICD-9-CM=426), supraventricular tachyarrhythmias, ventricular tachyarrhythmias and sinus node dysfunction (ICD-9-CM=427). Ventricular tachyarrhythmias alone (ICD-9-CM=427.1, 427.4–427.5) was also analyzed as secondary outcome. The study period was from the index date to the first onset of arrhythmia, withdraw from the national health insurance system, or 2013/12/31, which came first.

Covariates and Propensity Score Matching

To minimize the effect of confounding factors, we used propensity score (PS) matching to obtain a 1:1 matched by the age, gender, comorbidities such as hypertension (HTN: ICD-9-CM=401–405), hyperlipidemia (ICD-9-CM=272.0–272.4), chronic liver disease (ICD-9-CM=571), chronic kidney disease (CKD: ICD-9-CM=585), diabetes mellitus (DM: ICD-9-CM=250), chronic obstructive pulmonary disease (COPD: ICD-9-CM=491,492,496), ischemic heart disease (ICD-9-CM=410–414), heart failure (ICD-9-CM=428), stroke (ICD-9-CM=430–438), history of beta (β)-blocker usage, antibiotic macrolides treatment and index year. The pre-existing comorbidity was diagnosed one year before index date. The medications were used during the study period. PS matching is a statistical matching technique that can reduce potential confounding caused by unbalanced covariates in non-experimental settings. PS matching is the probability calculated *via* a logistic regression model. The score is a unit with certain characteristics, which can be used to reduce or eliminate selection bias.

Statistical Analysis

To compare the characteristics of HCQ and non-HCQ groups, Chi-square test for categorical variables and independent t test for continuous variables were used. The incidence of events was determined by the number of events divided by the observed person-years. The Kaplan-Meier method was applied to obtain the cumulative incidences of newly diagnosed arrhythmia and log-rank test to perform the significance. We used a Cox proportional hazard model to estimate the crude hazard ratios (HR), adjusted HR, and 95% confidence intervals (CIs) among the two groups. The per-day HCQ dosage was also calculated to perform the risk of arrhythmia. All statistical analyses were conducted using software SPSS version 18.0 (SPSS Inc., Chicago, IL, USA). A p value less than 0.05 between the two groups was considered to be statistically significant.

RESULTS

The flow chart for patient selection is demonstrated in **Figure 1**. Among the one million patients, a total of 15892 patients with newly
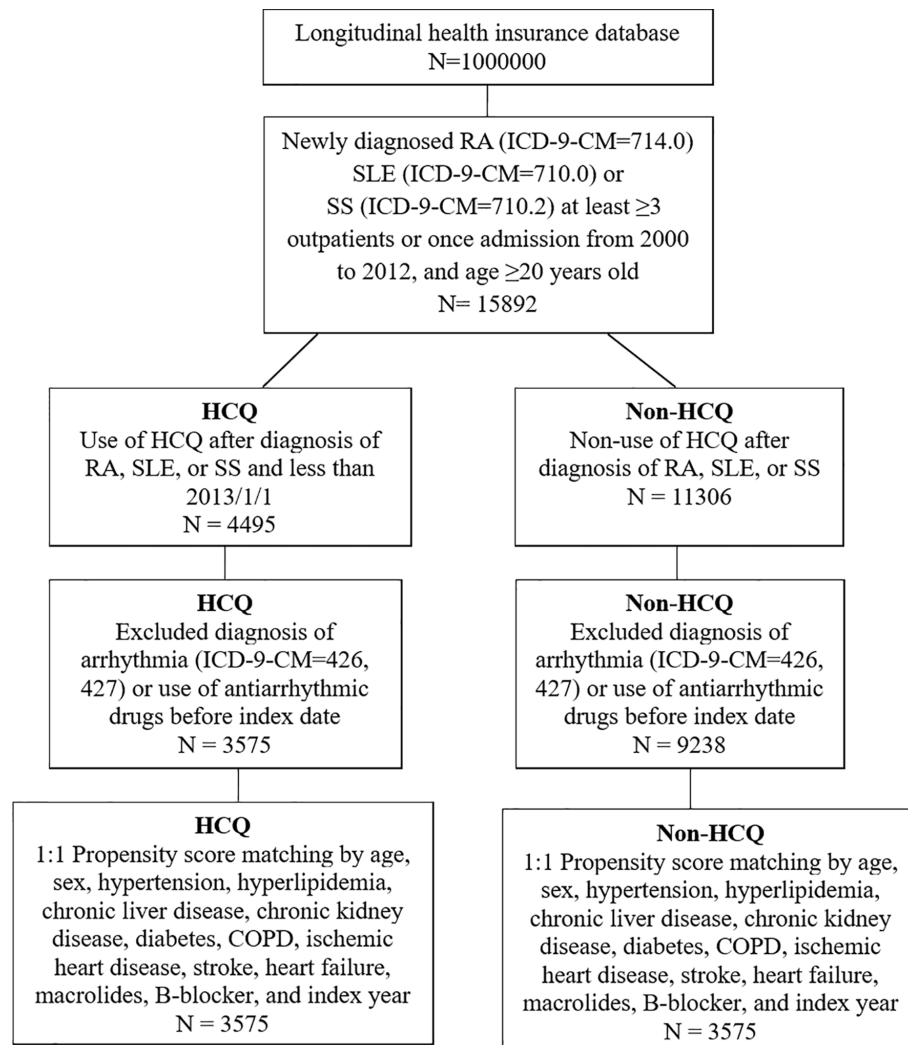
FIGURE 1 | Flow chart of patient selection for those with rheumatoid arthritis (RA), systemic lupus erythematosus (SLE) or Sjögren's syndrome (SS), who were using hydroxychloroquine (HCQ) (study group) and or not using HCQ (non-HCQ control group) from the National Health Insurance Research Database.

diagnosed RA, SLE and SS were selected to participate in the study. 2988 patients were excluded due to previous arrhythmia before their RA diagnosis, those using antiarrhythmic agents such as amiodarone, dronedarone, or propafenone. After PS matching with 1:1 ratio, a total of 3575 patients were enrolled in the both groups respectively.

Baseline demographic and clinical characteristics of the participants are summarized in **Table 1**. The mean (SD) age of the patients was 51.1 (13) years in the both groups. About 80% of the study population was female. Most underlying comorbidities were higher in non-HCQ group which were balanced after PS matching. 438 (12.3%) used a macrolide antibiotic combined with HCQ, whereas 420 (11.7%) patients used macrolide antibiotics in the non-HCQ group (p=0.512).

The main arrhythmias outcome was illustrated in **Figure 2**. The cumulative risk of both all arrhythmia (**Figure 2A**) and

ventricular tachyarrhythmia (**Figure 2B**) were not different in the HCQ group compared with non-HCQ group (log-rank test, p=0.165 and p=0.548 respectively).

The result of Cox regressions to determine the hazard ratios for arrhythmia is listed in **Table 2**. The incidence of arrhythmia did not increase in HCQ group with an adjusted HR of 0.81, 95% CI 0.61–1.07. The incidence of arrhythmia was 106 per 41916 person-months in the non-HCQ group and 87 per 42057 person-months in the HCQ group (**Table S1**). There was no different in ventricular arrhythmia in HCQ usage than in the non-HCQ group with an adjusted HR of 1.35, 95% CI 0.61–2.99 (**Table S2**). Age ≥50 years had higher risk of arrhythmia (adjusted HR 1.64, 95% CI 1.18–2.28). People with underlying hypertension, chronic kidney disease, ischemic heart disease, stroke and using β-blocker had significantly higher numbers of

TABLE 1 | Demographic characteristics of the HCQ and Non-HCQ groups.

	Before PS matching					After PS matching				
	HCQ (N= 3575)		Non-HCQ (N = 9238)		p-value	HCQ (N= 3575)		Non-HCQ (N = 3575)		p-value
	n	%	n	%		n	%	n	%	
Age					<0.001					0.255
<50	1647	46.1	3786	41.0		1647	46.1	1695	47.4	
≥50	1928	53.9	5452	59.0		1928	53.9	1880	52.6	
Mean ± SD	51 ± 15.1		53.8 ± 15.9		<0.001	51 ± 15.1		51 ± 15.6		0.937
Sex					<0.001					0.720
Female	2873	80.4	6271	67.9		2873	80.4	2885	80.7	
Male	702	19.6	2967	32.1		702	19.6	690	19.3	
Hypertension	620	17.3	2094	22.7	<0.001	620	17.3	595	16.6	0.431
Hyperlipidemia	271	7.6	720	7.8	0.685	271	7.6	270	7.6	0.964
Chronic liver disease	206	5.8	481	5.2	0.211	206	5.8	203	5.7	0.879
Chronic kidney disease	49	1.4	105	1.1	0.276	49	1.4	49	1.4	1
Diabetes mellitus	274	7.7	941	10.2	<0.001	274	7.7	262	7.3	0.590
COPD	103	2.9	318	3.4	0.110	103	2.9	114	3.2	0.448
Ischemic heart disease	159	4.4	504	5.5	0.021	159	4.4	171	4.8	0.499
Stroke	96	2.7	345	3.7	0.003	96	2.7	99	2.8	0.828
Heart failure	33	0.9	99	1.1	0.455	33	0.9	40	1.1	0.410
Macrolides	438	12.3	1275	13.8	0.021	438	12.3	420	11.7	0.512
B-blocker	645	18.0	1789	19.4	0.087	645	18.0	612	17.1	0.305

HCQ, Hydroxychloroquine; PS, propensity score; COPD, Chronic obstructive pulmonary disease.

FIGURE 2 | The cumulative incidence of all cardiac arrhythmia **(A)** and ventricular tachyarrhythmia **(B)** between the hydroxychloroquine (HCQ) group and the non-HCQ group (p-value=0.165 and p-value=0.548 respectively, Log-rank test).
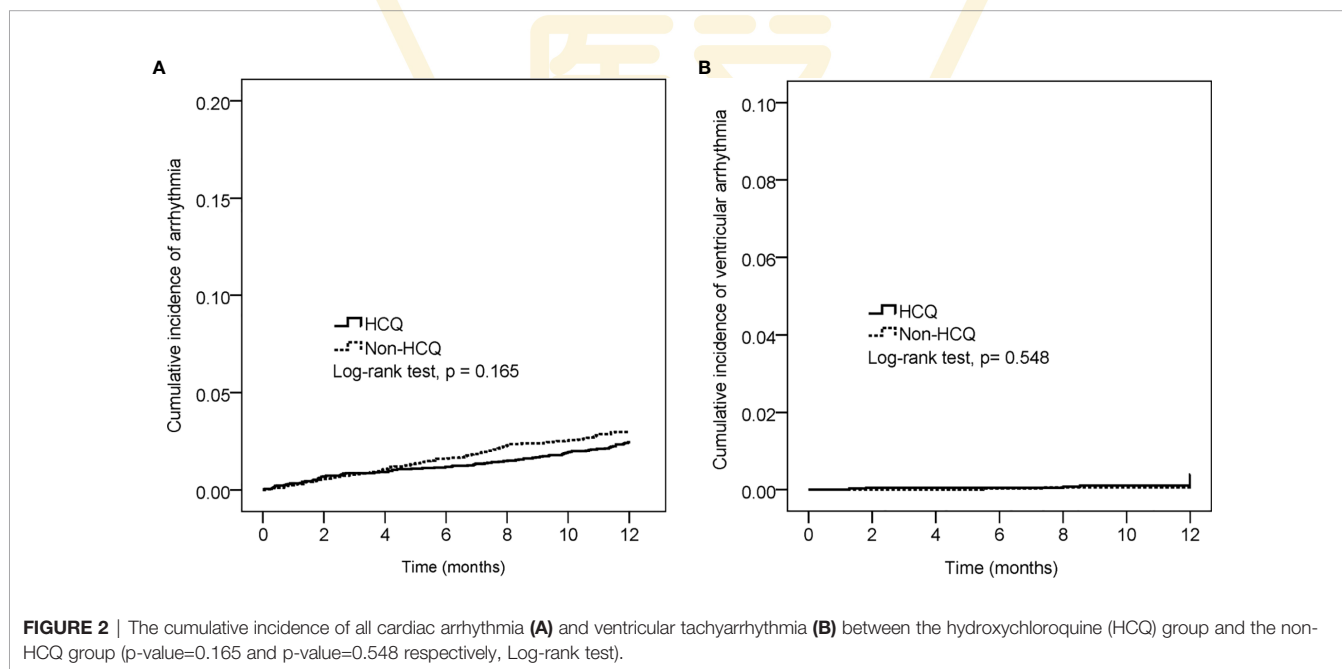
arrhythmias. Other comorbidities were not significantly different for the risk of arrhythmia.

The subgroup analysis for association of arrhythmia between HCQ and non-HCQ group is shown in **Figure 3** and **Table S3**. There was no statistically significant difference between the combination of HCQ and macrolide antibiotics and incidence of arrhythmia (only 13 events over 438 patients in HCQ group compared with 9 events among 420 patients in the non HCQ group) (adjusted HR of 1.38, 95% CI 0.59–3.23). Age above or below

50 years, gender and β-blocker usage also did not increase the risk of arrhythmia either patients using HCQ or not. **Figure 4**, **Tables S4**, **S5** provide the Cox regression hazard ratios for the relationships between arrhythmia and HCQ cumulative dose. All three diseases as well as individual RA, SLE and SS were also analyzed. We found that the risk of arrhythmia for HCQ did not significantly different regardless of the daily dose of <400 mg (adjusted HR 0.84, 95% CI 0.61–1.17) or ≥400 mg (adjusted HR 0.76, 95% CI 0.51–1.12), and follow-up duration of ≦4 months (adjusted HR 0.85, 95% CI 0.53–

TABLE 2 | Association of arrhythmia in RA, SLE or SS patients with multivariable analysis and Cox proportional hazard analysis.

	Crude HR (95% C.I.)	p-value	Adjusted HR† (95% C.I.)	p-value
HCQ				
No	Reference		Reference	
Yes	0.82 (0.62-1.09)	0.165	0.81 (0.61-1.07)	0.137
Age				
<50	Reference		Reference	
≥50	2.07 (1.52-2.82)	<0.001	1.64 (1.18-2.28)	0.003
Sex				
Female	Reference		Reference	
Male	1.01 (0.71-1.45)	0.940	0.95 (0.66-1.36)	0.760
Hypertension	1.58 (1.14-2.20)	0.006	0.61 (0.41-0.89)	0.011
Hyperlipidemia	2.01 (1.34-3.02)	<0.001	1.44 (0.93-2.22)	0.102
Chronic liver disease	1.20 (0.68-2.11)	0.522	0.92 (0.52-1.62)	0.765
Chronic kidney disease	4.22 (2.24-7.98)	<0.001	2.78 (1.42-5.42)	0.003
Diabetes	1.45 (0.91-2.30)	0.117	0.82 (0.50-1.34)	0.420
COPD	2.20 (1.23-3.95)	0.008	1.65 (0.90-3.02)	0.104
Ischemic heart disease	2.99 (1.95-4.58)	<0.001	1.65 (1.03-2.64)	0.036
Stroke	3.08 (1.82-5.22)	<0.001	2.00 (1.16-3.47)	0.013
Heart failure	3.46 (1.54-7.81)	0.003	1.50 (0.63-3.54)	0.361
Macrolides	0.94 (0.60-1.46)	0.778	0.80 (0.51-1.25)	0.329
B-blocker	3.87 (2.91-5.14)	<0.001	3.53 (2.59-4.80)	<0.001

HCQ, Hydroxychloroquine; RA, Rheumatoid arthritis; SLE, systemic lupus erythematosus; SS, Sjögren's syndrome; HR, hazard rati; COPD, Chronic obstructive pulmonary disease; †Adjusted for age, gender, hypertension, hyperlipidemia, chronic liver disease, chronic kidney disease, diabetes mellitus, COPD, ischemic heart disease, stroke, heart failure, macrolides, and B-blocker.

1.36) or >4 months (adjusted HR 0.78, 95% CI 0.55–1.12) compared with non HCQ usage. The different dose result was also consistent in all sub-analyzed individual disease.

DISCUSSION

The aim of this study was to determine the safety concern of HCQ treatment and the risk of arrhythmia. The results indicated that common rheumatic disease patients using HCQ did not

have higher risks of all kinds of cardiac arrhythmias including ventricular tachyarrhythmia. Furthermore, the risk of arrhythmia was not dependent on a longer duration of HCQ treatment >4 months or higher daily dose of ≥400mg.

HCQ has been used in many thousands of patients all over the world for the treatment of Covid-19 in early outbreak. However, recently observational and prospective studies have reported on the efficacy of HCQ treatment for Covid-19. Although some retrospective data disclosed use of HCQ alone and in combination with azithromycin decreased the Covid-19 associated mortality (21), most reports showed that HCQ treatment did not improve their clinical status or reduce the risk of intubation or death (13, 14, 16, 22). A recent systemic review and meta-analysis conducted by Putman et al. who collected 45 articles including 4 randomized controlled trials, 29 cohort studies and 12 case series, concluded that HCQ use was not associated with benefit or harm with regard to Covid-19 mortality (12). In addition, the safety of HCQ treatment in cardiac arrhythmia also had been discussed and results were inconsistent. Cavalcanti et al. conducted a prospective trial with 667 patients (13), and reported that prolongation of QTc interval was found more frequently in the HCQ group, but there was no increase in arrhythmia. Rosenberg et al. investigated 1438 hospitalized patients (14), reported 16% of patients in the HCQ experienced arrhythmias compared with 10% in the non-HCQ group. McGhie et al. analyzed 453 patients treated with antimalarial including HCQ and chloroquine which showed that cumulative antimalarial dose did not significant associate with ECG structural abnormalities, while was protective for ECG conduction abnormalities (15). Recent study from the RECOVERY collaborative group with 4716 hospitalized patients (16) showed that the risk of supraventricular tachycardia, ventricular arrhythmia and AV block were not increased in HCQ group. The study design, relatively small sample size and low event rate may have affected the outcomes and results. In the present study, we found no significant
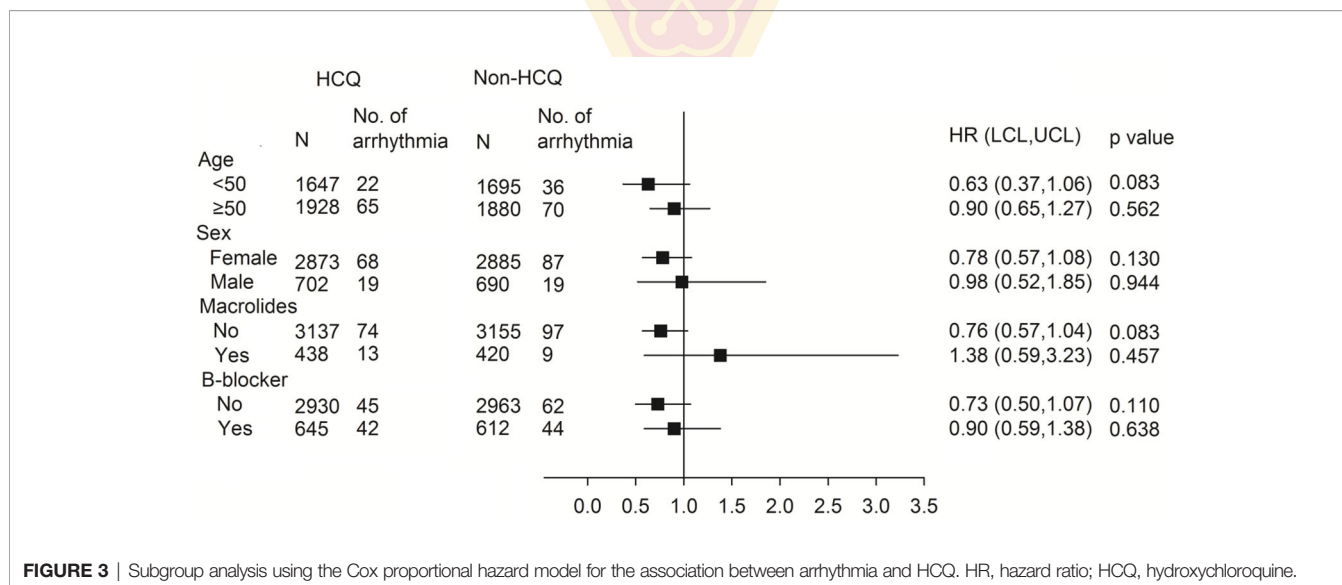
FIGURE 3 | Subgroup analysis using the Cox proportional hazard model for the association between arrhythmia and HCQ. HR, hazard ratio; HCQ, hydroxychloroquine.
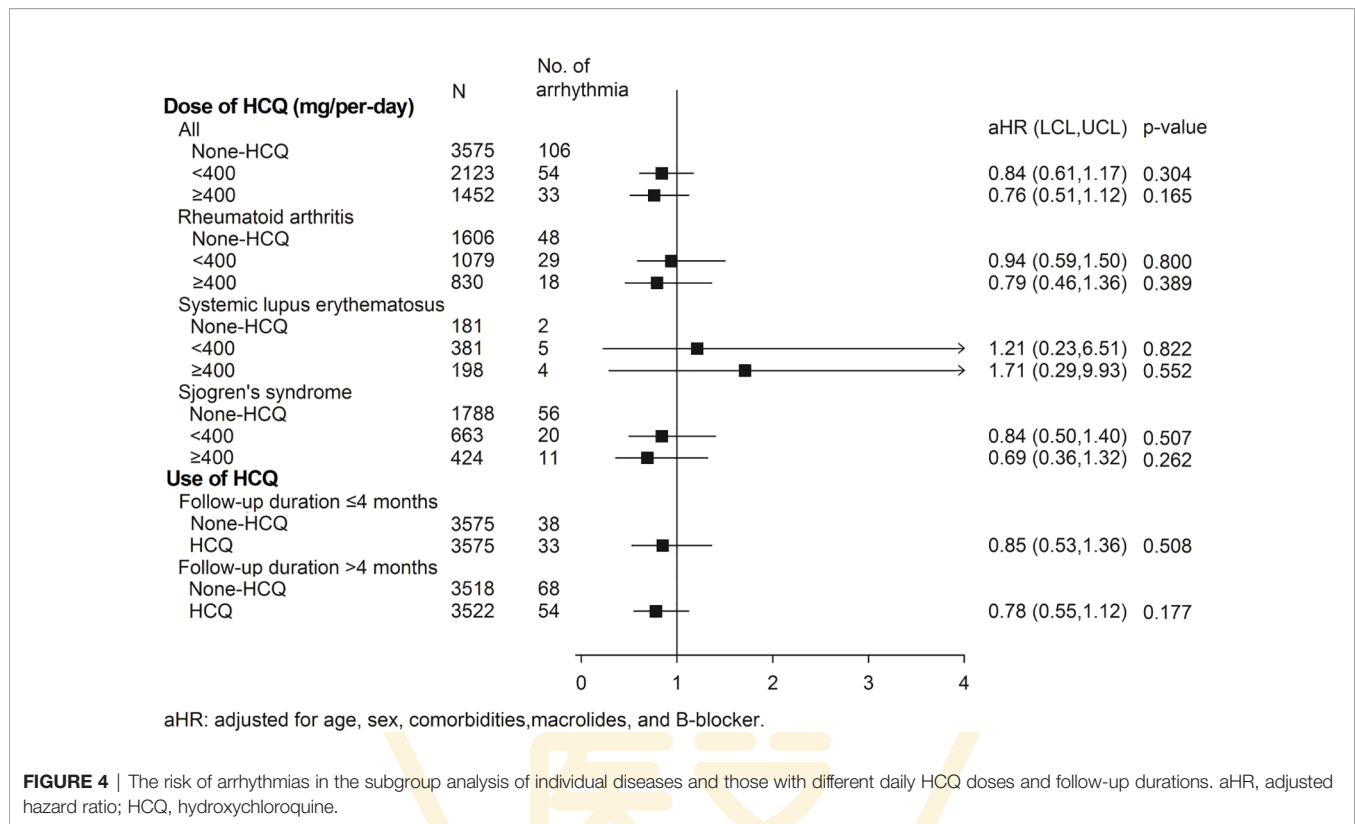
FIGURE 4 | The risk of arrhythmias in the subgroup analysis of individual diseases and those with different daily HCQ doses and follow-up durations. aHR, adjusted hazard ratio; HCQ, hydroxychloroquine.

different between cardiac arrhythmia and the use of HCQ in most rheumatic patients.

An open-label trial discloses azithromycin added to HCQ was significantly more efficient for virus elimination (23). HCQ with or without azithromycin were used as a treatment option for Covid-19 in several countries during early outbreak (23, 24). However, co-administration of HCQ with other drugs such as azithromycin might amplify the arrhythmia risk. Some antibiotics, including macrolides, show pharmacodynamic evidence of iKr inhibition, which results in QT prolongation and dispersion of recovery across the ventricular wall. This phenomenon also has the chance to induce TdP and increase the risk of cardiovascular death (25, 26). In animal studies, there are no synergistic arrhythmic effects of azithromycin with or without chloroquine (27). Nevertheless, one retrospective cohort study reported that patients taking azithromycin had increased risk of mortality, including cardiovascular death, compared with those without antibiotic use during the 5 days of therapy (26). Several studies report the combination of HCQ and azithromycin in Covid-19 treatment prolonged the QT interval, however inconsistent outcomes about the development of life-threatening arrhythmia and mortality were found (13, 28–30). Hence, we also analyzed whether arrhythmia increased or not in the specific subgroups using HCQ with added macrolide treatment for other reasons, which showed that combination therapy of HCQ with macrolides also did not increase any arrhythmia (**Figure 3** and **Table S3**). Nonetheless, the event numbers (arrhythmias) are low in both the HCQ and

non-HCQ groups. Even so, it may support the safety of HCQ combined with macrolide therapy.

Regarding comorbidities (**Table 2**), patients with CKD, ischemic heart disease and stroke had a significantly increased risk of arrhythmia. The anticipated result of CKD come from CKD related various arrhythmogenic alternation including autonomic nervous system, metabolic hemostasis, pharmacokinetics and pharmacodynamics of drugs that may facilitate cardiac arrhythmias (31, 32). β-blockers provide an antiarrhythmic effect because they decrease sympathetic activity by inhibition of the β1 adrenergic receptor and reduce atrial also ventricular tachyarrhythmia (33, 34). But they are also widely used in other cardiovascular diseases rather than arrhythmia such as post myocardial infarction, heart failure, and hypertension (35, 36). In our study, β-blockers were matched by PS matching to reduce possible confounding bias. We found that patients taking β-blocker developed more arrhythmia with an adjusted hazard ratio of 3.53. It may be due to patients taking β-blocker had more underlying comorbidities. In the subgroup analysis, β-blocker did not further increase or decrease risk of arrhythmia either patients using HCQ or not.

Recently we have reported that patients with RA using HCQ did not have a higher risk of cardiac arrhythmia regardless of the daily HCQ dose or follow-up duration (37), which result is consistent with the current study. In addition to RA population, our study includes SLE and SS which increase the sample size,

better matching between the 2 groups and further subgroup analysis. We also determined the sensitivity analysis for development of only ventricular tachyarrhythmia as secondary outcome, which also disclosed consistent outcome. The sub-group analysis of the individual disease of RA, SLE and SS, all revealed no significant increase risk of arrhythmia. Our data showed that the administration of HCQ had a neutral effect on the development of all arrhythmias and ventricular tachyarrhythmias. The previous study reports cardiotoxicity of HCQ was possibly associated with cumulative dose (38). The chronic use of HCQ has also been reported to provoke cardiac arrhythmia (10). According to the sub-analysis (**Figure 4**, **Tables S4** and **S5**), we did not find the incidence of cardiac arrhythmia increase with larger HCQ dose or longer follow-up duration. These data suggest the safety of HCQ regardless of different dose (<400mg or ≥400mg) or treatment duration (≤4 months or >4 months).

There are some strengths and limitations in our study. The strength of this study stands its large NHIRD system, covers 99% of the Taiwanese population, which minimize bias from selection, poor recall or participation (39). Limitations were also notified. First, electrocardiography (ECG) is recommended to measure the QTc interval in individuals receiving HCQ administration (40). In the database, we could not determine the QTc interval by ECG. Nevertheless, our result is safe for risk of arrhythmia in HCQ therapy even we did not provide a baseline ECG indicated that routine ECG data is not always required. Second, only macrolide antibiotics were analyzed as combination therapy, and we did not further investigate other possible drugs that could have prolonged QT. Third, duration and dose of macrolides are not reported as the event numbers is less. Thus claims of association between HCQ and macrolides should be limited. Fourth, diseases were defined according to ICD-9 codified data without any procedure codes, which may lead to over diagnosis. Thence, we added disease codes with at least three outpatient clinic visits or one admission to reduce this bias. Fifth, our study population limited for the patients with RA, SLE and SS hence the results should not be totally applied on patients using HCQ for other diseases. Finally, this is a retrospective cohort design so patient follow-up is not by protocol. There may remain as the possibility of having mild cases of arrhythmias in either group which may have gone undetected. Further larger prospective or randomized control trials are necessary to verify the outcomes of this study.

CONCLUSION

The administration of HCQ in patients with RA, SLE and SS did not increase the risk of cardiac arrhythmia as well as ventricular tachyarrhythmia regardless of the treatment duration (≤4 months or >4 months) or cumulative dose (<400mg or ≥400mg). The outcome is also consistent with others for combination HCQ with macrolide antibiotics.

DATA AVAILABILITY STATEMENT

The original contributions presented in the study are included in the article/**Supplementary Material**. Further inquiries can be directed to the corresponding author.

ETHICS STATEMENT

The studies involving human participants were reviewed and approved by Research Ethics Committee of Chung Shan Medical University and Hospital (approval no. CS-17114). Written informed consent for participation was not required for this study in accordance with the national legislation and the institutional requirements.

AUTHOR CONTRIBUTIONS

C-HL and JC-CW designed the study, generated the figures and wrote the manuscript. Y-HW analyzed the data and generated the figures. C-FT, K-CC, L-CL and T-HL performed the bioinformatics analysis and wrote the manuscript. C-HS made substantial contributions to the design of the study, conducted the data analysis and figure generation, and wrote the manuscript. All authors contributed to the article and approved the submitted version.

SUPPLEMENTARY MATERIAL

The Supplementary Material for this article can be found online at: https://www.frontiersin.org/articles/10.3389/fimmu.2021. 631869/full#supplementary-material

REFERENCES

1. Ben-Zvi I, Kivity S, Langevitz P, Shoenfeld Y. Hydroxychloroquine: from malaria to autoimmunity. *Clin Rev Allergy Immunol* (2012) 42:145–53. doi: 10.1007/s12016-010-8243-x
2. Alarcon GS, McGwin G, Bertoli AM, Fessler BJ, Calvo-Alen J, Bastian HM, et al. Effect of hydroxychloroquine on the survival of patients with systemic lupus erythematosus: data from LUMINA, a multiethnic US cohort (LUMINA L). *Ann Rheum Dis* (2007) 66:1168–72. doi: 10.1136/ard.2006.068676
3. Group CHS. A randomized study of the effect of withdrawing hydroxychloroquine sulfate in systemic lupus erythematosus. *N Engl J Med* (1991) 324:150–4. doi: 10.1056/NEJM199101173240303
4. Rempenault C, Combe B, Barnetche T, Gaujoux-Viala C, Lukas C, Morel J, et al. Metabolic and cardiovascular benefits of hydroxychloroquine in patients with rheumatoid arthritis: a systematic review and meta-analysis. *Ann Rheum Dis* (2018) 77:98–103. doi: 10.1136/annrheumdis-2017-211836
5. Wang SQ, Zhang LW, Wei P, Hua H. Is hydroxychloroquine effective in treating primary Sjogren's syndrome: a systematic review and meta-analysis. *BMC Musculoskelet Disord* (2017) 18:186. doi: 10.1186/s12891-017-1543-z
6. Yang DH, Leong PY, Sia SK, Wang YH, Wei JC. Long-Term Hydroxychloroquine Therapy and Risk of Coronary Artery Disease in Patients with Systemic Lupus Erythematosus. *J Clin Med* (2019) 8:796. doi: 10.3390/jcm8060796

7. Guan WJ, Ni ZY, Hu Y, Liang WH, Ou CQ, He JX, et al. Clinical Characteristics of Coronavirus Disease 2019 in China. *N Engl J Med* (2020) 382:1708–20. doi: 10.1056/NEJMoa2002032

8. Li Q, Guan X, Wu P, Wang X, Zhou L, Tong Y, et al. Early Transmission Dynamics in Wuhan, China, of Novel Coronavirus-Infected Pneumonia. *N Engl J Med* (2020) 382:1199–207. doi: 10.1056/NEJMoa2001316

9. Yanturali S, Aksay E, Demir O. Massive hydroxychloroquine overdose RA. *Acta Anaesthesiol Scand* (2004) 48:379–81. doi: 10.1111/j.0001-5172.2004.0302.x

10. Chen CY, Wang FL, Lin CC. Chronic hydroxychloroquine use associated with QT prolongation and refractory ventricular arrhythmia. *Clin Toxicol (Phila)* (2006) 44:173–5. doi: 10.1080/15563650500514558

11. Costedoat-Chalumeau N, Hulot JS, Amoura Z, Leroux G, Lechat P, Funck-Brentano C, et al. Heart conduction disorders related to antimalarials toxicity: an analysis of electrocardiograms in 85 patients treated with hydroxychloroquine for connective tissue diseases. *Rheumatol (Oxford)* (2007) 46:808–10. doi: 10.1093/rheumatology/kel402

12. Putman M, Chock YPE, Tam H, Kim AHJ, Sattui SE, Berenbaum F, et al. Antirheumatic Disease Therapies for the Treatment of COVID-19: A Systematic Review and Meta-Analysis. *Arthritis Rheumatol* (2021) 73:36–47. doi: 10.1002/art.41469

13. Cavalcanti AB, Zampieri FG, Rosa RG, Azevedo LCP, Veiga VC, Avezum A, et al. Hydroxychloroquine with or without Azithromycin in Mild-to-Moderate Covid-19. *N Engl J Med* (2020) 383:2041–52. doi: 10.1056/NEJMoa2019014

14. Rosenberg ES, Elizabeth M Dufort EM, Udo T, Wilberschied LA, Kumar J, Tesoriero J, et al. Association of Treatment With Hydroxychloroquine or Azithromycin With In-Hospital Mortality in Patients With COVID-19 in New York State. *JAMA* (2020) 23:2493–502. doi: 10.1001/jama.2020.8630

15. McGhie TK, Harvey P, Su J, Anderson N, Tomlinson G, Touma Z. Electrocardiogram abnormalities related to anti-malarials in systemic lupus erythematosus. *Clin Exp Rheumatol* (2018) 36:545–51.

16. Group RC, Horby P, Mafham M, Linsell L, Bell JL, Staplin N, et al. Effect of Hydroxychloroquine in Hospitalized Patients with Covid-19. *N Engl J Med* (2020) 383:2030–40. doi: 10.1056/NEJMoa2022926

17. Cheng TM. Taiwan's new national health insurance program: genesis and experience so far. *Health Aff* (2003) 22:61–76. doi: 10.1377/hlthaff.22.3.61

18. Chang YJ, Lee YH, Leong PY, Wang YH, Wei JC. Impact of Rheumatoid Arthritis on Alopecia: A Nationwide Population-Based Cohort Study in Taiwan. *Front Med (Lausanne)* (2020) 7:150. doi: 10.3389/fmed.2020.00150

19. Liu Y-T, Tsou H-K, Chiou JY, Wang YH, Chou MC, Wei JC. Association of Human Papillomavirus Infection With Risk for Rheumatoid Arthritis: A Population-Based Cohort Study. *Ann Rheum Dis* (2019) 78:1734–6. doi: 10.1136/annrheumdis-2019-215931

20. Wu CY, Tan M, Huang JY, Chiou JY, Wei JC. Hydroxychloroquine is neutral in risk of chronic kidney disease in patients with systemic lupus erythematosus. *Ann Rheum Dis* (2020) 217728. doi: 10.1136/annrheumdis-2020-217728

21. Arshad S, Kilgore P, Chaudhry ZS, Jacobsen G, Wang DD, Huitsing K, et al. Treatment with hydroxychloroquine, azithromycin, and combination in patients hospitalized with COVID-19. *Int J Infect Dis* (2020) 97:396–403. doi: 10.1016/j.ijid.2020.06.099

22. Geleris J, Sun Y, Platt J, Zucker J, Baldwin M, Hripcsak G, et al. Observational Study of Hydroxychloroquine in Hospitalized Patients with Covid-19. *N Engl J Med* (2020) 382:2411–8. doi: 10.1056/NEJMoa2012410

23. Gautret P, Lagier JC, Parola P, Hoang VT, Meddeb L, Mailhe M, et al. Hydroxychloroquine and azithromycin as a treatment of COVID-19: results of an open-label non-randomized clinical trial. *Int J Antimicrob Agents* (2020) 56:105949. doi: 10.1016/j.ijantimicag.2020.105949

24. Bhimraj A, Morgan R, Shumake A, Lavergne V, Baden L, Vincent CC, et al. Infectious Diseases Society of America Guidelines on the Treatment and Management of Patients with COVID-19. *Clin Infect Dis* (2020), ciaa478. doi: 10.1093/cid

25. Yap Y, Camm J. Risk of torsades de pointes with non-cardiac drugs. *BMJ* (2000) 320:1158–9. doi: 10.1136/bmj.320.7243.1158

26. Ray W, Murray K, Hall K, Arbogast P, Stein M. Azithromycin and the Risk of Cardiovascular Death. *N Engl J Med* (2012) 366:1881–90. doi: 10.1056/NEJMoa1003833

27. Fossa A, Wisialowski T, Duncan J, Deng S, Dunne M. Azithromycin/chloroquine combination does not increase cardiac instability despite an increase in monophasic action potential duration in the anesthetized guinea pig. *Am J Trop Med Hyg* (2007) 77:929–38. doi: 10.4269/ajtmh.2007.77.929

28. Cipriani A, Zorzi A, Ceccato D, Capone F, Parolin M, Donato F, et al. Arrhythmic profile and 24-hour QT interval variability in COVID-19 patients treated with hydroxychloroquine and azithromycin. *Int J Cardiol* (2020) 316:280–4. doi: 10.1016/j.ijcard.2020.05.036

29. Duska F, Waldauf P, Halacova M, Zvonicek V, Bala J, Balik M, et al. Azithromycin added to hydroxychloroquine for patients admitted to intensive care due to coronavirus disease 2019 (COVID-19)-protocol of randomised controlled trial AZIQUINE-ICU. *Trials* (2020) 21:631. doi: 10.1186/s13063-020-04566-x

30. Molina JM, Delaugerre C, Le Goff J, Mela-Lima B, Ponscarme D, Goldwirt L, et al. No evidence of rapid antiviral clearance or clinical benefit with the combination of hydroxychloroquine and azithromycin in patients with severe COVID-19 infection. *Med Mal Infect* (2020) 50:384. doi: 10.1016/j.medmal.2020.03.006

31. Potpara TS, Jokic V, Dagres N, Marin F, Prostran MS, Blomstrom-Lundqvist C, et al. Cardiac Arrhythmias in Patients With Chronic Kidney Disease: Implications of Renal Failure for Antiarrhythmic Drug Therapy. *Curr Med Chem* (2016) 23:2070–83. doi: 10.2174/0929867323666160309114246

32. Turakhia MP, Blankestijn PJ, Carrero JJ, Clase CM, Deo R, Herzog CA, et al. Chronic kidney disease and arrhythmias: conclusions from a Kidney Disease: Improving Global Outcomes (KDIGO) Controversies Conference. *Eur Heart J* (2018) 39:2314–25. doi: 10.1093/eurheartj/ehy060

33. Coumel P, Leclercq J-F, Escoubet B. Beta-blockers: Use for arrhythmias. *Eur Heart J* (1987) 8(supplment A):41–52. doi: 10.1093/eurheartj/8.suppl_A.41

34. Zicha S, Tsuji Y, Shiroshita-Takeshita A, Nattel S. Beta-blockers as antiarrhythmic agents. *Handb Exp Pharmacol* (2006) 171:235–66.

35. Borrello F, Beahan M, Klein L, Gheorghiade M. Reappraisal of beta-blocker therapy in the acute and chronic post-myocardial infarction period. *Rev Cardiovasc Med* (2003) 4(Suppl 3):S13–24. doi: 10.1016/j.amjcard.2004.01.021

36. Domanski M, Krause-Steinrauf H, Massie B, Deedwania P, Follmann D, Kovar D, et al. A comparative analysis of the results from 4 trials of beta-blocker therapy for heart failure BEST, CIBIS-II, MERIT-HF, and COPERNICUS. *J Card Fail* (2003) 9:354–63. doi: 10.1054/S1071-9164(03)00133-7

37. Lo CH, Wang YH, Tsai CF, Chan KC, Li LC, Lo TH, et al. Correspondence on 'Festina lente: hydroxychloroquine, COVID-19 and the role of the rheumatologist' by Graef et al. *Ann Rheum Dis* (2020) 218589. doi: 10.1136/annrheumdis-2020-218589

38. Chatre C, Roubille F, Vernhet H, Jorgensen C, Pers YM. Cardiac Complications Attributed to Chloroquine and Hydroxychloroquine: A Systematic Review of the Literature. *Drug Saf* (2018) 41:919–31. doi: 10.1007/s40264-018-0689-4

39. Hsing A, Ioannidis J. Nationwide Population Science: Lessons From the Taiwan National Health Insurance Research Database. *JAMA Intern Med* (2015) 175:1527–9. doi: 10.1001/jamainternmed.2015.3540

40. Kapoor A, Pandurangi U, Arora V, Gupta A, Jaswal A, Nabar A, et al. Cardiovascular risks of hydroxychloroquine in treatment and prophylaxis of COVID-19 patients: A scientific statement from the Indian Heart Rhythm Society. *Indian Pacing Electrophysiol J* (2020) 20:117–20. doi: 10.1016/j.ipej.2020.04.003

Correspondence on 'Festina lente: hydroxychloroquine, COVID-19 and the role of the rheumatologist' by Graef et al

We read with interest the study by Graef et al,[1] who mentioned about the treatment and safety of hydroxychloroquine (HCQ) for the current COVID-19 pandemic. They described that decades of research strongly support the well control of disease activity and survival benefit of HCQ use in rheumatic diseases, such as systemic lupus erythematosus and rheumatoid arthritis (RA). They also highlight that HCQ should be used with caution in patients with COVID-19, including the safety concern, especially when combined with administration of azithromycin because both of them are known corrected QT interval (QTc) prolongation agents.

During early outbreak, HCQ, combined with azithromycin, has been used as a treatment option for COVID-19.[2 3] Recently, an observational study with 1446 patients with COVID-19 reported that HCQ administration was not associated with a lower risk of intubation or death.[4] However, the reasons for mortality were not illustrated. Multiple confounding factors like histories of ischaemic heart disease, heart failure and cardiac arrhythmia were not well adjusted. The main functional site of HCQ in COVID-19 is the entry via ACE2 preceptor.[5 6] We believe that patient selection in early phases of COVID-19 infection would be more appropriate than well-established pneumonia or cytokines storm cases.

The risk of cardiac arrhythmias is an important safety issue. HCQ inhibits the 'funny' current of sinoatrial node and rapid component of the delayed rectifier potassium current, causing lengthening of the action potential and QTc prolongation, which results in potential life-threatening ventricular arrhythmias such as torsades de pointes.[7–10] Nevertheless, previous reports showed limited and inconsistent arrhythmia risk of HCQ treatment.[11 12]

We investigated a report to clarify whether HCQ increased the new onset of arrhythmia in patients with RA by using a large population-based dataset from the National Health Insurance Research Database in Taiwan from 1999 to 2013. We enrolled all people aged 20 years or more who were newly diagnosed with RA

(International Classification of Diseases, Ninth Revision, Clinical Modification (ICD-9-CM)=714.0)[13 14] with at least ≥3 outpatient clinic or once admission. Patients with previous arrhythmia history (ICD-9-CM=426–427) or usage of antiarrhythmic agents such as amiodarone, propafenone and dronedarone were excluded. The end point was set as the first cardiac arrhythmia or 1 year from the index date. To minimise the effect of confounding factors, we used propensity score matching (PSM) to obtain 1:1 ratio matched by age and gender, and comorbidities such as hypertension, hyperlipidaemia, chronic liver disease, chronic kidney disease, diabetes mellitus, chronic obstructive pulmonary disease, ischaemic heart disease, heart failure, stroke, history of β-blocker usage and antibiotic macrolide treatment. χ^2 test for categorical variables and independent t-test for continuous variables were used. The Kaplan-Meier method was applied to obtain the cumulative incidences of newly diagnosed arrhythmia and log-rank test to determine the significance. We used a Cox proportional hazard model to estimate crude HRs, adjusted HRs (aHRs) and 95% CIs between the two groups.

A total of 8564 patients with newly diagnosed RA were selected to participate in the study. We excluded 1559 patients who had arrhythmia before their RA diagnosis and those using antiarrhythmic agents. After PSM, 2111 patients were enrolled in both HCQ and non-HCQ groups, respectively (see online supplementary figure 1). Table 1 shows the baseline patient demographic and clinical characteristics. The mean age of the patients was 52.7 (SD 14.1) years in the HCQ group and 53.6 (SD 14.4) years in the non-HCQ group. The cumulative risk of arrhythmia was not significantly higher in the HCQ group than in the non-HCQ group (log-rank test, p=0.99) (figure 1).

The incidence of arrhythmia did not increase when a combination of HCQ with or without a macrolide antibiotic was taken (aHR 2.7, 95% CI 0.73 to 9.97, p=0.114). Age above or below 50 years, gender and β-blocker usage also did not increase the risk of arrhythmia in patients either using HCQ or not using HCQ (see online supplementary table 2). We found that the risk of arrhythmia for HCQ was not significantly different regardless of the daily dose of <400 mg (aHR 1.0, 95% CI 0.65 to 1.53) or ≥400 mg (aHR

Table 1 Demographic characteristics of patients in the HCQ and non-HCQ groups

| | Before PSM | | | | | After PSM | | | | |
| | HCQ (N=2112) | | Non-HCQ (N=4834) | | | HCQ (N=2111) | | Non-HCQ (N=2111) | | |
	n	%	n	%	P value	n	%	n	%	P value
Age (years)					<0.001					0.473
<50	872	41.3	1746	36.1		872	41.3	895	42.4	
≥50	1240	58.7	3088	63.9		1239	58.7	1216	57.6	
Mean±SD	52.8±14.1		55.8±14.8		<0.001	52.7±14.1		53.6±14.4		0.058
Gender					<0.001					0.514
Female	1607	76.1	3075	63.6		1606	76.1	1624	76.9	
Male	505	23.9	1759	36.4		505	23.9	487	23.1	
Hypertension	503	23.8	1528	31.6	<0.001	503	23.8	492	23.3	0.690
Hyperlipidaemia	318	15.1	726	15.0	0.967	318	15.1	314	14.9	0.863
Chronic liver disease	225	10.7	580	12.0	0.107	225	10.7	215	10.2	0.614
Chronic kidney disease	37	1.8	79	1.6	0.725	36	1.7	31	1.5	0.538
Diabetes mellitus	246	11.6	721	14.9	<0.001	246	11.7	257	12.2	0.601
COPD	132	6.3	404	8.4	0.002	132	6.3	89	4.2	0.003
Ischaemic heart disease	155	7.3	468	9.7	0.002	155	7.3	142	6.7	0.434
Stroke	86	4.1	299	6.2	<0.001	86	4.1	77	3.6	0.472
Heart failure	37	1.8	98	2.0	0.444	37	1.8	25	1.2	0.125
Macrolides	246	11.6	611	12.6	0.248	246	11.7	221	10.5	0.220
β blocker	368	17.4	1015	21.0	0.001	368	17.4	333	15.8	0.148

COPD, chronic obstructive pulmonary disease; HCQ, hydroxychloroquine; PSM, propensity score matching.
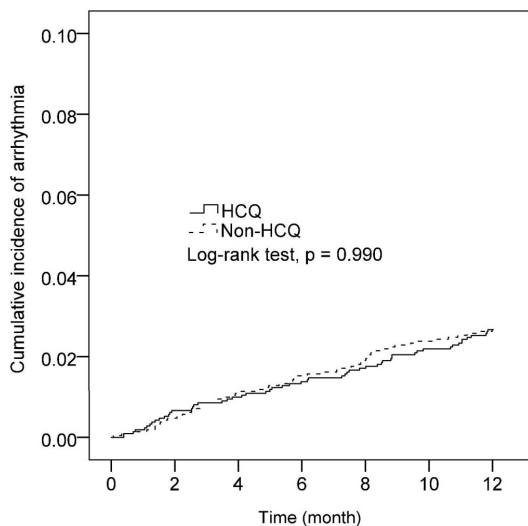
Figure 1 Cumulative incidence of cardiac arrhythmia between the HCQ group and the non-HCQ group (p value=0.99, log-rank test). HCQ, hydroxychloroquine.

0.85, 95% CI 0.52 to 1.4), and follow-up duration of <3 months (aHR 1.0, 95% CI 0.52 to 1.91) or ≥3 months (aHR 0.98, 95% CI 0.62 to 1.53) compared with non-HCQ usage (see online supplementary table 3).

This report may represent the first cohort study that used nationwide population-based data to assess the risk of arrhythmia with HCQ usage in patients with RA. The main results indicate that patients with RA using HCQ did not have a higher risk of cardiac arrhythmia. Larger daily HCQ dose, longer follow-up duration and combination therapy of HCQ with macrolides also did not increase any arrhythmia. Our result provides safety evidence of HCQ for rheumatic diseases. It may indirectly support the safety of HCQ therapy for other diseases such as COVID-19. Further prospective randomised controlled trial is required.

Chien Hsien Lo,[1,2] Yu-Hsun Wang,[3] Chin Feng Tsai,[1,2] Kuei Chuan Chan,[1,2] Li Ching Li,[4] Tse Hsien Lo,[4] Chun Hung Su ![ORCID] **,[1,2] James Cheng-Chung Wei[5,6,7]**

[1]Institute of Medicine, School of Medicine, Chung Shan Medical University, Taichung, Taiwan
[2]Division of Cardiology, Department of Internal Medicine, Chung Shan Medical University Hospital, Taichung, Taiwan
[3]Department of Medical Research, Chung Shan Medical University Hospital, Taichung, Taiwan
[4]Department of Internal Medicine, DaChien General Hospital, Miaoli, Taiwan
[5]Institute of Medicine, Chung Shan Medical University, Taichung, Taiwan
[6]Division of Allergy, Immunology and Rheumatology, Chung Shan Medical University Hospital, Taichung, Taiwan
[7]Graduate Institute of Integrated Medicine, China Medical University, Taichung, Taiwan

Correspondence to Dr James Cheng-Chung Wei, Institute of Medicine, Chung Shan Medical University, Taichung 40201, Taiwan; wei3228@gmail.comDr Chun Hung Su; such197408@gmail.com

► Additional material is published online only. To view, please visit the journal online (http://dx.doi.org/10.1136/annrheumdis-2020-218589).

Check for updates

► http://dx.doi.org/10.1136/annrheumdis-2020-218680

Ann Rheum Dis 2022;**81**:e163. doi:10.1136/annrheumdis-2020-218589

ORCID iD
Chun Hung Su http://orcid.org/0000-0003-4003-008X

REFERENCES

1 Graef ER, Liew JW, Putman MS, et al. *Festina lente*: hydroxychloroquine, COVID-19 and the role of the rheumatologist. *Ann Rheum Dis* 2020;79:734–6.
2 Gautret P, Lagier J-C, Parola P, et al. Hydroxychloroquine and azithromycin as a treatment of COVID-19: results of an open-label non-randomized clinical trial. *Int J Antimicrob Agents* 2020;105949.
3 Bhimraj A, Morgan R, Shumake A, et al. Infectious diseases Society of America guidelines on the treatment and management of patients with COVID-19. *Clin Infect Dis* 2020;4:ciaa478.
4 Geleris J, Sun Y, Platt J, et al. Observational study of hydroxychloroquine in hospitalized patients with Covid-19. *N Engl J Med* 2020;382:2411–8.
5 Klimke A, Hefner G, Will B, et al. Hydroxychloroquine as an aerosol might markedly reduce and even prevent severe clinical symptoms after SARS-CoV-2 infection. *Med Hypotheses* 2020;142:109783.
6 Picot S, Marty A, Bienvenu A-L, et al. Coalition: advocacy for prospective clinical trials to test the post-exposure potential of hydroxychloroquine against COVID-19. *One Health* 2020;100131.
7 Capel RA, Herring N, Kalla M, et al. Hydroxychloroquine reduces heart rate by modulating the hyperpolarization-activated current if: novel electrophysiological insights and therapeutic potential. *Heart Rhythm* 2015;12:2186–94.
8 Chugh SS, Reinier K, Singh T, et al. Determinants of prolonged QT interval and their contribution to sudden death risk in coronary artery disease: the Oregon sudden unexpected death study. *Circulation* 2009;119:663–70.
9 Morgan ND, Patel SV, Dvorkina O. Suspected hydroxychloroquine-associated QT-interval prolongation in a patient with systemic lupus erythematosus. *J Clin Rheumatol* 2013;19:286–8.
10 Simpson TF, Salazar JW, Vittinghoff E, et al. Association of QT-Prolonging medications with risk of autopsy-defined causes of sudden death. *JAMA Intern Med* 2020;180:698–9.
11 Yanturali S, Aksay E, Demir OF, et al. Massive hydroxychloroquine overdose. *Acta Anaesthesiol Scand* 2004;48:379–81.
12 Chen C-Y, Wang F-L, Lin C-C. Chronic hydroxychloroquine use associated with QT prolongation and refractory ventricular arrhythmia. *Clin Toxicol* 2006;44:173–5.
13 Chang Y-J, Lee Y-H, Leong P-Y, et al. Impact of rheumatoid arthritis on alopecia: a nationwide population-based cohort study in Taiwan. *Front Med* 2020;7:150.
14 Liu Y-T, Tsou H-K, Chiou J-Y, et al. Association of human papillomavirus infection with risk for rheumatoid arthritis: a population-based cohort study. *Ann Rheum Dis* 2019;78:1734–6.
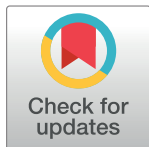
RESEARCH ARTICLE

Association of hydroxychloroquine and cardiac arrhythmia in patients with systemic lupus erythematosus: A population-based case control study

Chien-Hsien Lo[1,2], **Yu-Hsun Wang**[3], **Chin-Feng Tsai**[1,2], **Kuei-Chuan Chan**[1,2], **Li-Ching Li**[4], **Tse-Hsien Lo**[5], **James Cheng-Chung Wei**[6,7,8,9], **Chun-Hung Su**[1,2] *

1 Institute of Medicine, School of Medicine, Chung Shan Medical University, Taichung, Taiwan, **2** Division of Cardiology, Department of Internal Medicine, Chung-Shan Medical University Hospital, Taichung, Taiwan, **3** Department of Medical Research, Chung Shan Medical University Hospital, Taichung, Taiwan, **4** Department of Internal Medicine, Chung-Shan Medical University Hospital, Taichung, Taiwan, **5** Department of Internal Medicine, Da Chien General Hospital, Miaoli, Taiwan, **6** Department of Allergy, Immunology & Rheumatology, Chung Shan Medical University Hospital, Taichung, Taiwan, **7** Institute of Medicine, College of Medicine, Chung Shan Medical University, Taichung, Taiwan, **8** Graduate Institute of Integrated Medicine, China Medical University, Taichung, Taiwan, **9** Department of Medical Research, Taichung Veterans General Hospital, Taichung, Taiwan

☯ These authors contributed equally to this work.
* such197408@gmail.com

Abstract

Objectives

Hydroxychloroquine is widely used to treat certain viral and rheumatic diseases including systemic lupus erythematosus. Cardiac arrhythmia is an important safety issue with hydroxychloroquine. The aim of this study was to investigate whether hydroxychloroquine increases new-onset arrhythmia among patients with systemic lupus erythematosus.

Methods

This was a nested case-control study using data from the Longitudinal Health Insurance Database of Taiwan. A conditional logistic regression model was used to analyse differences in the risk of arrhythmia between systemic lupus erythematosus patients with and without hydroxychloroquine treatment after controlling for related variables.

Results

A total of 2499 patients with newly diagnosed systemic lupus erythematosus were identified (81% females), of whom 251 were enrolled in the new-onset arrhythmia group (mean age 50.4 years) and 251 in the non-arrhythmia group (mean age 49.1 years). There was no significantly increased risk of cardiac arrhythmia (adjusted odds ratio = 1.49, 95% confidence interval: 0.98–2.25) or ventricular arrhythmia (adjusted odds ratio = 1.02, 95% confidence interval: 0.19–5.41) between the patients with and without hydroxychloroquine treatment. In addition, there were no significant differences in the risk of arrhythmia between those

receiving hydroxychloroquine treatment for <180 days or ≥180 days, with a drug adherence rate of <50% or ≥50%, and receiving a daily dose of <400 mg or ≥400 mg.

Conclusion

In patients with systemic lupus erythematosus, hydroxychloroquine treatment did not significantly increase the risk of cardiac arrhythmia or life-threatening ventricular arrhythmia regardless of the different hydroxychloroquine treatment duration, drug adherence rate, or daily dose.

Introduction

The antimalarial drug hydroxychloroquine (HCQ) has been used as standard treatment to reduce disease activity and improve survival for certain inflammatory diseases such as systemic lupus erythematosus (SLE) and rheumatoid arthritis (RA) for more than half a century [1–3]. HCQ can modulate and protect against systemic inflammation and prothrombotic signalling pathways by inhibiting endosomal NADPH oxidase [4]. HCQ has also been demonstrated to reduce glycosylation of severe acute respiratory syndrome coronavirus (SARS-CoV) receptors that block the entry site via ACE2 preceptors [5, 6]. Coronavirus disease 2019 (Covid-19) is caused by SARS-CoV-2, which is transmitted rapidly and is widespread, and threatens the global population [7]. During the early outbreak, HCQ was used as a therapeutic option for Covid-19 treatment whether in combination with azithromycin or not [8, 9].

The risk of cardiac arrhythmias in patients receiving HCQ is an important safety issue. HCQ slows the rate of action potential firing in sinoatrial nodes through channels that inhibit the "funny" current (I_f) [10]. It has also been shown to cause inhomogeneous lengthening of the action potential and prolongation of corrected QT interval (QTc) by inhibiting the rapid component of the delayed rectifier potassium current (iKr), which potentially results in life-threatening ventricular arrhythmias such as torsades de pointes (TdP) [11–13]. Previous reports have shown that the risk of cardiac arrhythmia may be increased in patients using HCQ [14, 15], however the evidence is limited and the results have been inconsistent. Moreover, in everyday practice, very few arrhythmic events have been reported in patients taking HCQ. Therefore, the aim of this study was to clarify whether the risk of arrhythmia is increased in patients receiving HCQ therapy for SLE using a large population-based dataset from the National Health Insurance Research Database (NHIRD) in Taiwan.

Materials and methods

Data source

This retrospective case control study was conducted using data from the Taiwan National Health Insurance (NHI) program, which covers approximately 99% of the population in Taiwan. The NHIRD contains information on outpatient visits, inpatient care, medical procedures, and medications. We used the Longitudinal Health Insurance Database (LHID) which contains one million people randomly sampled from the NHIRD with International Classification of Diseases, 9th Revision, Clinical Modification (ICD-9-CM) diagnosis codes [16]. All data were completely anonymized, deidentified and aggregated before we accessed them. The Research Ethics Committee of Chung Shan Medical University and Hospital approved this study (CS-17114) and patient consent for publication is not required.

Patient selection

This study was conducted using claims data from 1999 to 2013 from the LHID. We enrolled all people who were newly diagnosed with SLE (ICD-9-CM = 710.0) [17, 18] with at least two outpatient clinic visits or one admission from 2000 to 2012. Patients with a diagnosis of arrhythmia (ICD-9-CM = 426, 427) before the diagnosis of SLE were excluded. The first date of newly diagnosed arrhythmia after a diagnosis of SLE was set as the index date. The comparison group included patients who had not been diagnosed with arrhythmia after a diagnosis of SLE. The study period was from the first date when SLE was diagnosed to the index date.

The main cardiac arrhythmia in this study was defined as a new diagnosis of all arrhythmias (ICD-9-CM = 426–427) [19], including conduction disorders such as atrioventricular block and bundle branch block (ICD-9-CM = 426), supraventricular tachyarrhythmias, ventricular tachyarrhythmias and sinus node dysfunction (ICD-9-CM = 427). Ventricular tachyarrhythmias alone (ICD-9-CM = 427.1, 427.4–427.5) were also analysed as sub-group data.

Covariates and matching

To minimise the effect of confounding factors, we performed simple matching to obtain a 1:1 ratio by age, sex and year of SLE diagnosis. The analysed covariates were underlying comorbidities including hypertension (ICD-9-CM = 401–405), hyperlipidemia (ICD-9-CM = 272.0–272.4), chronic liver disease (ICD-9-CM = 571), chronic kidney disease (ICD-9-CM = 585), diabetes mellitus (ICD-9-CM = 250), chronic obstructive pulmonary disease (ICD-9-CM = 491, 492, 496), ischaemic heart disease (ICD-9-CM = 410–414), heart failure (ICD-9-CM = 428), stroke (ICD-9-CM = 430–438), and alcoholism (ICD-9-CM = 305, 571.0–571.2).

Statistical analysis

To compare the characteristics of the patients with and without arrhythmias and HCQ therapy, the chi-square test was used for categorical variables and independent t test for continuous variables. We used a conditional logistic regression model to estimate crude odds ratios (ORs), adjusted ORs, and 95% confidence intervals (CIs) between the two groups. The per-day HCQ dosage was also calculated to analyse the risk of arrhythmia. All statistical analyses were conducted using SPSS version 18.0 (SPSS Inc., Chicago, IL, USA). The null hypothesis of no significant difference between two groups was rejected if $P < 0.05$.

Results

The flow chart of patient selection in this study is illustrated in Fig 1. Among the one million patients, 2499 with newly diagnosed SLE were selected to participate in the study. We excluded 328 patients who had arrhythmia before their SLE diagnosis, and the remaining patients with or without newly diagnosed arrhythmia were classified into two groups for further comparisons. After matching at a 1:1 ratio, a total of 251 patients were enrolled in each group.

The baseline patient demographic and clinical characteristics are summarised in Table 1. The mean (SD) age of the patients was 50.4 (17.9) years in the arrhythmia group and 49.1 (17.4) years in the non-arrhythmia group. Overall, 81% of the study population was female. Most underlying comorbidities were balanced after matching except for ischaemic heart disease and heart failure.

Table 2 shows the results of conditional logistic regression analysis to determine the ORs for arrhythmia. The patients who received HCQ therapy seemed to have a higher risk of arrhythmia, however the difference did not reach significance (adjusted OR 1.49 (95% CI

Fig 1. Flow chart of patient selection.

https://doi.org/10.1371/journal.pone.0251918.g001
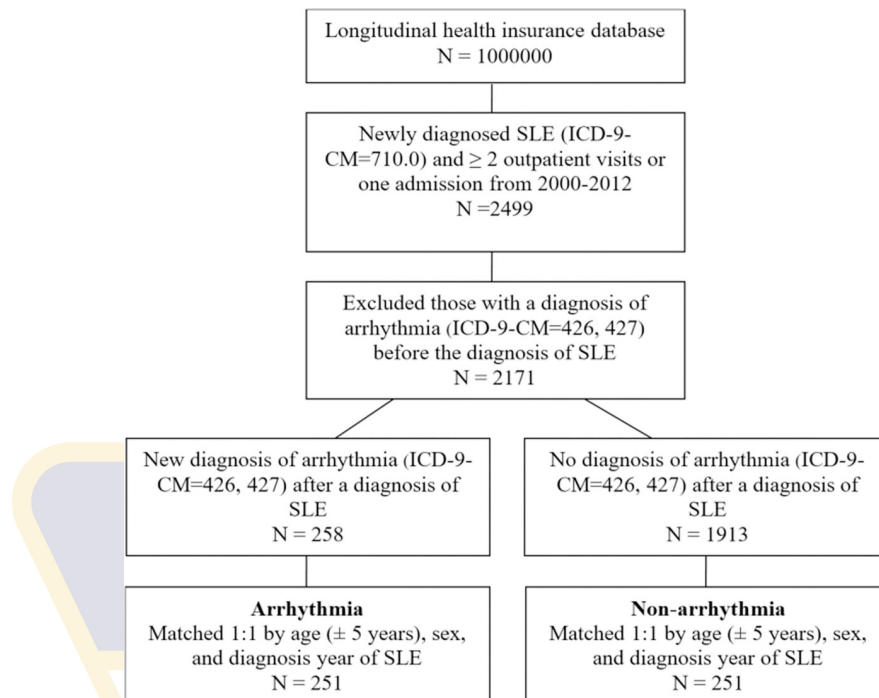
0.98–2.25, p = 0.060). The patients with underlying ischaemic heart disease had a significantly higher risk of arrhythmia (adjusted OR 4.82, 95% CI 2.16–10.74, p<0.001). The patients with underlying hypertension, chronic obstructive pulmonary disease and heart failure seemed to have higher risks of arrhythmia, however the differences did not reach significance after adjusting the ORs. There were no significant associations between other comorbidities and the risk of arrhythmia.

The ORs for the relationships between arrhythmia and HCQ adherence and cumulative dose are shown in Fig 2. Compared to the non-HCQ group, the risk of arrhythmia did not increase with HCQ treatment regardless of treatment duration <180 days or ≥180 days (adjusted ORs 1.61, and 1.44; p = 0.133 and 0.122, respectively), <50% or ≥50% adherence rate (adjusted ORs 1.62 and 1.37; p = 0.084 and 0.235, respectively) or daily dose of <400 mg or ≥400 mg (adjusted ORs 1.47 and 1.53; p = 0.096 and 0.210, respectively). In Table 3, we analyzed the sub-group for patients with ischaemic heart disease which found that the arrhythmia was not increased in HCQ treatment compared with non HCQ group (adjusted OR 1.1, 95% CI 0.298–4.08, p = 0.883). The sensitivity analysis about possible life-threatening ventricular arrhythmia is shown in Fig 3. Similarly, the results showed that the risk of events was not associated with HCQ treatment (adjusted OR 1.02, 95% CI 0.19–5.41, p = 0.985).

Discussion

The main purpose of this study was to clarify the controversy concerning the safety of HCQ treatment and the risk of cardiac arrhythmia in patients with SLE. The results indicated that the SLE patients using HCQ did not have higher risks of all kinds of cardiac arrhythmias or conduction disturbance. Moreover, the risk of arrhythmia was not affected by a longer duration of HCQ treatment, higher daily dose or better drug adherence rate. To the best of our knowledge, this is the first study to use nationwide population-based data to assess the risk of

Table 1. Demographic characteristics of the SLE patients with and without arrhythmia.

	With arrhythmia (N = 251)		Without arrhythmia (N 251)		
	n	%	n	%	p-value
Age (years)					0.412
<50	118	47.0	131	52.2	
≥50	133	53.0	120	47.8	
Mean ± SD	50.4 ± 17.9		49.1 ± 17.4		0.412
Sex					1
Female	205	81.7	205	81.7	
Male	46	18.3	46	18.3	
Hypertension	87	34.7	69	27.5	0.083
Hyperlipidemia	51	20.3	40	15.9	0.203
Chronic liver disease	51	20.3	49	19.5	0.823
Chronic kidney disease	19	7.6	9	3.6	0.052
Diabetes mellitus	40	15.9	27	10.8	0.088
COPD	31	12.4	18	7.2	0.051
Ischaemic heart disease	54	21.5	19	7.6	<0.001
Heart failure	14	5.6	1	0.4	0.001
Stroke	28	11.2	18	7.2	0.122
Alcoholism	5	2.0	2	0.8	0.450†
Hydroxychloroquine	104	41.4	87	34.7	0.118
Diagnosis year of SLE					1
2000	60	23.9	60	23.9	
2001	34	13.5	34	13.5	
2002	31	12.4	31	12.4	
2003	25	10.0	25	10.0	
2004	25	10.0	25	10.0	
2005	15	6.0	15	6.0	
2006	18	7.2	18	7.2	
2007	14	5.6	14	5.6	
2008	13	5.2	13	5.2	
2009	6	2.4	6	2.4	
2010	5	2.0	5	2.0	
2011	2	0.8	2	0.8	
2012	3	1.2	3	1.2	
Study period (years)	4.6 ± 3.5		4.6 ± 3.5		0.995

COPD: chronic obstructive pulmonary disease. SLE: systemic lupus erythematosus

†Fisher's exact test.

arrhythmia and HCQ treatment in patients with SLE. In our recent cohort study, patients with RA using HCQ did not have a higher risk of cardiac arrhythmia regardless of the daily HCQ dose or follow-up duration [19], which is consistent with the current study.

Subsequently, observational and prospective studies have reported on the efficacy and safety of HCQ treatment for Covid-19. In an observational study with 1446 Covid-19 patients, Geleris et al. reported that HCQ treatment did not reduce the risk of intubation or death, but the reasons for mortality were not illustrated [20]. In their study, the HCQ group received significantly more of the macrolide antibiotic azithromycin even after propensity score matching, and multiple confounding factors such as underlying ischaemic heart disease, heart failure and

Table 2. Multivariable logistic regression analysis of factors associated with arrhythmia in the SLE patients.
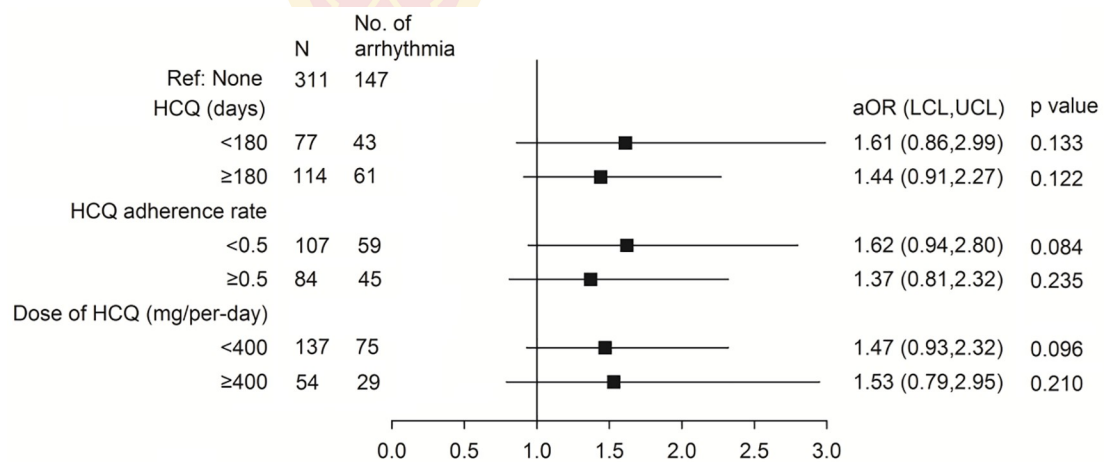
	Crude OR	95% CI	p-value	Adjusted OR[†]	95% CI	p-value
Hydroxychloroquine	1.33	0.93–1.92	0.120	1.49	0.98–2.25	0.060
Hypertension	1.58	1.01–2.48	0.046	1.07	0.63–1.83	0.797
Hyperlipidemia	1.48	0.87–2.51	0.148	1.22	0.62–2.38	0.566
Chronic liver disease	1.07	0.65–1.76	0.800	0.87	0.48–1.58	0.648
Chronic kidney disease	2.25	0.98–5.17	0.056	2.42	0.86–6.85	0.096
Diabetes mellitus	1.65	0.95–2.88	0.077	1.54	0.78–3.02	0.210
COPD	2.00	1.03–3.89	0.041	1.72	0.80–3.70	0.164
Ischaemic heart disease	5.37	2.53–11.43	<0.001	4.82	2.16–10.74	<0.001
Heart failure	14.00	1.84–106.46	0.011	6.62	0.82–53.37	0.076
Stroke	1.71	0.89–3.31	0.109	1.44	0.64–3.24	0.382
Alcoholism	2.50	0.49–12.89	0.273	4.13	0.60–28.36	0.149

COPD: chronic obstructive pulmonary disease. SLE: systemic lupus erythematosus

[†]Adjusted for hydroxychloroquine, hypertension, hyperlipidemia, chronic liver disease, chronic kidney disease, diabetes mellitus, COPD, ischemic heart disease, stroke, alcoholism, and heart failure.

https://doi.org/10.1371/journal.pone.0251918.t002

cardiac arrhythmia were not adjusted. Baseline QTc interval and heart rate were also important concerns before treatment, and cardiac death caused by new-onset arrhythmia was one of the possible reasons for negating the benefit of HCQ and azithromycin treatment. In addition, Cavalcanti et al. conducted a multicentre, open-label, randomised controlled trial with 667 patients [21], and reported that the use of HCQ in patients with mild-to-moderate Covid-19 did not improve their clinical status at 15 days. They found that prolongation of QTc interval was more frequent in the HCQ group, but that there was no increase in arrhythmia. The relatively small sample size and low event rate may have affected the outcomes of their study. In the present study, we found no correlation between cardiac arrhythmia and the use of HCQ in SLE patients. The strength of this study lies in its large dataset of patients enrolled in the NHI system, which covers 99% of the Taiwanese population and reduces bias from selection, participation, or poor recall [22]. Prospective clinical trials with a long follow-up period are difficult

Fig 2. Dose response relationship of hydroxychloroquine for risk of arrhythmia.

https://doi.org/10.1371/journal.pone.0251918.g002

Table 3. Subgroup multivariable logistic regression analysis of risk of arrhythmia in patients with ischaemic heart disease.

	HCQ		Non-HCQ		Adjusted OR		
	N	No. of arrhythmia	N	No. of arrhythmia		95% C.I.	p-value
Ischaemic heart disease							
No[†]	172	90	257	107	1.49	0.997–2.21	0.052
Yes[‡]	19	14	54	40	1.10	0.298–4.08	0.883

HCQ: hydroxychloroquine. COPD: chronic obstructive pulmonary disease.

†Adjusted for HCQ, hypertension, hyperlipidemia, chronic liver disease, chronic kidney disease, diabetes, COPD, stroke, and heart failure.

‡Adjusted for HCQ, hypertension, hyperlipidemia, chronic liver disease, diabetes, COPD, and stroke.

https://doi.org/10.1371/journal.pone.0251918.t003

to perform quickly to answer our study hypothesis, which is important for the clinical application of HCQ.

Although the risk of TdP with baseline QTc or drug-induced prolongation of the QTc interval is not a linear relationship, it is a potentially lethal polymorphic ventricular tachycardia that can cause sudden cardiac death. Previous case reports have described associations between HCQ and QTc prolongation and ventricular arrhythmia [12, 14, 15]. However, other studies have reported no significant differences in QTc interval and heart rate between normal values and patients treated with HCQ [23]. The main cardiac arrhythmia in our study was defined as a new diagnosis of all arrhythmias including conduction disorder, sinus node dysfunction, supraventricular and ventricular tachyarrhythmias. The greatest safety concern with HCQ is due to its action on iKr channels, causing QTc prolongation which may result in life-threatening ventricular arrhythmia and TdP. The sensitivity sub-analysis of only ventricular tachyarrhythmias also disclosed consistent outcomes. Our data showed that the administration of HCQ had a neutral effect on the development of all arrhythmias and especially ventricular tachyarrhythmias.

Regarding comorbidities, ischemic heart disease was associated with a significantly increased risk of arrhythmia, but the other comorbidities did not (Table 2). This anticipated result is likely due to acute or chronic ischaemic heart disease related to various arrhythmogenic alterations. A previous study reported that the cardiotoxicity of HCQ was possibly associated with the cumulative dose [24], and that conduction disorders including atrioventricular block, complete heart block, and bundle branch block are the main cardiac side effects [24]. The chronic use of HCQ has also been reported to provoke cardiac arrhythmia [15]. However our additional analysis disclosed HCQ did not increase arrhythmia whether in patients with ischemic heart disease or not (Table 3). Further sub-analysis did not show an increase in cardiac arrhythmia with a longer duration of HCQ use of ≥180 days, higher HCQ dose of ≥400 mg or better adherence (Fig 2). These results are also consistence with our previous report
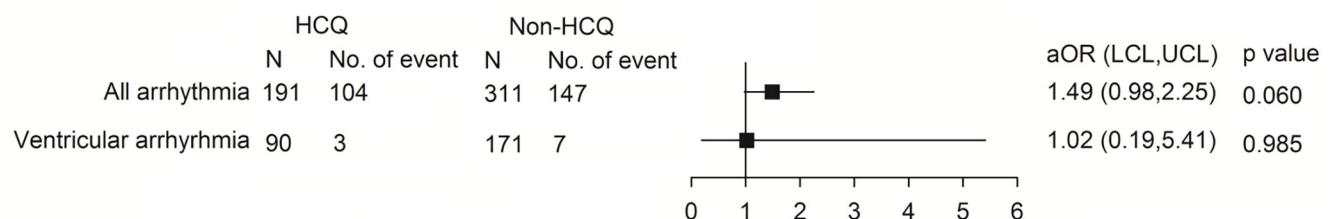
Fig 3. Sensitivity analysis of hydroxychloroquine for risk of ventricular arrhythmia and all kinds of arrhythmia.

https://doi.org/10.1371/journal.pone.0251918.g003

[19]. These data suggest the safety of HCQ regardless of the different cumulative dose and that there is no dose-dependent effect with long-term treatment for rheumatic diseases such as SLE and RA.

There are several limitations to this study. First, data on QTc interval as assessed by electro-cardiography (ECG) were not available in the LHID, although ECG is recommended to estimate the QTc interval in individuals receiving HCQ [25]. Nevertheless, we believe that our results are robust with regards to the risk of arrhythmia with HCQ therapy. Second, we did not investigate other drugs that could have prolonged QT, and this may have affected the results. Third, we did not have access to the results of serum blood tests, such as potassium, calcium, magnesium, glucose, or thyroid function, which may influence the development of arrhythmia. Fourth, our disease definition was based on codified data without any procedure codes, which may have led to over diagnosis. Therefore, we added SLE with at least two outpatient clinic visits or one admission to reduce this bias. Fifth, our study population consisted of patients with SLE, hence our results may not be totally applicable to patients who use HCQ for other diseases. Sixth, some baseline comorbidities were not balanced in the two groups. The study sample size was not large enough for further propensity score matching, as few SLE patients had arrhythmia (only 258 events of new arrhythmia in patients with underlying SLE among a population of one million). Finally, this study was hypothesis driven, so some unknown bias could exist. A larger randomised control trial is necessary to verify the outcomes of this study.

Conclusion

HCQ treatment in patients with SLE did not significantly increase all types of cardiac arrhythmias or ventricular tachyarrhythmias regardless of the higher cumulative dose. This neutral outcome may clarify the safety of HCQ regarding arrhythmias.

Acknowledgments

Author Contributions

Conceptualization: James Cheng-Chung Wei.

Data curation: Yu-Hsun Wang, Li-Ching Li, Tse-Hsien Lo.

Formal analysis: Yu-Hsun Wang.

Funding acquisition: Chun-Hung Su.

Supervision: Chin-Feng Tsai, Kuei-Chuan Chan.

Writing – original draft: Chien-Hsien Lo.

Writing – review & editing: James Cheng-Chung Wei, Chun-Hung Su.

References

1. Alarcon GS, McGwin G, Bertoli AM, Fessler BJ, Calvo-Alen J, Bastian HM, et al. Effect of hydroxychloroquine on the survival of patients with systemic lupus erythematosus: data from LUMINA, a multiethnic US cohort (LUMINA L). Ann Rheum Dis. 2007; 66:1168–72. Epub 2007/03/29. https://doi.org/10.1136/ard.2006.068676 PMID: 17389655; PubMed Central PMCID: PMC1955128.

2. Group CHS. A randomized study of the effect of withdrawing hydroxychloroquine sulfate in systemic lupus erythematosus. N Engl J Med. 1991; 324:150–4. https://doi.org/10.1056/NEJM199101173240303 PMID: 1984192

3. Rempenault C, Combe B, Barnetche T, Gaujoux-Viala C, Lukas C, Morel J, et al. Metabolic and cardio-vascular benefits of hydroxychloroquine in patients with rheumatoid arthritis: a systematic review and meta-analysis. Ann Rheum Dis. 2018; 77:98–103. Epub 2017/10/04. https://doi.org/10.1136/annrheumdis-2017-211836 PMID: 28970215.

4. Yang DH, Leong PY, Sia SK, Wang YH, Wei JC. Long-Term Hydroxychloroquine Therapy and Risk of Coronary Artery Disease in Patients with Systemic Lupus Erythematosus. J Clin Med. 2019; 8:796. Epub 2019/06/15. https://doi.org/10.3390/jcm8060796 PMID: 31195632; PubMed Central PMCID: PMC6616930.

5. Vincent MJ, Bergeron E, Benjannet S, Erickson BR, Rollin PE, Ksiazek TG, et al. Chloroquine is a potent inhibitor of SARS coronavirus infection and spread. Virol J. 2005; 2:69. Epub 2005/08/24. https://doi.org/10.1186/1743-422X-2-69 PMID: 16115318; PubMed Central PMCID: PMC1232869.

6. Picot S, Marty A, Bienvenu AL, Blumberg LH, Dupouy-Camet J, Carnevale P, et al. Coalition: Advocacy for prospective clinical trials to test the post-exposure potential of hydroxychloroquine against COVID-19. One Health. 2020; 100131. Epub 2020/04/16. https://doi.org/10.1016/j.onehlt.2020.100131 PMID: 32292817.

7. Guan WJ, Ni ZY, Hu Y, Liang WH, Ou CQ, He JX, et al. Clinical Characteristics of Coronavirus Disease 2019 in China. N Engl J Med. 2020; 382:1708–20. Epub 2020/02/29. https://doi.org/10.1056/NEJMoa2002032 PMID: 32109013; PubMed Central PMCID: PMC7092819.

8. Gautret P, Lagier JC, Parola P, Hoang VT, Meddeb L, Mailhe M, et al. Hydroxychloroquine and azithro-mycin as a treatment of COVID-19: results of an open-label non-randomized clinical trial. Int J Antimi-crob Agents. 2020:105949. Epub 2020/03/25. https://doi.org/10.1016/j.ijantimicag.2020.105949 PMID: 32205204; PubMed Central PMCID: PMC7102549.

9. Bhimraj A, Morgan R, Shumake A, Lavergne V, Baden L, Vincent CC, et al. Infectious Diseases Society of America Guidelines on the Treatment and Management of Patients with COVID-19. Clin Infect Dis. 2020; ciaa478. https://doi.org/10.1093/cid/ciaa478 PMID: 32338708

10. Capel RA, Herring N, Kalla M, Yavari A, Mirams GR, Douglas G, et al. Hydroxychloroquine reduces heart rate by modulating the hyperpolarization-activated current If: Novel electrophysiological insights and therapeutic potential. Heart Rhythm. 2015; 12:2186–94. Epub 2015/05/31. https://doi.org/10.1016/j.hrthm.2015.05.027 PMID: 26025323; PubMed Central PMCID: PMC4689153.

11. Chugh SS, Reinier K, Singh T, Uy-Evanado A, Socoteanu C, Peters D, et al. Determinants of prolonged QT interval and their contribution to sudden death risk in coronary artery disease: the Oregon Sudden Unexpected Death Study. Circulation. 2009; 119:663–70. Epub 2009/01/28. https://doi.org/10.1161/CIRCULATIONAHA.108.797035 PMID: 19171855; PubMed Central PMCID: PMC2734945.

12. Morgan ND, Patel SV, Dvorkina O. Suspected hydroxychloroquine-associated QT-interval prolongation in a patient with systemic lupus erythematosus. J Clin Rheumatol. 2013; 19:286–8. Epub 2013/07/23. https://doi.org/10.1097/RHU.0b013e31829d5e50 PMID: 23872551.

13. Simpson T, Salazar J, Vittinghoff E, Probert J, Iwahashi A, Olgin J, et al. Association of QT-Prolonging Medications With Risk of Autopsy-Defined Causes of Sudden Death. JAMA Intern Med. 2020; 180:1–9. https://doi.org/10.1001/jamainternmed.2020.0148 PMID: 32119028

14. Yanturali S, Aksay E, Demir O, R A. Massive hydroxychloroquine overdose. Acta Anaesthesiol Scand. 2004; 48:379–81. https://doi.org/10.1111/j.0001-5172.2004.0302.x PMID: 14982575

15. Chen CY, Wang FL, Lin CC. Chronic hydroxychloroquine use associated with QT prolongation and refractory ventricular arrhythmia. Clin Toxicol (Phila). 2006; 44:173–5. Epub 2006/04/18. https://doi.org/10.1080/15563650500514558 PMID: 16615675.

16. TM C. Taiwan's new national health insurance program: genesis and experience so far. Health Aff. 2003; 22:61–76. https://doi.org/10.1377/hlthaff.22.3.61 PMID: 12757273

17. Wu CY, Tan M, Huang JY, Chiou JY, Wei JC. Hydroxychloroquine is neutral in risk of chronic kidney disease in patients with systemic lupus erythematosus. Ann Rheum Dis. 2020. Epub 2020/05/22. https://doi.org/10.1136/annrheumdis-2020-217728 PMID: 32434824.

18. Yang DH, Leong PY, Sia SK, Wang YH, Wei JC. Long-Term Hydroxychloroquine Therapy and Risk of Coronary Artery Disease in Patients with Systemic Lupus Erythematosus. J Clin Med. 2019; 8. Epub 2019/06/15. https://doi.org/10.3390/jcm8060796 PMID: 31195632; PubMed Central PMCID: PMC6616930.

19. Lo CH, Wang YH, Tsai CF, Chan KC, Li LC, Lo TH, et al. Correspondence on 'Festina lente: hydroxy-chloroquine, COVID-19 and the role of the rheumatologist' by Graef et al. Ann Rheum Dis. 2020. Epub 2020/08/10. https://doi.org/10.1136/annrheumdis-2020-218589 PMID: 32769154.

20. Geleris J, Sun Y, Platt J, Zucker J, Baldwin M, Hripcsak G, et al. Observational Study of Hydroxychloro-quine in Hospitalized Patients with Covid-19. N Engl J Med. 2020; 382:2411–8. Epub 2020/05/08. https://doi.org/10.1056/NEJMoa2012410 PMID: 32379955.

21. Cavalcanti AB, Zampieri FG, Rosa RG, Azevedo LCP, Veiga VC, Avezum A, et al. Hydroxychloroquine with or without Azithromycin in Mild-to-Moderate Covid-19. N Engl J Med. 2020. Epub 2020/07/25. https://doi.org/10.1056/NEJMoa2019014 PMID: 32706953; PubMed Central PMCID: PMC7397242.

22. Hsing A, Ioannidis J. Nationwide Population Science: Lessons From the Taiwan National Health Insurance Research Database. JAMA Intern Med. 2015; 175:1527–9. https://doi.org/10.1001/jamainternmed.2015.3540 PMID: 26192815

23. Costedoat-Chalumeau N, Hulot JS, Amoura Z, Leroux G, Lechat P, Funck-Brentano C, et al. Heart conduction disordersrelated to antimalarials toxicity: an analysis of electrocardiograms in 85 patients treated with hydroxychloroquine for connective tissue diseases. Rheumatology (Oxford). 2007; 46:808–10. Epub 2007/01/05. https://doi.org/10.1093/rheumatology/kel402 PMID: 17202178.

24. Chatre C, Roubille F, Vernhet H, Jorgensen C, Pers YM. Cardiac Complications Attributed to Chloroquine and Hydroxychloroquine: A Systematic Review of the Literature. Drug Saf. 2018; 41:919–31. Epub 2018/06/03. https://doi.org/10.1007/s40264-018-0689-4 PMID: 29858838.

25. Kapoor A, Pandurangi U, Arora V, Gupta A, Jaswal A, Nabar A, et al. Cardiovascular risks of hydroxychloroquine in treatment and prophylaxis of COVID-19 patients: A scientific statement from the Indian Heart Rhythm Society. Indian Pacing Electrophysiol J. 2020. Epub 2020/04/12. https://doi.org/10.1016/j.ipej.2020.04.003 PMID: 32278018; PubMed Central PMCID: PMC7141642.
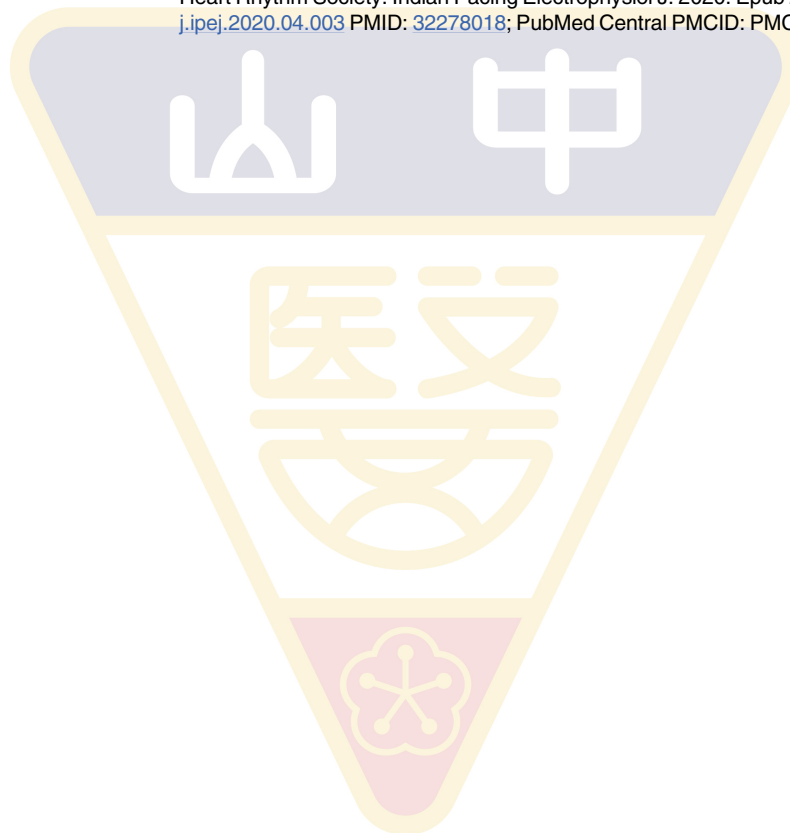
Research Paper

Oral treatment for diabetes using α-glucosidase inhibitors was a risk factor for chronic obstructive pulmonary disease: a cohort study

Sheng-Wen Wu, MD, PhD[1,2]; Yung-Chyuan Ho, PhD[3]; Ci-Wen Luo, MS[4,5]; Hung-Yi Chen, PhD[6]; Chun-Hung Su, MD, PhD[7,8,9,#]; Yu-Hsiang Kuan, PhD[4,5, #,✉]

1. Division of Nephrology, Department of Internal Medicine, Chung Shan Medical University Hospital, Taichung, Taiwan
2. The School of Medicine, Chung Shan Medical University, Taichung, Taiwan
3. School of Medical Applied Chemistry, Chung Shan Medical University, Taichung, Taiwan.
4. Department of Pharmacology, School of Medicine, Chung Shan Medical University, Taichung, Taiwan
5. Department of Pharmacy, Chung Shan Medical University Hospital, Taichung, Taiwan
6. School of Pharmacy, China Medical University, Taichung, Taiwan.
7. Department of Internal Medicine, Chung Shan Medical University Hospital, Taichung, Taiwan
8. Department of Internal Medicine, School of Medicine, Chung Shan Medical University, Taichung, Taiwan
9. Institute of Medicine, Chung Shan Medical University, Taichung, Taiwan

# The authors contributed equally to this work

✉ Corresponding author: Yu-Hsiang Kuan. Address: Department of Pharmacology, School of Medicine, Chung Shan Medical University and Chung Shan Medical University Hospital, No. 110, Sec. 1, Jianguo N. Rd., Taichung 402, Taiwan, ROC. Tel.: +886-4-24730022 Ext. 11662. Fax: +886-4-24739030. E-mail address: kuanyh@csmu.edu.tw (Yu-Hsiang Kuan)

Abstract

Objectives: Currently, diabetes mellitus (DM) and chronic obstructive pulmonary disease (COPD) have proven to be risk factors for each other. This study aimed to determine the risk relationship between COPD and five common oral medications for DM among patients with DM.

Methods: This population-based cohort study was conducted from 2008 to 2013. Patient data were retrieved from the Longitudinal Health Insurance Database (LHID) of the National Health Insurance Research Database (NHIRD). After pairing by gender, age, and index date, time-to-event analysis and multiple regression analysis were performed to determine the factors associated with COPD in patients taking oral medication for DM, including age, gender, income, and comorbidities. We identified 1,028 patients who took oral medication for DM and 1,028 controls who did not take oral medication for DM.

Results: We observed that the use of α-glucosidase inhibitors was associated with a higher risk of COPD (hazard ratio [HR]: 1.964, 95% confidence interval [CI]: 1.207–2.380). Furthermore, compared with the control group, α-glucosidase inhibitor users had a higher risk of COPD (HR: 2.295, 95% CI: 1.304–4.038), and no significant difference was observed in other oral medications for DM.

Conclusions: Based on present results, we could suggest that patients with DM who used α-glucosidase inhibitors are probably a higher risk of COPD. We recommend that in the future, treatment with α-glucosidase inhibitors upregulate the occurrence of COPD might through gastrointestinal side effects and malnutrition.

Key words: diabetes mellitus, chronic obstructive pulmonary disease, α-glucosidase inhibitor, cohort study, cox regression

Introduction

The relationship between diabetes mellitus (DM) and chronic obstructive pulmonary disease (COPD) has currently been confirmed.[1,2] The literature has also reported that the risk of death in patients with COPD and DM is higher than that in patients with general COPD.[3] Several medicines have yielded satisfactory

results in the treatment of COPD. Potassium channel modulators can effectively dilate the bronchi, reduce cough and mucus production, and inhibit tracheal inflammation[4]. A corresponding study was also conducted on oral medicines for DM. The use of metformin was not related to the deterioration of COPD, but the concentration of plasma lactic acid slightly increased in patients in a statistically significant manner.[5] Studies have also demonstrated that metformin can reduce mortality in patients with DM and in those with COPD and DM.[3]

Most reports investigated the effects of oral medicines for DM on patients with COPD. We studied the effect of oral medicines for DM on the subsequent development of COPD in patients. In the future, patients with DM should have more options and receive additional recommendations in the use of medicines. This study used the Taiwan National Health Insurance Research Database (NHIRD) to determine the relationship between oral medicines for DM and the development of COPD in patients after a series of adjustments.

Methods

Data source

The NHIRD is a claims database covering 98% of the population in Taiwan. The data are derived from the National Health Insurance programme implemented by the National Health Research Institutes. The Taiwan Longitudinal Health Insurance Database 2010 (LHID 2010) consists of a sample of 1 million claims randomly drawn from the NHIRD. No significant difference was observed in the statistical age, gender, annual births, and average insured amount. The strength of this database for research purposes hinges on its large sample size and vertical nature.[6] It provides information on patient characteristics, medical service, hospital drug compensation, general practice, community pharmacy, and International Classification of Diseases, Ninth Revision, Clinical Modification (ICD-9-CM) diagnostic codes. All NHIRD applicants must be researchers or clinicians in universities, research institutions, or hospitals. The data form NHIRD must be used for research purposes only. All applications should be reviewed by peer experts to ensure the rationality of the research. Ethical approval for this research was obtained from the institutional review board (IRB) of Chung Shan Medical University (CS2-15106).

Participants

Patients with DM were identified according to the ICD-9-CM code 250, A181. The identification of patients with COPD was conducted using ICD-9-CM codes 490.xx–496.xx. A patient with DM or COPD with at least one hospital admission or three or more outpatient claims was considered to be newly diagnosed as having DM or COPD. The index date was the date of DM diagnosis between 2008 and 2013, and the end point was the date of COPD diagnosis. Exclusion criteria were as follows: (1) missing data including gender and residential area, (2) patients younger than 20, (3) end point before the index date, (4) patients diagnosed as having DM or COPD before 2008, (5) and less than 90 days between the index date and the end point. The patients who used oral medication were defined as cases. We randomly selected individuals not using oral medicine, and we gender-matched, age-matched, and index date-matched them with the patients from the case group to form the control group. There were 1,028 and 1,028 controls.

Oral medicines for DM

Based on the Anatomical Therapeutic Chemical classification system, we divided patients between biguanides, α-glucosidase inhibitors, sulphonylureas, meglitinides, thiazolidinediones (TZDs), and no oral medicine use for DM. We excluded patients who used more than one medication or were treated with insulin during the follow-up period. Patients having taken medicine for at least a month were included in the study.

Comorbidity

COPD-related comorbidity[7] included hypertension (ICD-9-CM code: 401.xx, 402.xx, 403.xx, 404.xx, 405.xx), hyperlipidemia (ICD-9-CM code: 272.xx), cerebrovascular disease (CVD; ICD-9-CM code: 430.xx, 431.xx, 432.xx, 433.xx, 434.xx, 435.xx, 436.xx, 437.xx, 438.xx), anxiety (ICD-9-CM code: 300.0), substance abuse (ICD-9-CM code: 304.xx, 305.xx), congestive heart failure (ICD-9-CM code: 428.xx), peripheral vascular disease (ICD-9-CM code: 443.9), depression (ICD-9-CM code: 311.xx), gastro-esophageal refluxdisease (GERD; ICD-9-CM code: 530.81).

Statistical analysis

The chi-square test was used to analyse the category variables between the case and control groups. A two-tailed test was used to compare the continuous variables. Univariate and multivariate stratified Cox regression models were subsequently used to calculate the hazard ratio (HR) and 95% CI. Multivariable models were adjusted for COPD-related comorbidities, gender, age, low income, and urbanisation level.[8] A further analysis of the risk relationship between users of oral medicine for DM and their controls was conducted. Statistical

analyses were performed using the SAS 9.3 software package, and P < 0.05 was considered statistically significant.

Results

From 1 January 2008 to 31 December 2013, a total of 1,028 oral medicine users were compared with 1,028 controls. The descriptive demographic data namely age, gender, income, urbanization level, and comorbidities are presented in Table 1. Patients taking oral medicine were compared with their controls. No difference existed in age and gender. Patients were mostly male (55.88%) and 57 years old on average. There were more patients with a low income in the case group (50.58%) and more patients with a non–low income in the control group (50.88%). No difference was observed between the case and control groups. The patients generally lived in moderately urbanized areas (cases: 29.67%, controls: 30.64%).

Table 2 presents the Cox regression analysis of risk factors associated with COPD development. The HR of α-glucosidase inhibitor users was 1.697 (95% CI: 1.208–2.383) and was statistically significant (P = 0.0023). Low income was also a risk factor for COPD (HR: 1.143, 95% CI: 1.044–1.25, P = 0.0037). Compared with patients living in moderately urbanized areas, those living in agricultural areas had a higher risk of developing COPD (HR: 1.482, 95% CI: 1.197–1.835, P = 0.0003). Patients with hyperlipidaemia (HR: 0.808, 95% CI: 0.738–0.884, P < 0.0001) and cardiovascular disease (HR: 0.874, 95% CI: 0.771–0.991, P = 0.0352) had a lower risk of COPD development.

For further analysis, we compared the case group to the control group. Table 3 indicates that, apart from the α-glucosidase inhibitor users (crude HR: 1.718, 95% CI: 1.052–2.807; adjusted HR: 2.295, 95% CI: 1.304–4.038), no statistically significant differences were observed among the users of other medicines. A Kaplan–Meier curve was also used for analysis (Fig. 2). Only α-glucosidase inhibitor users had a significantly higher incidence of COPD than did the controls (log-rank test, P = 0.025).
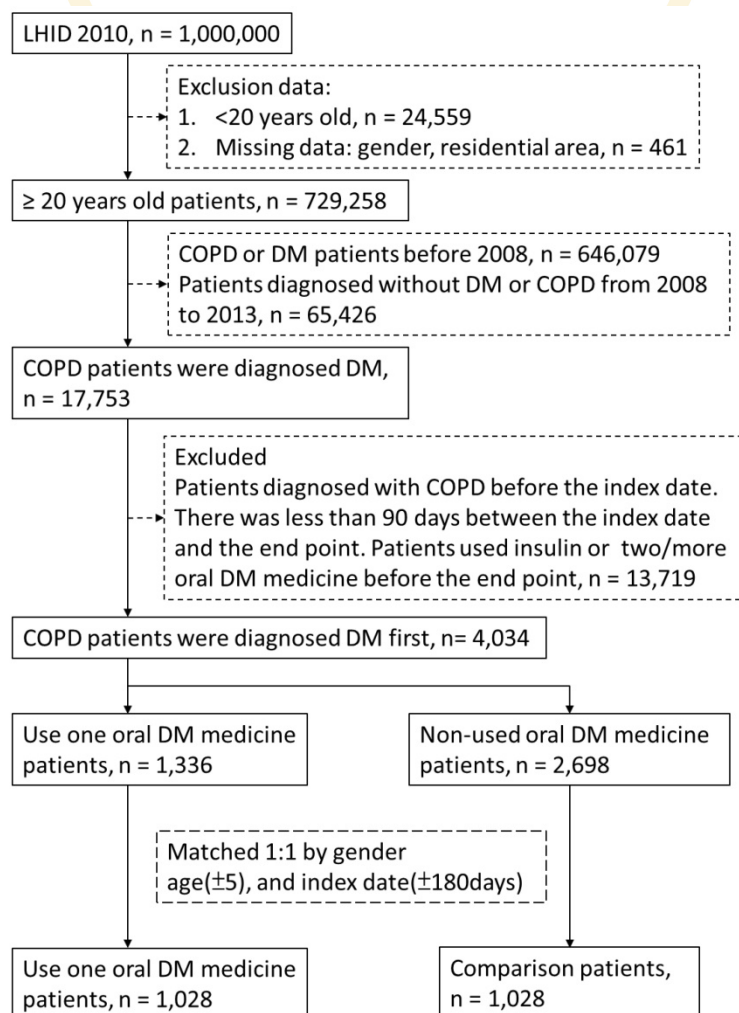
Figure 1. Flow-chart of participant selection.

Table 1. Basic characteristics of the study participants from 2008 to 2013.

	Oral medicine (n = 1,028)	Comparison (n = 1,028)	P
Gender			
female	505 (49.12%)	505 (49.12%)	1.0000
male	523 (50.88%)	523 (50.88%)	
Age in 2008 (Mean ± SD)	57.14±13.64	57.23±13.79	0.8773
Low-income			
Yes	505 (49.12%)	520 (50.58%)	0.5082
No	523 (50.88%)	508 (49.42%)	
Urbanization level			
Highly urbanization	303 (29.47%)	252 (24.51%)	0.0741
Moderate urbanization	315 (30.64%)	305 (29.67%)	
Emerging town	156 (15.18%)	167 (16.25%)	
General town	146 (14.2%)	159 (15.47%)	
Aged Township	20 (1.95%)	27 (2.63%)	
Agricultural town	42 (4.09%)	61 (5.93%)	
Remote township	46 (4.47%)	57 (5.54%)	
Comorbidity			
Hypertension	569 (55.35%)	693 (67.41%)	<.0001
Hyperlipidemia	514 (50%)	594 (57.78%)	0.0004
Osteoarthritis	410 (39.88%)	351 (34.14%)	0.0070
Cardiovascular disease	160 (15.56%)	195 (18.97%)	0.0411
Anxiety	340 (33.07%)	294 (28.6%)	0.0280
Substance abuse	32 (3.11%)	30 (2.92%)	0.7965
Congestive heart failure	54 (5.25%)	64 (6.23%)	0.3430
Peripheral vascular disease	30 (2.92%)	40 (3.89%)	0.2239
Depression	31 (3.02%)	27 (2.63%)	0.5942
GERD	28 (2.72%)	17 (1.65%)	0.0973

Abbreviation: SD, standard deviation.

Table 2. Hazards ratios of COPD with diabetes and compare with oral treatment medicine.

	Adjusted HR 95%CI	P-value
Diabetes medicine (reference: no used)		
Biguanides (n = 761)	1.089 (0.990-1.198)	0.0812
α-glucosidase inhibitor (n = 35)	1.694 (1.207-2.380)	0.0023
Sulfonylureas (n = 191)	1.080 (0.922-1.264)	0.3409
Meglitinides (n = 34)	1.054 (0.746-1.488)	0.7656
Thiazolidinediones (n = 7)	1.233 (0.584-2.604)	0.5828
Gender (reference: female)		
Male	1.015 (0.926-1.113)	0.7444
Age (reference: general population)		
Age	0.999 (0.995-1.003)	0.6085
Low income (reference: no)		
Yes	1.143 (1.044-1.250)	0.0036
Urbanization level (reference: moderate urbanization)		
Highly urbanization	1.085 (0.967-1.218)	0.1650
Emerging town	1.078 (0.941-1.236)	0.2764
General town	1.080 (0.940-1.241)	0.2755
Aged Township	0.972 (0.719-1.314)	0.8529
Agricultural town	1.482 (1.197-1.835)	0.0003
Remote township	1.041 (0.841-1.288)	0.7138
Comorbidity (reference: without)		
Hypertension	1.027 (0.929-1.135)	0.6052
Hyperlipidemia	0.808 (0.738-0.884)	<.0001
Osteoarthritis	0.926 (0.839-1.023)	0.1309
Cardiovascular disease	0.874 (0.771-0.991)	0.0352
Anxiety	0.954 (0.864-1.053)	0.3501
Substance abuse	0.930 (0.716-1.209)	0.5881
Congestive heart failure	0.977 (0.806-1.184)	0.8122
Peripheral vascular disease	0.900 (0.706-1.146)	0.3910
Depression	0.964 (0.737-1.261)	0.7916
GERD	1.097 (0.812-1.482)	0.5465

Abbreviation: CI, confidence interval.
Adjusted with gender, age, low income, urbanization level, comorbidity.

Figure 2. Kaplan–Meier curves estimating cumulative incidence of COPD patients between oral treatment medicine users and control cohorts.

Table 3. Oral treatment medicine subgroups of hazards ratios of COPD with diabetes.

	Event	Observed	Incidence Density	Crude		Adjusted	
		Person-months	(Per 1000 person-month)	HR 95%CI	*p*-value	HR 95%CI	*p*-value
Biguanides medicine							
Biguanides	761	16589	45.87	1.054 (0.953-1.166)	0.3056	1.063 (0.960-1.719)	0.2411
Comparison	761	17512	43.46	Reference		Reference	
α-glucosidase inhibitor medicine							
α-glucosidase inhibitors	35	546	64.10	1.718 (1.052-2.807)	0.0307	2.295 (1.304-4.038)	0.0040
Comparison	35	837	41.82	Reference		Reference	
Sulfonylureas medicine							
Sulfonylureas	191	4796	39.82	1.127 (0.921-1.379)	0.2471	1.172 (0.946-1.451)	0.1466
Comparison	191	4074	46.88	Reference		Reference	
Meglitinides medicine							
Meglitinides	34	710	47.89	1.112 (0.688-1.798)	0.6641	0.959 (0.538-1.711)	0.9590
Comparison	34	808	42.08	Reference		Reference	
Thiazolidinediones medicine							
Thiazolidinediones	7	159	44.03	0.948 (0.314-2.862)	0.9242	-	0.9993
Comparison	7	157	44.59	Reference		Reference	

Abbreviation: CI, confidence interval.

Adjusted with gender, age, low income, urbanization level, comorbidity.

Discussion

In this study, patients with DM using α-glucosidase inhibitors had a higher risk of developing COPD than those using other oral medicines. Sulphonylureas bind to and shut down the ATP-sensitive potassium channel on the cell membrane of the pancreatic beta cell, and they prevent the potassium from depolarising by blocking it.[9] In turn, the fusion of insulin particles with the cell membrane increases, and so does the secretion of mature insulin. The potassium channel has been proven to effectively alleviate the symptoms of COPD, such as decreased airway hyper responsiveness, bronchiectasis, decreased cough, and decreased mucus production as well as inhibition of airway inflammation and remodeling.[10] Therefore, closing the potassium channel may cause COPD to worsen. One of the sulphonylureas, glyburide, which binds to (+)-[³H] isradipine, causes pathological changes in the cardiopulmonary structure and function of rats with monocrotaline-induced pulmonary hypertension. This evidence suggests that sulphonylureas had a tendency to aggravate lung injury and related diseases such as COPD. Our results reveal that sulphonylureas were trending towards the development of COPD, but the statistics were nonsignificant. The mechanism of action of meglitinide was the same as that of sulphonylureas, that is, shutting down the ATP-dependent potassium channel.[11] In contrast to sulphonylureas, meglitinide has a fast onset and a short duration of action. Compared with those caused by sulphonylureas, the side effects of hypoglycaemia and weight gain caused by meglitinide are relatively mild.[12] This may also affect patients with COPD because of the inhibition of the potassium channels. Our results indicated that patients who used meglitinide did not face a risk of COPD; instead they exhibited a decreasing trend compared with their matched group. Studies have demonstrated that for patients with DM, repaglinide can replace meglitinide and treat early cystic fibrosis-related diseases.[13] Therefore, it may also be useful in the treatment of COPD. However, the detailed pathological relationship requires clarification.

One of the biguanides, metformin appears to be irrelevant for the treatment of COPD, regardless of whether the patient has diabetes.[14,15] However, studies have demonstrated that metformin can effectively inhibit the mortality of patients with COPD and the development of COPD.[16, 17] Therefore, whether biguanides inhibit the development of COPD remains to be discussed. In our results, there was no significant difference in the risk of COPD between biguanides cases and controls. Patients with COPD and DM who were exposed to TZDs had a small but significant risk of acute exacerbations of COPD.[18] TZDs exert antidiabetic effects by activating the mechanism of the γ isoform of the peroxisome proliferator-activated receptor (PPARγ) (nuclear receptor) and expression of PPARγ in alveolar macrophages, an in vitro alveolar macrophage model and in vivo associated with COPD Animal model studies have displayed the potential to fight inflammation.[19] However, studies have also indicated that the long-term use of TZDs in patients with type 2 diabetes causes pneumonia or lower respiratory tract infections as well as severe pneumonia or lower respiratory tract infections. The risk is increased.[20] TZDs also increases the risk of heart failure (HF)[21] and HF is often highly correlated with COPD.[22] In our results, TZDs were not associated with COPD in patients with DM.

The results indicated that patients with DM who used α-glucosidase inhibitors are probably a higher risk of COPD. α-Glucosidase inhibitors, the pseudo-carbohydrates, competitively inhibit activity

of α-glucosidases which hydrolyze non-absorbable oligosaccharides and polysaccharides into absorbable monosaccharides in the brush border of enterocytes.[23] α-Glucosidase inhibitors delay carbohydrate digestion and prolong the carbohydrate digestion duration, thus reducing monosaccharides absorption rates.[24,25] Therefore, patients taken with α-glucosidase inhibitors may have the potential to develop into malnutrition. Addition, α-glucosidase inhibitors cause the gastrointestinal side effects, such as bloating, nausea, diarrhea, and flatulence.[24] Malnutrition in COPD is described by variable prevalence rates ranging between 30-60%.[26] Malnutrition and poor nutrition play as the risk factor for patients with COPD. Compared with healthy individuals, patients with COPD had significantly higher rates of 0–3 hours of urinary lactulose to rhamnose and sucralose to erythritol and 5–24 hours of urinary galactooligosaccharide to erythritol.[25] These findings indicated that intestinal permeability would be significant reduction in carbohydrate metabolism in the patients with COPD[25] The patients with COPD also suffered by lower gastrointestinal symptoms, including constipation and bloating. The study suggests improving the management of gastrointestinal symptoms and maintaining a clear bowel to improve the condition of patients with COPD.[24] Based on these findings, the gastrointestinal side effects and malnutrition caused by α-glucosidase inhibitors may be one of the main reasons for the development of COPD, and further experiments need to be clarified. We recommend that patients with DM use α-glucosidase inhibitors in combination with other medicines to alleviate the gastrointestinal side effects and malnutrition.

In the analysis of multiple population studies, poor education systems, low-income families, and low composite socioeconomic status (SES) indices were associated with individuals with COPD whose annual income is below the minimum wage in the United States.[27] It have a much greater impact on smoking-related diseases, which is the same as ours.[28] In Poland, 8.5% of men and 4.9% of women have symptoms of chronic airflow obstruction. Livestock farmers have an increased risk of chronic bronchitis, COPD, and reduced forced expiratory volume in 1 second (FEV1).[29] Exposure to mineral dust by working in the soil has also been suggested to result in COPD.[30] This was also confirmed in our results. Interestingly, among the patients in the case group, those with DM with high blood lipids or cardiovascular disease had a lower risk of COPD. Studies have demonstrated that patients with hyperlipidaemia and COPD experience lung hyperinflation and airway obstruction less often than patients without hyperlipidaemia, but the effects of the drug need to be clarified.[29] In fact, α-glucosidase inhibitors can effectively reduce triglycerides and increase HDL; they can also inhibit the risk of cardiovascular disease[32] Moreover, biguanides and TZDs effectively reduce the risk of cardiovascular disease.[33,34] But, the risk of heart failure is increased by TZDs.[21] However, the relationship between the risk of cardiovascular disease and anti-diabetic agents including sulphonylureas and meglitinides are not clear.[35] At present, we also found that there are more patients using biguanides due to the lower risk of cardiovascular disease. Therefore, we further compared various drug users with their controls, but the results were similar.

There are several limitations to this study. We did not have a clear understanding of the lives or exercise habits of patients, for example, their cigarette smoking habit. We also could not accurately obtain the actual values of blood sugar levels, FVC, and FEV1 in patients with diabetes. Although we did not directly track the severity of diabetes and COPD from NHIRD could not directly track patients, adjusted these comorbidities of COPD for indirectly explain the severity. These comorbidities present high-risk factors for COPD. Despite the large sample size, the number of participants for whom a comparison between several medicines could be made remained limited after strict screening and matching. Especially for patients with DM who used TZDs, the result was unexpected. For other users of oral medicine for DM, we believe that there is credible by adjustment and matching.

Conclusion

In summary, we suggest that patients with DM who administration of the α-glucosidase inhibitors are probably a higher risk of COPD. Although α-glucosidase inhibitors have a satisfactory inhibitory effect on blood lipids and cardiovascular diseases. However, the gastrointestinal side effects and malnutrition of the α-glucosidase inhibitors probably results in higher incidence of COPD occur in the patients with DM. In future medications, the side effects of α-glucosidase inhibitors should be alleviated and the occurrence of COPD reduced.

Competing Interests

The authors have declared that no competing interest exists.

References

1. Rogliani P, Calzetta L, Segreti A, Barrile A, Cazzola M. Diabetes mellitus among outpatients with COPD attending a university hospital. Acta Diabetol. 2014; 51: 933-940.

2. Ho TW, Huang CT, Ruan SY, Tsai YJ, Lai F, Yu CJ. Diabetes mellitus in patients with chronic obstructive pulmonary disease-The impact on mortality. PLoS One. 2017; 12: e0175794.

3. Yen FS, Chen W, Wei JC, Hsu CC, Hwu CM. Effects of metformin use on total mortality in patients with type 2 diabetes and chronic obstructive pulmonary disease: A matched-subject design. PLoS One. 2018; 13: e0204859.

4. Malerba M, Radaeli A, Mancuso S, Polosa R. The potential therapeutic role of potassium channel modulators in asthma and chronic obstructive pulmonary disease. J Biol Regul Homeost Agents. 2010; 24: 123-130.

5. Hitchings AW, Archer JRH, Srivastava SA, Baker EH. Safety of Metformin in Patients with Chronic Obstructive Pulmonary Disease and Type 2 Diabetes Mellitus. COPD. 2015; 12: 126-131.

6. Hsing AW, John P, Ioannidins A. National population science lessons from Taiwan national health insurance research database. JAMA Internal Med. 2015; 175: 1527-1529.

7. Divo MJ, Casanova C, Marin JM, Pinto-Plata VM, de-Torres JP, Zulueta JJ, et al. COPD comorbidities network. Eur Respir J .2015; 46: 640-50.

8. Liu CY, Hung YT, Chuang YL, Chen YJ, Weng WS, Liu JS. Incorporating development stratification of Taiwan townships into sampling design of large scale health interview survey. J Health Manage. 2006; 4: 1-22.

9. Pelaia G, Gallelli L, Vatrella A, Grembiale RD, Maselli R, De Sarro GB, et al. Potential role of potassium channel openers in the treatment of asthma and chronic obstructive pulmonary disease. Life Sci. 2002; 70: 977-990.

10. Malerba M, Radaeli A, Mancuso S, Polosa R. The potential therapeutic role of potassium channel modulators in Asthma and chronic obstructive pulmonary disease. J Biol Regul Homeost Agents. 2010; 24: 123-130.

11. Blicklé JF. Meglitinide analogues: a review of clinical data focused on recent trials. Diabetes Metab. 2006; 32: 113-120.

12. Guardado-Mendoza R, Prioletta A, Jiménez-Ceja LM, Sosale A, Folli F. The role of nateglinide and repaglinide, derivatives of meglitinide, in the treatment of type 2 diabetes mellitus. Arch Med Sci. 2013; 9: 936-943.

13. Ballmann M, Hubert D, Assael BM, Staab D, Hebestreit A, Naehrlich L, et al. Repaglinide versus insulin for newly diagnosed diabetes in patients with cystic fibrosis: a multicentre, open-label, randomised trial. Lancet Diabetes Endocrinol. 2018; 6: 114-121.

14. Hitchings AW, Archer JR, Srivastava SA, Baker EH. Safety of Metformin in Patients with Chronic Obstructive Pulmonary Disease and Type 2 Diabetes Mellitus. COPD. 2015; 12: 126-131.

15. Hitchings AW, Lai D, Jones PW, Baker EH, Metformin in COPD Trial Team. Metformin in COPD Trial Team. Metformin in severe exacerbations Of chronic obstructive pulmonary disease: a randomised controlled trial. Thorax. 2016; 71: 587-593.

16. Yen FS, Chen W, Wei JC, Hsu CC, Hwu CM. Effects of metformin use on total mortality in patients with type 2 diabetes and chronic obstructive pulmonary disease: A matched-subject design. PLoS One. 2018; 13: e0204859.

17. Tseng CH. Metformin and risk of chronic obstructive pulmonary disease in diabetes patients. Diabetes Metab. 2019; 45: 184-190.

18. Rinne ST, Liu CF, Feemster LC, Collins BF, Bryson CL, O'Riordan TG, et al. Thiazolidinediones are associated with a reduced risk of COPD exacerbations. Int J Chron Obstruct Pulmon Dis. 2015; 10: 1591-1597.

19. Lea S, Plumb J, Metcalfe H, Spicer D, Woodman P, Fox JC, et al. The effect of peroxisome proliferator-activated receptor-γ ligands on in vitro and in vivo models of COPD. Eur Respir J. 2014; 43: 409-420.

20. Singh S, Loke YK, Furberg CD. Long-term use of thiazolidinediones and the associated risk of pneumonia or lower respiratory tract infection: systematic review and meta-analysis. Thorax. 2011; 66: 383-388.

21. Hernandez AV, Usmani A, Rajamanickam A, Moheet A. Thiazolidinediones and risk of heart failure in patients with or at high risk of type 2 diabetes mellitus: a meta-analysis and meta-regression analysis of placebo-controlled randomized clinical trials. Am J Cardiovasc Drugs. 2011; 11: 115-128.

22. de Miguel Díez J, Chancafe Morgan J, Jiménez García R. The association between COPD and heart failure risk: a review. Int J Chron Obstruct Pulmon Dis. 2013; 8: 305-312.

23. Derosacor G, Maffioli P. α-Glucosidase Inhibitors and Their Use in Clinical Practice. Arch Med Sci. 2012 ; 8: 899-906.

24. Sun Y, Zheng F, Li Y, Wu R, Liu Y, Liu M, et al. Correlation between lower gastrointestinal tract symptoms and quality of life in patients with stable chronic obstructive pulmonary disease. J Tradit Chin Med. 2013; 33: 608-614.

25. Rutten EPA, Lenaerts K, Buurman WA, Wouters EFM. Disturbed Intestinal Integrity in Patients With COPD: Effects of Activities of Daily Living. Chest. 2014; 145: 245-252.

26. Hancu A. Nutritional Status as a Risk Factor in COPD. Maedica (Buchar). 2019 Jun;14: 140-143.

27. Grigsby M, Siddharthan T, Chowdhury MA, Siddiquee A, Rubinstein A, Sobrino E, et al. Socioeconomic status and COPD among low- and middle-income countries. Int J Chron Obstruct Pulmon Dis. 2016; 11: 2497-2507.

28. Lowe KE, Make BJ, Crapo JD, Kinney GL, Hokanson JE, Kim V, et al. Association of low income with pulmonary disease progression in smokers with and without chronic obstructive pulmonary disease. ERJ Open Res. 2018; 4.

29. Szczyrek M, Krawczyk P, Milanowski J, Jastrzębska I, Zwolak A, Daniluk J, et al. Chronic obstructive pulmonary disease in farmers and agricultural workers - an overview. Ann Agric Environ Med. 2011; 18: 310-313.

30. Weinhold B. Occupational Health: Agriculture–COPD Link Bolstered. Environ Health Perspect. 2007; 115: A444.

31. Kahnert K, Lucke T, Huber RM, Behr J, Biertz F, Vogt A, et al. Relationship of hyperlipidemia to comorbidities and lung function in COPD: Results of the COSYCONET cohort. PLoS One. 2017; 12: e0177501.

32. Standl E, Theodorakis MJ, Erbach M, Schnell O, Tuomilehto J. On the potential of acarbose to reduce cardiovascular disease. Cardiovasc Diabetol. 2014; 13: 81.

33. Lamanna C, Monami M, Marchionni N, Mannucci E. Effect of metformin on cardiovascular events and mortality: a meta-analysis of randomized clinical trials. Diabetes Obes Metab. 2011;13:221–228.

34. Wilcox R, Bousser MG, Betteridge DJ, Schernthaner G, Pirags V, Kupfer S, et al. Effects of pioglitazone in patients with type 2 diabetes with or without previous stroke: results from proactive (prospective pioglitazone clinical trial In macrovascular events 04) Stroke. 2007; 38: 865–873.

35. James Xu, Rohan Rajaratnam. Cardiovascular safety of non-insulin pharmacotherapy for type 2 diabetes. Cardiovasc Diabetol. 2017; 16: 18.

Classification of Photoplethysmographic Signal Quality with Deep Convolution Neural Networks for Accurate Measurement of Cardiac Stroke Volume

Shing-Hong Liu [1] [ORCID]**, Ren-Xuan Li** [1]**, Jia-Jung Wang** [2,*]**, Wenxi Chen** [3] **and Chun-Hung Su** [4,5,*]

[1]   Department of Computer Science and Information Engineering, Chaoyang University of Technology, Taichung City 41349, Taiwan; shliu@cyut.edu.tw (S.-H.L.); s10830624@gm.cyut.edu.tw (R.-X.L.)
[2]   Department of Biomedical Engineering, I-Shou University, Kaohsiung City 82445, Taiwan
[3]   Biomedical Information Engineering Laboratory, The University of Aizu, Aizu-Wakamatsu City, Fukushima 965-8580, Japan; wenxi@u-aizu.ac.jp
[4]   Institute of Medicine, School of Medicine, Chung-Shan Medical University, Taichung 402, Taiwan
[5]   Department of Internal Medicine, Chung-Shan Medical University Hospital, Taichung 402, Taiwan
*   Correspondence: wangjj@isu.edu.tw (J.-J.W.); such197408@gmail.com (C.-H.S.);
    Tel.: +886-7-6151-100-7464 (J.-J.W.); +886-4-247-39595 (ext. 34711) (C.-H.S.)

check for updates

Abstract: As photoplethysmographic (PPG) signals are comprised of numerous pieces of important physiological information, they have been widely employed to measure many physiological parameters. However, only a high-quality PPG signal can provide a reliable physiological assessment. Unfortunately, PPG signals are easily corrupted by motion artifacts and baseline drift during recording. Although several rule-based algorithms have been developed for evaluating the quality of PPG signals, few artificial intelligence-based algorithms have been presented. Thus, this study aims to classify the quality of PPG signals by using two two-dimensional deep convolution neural networks (DCNN) when the PPG pulse is used to measure cardiac stroke volume (SV) by impedance cardiography. An image derived from a PPG pulse and its differential pulse is used as the input to the two DCNN models. To quantify the quality of individual PPG pulses, the error percentage of the beat-to-beat SV measured by our device and medis® CS 2000 synchronously is used to determine whether the pulse quality is high, middle, or low. Fourteen subjects were recruited, and a total of 3135 PPG pulses (1342 high quality, 73 middle quality, and 1720 low quality) were obtained. We used a traditional DCNN, VGG-19, and a residual DCNN, ResNet-50, to determine the quality levels of the PPG pulses. Their results were all better than the previous rule-based methods. The accuracies of VGG-19 and ResNet-50 were 0.895 and 0.925, respectively. Thus, the proposed DCNN may be applied for the classification of PPG quality and be helpful for improving the SV measurement in impedance cardiography.

Keywords: photoplethysmography (PPG); deep convolution neural network (DCNN); signal quality index (SQI); impedance cardiography (ICG); stroke volume (SV)

1. Introduction

The photoplethysmographic (PPG) signal has been widely used to measure many physiological parameters, such as pulse rate [1], blood oxygen saturation [2], blood pressure [3], respiration rate [4], and left ventricular ejection time (LVET) [5]. The noninvasive techniques for photoplethysmography include two optical types, transmission and reflection [6], as shown in Figure 1. A light-emitting diode (LED) is often used to generate low-intensity infrared light on the skin, and a portion of the light will be absorbed mainly by both arterial and venous blood. For the reflection PPG, the nonabsorbed light

will be reflected and detected by a photo diode. The LED and photo diode are placed on the same side, as shown in Figure 1a. For the transmission PPG, the nonabsorbed light will be transmitted and detected by a photo diode. The LED and photo diode are placed on the opposite side, as shown in Figure 1b. In either the reflection or the transmission method, the PPG signal represents the changes in blood volume (Figure 1), although it cannot be used to quantify the amount of blood.
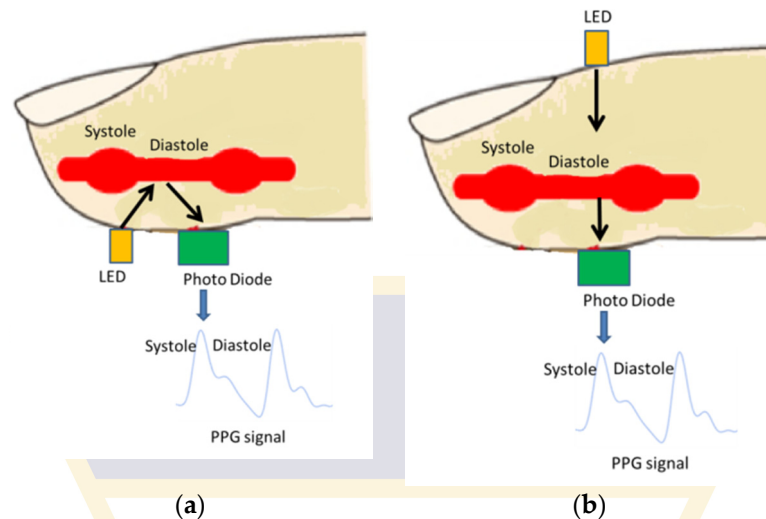

Figure 1. Schematic illustration of the photoplethysmography. The LED illuminates the skin and the nonabsorbed light will be detected by the photo diode. (**a**) For the reflected method, the LED and photo diode are on the same side. (**b**) For the transmitted method, the LED and photo diode are on the opposite side.

The PPG signal measured by the reflection method is more easily corrupted by the motion noise than the transmission method. Currently, the wearable device with the PPG sensor usually uses the reflection method to perform the physiological measurement. When the users wear these devices to do the exercise, PPG signals are very vulnerable to motion artifacts. The common solution is to improve device mechanisms to reduce the motion effect on the recoded PPG signal and to raise the measured accuracy. However, the higher the quality of the PPG signal, the better the accuracy of the measured parameters extracted from such a PPG signal. Therefore, how to classify the quality of PPG signals is an important issue for the development of wearable devices.

PPG is a noninvasive optical measurement method in which the change of blood volume interconnects the physiological responses to circulatory events in peripheral blood vessels. Thus, its waveform bears regular morphological characteristics [7,8]. As shown in Figure 2, there are a lot of physiological characteristics in a PPG pulse, including the main peak, dicrotic notch, pulse width, and amplitude, and so on. As a result, many researchers have used those significant characteristics (i.e., the rule-based methods) to determine the quality of each PPG pulse. In addition, the signal quality index (SQI) represents the corrupted degree of the PPG pulse. Liu et al. have employed fuzzy rules to determine the SQI of PPG pulses [9], and Fischer et al. have applied the characteristics of PPG waveform and the decision tree to classify its SQI [10]. Li et al. have used the Bayesian hypothesis testing method to analyze the SQI [11]. In these studies, they all needed to adjust the thresholds of the rule-base method to get the best results. Recently, Liu et al. used a fuzzy neural network to evaluate the SQI [12]. Although they used the artificial intelligence method to gauge the quality of the minorly corrupted PPG pulse, the rule-base method was also used to delete the majorly corrupted PPG pulses.

The traditional approach for the SQI assessment is to extract the features from the PPG signal. It is well known that the morphological approach is sensitive to signal noise and has many limitations on the performance robustness of the classification model [8]. Currently, deep learning techniques have been used to process feature extraction tasks by convolution computation [13]. As the

physiological signals, such as electrocardiograms (ECGs), electroencephalograms, and PPGs, belong to one-dimensional signals, several studies have used a one-dimensional deep convolution neural network (1D DCNN) to classify the different arrhythmic types and the signal quality [14–17]. Some studies have transferred the 1D signal to a two-dimensional (2D) signal by short time frequency transform [18], wavelet transform [19], and power spectral density [20]. Then, the 2D DCNN employed these images as the input to do the classifications. However, in these studies, a segment signal of about 2 to 5 s was transferred to an image. Thus, the methods only were suitable for processing consistent, continuous signals.
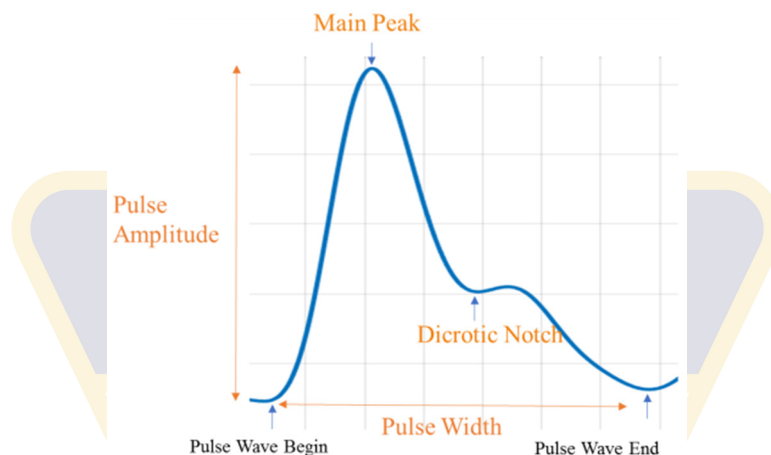
Figure 2. The characteristics of a PPG pulse chiefly include the main peak, dicrotic notch, pulse width, and pulse amplitude.

When the heart is in the systolic phase, an amount of blood, which is called the stroke volume (SV), is pumped into systematic circulation. In this period, the volume of the thoracic cavity will change. Thus, impedance cardiography (ICG) was proposed by Kubicek et al., which is a noninvasive measurement technique to measure cardiac hemodynamic parameters [21]. In the SV calculation with ICG technology, LVET is one of the most important parameters, which is measured by the ICG signal. As the signal-to-noise ratio of the ICG signal is very low, the accuracy of LVET is not high enough. Liu et al. used a reflective PPG sensor placed on the neck to measure the LVET [5]. The LVETs measured by the PPG pulses were more accurate than those by the ICG pulses. Therefore, the accuracy of SV measured by their proposed technique was higher than the traditional ICG technique.

According to previous mentions, the higher the SQI of the PPG signal, the more accurate the physiological parameters measured by the PPG signal. Unlike previous rule-based methods, our proposed approach does not require any predetermined features in the PPG signal. In this study, we used the raw morphology of PPG pulses to determine their quality levels. Thus, the aim of this study is to develop a novel SQI approach to access the quality of PPG pulses for improvement of SV measurement with a 2D DCNN. The PPG pulse and its differential pulse were segmented from the continuous PPG signal, and then they were merged into an image. Both the 2D deep residual neural network (DRNN) and 2D DCNN were used to determine the quality level of each PPG pulse. Fourteen healthy adult males participated in this experiment. The beat-to-beat SVs were measured by our ICG device [5] and medis$^{®}$ CS2000 for about three minutes, simultaneously. We utilized the error percentage of measured SVs to define the levels of SQI for each PPG pulse. The error percentage represents the accuracy of the SV measurements. The results showed that the 2D DRNN could assess the levels of SQI for the PPG pulses more easily than the rule-base method and the general DCNN.

2. Impedance Cardiography

In 1966, Kubicek et al. proposed an ICG, a noninvasive technique, to assess the continuous SV [16]. Equation (1) governs the ICG method,

$$SV = r_b \cdot \left(\frac{L}{Z_0}\right)^2 \cdot LVET \cdot dZ/dt_{(max)},$$ (1)

where r_b is the blood resistivity that is assumed to be a constant value of 150 ohm × cm, L is the distance (cm) between two recording electrodes on the neck and chest, Z_0 is the base impedance (ohm) between the recording electrodes indicating initial thoracic cavity, and dZ/dt(max) is the absolute value (ohm/sec) of the maximum change of the ICG impedance signal. According to Equation (1), the SV has an absolute linear relationship with the LVET and dZ/dt(max). Figure 3 shows the synchronous ECG, ICG, and PPG signals, and the differential ICG (DICG) and differential PPG (DPPG) signals. In this figure, the PPG signal seems to be corrupted by fewer motion artifacts than the ICG signal [5]. The LVET is defined in the DPPG signal as the time interval between the first zero crossing point and the minimum point. The LVETs of heartbeats measured by high-quality PPG pulses would become more accurate.
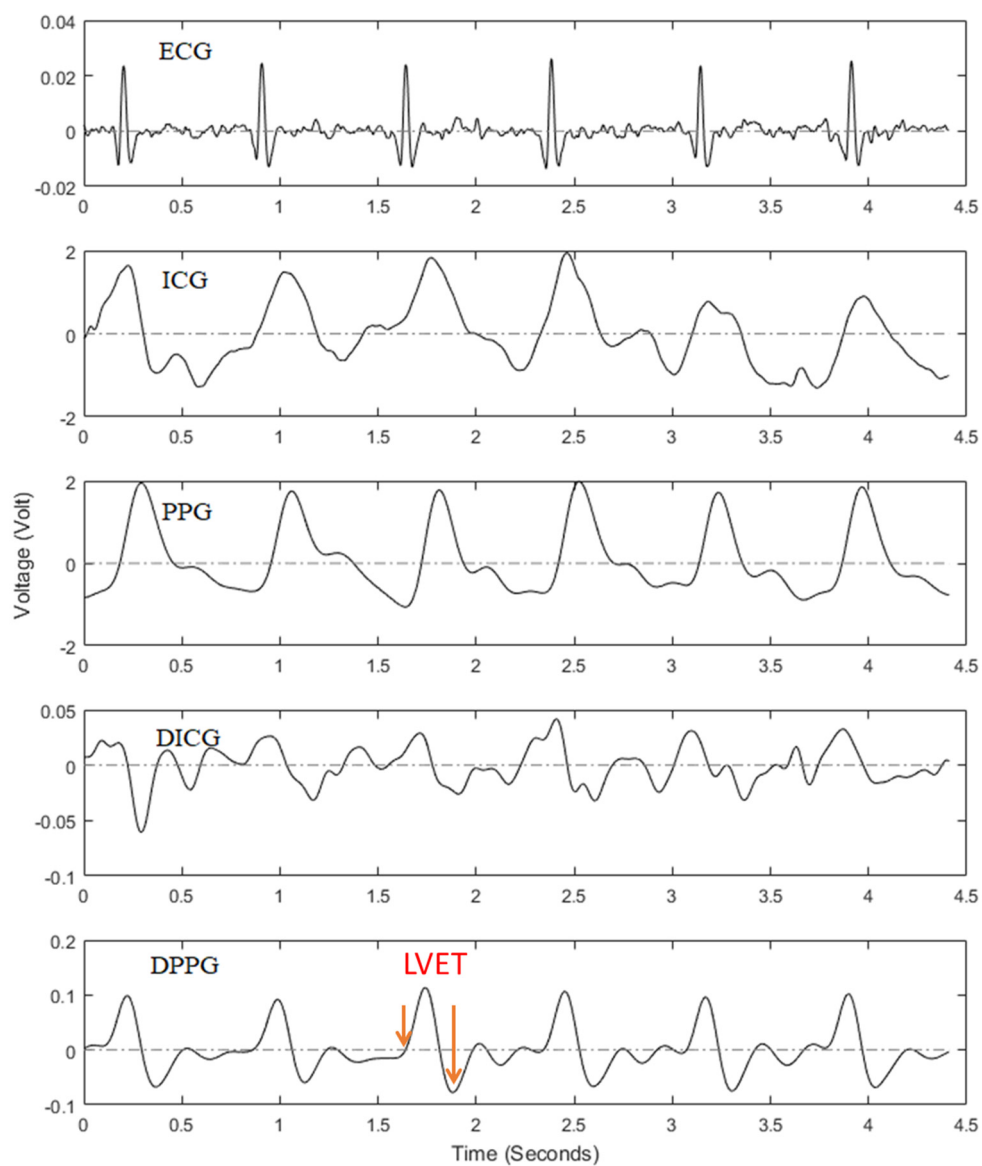
Figure 3. Typical signal registration in the study. From the first row to the fifth row are the electrocardiogram (ECG), impedance cardiography (ICG), photoplethysmography (PPG), differential ICG (DICG), and differential PPG (DPPG), respectively. The left ventricular ejection time (LVET) is defined as the time interval between the first zero crossing point (short arrow) and the minimum point (long arrow) in the DPPG signal.

3. Method

The overall procedure of the proposed SQI classification model for PPG pulses is shown in Figure 4. The original ICG and PPG signals are measured by our ICG device [5]. The input PPG and DPPG signals are segmented as the pulses by the zero-crossing points of the DPPG signal. Both the PPG and DPPG signals during one heart cycle are merged and transformed into images. These images are then used as the input to the 2D DCNN to perform the classification of the three SQI levels (high, middle, and low), which are defined by the error percentage of the measured SV as compared with the reference.
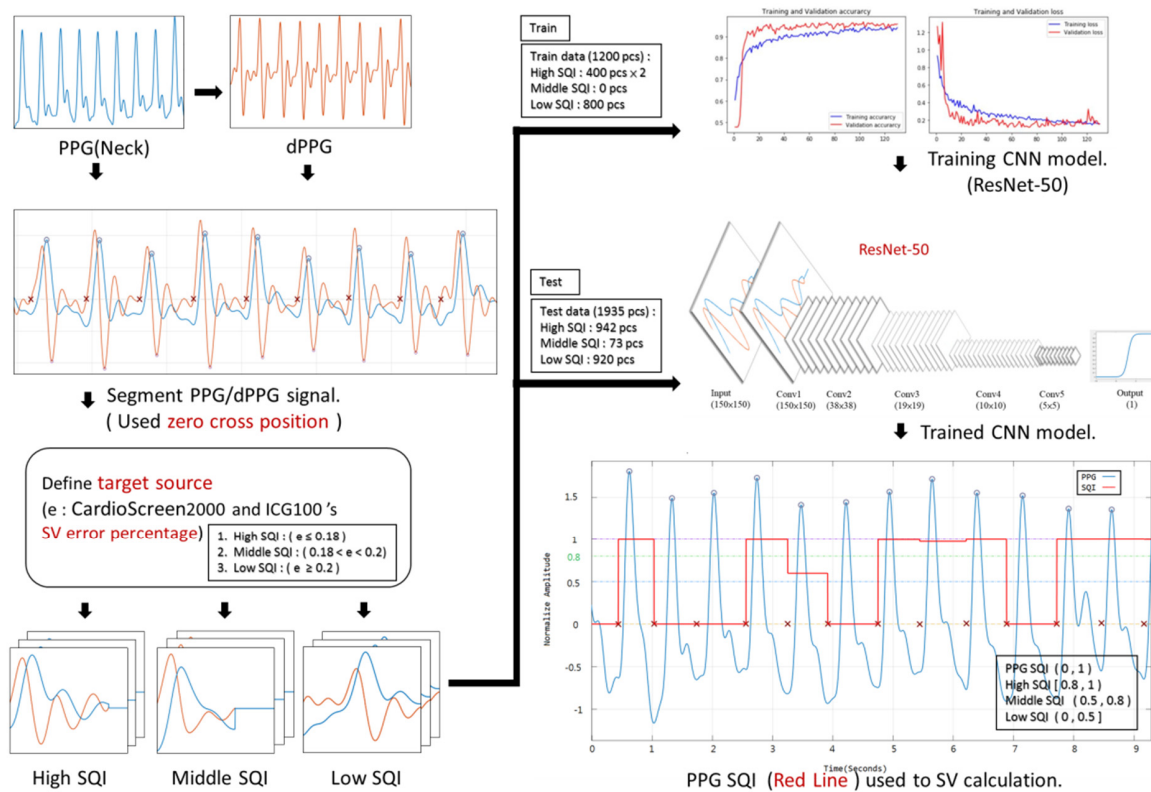

Figure 4. Overall procedure for signal quality index (SQI) classification of PPG pulses.

3.1. Data Acquisition

Our ICG device was described in a previous study [5] in which analog ICG and PPG signals were all digitalized with a sampling frequency of 500 Hz. The PPG sensors were placed on the neck of the subject. The ICG and PPG signals were filtered to remove the baseline drift and the high-frequency noise using a second-order Butterworth bandpass filter in which the lower and upper cutoff frequencies were 0.2 and 10 Hz, respectively. Then, the DPPG and DICG signals were gotten from the PPG and ICG signals by the first-order discrete derivative, which passed a zero-phase forward and reverse second-order Butterworth lowpass filter. Its cutoff frequency was 10 Hz. The first zero crossing point for the DPPG signal during one heart cycle was used to segment the pulse. As the heart rates of the included subjects were not lower than 60 beats/minute, an image consisted of two pulses, PPG and DPPG, whose length (size) was set to 500 points. If the length of a pulse was less than 500 points, it was padded to become 500-points long with zero points. Figure 5 shows different 150×150 images obtained from the segmented PPG (blue line) and DPPG (orange line) signals with three different SQI levels. In Figure 5a, because the morphologies of the two PPG pulses within the systolic phase are perfect (i.e., the morphologies have a clear, distinct dicrotic notch and starting ejection point), their SQIs are high. The two PPG pulses in Figure 5b belong to the middle SQI ones, due to good morphology at the starting ejection point. However, their dicrotic notches are not distinct in the PPG signals. Therefore, the values of their differential signals at the dicrotic notch zone may not be larger

than zero. As shown in Figure 5c, the two PPG pulses own low SQIs since their amplitudes or baselines have been greatly distorted due to severe motion artifacts.
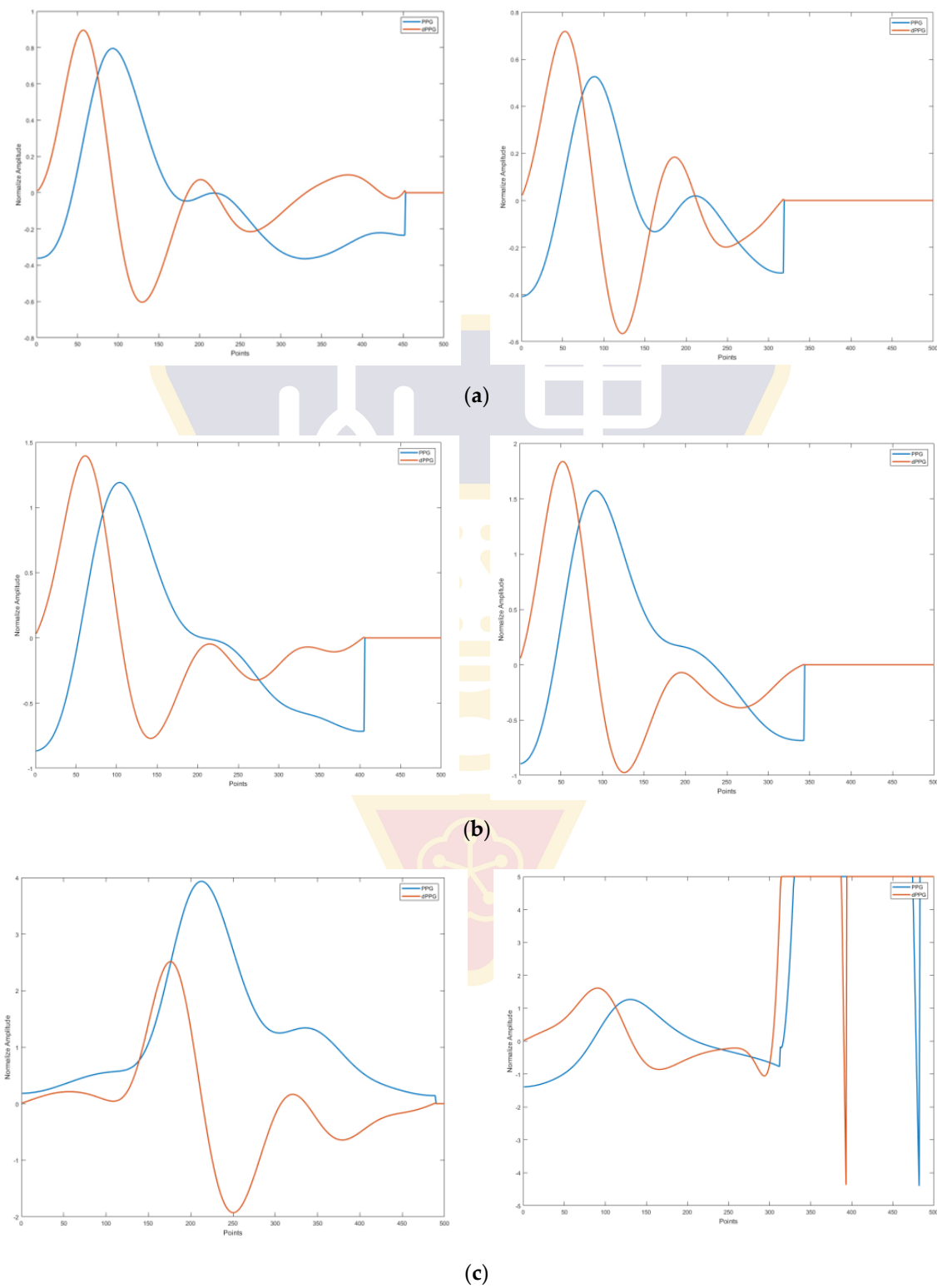
Figure 5. PPG (blue line) and DPPG (orange line) pulses with different quality levels. (**a**) High quality, (**b**) middle quality, (**c**) low quality.

3.2. Network Architectures

Since the number of samples was not large and there were not many differences in the characteristics of patterns, 2D DCNNs were chosen to perform the classification task in the study. We built two 2D DCNNs based on the trained DRNN architecture with a 50-layer network (ResNet-50) [22] and the trained DCNN architecture with a 19-layer network (VGG-19) [23]. In the output layer, we replaced the 1000 fully-connected with softmax activation by a 1 fully-connected with sigmoid activation. The VGG-19 and ResNet-50 are the base models in this study that were pretrained for object detection tasks on the ImageNet dataset [24]. The architectures of the two 2D DCNNs are shown in Figure 6, with detailed descriptions shown in Tables 1 and 2, respectively. In Table 1, the filters in the VGG-19 all are of 3×3 size. The downsampling is performed directly by the maximum pooling layers that have a stride of 2, and batch normalization is performed right after each convolution and before ReLU activation. Two fully connected layers have sizes of 1024. For the ResNet-50, the main theme is to skip blocks of convolutional layers by using shortcut connections, as shown in Figure 6. The dot lines indicate that the dimensions of input and output are different. Thus, the 1×1 convolution with a stride of 2 is used to perform the projection shortcut. The solid lines represent that the dimensions of input and output are the same. Then, the identity shortcut is used. In Table 2, the filters in ResNet-50 follow two design rules. First, when the feature sizes of input and output are the same, the layers have the same number of filters. Second, when the feature map size is halved, the number of filters is doubled. The downsampling is performed directly by convolutional layers that have a stride of 2, and batch normalization is performed right after each convolution and before ReLU activation. The network ends with a global average pooling layer with a 7×7 filter.
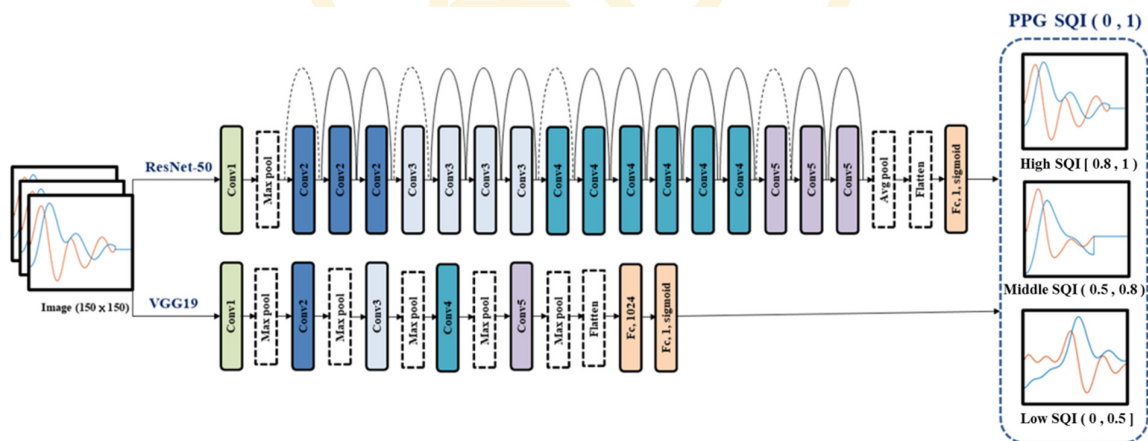
Figure 6. The architectures of the ResNet-50 and VGG-19.

Table 1. Fundamental information about the VGG-19 layers and associated parameters of the network architecture.

Type	Filter Size	Channel Number	Input Size
Conv1	3×3	64	$150 \times 150 \times 3$
	3×3	64	$150 \times 150 \times 64$
Max pool	3×3	-	$150 \times 150 \times 64$
Conv2	3×3	128	$75 \times 75 \times 64$
	3×3	128	$75 \times 75 \times 128$
Max pool	3×3	-	$75 \times 75 \times 128$
	3×3	256	$37 \times 37 \times 128$
Conv3	3×3	256	$37 \times 37 \times 256$
	3×3	256	$37 \times 37 \times 256$
	3×3	256	$37 \times 37 \times 256$
Max pool	3×3	-	$37 \times 37 \times 256$

Table 1. *Cont.*

Type	Filter Size	Channel Number	Input Size
	3×3	512	$18 \times 18 \times 256$
	3×3	512	$18 \times 18 \times 512$
Conv4	3×3	512	$18 \times 18 \times 512$
	3×3	512	$18 \times 18 \times 512$
Max pool	3×3	-	$18 \times 18 \times 512$
	3×3	512	$9 \times 9 \times 512$
Conv5	3×3	512	$9 \times 9 \times 512$
	3×3	512	$9 \times 9 \times 512$
	3×3	512	$9 \times 9 \times 512$
Max pool	3×3	-	$9 \times 9 \times 512$
Flattn	-	1	$4 \times 4 \times 512$
Fc	-	1	8192
Out	-	1	1024

Table 2. Fundamental information about the ResNet-50 layers and associated parameters of the network architecture.

Type	Filter Size	Channel Number	Input Size	Times
Conv1	7×7	64	$156 \times 156 \times 3$	1
Max pool	3×3	-	$77 \times 77 \times 64$	1
	1×1	64	$38 \times 38 \times 64$	
Conv2	3×3	64	$38 \times 38 \times 64$	3
	1×1	256	$38 \times 38 \times 256$	
	1×1	128	$19 \times 19 \times 128$	
Conv3	3×3	128	$19 \times 19 \times 128$	4
	1×1	512	$19 \times 19 \times 512$	
	1×1	256	$10 \times 10 \times 256$	
Conv4	3×3	256	$10 \times 10 \times 256$	6
	1×1	1024	$10 \times 10 \times 1024$	
	1×1	512	$5 \times 5 \times 512$	
Conv5	3×3	512	$5 \times 5 \times 512$	3
	1×1	2048	$5 \times 5 \times 2048$	
Avg pool	7×7	-	$5 \times 5 \times 2048$	1
Flattn	-	1	$5 \times 5 \times 2048$	1
Out	-	1	51200	1

3.3. Experimental Protocol

This study recruited fourteen healthy male subjects without cardiovascular disease or injured limbs. Their ages were between 22 and 29 years (22.7 ± 2.1 years, mean ± standard deviation), weight between 46 and 78 Kg (61.8 ± 8.8 Kg), height between 165 and 188 cm (173.1 ± 6.1 cm), and heart rates between 65 and 78 beats/minute (70.5 ± 3.4 beats/minute). A commercial medical device (medis® CS2000, medis, Germany) with the ICG technology was utilized to measure the beat-to-beat SV that was considered as the reference value in the study. This experiment was approved by the Research Ethics Committee of China Medical University and Hospital (No. CMUH107-REC3-061), Taichung, Taiwan.

The measurement duration for each subject lasted for three minutes. During the measurement, four electrodes of medis® CS2000 were placed on the left side of the body. The other four electrodes of our designed ICG device were put at the right side of the body, and the PPG sensor was placed on the neck. The details of the measurement for the placement of those ICG electrodes were described in our previous study [12]. We recorded the beats of medis® CS2000 and our ICG device synchronously. The data statistics are described as mean ± standard deviation (SD).

3.4. Statistical Analysis

In this study, PPG pulses are considered as high-quality when their error percentages of the SV measured by our ICG device and the medis® CS2000 device are less than 18%. There were 1342 high-quality pulses. PPG pulses are considered as middle-quality when their error percentages are between 18% and 20%. There were 73 middle-quality pulses. PPG pulses are considered as low-quality when their error percentages are larger than 20%. There were 1720 low-quality pulses. Table 3 shows the three levels of SQI for all subjects. According to our proposed method, a PPG pulse is considered true-positive (TP) when its quality level is correctly identified, false-positive (FP) when its quality level is incorrectly identified, true-negative (TN) when its quality level is correctly rejected, and false-negative (FN) when its quality level is incorrectly rejected. Here, the performance of the proposed method was evaluated using accuracy, $(TP + TN)/(TP + FP + FN + TN)$, precision, $TP/(TP + FP)$, sensitivity, $TP/(TP + FN)$, and specificity, $TN/(FN + TN)$.

Table 3. Quality information of PPG pulses for fourteen subjects.

| Subjects	Number of Pulses	High SQI	Middle SQI	Low SQI
1	213	97	7	109
2	231	160	7	64
3	198	52	6	140
4	235	132	8	95
5	303	160	7	136
6	234	79	6	149
7	235	81	6	148
8	193	112	3	78
9	209	8	1	200
10	249	105	6	138
11	261	79	7	175
12	159	32	4	123
13	205	93	2	110
14	210	152	3	55
All	**3135**	**1342**	**73**	**1720**

4. Results

4.1. Training Outcomes of Deep Convolution Neural Networks

The proposed VGG-19 and ResNet-50 were trained by 1200 PPG pulses that were divided into two categories, high-quality $(d = 1)$ and low-quality $(d = 0)$. The high-quality samples included 400 pulses randomly chosen from the 1342 samples, and the low-quality samples comprised 800 pulses randomly chosen from the 1720 samples. We did not use the pulses belonging to middle-quality to train the networks in this study because the sample number of this level was too few, only 73 pulses. In order to balance the sample numbers for the two levels, the high-quality samples were extended to 800 using the 400 samples. Figure 7a shows the training results for the VGG-19 model. The training and validation accuracies are 0.88 and 0.90 after training 105 times to avoid the model overfitting the data, respectively. The training and validation loss errors are 0.28 and 0.29, respectively. Figure 7b shows the training results for the ResNet-50 model. The training and validation accuracies are 0.94 and 0.96, and loss errors are 0.15 and 0.16 after training 130 times.

4.2. Testing Outcomes of Deep Convolution Neural Networks

The testing samples included 1935 PPG pulses and did not overlap the training samples. The high-quality, middle-quality, and low-quality samples comprised 942, 73, and 920 PPG pulses, respectively. When the output value of the 2D DCNN was between 0.8 and 1.0, between 0.5 and 0.8, or between 0 and 0.5, the PPG pulse was classified as a high-quality, middle-quality, or low-quality,

respectively. Table 4 shows the performance of the VGG-19 and ResNet-50 models in the classification of the high- and low-quality levels. The average accuracy (0.895) of the VGG-19 model is lower than that (0.925) of the ResNet-50 model. However, the sensitivity (0.970) and specificity (0.970) of the VGG-19 model are higher than those (0.915 and 920) of the ResNet-50 model, respectively. For all the testing data, the statistic error of SV is pretty high and found to be 33.5 ± 76.8 mL. Table 5 shows the statistic errors of SV for the three groups (high-quality, middle-quality, and low-quality), as classified by the VGG-19 and ResNet-50 models. With either of the two models, the high-quality group obviously resulted in the least SV errors. Additionally, the SV errors using the ResNet-50 model were lower than those using the VGG-19 model for the three groups with different quality levels.
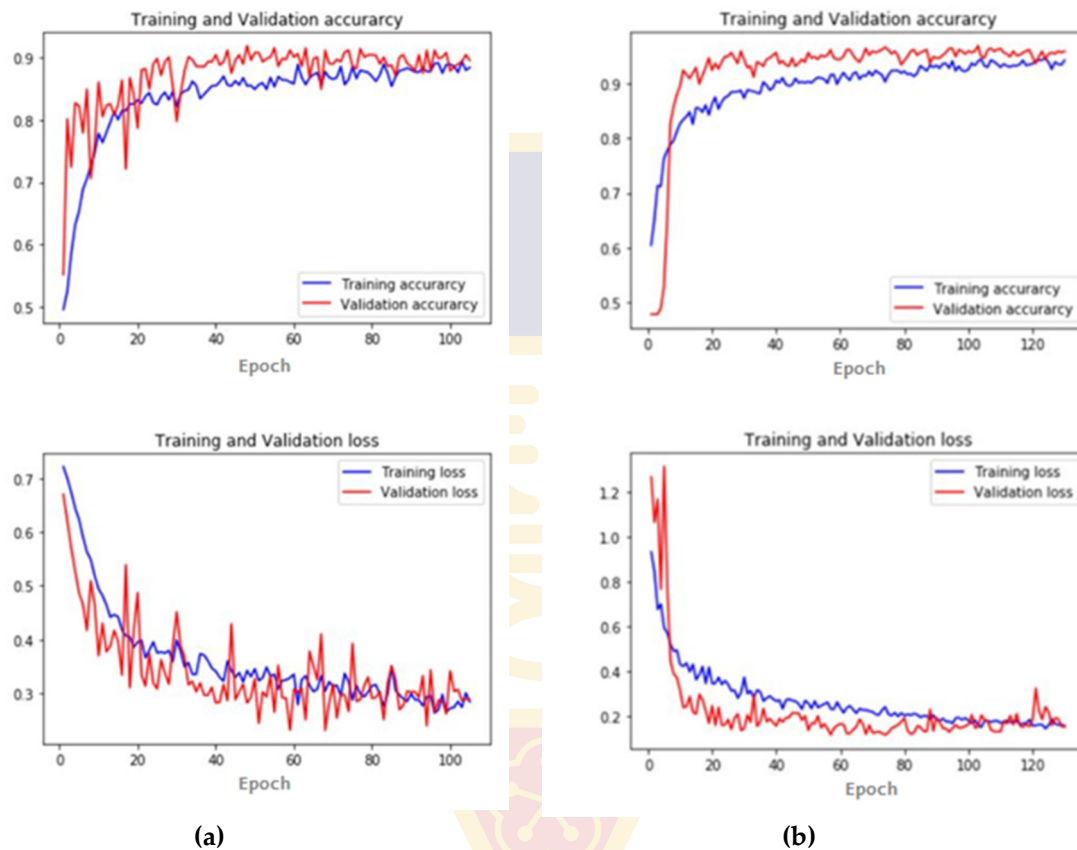
Figure 7. Accuracy and loss profiles of training and validation in the two models. (**a**) VGG-19 model; (**b**) ResNet-50 model.

Table 4. The testing results for the VGG-19 and ResNet-50 models. TP, TN, FP, and FN denote the true positive, true negative, false positive and false negative pulses, respectively.

Model	TP (N)	TN (N)	FP (N)	FN (N)	Accuracy (%)	Precision (%)	Sensitivity (%)	Specificity (%)
VGG-19 High vs. (Middle + Low)	897	780	213	45	0.87	0.81	0.95	0.95
VGG-19 (High + Middle) vs. Low	1006	774	146	9	0.92	0.87	0.99	0.99
ResNet-50 High vs. (Middle + Low)	860	910	83	82	0.91	0.91	0.91	0.92
ResNet-50 (High + Middle) vs. Low	933	886	34	82	0.94	0.96	0.92	0.92

Figure 8 shows the results of SQI classification with the ResNet-50 model for the PPG (blue line) and DPPG (orange line) signals moderately corrupted by the baseline drift. The SQI level of each

pulse was determined according to the error percentage between the reference SV by medis® CS2000 and the measured SV by our ICG device. An error percentage of below 18%, between 18% and 20%, or above 20% represents a high-quality, middle-quality, or low-quality PPG pulse, respectively. The first and third rows, and the second and fourth rows of the data correspond to the two SVs, and the two LVETs measured by medis® CS 2000 and our ICG device, respectively. The fifth row of the data denotes the error percentage of the SV. The red line represents the output value of the ResNet-50 model. If the output value is larger than 0.8, between 0.5 and 0.8, and less than 0.5, then the PPG pulse will be classified as a high-, middle- and low-quality one, respectively. The cross and circle symbols denote the first zero-crossing point and minimum-value point of the DPPG pulse, respectively. For the seventh PPG pulse in the figure, it belongs to one of the PPG pulses with high quality because it has a sharp valley in the starting ejection zone and a clear dicrotic notch. Thus, its corresponding SV error percentage is found to be relatively low, 0.02, and the output value of the ResNet-50 model for this pulse is 1.0. In addition, the second and third pulses both belong to low SQI ones, although they have clear dicrotic notches and flat shape in the starting ejection zones. Since their LVET errors are 80 and 97 ms, their corresponding SV error percentages are found to be 0.49 and 0.42, respectively. Thus, two output values of the ResNet-50 model for these two pulses are both 0. For the fifth pulse, it belongs to a middle SQI one because it does not have a sharp valley in the starting ejection zone. Thus, its SV error percentage is 0.2, and the output value of the ResNet-50 model for this pulse is 0.6.

Table 5. The statistic errors of SV in the three groups as classified by the VGG-19 and ResNet-50 models.

Group	SV Error (mL)	
	VGG-19	ResNet-50
High-quality group (N = 942)	4.5 ± 14.7	2.6 ± 14.2
Middle-quality group (N = 73)	25.4 ± 42.3	19.9 ± 35.1
Low-quality group (N = 920)	64.6 ± 102.1	57.67 ± 95.4
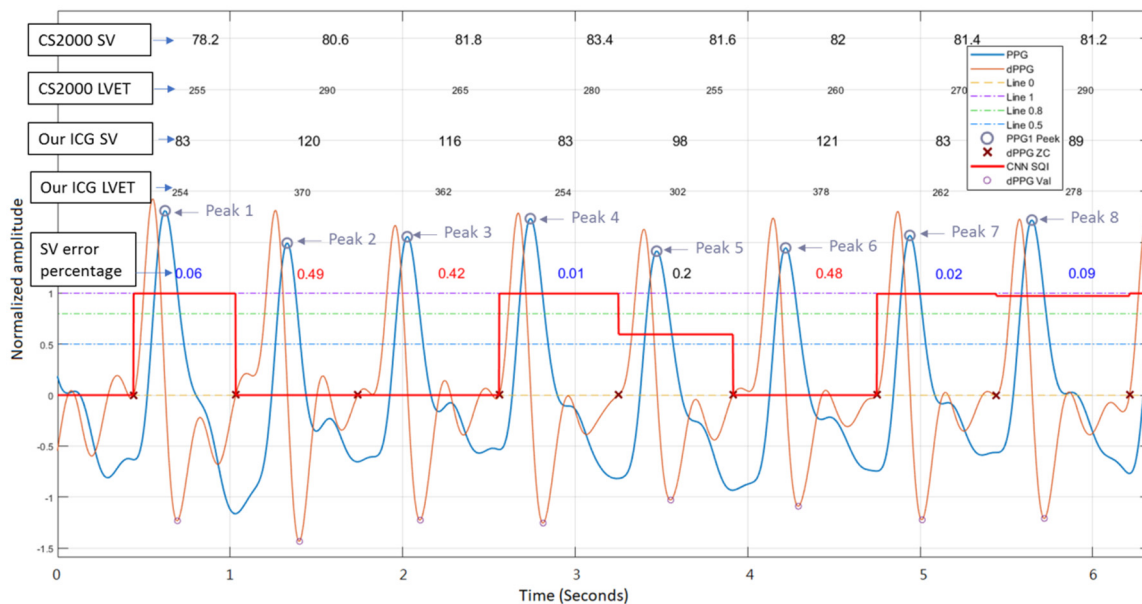
Figure 8. The results of SQI classification with the ResNet-50 model for the PPG (blue line) and DPPG (orange line) signals moderately corrupted by the baseline drift. The first and third rows of the data are the two SVs with medis® CS 2000 and our ICG device, respectively, while the second and fourth rows are the two LVETs with medis® CS 2000 and our ICG device, respectively. The fifth row denotes the error percentages of SV. The red line is the output value of the ResNet-50 model. The cross and circle symbols represent the first zero-crossing point and minimum-value point of the DPPG pulse, respectively.

Figure 9 shows the results of SQI classification with the ResNet-50 model for the PPG (blue line) and DPPG (orange line) signals in the presence of serious baseline drift. When the baseline of the PPG pulses is heavily wandered, the proposed ResNet-50 can still successfully identify these pulses as low SQI ones. Thus, the output values of the ResNet-50 model for these pulses are all 0.
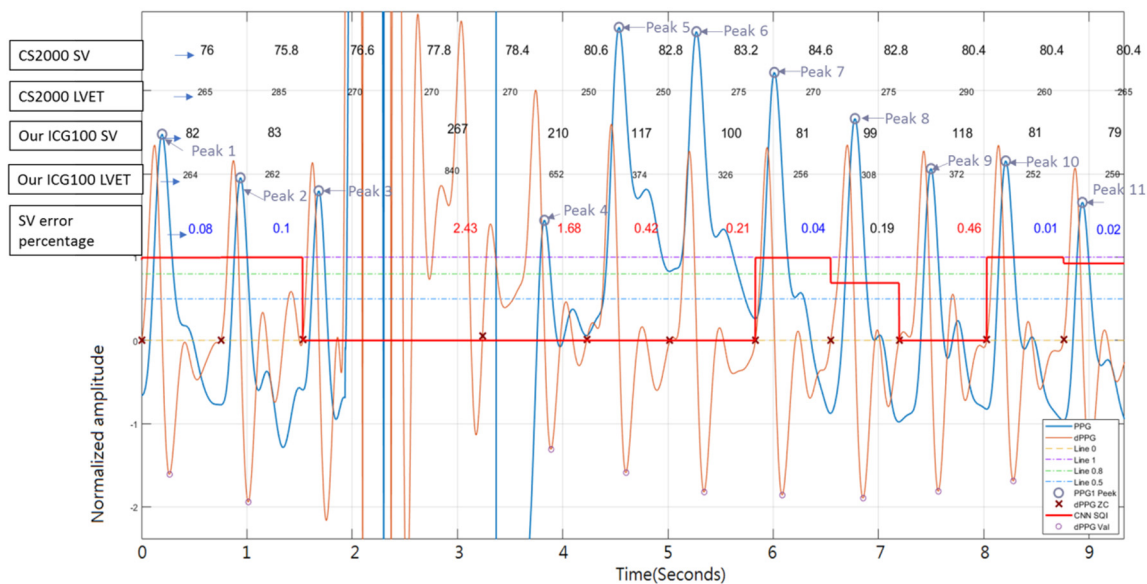
Figure 9. The results of SQI classification with the ResNet-50 model for the PPG (blue line) and DPPG (orange line) signals corrupted by serious baseline drift. The first and third rows of the data are the two SVs with medis® CS 2000 and our ICG device, respectively, while the second and fourth rows are the two LVETs with medis® CS 2000 and our ICG device, respectively. The fifth row represents the error percentages of SV. The red line denotes the output value of the ResNet-50 model. The cross and circle symbols represent the first zero-crossing point and minimum-value point of the DPPG pulse, respectively.

5. Discussion

In a rule-based classification approach, only finite characteristics in time or frequency domains are extracted from a PPG pulse. Therefore, the performance of such a rule-based classification approach depends on the kind and number of characteristics. Since the number of the selected characteristics is always limited, all the information that exists in the PPG pulse is not fully utilized in the rule-based approaches [3,10,12]. Essentially, the main characteristics of a high-quality PPG pulse directly affect the measuring physiological parameter. In this study, LVET is defined as the time interval initiated at the opening of the aortic valve and terminated at the closing of the aortic valve. Thus, for the morphology of a PPG pulse, the starting ejection point is the first zero-crossing point of the DPPG pulse during systole. The ending ejection point is the time for the first minimum valley of the DPPG pulse during systole, which happens before the dicrotic notch. Thus, the clear foot and dicrotic notch are the main characteristics of the high-quality PPG pulse. In the 2D DCNN, the convolution layers can automatically classify the different feature patterns from the raw image. Thus, the performance of the 2D DCNN in this study is found to be better than that of our previous study using the rule-based method [12].

In the previous study [5], we found that a substantial error is usually present in the LVET measured by the PPG or ICG, as compared with the standard reference measured by phonocardiography. Although the SV has a linear relation with the LVET according to Equation (1), the SV measured by medis® CS2000 is calibrated through some parameters. In this study, both SV and LVET measured by medis® CS2000 are used as the references to compare with those measured by our ICG device. In the study, one of our findings is that the application of high-quality PPG pulses leads to relatively lower errors

in the SV and LVET measurement, as shown in Figures 8 and 9. Thus, only the PPG pulse with high quality can be used to obtain a reliable LVET and, subsequently, yield an accurate SV. In Table 5, the SV is measured by high-quality PPG pulses in which the statistic errors of SV for the VGG-19 and ResNet-50 models are found to be relatively low (4.5 ± 14.7 and 2.6 ± 14.2 mL), respectively.

In previous studies [10,25,26], the quality level of a PPG pulse was defined by experts in a manual fashion. However, in the validation of their algorithms, a direct comparison of performance between two published algorithms is restricted due to the different cognitive abilities of such experts. In this study, we use three error percentage degrees, below 18%, between 18% and 20%, and above 20%, to classify individual PPG pulse's SQI (low, middle, or high). Based on the quantitative degrees of error percentage, the proposed algorithm can effectively differentiate the quality level of each PPG pulse. Additionally, the accuracy in the SV measurement with a high SQI PPG pulse classified by the algorithm is found to be higher than that with a low SQI PPG pulse.

A classification approach using the DCNN does not need predetermined characteristics or features and makes full use of the information embedded in the PPG pulse by taking advantage of a deep learning process [27,28]. In our previous study, we proposed a rule-based method combined with a fuzzy neural network to determine the SQIs of PPG pulses [12]. In order to increase the tolerance of the rule-based method, a PPG pulse with an error percentage of SV less than 40% was considered to be of high quality. In the test data, the statistic error of PPG pulses classified to be of high quality was set 6.4 ± 12.8 mL. However, the accuracies for successfully determining high- and low-quality pulses achieved only 0.83 and 0.86, respectively. On the other hand, in the present work, we label a PPG pulse as high quality when its error percentage of SV is less than 20%. In the test data, the statistic error of pulses classified as high quality with the proposed ResNet-50 model is 2.6 ± 14.2 mL. The accuracies for successfully classifying high- and low-quality PPG pulses are 0.91 and 0.94, respectively. Since the performance of the proposed 2D DCNN approach for the SQI classification seems to be better than the rule-base method, the DCNN method may be applied to increase the measurement accuracy of SV.

Moreover, when the PPG signals are corrupted by serious baseline drift, these PPG pulses should be removed by some algorithms before classifying their SQIs using the rule-based method. In the study, the proposed 2D DCNN approaches (VGG-19 or ResNet-50) can make use of the morphologies of PPG and DPPG waveforms to determine their SQIs. The PPG and DPPG signals are first merged and transformed into an image, as shown in Figure 5, before we can use them to perform the classification task. As shown in Figure 5c, the image is constructed by the PPG and DPPG pulses in which the PPG pulse almost lacks the fundamental morphology of a traditional PPG waveform, but it can still be correctly classified as a low-quality one by the proposed ResNet-50 model (Figure 9). This suggests that the proposed 2D DCNN approaches may be useful for quality classification of the PPG pulses, even for those seriously corrupted by motion artifacts and power line interference.

It is assumed that in a continuous PPG signal, the morphology of a high-quality PPG pulse may be gradually changed to a low-quality PPG one. Hence, a middle-quality pulse can be considered as a transitional one between the high- and low-quality pulses. In the present work, we define the error percentage of the measured SV with middle-quality pulses to be between 18% and 20%. Therefore, both the ResNet-50 and VGG-19 models are trained only using high- and low-quality PPG pulses, excluding the middle-quality ones. The output layers of the VGG-19 and ResNet-50 models use the sigmoid function as the active function. Thus, the current VGG-19 or ResNet-50 model can be considered as a regression model for determining the morphologic change of the PPG pulse. We define the output ranges of high- and low-quality pulses as between 1.0 and 0.8 and between 0.5 and 0.0, respectively. Of course, some testing pulses may be classified as the middle-quality ones when their testing outputs are between 0.8 and 0.5. Therefore, in Table 4, we test the performance of the VGG-19 or ResNet-50 model with the high-quality class and the not-high-quality class, and with the not-low-quality class and the low-quality class.

Although the ResNet-50 model is constructed by a trained DRNN architecture with a 50-layer network, its average accuracy (0.940) for classifying the high- plus middle-quality and the low-quality

PPG pulses is higher than that (0.92) of the VGG-19 model with a 19-layer network. However, both sensitivity (0.915) and specificity (0.92) of the ResNet-50 model are lower than those (0.97, 0.97) of the VGG-19 model for classifying these two quality groups. It seems that due to few samples included in the study, no significant difference exists between the performances of the ResNet-50 and VGG-19 models.

There are some limitations to the present study. First, because the subjects recruited in this study all are healthy males, the pulses with the middle- or low-quality are all corrupted, mostly by the motion artifacts. In the study, we did not acquire the PPG pulses belonging to arrhythmic beats. Thus, gender and cardiovascular disease may somewhat affect the current results. Second, PPG pulse morphology would be varied with vascular compliance, which is closely associated with age and hypertension [29,30]. The ages of the included subjects are between 22 and 29 years, and their systolic and diastolic blood pressure are all in a normal range. Thus, subjects of different ages or with hypertension may have various pulse morphologies that may consequently influence the present outcome. Third, only 1-second episodes of PPG signals are employed in the current study. To make sure that each 1-second PPG signal contains at least one cardiac cycle data, the heart rates of the recruited participants must be higher than 60 beats/minute.

6. Conclusions

In order to quantify the level of SQI for each PPG pulse, the error percentage of measured SV for each beat was used to define the level of SQI for each PPG pulse. The morphologies of PPG and DPPG pulses were combined into an image, which was used to determine the quality level of each PPG pulse. The proposed VGG-19 and ResNet-50 models can be used to successfully determine the SQI of each PPG pulse. Thus, we did not need to explore the characteristics of the PPG pulse to determine the pulse SQI when using the 2D DRNN. Moreover, comparing with the results of our study, the performance of the 2D DRNN was better than that of a traditional rule-based method. Noticeably, the main limitation of the study is the small number of PPG pulses. If more PPG pulses are used in the training process of the 2D DRNN, better results can be expected.

Author Contributions: Conceptualization, S.-H.L. and J.-J.W.; methodology, S.-H.L. and R.-X.L.; software, R.-X.L.; validation, C.-H.S. writing—original draft preparation, S.-H.L. and J.-J.W.; writing—review and editing, S.-H.L., J.-J.W., and W.C. All authors have read and agreed to the published version of the manuscript.

**Conflicts of Interest:** The authors declare no conflict of interest.

References

1. Majumder, S.; Mondal, T.; Deen, M.J. Wearable sensors for remote health monitoring. *Sensors* **2017**, *17*, 130. [CrossRef] [PubMed]
2. Sharwood-Smith, G.; Bruce, J.; Drummond, G. Assessment of pulse transit time to indicate cardiovascular changes during obstetric spinal anesthesia. *Br. J. Anaesth.* **2006**, *96*, 100–105. [CrossRef] [PubMed]
3. Shelley, K.H. Photoplethysmography: Beyond the calculation of arterial oxygen saturation and heart rate. *Anesth. Analg.* **2007**, *105*, S31–S36. [CrossRef]
4. Chon, K.H.; Dash, S.; Ju, K. Estimation of respiratory rate from photoplethysmogram data using time-frequency spectral estimation. *IEEE Trans. Biomed. Eng.* **2009**, *56*, 2054–2063. [CrossRef] [PubMed]
5. Liu, S.-H.; Wang, J.-J.; Su, C.-H.; Cheng, D.-C. Improvement of left ventricular ejection time measurement in the impedance cardiography combined with the reflection photoplethysmography. *Sensors* **2018**, *18*, 3036. [CrossRef] [PubMed]

6. Biswas, D.; Simões-Capela, N.; Hoof, C.V.; Helleputte, N.V. Heart rate estimation from wrist-worn photoplethysmography: A review. *IEEE Sens. J.* **2019**, *19*, 6560–6570. [CrossRef]

7. Allen, J.; Murray, A. Similarity in bilateral photoplethysmographic peripheral pulse wave characteristics at the ears, thumbs and toes. *Physiol. Meas.* **2000**, *21*, 369–377. [CrossRef]

8. Allen, J. Photoplethysmography and its application in clinical physiological measurement. *Physiol. Meas.* **2007**, *28*, R1–R39. [CrossRef]

9. Liu, S.-H.; Chang, K.-M.; Fu, T.-H. Heart rate extraction from photoplethysmogram on fuzzy Logic discriminator. *Eng. Appl. Artif. Intell.* **2010**, *23*, 968–977. [CrossRef]

10. Fischer, C.; Domer, B.; Wibmer, T.; Penzel, T. An algorithm for real-time pulse waveform segmentation and artifact detection in photoplethysmograms. *IEEE J. Biomed. Health Inform.* **2017**, *21*, 372–381. [CrossRef]

11. Li, K.; Warren, S.; Natarajan, B. Onboard tagging for real-time quality assessment of photoplethysmograms acquired by a wireless reflectance pulse oximeter. *IEEE Trans. Biomed. Circuits Syst.* **2012**, *6*, 54–63. [CrossRef] [PubMed]

12. Liu, S.-H.; Wang, J.-J.; Chen, W.; Pan, K.-L.; Su, C.-H. Classification of photoplethysmographic signal quality with fuzzy neural network for improvement of stroke volume measurement. *Appl. Sci.* **2020**, *10*, 1476. [CrossRef]

13. Pourbabaee, B.; Roshtkhari, M.J.; Khorasani, K. Deep convolutional neural networks and learning ECG features for screening paroxysmal atrial fibrillation patients. *IEEE Trans. Syst. Man Cybern. Syst.* **2018**, *48*, 2095–2104. [CrossRef]

14. Kiranyaz, S.; Ince, T.; Gabbouj, M. Real-time patient-specific ECG classification by 1-D convolutional neural networks. *IEEE Trans. Biomed. Eng.* **2016**, *63*, 664–675. [CrossRef]

15. Yildirim, O.; Plawiak, P.; Tan, S.; Acharya, U. Arrhythmia detection using deep convolutional neural network with long duration ECG signals. *Comput. Biol. Med.* **2018**, *102*, 411–420. [CrossRef]

16. Jimenez-Serrano, S.; Yagüe-Mayans, J.; Simarro-Mondéjar, E.; Calvo, C.J.; Castells, F.; Millet, J. Atrial fibrillation detection using feedforward neural networks and automatically extracted signal features. *Comput. Cardiol. Conf.* **2017**, *389*. [CrossRef]

17. Giorgio, A.; Rizzi, M.; Guaragnella, C. Efficient detection of ventricular late potentials on ECG signals based on wavelet denoising and SVM classification. *Information* **2019**, *10*, 328. [CrossRef]

18. Huang, J.; Chen, B.; Yao, B.; He, W. Arrhythmia classification using STFT-based spectrogram and convolutional neural network. *IEEE Access* **2019**, *7*, 92871–92880. [CrossRef]

19. Zhang, Q.; Zhou, D.; Zeng, X. A multiresolution convolutional neural network for ECG-based biometric human identification in smart health applications. *IEEE Access* **2017**, *5*, 11805–11816. [CrossRef]

20. Abdeldayem, S.S.; Bourlai, T. A novel approach for ECG-based human identification using spectral correlation and deep learning. *IEEE Trans. Biogr. Behav. Iden. Sci.* **2020**, *2*, 1–14. [CrossRef]

21. Kubicek, W.G.; Karnegis, J.N.; Patterson, R.P.; Witsoe, D.A.; Mattson, R.H. Development and evaluation of an impedance cardiograph system. *Aerosp. Med.* **1966**, *37*, 1208–1212.

22. He, K.; Zhang, X.; Ren, S.; Sun, J. Deep residual learning for image recognition. *Proc. IEEE Conf. Comput. Vis. Pattern Recognit.* **2016**, 770–778. [CrossRef]

23. Simonyan, K.; Zisserman, A. Very deep convolutional networks for large-scale image recognition. *arXiv* **2014**, *1556*, 1409.

24. Keras Applications. Available online: https://keras.io/applications/ (accessed on 14 May 2020).

25. Chong, J.W.; Dao, D.K.; Salehizadeh, S.M.A.; Mcmanus, D.D.; Darling, C.E.; Chon, K.H.; Mendelson, Y. Photoplethysmograph signal reconstruction based on a novel hybrid motion artifact detection-reduction approach part I: Motion and noise artifact detection. *Ann. Biomed. Eng.* **2014**, *42*, 2238–2250. [CrossRef] [PubMed]

26. Karlen, W.; Kobayashi, K.; Ansermino, J.M.; Dumont, G.A. Photoplethysmogram signal quality estimation using repeated Gaussian filters and cross-correlation. *Physiol. Meas.* **2012**, *33*, 1617–1629. [CrossRef]

27. Pereira, T.; Ding, C.; Gadhoumi, K.; Tran, N.; Colorado, R.A.; Meisel, K.; Hu, X. Deep learning approaches for plethysmography signal quality assessment in the presence of atrial fibrillation. *Physiol. Meas.* **2019**, *40*, 125002. [CrossRef] [PubMed]

28. Pereira, T.; Gadhoumi, K.; Ma, M.; Liu, X.; Xiao, R.; Colorado, R.A.; Keenan, K.J.; Meisel, K.; Hu, X. A supervised approach to robust photoplethysmography quality assessment. *IEEE J. Biomed. Health Inform.* **2020**, *24*, 649–657. [CrossRef] [PubMed]

29. McVeigh, G.E. Pulse waveform analysis and arterial wall properties. *Hypertension* **2003**, *41*, 1010–1011. [CrossRef] [PubMed]

30. Resnick, L.M.; Militianu, D.; Cunnings, A.J.; Pipe, J.G.; Evelhoch, J.L.; Soulen, R.L.; Lester, M.A. Pulse waveform analysis of arterial compliance: Relation to other techniques, age, and metabolic variables. *Am. J. Hyperten.* **2000**, *13*, 1243–1249. [CrossRef]
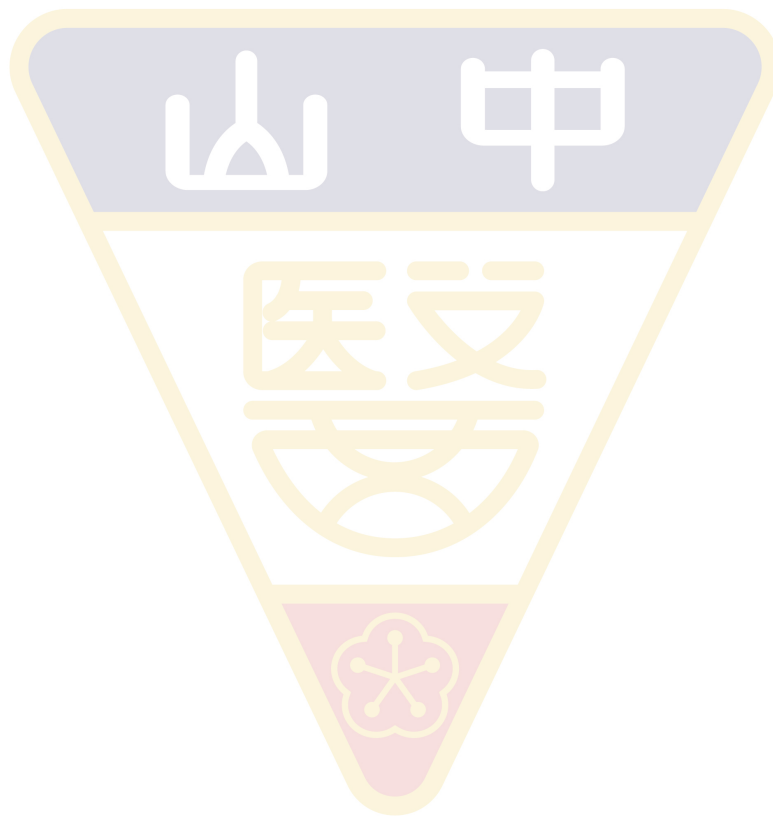
Genotoxic effects of 1-nitropyrene in macrophages are mediated through a p53-dependent pathway involving cytochrome *c* release, caspase activation, and PARP-1 cleavage

Sheng-Wen Wu [a,b], Chun-Hung Su [c,d], Yung-Chuan Ho [e], Rosa Huang-Liu [f], Ching-Chi Tseng [g], Yun-Wei Chiang [h], Kun-Lin Yeh [i], Shiuan-Shinn Lee [j], Wen-Ying Chen [i], Chun-Jung Chen [k], Yi-Ching Li [l,m], Chien-Ying Lee [l,m,1], Yu-Hsiang Kuan [l,m,*,1]

[a] *Division of Nephrology, Department of Internal Medicine, Chung Shan Medical University Hospital, Taichung, Taiwan*
[b] *The School of Medicine, Chung Shan Medical University, Taichung, Taiwan*
[c] *Department of Internal Medicine, Chung Shan Medical University Hospital, Taichung, Taiwan*
[d] *Department of Internal Medicine, School of Medicine, Chung Shan Medical University, Taichung, Taiwan*
[e] *School of Medical Applied Chemistry, Chung Shan Medical University, Taichung, Taiwan*
[f] *School of Nutrition, Chung Shan Medical University, Taichung, Taiwan*
[g] *Aerospace Center Hospital, Peking University, Beijing, China*
[h] *Department of life sciences, National Chung-Hsing University, Taichung, Taiwan*
[i] *Department of Veterinary Medicine, National Chung Hsing University, Taichung, Taiwan*
[j] *School of Public Health, Chung Shan Medical University, Taichung, Taiwan*
[k] *Department of Education and Research, Taichung Veterans General Hospital, Taichung, Taiwan*
[l] *Department of Pharmacology, School of Medicine, Chung Shan Medical University, Taichung, Taiwan*
[m] *Department of Pharmacy, Chung Shan Medical University Hospital, Taichung, Taiwan*

ARTICLE INFO

ABSTRACT

Genotoxic stress from environmental pollutants plays a critical role in cytotoxicity. The most abundant nitro-polycyclic aromatic hydrocarbon in environmental pollutants, 1-nitropyrene (1-NP), is generated during fossil fuel, diesel, and biomass combustion under sunlight. Macrophages, the key regulators of the innate immune system, provide the first line of defense against pathogens. The toxic effects of 1-NP on macrophages remain unclear. Through a lactate dehydrogenase assay, we measured the cytotoxicity induced by 1-NP. Our results revealed that 1-NP induced genotoxicity also named DNA damage, including micronucleus formation and DNA strand breaks, in a concentration-dependent manner. Furthermore, 1-NP induced p53 phosphorylation and nuclear accumulation; mitochondrial cytochrome *c* release; caspase-3 and -9 activation and cleavage; and poly (ADP-ribose) polymerase-1 (PARP-1) cleavage in a concentration-dependent manner. Pretreatment with the PARP inhibitor, 3-aminobenzamide, significantly reduced cytotoxicity, genotoxicity, and PARP-1 cleavage induced by 1-NP. Pretreatment with the caspase-3 inhibitor, z-DEVD-fmk, significantly reduced cytotoxicity, genotoxicity, PARP-1 cleavage, and caspase 3 activation induced by 1-NP. Pretreatment with the p53 inhibitor, pifithrin-α, significantly reduced cytotoxicity, genotoxicity, PARP-1 cleavage, caspase 3 activation, and p53 phosphorylation induced by 1-NP. We propose that cytotoxicity and genotoxicity induced by 1-NP by PARP-1 cleavage via caspase-3 and -9 activation through cytochrome *c* release from mitochondria and its upstream p53-dependent pathway in macrophages.

* Correspondence to: Department of Pharmacology, School of Medicine, Chung Shan Medical University, No. 110, Section 1, Jianguo N. Rd., Taichung 402, Taiwan.
E-mail address: kuanyh@csmu.edu.tw (Y.-H. Kuan).
[1] These authors contributed equally to this work.

1. Introduction

Genotoxic stress, generated from environmental pollutants, plays a critical role in cytotoxicity and tumorigenicity (Huang et al., 2018; Wang et al., 2020; Zhao et al., 2019). Genotoxicity is the ability of genotoxic stress to damage genetic material. DNA damage is an important indicator of genotoxicity (Wu et al., 2007; Huang, 2018). The p53 tumor suppressor protein is at the center of cellular signaling networks that respond to genotoxic stress (Murray-Zmijewski et al., 2008). DNA damage-induced phosphorylation of p53 leads to cytochrome *c* release from the mitochondria (Schuler et al., 2000). The release of cytochrome *c* induces cysteine-aspartic protease (caspase) activation and the subsequent cleavage and inactivation of poly (ADP-ribose) polymerase-1 (PARP-1) (Schuler et al., 2000; Weaver and Yang, 2013), which is a signaling molecule that participates in cytotoxic DNA damage (Weaver and Yang, 2013). Thus, these evidence indicated that the p53 and genotoxicity mediated by cytochrome *c* release, caspase activation, and PARP-1 cleavage results in cytotoxicity.

The most abundant nitro-polycyclic aromatic hydrocarbon (nitro-PAH) in environmental pollutants, 1-nitropyrene (1-NP), is generated during fossil fuel, diesel, and biomass combustion under sunlight (Gao and Ji, 2018). Studies have demonstrated the genotoxic effects of 1-NP in tilapia, human alveolar basal epithelial cells, and human placental trophoblasts (Wang et al., 2020; Bacolod et al., 2017; Rossner et al., 2016). However, the effects of 1-NP on macrophages are unclear. Macrophages are the key regulators of the peripheral innate immune system and provide the first line of defense against pathogens (Sato et al., 2020). However, excessive or prolonged activation of macrophages challenged by environmental pollutants induces cytotoxicity and genotoxicity (André et al., 2011). Further studies are necessary to identify the role of genotoxic stress in macrophages treated with 1-NP.

2. Materials and methods

2.1. Materials

All reagents for cell cultures, including Dulbecco's modified Eagle's medium (DMEM), fetal bovine serum (FBS), trypsin protease, phosphate buffered saline (PBS), and antibiotic antimycotic solution were purchased from HyClone Laboratories, Inc. (Logan, UT, USA). Lactate dehydrogenase (LDH) assay kit, 1-nitropyrene (1-NP), dimethyl sulfoxide (DMSO), low-melting agarose, and other reagents of analytical grade were obtained from Sigma-Aldrich (St. Louis, MO, USA). Caspase-3, caspase-8, and caspase-9 fluorometric assay kits were purchased from Biovision, Inc. (Mountain View, Calif., USA). Primary antibodies for the detection of PARP-1, β-actin, caspase-3, caspase-8, caspase-9, cytochrome C, COX-IV, phosphoryl (P)-p53, p53 were obtained from Santa Cruz (Santa Cruz, CA, USA). The PARP inhibitor, 3-aminobenzamide, the caspase 3 inhibitor, z-DEVD-fmk, and the p53 inhibitor, pifithrin-α, were purchased from Santa Cruz (Santa Cruz, CA, USA). Horseradish peroxidase (HRP)-conjugated anti-rabbit IgG or anti-mouse IgG were purchased from Jackson ImmunoResearch Laboratories (Baltimore, MD, USA). The 1-NP, 3-aminobenzamide, z-DEVD-fmk, and pifithrin-α solution was prepared by dissolving in DMSO. The DMSO final concentration was less than 0.05% (v/v).

2.2. Cell culture and treatment

The mouse macrophage-like cell line RAW264.7 was purchased from the Bioresource Collection and Research Centre (BCRC, Hsinchu, Taiwan). The cells were maintained in Dulbecco's modified Eagle's medium with 10% FBS and a 1% antibiotic antimycotic solution at 37 °C in a 5% CO_2 incubator (Huang et al., 2020). For the cytotoxicity assay, the cells were treated with 0, 3, 10, 30, or 50 μM 1-NP for 6, 12, 24, or

48 h. For other assays, the cells were treated with 0, 3, 10, 30, or 50 μM 1-NP for 24 h. For protection assays, the cells were treated with vehicle, 3-aminobenzamide at 10 mM, z-DEVD-fmk at 1 μM, and pifithrin-α at 10 μM. After 30 min, the cells were incubated with 1-NP at 30 μM for 24 h.

2.3. Cytotoxicity assay

Cytotoxicity was evaluated using a lactate dehydrogenase (LDH) assay (Chang et al., 2020). In brief, the culture medium was aspirated and replaced with medium containing 3, 10, 30, or 50 μM 1-NP and 1% Triton X-100 for 6, 12, 24, or 48 h. The supernatant was transferred to a new plate and mixed with the reaction mixture, consisting of a catalyst and dye solution, and incubated for 30 min at room temperature. LDH activity in the supernatant was quantified using a microplate reader (Synergy HT Multi-Mode Microplate Reader, Biotek, Winooski, VT, USA) at 490 nm.

2.4. Cytokinesis-block micronucleus assay

Cells treated with various concentrations of 1-NP were incubated with 3 μg/mL cytochalasin-B for 24 h, washed twice with PBS, resuspended in 75 mM potassium chloride, fixed, and placed in a mixture of glacial acetic acid:methanol (1:3). The pellet was resuspended and pipetted on a cold, dry glass slide. The slides were stained with 2% Giemsa stain for 15 min and then analyzed under a microscope with transmitted light. On each slide, at least 500 binucleated macrophages were scored per culture to determine the micronucleus (MN) frequency (Tsai et al., 2020).

2.5. Alkaline single cell gel electrophoresis assay

Cells treated with various concentrations of 1-NP for 24 h were embedded in 1% low melting agarose on microscope slides precoated with 1% normal melting point agarose. The slides were first placed in a cold tray for agarose to solidification and then in a lysis buffer, pH 10 (2.5 M NaCl, 100 mM EDTA, 10 mM Tris-HCl, 1% Triton X-100, 200 mM NaOH, 34.1 mM *N*-lauroylsarcosine, and 10% DMSO) for 1 h on ice in the dark. The slides were washed and incubated in an alkaline solution (0.3 M NaOH and 1 mM EDTA) for 40 min at 4 °C. After horizontal electrophoresis (29 V, 1.15 V/cm electrophoresis platform) at room temperature, the slides were stained with ethidium bromide and observed under a fluorescence microscope. DNA damage was analyzed using the image analysis system Comet v.3. To quantify DNA damage, single cell gel electrophoresis (COMET) parameters, including tail length, tail moment, olive moment, and percent tail DNA (% tail DNA), were evaluated (Tsai et al., 2020).

2.6. Caspase-3 and -9 activity assay

Caspase activity was assayed using a fluorometric assay kit in accordance with the manufacturer's instructions. Cells treated with various concentrations of 1-NP for 24 h were washed, collected, and lysed. The lysate was centrifuged, and the protein content was detected through the Bradford assay. Equal amounts of protein lysate were incubated with the fluorogenic substrates of caspase-3 and -9. The fluorescence intensity of each sample was measured using a Synergy HT Multi-Mode Microplate Reader (Biotek, Winooski, VT, USA) at 400-nm excitation and 505-nm emission wavelengths. Fluorescence intensity was expressed as a relative fluorescence unit (Huang et al., 2020).

2.7. Preparation of nuclear fractions and Western blot assay

After treatment with the indicated concentration of 1-NP for 24 h,

total protein from whole cells was extracted in the RIPA lysis buffer containing protease and phosphatase inhibitors. The cytosolic and nuclear fraction was isolated using the cytoplasmic and nuclear protein extraction kit. Protein extracts were resolved on SDS–PAGE gels, transferred to polyvinylidene fluoride membranes, and fixed in 5% skim milk, as described previously (Huang et al., 2020). The membranes were treated with antibodies against caspase-3, caspase-8, caspase-9, p53, phospho-p53, PARP-1, β-actin, and GAPDH for 2 h. The membranes were washed before the addition of the horseradish peroxidase–conjugated secondary antibody. The protein bands were visualized and quantified with enhanced chemiluminescence labeling using an Infinity CX5 detection system (Vilber Lourmat, France).

2.8. Statistical analysis

Statistical analysis was performed with SPSS software (SPSS inc., Chicago, IL, USA). One-way analysis of variance followed by the posthoc Bonferroni's test was used to multiple group comparisons. Data are expressed as the mean ± standard deviation (S.D.) of results obtained from three independent experiments. $P < .05$ indicated statistical significance for all tests.

3. Results

3.1. Cytotoxic effects of 1-NP on RAW 264.7 macrophages

The cytotoxic effect of 1-NP on RAW 264.7 macrophages was measured through an LDH assay (Fig. 1). RAW 264.7 cells incubated with 3 μM 1-NP for 48 h or 10 μM 1-NP for 6 h exhibited significant cytotoxicity ($P < .05$). Thus, 1-NP induced cytotoxicity in a concentration- and time-dependent manner.

3.2. Effects of 1-NP on DNA damage in RAW 264.7 macrophages

The DNA damage of 1-NP on RAW264.7 macrophages was measured through MN formation and COMET assay. The formation assay was used to study the effect of 1-NP–induced genotoxicity and chromosomal instability in RAW 264.7 macrophages. The induction of MN formation in the presence of 1-NP for 24 h was concentration dependent, and a significant increase was observed at 10 μM ($P < .05$; Fig. 2A). The COMET assay was used to assess the effects of 1-NP–induced DNA single-strand breaks in RAW 264.7 macrophages. A statistically significant and concentration-dependent upregulation in tail length, tail moment, olive moment, and % tail DNA was induced by 1-NP. The increase was significant when the cells were treated with 10 μM 1-NP for 24 h ($P < .05$; Fig. 2B and C).

3.3. Effects of 1-NP on the nuclear accumulation and phosphorylation of p53 in RAW 264.7 macrophages

DNA damage induces the nuclear accumulation and phosphorylation of p53 (Sborchia et al., 2019; Guttenplan et al., 2019). We measured the nuclear accumulation of p53 induced by 1-NP in RAW264.7 macrophages. As shown in Fig. 3A, the cytosolic level of p53 remained unchanged in the presence of up to 50 μM 1-NP. By contrast, 1-NP induced the nuclear accumulation of p53 in a concentration-dependent manner, and a significant increase was observed at 10 μM (Fig. 3B, $P < .05$). The values for p53 phosphorylation levels are shown in Fig. 3C. Phosphorylation of p53 was induced by 1-NP in a concentration-dependent manner, and a significant increase was observed at 10 μM ($P < .05$).

3.4. Effects of 1-NP on mitochondrial cytochrome c release in RAW 264.7 macrophages

Mitochondrial cytochrome *c* release was induced by p53 phosphorylation (Deng et al., 2006). Changes in the level of mitochondrial cytochrome *c* release induced by 1-NP are displayed in Fig. 4. The decrease in mitochondrial cytochrome *c* levels by 1-NP was concentration dependent, and a significant decrease was observed at 10 μM ($P < .05$). However, the increase in cytosolic cytochrome *c* levels in the presence of 1-NP was concentration dependent, and a significant increase was observed at 10 μM ($P < .05$).

3.5. Effects of 1-NP on the activation and cleavage of procaspase-3 and -9 in RAW 264.7 macrophages

The activation and cleavage of procaspase-3 and -9 were induced by mitochondrial cytochrome *c* release (Reiners Jr et al., 2002; Chipoy et al., 2007). To study the effect of 1-NP on the activation and cleavage of procaspase-3 and procaspase-9, we used a fluorometric assay and Western blot assay, respectively. The activation (Fig. 5A) and cleavage (Fig. 5B) of procaspase-3 and -9 were induced by 1-NP in a concentration-dependent manner, with a significant increase at 10 μM ($P < .05$).

3.6. Effects of 1-NP on PARP-1 cleavage in RAW 264.7 macrophages

PARP-1 cleavage was induced by caspase-3 activation (Li et al., 2020). We used Western blotting to study the effect of 1-NP on PARP-1 cleavage. As shown in Fig. 8, 1-NP induced PARP-1 cleavage in a concentration-dependent manner, and a significant increase was observed at 10 μM (Fig. 6, $P < .05$).

3.7. Effects of PARP inhibitor, caspase-3 inhibitor, p53 inhibitor on 1-NP-induced cytotoxicity and genotoxicity via PARP-1 cleavage, caspase-3 activation, p53 phosphorylation

To demonstrate the effects of PARP-1, caspase-3, and p53 involved in cytotoxicity and genotoxicity induced by 1-NP. We used the PARP-1 inhibitor, caspase-3 inhibitor, and p53 inhibitor containing 3-aminobenzamide at 10 mM, z-DEVD-fmk at 1 μM, and pifithrin-α at 10 μM, respectively, pretreatment with the RAW264.7 cells for 30 min and then incubated with 1-NP at 30 μM for 24 h. As shown in Fig. 7(A) and (B), the cytotoxicity and genotoxicity were significantly induced by 1-NP ($P < .05$). Pretreatment with 3-aminobenzamide, z-DEVD-fmk, pifithrin-α markedly reduced the cytotoxicity and genotoxicity induced by 1-NP ($P < .05$). In addition, pretreatment with 3-aminobenzamide, z-DEVD-fmk, pifithrin-α markedly reduced the PARP-1 cleavage induced
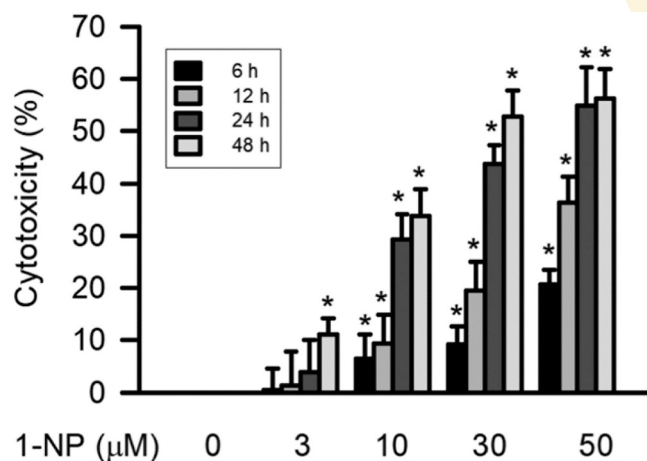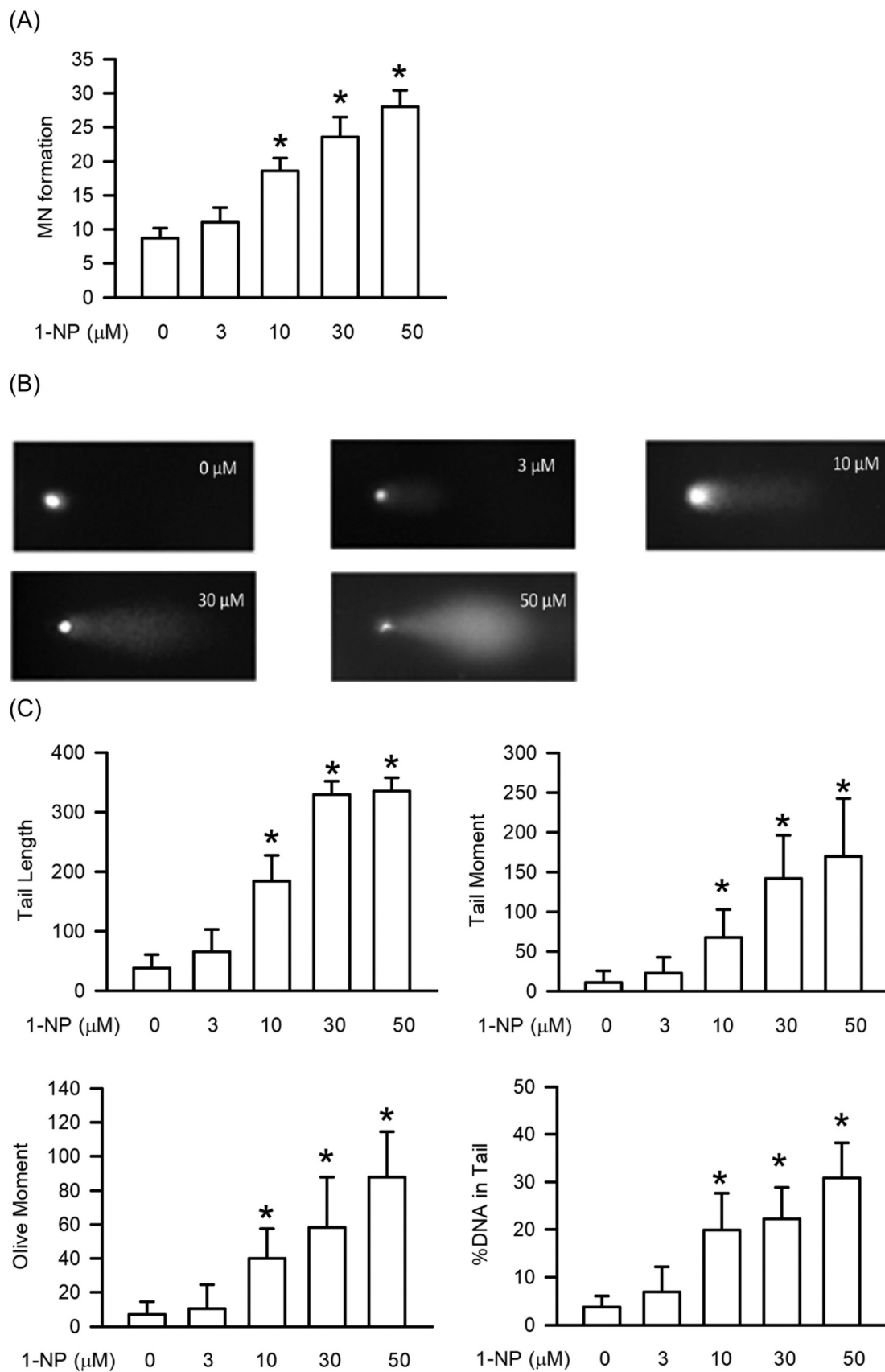

Fig. 1. Effects of 1-NP on cytotoxic effect. RAW264.7 macrophages were incubated with 1-NP at indicated concentration for various duration. Cytotoxicity was detected by the LDH assay. Values are expressed as mean ± S.D. (n = 3). *$P < .05$ considered significantly different from the control values.

(A)

(B)

(C)

Fig. 2. Effects of 1-NP on DNA damage. (A) MN formation of RAW264.7 macrophages were incubated with 1-NP at indicated concentration for 24 h. (A) Gel electrophoresis of RAW264.7 macrophages were incubated with 1-NP at indicated concentration for 24 h. (B) DNA damage was quantified as tail length, tail moment, olive moment, and % tail DNA Values are expressed as mean ± S.D. (n = 3). *$P < .05$ considered significantly different from the control values.
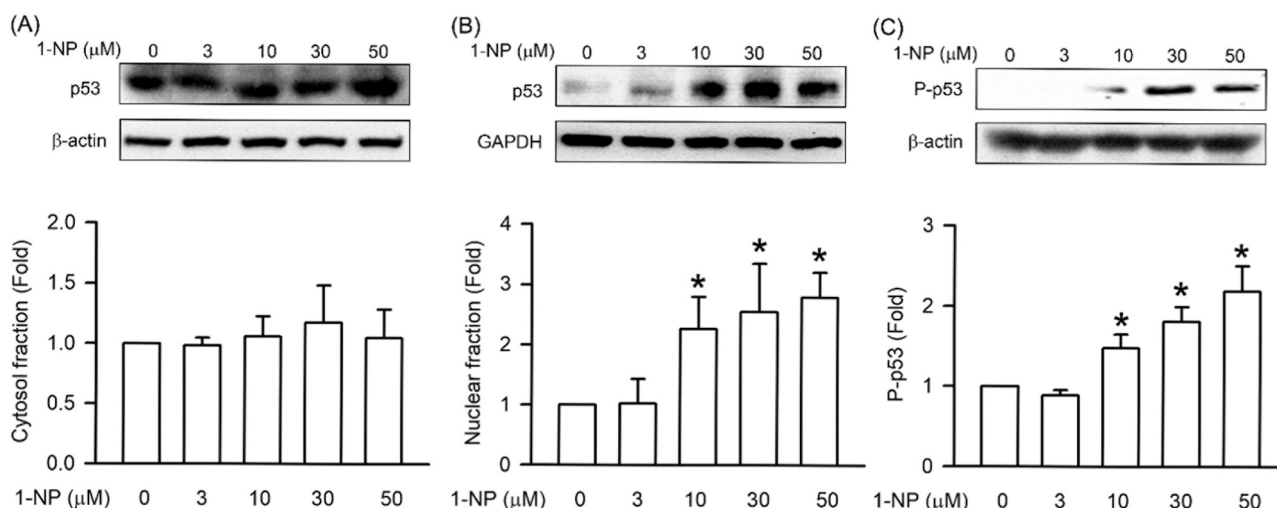
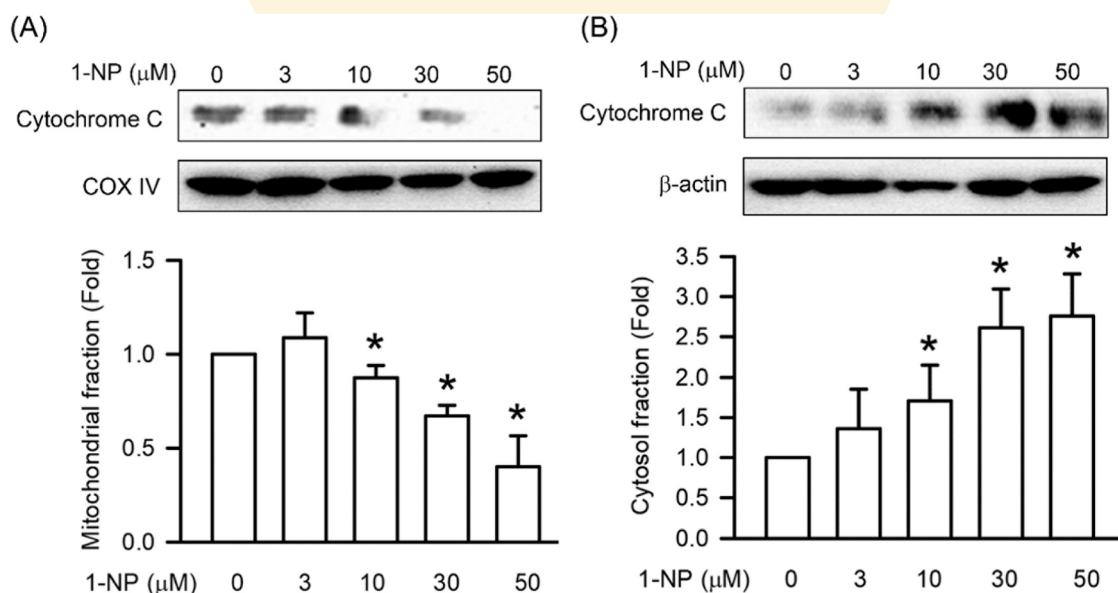**Fig. 3.** Effects of 1-NP on nuclear accumulation and phosphorylation of p53. RAW264.7 macrophages were incubated with 1-NP at indicated concentration for 24 h. Cytosolic expression (A), nuclear expression (B), and phosphorylation (C) of p53 were measured by Western blot assay. The change in fold of p53 expression and phosphorylation between the treated and control groups were calculated. Values are expressed as mean ± S.D. (n = 3). *$P < .05$ considered significantly different from the control values.


Fig. 4. Effects of 1-NP on mitochondrial cytochrome *c* release. RAW264.7 macrophages were incubated with 1-NP at indicated concentration for 24 h. Mitochondrial expression (A) and cytosolic expression (B) of cytochrome *c* were measured by Western blot assay. The change in fold of cytochrome *c* expression between the treated and control groups were calculated. Values are expressed as mean ± S.D. (n = 3). *$P < .05$ considered significantly different from the control values.

by 1-NP (Fig. 7(C), $P < .05$). Pretreatment with z-DEVD-fmk and pifi-thrin-α markedly reduced the caspase-3 activity induced by 1-NP (Fig. 7 (D), $P < .05$). Pretreatment with 3-aminobenzamide could not effectively inhibit the caspase-3 activity induced by 1-NP (Fig. 7(D)). Pretreatment with pifithrin-α markedly reduced the p53 phosphorylation induced by 1-NP (Fig. 7(E), $P < .05$). Pretreatment with 3-aminobenzamide and z-DEVD-fmk could not effectively inhibit the p53 phosphorylation induced by 1-NP (Fig. 7(E)).

4. Discussion

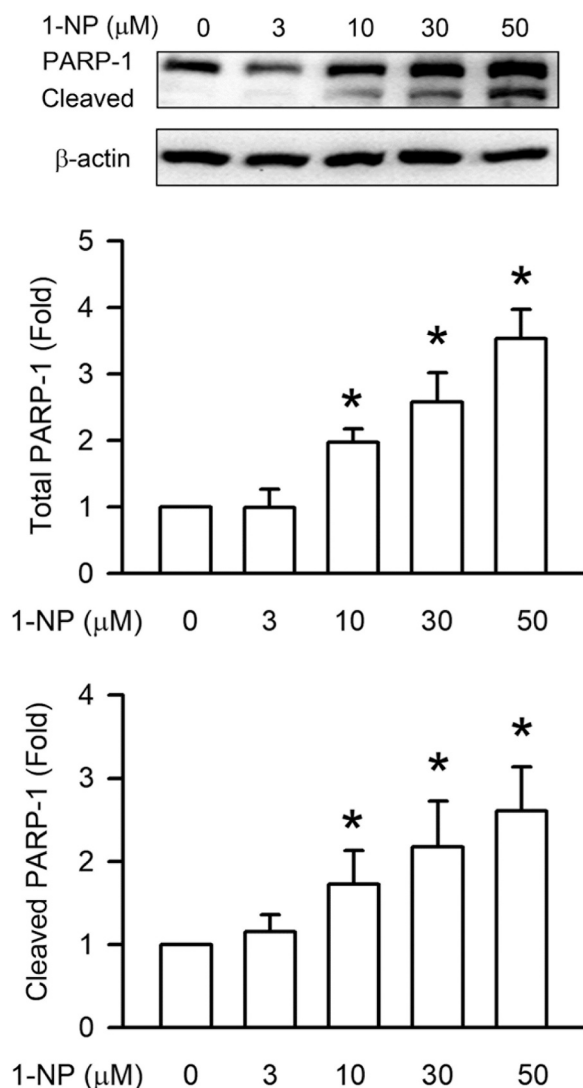Immunotoxicity induced by environmental pollutants is a major health concern worldwide. Diesel exhaust, a mixture of particles and gases, is the main source of environmental pollutants. Of the more than 200 nitro-PAHs present in diesel exhaust, 1-NP is the most abundant (Scheepers et al., 1995). Therefore, 1-NP is a chemical indicator for diesel exhaust in the environment and human body (Scheepers et al.,

(A)

(B)
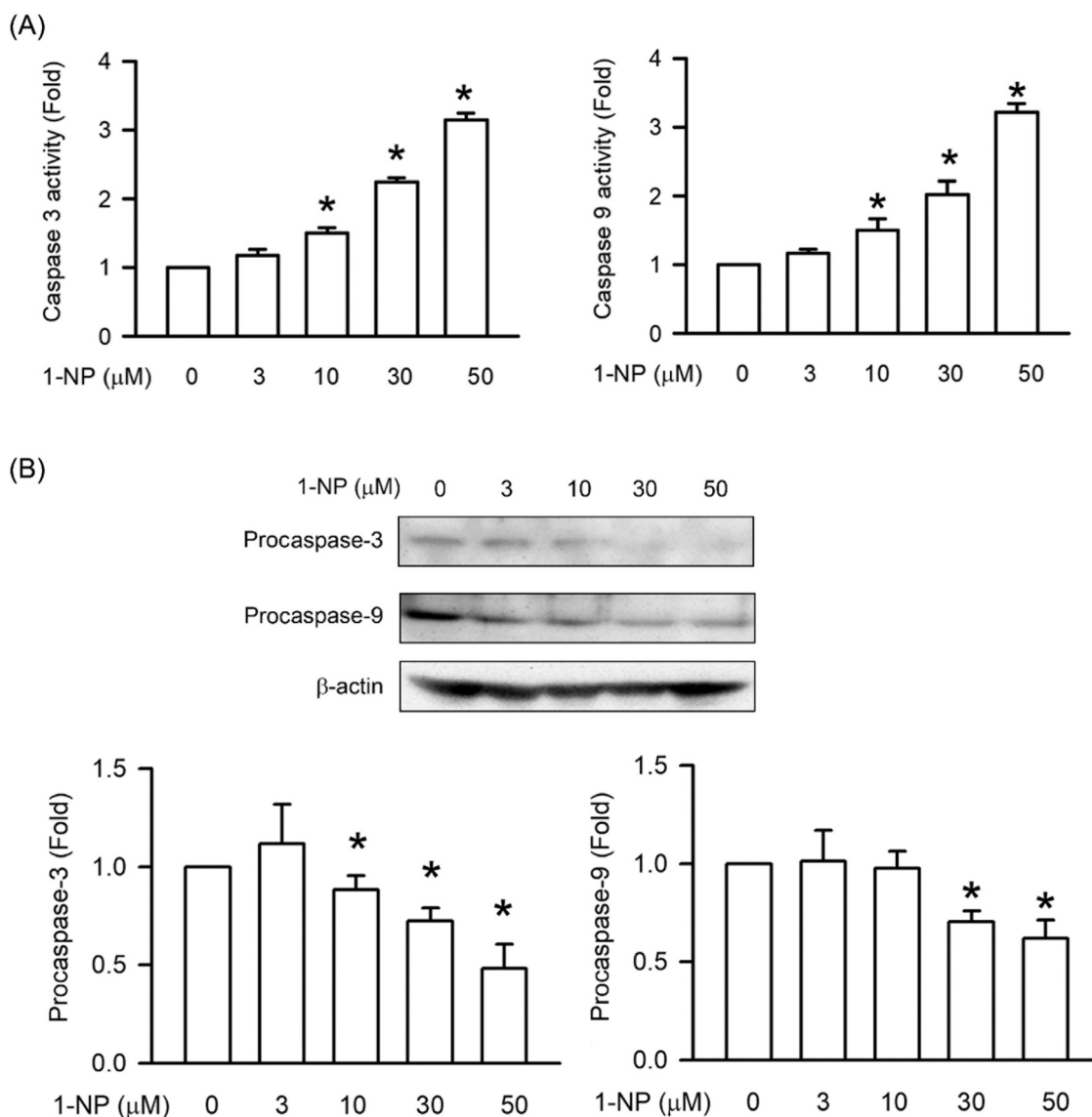
Fig. 5. Effects of 1-NP on activation and cleavage of procaspase-3 and -9. RAW264.7 macrophages were incubated with 1-NP at indicated concentration for 24 h. (A) Activation of caspase-3 and -9 were measured by fluorometric assay kit. (B) Cleavage of procaspase-3 and -9 were measured by Western blot assay. (C) The change in fold of procaspase-3 and -9 cleavage between the treated and control groups were calculated. Values are expressed as mean ± S.D. (n = 3). *$P < .05$ considered significantly different from the control values.

1995). In previous study, 1-NP has been found at concentrations of up to 57 pg/m^3 from air particle over urban and suburban areas in Michigan (Gibson, 1986). Recent retrospective research has found that the concentration of 1-NP exposures in air ranged from 10 to 1000 pg/m^3 and 1 to 100 pg/m^3 in urban areas and rural areas, respectively (IARC, 2014). Due to daily exposure would be resulted in the accumulation of toxic concentrations in humans or animals. After 13 weeks, there is no death case in 20 F344/N rats which are exposed to 1-NP aerosol, 6 h per day, 5 days per week (Chan, 1996). At the same study purpose that squamous metaplasia of the laryngeal and bronchial respiratory epithelium induced by 1-NP in the rats (Chan, 1996). Cellular morphology exchange, proliferation downregulation, and cytotoxicity upregulation exist in 1-NP-treated hepatoma cell lines, Hepa1c1c7 cells (Asare et al., 2008). The approximately 50% cytotoxic effect induced by 1-NP after 2 h incubation at 1 μM in the primary culture of rat hepatocytes (de

Mejía and Ramírez-Mares, 2002). In the primary culture of rat tracheal epithelial cells, approximately 50% cytotoxic effect induced by 1-NP after 24 h incubation at the concentration of 9 μM (Mitchell and Thomassen, 1990). 1-NP could not induce cytotoxicity in Chinese hamster lung fibroblast for concentration up to 240 μM and 12 h incubation (Edwards et al., 1986). Based on these studies suggested that the different degree of toxic effects induced by 1-NP in various cell types. Due to no evidence showing the toxic effect was induced by 1-NP in RAW264.7 macrophages. Therefore, we have further studied the toxic effects in RAW264.7 macrophages incubated with 1-NP at the concentration from 3 to 50 μM for 6 to 48 h. The cytotoxicity induced by 1-NP is concentration- and time- dependent manner in RAW 264.7 macrophages. According to the results of cytotoxicity at present study, the concentration of 1-NP required to achieve an approximately 50% cytotoxicity was 30 μM after a 24 h or 48 h incubation. These results suggest

Fig. 6. Effects of 1-NP on PARP-1 cleavage. RAW264.7 macrophages were incubated with 1-NP at indicated concentration for 24 h. Cleavage of PARP-1 was measured by Western blot assay. The change in fold of PARP-1 cleavage between the treated and control groups were calculated. Values are expressed as mean ± S.D. (n = 3). *$P < .05$ considered significantly different from the control values.

strand breakage, and DNA fragmentation in a concentration-dependent manner. Moreover, genotoxicity induced by various concentrations of 1-NP exhibits a similar trend to cytotoxicity, suggesting that genotoxicity is partially involved in 1-NP-induced cytotoxicity in RAW 264.7 macrophages.
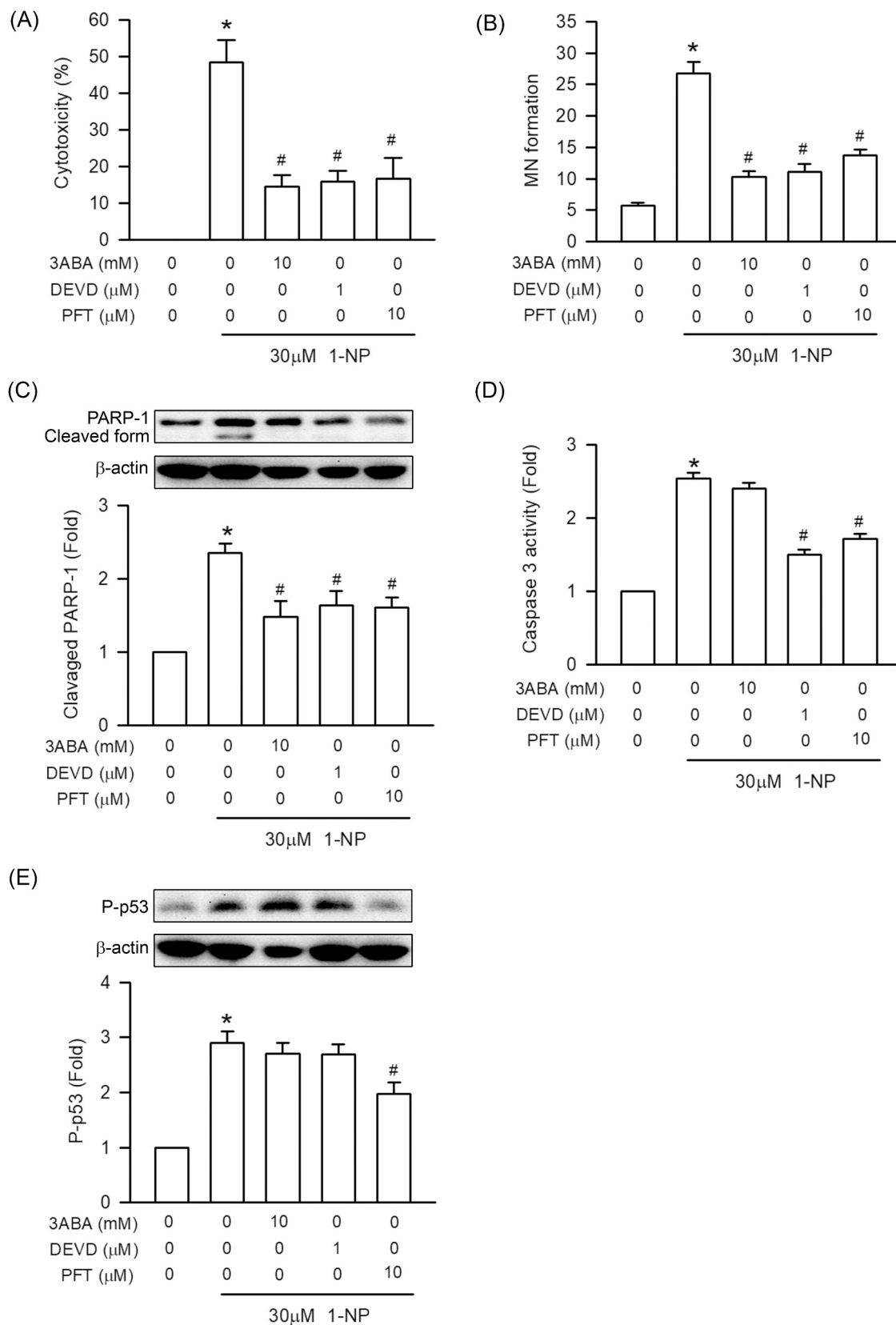
The protein p53 is a key sensor of genotoxic stress (Murray-Zmijewski et al., 2008). Under genotoxic stress, p53 phosphorylation and nuclear translocation promote the accumulation of DNA damage, leading to mutagenicity and carcinogenicity (Sborchia et al., 2019; Guttenplan et al., 2019). The phosphorylation of p53 is stimulated by 1-NP in 2 hepatoma cell lines, HepG2 and Hepa1c1c7 (Su et al., 2008; Asare et al., 2008, 2009). Our finding that 1-NP-induces p53 phosphorylation is consistent with those of previous studies. To the best of our knowledge, this is the first evidence that shows the nuclear translocation of p53 induced by 1-NP in RAW 264.7 macrophages.

Under genotoxic stress, cytoplasmic p53 interacts with members of the B cell lymphoma-2 (bcl-2) family, which leads to the permeabilization of the outer mitochondrial membrane (Kroemer et al., 2015). Cytochrome *c* released from the mitochondrial intermembrane space through the bcl-2 protein family integral insertion into the outer mitochondrial membrane induced by p53 phosphorylation (Kroemer et al., 2015). No study has reported that 1-NP treatment induces cytochrome *c* release (Deng et al., 2006). We have shown for the first time that 1-NP–induced cytochrome *c* release induces genotoxicity and cytotoxicity in RAW 264.7 macrophages. The cleavage of procaspase-9, facilitated by cytoplasmic cytochrome *c*, converts it into the enzymatically active caspase-9, which processes procaspase-3 into activated caspase-3 (Reiners et al., 2002). A study reported that 1-NP activates caspase-3 in hepatoma cells and bronchial epithelial cells (Oya et al., 2011; Asare et al., 2009). In RAW 264.7 macrophages treated with 1-NP for 24 h, the activation and upregulation of caspase-3 and -9 were observed to be concentration dependent. Thus, 1-NP–induced genotoxicity activates caspase-3 and -9 through p53 phosphorylation and cytochrome *c* release.

PARP-1, an abundant and ubiquitous nuclear protein, is highly sensitive to DNA damage and genotoxicity. PARP-1 initiates poly (ADP-ribosylation) to synthesize poly (ADP-ribose), which facilitates DNA repair and replication or triggers DNA degradation (Wang et al., 2019; Caron et al., 2019). PARP-1 cleavage by caspase-3 inhibits DNA damage repair and replication and increases DNA damage (Li et al., 2020). Moreover, 1-NP was shown to induce PARP-1 cleavage in hepatoma and bronchial epithelial cells (Su et al., 2008; Oya et al., 2011). In the present study, 1-NP induced PARP-1 cleavage in a concentration-dependent manner in RAW 264.7 macrophages. Thus, PARP-1 cleavage is induced by 1-NP through caspase-3 activation and leads to genotoxicity.

The various inhibitors can be used to the intracellular signal pathway involved in cytotoxicity and genotoxicity induced by 1-NP. 3-aminobenzamide is the inhibitor of PARP. z-DEVD-fmk is the inhibitor of caspase-3. Pifithrin-α is the inhibitor of p53. The first, cytotoxicity and genotoxicity were reduced by the 3-aminobenzamide, z-DEVD-fmk, pifithrin-α in 1-NP-treated RAW264.7 macrophages. The second, 1-NP-induced PARP-1 cleavage was inhibited by 3-aminobenzamide, z-DEVD-fmk, pifithrin-α. The third, 1-NP-induced caspase-3 activation was inhibited by z-DEVD-fmk and pifithrin-α not 3-aminobenzamide. The last, 1-NP induced p53 phosphorylation was inhibited by pifithrin-α, not 3-aminobenzamide and z-DEVD-fmk. These results indicated cytotoxicity and genotoxicity induced by 1-NP via PARP-1 through caspase-3 and its upstream p53.

As shown in Fig. 8, our results revealed that cytotoxicity induced by 1-NP follows a similar trend in terms of concentration as genotoxicity, including MN formation and DNA strand breakage, in the RAW264.7 macrophages. Western blot analysis revealed phosphorylation and nuclear translocation of p53, mitochondrial cytochrome *c* release into cytosol, and procaspase-3 and -9 cleavage could be induced by 1-NP. In addition, the caspase-3 and -9 activation would be induced by 1-NP. Cytotoxicity, genotoxicity, and PARP-1 cleavage were reduced by 3-

that the cytotoxic effect of 1-NP reaches saturation by 24 h in RAW264.7 macrophages. Therefore, following-up research of toxic mechanism induced by 1-NP was carried out for 24 h incubation.

Genotoxicity is an important type of cytotoxicity. Genotoxic compounds exert various biological changes, including mutagenicity, carcinogenicity, and DNA damage (Botero et al., 2020). The International Agency for Research on Cancer classified 1-NP as a group 2A agent, suggesting that it is carcinogenic to humans (IARC, 2014). Genotoxicity is the ability of a compound to induce DNA damage, including MN formation, DNA strand breakage, and DNA fragmentation (Wu et al., 2007; Huang, 2018). A study revealed that 1-NP induces MN formation during the germination of barley (*Hordeum vulgare*) and early growth of tilapia (*Oreochromis niloticus*) (Bacolod et al., 2017; Yun et al., 2019). Moreover, 1-NP causes DNA single-strand damage, as measured through a COMET assay, in keratinocytes, human umbilical vein endothelial cells, alveolar basal epithelial cells, and placental trophoblasts (Shang et al., 2017; Andersson et al., 2009; Fullove and Yu, 2013; Wang et al., 2020). Our results demonstrate that 1-NP induces MN formation, DNA

Fig. 7. Effects of PARP inhibitor, caspase-3 inhibitor, p53 inhibitor on cytotoxicity, genotoxicity, PARP-1 cleavage, caspase-3 activation, p53 phosphorylation induced by 1-NP. The RAW264.7 macrophages incubated with 3-aminobenzamide (3ABA) at 10 mM, z-DEVD-fmk (DEVD) at 1 μM, or pifithrin-α (PFT) at 10 μM for 30 min, and then the cells treated with 1-NP at 30 μM for 24 h. (A) Cytotoxicity was detected by LDH assay. (B) Genotoxicity was detected by MN formation assay, respectively. (C) Cleavage of PARP-1 and (E) phosphorylation of p53 were measured by Western blot assay. (D) Activation of caspase-3 was measured by fluorometric assay kit. Values are expressed as mean ± S.D. (n = 3). *$P < .05$ considered significantly different from the control values. #$P < .05$ considered significantly different from the 1-NP group.
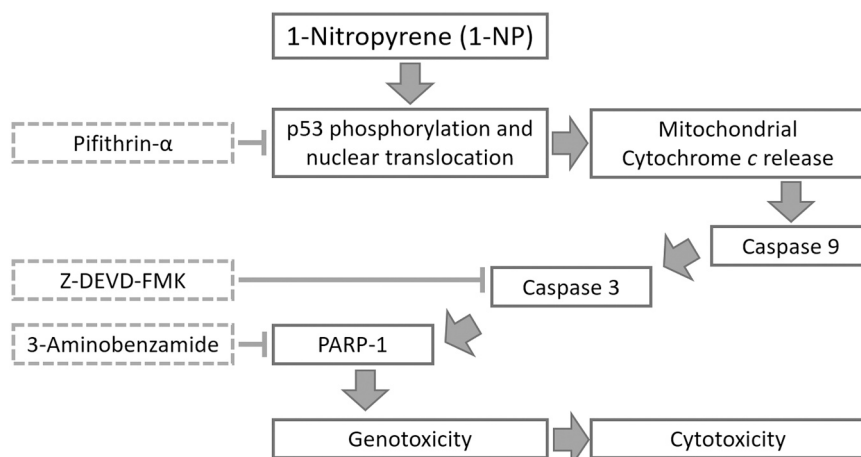
Fig. 8. Schemes of the mechanism of the 1-NP-induced genotoxicity and cytotoxicity in RAW264.7 cells.

aminobenzamide, z-DEVD-fmk, pifithrin-α in 1-NP-treated RAW264.7 macrophages. Activation of caspase-3 was reduced by z-DEVD-fmk and pifithrin-α. Phosphorylation of p53 was reduced by pifithrin-α. These results suggested 1-NP induced cytotoxicity and DNA damage via PARP-1 cleavage through caspase-3 activation. More, 1-NP induced caspase-3 and -9 activation through p53-dependent mitochondrial cytochrome *c* release. Our findings suggested that 1-NP-mediates cytotoxicity and genotoxicity by PARP-1 cleavage via caspase-3 and -9 activation through cytochrome *c* release from mitochondria and its upstream factors p53-dependent pathway in macrophages.

CRediT authorship contribution statement

Sheng-Wen Wu: Conceptualization, Formal analysis, Investigation, Data curation, Writing - original draft, Writing - review & editing, Supervision, Funding acquisition. **Chun-Hung Su:** Conceptualization, Formal analysis, Investigation, Data curation, Writing - original draft, Writing - review & editing. **Yung-Chyuan Ho:** Formal analysis, Investigation, Data curation, Writing - original draft. **Rosa Huang-Liu:** Formal analysis, Data curation, Writing - original draft. **Ching-Chi Tseng:** Formal analysis, Investigation, Data curation, Writing - original draft. **Yun-Wei Chiang:** Investigation, Data curation. **Kun-Lin Yeh:** Investigation, Data curation. **Shiuan-Shinn Lee:** Investigation, Data curation, Visualization. **Wen-Ying Chen:** Data curation, Visualization. **Chun-Jung Chen:** Investigation, Visualization. **Yi-Ching Li:** Investigation, Visualization. **Chien-Ying Lee:** Writing - review & editing, Supervision, Project administration. **Yu-Hsiang Kuan:** Conceptualization, Writing - review & editing, Supervision, Project administration, Funding acquisition.

Declaration of Competing Interest

The authors declare that they have no known competing financial interests or personal relationships that could have appeared to influence the work reported in this paper.

Acknowledgement

References

Andersson, H., Piras, E., Demma, J., Hellman, B., Brittebo, E., 2009. Low levels of the air pollutant 1-nitropyrene induce DNA damage, increased levels of reactive oxygen species and endoplasmic reticulum stress in human endothelial cells. Toxicology 262, 57–64.

André, V., Billet, S., Pottier, D., Le Goff, J., Pottier, I., Garçon, G., Shirali, P., Sichel, F., 2011. Mutagenicity and genotoxicity of PM2.5 issued from an urbano-industrialized area of Dunkerque (France). J. Appl. Toxicol. 31, 131–138.

Asare, N., Landvik, N.E., Lagadic-Gossmann, D., Rissel, M., Tekpli, X., Ask, K., Låg, M., Holme, J.A., 2008. 1-Nitropyrene (1-NP) induces apoptosis and apparently a non-apoptotic programmed cell death (paraptosis) in Hepa1c1c7 cells. Toxicol. Appl. Pharmacol. 230, 175–186.

Asare, N., Tekpli, X., Rissel, M., Solhaug, A., Landvik, N., Lecureur, V., Podechard, N., Brunborg, G., Låg, M., Lagadic-Gossmann, D., Holme, J.A., 2009. Signalling pathways involved in 1-nitropyrene (1-NP)-induced and 3-nitrofluoranthene (3-NF)-induced cell death in Hepa1c1c7 cells. Mutagenesis 24, 481–493.

Bacolod, E.T., Uno, S., Villamor, S.S., Koyama, J., 2017. Oxidative stress and genotoxicity biomarker responses in tilapia (Oreochromis niloticus) exposed to environmental concentration of 1-nitropyrene. Mar. Pollut. Bull. 124, 786–791.

Botero, M.L., Mendoza, C., Arias, S., Hincapié, O.D., Agudelo, J.R., Ortiz, I.C., 2020. In vitro evaluation of the cytotoxicity, mutagenicity and DNA damage induced by particle matter and gaseous emissions from a medium-duty diesel vehicle under real driving conditions using palm oil biodiesel blends. Environ. Pollut. 265, 115034.

Caron, M.C., Sharma, A.K., O'Sullivan, J., Myler, L.R., Ferreira, M.T., Rodrigue, A., Coulombe, Y., Ethier, C., Gagné, J.P., Langelier, M.F., Pascal, J.M., Finkelstein, I.J., Hendzel, M.J., Poirier, G.G., Masson, J.Y., 2019. Poly(ADP-ribose) polymerase-1 antagonizes DNA resection at double-strand breaks. Nat. Commun. 10, 2954.

Chan, Po, 1996. NTP Technical Report on the Toxicity Studies of 1-Nitropyrene (CAS No. 5522-43-0) Administered by Inhalation to F344/N Rats. Toxic Report Sereis, 34. pp. 1-D2.

Chang, C.Y., Chiang, C.Y., Chiang, Y.W., Lee, M.W., Lee, C.Y., Chen, H.Y., Lin, H.W., Kuan, Y.H., 2020. Toxic effects of urethane dimethacrylate on macrophages through caspase activation, mitochondrial dysfunction, and reactive oxygen species generation. Polymers 12, 1398.

Chipoy, C., Brounais, B., Trichet, V., Battaglia, S., Berreur, M., Oliver, L., Juin, P., Rédini, F., Heymann, D., Blanchard, F., 2007. Sensitization of osteosarcoma cells to apoptosis by oncostatin M depends on STAT5 and p53. Oncogene 26, 6653–6664.

Deng, X., Gao, F., Flagg, T., Anderson, J., May, W.S., 2006. Bcl2's flexible loop domain regulates p53 binding and survival. Mol. Cell. Biol. 26, 4421–4434.

Edwards, M.J., Parry, J.M., Batmanghelich, S., Smith, K., 1986. Toxicity and DNA damage induced by 1-nitropyrene and its derivatives in Chinese hamster lung fibroblasts. Mutat. Res. 163, 81–89.

Fullove, T.P., Yu, H., 2013. DNA damage and repair of human skin keratinocytes concurrently exposed to pyrene derivatives and UVA light. Toxicol. Res. 2, 193–199.

Gao, Y., Ji, H., 2018. Characteristics of polycyclic aromatic hydrocarbons components in fine particle during heavy polluting phase of each season in urban Beijing. Chemosphere 212, 346–357.

Gibson, T.L., 1986. Sources of nitroaromatic mutagens in atmosphere polycyclic organic matter. J. Air Pollut. Control Assoc. 36, 1022–1025.

Guttenplan, J.B., Chen, K.M., Sun, Y.W., Shalaby, N.A.E., Kosinska, W., Desai, D., Gowda, K., Amin, S., El-Bayoumy, K., 2019. Effects of the tobacco carcinogens N′-nitrosonornicotine and dibenzo(a,l)pyrene individually and in combination on DNA damage in human oral leukoplakia and on mutagenicity and mutation profiles in lacI mouse tongue. Chem. Res. Toxicol. 32, 1893–1899.

Huang, F.M., Chang, Y.C., Lee, S.S., Ho, Y.C., Yang, M.L., Lin, H.W., Kuan, Y.H., 2018. Bisphenol A exhibits cytotoxic or genotoxic potential via oxidative stress-associated

mitochondrial apoptotic pathway in murine macrophages. Food Chem. Toxicol. 122, 215–224.

Huang, F.M., Chang, Y.C., Su, C.H., Wu, S.W., Lee, S.S., Lee, M.W., Yeh, K.L., Chiang, C. Y., Tu, D.G., Lu, Y.C., Kuan, Y.H., 2020. Rutin-protected BisGMA-induced cytotoxicity, genotoxicity, and apoptosis in macrophages through the reduction of the mitochondrial apoptotic pathway and induction of antioxidant enzymes. Environ. Toxicol. 36, 45–54. https://doi.org/10.1002/tox.23009.

IARC, 2014. Diesel and Gasoline Engine Exhausts and Some Nitroarenes. IARC Monographs on the Evaluation of Carcinogenic Risks to Humans, No. 105, pp. 9–699.

Kroemer, G., Bravo-San Pedro, J.M., Galluzzi, L., 2015. Novel function of cytoplasmic p53 at the interface between mitochondria and the endoplasmic reticulum. Cell Death Dis. 6 (3), e1698.

Li, Y., Yang, M., Meng, T., Niu, Y., Dai, Y., Zhang, L., Zheng, X., Jalava, P., Dong, G., Gao, W., Zheng, Y., 2020. Oxidative stress induced by ultrafine carbon black particles can elicit apoptosis in vivo and vitro. Sci. Total Environ. 709 (709), 135802.

de Mejía, E.G., Ramírez-Mares, M.V., 2002. Leaf extract from Ardisia compressa protects against 1-nitropyrene-induced cytotoxicity and its antioxidant defense disruption in cultured rat hepatocytes. Toxicology 179, 151–162.

Mitchell, C.E., Thomassen, D.G., 1990. Cytotoxic and transformation responses of rat tracheal epithelial cells exposed to nitrated polycyclic aromatic hydrocarbons in culture. Carcinogenesis 11, 155–158.

Murray-Zmijewski, F., Slee, E.A., Lu, X., 2008. A complex barcode underlies the heterogeneous response of p53 to stress. Nat. Rev. Mol. Cell Biol. 9, 702–712.

Oya, E., Ovrevik, J., Arlt, V.M., Nagy, E., Phillips, D.H., Holme, J.A., 2011. DNA damage and DNA damage response in human bronchial epithelial BEAS-2B cells following exposure to 2-nitrobenzanthrone and 3-nitrobenzanthrone: role in apoptosis. Mutagenesis 26, 697–708.

Reiners Jr, J.J., Caruso, J.A., Mathieu, P., Chelladurai, B., Yin, X.M., Kessel, D., 2002. Release of cytochrome c and activation of pro-caspase-9 following lysosomal photodamage involves Bid cleavage. Cell Death Differ. 9, 934–944.

Rossner, P., Strapacova, S., Stolcpartova, J., Schmuczerova, J., Milcova, A., Neca, J., Vlkova, V., Brzicova, T., Machala, M., Topinka, J., 2016. Toxic effects of the major components of diesel exhaust in human alveolar basal epithelial cells (A549). Int. J. Mol. Sci. 17, 1393.

Sato, R., Reuter, T., Hiranuma, R., Shibata, T., Fukui, R., Motoi, Y., Murakami, Y., Tsukamoto, H., Yamazaki, S., Liu, K., Saitoh, S.I., Latz, E., Miyake, K., 2020. The impact of cell maturation and tissue microenvironments on the expression of endosomal Toll-like receptors in monocytes and macrophages. Int. Immunol. 32, 785–798. https://doi.org/10.1093/intimm/dxaa055.

Sborchia, M., Keun, H.C., Phillips, D.H., Arlt, V.M., 2019. The impact of p53 on aristolochic acid I-induced gene expression in vivo. Int. J. Mol. Sci. 20, 6155.

Scheepers, P.T., Martens, M.H., Velders, D.D., Fijneman, P., van Kerkhoven, M., Noordhoek, J., Bos, R.P., 1995. 1-Nitropyrene as a marker for the mutagenicity of diesel exhaust-derived airborne particulate matter in workplace atmospheres. Environ. Mol. Mutagen. 25, 134–147.

Schuler, M., Bossy-Wetzel, E., Goldstein, J.C., Fitzgerald, D.R, P., 2000. Green p53 induces apoptosis by caspase activation through mitochondrial cytochrome c release. J. Biol. Chem. 275, 7337–7342.

Shang, Y., Zhou, Q., Wang, T., Jiang, Y., Zhong, Y., Qian, G., Zhu, T., Qiu, X., An, J., 2017. Airborne nitro-PAHs induce Nrf2/ARE defense system against oxidative stress and promote inflammatory process by activating PI3K/Akt pathway in A549 cells. Toxicol. Vitr. 44, 66–73.

Su, J.G., Liao, P.J., Huang, M.C., Chu, W.C., Lin, S.C., Chang, Y.J., 2008. Aldo-keto reductase 1C2 is essential for 1-nitropyrene's but not for benzo(a)pyrene's induction of p53 phosphorylation and apoptosis. Toxicology 244 (2–3), 257–270.

Tsai, P.K., Wu, S.W., Chiang, C.Y., Lee, M.W., Chen, H.Y., Chen, W.Y., Chen, C.J., Yang, S.F., Yeh, C.B., Kuan, Y.H., 2020. Evaluation of cytotoxicity, apoptosis, and genotoxicity induced by indium chloride in macrophages through mitochondrial dysfunction and reactive oxygen species generation. Ecotoxicol. Environ. Saf. 193, 110348.

Wang, B., Xu, S., Lu, X., Ma, Gao, L., Zhang, S.Y., Li, R., Fu, L., Wang, H., Sun, G.P., Xu, D. X., 2020. Reactive oxygen species-mediated cellular genotoxic stress is involved in 1-nitropyrene-induced trophoblast cycle arrest and fetal growth restriction. Environ. Pollut. 260, 113984.

Wang, Y., Luo, W., Wang, Y., 2019. PARP-1 and its associated nucleases in DNA damage response. DNA Repair 81, 102651.

Weaver, A.N., Yang, E.S., 2013. Beyond DNA repair: additional functions of PARP-1 in cancer. Front. Oncol. 3, 290.

Wu, F.Y., Wu, H.D., Yang, H.L., Kuo, H.W., Ying, J.C., Lin, C.J., Yang, C.C., Lin, L.Y., Chiu, T.H., Lai, J.S., 2007. Associations among genetic susceptibility, DNA damage, and pregnancy outcomes of expectant mothers exposed to environmental tobacco smoke. Sci. Total Environ. 386, 124–133.

Yun, Y., Liang, L., Wei, Y., Luo, Z., Yuan, F., Li, G., Sang, N., 2019. Exposure to Nitro-PAHs interfere with germination and early growth of Hordeum vulgare via oxidative stress. Ecotoxicol. Environ. Saf. 180, 756–761.

Zhao, L., Zhang, L., Chen, M., Dong, C., Li, R., Cai, Z., 2019. Effects of ambient atmospheric (PM2.5) 1-nitropyrene and 9-nitroanthracene on DNA damage and oxidative stress in hearts of rats. Cardiovasc. Toxicol. 19, 178–190.

RESEARCH ARTICLE

Bisphenol A induced apoptosis via oxidative stress generation involved Nrf2/HO-1 pathway and mitochondrial dependent pathways in human retinal pigment epithelium (ARPE-19) cells

Yun-Wei Chiang[1,2] | Chun-Hung Su[3,4] | Han-Yin Sun[5,6] | Shih-Pin Chen[3,4] | Chun-Jung Chen[7] | Wen-Ying Chen[8] (ID) | Chia-Che Chang[9,10,11,12] | Chuan-Mu Chen[1] | Yu-Hsiang Kuan[13,14] (ID)

[1]Department of Life Sciences, National Chung-Hsing University, Taichung, Taiwan

[2]Department of Optometry, Central Taiwan University of Science and Technology, Taichung, Taiwan

[3]Department of Internal Medicine, Chung Shan Medical University Hospital, Taichung, Taiwan

[4]Department of Internal Medicine, School of Medicine, Chung Shan Medical University, Taichung, Taiwan

[5]Department of Optometry, Chung Shan Medical University, Taichung, Taiwan

[6]Department of Ophthalmology, Chung Shan Medical University Hospital, Taichung, Taiwan

[7]Department of Education and Research, Taichung Veterans General Hospital, Taichung, Taiwan

[8]Department of Veterinary Medicine, National Chung Hsing University, Taichung, Taiwan

[9]Institute of Biomedical Sciences, National Chung Hsing University, Taichung, Taiwan

[10]Department of Biotechnology, Asia University, Taichung, Taiwan

[11]Department of Medical Research, China Medical University Hospital, Taichung, Taiwan

[12]Traditional Herbal Medicine Research Center, Taipei Medical University Hospital, Taipei, Taiwan

[13]Department of Pharmacology, School of Medicine, Chung Shan Medical University, Taichung, Taiwan

[14]Department of Pharmacy, Chung Shan Medical University Hospital, Taichung, Taiwan

Correspondence
Yu-Hsiang Kuan, Department of Pharmacology, School of Medicine, Chung Shan Medical University, No. 110, Sec. 1, Jianguo N. Rd., Taichung 402, Taiwan.
Email: kuanyh@csmu.edu.tw

Abstract

Bisphenol A (BPA) is an estrogen-like compound, and an environmental hormone, that is commonly used in daily life. Therefore, it may enter the human body through food or direct contact, causing BPA residues in blood and urine. Because most studies focused on the analysis of BPA in reproductive cells or tissues, regarding evidence the effect of BPA on human retinal pigment epithelium (ARPE-19) cells unavailable. Accordingly, the present study explored the cytotoxicity of BPA on ARPE-19 cells. After BPA treatment, the expression of Bcl-XL an antiapoptotic protein, in the mitochondria decreased, and the expression of Bax, a proapoptotic protein increased. Then the mitochondrial membrane potential was affected. BPA changed in mitochondrial membrane potential led to the release of cytochrome C, which activated caspase-9 to promote downstream caspase-3 leading to cytotoxicity. The nuclear factor (erythroid-derived 2)-like 2 (Nrf2) and heme oxygenase 1 (HO-1) pathway play a major role in age-related macular degeneration. Our results showed that expression of HO-1 and Nrf2 suppressed by BPA. Superoxide dismutase and catalase, which

Nrf2 downstream antioxidants, were degraded by BPA. AMP-activated kinase (AMPK), which can regulate the phosphorylation of Nrf2, and the phosphorylation of AMPK expression was reduced by BPA. Finally, BPA-induced ROS generation and cytotoxicity were reduced by N-acetyl-L-cysteine. Taken together, these results suggest that BPA induced ARPE-19 cells via oxidative stress, which was associated with down regulated Nrf2/HO-1 pathway, and the mitochondria dependent apoptotic signaling pathway.

KEYWORDS

apoptosis, ARPE-19 cells, bisphenol A, mitochondrial dysfunction, Nrf2/HO-1 pathway

1 | INTRODUCTION

Bisphenol A (BPA) is often used to manufacture consumable items such as pots, bottles, and tableware. BPA can even be added to the food.[1,2] Research has revealed that BPA remains in human blood and urine.[3] A study reported that BPA binds to estrogen receptor α and affects the reproductive system.[4] Another study demonstrated that amount of residual BPA in human urine and blood is related to obesity, cardiovascular disease, and type 2 diabetes.[5]

Age-related macular degeneration (AMD) is a progressive degeneration of retinal pigment epithelial cells, Bruch's membrane, and choroidal microvascular plexus due to aging.[6] AMD also causes visual distortion, and macular holes that appear gradually in the vision, and eventually cause vision loss, usually through bilateral attacks. In developed countries, AMD is the most common cause of irreversible vision loss in people aged older than 50 years. Oxidative stress and inflammation are associated with AMD. The retinal pigment epithelium (RPE) is a cell layer that closely adheres to the photoreceptor cell layer and is connected to the choroidal microvascular plexus. The RPE can absorb light, act as a blood-retinal barrier, induce phagocytosis of the outer photoreceptor segment, and secrete and provide nutrients to the retinal photoreceptor cells.[7] The RPE is crucial immunoprotected layer in the macula. Impairment of RPE function, is the primary factor leading to clinical AMD.[8]

Studies have indicated that the apoptosis of the RPE, photoreceptor cells, and inner nuclear layer in human AMD.[9] The apoptotic pathway could be mediated by mitochondria. In this pathway, cytochrome C is released from the space between mitochondrial membranes and enters the cytoplasm to activate caspase. The Bcl-2 protein family plays a role in regulating mitochondrial apoptosis.[10] Antioxidant enzymes such as superoxide dismutase (SOD) and catalase (CAT) can protect RPE and photoreceptor cells against oxidative damage.[11] Additionally, nuclear factor (erythroid-derived 2)-like 2 (Nrf2) is a vital antioxidant pathway. Under normal conditions, Nrf2 is repressed by Kelch-like ECH-associated protein 1, which exhibits a stable low concentration. Under oxidative stress, Nrf2 is transcribed, and it activates cytoprotective genes, such as heme oxygenase 1 (HO-1).[12] The Nrf2 pathway also plays a key role in many diseases, including AMD.[13] AMP-activated kinase (AMPK) has a crucial role in regulating antioxidant defense during oxidative stress. Recent studies have shown that AMPK is the potential target for inducing Nrf2 antioxidant defense.[14,15] AMD progression is due to the excessive production of free radicals and other reactive oxygen species (ROS), resulting in imbalanced antioxidant degradation.[11]

BPA is an environmental hormone that can enter the human body through food. However, the harmful effects of BPA on the retina have not been clarified. To fill this research gap, we investigated the effect of BPA induced oxidative stress and mitochondrial dysfunction through caspase and Nrf2/HO-1 pathways activation in ARPE-19 cells.

2 | MATERIALS AND METHODS

2.1 | Materials

All reagents for cell cultures, including Dulbecco's modified Eagle's medium, fetal bovine serum (FBS), trypsin protease, phosphate buffered saline (PBS), and antibiotic antimycotic solution were purchased from HyClone Laboratories (Logan, UT, USA). Anti-cytochrome C antibody was purchased from Biolegend (San Diego, California, USA). Antibody cysteine-aspartic proteases caspase-3 and caspase-9 fluorometric assay kits were purchased from Biovision (Mountain View, Calif., USA). Primary antibodies for the detection of Bcl-XL, Bax, phosphorylation of AMPK (p-AMPK), Nrf2, CAT, SOD, HO-1, and β-actin were obtained from Santa Cruz (Santa Cruz, CA, USA). BPA (HPLC grade, purity ≥96.5%), dimethyl sulfoxide (DMSO), low-melting agarose, 3-(4,5-Dimethylthiazol-2-yl)-2,5-diphenyltetrazolium bromide (MTT), propidium iodide, 2′,7′-dichlorofluorescin diacetate (DCFH-DA), thiobarbituric acid reactive substance (TBARS) assay kit, tetraethylbenzimidazolylcarbocyanine iodide (JC-1), N-acetyl-L-cysteine (NAC), and other reagents were obtained from Sigma-Aldrich (St. Louis, MO, USA). The BPA was prepared by dissolving in DMSO. The DMSO final concentration was less than 0.05% (v/v).

2.2 | Cell culture and cell treatment

The human retinal epithelial cells line, ARPE-19 cells, was purchased from the Bioresource Collection and Research Center (Hsinchu, Taiwan). The cells were cultured in Dulbecco's modified Eagle's

medium supplemented with 10% FBS, at 37°C in a humidified atmosphere containing 5% CO_2 and 95% air. After the ARPE-19 cells were incubated with or without NAC at 0.2 mM for 1 h, the cells were treated with BPA at the concentration of 0, 10, 25, 50, and 100 μM for 0, 2, 4, 8, and 24 h.

2.3 | Cell viability assay

Cell viability was assessed through a MTT reduction assay, as described previous.[16] After treatment without or with BPA, the cells were incubated with MTT at 5 mg/ml for 2 h. After the supernatant was discarded, the blue formazan intracellular crystals were dissolved in DMSO. Optical density measurements were performed at 570 nm by using a Synergy HT multi-mode microplate reader (Biotek, Winooski, VT).

2.4 | Sub-G1 formation analysis through PI staining

Apoptosis was assessed through PI staining for sub-G1, as described previously.[17] After treatment without or with BPA, the cells were fixed in 75% ethanol at −20°C for 24 h. After being washed, the cells were incubated with 1 mg/ml RNAase A and 5 μg/ml PI at 37°C for 0.5 h. Sub-G1 fluorescence was measured using BD accouri C6 flow Plus software (BD Bioscience, San Jose, CA, USA).

2.5 | Determination of ROS production

ROS generation was assessed through a semiquantitative DCFH-DA fluorescence assay, as described previously.[18] The ARPE-19 cells were incubated with 10 μM DCFH-DA for 30 min at 37°C, after which they were washed three times and then resuspended in PBS. The cells were monitored using flow cytometry at excitation and emission wavelengths of 488 and 525 nm, respectively.

2.6 | Lipid peroxidation assay

The presence of malondialdehyde (MDA) and the production of lipid peroxidation were using the TBARS assay kit as described previously.[19] After treatment, the ARPE-19 cells were homogenized and incubated with thiobarbituric acid reactive substances, including thiobarbituric acid and trichloroacetic acid. According to the manufacturer's instructions, read the absorbance at 530–540 nm by using a Synergy HT multi-mode microplate reader (Biotek, Winooski, VT).

2.7 | Caspase-3 and -9 activity assays

Caspase activity was assayed using a caspase fluorometric assay kit (Alexis Biochemicals, Enzo Life Sciences, Plymouth Meeting, PA,
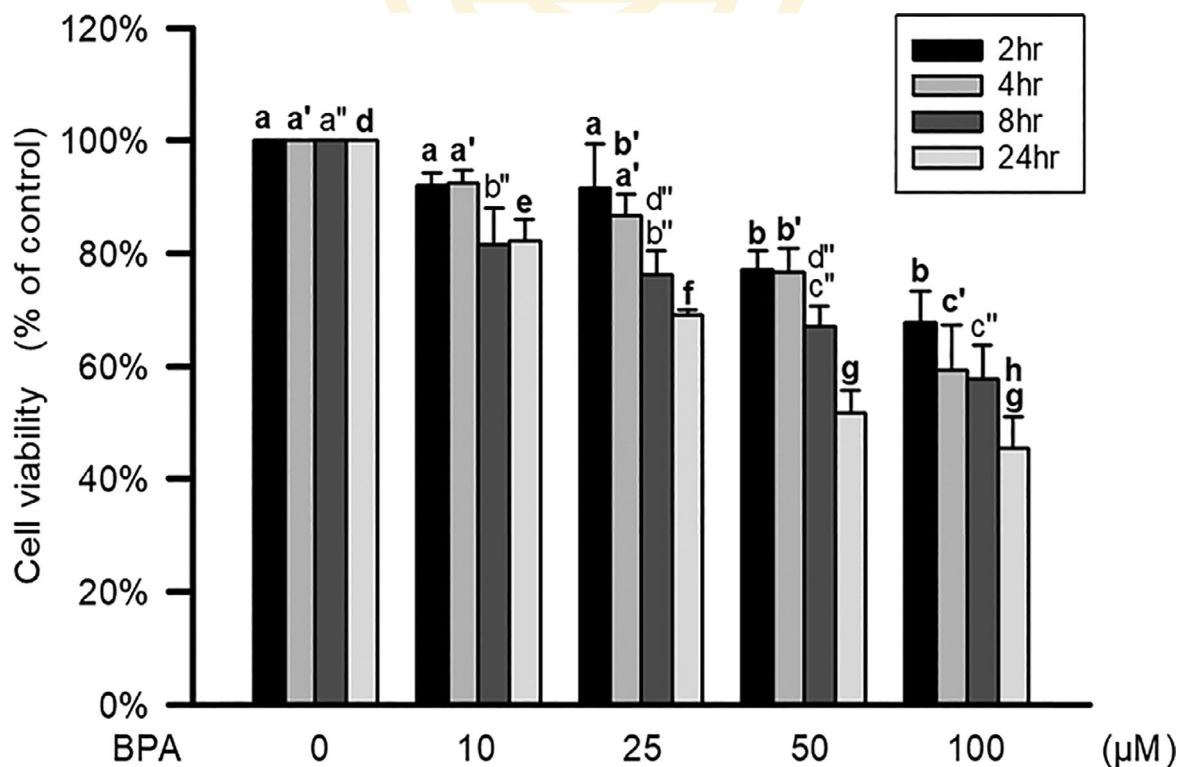
FIGURE 1 Effects of BPA on the survival rate in ARPE-19 cells. As the exposure time increased or BPA concentration increased, the survival rate had a significant decreased ($p < .05$). Data are expressed as mean ± SE ($n = 5$). The values without a common superscript letter are significantly different ($p < .05$), but they are limited to groups with the same treatment time

USA), as described previously.[20] After treatment, the cells were collected and lysed with the lysis buffer which including 250 mM HEPES pH 7.4, 25 mM CHAPS, 25 mM DTT. The cells were then incubated with DEVD-AFC (caspase-3 substrate) and LEHD-AFC (caspase-9 substrate) for 1 h. The samples were incubator for 1 h at 37°C. according to the manufacturers' instructions. The samples were assessed using a fluorescence microplate reader (Molecular Devices, CA) at excitation and emission wavelengths of 400 and 505 nm, respectively. The data are expressed as relative fluorescence units.

## 2.8 | Mitochondrial membrane potential assay

Mitochondrial membrane potential (MMP) was measured using JC-1 fluorimetry, as described previously.[17] After treatment, the ARPE-19 cells were incubated with 5 μM JC-1 at 37°C for 30 min in the dark, washed twice with PBS, then assessed using a flow cytometer (Beckton Dickinson, San Jose, CA). Upregulation enhanced green fluorescence indicated mitochondrial dysfunction.

2.9 | Cytochrome C assessment in the cytoplasm

After treatment, the cells were collected and fixed solution. The cells were permeabilized with Perm buffer and incubated with anti-cytochrome C antibody for 30 min according to the manufacturer's instruction (Biolegend, USA). Fluorescence emitted from the cytochrome C formation was measured using BD accouri C6 flow Plus software (BD Bioscience, San Jose, CA, USA).

2.10 | Western blot assay

A Western blot assay was performed as described previously.[21] After treatment, the cells were collected and lysed on ice for 30 min. Protein extracts were resolved using sodium dodecyl sulfate–polyacrylamide gel electrophoresis and then immediately transferred by electrophoresis to polyvinylidene difluoride membranes. The membranes were blocked and incubated with the indicated primary antibodies, including Bcl-XL, Bax, p-AMPK, Nrf2, CAT, SOD, HO-1, and β-actin. After being washed, the membranes were incubated with horseradish peroxidase-conjugated
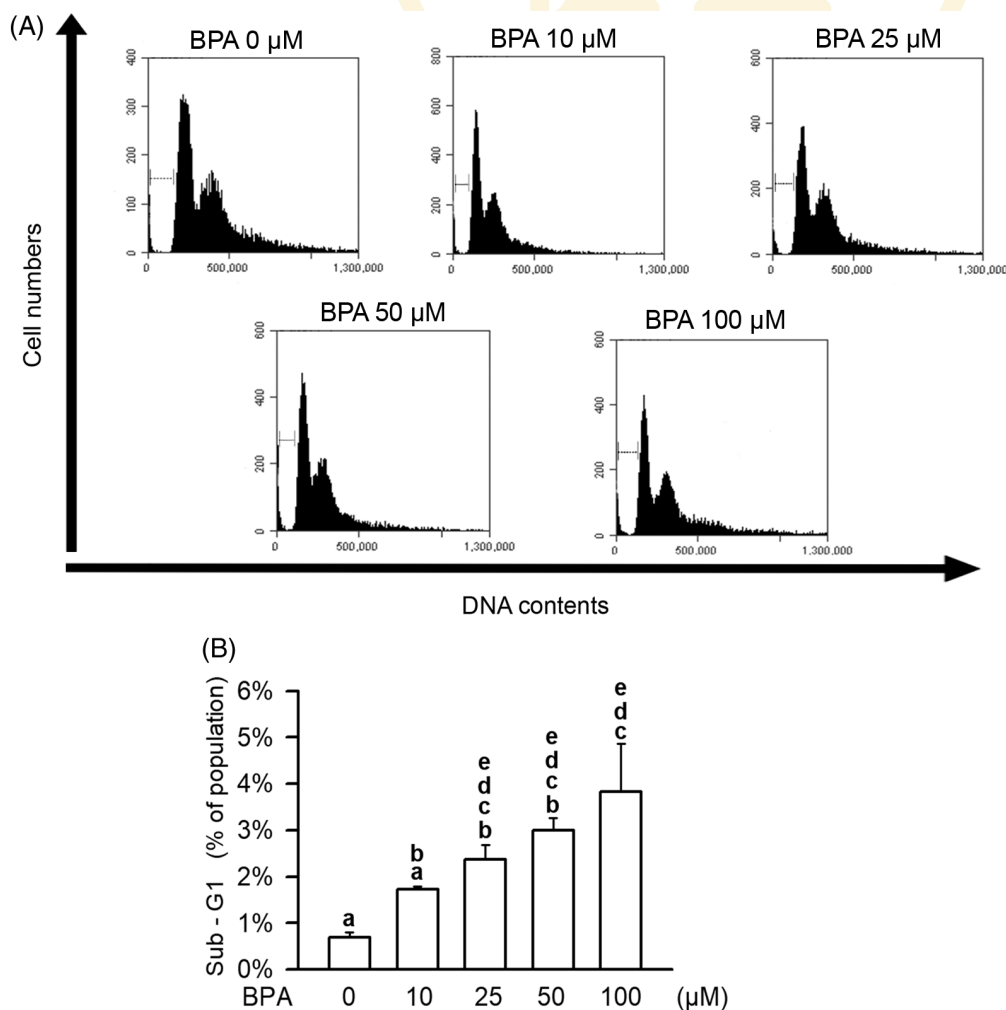
FIGURE 2 Effects of BPA on the sub-G1 phase in ARPE-19 cells. (A) BPA treatment increased ARPE-19 cells in sub-G1 population. (B) Quantitatively, the percentage of sub G1 phase were calculated and analyzed. Data are expressed as mean ± SE ($n = 3$). Values without a common superscript letter are significantly different ($p < .05$)

secondary antibody (rabbit, mouse) for 1 h. The blots were visualized using enhanced luminal reagent detection kit.

2.11 | Statistical analysis

All experimental data are expressed as mean ± standard error (SE). A one-way ANOVA analysis of variance was used for statistical analysis, and the differences between groups were determined using Bonferroni's post-hoc test. A p value of <.05 was considered to indicate statistically significant results.

3 | RESULTS

3.1 | Effects of BPA on ARPE-19 cell survival

To evaluate the cytotoxicity of BPA against ARPE-19 cells, the ARPE-19 cells were treated with BPA at various concentrations for different treatment durations. When the cells were treated with BPA for 8 h, the survival rate decreased start significantly at the BPA concentration was 10 μM ($p < .05$; Figure 1). At the BPA concentration treatment of 50 μM, the cell survival rate decreased significantly has been exposed after 2 h of exposure treatment decreased significantly ($p < .05$).

3.2 | Effect of BPA of sub-G1 formation in ARPE-19

Normally, the cell cycle of healthy cells can be divided into G0/G1, S, G2, and M phases. The cell cycle could be determined by detecting the amount of DNA. DNA double-strand breaks engender apoptosis or necrosis, resulting in an increase in DNA content in the sub-G1 phase. As the BPA concentration increased, the sub-G1 phase population increased for the cells treated for 24 h (Figure 2A). At the BPA concentration of 25 μM, the sub-G1 phase population start differed significantly between the treated cells and control group ($p < .05$, Figure 2B).

3.3 | Effects of BPA on caspase-3 and -9 expression in ARPE-19 cells

Apoptosis is mainly regulated by the protein caspase. This study explored whether BPA affects the expression of caspase-3 and caspase-9 in ARPE-19 cells. When the cells were treated with BPA for 24 h, the caspase-3 and caspase-9 expression levels increased as the BPA concentration increased from 25 μM ($p < .05$, Figure 3A,B).

3.4 | BPA caused mitochondrial dysfunction and release of cytochrome C in ARPE-19 cells

The distinguishing feature of early cell apoptosis is the mitochondria destruction. Mitochondrial destruction includes changes in

MMP and mitochondrial redox potential. When the cells were treated with BPA, the JC1 green fluorescence intensity increased significantly at 100 μM ($p < .05$, Figure 4A,B). When cells were subjected to extracellular or intracellular pressure and sustained damage, the MMP changed, and cytochrome C was released from the intermembrane space of the mitochondria into the cytoplasm. When the APRE-19 cells were treated with 100 μM BPA for 24 h, the cytochrome C concentration in the cytoplasm increased significantly ($p < .05$, Figure 4C).

3.5 | BPA caused cells to follow the Bcl-2 family pathway and promoted apoptosis

The Bcl-2 family plays a major role in cell survival and in the mitochondrial apoptotic pathway.[22] This study revealed that when the cells were treated with 50 μM BPA for 24 h, the protein expression of Bcl-XL decreased significantly but the protein expression of Bax increased significantly when the BPA concentration was at 100 μM ($p < .05$, Figure 5).

3.6 | BPA increased intracellular ROS generation

Oxidative stress is characterized by high intracellular ROS expression levels, which could engender lipids, proteins, and DNA damage.[23] Moreover, oxidative stress is related to a various pathological factor.[24] This study revealed that BPA could induce ROS production in
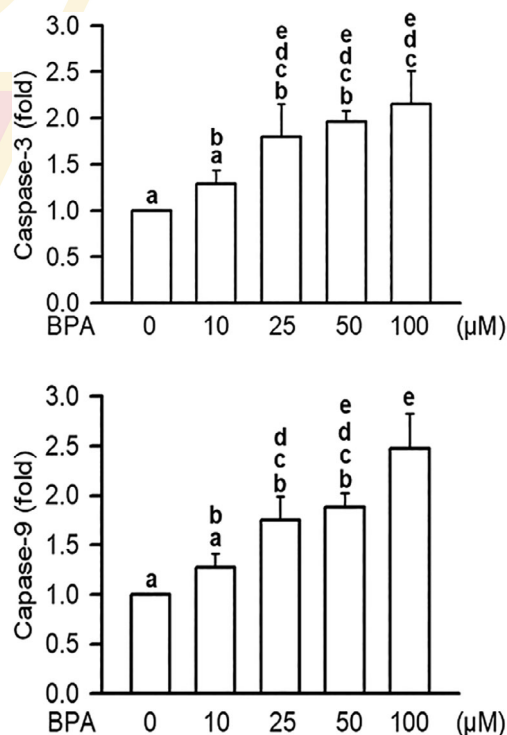
FIGURE 3 Effects of BPA on caspase-3 and -9 activity in ARPE-19. Data are expressed as mean ± SE ($n = 5$). Values without a common superscript letter are significantly different ($p < .05$)

(A)

(B)

(C)
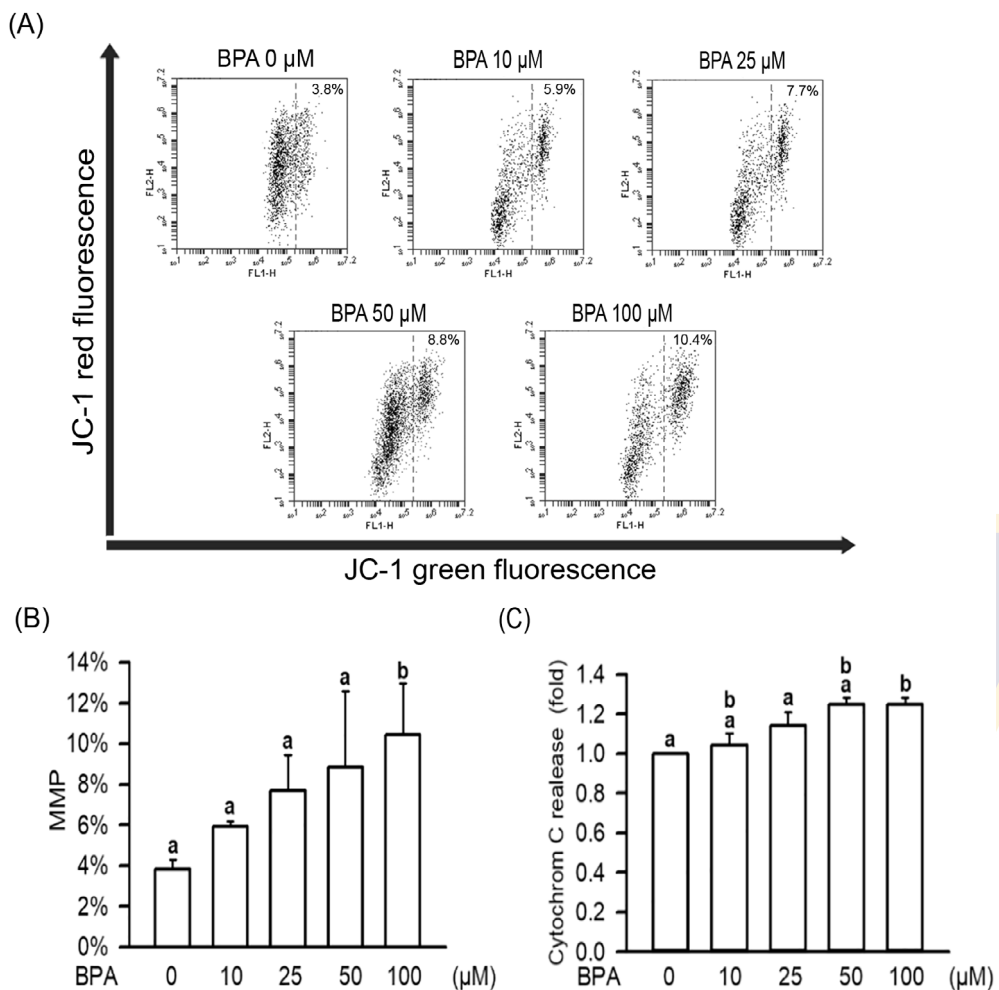
FIGURE 4 Effects of BPA on MMP and cytochrome C in ARPE-19 cells. (A) BPA treatment increased the percentage of ARPE-19 cells labeled with JC-1 stain. (B) Quantitatively, the percentage of MMP was calculated and analyzed. (C) BPA treatment increased cytochrome C expression in the cytoplasm. Data are expressed as mean ± SE ($n = 3$). Values without a common superscript letter are significantly different ($p < .05$)

the ARPE-19 cells ($p < .05$, Figure 6). When the ARPE-19 cells were treated with 100 μM BPA for 24 h, the ROS production level in the cells increased significantly.

3.7 | BPA caused lipid peroxidation in ARPE-19 cells

MDA is the product of lipid peroxidation and induce cytotoxicity in RPE cells.[25] This study revealed that BPA could induce MDA level in the ARPE-19 cells (Figure 7). When the ARPE-19 cells were treated with 100 μM BPA for 24 h, the MDA production level in the cells increased significantly ($p < .05$).

3.8 | BPA could degrade SOD and CAT expression in ARPE-19 cells

SOD and CAT constitute a system that can maintain the cellular concentration of the products of partial oxygen reduction (superoxide and hydrogen peroxide). Under oxidative stress, increased concentrations of free radicals can lead to the destruction of antioxidant enzymes.[26] The study found that when the ARPE-19 cells were

treated with 50 μM BPA for 24 h, SOD and CAT expression decreased significantly in the cells ($p < .05$, Figure 8).

3.9 | BPA repressed expression of Nrf2 and HO-1 in ARPE-19 cells

Nrf2 is a major antioxidant pathway that plays a key role in AMD.[13] HO-1 is an antioxidative protein which is regulated by the transcription factor Nrf2.[19] This study indicated that both Nrf2 and HO-1 expression decreased significantly ($p < .05$, Figure 9), when the ARPE-19 cells were treated with 100 μM BPA for 24 h.

3.10 | BPA repressed expression of AMPK phosphorylation in ARPE-19 cells

AMPK leads to phosphorylation of the transcription factor Nrf2.[27] To understand whether the effects on Nrf2 during BPA induced ARPE-19 cells were dependent on AMPK activity, we investigate AMPK phosphorylation using our experimental setup. When the ARPE-19 cells were treated with 50 μM BPA for 24 h, the p-AMPK levels were significantly decreased ($p < .05$, Figure 10).

(A)

BPA (μM) 0 10 25 50 100

Bcl-XL

Bax

β-actin

(B)

Bcl-XL (fold)

(C)

Bax (fold)

FIGURE 5 Effects of BPA on Bcl-XL and Bax expression. (A) Bcl-XL and Bax protein expression were measured by western blot. (B, C) Quantitatively, Bcl-XL and Bax protein expression were calculated and analyzed. Data are expressed as mean ± SE ($n = 3$). Values without a common superscript letter are significantly different ($p < .05$)

ROS generation (fold)
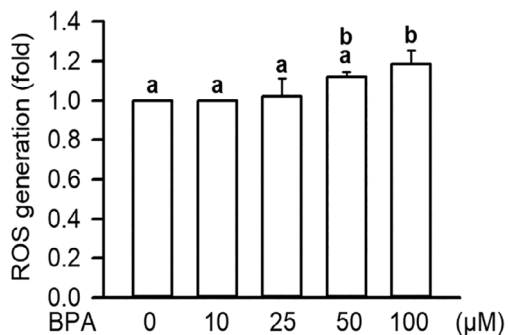
FIGURE 6 Effects of BPA on intracellular ROS generation in ARPE-19. Data are expressed as mean ± SE ($n = 5$). Values without a common superscript letter are significantly different ($p < .05$)

MDA (fold)

FIGURE 7 Effects of BPA on the production of lipid peroxidation level in ARPE-19. Data are expressed as mean ± SE ($n = 3$). Values without a common superscript letter are significantly different ($p < .05$)

(A)

BPA (μM) 0 10 25 50 100

SOD

CAT

β-actin

(B)

SOD (fold)

(C)

CAT (fold)
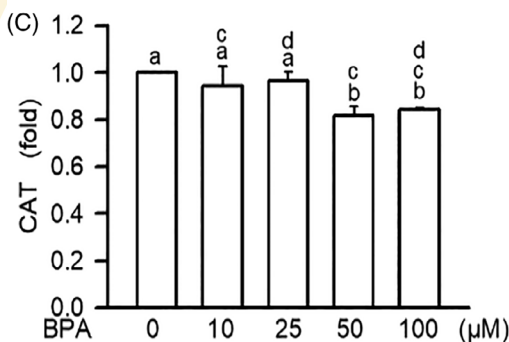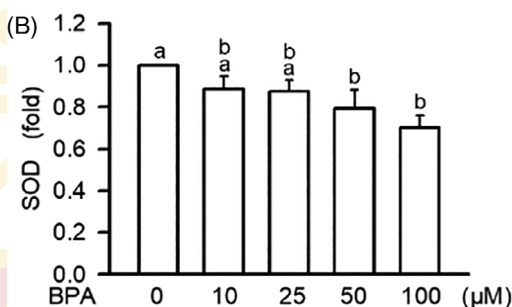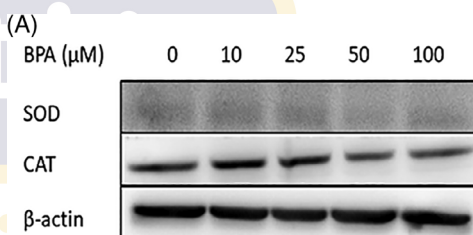
FIGURE 8 Effects of BPA on SOD and CAT expression. in ARPE-19 cells. (A) SOD and CAT protein expression were measured by western blot. (B, C) Quantitatively, SOD and CAT protein expression were calculated and analyzed. Data are expressed as mean ± SE ($n = 3$). Values without a common superscript letter are significantly different ($p < .05$)

(A)

(B)

(C)
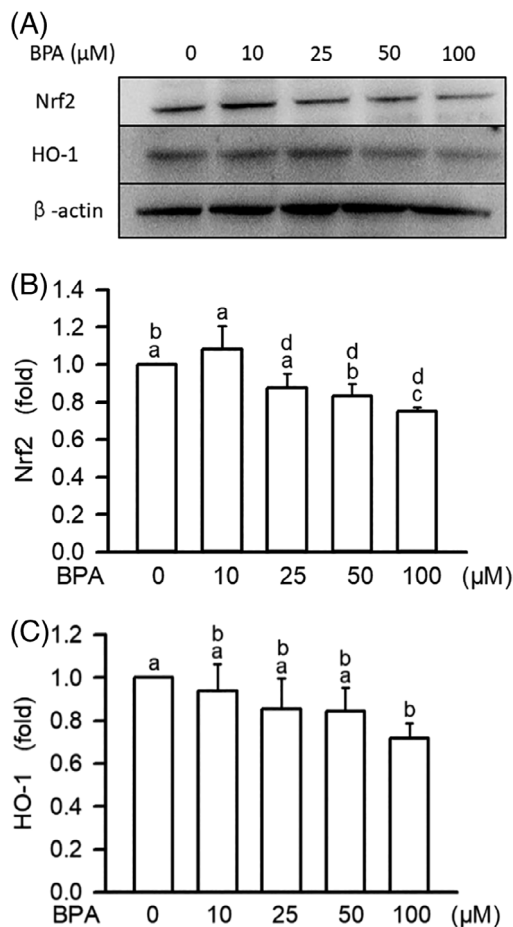
FIGURE 9 Effects of BPA on Nrf2 and HO-1 expression in ARPE-19 cells. (A) Nrf2 and HO-1 protein expression were measured by western blot. (B, C) Quantitatively, the Nrf2 and HO-1 protein expression were calculated and analyzed. Data are expressed as mean ± SE ($n = 3$). Values without a common superscript letter are significantly different ($p < .05$)

(A)

(B)

FIGURE 10 Effects of BPA on p-AMPK expression in ARPE-19 cells. (A) p-AMPK protein expression was measured by western blot. (B) Quantitatively, p-AMPK protein expression was calculated and analyzed. Data are expressed as mean ± SE ($n = 3–5$). Values without a common superscript letter are significantly different ($p < .05$)

3.11 | Effects of ROS scavenger, NAC, on BPA-induced intracellular ROS generation and cytotoxicity in ARPE-19 cells

To demonstrate the effects of ROS generation involved in cytotoxicity induced by BPA. NAC is the scavenger of ROS.[28] We pretreated ARPE-19 cells with NAC at 0.2 mM for 1 h and then incubated with BPA at 100 μM for 24 h. As shown in Figure 11, the intracellular ROS generation and cytotoxicity were significantly induced by BPA ($p < .05$). Pretreatment with NAC markedly reduced the intracellular ROS generation and cytotoxicity induced by BPA ($p < .05$).

4 | DISCUSSION

Apoptosis is the mechanism of cell death in human retinitis pigmentosa. In AMD, RPE cells gradually undergo apoptosis.[9] The pathogenesis of AMD is also related to the oxidative damage of RPE

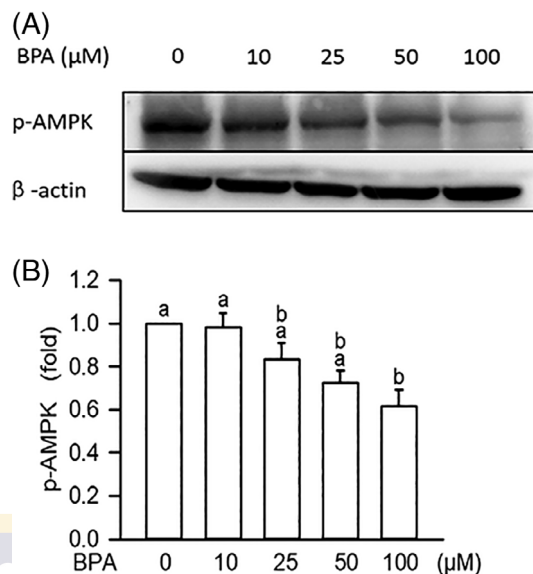cells and photoreceptor cells. The RPE is a vital retinal blood barrier.[29] BPA is a compound similar to estrogen and is an environmental hormone. It might enter the human body through food and might remain as a residue in blood and urine.[30] Previous studies have reported that BPA could cause cytotoxicity in human promyelocytic leukemia cells, mouse macrophages and male germ cells.[20,31,32] DNA double strands breaks engender cell apoptosis or necrosis, resulting in an increase in the sub-G1 phase. Moreover, a previous study indicated that BPA induced DNA damage in insulinoma-1 (INS-1) cells.[33] Our study also reveal that BPA could cause cytotoxicity and DNA damage in ARPE-19 cells, resulting in a decrease in cell viability.

Apoptosis could occur through the caspase-dependent pathway.[34] It was regulated by a group of proteins between the mitochondrial membrane and the cytoplasm.[35] When a cell is subjected to oxidative pressure, changes in MMP induce the release of cytochrome C from the intermembrane space of the mitochondria into the cytoplasm, as well as Apaf-1 and caspase-9 to stimulate the formation of an apoptosome. Subsequently, ATP activates the complex of caspase-9, which also promotes the activation of downstream caspase finally, apoptosis induced.[36] Exposure of HepG2 cells to BPA could change the MMP of cells and generate oxidative stress.[37] Furthermore, BPA induced INS-1 cell mitochondrial dysfunction and the release cytochrome C apoptosis.[38] A previous Study had reported that BPA in the diet could increase caspase-3 and caspase-9, apoptosis and mitochondrial dysfunction in the colon and liver of mice.[39] Our results reveal that BPA affected the MMP and caused an increase in cytochrome C, caspase-9, and caspase-3, which implies that BPA leads to apoptosis through the caspase pathway.
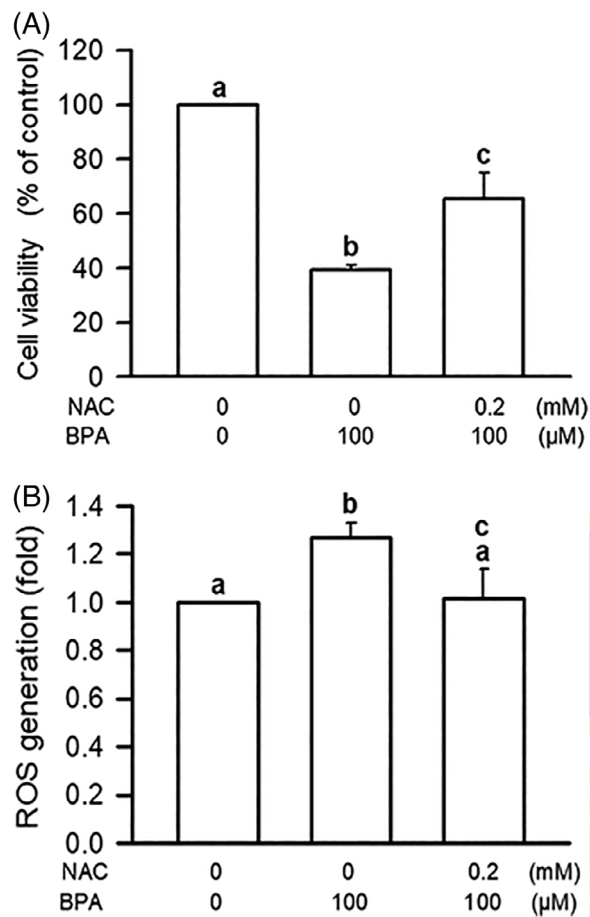
FIGURE 11   Effects of NAC on BPA-induced intracellular ROS generation and cytotoxicity. (A) NAC pretreated in ARPE-19 increased the cell viability. (B) NAC also inhibited ROS generation in BPA treated cell. Data are expressed as mean ± SE ($n = 4$). Values without a common superscript letter are significantly different ($p < .05$)

FIGURE 12   Schemes of the mechanism of the BPA-induced apoptosis and cytotoxicity in RAW264.7 cells. Cytotoxicity is induced by BPA via apoptosis and associated with mitochondrial dysfunction and oxidative stress generation. BPA induces mitochondrial dysfunction which including cytochrome C release, BCL2 family expression exchange, and caspase-3/9 activation. Oxidative stress generation is induced by BPA via inhibition of AMPK phosphorylation, Nrf2 expression, HO-1 expression, SOD, and CAT expression

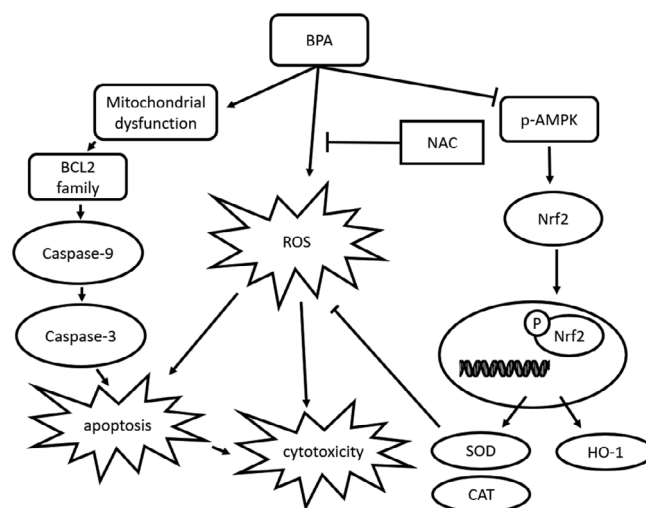Mitochondrial dysfunction in RPE cells is related to AMD.[40] The Bcl-2 family is most crucial component of the mitochondrial apoptotic pathway. Bcl-2 located in the outer layer of the mitochondrial membrane and regulates cell apoptosis information. The Bcl-2 family comprises two groups: the executioner proteins Bax and Bak that activate the final effector caspases of apoptosis, and the antiapoptotic members such as Bcl-2 and Bcl-XL.[41] BPA exposure can increase rat sperm cell cytochrome C, apoptosis-inducing factor, caspase-3, caspase-9, and Bax protein concentrations and decrease Bcl-2 protein concentrations.[42] Upregulation of Bax and Downregulation of Bcl-2 are induced by maternal exposure to BPA in the testis and ovarian tissues of offspring mice.[43] The findings of the present study demonstrate that BPA reduced the expression of the antiapoptotic protein Bcl-XL but increased the expression of the pro-proapoptotic protein Bax.

A previous study indicated that apoptosis is induced by ROS.[44] An increase in oxidative stress was reported found to be closely related to AMD.[8] Nrf2 regulates several crucial enzymes in antioxidant reactions including CAT, SOD, and glutathione.[45] CAT can prevent cell apoptosis caused by hydrogen peroxide.[44] AMPK functions as a central regulator of cell survival in response to stressful stimuli and directly phosphorylates Nrf2.[15] Previous research showed that aging RPE cell are susceptible to oxidative damage due to Nrf2 signaling.[46] Another study found that BPA could increase overall oxidative stress and engender a decrease in malondialdehyde and glutathione in chicken embryo brain tissue.[47] In male germ cells, exposure to BPA was reported to increase ROS expression.[32] However, no studies have evaluated the effects of BPA on RPE systems. The results of our study demonstrate that BPA increased ROS and MDA accumulation. BPA reduced the SOD and CAT expression. It also found that Nrf2 and HO-1 expression decreased in BPA treated cell. It indicated that BPA treatment was associated with the down-regulation of the Nrf2 transcription response. More, we also found BPA-induced intracellular ROS generation and cytotoxicity inhibited by NAC. Based on these findings, we suggest that cytotoxicity induced by BPA via intracellular ROS generation in ARPE-19 cells.

In conclusion, BPA affected ARPE-19 cell survival rates and induced ROS production (Figure 12). Regarding the mechanisms underlying the induction of oxidative stress and apoptosis, we propose the following: (a) BPA reduced the expression of the anti-apoptotic protein Bcl-XL, and increased the expression of the proapoptotic proteins Bax, which could change the MMP and release cytochrome C to bind to caspase-9 thereby causing apoptosis. (b) BPA induced oxidative stress degrade SOD and CAT expression, repressed Nrf2/HO-1 expression and AMPK phosphorylation.

CONFLICT OF INTEREST

The authors declare no potential conflict of interest.

DATA AVAILABILITY STATEMENT

We declare that the data that support the findings of this study are available from the corresponding author upon reasonable request.

ORCID

Wen-Ying Chen https://orcid.org/0000-0002-5105-5285
Yu-Hsiang Kuan https://orcid.org/0000-0002-8991-6394

REFERENCES

1. Cao X-L, Corriveau J, Popovic S. Levels of bisphenol A in canned soft drink products in Canadian markets. *J Agric Food Chem*. 2009;4:1307-1311.
2. Vandenberg LN, Hauser R, Marcus M, Olea N, Welshons WV. Human exposure to bisphenol A (BPA). *Reprod Toxicol*. 2007;24:139-177.
3. He Y, Miao M, Herrinton LJ, et al. Bisphenol A levels in blood and urine in a Chinese population and the personal factors affecting the levels. *Environ Res*. 2009;109:629-633.
4. Gould JC, Leonard LS, Maness SC, et al. Bisphenol A interacts with the estrogen receptor a in a distinct manner from estradiol. *Mol Cell Endocrinol*. 1998;142:203-214.
5. Takeuchi T, Tsutumi O, Ikezuki Y, Takai Y, Taketani Y. Positive relationship positive relationship. *Endocr J*. 2004;51:165-168.
6. Klein R, Klein BEK, Linton KLP. Prevalence of age-related maculopathy: the beaver dam eye study. *Ophthalmology*. 2020;127:S122-S132.
7. Jaadane I, Villalpando Rodriguez GE, Boulenguez P, et al. Effects of white light-emitting diode (LED) exposure on retinal pigment epithelium in vivo. *J Cell Mol Med*. 2017;21:3453-3466.
8. Kauppinen A, Niskanen H, Suuronen T, Kinnunen K, Salminen A, Kaarniranta K. Oxidative stress activates NLRP3 inflammasomes in ARPE-19 cells—implications for age-related macular degeneration (AMD). *Immunol Lett*. 2012;147:29-33.
9. Joshua L, Dunaief M, Tzvete Dentchev M, Ying G-S, Milam AH, Milam P. The role of apoptosis in age-related macular degeneration. *Clin Sci*. 2002;120:1435-1442.
10. Sparrow JR, Cai B. Blue light–induced apoptosis of A2E-containing RPE involvement of caspase-3 and protection by Bcl-2. *Invest Ophthalmol Vis Sci*. 2001;42:1356-1362.
11. Tokarz P, Kaarniranta K, Blasiak J. Role of antioxidant enzymes and small molecular weight antioxidants in the pathogenesis of age-related macular degeneration (AMD). *Biogerontology*. 2013;14:461-482.
12. Suzuki T, Motohashi H, Yamamoto M. Toward clinical application of the Keap1-Nrf2 pathway. *Trends Pharmacol Sci*. 2013;34:340-346.
13. Lambros ML, Plafker SM. Oxidative stress and the nrf2 anti-oxidant transcription factor in age-related macular degeneration. *HHS Publ Access*. 2016;10:67-72.
14. Zimmermann K, Baldinger J, Mayerhofer B, Atanasov AG, Dirsch VM, Heiss EH. Activated AMPK boosts the Nrf2/HO-1 signaling axis—a role for the unfolded protein response. *Free Radic Biol Med*. 2015;88:417-426.
15. Joo MS, Kim WD, Lee KY, Kim JH, Koo JH, Kim SG. AMPK facilitates nuclear accumulation of Nrf2 by phosphorylating at serine 550. *Mol Cell Biol*. 2016;36:1931-1942.
16. Liu Y, Peterson DA, Kimura H, Schubert D. Mechanism of cellular 3-(4,5-dimethylthiazol-2-yl)-2,5-diphenyltetrazolium bromide (MTT) reduction. *J Neurochem*. 1997;69:581-593.
17. Huang FM, Chang YC, Su CH, et al. Rutin-protected BisGMA-induced cytotoxicity, genotoxicity, and apoptosis in macrophages through the reduction of the mitochondrial apoptotic pathway and induction of antioxidant enzymes. *Environ Toxicol*. 2020;36:45-54.
18. Lee CY, Su CH, Tsai PK, et al. Cadmium nitrate-induced neuronal apoptosis is protected by N-acetyl-l-cysteine via reducing reactive oxygen species generation and mitochondria dysfunction. *Biomed Pharmacother*. 2018;108:448-456.
19. Ni YL, Shen HT, Su CH, et al. Nerolidol suppresses the inflammatory response during lipopolysaccharide-induced acute lung injury via the modulation of antioxidant enzymes and the AMPK/Nrf-2/HO-1 pathway. *Oxid Med Cell Longev*. 2019;2019:9605980.
20. Huang FM, Chang YC, Lee SS, et al. Bisphenol A exhibits cytotoxic or genotoxic potential via oxidative stress-associated mitochondrial apoptotic pathway in murine macrophages. *Food Chem Toxicol*. 2018;122:215-224.
21. Huang FM, Chang YC, Lee SS, Yang ML, Kuan YH. Expression of pro-inflammatory cytokines and mediators induced by bisphenol A via ERK-NFkappaB and JAK1/2-STAT3 pathways in macrophages. *Environ Toxicol*. 2019;34:486-494.
22. Sassone J, Maraschi A, Sassone F, Silani V, Ciammola A. Defining the role of the Bcl-2 family proteins in Huntington's disease. *Cell Death Dis*. 2013;4:e772.
23. Zhang J, Wang X, Vikash V, et al. ROS and ROS-mediated cellular signaling. *Oxid Med Cell Longev*. 2016;2016:4350965.
24. Ilaria L, Gennaro R, Francesco C, et al. Oxidative stress, aging, and diseases. *Clin Interv Aging*. 2018;13:757-772.
25. Ye F, Kaneko H, Hayashi Y, et al. Malondialdehyde induces autophagy dysfunction and VEGF secretion in the retinal pigment epithelium in age-related macular degeneration. *Free Radic Biol Med*. 2016;94:121-134.
26. Escobar JA, Rubio MA, Lissi EA. SOD and catalase inactivation by singlet oxygen and peroxyl radicals. *Free Radic Biol Med*. 1996;20:285-290.
27. Matzinger M, Fischhuber K, Poloske D, Mechtler K, Heiss EH. AMPK leads to phosphorylation of the transcription factor Nrf2, tuning transactivation of selected target genes. *Redox Biol*. 2020;29:101393.
28. Halasi M, Wang M, Chavan TS, Gaponenko V, Hay N, Gartel AL. ROS inhibitor N-acetyl-L-cysteine antagonizes the activity of proteasome inhibitors. *Biochem J*. 2013;454:201-208.
29. Jia L, Liu Z, Sun L, et al. Acrolein, a toxicant in cigarette smoke, causes oxidative damage and mitochondrial dysfunction in RPE cells: protection by (R)-alpha-lipoic acid. *Invest Ophthalmol Vis Sci*. 2007;48:339-348.
30. Calafat AM, Kuklenyik Z, Reidy JA, Caudill SP, Ekong J, Needham LL. Urinary concentrations of bisphenol A and 4-nonylphenol in a human reference population. *Environ Health Perspect*. 2005;113:391-395.
31. Terasaka H, Kadoma Y, Sakagami H, Fujisawa S. Cytotoxicity and apoptosis-inducing activity of bisphenol A and hydroquinone in HL-60 cells.pdf. *Anticancer Res*. 2005;25:2241-2248.
32. Yin L, Dai Y, Cui Z, et al. The regulation of cellular apoptosis by the ROS-triggered PERK/EIF2alpha/chop pathway plays a vital role in bisphenol A-induced male reproductive toxicity. *Toxicol Appl Pharmacol*. 2017;314:98-108.
33. Xin F, Jiang L, Liu X, et al. Bisphenol A induces oxidative stress-associated DNA damage in INS-1 cells. *Mutat Res Genet Toxicol Environ Mutagen*. 2014;769:29-33.
34. Li YJ, Song TB, Cai YY, et al. Bisphenol A exposure induces apoptosis and upregulation of Fas/FasL and caspase-3 expression in the testes of mice. *Toxicol Sci*. 2009;108:427-436.
35. Li YC, Kuan YH, Huang FM, Chang YC. The role of DNA damage and caspase activation in cytotoxicity and genotoxicity of macrophages induced by bisphenol-A-glycidyldimethacrylate. *Int Endod J*. 2012;45:499-507.
36. Wang Q, Zhao XF, Ji YL, et al. Mitochondrial signaling pathway is also involved in bisphenol A induced germ cell apoptosis in testes. *Toxicol Lett*. 2010;199:129-135.
37. Huc L, Lemarie A, Gueraud F, Helies-Toussaint C. Low concentrations of bisphenol A induce lipid accumulation mediated by the production of reactive oxygen species in the mitochondria of HepG2 cells. *Toxicol In Vitro*. 2012;26:709-717.

38. Lin Y, Sun X, Qiu L, et al. Exposure to bisphenol A induces dysfunction of insulin secretion and apoptosis through the damage of mitochondria in rat insulinoma (INS-1) cells. *Cell Death Dis*. 2013;4:e460.

39. Wang K, Zhao Z, Ji W. Bisphenol A induces apoptosis, oxidative stress and inflammatory response in colon and liver of mice in a mitochondria-dependent manner. *Biomed Pharmacother*. 2019;117: 109182.

40. Miceli MV, Jazwinski SM. Nuclear gene expression changes due to mitochondrial dysfunction in ARPE-19 cells: implications for age-related macular degeneration. *Investig Opthalmol Vis Sci*. 2005;46: 1765-1772.

41. Shamas-Din A, Kale J, Leber B, Andrews DW. Mechanisms of action of Bcl-2 family proteins. *Cold Spring Harb Perspect Biol*. 2013;5: a008714.

42. Wang P, Luo C, Li Q, Chen S, Hu Y. Mitochondrion-mediated apoptosis is involved in reproductive damage caused by BPA in male rats. *Environ Toxicol Pharmacol*. 2014;38:1025-1033.

43. Ma S, Shi W, Wang X, Song P, Zhong X. Bisphenol A exposure during pregnancy alters the mortality and levels of reproductive hormones and genes in offspring mice. *Biomed Res Int*. 2017;2017: 3585809.

44. Simon H-U, Haj-Yehia A, Levi-Schaffer F. Role of reactive oxygen species (ROS) in apoptosis induction. *Cold Spring Harb Perspect Biol*. 2000;5:415-418.

45. Cano M, Thimmalappula R, Fujihara M, et al. Cigarette smoking, oxidative stress, the anti-oxidant response through Nrf2 signaling, and age-related macular degeneration. *Vision Res*. 2010;50:652-664.

46. Sachdeva MM, Cano M, Handa JT. Nrf2 signaling is impaired in the aging RPE given an oxidative insult. *Exp Eye Res*. 2014;119:111-114.

47. Gharibi S, Dilmaghanian A, Sadighara P, et al. The effect of Bisphenol A on oxidative stress indices and pathological changes in the brain of chicken embryos. *World Appl Sci J*. 2013;26:345-351.

Research Article

Observation of the Expression of Vascular Endothelial Growth Factor and the Potential Effect of Promoting Hair Growth Treated with Chinese Herbal BeauTop

Chien-Ying Lee,[1,2] Chun-Hung Su,[1] Chien-Ying Chiang,[3] Chun-Nan Wu,[2] and Yu-Hsiang Kuan [1,2]

[1]*Department of Pharmacology, School of Medicine, Chung Shan Medical University, Taichung, Taiwan*
[2]*Department of Pharmacy, Chung Shan Medical University Hospital, Taichung, Taiwan*
[3]*Brion Research Institute, New Taipei, Taiwan*

Correspondence should be addressed to Yu-Hsiang Kuan; kuanyh@csmu.edu.tw

Despite minoxidil and finasteride already being approved by the Food and Drug Administration (FDA) for the treatment of hair loss, it is important to identify new and innovative treatments for hair loss, such as looking for a solution in Chinese herbal medicine. One such treatment to consider is BeauTop (BT), whose primary ingredients include *Panax japonicus* (T.Nees), C.A. Mey. (Araliaceae), *Astragalus membranaceus* (Fisch) Bunge (Fabaceae), *Angelica sinensis* (Oliv.) Diels (Apiaceae), *Ligustrum lucidum* W.T. Aiton (Oleaceae), *Rehmannia glutinosa* (Gaertn.) DC. (Plantaginaceae), and *Eclipta prostrata* (L.) *L.* (Compositae). The aim of this study was to evaluate whether BT can promote hair growth in C57BL/6 mice and to investigate hair coverage, the expression of vascular endothelial growth factor (VEFG), and the numbers of hair follicles in growth phase after oral administration. A total of 12 C57BL/6 mice were divided into two groups: control group and treatment group BT. BT was administered orally as an extract at a volume of 0.6 g/kg. The control group was treated with distilled water. Each group was treated once a day for 12 consecutive days. To observe the expression of VEGF distribution, the number of hair follicles and the hair coverage were examined on days 4, 8, and 12. By comparing the treatment group and control group, we found that VEGF in the BT group on day 8 presented with a higher area percentage than the control group (p value = 0.003). Hair follicle counting results showed that the BT group was significantly higher than the control group on day 8 (p value = 0.031). Furthermore, hair coverage was shown to be significantly increased in the treatment group BT on day 8 (p value = 0.013). Taken together, these results suggest that Chinese medicine (BT) possesses the potential effect of promoting hair growth through VEGF expression. VEGF is considered the most important mediator for the process of angiogenesis involved in hair growth development.

1. Introduction

Hair is thought to be an important component of an individual's feeling of attractiveness. The significant psychological effect of hair loss has a measurably negative change in self-esteem [1]. Androgenetic alopecia (AGA) is a common form of hair loss in both men and women. Approximately 50% of the male population are affected to some extent. AGA is a physiologic androgen-stimulated condition that occurs in genetically predisposed areas of the scalp [2]. The conversion of circulating testosterone into dihydrotestosterone (DHT) is mainly by the action of 5α-reductase type 2 [3]. DHT plays a major role in the pathogenesis of AGA, while elevated DHT level can be observed in men with AGA [4].

There are three phases of hair growth in the cycle, including the anagen, catagen, and telogen phases [5]. The hair growth cycle is regulated by several growth factors, including vascular endothelial growth factor (VEFG) [6], epithelial growth factor (EGF) [7], insulin-like growth factor (IGF)-1

[8], and fibroblast growth factor (FGF)-5 and -7 [9]. Dysregulation of these growth factors results in hair loss.

Evidence has established the fundamental role of VEGF as a key regulator of physiological and pathological angiogenesis during cutaneous development. VEGF receptor-2 is the primary receptor for VEGF and most functional effects were mediated by VEGF [10]. Importantly, transgenic mice overexpression of VEGF in keratinocytes of hair follicles strongly induced perifollicular vascularization during hair growth cycle, led to accelerated hair regrowth after depilation, and increased hair follicle size and hair shaft diameter. These findings suggested that VEGF plays an important role in the regulation of perifollicular vascularization during hair growth [11]. In addition, hair growth is induced by topical tofacitinib, the JAK3 inhibitor, via the increased concentration of VEGF and the lowered level of inflammation [12]. Based on these findings, we hypothesized that VEGF is considered the key mediator for the process of angiogenesis involved in cutaneous development and physiological and pathological processes.

In our study, the ingredients of the Chinese herbal medicine, BeauTop (BT), included *Panax japonicus* (T.Nees) C.A. Mey. (Araliaceae), *Astragalus membranaceus* (Fisch) Bunge (Fabaceae), *Angelica sinensis* (Oliv.) Diels (Apiaceae), *Ligustrum lucidum* W.T. Aiton (Oleaceae), *Rehmannia glutinosa* (Gaertn.) DC. (Plantaginaceae), and *Eclipta prostrata* (L.) *L.* (Compositae). Reports suggest that *Panax japonicus* is an immunological modulator [13]. *Astragalus membranaceus* is well known to strengthen a host's defense system [14]. *Angelica sinensis* is commonly used to promote blood circulation in the treatment of menstrual disorders [15]. Many reports have shown the pharmacological functions of *Rehmannia glutinosa* on the blood system, anti-inflammatory, and immune system [16, 17]. *Eclipta prostrata* could effectively reduce cholesterol levels in the blood and improve the antioxidant activities in rats [18].

Research in the field of reversing hair loss still remains a challenging subject. Even though topical minoxidil solution and oral finasteride have been approved by the Food and Drug Administration (FDA) as effects treatment options for androgenetic alopecia in men, it is important to improve the therapeutic approach for hair loss by looking at Chinese herbal medicine, for example. Our previous study had shown that the mechanism of BT improving hair growth is associated with the expression, in EGF and FGF-7, BT may have a potential effect to stimulate hair growth [19].

The aim of this study was to evaluate whether the Chinese herbal medicine BT can promote hair growth through the expression of VEGF in hair follicles in C57BL/6J mice. To achieve this aim, we will examine hair coverage, expression of VEFG, and the number of hair follicles in the growth phase after oral administration.

2. Materials and Methods

2.1. Animals and Skin Collection. We chose C57BL/6 mice for our study based on our review of prior related studies [11, 20]. Female C57BL/6 mice weighing 15–20 g (six weeks old) were obtained from the National Laboratory Animal Center (Taipei, Taiwan); mice were randomly grouped and cared for in a sterilized cage independent animal unit under a 12-hour light/darkness cycle in the Animal Technology Institute Taiwan (ATIT). Mice were fed mouse chow and water *ad libitum*. The environment was maintained at a temperature of around $24 \pm 2^\circ$C and the humidity range was maintained from 30 to 70%. The animals were killed by cervical dislocation under an overdose of anesthesia and the skin was harvested at the level of subcutis and stored at -80°C until further use. This study was approved by the research ethics committee of the Agricultural Technology Research Institute (No. 97011) before the study begins.

2.2. Preparation of Chinese Herbal Medicine Formulations. The BeauTop samples were provided by the Brion Research Institute. A mixture of *Panax japonicus*, *Astragalus membranaceus*, *Angelica sinensis*, *Ligustrum lucidum*, *Rehmannia glutinosa*, and *Eclipta prostrata* at a ratio of $7 : 9 : 7 : 10 : 7 : 10$ [19] was prepared. The process of making BeauTop is described in Patent US 7,828,048 B2 (reference: Patent US 7,828,048 B2, column 4, lines 59-67). All components were purchased from Sun Ten Pharmaceutical Co. Ltd. (Taipei, Taiwan).

2.3. Experimental Design

2.3.1. Screening the Best Formulation of Chinese Herbal Medicine by Hair Follicle Counting. A total of 12 mice of C57BL/6 were divided into 2 groups, a control group and a treatment group BT. Mice were anesthetized with 2, 2, 2-tribromoethanol (Avertin®) by intraperitoneal injection at a dose of 250 mg/kg. Hot rosin and paraffin mixture depilation were used to induce hair follicles to enter from telogen into anagen and each depilatory area was fixed upon 2 cm × 2 cm. Treatment groups (BT) were orally administrated quantitative Chinese herbal medicine extract powder at 0.6 g/kg body weight. The control group received distilled water. Each group was treated once a day for 12 consecutive days.

Three mice from each group were taken for photos and skin sampling on day 4, day 8, and day 12. The samples of skin were fixed in 10% formalin solution for at least 24 hours. Each skin texture sample was sliced into three pieces and put in the same embedding box. The sliced samples were prepared for further immunohistochemical stain and counting of hair follicle number. The number of follicles per mm^2 was then calculated using an AxioCam ICc3 microscope at × 100 magnification.

2.3.2. Analysis of Growth Factor Expression of VEGF during Treatment with Chinese Herbal Medicine. A total of 12 mice of C57BL/6 were separated into 2 groups, one control group and one treatment BT group. The protocol for this is described as Step 2.1 and the same embedding box (including 3 sliced skin samples) was prepared for growth factors such as VEGF immunohistochemical stain. Fixed sections were immunostained with antimouse VEGF (Millipore, Billerica, MA), according to the manufacturer's instructions.

2.4. Image Analysis. Immunohistochemical stain was used in the evaluation of growth factors on each slide. All the growth factors were stained a brown color. An Olympus microscope equipped with an AxioCam ICc3 imagine system was used to randomly screen in the field and Image-Pro Plus software was utilized to calculate the percentage of color area.

2.5. Statistical Analysis. The summary data are presented as the mean and standard deviation unless otherwise stated. Statistical analysis for group comparison was performed via Independent t-test analysis for a comparison between the treatment and control group (SPSS version 12.0, Claritas Inc. USA.).

3. Results

We compared the treatment group and placebo group on day 8, and we observed that the accelerated hair growth in the BT group was greater than the control group (Figure 1).

The immunohistochemical stain results showed that in mice treated with BeauTop, the expression in VEGF was significantly greater than the control group on day 8. In the control group, many of the hair follicles had the normal structure characteristics of the anagen phase, and both the hair bulb and the inner and outer root sheaths were clearly identified. After treatment on day 8, we observed the rapid growth of hair follicles and these enlarged primordial follicles with hypertrophy appeared to be larger in the anagen phase (Figure 2).

Histopathological results, comparing the treatment group and placebo group, showed that the growth factors during the study period indicated that VEGF in the BT group on day 8 presented a higher area percentage than the control group, respectively (p value = 0.003). The expression of VEGF did not significantly increase in BT on day 12 (p value = 0.058) (Figure 3).

Based on prior data, we hypothesized that the BT had possessed superior hair growth effectiveness. Therefore, we took a close look at the BT formulation with regard to growth factor analysis. When examining the follicle counting results, we found that when comparing the treatment group and placebo group, the hair follicle counting in the BT group was significantly higher than the control group on day 8 (p value = 0.031). The difference between the control group and the BT group was not significantly on day 12 (p value = 0.081) (Figure 4).

Hair coverage also significantly increased in the treatment group BT on day 8 (p value = 0.013) but did not significantly increase in the BT group on day 12 (p value = 0.081) (Figure 5).

4. Discussion

Even though minoxidil and finasteride have been approved for the treatment of hair loss, we compared Chinese herbal medicine BT treatment group and control group to explore the therapeutic effect of accelerated hair growth. Our study demonstrated that the expression in VEGF in the BT group was significantly greater than the control group on day 8, presenting a higher area percentage than the control group. We also found that hair follicle counting in the BT group was significantly higher than the control group, and hair coverage was shown to be significantly increased in the treatment group BT on day 8. Based on these findings, we suggest that BT had possessed superior hair growth effectiveness through VEGF expression, and VEGF is considered as the most important mediator for the process of angiogenesis involved in hair growth development.

Our previous study had shown that the expression of EGF and FGF-7 in the BT group was increased on day 8. However, FGF-5 in the BT group was reduced on day 12. There were no effects on the expression of IGF-1. This study indicated that BT might have a potential effect to stimulate hair growth. Taken together, the results suggest the mechanism of BT improving hair growth via the expression in EGF and FGF-7 [19]. From these data, it can be suggested that BT had a potential effect to improve hair growth via the induction of several growth factors (VEGF, EGF, and FGF), especially the expression of VEGF as the key mediator in hair growth development.

During embryonic development, VEFG is one of the most important mediators that regulate blood vessel formation on wound repair and in maintaining vascular homeostasis [21]. Deficiency in various VEGF receptors or their ligands shows serious problems in the vascular formation that causes many diseases [22]. It was demonstrated that VEGF expression in human follicles significantly decreased when compared to normal follicles [23]. From our study data, the increased expression of VEGF was significant on day 8 and presented with a higher area percentage in the treatment group as compared to the control group. It was revealed that the BT has the potential effect of stimulating hair growth via upregulation of VEGF expression. In the normal hair growth cycle, VEGF expression will stop increasing to prevent hair overgrowth, and we observed that the expression of VEGF did not significantly increase on day 12.

VEGF plays a key role in mediating the process of angiogenesis during development, and in a number of inflammatory diseases and neoplastic diseases that are associated with neovascularization [24]. In our study, we also found that the change in the number of hair follicles significantly increased the rapid growth of hair follicles and these enlarged primordial follicles with hypertrophy appeared to be larger in the BT group on day 8, revealing that BT has the potential effect of promoting VEGF expression in follicular follicles resulting in accelerated hair regrowth and increased hair follicle size in mice. As per the previous study [12], we also found similar results which show that the promotion of angiogenesis can promote hair growth through VEGF expression. We observed that the accelerated hair growth in the BT group was greater than the control group, and the hair coverage significantly increased in the treatment group BT on day 8.

A number of hair conditions are caused by hair follicles. Hair follicle affects skin conditions through the immune system and hormone system. The immune system of hair
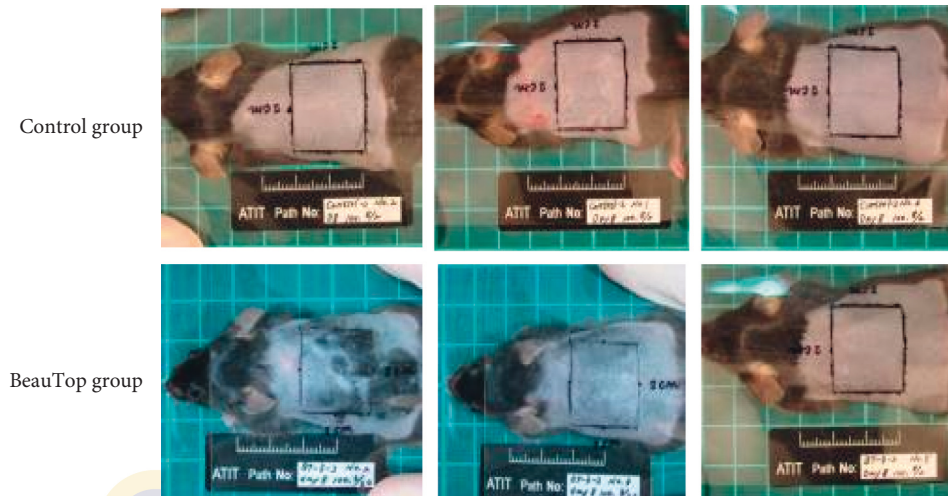
FIGURE 1: Comparison of the hair growth between control group and BeauTop group on Day 8.

follicle is associated with the hair follicle hormone system. Certain conditions can affect hair follicles and cause hair loss. Importantly, environmental stress may influence both the immune system and hormone system of the hair follicle and lead to the induction of cell-mediated autoimmune hair disease, such as alopecia areata (AA) [25]. It is important to note that AA and alopecia universally appear to be autoimmune diseases and are not associated with androgen [26].

In our study, BT is formulated from the following six ingredients: *Panax japonicus*, *Astragalus membranaceus*, *Angelica sinensis*, *Ligustrum lucidum*, *Rehmannia glutinosa*, and *Eclipta prostrata*. One study reported the effects of saponin from *Panax japonicus* that increase the activation and synthesis of TGF-beta1 and modify the expression of TGF-beta receptors in fibroblasts [27]. A formulation containing *Panax japonicus* and *Panax notoginseng* (Burkill) F. H. Chen (Araliaceae) can promote the secretion of VEGF and the expression of VEGF receptor 2, which indicated that one of the underlying mechanisms of *Panax japonicus* and *Panax notoginseng* formula might be associated with the promotion of angiogenic processes [28]. One study demonstrated that ginseng was capable of regulating antibody production by augmentation of *T* helper type 1 immune response (IL-2, IFN-gamma) and *T* helper type 2 immune response (IL-4, IL-10) cytokine production [29]. One study suggests that Radix Astragali extract (RAE) is a potent stimulator of angiogenesis and that it exerts its potential proangiogenic effects involving the VEGF and Akt-dependent signaling pathways [30]. Another review revealed that *Angelica sinensis* is an alternative treatment available for hair loss that acts through hair cycle pathways associated with hair follicle apoptosis regression during the catagen phase [31]. Adipose-derived mesenchymal stem cells (ADMSCs) can provide a promising future in the field of tissue engineering and regenerative medicine and may serve a wide variety of applications. A study showed that Rehmannia glutinosa oligosaccharide (RGO) might increase the viability and proliferative capacity and alleviate H_2O_2-induced apoptosis of human ADMSCs via the secretion of VEGF and

hepatocyte growth factor. The results indicate that the application of RGO will enhance stem cell preservation and improve their therapeutic effects of cell therapy [32]. Various extracts and individual compounds derived from *Ligustrum lucidum* have been reported to possess a variety of pharmacological effects, e.g., immune regulation, antioxidative effect, antiaging effect, and anti-inflammation effect [33]. Another review also showed that *Ligustrum lucidum* could modulate estrogen receptor expression with no uterotrophic effect in ovariectomized rats [34] and improve bone quality in type 1 diabetic mice via stimulating parathyroid production [35]. Butanol extract from *Eclipta prostrata* has an antioxidative effect in rats, and saponin is a primary ingredient in butanol extract that has antioxidative effects in vitro [36].

From the above and previous information, we hypothesized that BT had a potential effect of improving hair growth via the induction of several growth factors (VEGF, EGF, and FGF), especially the expression of VEGF as the key mediator in hair growth development, physiological, and pathological processes. We also hypothesized that BT may have the potential effect for AGA through the immunomodulating effect that protects hair follicles from immune attacks and may have the potential effect for AGA through anti-inflammatory properties that protect hair follicles from inflammation. However, further studies are needed to evaluate this phenomenon.

Our previous randomized, double-blind placebo-controlled clinical trial revealed that in the BT treatment group, 52.9% of participants showed an increase in hair growth. The changes in hair growth are as follows: 5.9% slightly improved, 29.4% moderately improved, and 17.6% markedly improved [37]. This represents that the composition of formula mode is an important meaning for improving the research of treating diseases by integrated syndrome differentiation via the new clinical trial design [38].

In traditional Chinese medicine culture, qi (also chi) is an active principle forming part of any living organism. *Panax japonicus* could offer a sweet flavor and warming

Sample 1

Control group

BeauTop group

Sample 2

Control group

BeauTop group

Sample 3

Control group
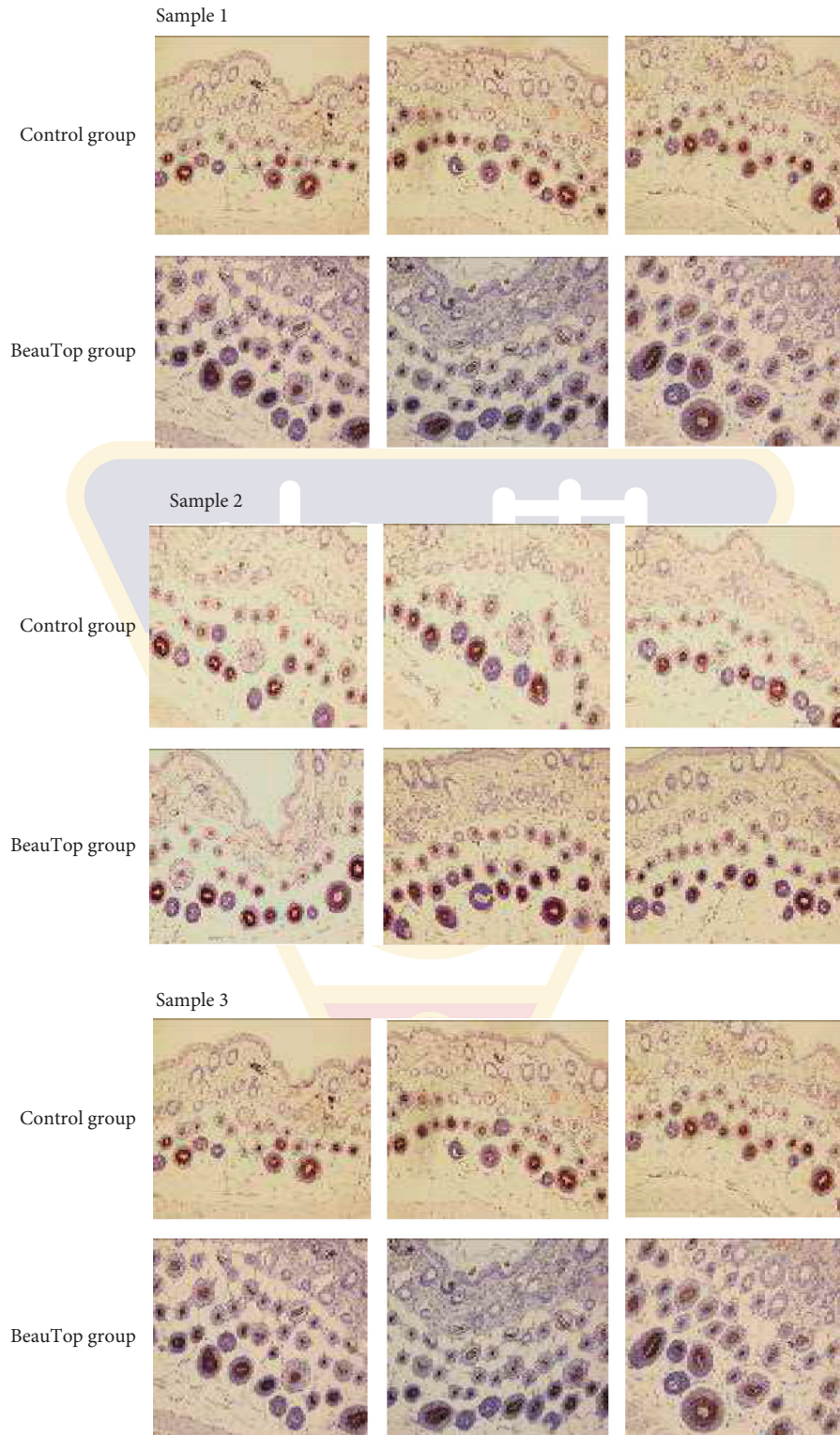
BeauTop group

Figure 2: Comparison of Immunohistochemistic stain of VEGF between control group and BeauTop group on Day 8.

property effects, strongly invigorate primordial qi and is the principal herb formula [38]. Interestingly, a study indicated that Shengfaling Tincture acts to increase blood circulation and hair growth in rats with hair depilation. This study also expressed a significant reduction in blood viscosity and hematocrit in qi-deficiency rats who received Shengfaling

treatment [39]. Danggui Buxue Tang (DBT) is an ancient Chinese medicinal decoction containing *Astragalus membranaceus* and *Angelica sinensis* (weight ratio of 5 : 1) that is being commonly prescribed as hematopoietic medicine to treat women with menopausal symptoms [40]. Pharmacological results indicate that DBT can stimulate the
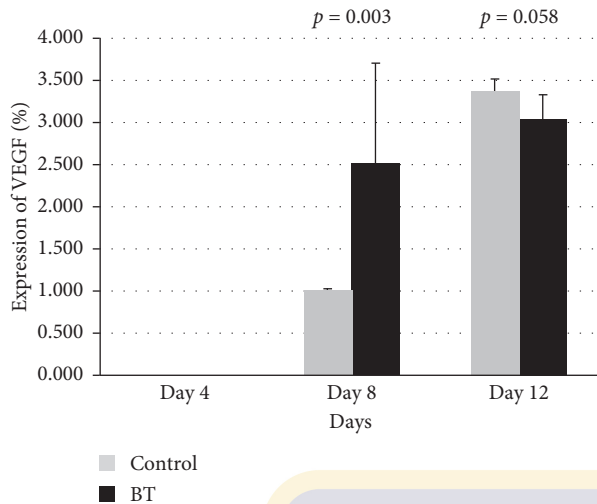
FIGURE 3: The area percentage (%) of VEGF distribution among treatment groups (BT) and control group, after being treated with the Chinese herbal medicines on Day 4, Day 8 and Day 12.
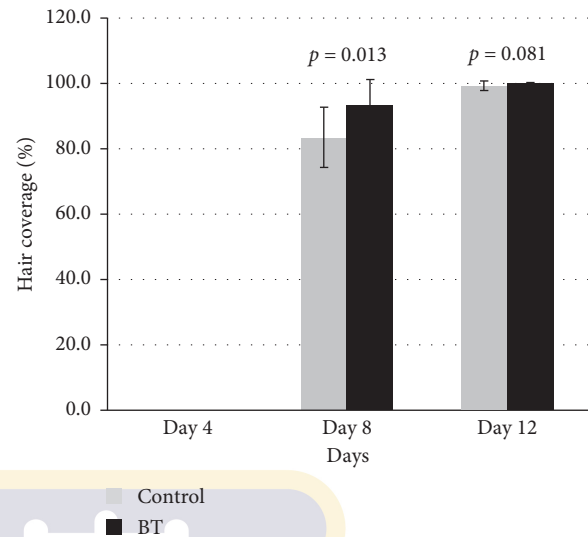
FIGURE 5: The hair coverage among treatment groups (BT) and control group, after being treated with the Chinese herbal medicines on Day 4, Day 8 and Day 12.
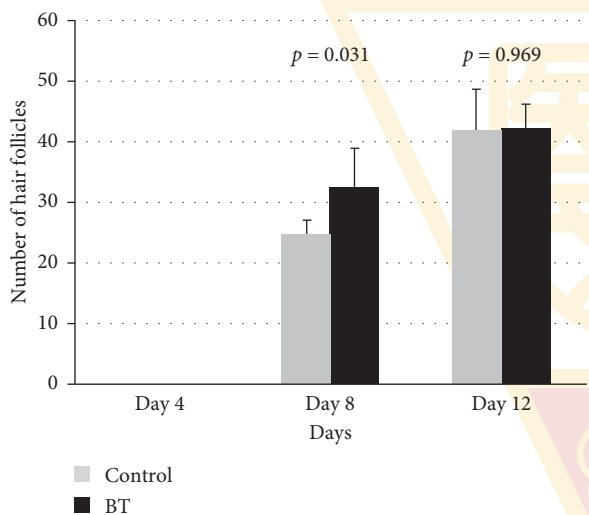
FIGURE 4: The number of hair follicle among treatment groups (BT) and control group, after treated being with the Chinese herbal medicines on Day 4, Day 8 and Day 12.

and the available liposome preparations for their ability to target the follicle, the topical gene therapy approach seems feasible [43]. A change in diet or taking the appropriate herbal health products or natural supplements will correct this widespread problem, need for further development in this area. Therefore, there will be more studies that will attempt to better understand the molecular mechanisms of hair-growth-promoting effects of BT.

5. Conclusion

We suggest that BT had possessed superior hair growth effectiveness through VEGF expression, and VEGF is considered as the most important mediator for the process of angiogenesis involved in hair growth development. This study presented a higher area percentage in the change of the number of hair follicles in the treatment group as compared to the control group. It was revealed that the BT has the potential effect of stimulating hair growth via upregulation of VEGF expression.

Data Availability

The results are collected from basic research studies shown in the manuscript.

Conflicts of Interest

All authors declare no conflicts of interest.

Authors' Contributions

Chun-Nan Wu and Yu-Hsiang Kuan is the author who contributed equally to this work.

production of hematopoietic growth factor erythropoietin (EPO) [41]. Another study suggests that DBT improves immune function through the regulatory effects on immune function parameters, such as TNF-α, IL-12, NO production, and NF-κB -mediated immune response [42]. We hypothesized that BT might have another potential effect to improve hair growth via increasing blood flow and qi.

Additional therapies for hair loss will become available in the future (e.g., topically effective Chinese herbal medicine). A better understanding of the causes and pathophysiology of alopecia should lead to more successful treatments involving the use of natural supplements that alter hair follicle cycling that provides protection from hair follicle immune attack. Given the accessibility of the follicle

Acknowledgments

References

[1] T. F. Cash, "The psychological effects of androgenetic alopecia in men," *Journal of the American Academy of Dermatology*, vol. 26, no. 6, pp. 926–931, 1992.

[2] N. Otberg, A. M. Finner, and J. Shapiro, "Androgenetic alopecia," *Endocrinology and Metabolism Clinics of North America*, vol. 36, no. 2, pp. 379–398, 2007.

[3] A. Tosti, F. Camaeho-Martinez, and R. Dawber, "Management of androgenetic alopecia," *Journal of the European Academy of Dermatology and Venereology*, vol. 12, no. 3, pp. 205–214, 1999.

[4] J. Ondrácek and J. Prixová, "The effect of neomycin and chloramphenicol against phagocytized Shigella in mouse macrophagues," *Sbornik Vedeckych Praci Lekarske Fakulty Karlovy University V Hradci Kralove*, vol. 11, no. 3, pp. 303–306, 1968.

[5] L. Alonso and E. Fuchs, "The hair cycle," *Journal of Cell Science*, vol. 119, no. 3, pp. 391–393, 2006.

[6] M. Ozeki and Y. Tabata, "Promoted growth of murine hair follicles through controlled release of vascular endothelial growth factor," *Biomaterials*, vol. 23, no. 11, pp. 2367–2373, 2002.

[7] D. T. Alexandrescu, C. L. Kauffman, and C. A. Dasanu, "The cutaneous epidermal growth factor network: can it be translated clinically to stimulate hair growth?" *Dermatology Online Journal*, vol. 15, no. 3, p. 1, 2009.

[8] J. Zhao, N. Harada, and K. Okajima, "Dihydrotestosterone inhibits hair growth in mice by inhibiting insulin-like growth factor-I production in dermal papillae," *Growth Hormone & IGF Research*, vol. 21, no. 5, pp. 260–267, 2011.

[9] Y. R. Yun, J. E. Won, E Jeon et al., "Fibroblast growth factors: biology, function, and application for tissue regeneration," *Journal of Tissue Engineering*, vol. 2010, Article ID 218142, 2010.

[10] W. Li, Z.-F. Lu, X.-Y. Man et al., "VEGF upregulates VEGF receptor-2 on human outer root sheath cells and stimulates proliferation through ERK pathway," *Molecular Biology Reports*, vol. 39, no. 9, pp. 8687–8694, 2012.

[11] K. Yano, L. F. Brown, and M. Detmar, "Control of hair growth and follicle size by VEGF-mediated angiogenesis," *Journal of Clinical Investigation*, vol. 107, no. 4, pp. 409–417, 2010.

[12] J. Meephansan, J. Thummakriengkrai, S. Ponnikorn, W. Yingmema, R. Deenonpoe, and P. Suchonwanit, "Efficacy of topical tofacitinib in promoting hair growth in non-scarring alopecia: possible mechanism via VEGF induction," *Archives of Dermatological Research*, vol. 309, no. 9, pp. 729–738, 2017.

[13] C.-J. Liou, W.-C. Huang, and J. Tseng, "Long-term oral administration of ginseng extract modulates humoral immune response and spleen cell functions," *The American Journal of Chinese Medicine*, vol. 33, no. 04, pp. 651–661, 2005.

[14] R. Jin and S. Kurashige, "Effects of Chinese herbs on macrophage functions in N-butyl-N-butanolnitrosoamine treated mice," *Immunopharmacology and Immunotoxicology*, vol. 18, no. 1, pp. 105–114, 1996.

[15] T. K. Yim, W. K. Wu, W. F. Pak, D. H. F. Mak, S. M. Liang, and K. M. Ko, "Myocardial protection against ischaemia-reperfusion injury by a Polygonum multiflorum extract supplemented ?Dang-Gui decoction for enriching blood?, a compound formulation, ex vivo," *Phytotherapy Research*, vol. 14, no. 3, pp. 195–199, 2000.

[16] R.-X. Zhang, M.-X. Li, and Z.-P. Jia, "Rehmannia glutinosa: review of botany, chemistry and pharmacology," *Journal of Ethnopharmacology*, vol. 117, no. 2, pp. 199–214, 2008.

[17] X. Zhang, A. Zhang, B. Jiang, Y. Bao, J. Wang, and L. An, "Further pharmacological evidence of the neuroprotective effect of catalpol from Rehmannia glutinosa," *Phytomedicine*, vol. 15, no. 6-7, pp. 484–490, 2008.

[18] D.-I. Kim, S.-H. Lee, J.-H. Choi, H. S. Lillehoj, M.-H. Yu, and G.-S. Lee, "The butanol fraction of Eclipta prostrata (Linn) effectively reduces serum lipid levels and improves antioxidant activities in CD rats," *Nutrition Research*, vol. 28, no. 8, pp. 550–554, 2008.

[19] C. Y. Lee, C. Y. Yang, C. C. Lin, M. C. Yu, S. J. Sheu, and Y. H. Kuan, "Hair growth is promoted by BeauTop via expression of EGF and FGF7," *Molecular Medicine Reports*, vol. 17, no. 6, pp. 8047–8052, 2018.

[20] Y. K. Sung, S. Y. Hwang, S. Y. Cha et al., "The hair growth promoting effect of ascorbic acid 2-phosphate, a long-acting Vitamin C derivative," *Journal of Dermatological Science*, vol. 41, no. 2, pp. 150–152, 2006.

[21] S. Cébe-Suarez, A. Zehnder-Fjällman, and K. Ballmer-Hofer, "The role of VEGF receptors in angiogenesis; complex partnerships," *Cellular and Molecular Life Sciences*, vol. 63, no. 5, pp. 601–615, 2006.

[22] M. Kowanetz and N. Ferrara, "Vascular endothelial growth factor signaling pathways: therapeutic perspective: fig. 1," *Clinical Cancer Research*, vol. 12, no. 17, pp. 5018–5022, 2006.

[23] C. K. Goldman, J.-C. Tsai, L. Soroceanu, and G. Y. Gillespie, "Loss of vascular endothelial growth factor in human alopecia hair follicles," *Journal of Investigative Dermatology*, vol. 104, no. 5, pp. 18–20, 1995.

[24] H. F. Dvorak, L. F. Brown, M. Detmar, and A. M. Dvorak, "Vascular permeability factor/vascular endothelial growth factor, microvascular hyperpermeability, and angiogenesis," *The American Journal of Pathology*, vol. 146, no. 5, pp. 1029–1039, 1995.

[25] T. Ito, "Hair follicle is a target of stress hormone and autoimmune reactions," *Journal of Dermatological Science*, vol. 60, no. 2, pp. 67–73, 2010.

[26] M. C. Jones, "Treatment options for androgenic alopecia," *U.S. Pharmacopeia*, vol. 43, no. 8, pp. 12–16, 2018.

[27] T. Kanzaki, N. Morisaki, R. Shiina, and Y. Saito, "Role of transforming growth factor-β pathway in the mechanism of wound healing by saponin from Ginseng Radix rubra," *British Journal of Pharmacology*, vol. 125, no. 2, pp. 255–262, 1998.

[28] Y. Lei, W. Tian, L. Q. Zhu, J. Yang, and K. J. Chen, "Effects of Radix Ginseng and Radix Notoginseng formula on secretion of vascular endothelial growth factor and expression of vascular endothelial growth factor receptor-2 in human umbilical vein endothelial cells," *Journal of Chinese Integrative Medicine*, vol. 8, no. 4, pp. 368–372, 2010.

[29] C.-J. Liou, M.-L. Li, and J. Tseng, "Intraperitoneal injection of ginseng extract enhances both immunoglobulin and cytokine production in mice," *The American Journal of Chinese Medicine*, vol. 32, no. 1, pp. 75–88, 2004.

[30] Y. Zhang, G. Hu, H. C. Lin, S. J. Hong, Y. H. Deng, and J. Y. Tang, "Radix Astragali extract promotes angiogenesis involving vascular endothelial growth factor receptor-related phosphatidylinositol 3-kinase/Akt-dependent pathway in human endothelial cells," *Phytotherapy Research*, vol. 23, no. 9, pp. 205–213, 2009.

[31] M. H. Kim, Y. Y. Choi, I.-H. Cho, J. Hong, S.-H. Kim, and W. M. Yang, "Angelica sinensis induces hair regrowth via the inhibition of apoptosis signaling," *The American Journal of Chinese Medicine*, vol. 42, no. 4, pp. 1021–1034, 2014.

[32] Y. Zhang, Y. Wang, L. Wang, Y. Zhang, Y. Qin, and T. Chen, "Effects of Rehmannia glutinosa oligosaccharide on human adipose-derived mesenchymal stem cells in vitro," *Life Sciences*, vol. 91, no. 25-26, pp. 1323–1327, 2012.

[33] L. Gao, C. Li, Z. Wang et al., "Ligustri Lucidi Fructusas a traditional Chinese medicine: a review of its phytochemistry and pharmacology," *Natural Product Research*, vol. 29, no. 6, pp. 493–510, 2015.

[34] Y. Q. Tang, C. Li, X. J. Sun, Y. Liu, X. T. Wang, and Y. B. Guo, "Fructus Ligustri Lucidi modulates estrogen receptor expression with no uterotrophic effect in ovariectomized rats," *BMC Complementary Medicine and Therapies*, vol. 18, no. 1, p. 118, 2018.

[35] Y. Zhang, T.-Y. Diao, L. Wang, C.-T. Che, and M.-S. Wong, "Protective effects of water fraction of Fructus Ligustri Lucidi extract against hypercalciuria and trabecular bone deterioration in experimentally type 1 diabetic mice," *Journal of Ethnopharmacology*, vol. 158, pp. 239–245, 2014.

[36] D.-I. Kim, S.-H. Lee, J.-H. Hong et al., "The butanol fraction of Eclipta prostrata (Linn) increases the formation of brain acetylcholine and decreases oxidative stress in the brain and serum of cesarean-derived rats," *Nutrition Research*, vol. 30, no. 8, pp. 579–584, 2010.

[37] C.-Y. Lee, C.-C. Wei, M.-C. Yu et al., "Hair growth effect of traditional Chinese medicine BeauTop on androgenetic alopecia patients: a randomized double-blind placebo-controlled clinical trial," *Experimental and Therapeutic Medicine*, vol. 13, no. 1, pp. 194–202, 2017.

[38] C. M. Chen, C. Y. Lee, P. J. Lin, C. L. Hsieh, and H. C. Shih, "Evaluation on the pharmacological effect of traditional Chinese medicine SiJunZiTang on stress-induced peptic ulcers," *Evidence-Based Complementary and Alternative Medicine*, vol. 2013, Article ID 186076, , 2013.

[39] P. B. Ma, "Experimental study on the role of Shengfaling tincture in promoting blood circulation and hair growth in rats," *Di 1 jun yi da xue xue bao = Academic journal of the first medical college of PLA*, vol. 22, no. 5, pp. 421-422, 2002.

[40] O. Zierau, K. Y. Zheng, A. Papke, T. T. Dong, K. W. Tsim, and G. Vollmer, "Functions of danggui buxue tang, a Chinese herbal decoction containing Astragali radix and angelicae sinensis radix, in uterus and liver are both estrogen receptor-dependent and -independent," *Evidence-Based Complementary and Alternative Medicine*, vol. 2014, Article ID 438531, , 2014.

[41] K. Y. Z. Zheng, R. C. Y. Choi, H. Q. H. Xie et al., "The expression of erythropoietin triggered by danggui buxue tang, a Chinese herbal decoction prepared from radix Astragali and radix Angelicae Sinensis, is mediated by the hypoxia-inducible factor in cultured HEK293T cells," *Journal of Ethnopharmacology*, vol. 132, no. 1, pp. 259–267, 2010.

[42] M.-C. Kim, G.-H. Lee, S.-J. Kim et al., "Immune-enhancing effect of Danggwibohyeoltang, an extract fromAstragali RadixandAngelicae gigantis Radix,in vitroandin vivo,"

[43] L. Li and R. M. Hoffman, "The feasibility of targeted selective gene therapy of the hair follicle," *Nature Medicine*, vol. 1, no. 7, pp. 705-706, 1995.

Immunopharmacology and Immunotoxicology, vol. 34, no. 1, pp. 66–73, 2012.

Research Paper

Risk of peripheral artery disease and stroke in migraineurs with or without aura: a nationwide population-based cohort study

Wun-Zhih Siao[1,2,3], Chun-Hung Su[1,2*], Yu-Hsiang Kuan[4,5], Tung-Han Tsai[6], Kuang-Hua Huan[6#], Chien-Ying Lee[4,5✉]

1. Department of Internal Medicine, School of Medicine, Chung Shan Medical University, Taichung, Taiwan
2. Division of Cardiology, Department of Internal Medicine, Chung Shan Medical University Hospital, Taichung, Taiwan
3. Institute of Medicine, College of Medicine, Chung Shan Medical University, Taichung, Taiwan
4. Department of Pharmacology, School of Medicine, Chung Shan Medical University, Taichung, Taiwan
5. Department of Pharmacy, Chung Shan Medical University Hospital, Taichung, Taiwan
6. Department of Health Services Administration, China Medical University, Taichung, Taiwan

*equal to first author

#equal to corresponding author

✉ Corresponding author: Chien-Ying Lee: cshd015@csmu.edu.tw

Abstract

Background: Migraine is deemed a neurovascular disorder and there is growing evidence on the increased risk of cardiovascular disease, especially ischemic stroke, in patients with migraine. However the risk of peripheral artery disease (PAD) and stroke in migraineurs and the association between migraineurs with or without aura is still under debate. Our study aimed to identify the risk of PAD and stroke in migraineurs with or without aura.

Methods: This was a population-based cohort study utilizing Taiwan Longitudinal Health Insurance Database (LHID2010). Patients with coding of migraine from 2002 to 2011 were enrolled and those with established cardiovascular disease defined as myocardial infarction, stroke, PAD, venous thromboembolism, atrial fibrillation and heart failure diagnosis before the index date were excluded. Participants were categorized into migraine group, migraine without aura group, and migraine with aura group respectively. The subjects in the three groups were propensity score-matched randomly to their counterparts without migraine. The study outcome was PAD and stroke. The Cox proportional hazard model was used to estimate the hazard ratios with 95% confidence interval (CI) for the association between migraine and the incident events of disease, after controlling for related variables.

Results: The migraine, migraine without aura, and migraine with aura group included 5,173 patients, 942 patients and 479 patients respectively after propensity score-matching. The migraine group had an increased risk of PAD [adjusted hazard ratio (aHR): 1.93; 95% confidence interval (CI): 1.45–2.57; p < 0.001] and stroke (aHR: 1.55; 95% CI: 1.35–1.77; p < 0.001) compared to their non-migraine controls. Both the groups of migraine without aura and with aura had an increased risk of stroke (aHR: 1.49, 95% CI: 1.11–2.00; p = 0.008; aHR: 1.63, 95% CI: 1.10–2.43; p = 0.016). With regards to the outcome of PAD, the group of migraine with aura had a trend of an increased risk but did not reach statistical significance (aHR: 1.95, 95% CI: 0.86–4.40; p = 0.108).

Conclusion: Migraineurs without established cardiovascular disease had a significantly increased risk of PAD and stroke, and the risk of stroke persists in migraineurs with or without aura, with an increased trend of PAD in migraineurs with aura. Our study result should remind clinical physicians of the risk of PAD in the future among migraineurs even without established cardiovascular disease currently, and screening for PAD and stroke may be needed in caring patients with migraine.

Introduction

Migraine is deemed as a neurovascular disorder that is more common in women than men [1]. A population-based study showed high prevalence of migraine in Taiwan, with prevalence rate of 14.4% in woman and 9.1% in men aged more than 15 years old respectively [2]. Migraine can lead to disability, impair life quality, and carry large healthcare and economic burden. The association between migraine and cardiovascular disease has been studied. Strong evidence suggested migraine as a risk factor for ischemic stroke. Researches have also shown the positive link between migraine and ischemic heart disease, especially in migraineurs with aura [3-5].

PAD has approximately 20% prevalence rate and the risk increased in elderly. Atherosclerosis is the major pathogenesis that implicated in the development of PAD. Risk factors such as cigarette smoking, diabetes, hypertension, dyslipidemia, and hyperhomocysteinemia contribute to the develop-ment of PAD [6, 7]. Severe PAD increased the risk of limb amputation or percutaneous transluminal intervention that result in poor life quality and heavy burden of economic. Once patients with PAD develop critical limb ischemia, the mortality rate within the first year was as higher as 20-25%, and the five-year survival rate was less then 30% [8]. There was substantial evidence supporting the higher risk of stroke among migraineurs, and mostly migraineurs with aura [5]. Historical researches demonstrated undetermined results as regard the association of migraine and PAD. Evidence from observation studies found migraineurs had lower ankle-brachial index (ABI) or higher risk with symptom of claudication suggesting presence of PAD [9, 10]. However a population-based cohort study did not showed a statistically significant correlation between migraine and PAD [11]. Moreover, there is little data addressing the risk of PAD in migraineurs with or without aura. Thus the aim of this study was to evaluate the risk of PAD and stroke in migraineurs without established cardiovascular disease, and the risk between migraineurs with or without aura, by analyzing a nationwide population-based retrospect-ive cohort from the National Health Insurance Research Database (NHIRD) in Taiwan.

Materials and Methods

Database

This was a retrospective cohort study, in which secondary data analysis was conducted. Data were obtained from the 2000-2013 Longitudinal Health Insurance Database (LHID) provided by the National Health Insurance Administration, Ministry of Health and Welfare and managed by National Health Research Institutes (Registered number NHIRD-104-004). The LHID comprises the information of one million beneficiaries randomly selected from the Taiwan National Health Insurance (NHI) program. The NHI program is a nationwide social insurance program that has covered up to 99% of citizens since 1995. Hence, the database is nationally representative of Taiwan. Owing to the anonymity of the database, the requirement for informed consent was waived, and this study was approved as an ethical review by the Institutional Review Board of China Medical University Hospital, Taiwan.

Study Subjects

The participants were the new-onset migraine patients who aged above 20 years old. The definition of migraine was migraine diagnosis three times a year, which according to the International Classification of Diseases, Ninth Revision, Clinical Modification (ICD-9-CM) code 346), and concurrent use of antimigraine preparations. We excluded patients who had suffered cardiovascular diseases before had migraine to reduce the study bias. The cardiovascular diseases contained myocardial infarction (ICD-9-CM code 410), stroke (ICD-9-CM code 430-438), peripheral artery disease (ICD-9-CM) code 443.9), venous thromboembolism (ICD-9-CM code 453), atrial fibrillation (ICD-9-CM code 427.31), and heart failure (ICD-9-CM code 428). Furthermore, we used the propensity score matching (PSM) to obtain the patients without migraine in 1:5 matching for each migraine patient on the year of enrollment, via gender, age and Charlson comorbidities index (CCI), as the comparison. In addition, the patients who we selected for the comparison was had no received any migraine diagnosis during the study period. The study is an epidemiologic study based on the LHID [12, 13]. We adopted the PSM to obtain the comparison group the same method as previous population-based studies conducted on LHID. The PSM is a statistical matching technique that is available to reduce potential confounding caused by unbalanced covariates in non-experimental settings. The PSM is the probability calculated via the Logistic regression model. A score is a unit with certain characteristics that will be assigned to migraine patients. The scores could be used to reduce or eliminate selection bias in observational studies on the characteristics of migraine and non-migraine.

We enrolled 5,173 patients with migraine and 25,865 patients without migraine, respectively. Besides, we classified subgroups of migraine patients into migraine without aura (ICD-9 CM code 346.1,

346.7), and migraine with aura (ICD-9 CM code 346.0, 346.5, 346.6). Figure 1 was the flowchart of selection of patients.

Study Designs

This study was conducted using 2000-2013 claim data from LHID. We enrolled patients with migraine and the comparison from 2002-2011 as the study subject, to ensure that exclusion condition and each patient had least two years of follow-up. Each patient was follow-up until the date of the incident events of disease, death, or the end of 2013, whichever occurred first. We estimated the risk of the incident events of disease contained peripheral artery disease and stroke. The definition of peripheral artery disease in the study was based on the diagnosis according to the ICD-9-CM codes 443.9, and the stroke was according to the ICD-9-CM codes 430-438.

The control variables in the study were gender, age, and comorbidity diseases. The comorbidity disease contained diabetes mellitus (ICD-9-CM codes 250), hypertension (ICD-9-CM codes 401-405), hyperlipidemia (ICD-9-CM code 272.0-272.4), valvular heart disease (ICD-9-CM code 394-396, 424,

746), obesity (ICD-9-CM code 278), chronic obstructive pulmonary disease (COPD) (ICD-9-CM code 490-492, 494-496), liver disease (ICD-9-CM code 070, 571, 573.3), cancer (ICD-9-CM code 140-239), thyroid disease (ICD-9-CM code 240-246, 759.1-759.2), autoimmune disease (ICD-9-CM code 279.4), renal failure (ICD-9-CM code 584-585), and Helicobacter pylori (ICD-9-CM code 041.86).

Statistical analysis

All statistical analyses in the study were using SAS software version 9.4 (SAS Institute Inc., Cary, NC, USA). Descriptive statistics were used to perform descriptive analysis of the number and percentage of patient characteristics (gender, age, and comorbidity disease). The Chi-square test was used to compare the differences between migraine patients and the comparison after matching. The study used the Cox proportional hazard model to estimate the hazard ratios with 95% confidence interval (CI) for the association between migraine and the incident events of disease, after controlling for related variables. Statistical significance in this study was defined as $p < 0.05$.
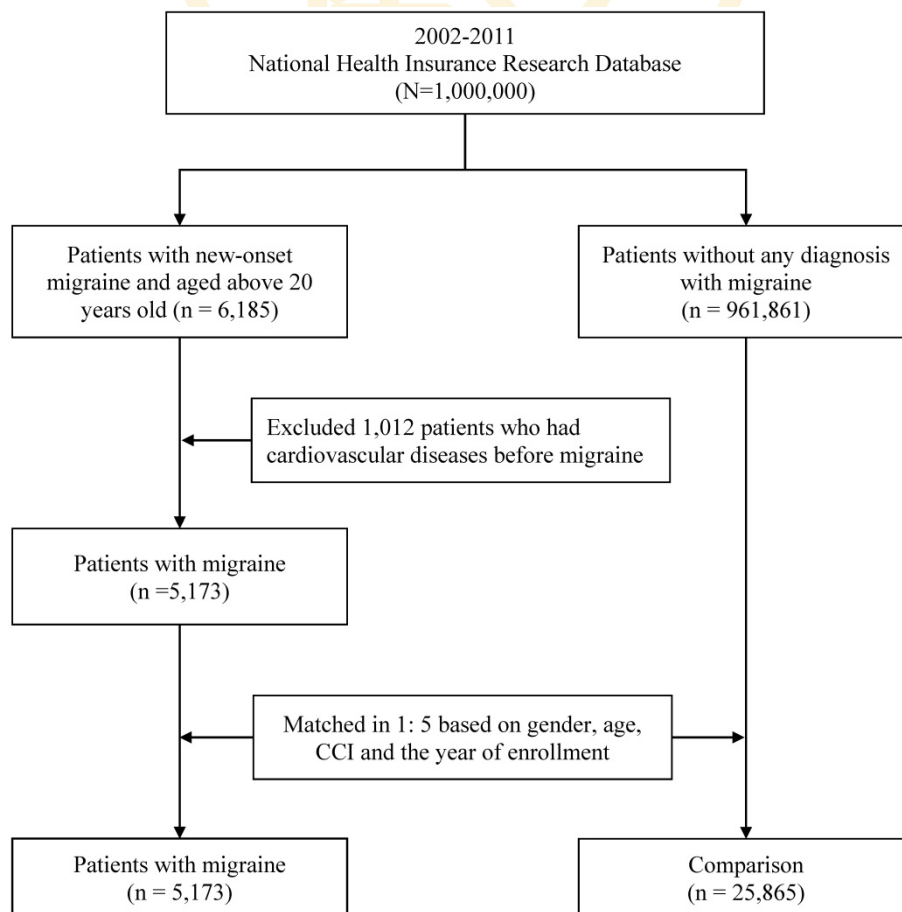
Figure 1. Flowchart of the study subject selection process.

Table 1. The baseline characteristics of patients with migraine after matching

Variables	Comparison		Migraine patients								p-value [b]
			subtotal		Migraine		Without aura		With aura		
	n	%	n	%	n	%	n	%	n	%	
Total	25,865	83.33	5,173	16.67	3,752	12.09	942	3.03	479	1.54	
Gender [a.]											1.000
Female	18,835	72.82	3,767	72.82	2,697	71.88	708	75.16	362	75.57	
Male	7,030	27.18	1,406	27.18	1,055	28.12	234	24.84	117	24.43	
Age (year) [a.]	45.00 ± 14.38		44.97 ± 13.36		45.64 ± 13.46		43.13 ± 12.98		43.32 ± 12.93		1.000
20-34	6,545	25.30	1,309	25.30	887	23.64	282	29.94	140	29.23	
35-49	10,700	41.37	2,140	41.37	1,555	41.44	379	40.23	206	43.01	
50-64	6,395	24.72	1,279	24.72	956	25.48	223	23.67	100	20.88	
≥65	2,225	8.60	445	8.60	354	9.43	58	6.16	33	6.89	
CCI [a.]											1.000
0	12,025	46.49	2,405	46.49	1,734	46.22	455	48.30	216	45.09	
1	7,535	29.13	1,507	29.13	1,071	28.54	279	29.62	157	32.78	
2	3,265	12.62	653	12.62	488	13.01	110	11.68	55	11.48	
≥3	3,040	11.75	608	11.75	459	12.23	98	10.40	51	10.65	
Diabetes mellitus											<0.001
No	22,923	88.63	4,711	91.07	3,396	90.51	873	92.68	442	92.28	
Yes	2,942	11.37	462	8.93	356	9.49	69	7.32	37	7.72	
Hypertension											<0.001
No	20,692	80.00	3,702	71.56	2,610	69.56	723	76.75	369	77.04	
Yes	5,173	20.00	1,471	28.44	1,142	30.44	219	23.25	110	22.96	
Hyperlipidemia											<0.001
No	21,917	84.74	4,229	81.75	3,049	81.26	799	84.82	381	79.54	
Yes	3,948	15.26	944	18.25	703	18.74	143	15.18	98	20.46	
Valvular heart disease											<0.001
No	24,995	96.64	4,915	95.01	3,577	95.34	881	93.52	457	95.41	
Yes	870	3.36	258	4.99	175	4.66	61	6.48	22	4.59	
Obesity											<0.001
No	25,603	98.99	5,085	98.30	3,695	98.48	921	97.77	469	97.91	
Yes	262	1.01	88	1.70	57	1.52	21	2.23	10	2.09	
COPD											<0.001
No	22,349	86.41	4,316	83.43	3,146	83.85	784	83.23	386	80.58	
Yes	3,516	13.59	857	16.57	606	16.15	158	16.77	93	19.42	
Liver disease											<0.001
No	20,653	79.85	3,930	75.97	2,857	76.15	721	76.54	352	73.49	
Yes	5,212	20.15	1,243	24.03	895	23.85	221	23.46	127	26.51	
Cancer											<0.001
No	24,675	95.40	5,016	96.97	3,637	96.93	913	96.92	466	97.29	
Yes	1,190	4.60	157	3.03	115	3.07	29	3.08	13	2.71	
Thyroid disease											<0.001
No	24,282	93.88	4,755	91.92	3,457	92.14	862	91.51	436	91.02	
Yes	1,583	6.12	418	8.08	295	7.86	80	8.49	43	8.98	
Autoimmune disease											0.793
No	25,805	99.77	5,160	99.75	3,742	99.73	942	100.00	476	99.37	
Yes	60	0.23	13	0.25	10	0.27	-	-	3	0.63	
Renal failure											0.016
No	25,578	98.89	5,135	99.27	3,723	99.23	935	99.26	477	99.58	
Yes	287	1.11	38	0.73	29	0.77	7	0.74	2	0.42	
Helicobacter pylori											0.014
No	25,790	99.71	5,147	99.50	3,737	99.60	935	99.26	475	99.16	
Yes	75	0.29	26	0.50	15	0.40	7	0.74	4	0.84	

a. Variables for propensity score matching.

b. The difference between migraine patients and comparison after matching.

Results

The baseline characteristics of patients with migraine after matching

Table 1 show the distribution of the variables of the study subjects. Among all patients with migraine, there were 942 patients without aura (3.03%), and 479 patients with aura (1.54%). In patients with migraine, the age was 44.97 ± 13.36, and most patients were female (72.82%). In terms of comorbidities, 8.93% of patients with migraine had diabetes mellitus, 28.44% had hypertension, 18.25% had hyperlipidemia, 4.99% had valvular heart disease, and 24.03% had liver disease. the gender, age and CCI were the matched and the Chi-square test was used to verify the difference between the paired migraine patients and the comparison, which there was no statistically significant difference (p >0.05).

Risk of related health outcomes in migraine patients with or without aura

This study explores the correlation between

migraine patients and the occurrence of peripheral artery disease and stroke. Figure 2 illustrated the cumulative risk of stroke was significantly higher in migraine patients than in the comparison. As well, Figure 3 illustrated the cumulative risk of peripheral artery disease was higher in migraine patients than in the comparison.

Table 2 shows the risk of each variable and the occurrence of peripheral artery disease and stroke, respectively. After controlling other related variables, the adjusted hazard ratio (aHR) of migraine patients in developing peripheral artery disease was 1.93 times (95 % CI =1.45-2.57), and stroke was 1.55 times (95% CI=1.35-1.77). In terms of subgroup, migraine without aura and with aura patients had no statistic significant on developing peripheral artery disease, but migraine without aura patients (aHR =1.49, 95% CI =1.11-2.00) and migraine with aura patients (aHR =1.63, 95% CI =1.10-2.43) both had a higher risk on developing stroke. The more old age, the higher the relative risk of developing peripheral artery disease and stroke. Compared with patients aged 20-34, the relative risk of patients in ≥65 years old was 8.37 times (95% CI =4.62-15.18) on developing peripheral artery disease and 17.81 times (95% CI =13.19-24.06) on developing stroke.

Table 2. Risk of related health outcomes in migraine patients with or without aura.

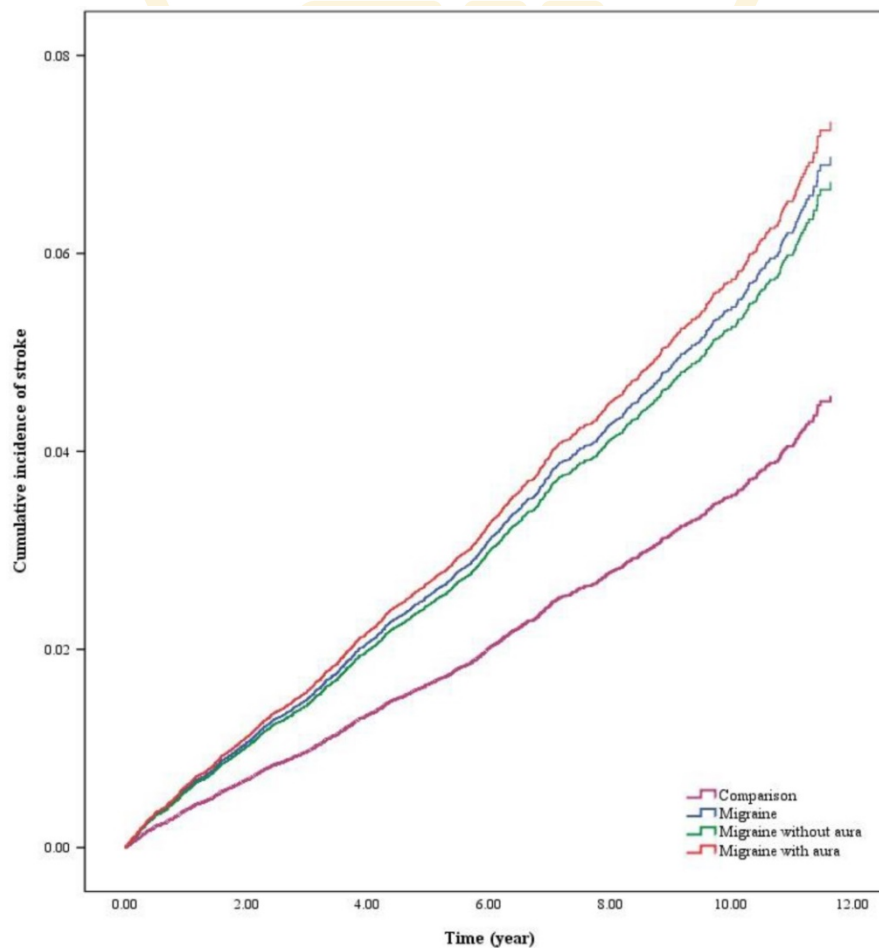| Variables	Peripheral artery disease				Stroke				
	Events	aHR [a]	95% CI		p-value	Events	aHR [a]	95% CI		p-value
Patients group										
Comparison (REF)	206	1				1,105	1			
Migraine	63	1.93	1.45	- 2.57	<0.001	268	1.55	1.35	- 1.77	<0.001
Migraine without aura	5	0.84	0.35	- 2.04	0.700	47	1.49	1.11	- 2.00	0.008
Migraine with aura	6	1.95	0.86	- 4.40	0.108	25	1.63	1.10	- 2.43	0.016
Gender										
Female (REF)	202	1				926	1			
Male	78	0.92	0.71	- 1.21	0.556	519	1.34	1.20	- 1.49	<0.001
Age (year)										
20-34 (REF)	15	1				52	1			
35-49	79	2.76	1.58	- 4.80	<0.001	287	3.04	2.26	- 4.08	<0.001
50-64	111	5.19	2.96	- 9.08	<0.001	623	9.47	7.09	- 12.65	<0.001
≥65	75	8.37	4.62	- 15.18	<0.001	483	17.81	13.19	- 24.06	<0.001
Diabetes mellitus										
No (REF)	214	1				1,083	1			
Yes	66	1.23	0.90	- 1.69	0.193	362	1.29	1.13	- 1.48	<0.001
Hypertension										
No (REF)	144	1				684	1			
Yes	136	1.65	1.24	- 2.19	<0.001	761	1.65	1.46	- 1.87	<0.001
Hyperlipidemia										
No (REF)	199	1				1,036	1			
Yes	81	1.16	0.86	- 1.56	0.336	409	0.98	0.86	- 1.12	0.788
Valvular heart disease										
No (REF)	267	1				1,348	1			
Yes	13	1.01	0.58	- 1.78	0.970	97	1.42	1.15	- 1.76	0.001
Obesity										
No (REF)	278	1				1,423	1			
Yes	2	0.55	0.14	- 2.23	0.406	22	1.33	0.87	- 2.03	0.190
COPD										
No (REF)	223	1				1,096	1			
Yes	57	1.01	0.75	- 1.37	0.947	349	1.12	0.99	- 1.27	0.080
Liver disease										
No (REF)	205	1				1,083	1			
Yes	75	1.12	0.85	- 1.48	0.421	362	0.95	0.84	- 1.07	0.389
Cancer										
No (REF)	265	1				1,346	1			
Yes	15	0.91	0.54	- 1.53	0.715	99	1.04	0.85	- 1.28	0.697
Thyroid disease										
No (REF)	261	1				1,359	1			
Yes	19	1.05	0.65	- 1.68	0.853	86	0.95	0.76	- 1.19	0.650
Autoimmune disease										
No (REF)	279	1				1,442	1			
Yes	1	1.98	0.28	- 14.13	0.498	3	0.92	0.23	- 3.67	0.901
Renal failure										
No (REF)	268	1				1,409	1			
Yes	12	2.49	1.38	- 4.51	0.003	36	1.19	0.85	- 1.67	0.300
Helicobacter pylori										
No (REF)	280					1,444	1			
Yes	-	-	-	-	-	1	0.27	0.04	- 1.92	0.191

a. aHR, adjusted hazard ratio.

In terms of comorbidity analysis, patients with hypertension showed the higher relative risk of developing peripheral artery disease (aHR=1.65, 95% CI=1.24-2.19); patients with diabetes mellitus (aHR= 1.29, 95% CI=1.13-1.48), hypertension (aHR=1.65, 95% CI=1.46-1.87), and valvular heart disease (aHR= 1.42, 95% CI=1.15-1.76) had the higher risk of developing stroke.

Discussion

Our study showed migraineurs without established cardiovascular disease had a 1.93-fold risk increment of PAD. The increased risk of stroke in migraineurs was also observed (aHR: 1.55; 95% CI: 1.35–1.77; p < 0.001), which was compatible with the data from meta-analysis study (aHR: 1.73; 95% CI: 1.31–2.29; p : 0.004) [14]. Evidence had showed migraineurs had higher risk of ischemic stroke particularly those with aura [14, 15]. Our study revealed both migraineurs with or without aura had increased risk of stroke, with 1.63-fold risk increment and 1.49-fold risk increment respectively. Although

no statistical significant association between PAD and migraineurs with aura was found, the increased trend of risk of PAD in migraineurs with aura was observed in our study.

There are several possible mechanisms link between migraine and PAD. Endothelial microparticles (EMP) are small vesicles generated from endothelial cells and play important roles in inflammation, coagulation and endothelial function. Elevated EMP was observed among woman with migraine and aura, and was correlated with higher heart rate-adjusted augmentation index, which is an indirect measure of arterial stiffness [16]. The vascular biomarker that implicated in the pathogenesis of coagulation-specific disorder has also contributed the association of migraine and PAD. A population-based study showed woman with migraine and aura had elevated Fibrinogen and Factor II level, and the increased frequency of aura attack predicted higher vascular biomarker [17]. The molecular basis may provide support of our result that increased risk of PAD in migraineurs and especially those with aura.

Figure 2. The cumulative risk of stroke in migraine patients with or without aura.
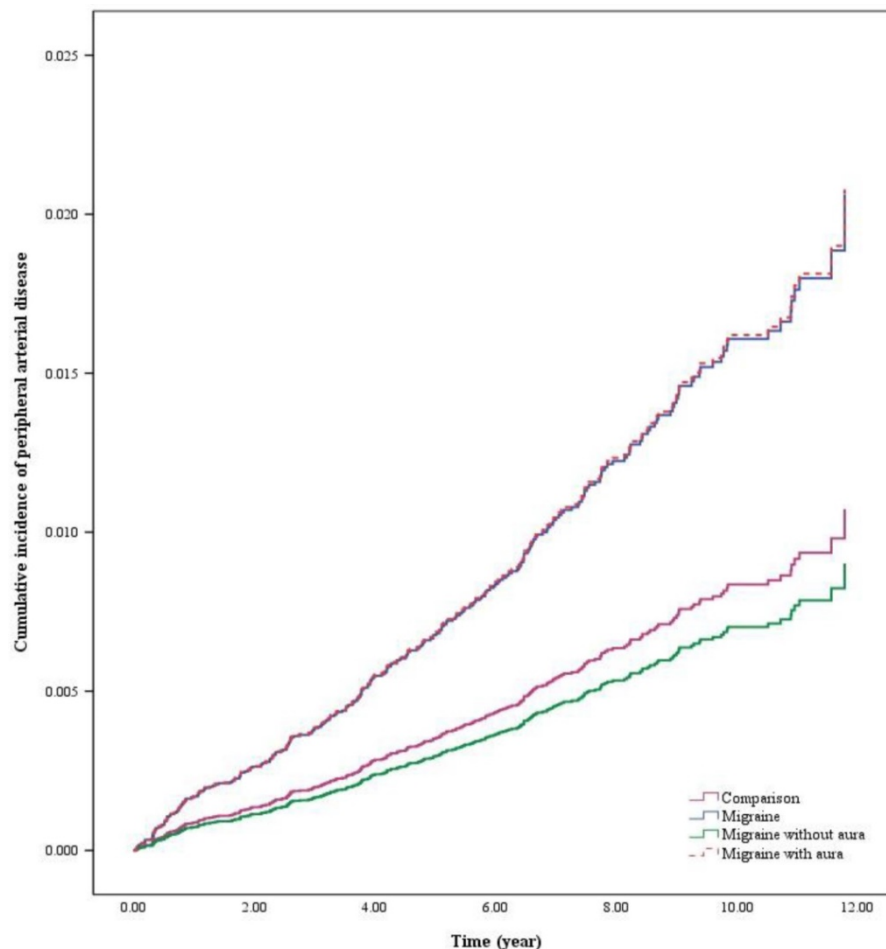
Figure 3. The cumulative risk of peripheral artery disease in migraine patients with or without aura.

Accumulating evidence also suggested the genetic overlaping between migraine and coronary artery disease [18]. Since potential pathophysiology that promote atherosclerotic cardiovascular disease is involved in the shared genetic factors between coronary artery disease and PAD [19], the investigation of genetic basis may provide our understanding on the contributing mechanism between the two entities of disease.

Selvin, Elizabeth and Thomas P. Erlinger had described diabetes, hypertension, hypercholesterolemia, and impaired renal function as the risk factors of PAD [20]. In our study, participants with history of diabetes, hypertension and renal failure were positive associated with PAD, which was compatible the result of the previous study. Subjects with chronic obstructive pulmonary disease and hypercholesterolemia also have higher risk of PAD albeit non-statistical significance. Of note, the obesity paradox has been mentioned [21] and Selvin, Elizabeth and Thomas P. Erlinger showed obesity was negative associated with PAD [20]. Our study also demonstrated the trend of negative association between PAD and obesity.

Previous study had suggested the strong evidence of positive correlation between migraine and stroke. A case-control study demonstrated the association between migraine and stroke (OR 1.5, 95% CI 1.2–2.1), and claudication (OR 2.69, 95% CI 1.98–3.23) [10]. Of note, the study population did not exclude those with established cardiovascular disease. Evidence from meta-analysis study found the higher risk of ischemic stroke among patients with migraine and the risk was increased by being female gender and younger age [14]. The result from the meta-analysis disclosed the underlying pathophysiology beyond atherosclerosis between migraine and stroke, since atherosclerosis is classed as a disease of aging.

The historical studies aimed to investigate the relationship between migraine and PAD but the result was conflicting. A small study demonstrated that migraineurs tended to have lower ABI significantly. More specifically, participants in this study had no history of cardiac vascular events such as angina, heart disease or stroke [9]. A cross-sectional case-control study was designed to identify the risk of atherosclerosis in migraineurs. Atherosclerosis was quantified by intima media thickness, pulse wave velocity and ABI. The result showed the risk of

atherosclerosis did not increase among those with migraine compared with those without migraine, although subjects with migraine are more likely to have diabetes and smoking [22].

A population-based cohort study demonstrated the increased risk of PAD among subjects with migraine [23]. In the study, patients with cardiovascular disease or cardiovascular risk were included. The bias of underlying cardiovascular disease attributed to the positive result cannot be ignored, since both cardiovascular disease and PAD shared pathogenic mechanisms. Otherwise there were still potential residues confounding bias such as autoimmune disease in the study. The autoimmune disease shared an inflammatory process that lead to development of atherosclerosis contributing to PAD risk [24]. A retrospective study also conducted that rheumatoid arthritis as a significant risk factor of PAD [25]. In our study, we excluded those with established cardiovascular disease to attenuate the influence of atherosclerosis. Otherwise, obesity and autoimmune disease were matched between the study groups to eliminate the effect of confounding bias. Another population-based cohort study showed the trend of lower incidence of peripheral artery disease in migraineurs but did not reach statistical significance. In the study, migraineurs with aura seems to have higher risk of peripheral artery disease compared with those without aura. The reasons for insignificant result maybe explain by the fewer events [11].

Otherwise, the frequency of infections may link the association between migraine and PAD. A study has yielded the increased likelihood of peripheral arterial disease when exposure more infection [26]. A case-control study has also described the positive relationship between infections, such as Helicobacter pylori (*H. pylori*), and PAD, with odds ratio from 1.6-2.0 in young woman, and the risk is correlated with the cumulative number of infections [27]. The clinical evidence also supported *H. pylori* to be a potential risk factor of PAD [28, 29]. On the other hand, *H. pylori* infection was common in those with migraine, and eradication therapy lead to improved symptom of migraine [30, 31]. During the era of the coronavirus disease 2019 (COVID-19) pandemic, headache was reported as a symptom of COVID-19 illness. Observation study has proposed the possible pathophysiology linked between COVID-19 infection and migraine, included calcitonin gene-related peptide, angiotensin system, inflammatory cytokines and trigeminovascular activation [32]. In addition, patients with COVID-19 are at increased risk of PAD, even acute limb ischemia, particular those with higher inflammatory markers [33, 34]. Inflammation may play a role linking migraine and PAD and more

evidence needed to investigate the association.

PAD has potential risk to carry impairment in the quality of life and the prevalence rate is higher in woman at young age. Our study found increased risk of PAD in those with migraine and it's important to early screen the presence of PAD among migraineurs especially with aura, since the disease onset of migraine starting during young onset, and the underdiagnose of PAD may contribute to worse outcome [35, 36].

There are some strengths in our study. We examine the risk of PAD in migraineurs with and without aura, and the group of migraine with aura tended to have higher risk of PAD, albeit non-statistical significance which was related to limited events. As regard of the other study outcome of stroke, our study showed the same result of relationship between stroke and migraine, which makes our study more convincing. Our study also aimed to eliminate the possible confounding bias as much as possible and excluded those with underlying cardiovascular disease to attenuate the effect of atherosclerosis.

We highlight the following limitations in our study. First, the study was designed to attenuate the effect of established cardiovascular disease on the development of PAD among migraineurs. However, our study did not exclude migraineurs with cardiovascular risk such hypertension or diabetes, due to the limitation of effective sample size. However, the study groups were propensity score-matched by cardiovascular risk and Charlson Comorbidity Index to eliminate the possible confounding bias. Second, the drug effect, such as beta-blocker and ergot which may be used for treatment of migraine, may influence the result of our study on the risk of PAD in migraineurs. Third, the other residual biases still exist, such as the experience of infection frequency or inflammation biomarkers that are not available from database, which may be associated with risk factors for PAD. Fourth, among all migraine patients, a portion of patients were not identified as migraine with or without aura, due to the ICD code of the NHIRD. It may be an underestimation of our study regarding the risk of PAD among migraineurs with/without aura since there were some migraineurs, especially those without aura, not classified into their corresponding groups. Finally, we did not include cigarette smoking as a covariate because the NHIRD does not contain information on the quality of life, education, and living habits. However, we aimed to attenuate the bias of smoking between study and control groups by selecting chronic obstructive pulmonary disease (COPD) as the covariant.

Conclusion

In summary, migraineurs without established cardiovascular disease had a significant increased risk of PAD and stroke, and the risk of stroke persists among migraineurs with or without aura, albeit the trend is toward higher likelihood of PAD in migraineurs with aura, but the result did not reach statistical significance. Our study result should remind clinical physicians the risk of PAD in the future among migraineurs even without established cardiovascular disease currently. More, screening for peripheral artery disease may be needed in caring for patients with migraine.

Abbreviations

aHR: adjusted hazard ratio; CI: confidence interval; PAD: peripheral artery disease; ABI: ankle-brachial index; EMP: endothelial microparticles; *H. pylori*: Helicobacter pylori; COVID-19: coronavirus disease 2019.

Supplementary Material

Supplementary table.
https://www.medsci.org/v19p1163s1.pdf

Acknowledgments

We are grateful to Chung Shan Medical University, Taiwan, China Medical University, Taiwan, Asia University, Taiwan, and the Health Data Science Center, China Medical University Hospital, for providing administrative, technical, and funding support that has contributed to the completion of this study. This study is based, in part, on data released by the Health and Welfare Data Science Center, Ministry of Health and Welfare. The interpretation and conclusions contained herein do not represent those of the Ministry of Health and Welfare.

Institutional Review Board Statement

This study protocol was approved as a completely ethical review by the Central Regional Research Ethics Committee of China Medical University, Taiwan (No. CRREC-109-011). Due to the database is anonymous, the requirement for informed consent was waived.

Data Availability Statement

The National Health Insurance Database used to support the findings of this study were provided by the Health and Welfare Data Science Center, Ministry of Health and Welfare (HWDC, MOHW) under license and so cannot be made freely available. Requests for access to these data should be made to HWDC (https://dep.mohw.gov.tw/dos/np-2497-113.html).

Competing Interests

The authors have declared that no competing interest exists.

References

1. Feigin V. Global, regional, and National Incidence, prevalence, and years lived with disability for 310 acute and chronic diseases and injuries, 1990-2015: a systematic analysis for the global burden of disease study 2015. The Lancet. 2016; 388: 1545-602.
2. Wang SJ, Fuh JL, Young YH, Lu SR, Shia BC. Prevalence of migraine in Taipei, Taiwan: a population-based survey. Cephalalgia. 2000; 20: 566-72.
3. Saeed A, Rana KF, Warriach ZI, Tariq MA, Malik BH. Association of Migraine and Ischemic Heart Disease: A Review. Cureus. 2019; 11.
4. Sacco S, Ornello R, Ripa P, Tiseo C, Degan D, Pistoia F, et al. Migraine and risk of ischaemic heart disease: a systematic review and meta-analysis of observational studies. European journal of neurology. 2015; 22: 1001-11.
5. Mahmoud AN, Mentias A, Elgendy AY, Qazi A, Barakat AF, Saad M, et al. Migraine and the risk of cardiovascular and cerebrovascular events: a meta-analysis of 16 cohort studies including 1 152 407 subjects. BMJ open. 2018; 8: e020498.
6. Norman PE, Eikelboom JW, Hankey GJ. Peripheral arterial disease: prognostic significance and prevention of atherothrombotic complications. Medical Journal of Australia. 2004; 181: 150-4.
7. Bergiers S, Vaes B, Degryse J. To screen or not to screen for peripheral arterial disease in subjects aged 80 and over in primary health care: a cross-sectional analysis from the BELFRAIL study. BMC family practice. 2011; 12: 39.
8. Hirsch AT, Haskal ZJ, Hertzer NR, Bakal CW, Creager MA, Halperin JL, et al. ACC/AHA 2005 guidelines for the management of patients with peripheral arterial disease (lower extremity, renal, mesenteric, and abdominal aortic): a collaborative report from the American Association for Vascular Surgery/Society for Vascular Surgery, Society for Cardiovascular Angiography and Interventions, Society for Vascular Medicine and Biology, Society of Interventional Radiology, and the ACC/AHA Task Force on Practice Guidelines (Writing Committee to Develop Guidelines for the Management of Patients With Peripheral Arterial Disease). Journal of the American College of Cardiology. 2006; 47: e1-e192.
9. Jurno ME, Chevtchouk L, Nunes AA, De Rezende DF, da Cunha Jevoux C, De Souza JA, et al. Ankle-brachial index, a screening for peripheral obstructive arterial disease, and migraine–a controlled study. Headache: The Journal of Head and Face Pain. 2010; 50: 626-30.
10. Bigal M, Kurth T, Santanello N, Buse D, Golden W, Robbins M, et al. Migraine and cardiovascular disease: a population-based study. Neurology. 2010; 74: 628-35.
11. Adelborg K, Szépligeti SK, Holland-Bill L, Ehrenstein V, Horváth-Puhó E, Henderson VW, et al. Migraine and risk of cardiovascular diseases: Danish population based matched cohort study. bmj. 2018; 360: k96.
12. Lee T-Y, Hsu Y-C, Tseng H-C, Yu S-H, Lin J-T, Wu M-S, et al. Association of daily aspirin therapy with risk of hepatocellular carcinoma in patients with chronic hepatitis B. JAMA internal medicine. 2019; 179: 633-40.
13. Cheng Y-T, Cheng C-T, Wang S-Y, Wu VC-C, Chu P-H, Chou A-H, et al. Long-term outcomes of endovascular and open repair for traumatic thoracic aortic injury. JAMA network open. 2019; 2: e187861-e.
14. Schürks M, Rist PM, Bigal ME, Buring JE, Lipton RB, Kurth T. Migraine and cardiovascular disease: systematic review and meta-analysis. Bmj. 2009; 339: b3914.
15. Sacco S, Ripa P, Grassi D, Pistoia F, Ornello R, Carolei A, et al. Peripheral vascular dysfunction in migraine: a review. The journal of headache and pain. 2013; 14: 80.
16. Liman TG, Bachelier-Walenta K, Neeb L, Rosinski J, Reuter U, Böhm M, et al. Circulating endothelial microparticles in female migraineurs with aura. Cephalalgia. 2015; 35: 88-94.
17. Tietjen GE, Khubchandani J, Herial N, Palm-Meinders IH, Koppen H, Terwindt GM, et al. Migraine and vascular disease biomarkers: a population-based case-control study. Cephalalgia. 2018; 38: 511-8.
18. Winsvold BS, Bettella F, Witoelar A, Anttila V, Gormley P, Kurth T, et al. Shared genetic risk between migraine and coronary artery disease: a genome-wide analysis of common variants. PloS one. 2017; 12: e0185663.
19. Kullo IJ, Leeper NJ. The genetic basis of peripheral arterial disease: current knowledge, challenges, and future directions. Circulation research. 2015; 116: 1551-60.

20. Selvin E, Erlinger TP. Prevalence of and risk factors for peripheral arterial disease in the United States: results from the National Health and Nutrition Examination Survey, 1999–2000. Circulation. 2004; 110: 738-43.

21. Ludhwani D, Wu J. Obesity paradox in peripheral arterial disease: results of a propensity match analysis from the national inpatient sample. Cureus. 2019; 11.

22. Stam AH, Weller CM, Janssens ACJ, Aulchenko YS, Oostra BA, Frants RR, et al. Migraine is not associated with enhanced atherosclerosis. 2013; 33: 228-35.

23. Kuo F-H, Lee C-Y, Li J-P, Chung J-F, Wang Y-H, Hsieh M-J, et al. Migraine as a Risk Factor for Peripheral Artery Occlusive Disease: A Population-Based Cohort Study. International Journal of Environmental Research and Public Health. 2020; 17: 8549.

24. Brevetti G, Giugliano G, Brevetti L, Hiatt WR. Inflammation in peripheral artery disease. Circulation. 2010; 122: 1862-75.

25. Liang KP, Liang KV, Matteson EL, McClelland RL, Christianson TJ, Turesson C. Incidence of noncardiac vascular disease in rheumatoid arthritis and relationship to extraarticular disease manifestations. Arthritis & Rheumatism: Official Journal of the American College of Rheumatology. 2006; 54: 642-8.

26. Bloemenkamp DG, van den Bosch MA, Mali WP, Tanis BC, Rosendaal FR, Kemmeren JM, et al. Novel risk factors for peripheral arterial disease in young women. The American journal of medicine. 2002; 113: 462-7.

27. Bloemenkamp DG, Willem PTM, Tanis BC, Rosendaal FR, van den Bosch MA, Kemmeren JM, et al. Chlamydia pneumoniae, Helicobacter pylori and cytomegalovirus infections and the risk of peripheral arterial disease in young women. Atherosclerosis. 2002; 163: 149-56.

28. Gasbarrini A, Franceschi F, Armuzzi A, Ojetti V, Candelli M, Torre ES, et al. Extradigestive manifestations of Helicobacter pylori gastric infection. Gut. 1999; 45: I9-I12.

29. Sawayama Y, Hamada M, Otaguro S, Maeda S, Ohnishi H, Fujimoto Y, et al. Chronic Helicobacter pylori infection is associated with peripheral arterial disease. Journal of Infection and Chemotherapy. 2008; 14: 250-4.

30. Gasbarrini A, De AL, Fiore G, Gambrielli M, Franceschi F, Ojetti V, et al. Beneficial effects of Helicobacter pylori eradication on migraine. Hepato-gastroenterology. 1998; 45: 765-70.

31. Gasbarrini A, Serricchio M, Tondi P, De AL, Franceschi F, Ojetti V, et al. Raynaud's Phenomenon and Helicobacter Pylori Infection. The International journal of angiology: official publication of the International College of Angiology, Inc. 1998; 7: 307-9.

32. Toptan T, Aktan Ç, Başarı A, Bolay H. Case Series of Headache Characteristics in COVID-19: Headache Can Be an Isolated Symptom. Headache: The Journal of Head and Face Pain. 2020; 60: 1788-92.

33. Ogawa M, Doo FX, Somwaru AS, Roudenko A, Kamath A, Friedman B. Peripheral arterial occlusion due to COVID-19: CT angiography findings of nine patients. Clinical Imaging. 2021; 73: 43-7.

34. Bellosta R, Luzzani L, Natalini G, Pegorer MA, Attisani L, Cossu LG, et al. Acute limb ischemia in patients with COVID-19 pneumonia. Journal of vascular surgery. 2020; 72: 1864-72.

35. Teodorescu VJ, Vavra AK, Kibbe MR. Peripheral arterial disease in women. Journal of vascular surgery. 2013; 57: 18S-26S.

36. Bush RL, Kallen MA, Liles DR, Bates JT, Petersen LA. Knowledge and awareness of peripheral vascular disease are poor among women at risk for cardiovascular disease. Journal of Surgical Research. 2008; 145: 313-9.

Research Article

Nerolidol Suppresses the Inflammatory Response during Lipopolysaccharide-Induced Acute Lung Injury via the Modulation of Antioxidant Enzymes and the AMPK/Nrf-2/HO-1 Pathway

Yung-Lun Ni,[1] Huan-Ting Shen,[1,2] Chun-Hung Su,[3,4] Wen-Ying Chen,[5] Rosa Huang-Liu,[6] Chun-Jung Chen,[7] Shih-Pin Chen,[3,4] and Yu-Hsiang Kuan [8,9]

[1]Department of Pulmonary Medicine, Taichung Tzu Chi Hospital, Buddhist Tzu Chi Medical Foundation, Taichung, Taiwan
[2]Institute of Biochemistry, Microbiology, and Immunology, Chung Shan Medical University, Taichung, Taiwan
[3]Department of Internal Medicine, School of Medicine, Chung Shan Medical University, Taichung, Taiwan
[4]Department of Internal Medicine, Chung Shan Medical University Hospital, Taichung, Taiwan
[5]Department of Veterinary Medicine, National Chung Hsing University, Taichung, Taiwan
[6]School of Nutrition, Chung Shan Medical University, Taichung, Taiwan
[7]Department of Education and Research, Taichung Veterans General Hospital, Taichung, Taiwan
[8]Department of Pharmacology, School of Medicine, Chung Shan Medical University, Taichung, Taiwan
[9]Department of Pharmacy, Chung Shan Medical University Hospital, Taichung, Taiwan

Correspondence should be addressed to Yu-Hsiang Kuan; kuanyh@csmu.edu.tw

Shih-Pin Chen and Yu-Hsiang Kuan contributed equally to this work.

Acute lung injury (ALI) is a life-threatening disease that is characterised by the rapid onset of inflammatory responses. Lipopolysaccharide (LPS) is an endotoxin that plays an important role in triggering ALI via pneumonia and sepsis. However, no effective therapeutic strategies are currently available to treat ALI. Nerolidol is an aliphatic sesquiterpene alcohol that is found in the essential oils of many flowers as well as floral plants. It has been shown to exhibit anti-inflammatory, antioxidant, and anticancer properties. Herein, we show that nerolidol pretreatment counteracted the histopathological hallmarks in LPS-induced ALI mice. Indeed, nerolidol pretreatment inhibited LPS-induced alveolar-capillary barrier disruption, lung edema, and lipid peroxidation. Moreover, nerolidol pretreatment prevented the LPS from decreasing the enzymatic activities of superoxide dismutase, catalase, and glutathione peroxidase. Importantly, nerolidol treatment enhanced phosphorylation of AMP-activated protein kinase (AMPK) and expression of nuclear factor erythroid-derived 2-related factor 2 (Nrf-2) and heme oxygenase-1 (HO-1). Taken together, our study reveals the novel protective effects of nerolidol in LPS-induced ALI via the induction of antioxidant responses and activation of the AMPK/Nrf-2/HO-1 signalling pathway.

1. Introduction

Acute lung injury (ALI) is generally characterised by the rapid onset of inflammatory responses, including bilateral pulmonary neutrophil infiltration, haemorrhage, hyaline membrane formation, lung edema, and hypothermia [1]. In humans, ALI and acute respiratory distress syndrome (a more severe form of ALI) score highly in terms of morbidity and mortality rates worldwide [2, 3]. ALI can lead to the development of pneumonia as well as sepsis. However, no

effective therapeutic strategies for ALI are currently available. Lipopolysaccharide (LPS) is a glucosamine-based saccharolipid and the main element of the outer lipid membrane in Gram-negative bacteria [4]. Consequently, LPS may play an important role in triggering pneumonia and sepsis [2].

In an animal experimental model, LPS instillation causes the activation of tissue-resident leukocytes and the recruitment of peripheral blood leukocytes to the lungs through the disrupted alveolar-capillary barrier [5–7]. The activation of leukocytes induces degranulation and a respiratory burst for the robust production of reactive oxygen species (ROS) such as superoxide anion, hydrogen peroxide, and hydroxyl radical [8]. In cells, the nuclear factor erythroid-derived 2-related factor 2 (Nrf-2)/heme oxygenase-1 (HO-1) pathway, as well as the activities of antioxidant enzymes (AOEs) such as superoxide dismutase (SOD), catalase (CAT), and glutathione peroxidase (GPx), are activated during oxidative stress. These enzymes catalyse chemical reactions to counteract ROS-induced oxidative damages, including lipid peroxidation and tissue damage [5, 9–11]. The nuclear accumulation and phosphorylation of Nrf-2 is facilitated by AMP-activated protein kinase (AMPK) signalling [10]. Interestingly, in murine ALI models, LPS has been shown to inactivate AMPK signalling and downregulate AOEs [12, 13].

Nerolidol (3,7,11-trimethyl-1,6,10-dodecatrien-3-ol) is an aliphatic sesquiterpene alcohol found in the essential oils of many flowers and plants with a floral scent. Nerolidol is present in neroli, ginger, citronella, lemongrass, rose, and tea tree [14, 15]. Despite the well-documented anti-inflammatory, antioxidant, antimicrobial, and anticancer properties of nerolidol [16], no studies have so far evaluated the protective effects as well as the molecular mechanisms of nerolidol on ALI. Herein, we report a previously uncharacterised protective role of nerolidol during LPS-induced ALI in mice that is associated with the AMPK/Nrf-2/HO-1 pathway and antioxidant responses.

2. Materials and Methods

2.1. Materials. Antibody against phospho-AMPK (catalog Number 2535) was acquired from Cell Signalling Technology, Inc. (Beverly, MA). Nerolidol and antibodies against AMPK (catalog Number SC-25792), Nrf-2 (catalog Number SC-13032), HO-1 (catalog Number SC-10789), and β-actin (catalog Number SC-47778) were acquired from Santa Cruz Biotechnology Inc. (Santa Cruz, CA). A thiobarbituric acid reactive substance (TBARS) assay kit, CAT assay kit, SOD assay kit, and GPx assay kit were obtained from Cayman Chemical Co. (Ann Arbor, MI). Lipopolysaccharide (LPS; *Escherichia coli*, serotype 0111:B4) and other reagents were purchased from Sigma-Aldrich (St. Louis, MO).

2.2. Mice and Experimental Design. Male BALB/c mice aged 8–10 weeks weighing 25–35 g were obtained from the National Laboratory Animal Center (Taipei, Taiwan). Mice were housed under a 12 : 12 h light-dark cycle with free access to a laboratory rodent diet. All animal experiments were conducted in accordance with the Institutional Animal Ethics

Committee of Chung Shan Medical University. The mice were randomly divided into six groups as follows: control, LPS, nerolidol (10, 30, and 100 μmol/kg)+LPS, and dexamethasone (1 mg/kg)+LPS groups. The control group received vehicle intraperitoneally (IP) for 30 min followed by the intranasal administration of 20 μL saline by drops applied with a pipette. The LPS, nerolidol+LPS, and dexamethasone+LPS groups received vehicle, nerolidol, and dexamethasone IP for 30 min followed by the intranasal administration of LPS at 100 μg/20 μL of saline by drops applied with a pipette. Mice were euthanised by pentobarbital after LPS treatment for 24 h [7]. Bronchoalveolar lavage fluid (BALF) and lung tissues were collected. Bronchoalveolar lavage was collected by flushing 1 mL of sterile saline via the tracheal cannula three times. After the collection and centrifugation steps were completed, the protein concentrations were determined using the Bradford protein assay (Bio-Rad Laboratories) in a supernatant of BALF [7].

2.3. Lung Histopathology. The lungs were excised, soaked in 10% formalin, and embedded in paraffin. Tissue blocks were sectioned into 4 μm thick sections using the rotary microtome. Sections were stained with hematoxylin-eosin. Under a light microscope, the level of histopathological changes was evaluated by leukocyte infiltration, alveolar wall thickness, and hyaline membrane formation in a blind manner by 50 microscopic fields randomly [5].

2.4. Wet-to-Dry Lung Weight Ratio. The index of lung edema after LPS administration was measured using a wet-to-dry (W/D) weight ratio [6], obtained by the weight measured immediately after excision (wet) and the weight after dehydration for 48 h at 80°C (dry).

2.5. Myeloperoxidase (MPO) Assay. Twenty-four hours after LPS administration, the lungs were excised and homogenised in MPO extractive phosphate buffer containing guaiacol and cetyltrimethylammonium bromide. After being subjected to centrifugation, the supernatant was reacted with hydrogen peroxide. The levels of MPO were indicated by absorbance at 470 nm [5].

2.6. Lipid Peroxidation Assay. The presence of malondialdehyde (MDA) and the production of lipid peroxidation were evaluated in the lungs using the TBARS assay kit following the manufacturer's protocol as described previously [5]. The lung homogenate was incubated with thiobarbituric acid reactive substances, including thiobarbituric acid and trichloroacetic acid. The chromogenic reaction was carried out at 100°C for 1 h, and the absorbance was measured at 530 nm.

2.7. Antioxidative Enzyme (AOE) Assay. The activities of antioxidative enzymes (AOEs), including SOD, CAT, and GPx, were measured using commercial assay kits for SOD, CAT, and GPx, respectively, according to the manufacturer's instructions [5].

2.8. Western Blot Assay. The total proteins in the harvested lungs were homogenised and extracted using the T-PER solution (Pierce, Rockford, IL). Equal amounts of protein

were separated using SDS-PAGE at 7.5% and transferred onto PVDF membranes. Membranes were blocked using 5% nonfat milk in phosphate-buffered saline containing 0.1% Tween-20 for 1 h at room temperature, and probed with primary antibodies including phospho-AMPK, AMPK, Nrf-2, HO-1, and β-actin. Membranes were washed and incubated with horseradish peroxidase- (HRP-) labelled secondary antibodies for 1 h. The membranes were detected using ECL Plus Western blotting detection reagents [6].

2.9. Statistical Analysis. In this study, at least three separate repetitions of each experiment were performed. Unless otherwise specified, the data are presented as mean ± standard deviation. Statistical analyses were performed using SPSS 14.0 statistical software (SPSS, Chicago, IL). One-way analysis of variance and the Bonferroni t-test for multigroup comparisons were used to calculate the P values. $P < 0.05$ was considered statistically significant.

3. Results

3.1. Nerolidol Protects against LPS-Induced ALI. To evaluate the protective effects of nerolidol on acute pulmonary inflammation, the murine model of LPS-induced ALI was implemented. Thirty minutes after the IP administration of nerolidol at differential concentrations, the mice were subjected to intranasal instillation with either saline (control) or LPS. After 24 h, we observed normal pulmonary structures and no histopathological changes using light microscopy in the control group (Figure 1(a)). As expected, we observed neutrophil infiltration, alveolar wall thickening, haemorrhage, and hyaline membrane formation after LPS administration (Figure 1(b)). Notably, nerolidol pretreatment alleviated the LPS-mediated histopathological hallmarks in a dose-dependent manner (Figures 1(c)–1(e)). The LPS-induced histopathology was also reduced in the presence of dexamethasone, which is an anti-inflammatory steroid (Figure 1(f)), suggesting that nerolidol exhibited anti-inflammatory effects in the lungs during LPS-induced ALI.

3.2. Nerolidol Protects against LPS-Induced Alveolar-Capillary Barrier Disruption and Leukocyte Infiltration. Neutrophil activation and infiltration play an essential role in LPS-induced ALI. Alveolar-capillary barrier disruption by activated neutrophils and LPS results in plasma protein and neutrophil leakage into the alveolar space [7]. We found that LPS-treated mice exhibited a significantly higher protein concentration in the BALF compared with control mice ($P < 0.05$). However, this was significantly reduced in mice pretreated with nerolidol at a concentration of 30 μmol/kg; the protein concentration in BALF was also significantly reduced ($P < 0.05$; Figure 2(a)). Furthermore, we found that while the MPO content in the lungs increased significantly after LPS administration ($P < 0.05$), this was significantly inhibited by nerolidol pretreatment at 30 μmol/kg ($P < 0.05$; Figure 2(b)), suggesting that the activation and recruitment of neutrophils were suppressed by nerolidol.

3.3. Nerolidol Protects against LPS-Induced Lung Edema. Lung edema, an excess accumulation of fluid in the lungs, is caused by the disruption of the alveolar-capillary barrier and is a critical pathological feature in ALI [6]. By characterising the wet and dry weights of the lungs (see Materials and Methods), we found that LPS-treated mice exhibited increased W/D ratio compared with control mice ($P < 0.05$), indicating the manifestation of lung edema in these mice. Similar to our previous observation, pretreatment with nerolidol inhibited LPS-induced lung edema in a dose-dependent manner; a significant effect started at 30 μmol/kg ($P < 0.05$; Figure 3).

3.4. Nerolidol Protects against LPS-Induced Lipid Peroxidation in the Lungs. Leukocyte activation and infiltration result in lipid peroxidation, which is a critical risk factor in the pathogenesis of ALI [5]. MDA is the product of lipid peroxidation and can be used as an indicator for lipid peroxidation rate. We observed that while LPS treatment led to a significant increase in MDA levels in mice ($P < 0.05$), this effect was significantly inhibited by nerolidol pretreatment in a dose-dependent manner; a significant effect started at 30 μmol/kg ($P < 0.05$; Figure 4), suggesting that nerolidol pretreatment could effectively suppress lipid peroxidation induced by ALI-mediated leukocyte infiltration.

3.5. Nerolidol Counteracts LPS-Mediated AOE Inhibition. Given the seemingly potent anti-inflammatory efficacy, we next asked how nerolidol pretreatment might exert such effects. Oxidative stress that facilitates lipid oxidation can be opposed by the activities of AOEs, such as SOD, CAT, and GPx [5]. We noted that the activities of SOD, CAT, and GPx were suppressed in LPS-treated mice compared with control mice ($P < 0.05$; Figure 5), indicating that LPS-induced ALI and leukocyte recruitment were associated with decreased AOE activities. Importantly, we found that nerolidol pretreatment was sufficient to prevent the decrease of AOE activities in a dose-dependent manner; a significant effect started at 30 μmol/kg ($P < 0.05$; Figure 5), indicating that nerolidol might reduce inflammatory tissue damage via the upregulation of the antioxidant response.

3.6. Nerolidol Prevented the LPS-Induced Repression of Nrf-2 and HO-1 Expression. HO-1 is an antioxidative protein involved in the resolution of inflammation. Its expression is regulated by the transcription factor Nrf-2 [5]. We found that both Nrf-2 and HO-1 expressions were significantly reduced in LPS-treated mice compared with control mice ($P < 0.05$), indicating that LPS treatment was associated with the downregulation of the Nrf-2/HO-1 transcription response. Importantly, pretreatment with nerolidol prevented the LPS-induced repression of Nrf-2 and HO-1 and enhanced LPS-reduced repression in a dose-dependent manner; a significant effect started at 30 μmol/kg ($P < 0.05$; Figure 6), suggesting that nerolidol-mediated protective response involved the Nrf-2/HO-1 transcription axis.

3.7. Nerolidol Prevented the LPS-Induced Repression of AMPK Phosphorylation. AMPK signalling induces the nuclear accumulation of Nrf-2 [17]. To determine whether the effects on Nrf-2 during LPS-induced ALI were dependent on AMPK activity, we measured AMPK phosphorylation
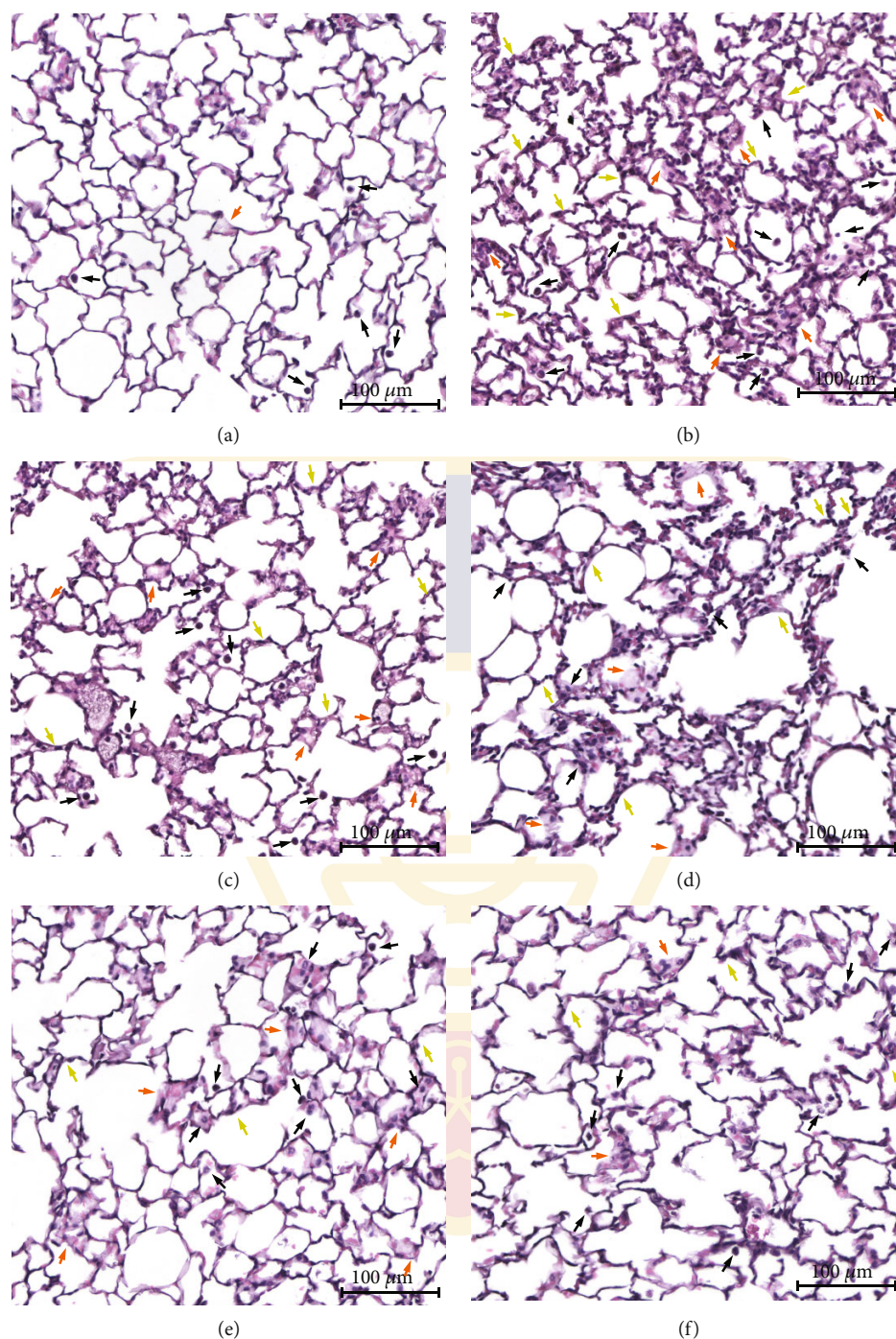
FIGURE 1: Nerolidol protects against the histopathological exchange of lungs in LPS-induced ALI. (a) Control, (b) LPS, (c) 10 μmol/kg nerolidol+LPS, (d) 30 μmol/kg nerolidol+LPS, (e) 100 μmol/kg nerolidol+LPS, and (f) 1 mg/kg dexamethasone+LPS. Hematoxylin-eosin staining of lung sections of each experimental group (magnification: ×100; scale bars represent 100 μm). Black arrow, neutrophil infiltration; orange arrow, haemorrhage and hyaline membrane formation; green arrow, alveolar wall thickness and edema.

using our experimental setup. Consistent with our hypothesis, we found that the phosphorylation of AMPK was significantly reduced in LPS-treated mice compared with control mice ($P < 0.05$), suggesting that LPS-induced ALI was associated with the downregulation of AMPK signalling. Notably, nerolidol pretreatment inhibited LPS-induced AMPK silencing and enhanced phosphorylation of AMPK in a dose-

dependent manner; a significant effect started at 30 μmol/kg ($P < 0.05$; Figure 7).

4. Discussion

Nerolidol is the sesquiterpene compound found in essential oils from flowers and plants [14, 15]. Nerolidol is widely used
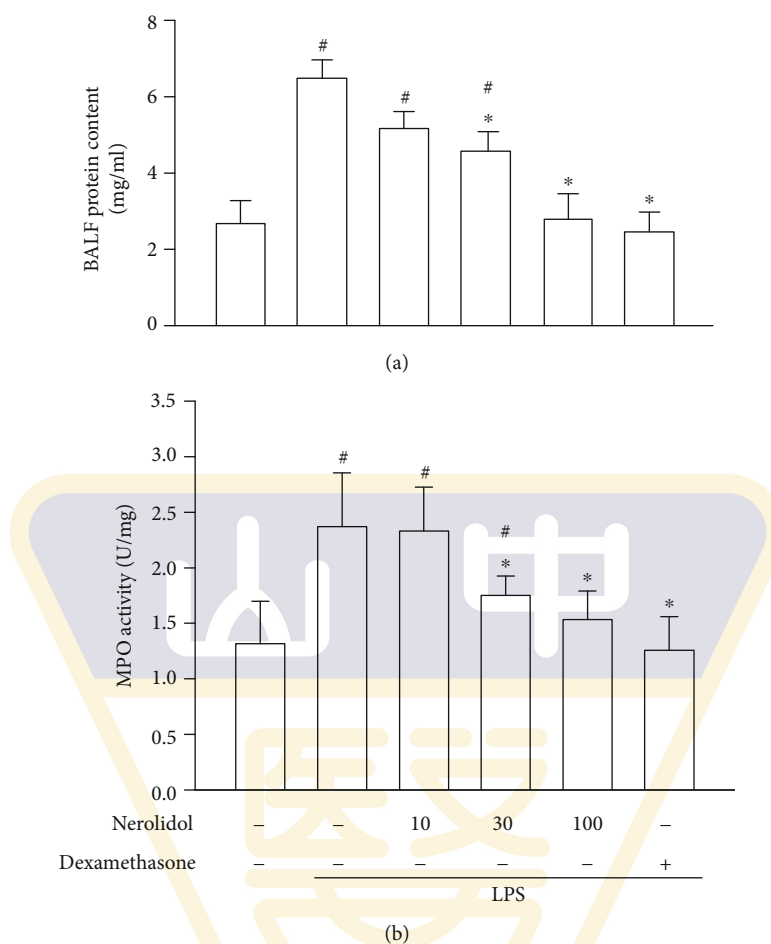
FIGURE 2: Nerolidol protects against LPS-induced alveolar-capillary barrier disruption and leukocyte infiltration. (a) Alveolar-capillary barrier disruption was determined by protein leakage via a Bradford protein assay. (b) Leukocyte infiltration was determined by MPO activity in BALF. Values are expressed as mean ± S.D. of 3-4 mice per group. #$P < 0.05$ represents a significant difference between the indicated group and the control group; *$P < 0.05$ represents a significant difference between the indicated group and the LPS groups.

as a fragrant ingredient and flavouring and as a fixative reagent in detergents and perfumes [18, 19]. It is also used in many food products as a flavour enhancer, and its use is permitted by both the United States Food and Drug Administration and the European Food Safety Authority [20]. In addition, nerolidol has several pharmacological effects, such as anti-inflammatory and antioxidant activities. In a previous study, nerolidol at concentrations of 100 and 200 mg/kg has been shown to suppress LPS-induced acute kidney inflammation in rat models [21]. Moreover, nerolidol reduces the generation of proinflammatory mediators in LPS-activated peritoneal macrophages [22]. ALI is the pulmonary disorder of acute inflammation directly induced by LPS instillation in mouse models [22]. LPS instillation causes apparent histopathology including neutrophil infiltration, haemorrhage, hyaline membrane formation, and lung edema [1]. These pathological characteristics are similar to clinical signs in ALI patients [23]. In this study, the histopathological results of LPS-induced ALI correlated well with those of previous studies [1, 6]. In addition, we showed that the LPS-induced histopathological characteristics of ALI could be counteracted by nerolidol *in vivo* in a dose-dependent manner.

Importantly, these results indicated that LPS-induced inflammatory responses in ALI could be reversed by nerolidol.

Leukocytes, especially neutrophils, are the prime culprit in the pathogenesis of ALI. After the administration of LPS, proinflammatory mediators from alveolar macrophages and pulmonary cells stimulate neutrophil activation within peripheral circulation [6]. Migration, respiratory burst, and degranulation of neutrophils are critical to the innate immune system [24]. Essential oil extracted from *Peperomia serpens* Loud (EOP), which mainly contains nerolidol, has been shown to modulate acute inflammatory responses through the interference of leukocyte migration, rolling, and adhesion in rodent models [25]. EOP inhibits the paw edema induced by carrageenan and dextran, as well as the ear edema induced by croton oil [25]. Consistent with previous data, our results suggested that LPS-induced neutrophil infiltration into the lungs and the disruption of the alveolar-capillary barrier could be reduced by nerolidol, as revealed by MPO and protein leakage assays, respectively. Moreover, lung edema was also ameliorated by nerolidol in our LPS-induced ALI model. These results indicated that
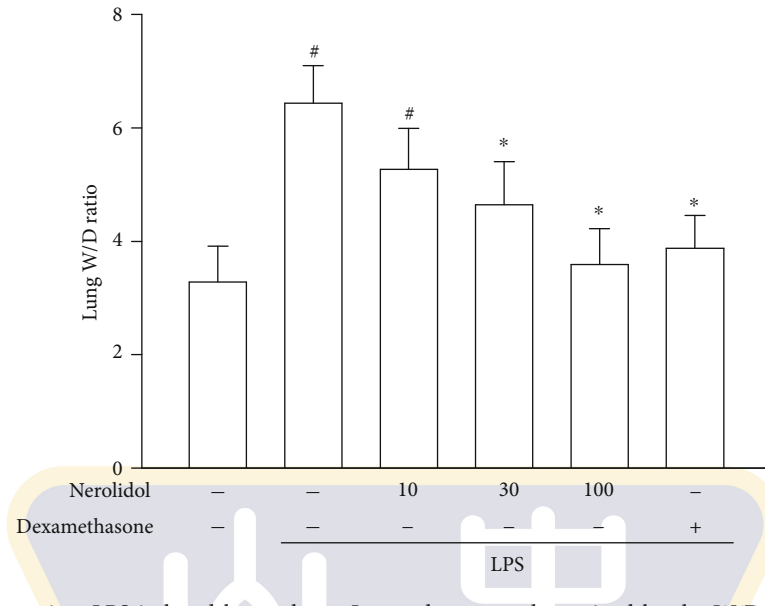
FIGURE 3: Nerolidol protects against LPS-induced lung edema. Lung edema was determined by the W/D ratio. Values are expressed as mean ± S.D. of 3-4 mice per group. #$P < 0.05$ represents a significant difference between the indicated group and the control group; *$P < 0.05$ represents a significant difference between the indicated group and the LPS groups.
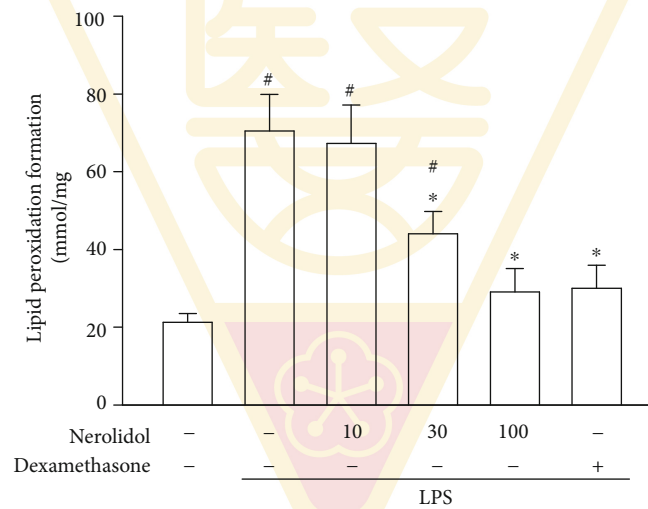

FIGURE 4: Nerolidol protects against LPS-induced lipid peroxidation in the lungs. Lipid peroxidation was determined by the MDA formation. Values are expressed as mean ± S.D. of 3-4 mice per group. #$P < 0.05$ represents a significant difference between the indicated group and the control group; *$P < 0.05$ represents a significant difference between the indicated group and the LPS groups.

nerolidol reduced LPS-induced lung edema through inhibiting neutrophil infiltration and alveolar-capillary barrier disruption.

During inflammation, leukocytes produce large quantities of ROS in response to an invasive pathogen. While exhibiting antimicrobial effects, excessive oxidative stress can also cause injury to peripheral tissues. Lipid peroxidation is the most common readout of oxidative stress and potential tissue damage [26]. Studies have indicated that nerolidol inhibits lipid peroxidation in rotenone-induced midbrain tissue damage and *Trypanosoma evansi*-mediated brain and hepatic damage [27–29]. In this current study, we found that lipid

peroxidation induced by LPS in the lungs could be inhibited by nerolidol in a dose-dependent manner. In cells, oxidative stress, or the level of ROS, is generally counterbalanced by antioxidant responses. These include the AOEs and signalling pathways such as the Nrf-2/HO-1 axis [9, 10]. It has been shown that ROS generation reduces the capacities of AOEs, including SOD, CAT, and GPx [5]. Interestingly, rotenone- or *Trypanosoma evansi*-induced AOE suppression could be reversed by nerolidol in the brain or liver [27–29]. Herein, we show that pretreatment with nerolidol significantly prevented the decrease of AOE activities in the lungs of mice treated with LPS using our ALI model. These results
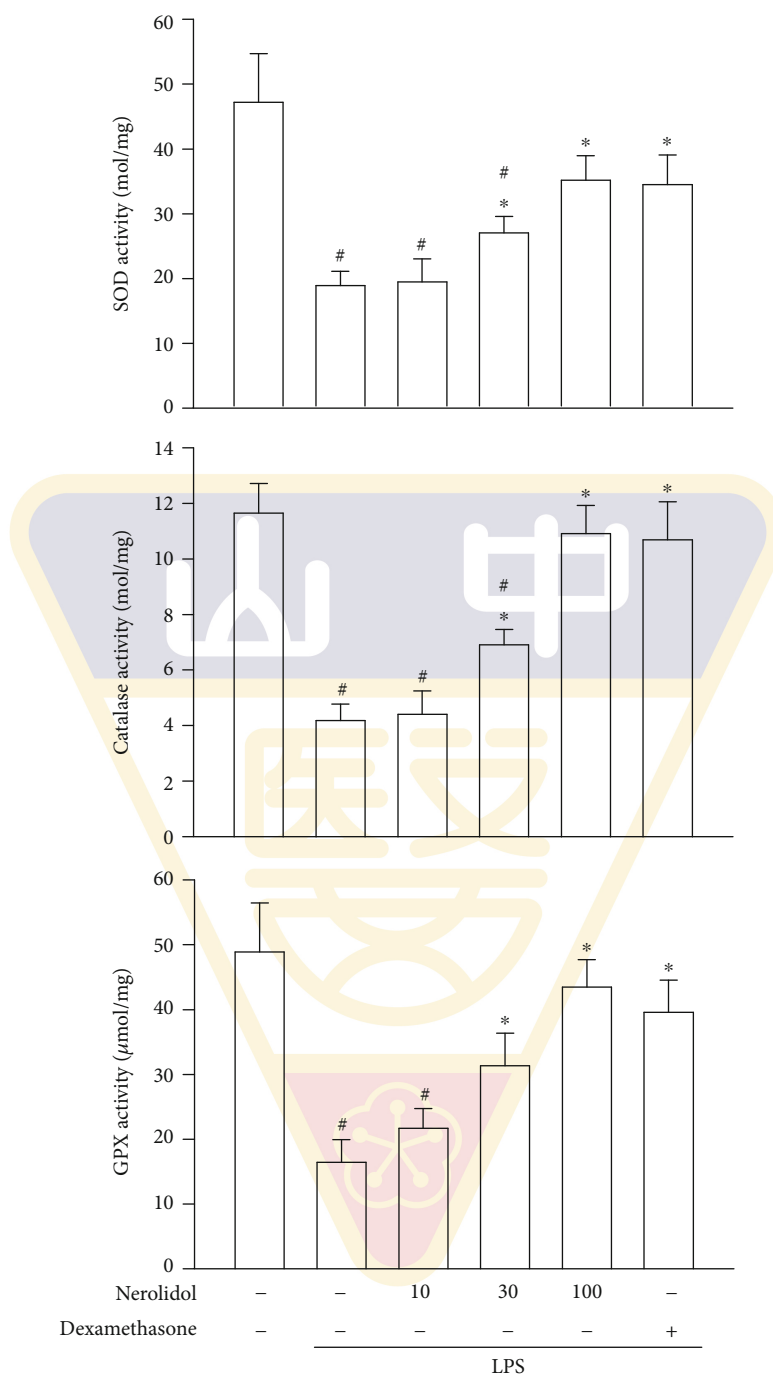
FIGURE 5: Nerolidol protects against LPS-reduced AOE activities. The AOEs represented are SOD, CAT, and GPx. Values are expressed as mean ± S.D. of 3-4 mice per group. $^{\#}P < 0.05$ represents a significant difference between the indicated group and the control group; $^{*}P < 0.05$ represents a significant difference between the indicated group and the LPS groups.

suggested that nerolidol prevented neutrophil-associated tissue damage likely through the reduction of lipid peroxidation and upregulation of AOE activities during LPS-induced ALI in mice.

Nrf-2 is an important transcription factor and the master regulator of antioxidant defence molecules [30]. The ROS-mediated activation of Nrf-2 induces the expression of many different proteins, including HO-1, the phase-II detoxifying and antioxidative protein. The activation, nuclear translocation, and stabilisation of Nrf-2 are enhanced by 3S-(+)-9-oxonerolidol, a derivative of nerolidol, in human lung epithelial cells [31]. In the present study, we showed that LPS inhibited the expression of Nrf-2 and HO-1 and that these were rescued and further enhanced by nerolidol in a dose-dependent manner. In addition, our results indicated that oxidative stress induced the activation and expression of
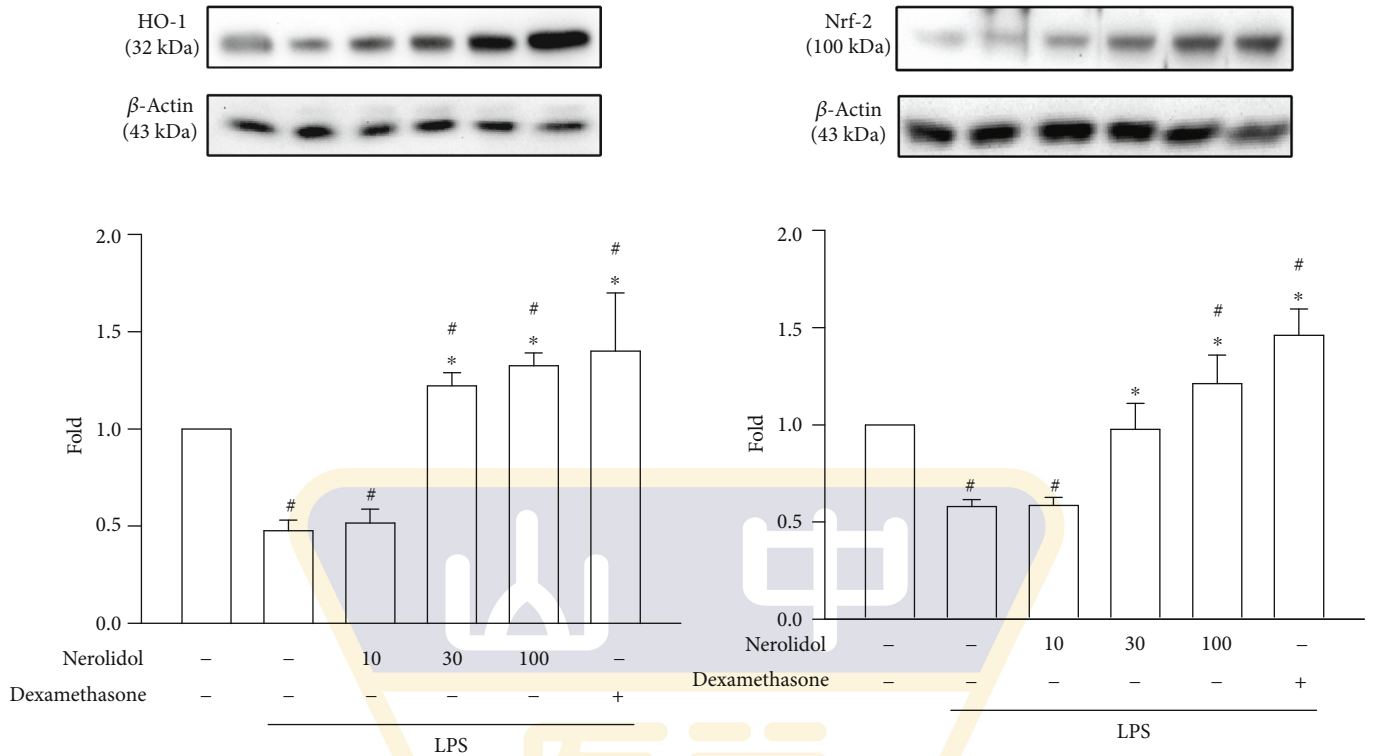
FIGURE 6: Nerolidol enhances LPS-induced Nrf2 and HO-1 expression. The lung lysates were analyzed by Western blotting. Values are expressed as mean ± S.D. of 3-4 mice per group. [#]$P < 0.05$ represents a significant difference between the indicated group and the control group; [*]$P < 0.05$ represents a significant difference between the indicated group and the LPS groups.

FIGURE 7: Nerolidol enhances LPS-induced AMPK phosphorylation. The lung lysates were analyzed by Western blotting. Values are expressed as mean ± S.D. of 3-4 mice per group. [#]$P < 0.05$ represents a significant difference between the indicated group and the control group; [*]$P < 0.05$ represents a significant difference between the indicated group and the LPS groups.
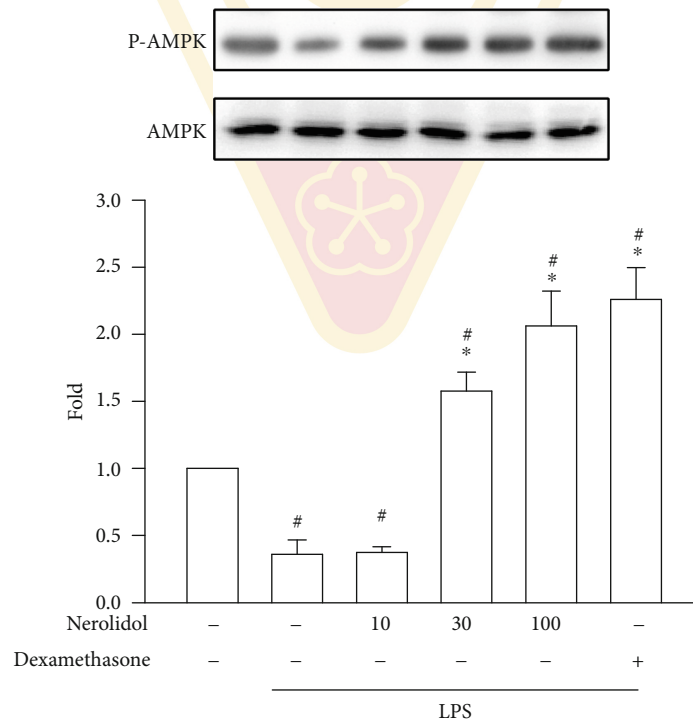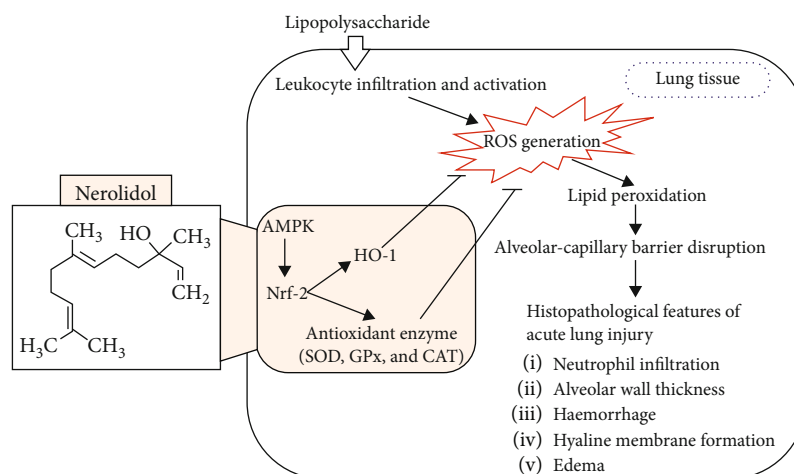
Figure 8: Scheme of the mechanisms in the protective effect of nerolidol on LPS-induced ALI.

Nrf-2 through the activation of AMPK signalling, which is a crucial player during various inflammatory and oxidative stresses [17]. As shown in our results, we found that the level of AMPK phosphorylation in the presence of nerolidol was positively correlated with the expression of Nrf-2 in LPS-treated mice. These results further indicated that HO-1 expression was likely influenced by the AMPK/Nrf-2 pathway in our model.

In conclusion, we have demonstrated that nerolidol pretreatment effectively protected against the exacerbation of lung histopathology, including neutrophil infiltration, alveolar wall thickening, haemorrhage, hyaline membrane formation, and edema, during LPS-induced ALI. The protective mechanisms of nerolidol include (1) the inhibition of alveolar-capillary barrier disruption and leukocyte infiltration; (2) the reduction of lipid peroxidation; (3) the prevention of AOE activities; and (4) the prevention of the decrease and increase of HO-1 expression, Nrf-2 expression, and AMPK phosphorylation. Taken together, our findings suggested that the beneficial effects of the application of nerolidol in the prevention of ALI inflammation most likely involves the restoration of the AMPK/Nrf-2/HO-1 pathway and AOE activities (model illustrated in Figure 8). The protective effects of nerolidol are similar as the monocyclic sesquiterpene derivative, zerumbone, on LPS-induced ALI mice. A previous study has proposed that the protective mechanism of zerumbone on LPS-induced ALI was via the upregulation of AOEs and the Nrf-2/HO-1 pathway [5]. This evidence could be used to propose that ALI could be reduced by sesquiterpene derivatives, including nerolidol and zerumbone, via the restoration of the AOE activities, HO-1, and the relative upstream pathway.

Data Availability

The data of this manuscript entitled "Nerolidol Suppresses the Inflammatory Response during Lipopolysaccharide-Induced Acute Lung Injury via the Modulation of Antioxidant Enzymes and the AMPK/Nrf-2/HO-1 Pathway" (manuscript No. 9605980) is under license and so cannot be made freely available. Requests for access to these data should

be made to Yu-Hsiang Kuan through the following E-mail address: kuanyh@csmu.edu.tw.

Conflicts of Interest

The authors declare no conflict of interest.

Authors' Contributions

Shih-Pin Chen and Yu-Hsiang Kuan contributed equally to this work.

Acknowledgments

References

[1] Y. Butt, A. Kurdowska, and T. C. Allen, "Acute lung injury: a clinical and molecular review," *Archives of Pathology & Laboratory Medicine*, vol. 140, no. 4, pp. 345–350, 2016.

[2] E. R. Johnson and M. A. Matthay, "Acute lung injury: epidemiology, pathogenesis, and treatment," *Journal of Aerosol Medicine and Pulmonary Drug Delivery*, vol. 23, no. 4, pp. 243–252, 2010.

[3] E. Rezoagli, R. Fumagalli, and G. Bellani, "Definition and epidemiology of acute respiratory distress syndrome," *Annals of Translational Medicine*, vol. 5, no. 14, p. 282, 2017.

[4] T. Yokochi, "A new experimental murine model for lipopolysaccharide-mediated lethal shock with lung injury," *Innate Immunity*, vol. 18, no. 2, pp. 364–370, 2012.

[5] W. S. Leung, M. L. Yang, S. S. Lee et al., "Protective effect of zerumbone reduces lipopolysaccharide-induced acute lung injury via antioxidative enzymes and Nrf2/HO-1 pathway,"

International Immunopharmacology, vol. 46, pp. 194–200, 2017.

[6] Y. C. Ho, S. S. Lee, M. L. Yang et al., "Zerumbone reduced the inflammatory response of acute lung injury in endotoxin-treated mice via Akt-NFκB pathway," *Chemico-Biological Interactions*, vol. 271, pp. 9–14, 2017.

[7] C. Y. Lee, S. P. Chen, C. H. Su et al., "Zerumbone from *Zingiber zerumbet* ameliorates lipopolysaccharide-induced ICAM-1 and cytokines expression via p38 MAPK/JNK-IκB/NF-κB pathway in mouse model of acute lung injury," *Chinese Journal of Physiology*, vol. 61, no. 3, pp. 171–180, 2018.

[8] A. Nunes-Silva, P. T. T. Bernardes, B. M. Rezende et al., "Treadmill exercise induces neutrophil recruitment into muscle tissue in a reactive oxygen species-dependent manner. An intravital microscopy study," *PLoS One*, vol. 9, no. 5, article e96464, 2014.

[9] O. M. Ighodaro and O. A. Akinloye, "First line defence antioxidants-superoxide dismutase (SOD), catalase (CAT) and glutathione peroxidase (GPX): their fundamental role in the entire antioxidant defence grid," *Alexandria Journal of Medicine*, vol. 54, no. 4, pp. 287–293, 2018.

[10] A. Loboda, M. Damulewicz, E. Pyza, A. Jozkowicz, and J. Dulak, "Role of Nrf2/HO-1 system in development, oxidative stress response and diseases: an evolutionarily conserved mechanism," *Cellular and Molecular Life Sciences*, vol. 73, no. 17, pp. 3221–3247, 2016.

[11] M. Schieber and N. S. Chandel, "ROS function in redox signaling and oxidative stress," *Current Biology*, vol. 24, no. 10, pp. R453–R462, 2014.

[12] G. Wang, Y. Song, W. Feng et al., "Activation of AMPK attenuates LPS-induced acute lung injury by upregulation of PGC1α and SOD1," *Experimental and Therapeutic Medicine*, vol. 12, no. 3, pp. 1551–1555, 2016.

[13] Y. L. Qiu, X. N. Cheng, F. Bai, L. Y. Fang, H. Z. Hu, and D. Q. Sun, "Aucubin protects against lipopolysaccharide-induced acute pulmonary injury through regulating Nrf2 and AMPK pathways," *Biomedicine & Pharmacotherapy*, vol. 106, pp. 192–199, 2018.

[14] S. Pacifico, B. D'Abrosca, A. Golino et al., "Antioxidant evaluation of polyhydroxylated nerolidols from redroot pigweed (*Amaranthus retroflexus*) leaves," *LWT - Food Science and Technology*, vol. 41, no. 9, pp. 1665–1671, 2008.

[15] J. Azzi, L. Auezova, P. E. Danjou, S. Fourmentin, and H. Greige-Gerges, "First evaluation of drug-in-cyclodextrin-in-liposomes as an encapsulating system for nerolidol," *Food Chemistry*, vol. 255, pp. 399–404, 2018.

[16] W.-K. Chan, L. Tan, K. G. Chan, L. H. Lee, and B. H. Goh, "Nerolidol: a sesquiterpene alcohol with multi-faceted pharmacological and biological activities," *Molecules*, vol. 21, no. 5, p. 529, 2016.

[17] D. G. Hardie, F. A. Ross, and S. A. Hawley, "AMPK: a nutrient and energy sensor that maintains energy homeostasis," *Nature Reviews Molecular Cell Biology*, vol. 13, no. 4, pp. 251–262, 2012.

[18] A. Lapczynski, S. P. Bhatia, C. S. Letizia, and A. M. Api, "Fragrance material review on nerolidol (isomer unspecified)," *Food and Chemical Toxicology*, vol. 46, no. 11, pp. S247–S250, 2008.

[19] D. McGinty, C. S. Letizia, and A. M. Api, "Addendum to fragrance material review on nerolidol (isomer unspecified)," *Food and Chemical Toxicology*, vol. 48, pp. S43–S45, 2010.

[20] A. Y. Saito, A. A. Marin Rodriguez, D. S. Menchaca Vega, R. A. C. Sussmann, E. A. Kimura, and A. M. Katzin, "Antimalarial activity of the terpene nerolidol," *International Journal of Antimicrobial Agents*, vol. 48, no. 6, pp. 641–646, 2016.

[21] L. Zhang, D. Sun, Y. Bao, Y. Shi, Y. Cui, and M. Guo, "Nerolidol protects against LPS-induced acute kidney injury via inhibiting TLR4/NF-κB signaling," *Phytotherapy Research*, vol. 31, no. 3, pp. 459–465, 2017.

[22] D. V. Fonsêca, P. R. R. Salgado, F. L. de Carvalho et al., "Nerolidol exhibits antinociceptive and anti-inflammatory activity: involvement of the GABAergic system and proinflammatory cytokines," *Fundamental & Clinical Pharmacology*, vol. 30, no. 1, pp. 14–22, 2016.

[23] M. Rojas, C. R. Woods, A. L. Mora, J. Xu, and K. L. Brigham, "Endotoxin-induced lung injury in mice: structural, functional, and biochemical responses," *American Journal of Physiology-Lung Cellular and Molecular Physiology*, vol. 288, no. 2, pp. L333–L341, 2005.

[24] T. S. Teng, A. L. Ji, X. Y. Ji, and Y. Z. Li, "Neutrophils and immunity: from bactericidal action to being conquered," *Journal of Immunology Research*, vol. 2017, Article ID 9671604, 14 pages, 2017.

[25] B. G. Pinheiro, A. S. B. Silva, G. E. P. Souza et al., "Chemical composition, antinociceptive and anti-inflammatory effects in rodents of the essential oil of *Peperomia serpens* (Sw.) Loud," *Journal of Ethnopharmacology*, vol. 138, no. 2, pp. 479–486, 2011.

[26] M. Mittal, M. R. Siddiqui, K. Tran, S. P. Reddy, and A. B. Malik, "Reactive oxygen species in inflammation and tissue injury," *Antioxidants & Redox Signaling*, vol. 20, no. 7, pp. 1126–1167, 2014.

[27] H. Javed, S. Azimullah, S. B. Abul Khair, S. Ojha, and M. E. Haque, "Neuroprotective effect of nerolidol against neuroinflammation and oxidative stress induced by rotenone," *BMC Neuroscience*, vol. 17, no. 1, p. 58, 2016.

[28] M. D. Baldissera, C. F. Souza, T. H. Grando et al., "Nerolidol-loaded nanospheres prevent hepatic oxidative stress of mice infected by *Trypanosoma evansi*," *Parasitology*, vol. 144, no. 2, pp. 148–157, 2017.

[29] M. D. Baldissera, C. F. Souza, T. H. Grando et al., "Nerolidol-loaded nanospheres prevent behavioral impairment via ameliorating Na+, K+-ATPase and AChE activities as well as reducing oxidative stress in the brain of *Trypanosoma evansi*-infected mice," *Naunyn-Schmiedeberg's Archives of Pharmacology*, vol. 390, no. 2, pp. 139–148, 2017.

[30] A. T. Dinkova-Kostova and P. Talalay, "Direct and indirect antioxidant properties of inducers of cytoprotective proteins," *Molecular Nutrition & Food Research*, vol. 52, pp. S128–S138, 2008.

[31] M. X. Zhou, G. H. Li, B. Sun et al., "Identification of novel Nrf2 activators from *Cinnamomum chartophyllum* H.W. Li and their potential application of preventing oxidative insults in human lung epithelial cells," *Redox Biology*, vol. 14, pp. 154–163, 2018.
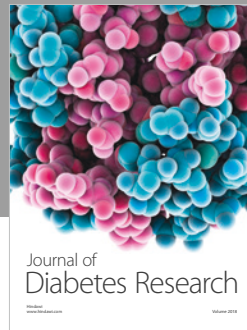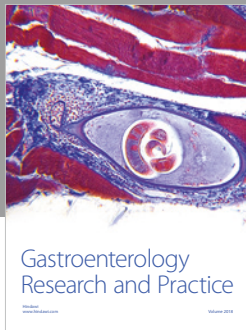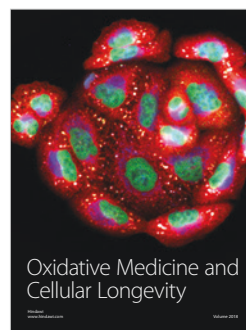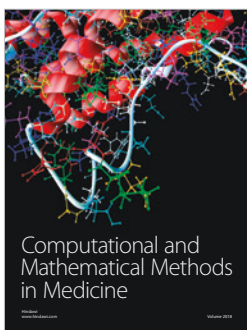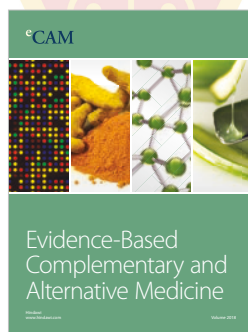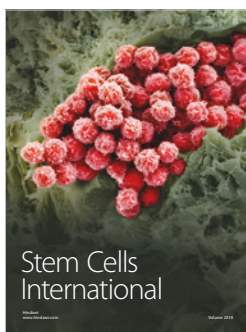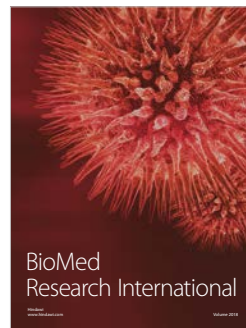
Ruptured Sinus of Valsalva Aneurysm Presenting as Acute Coronary Syndrome with Cardiogenic Shock and aVR ST-Elevation – A Case Report

Sheng-Wei Huang,[1] Chien-Hsien Lo,[1] Chin-Feng Tsai[1,2] and Chun-Hung Su[1,2]

INTRODUCTION

A ruptured sinus of Valsalva aneurysm can present as a clinical emergency and can lead to progressively deteriorating dyspnea. We describe an unusual case of sinus of Valsalva aneurysm (SOVA) presenting with acute chest pain and dyspnea with electrocardiographic ST-segment elevation in the V1 and aVR leads. Diagnostic angiography and cardiac computed tomography angiography showed contrast enhancement from the aorta to the right ventricle and pulmonary artery. The patient was referred to a cardiovascular surgeon for immediate surgical excision and repair. This case highlights the importance of physical examination and echocardiography, especially in the emergency setting, since the disease can manifest in various presentations. To the best of our knowledge, this report may be the first described case to suggest an acute coronary syndrome with aVR ST-elevation occurring from an acute ruptured SOVA.

CASE

A 53-year-old man with a history of hypertension and chronic renal insufficiency was admitted to the emergency department because of acute onset of chest pain. The symptoms began while he started working at his office for a few minutes in the morning, and then he developed central chest tightness and shortness of breath while sitting in his chair. At the same time, he also felt weak and diaphoretic. These symptoms did not subside with rest. This sudden onset of substernal, anterior chest discomfort, non-radiating pain persisted until he presented to the emergency department more than 30 minutes later.

On physical examination, he appeared pale-faced, and he had a continuous cardiac murmur detected on cardiac auscultation with clear breath sounds. He had tachycardia (heart rate: 136 beats per minute) and profound shock (blood pressure: 80/46 mmHg) without a significant blood pressure gradient (< 10 mmHg) in his four limbs or engorged jugular vein. His initial 12-lead electrocardiogram revealed > 1.5 mm ST-segment elevation in the V1 and aVR leads with ST depression in leads I, II, and V4 to V6. The ST-segment elevation in the aVR was more prominent than in V1 (Figure 1A). An admission troponin I level of 0.11 ng/ml was reported.

Given the patient's typical electrocardiographic findings of left main coronary artery occlusion, dual antiplatelet therapy with aspirin and ticagrelor were administered. The patient was referred for emergent coronary angiography, which illustrated insignificant coronary artery disease. Left ventriculography with contrast was performed via a 6F pigtail catheter inserted into ascending aorta. Surprisingly, the contrast test revealed a right ventricular image; therefore, we removed the pigtail catheter and performed a manual contrast injection, and the image showed contrast enhancement from the ascending aorta into the right ventricle and pulmonary artery. Thus, we considered a shunt connection from the aorta to the right ventricle (Figure 1B).

Transthoracic echocardiography detected a continuous shunt from the aorta to the right ventricle,

normal left ventricular systolic function without regional wall motion abnormality or chamber dilatation. These findings suggest a ruptured SOVA on right coronary sinus (Figure 2A, 2B). The patient's previous echocardiographic images were reviewed. They showed moderate aortic regurgitation and an unruptured SOVA on right coronary sinus for at least 5 years (Figure 2C, 2D). Aortic regurgitation had disappeared in the present echocardiography study.

The patient's chest discomfort deteriorated, and profound shock persisted. Cardiac computed tomography angiography (CCTA) confirmed the diagnosis of a ruptured SOVA with a shunt from the aorta to the right ventricle (Figure 1C). The patient underwent emergent excision of the right coronary sinus aneurysm, patch repair, and pericardial effusion drainage. He was discharged without symptoms 7 days later. Follow-up echocardiography after 10 months demonstrated a normal sinus of Valsalva without residual pericardial effusion. He was hemodynamically stable and without chest discomfort 12 months after surgery (Supplementary Figure 1).
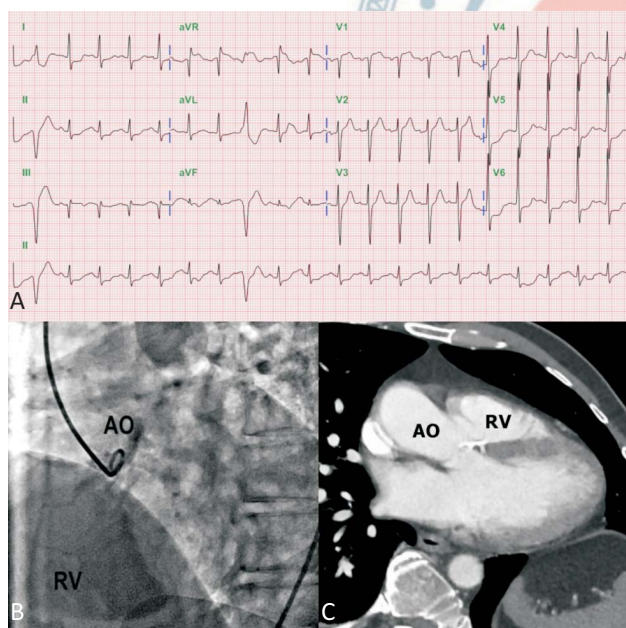
Figure 1. *(A) Initial 12-lead electrocardiography revealed ST-segment elevation in the V1 and aVR leads with V4 to V6, Lead I and II ST depressions. Note the ST-segment elevation in the aVR lead is more prominent than in the V1 lead. (B) Contrast enhancement from ascending aorta to right ventricle and pulmonary artery, suggestive of a shunt connection from the aorta to the right ventricle. (C) Cardiac computed tomography angiography (CCTA) confirmed the ruptured sinus of Valsalva aneurysm with a shunt from the aorta to the right ventricle.*

DISCUSSION

Ruptured SOVAs can present as a clinical emergency because of formation of aortic-cardiac shunting, primarily toward the right atrium and right ventricle, which can rapidly affect the hemodynamic status. SOVA is rarely considered in the differential diagnosis of acute chest pain with ST-segment elevation on ECG and has been reported in few literature in conjunction with acute ST-elevation myocardial infarction.[1]

Our patient was treated for hypertension and chronic aortic regurgitation according to his previous echocardiography in 2013. The SOVA in our patient was not recognized on his first echocardiogram, and his symptoms stayed stationary until acute chest discomfort developed during this emergency episode. Acute chest pain with lead aVR ST-segment elevation and ST-segment depression in several other leads may predict acute left main coronary artery obstruction.[2,3] The guideline suggests that early initiation of aspirin and P2Y12 inhibitor loading may help to achieve early efficacy. But in cases of ST-segment elevation and myocardial infarction, the diagnoses is not clear yet, delaying P2Y12 inhibitor loading until other etiologies are excluded (e.g.,
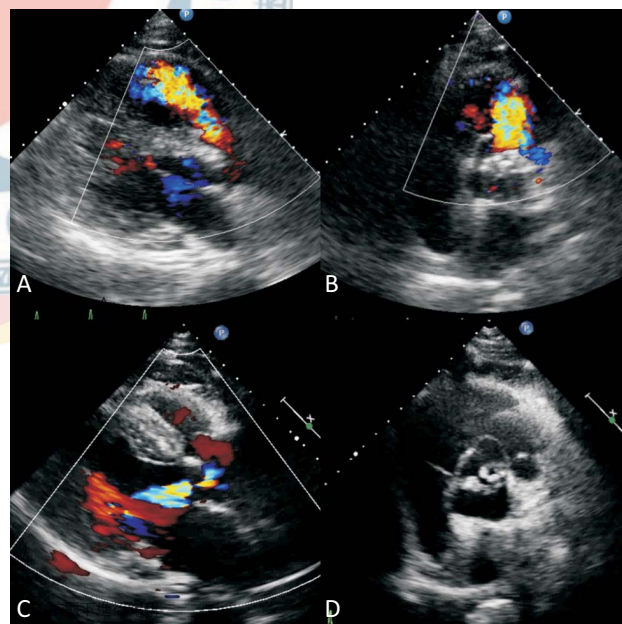
Figure 2. *(A, B) Transthoracic echocardiography detected a continuous shunt connection from the aorta to the right ventricle. No significant aortic regurgitation. (C, D) Previous transthoracic echocardiography detected significant aortic regurgitation and unruptured sinus of Valsalva aneurysm.*

aortic dissection) should be considered.[4] Our treatment strategy for the patient was to send him immediately for emergent coronary angioraphy, which met the percutaneous coronary intervention-mediated reperfusion (wire crossing) time of less than 90 minutes.[5] However, asymmetric radial pulsations (blood pressure) can present in aortic dissection but not in ruptured SOVA, and this phenomenon emphasizes the importance of early differential diagnosis. Early diagnosis and recognition that a patient with possible predictors and risk factors such as previous knowledge of an echocardiogram with an unruptured SOVA, poorly controlled blood pressure and the presence of a new cardiac murmur are critical for early diagnosis. Echocardiography, electrocardiographically gated CCTA, and cardiac magnetic resonance (CMR) imaging can provide an accurate diagnosis. Because the patient presented with persistent, profound cardiogenic shock, we chose CCTA rather than CMR imaging for efficiency and to rush the patient to surgery as soon as possible, even though transesophageal echocardiography is another good methods to detect SOVA and CMR imaging can provide excellent anatomic and functional information.[6]

With our patient, after dual antiplatelet therapy with aspirin 300 mg and ticagrelor 180 mg, the cardiac surgeon confronted numerous difficulties with hemostasis during the operation. Fortunately, the patient was discharged smoothly with no residual symptoms.

Reviewing the entire clinical course and management of the patient showed that there are many points to be learned. Firstly, lack of experience with echocardiography to recognize the presence of SOVA on the initial echocardiogram and the patient's lack of awareness of the danger of aneurysm rupture is extremely dangerous. Unruptured SOVA is usually asymptomatic or presents with symptoms of dyspnea, easy fatigability, palpitations, or chest pain.[7] Asymptomatic SOVA is often detected serendipitously by routine 2-dimensional echocardiography. Aortic regurgitation is one of the most common cardiac anomalies that occur in conjunction with SOVA, like in this case. Second, a detailed, symptom-oriented and focused physical examination in the emergency department could reveal a significant continuous murmur in the left lower sternal border that differed from aortic insufficiency.[8] However, both the careful auscultation and bedside echocardiography were both ignored in order to shorten the door to wire crossing time. When patients presented with an acute myocardial infarction with shock and cardiac murmur, mechanical complication is important differential diagnosis. Eventually a continuous murmur firstly recorded and described in the cardiac care unit in the left lower sternal border, after coronary angiography. The lead aVR is to obtain specific information from the right side of the heart, such as the right ventricle outflow tract and the basal part of the interventricular septum. Rupture of the SOVA could cause an acute interruption of coronary artery blood flow that contributing to the electrocardiographic changes. After the aneurysm has ruptured, the flow into the right ventricle (RV) would be continuous during both systole and diastole according to continuous pressure gradient. The acute left-to-right shunting may cause coronary flow supply-demand mismatch and more severely, cardiogenic shock and then deteriorated coronary insufficiency, contributing to aVR ST elevation and diffuse ST depressions. The mechanism include increased myocardial oxygen consumption because of overactived sympathetic tone and acute RV injury resulting from acute left-to-right shunting that may induce RV transmural ischemia. Those leads being remote from the RV like lead I and V4 to V6, will record ST depressions.[9] Additionally, all acute cardiovascular conditions should be assessed with echocardiography for differentiation between acute myocardial infarction, aortic dissection, acute pulmonary embolism, and cardiac tamponade.[10] However uncommon, SOVA rupture with shunting is also detected easily. Unnecessary medical prescription and intervention could be avoided by the careful use of these non-invasive examinations.

To the best of our knowledge, this report may be the first described case to suggest an acute aVR ST-elevation myocardial infarction occurring from an acute ruptured SOVA. Early diagnosis by accurate imaging and emergent surgical repair can provide good immediate and 1-year outcomes.

LEARNING POINTS

- A ruptured SOVA can present as a clinical emergency and can lead to progressively deteriorating dyspnea and acute coronary syndrome. Continuous heart mur-

mur with acute shock hints acute ruptured SOVA.

- Lead aVR ST elevation reflects reciprocal change from ischemia of the left ventricle and ischemia from the RV outflow tract or the right basal part of the interventricular septum region, possible caused not only by left main coronary artery stenosis and severe triple vessel obstructions but also any RV injury.
- All acute cardiovascular conditions should be assessed with echocardiography. However uncommon, SOVA rupture with shunting is also detected easily.
- Early diagnosis by accurate imaging and emergent surgical repair can provide good immediate and 1-year outcomes for ruptured SOVA.

ACKNOWLEDGMENT

None.

CONFLICT OF INTEREST

All the authors declare no conflict of interest.

REFERENCES

1. Nguyen TL, Thomas L. Acute myocardial infarction secondary to a spontaneous right coronary artery dissection resulting from a sinus of valsalva aneurysm. *Eur J Echocardiogr* 2010;11:E2.
2. Nia AM, Gassanov N, Reuter H, Er F. A sign to heaven: aVR lead elevation and myocardial infarction. *ScientificWorldJournal* 2011; 11:662-5.
3. Adar A, Onalan O, Cakan F. Relationship between ST-segment shifts in lead aVR and coronary complexity in patients with acute coronary syndrome. *Acta Cardiol Sin* 2019;35:11-9.
4. Ibanez B, James S, Agewall S, et al. 2017 ESC Guidelines for the management of acute myocardial infarction in patients presenting with ST-segment elevation: The Task Force for the management of acute myocardial infarction in patients presenting with ST-segment elevation of the European Society of Cardiology (ESC). *Eur Heart J* 2018;39:119-77.
5. Li YH, Chiu YW, Cheng JJ, et al. Changing practice pattern of acute coronary syndromes in Taiwan from 2008 to 2015. *Acta Cardiol Sin* 2019;35:1-10.
6. Bricker AO, Avutu B, Mohammed T-LH, et al. Valsalva sinus aneurysms: findings at CT and MR imaging. *RadioGraphics* 2010; 30:99-110.
7. Cheng TO, Yang YL, Xie MX, et al. Echocardiographic diagnosis of sinus of Valsalva aneurysm: a 17-year (1995-2012) experience of 212 surgically treated patients from one single medical center in China. *Int J Cardiol* 2014;173:33-9.
8. Topi B, John J, Agarwal A, et al. An uncommon cause of a continuous murmur. *Exp Clin Cardiol. 2* 2012;17:148-9.
9. Zhong-Qun Z, Chong-Quan W, Nikus KC, et al. A new electrocardiogram finding for massive pulmonary embolism: ST elevation in lead aVR with ST depression in leads I and V(4) to V(6). *Am J Emerg Med* 2013;31:456.e455-8.
10. Neskovic AN, Hagendorff A, Lancellotti P, et al. Emergency echocardiography: the European Association of Cardiovascular Imaging recommendations. *Eur Heart J Cardiovasc Imaging* 2013;14:1-11.

SUPPLEMENT
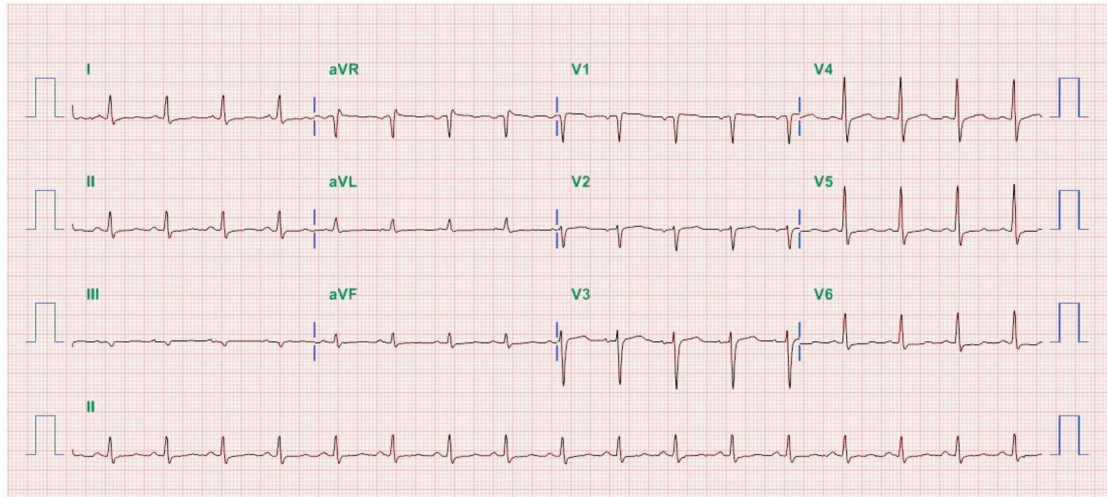
Supplementary Figure 1. *The post-operation electrocardiography shows those initial ST elevation at lead aVR and other ST depressions all normalized.*

Review Article

2020 Focused Update of the 2012 Guidelines of the Taiwan Society of Cardiology for the Management of ST-Segment Elevation Myocardial Infarction

Yi-Heng Li,[1] Cheng-Han Lee,[1,2] Wei-Chun Huang,[3,4,5] Yu-Chen Wang,[6,7,8] Chun-Hung Su,[9,10] Pei-Hsun Sung,[11,12] Shih-Chieh Chien[13] and Juey-Jen Hwang[14]

for The Writing Group of 2020 Focused Update of the 2012 Guidelines of the Taiwan Society of Cardiology for the Management of ST-segment Elevation Myocardial Infarction

One of the major missions of the Taiwan Society of Cardiology is to publish practice guidelines that are suitable for local use in Taiwan. The ultimate purpose is to continuously improve cardiovascular health care from the implementation of the recommendations in the guidelines. Despite recent improvement of medical care, patients with ST-segment elevation myocardial infarction (STEMI) still carry a high morbidity and mortality. There have been many changes in the concepts of STEMI diagnosis and treatment in recent years. The 2020 focused update of the 2012 guidelines of the Taiwan Society of Cardiology for the management of STEMI is an amendment of the 2012 guidelines based on the newest published scientific data. The recommendations in this focused update provide the diagnosis and treatment strategy for STEMI that should be generally implemented in Taiwan. Nevertheless, guidelines never completely replace clinical judgment and medical decision still should be determined individually.

Key Words: Acute myocardial infarction • Guideline • Taiwan

INTRODUCTION

Through early revascularization with primary percutaneous coronary intervention (PCI) and use of guideline-recommended secondary preventive medications, the mortality of ST-segment elevation myocardial infarction (STEMI) continues to decrease in Taiwan.[1] Since the publication of the 2012 Guidelines of the Taiwan Society of Cardiology (TSOC) for the Management of STEMI,[2] some concepts in treating the disease have been modi-

fied due to emerging new evidences. The purpose of this "focused update" is to revise the 2012 guideline specifically in several areas that the new study results bring in changes of STEMI management. The focused update began with a short review of epidemiology and recent treatment trends of STEMI in Taiwan. STEMI equivalents, defined as patients without typical ST segment elevation on electrocardiography (ECG), but need immediate triage and management as STEMI, were added in the diagnosis section. Revision on the section of pre-hospital management added new recommendations of early identification of STEMI by emergency medical service (EMS) field triage with prehospital ECG and direct transportation to the nearest PCI-available hospitals. In addition to clopidogrel and ticagrelor, prasugrel was introduced into Taiwan in the end of 2018. There were revised recommendations about the choice of P2Y12 inhibitors for STEMI. There were also revisions to the section on primary PCI, including adequate time intervals from diagnosis to intervention, vascular access and complete revascularization strategy. Cardiogenic shock is still a major cause of mortality in STEMI. Revision on section of cardiogenic shock was added because of recent advances in therapeutic options. For secondary preventive strategies, new pharmacological therapies for diabetes and hypercholesterolemia have been developed and proved to further reduce recurrent cardiovascular (CV) events in high risk patients such as STEMI. The section of long-term pharmacological treatment after discharge was revised and included all these new medical therapies. Finally, a new section of quality care of STEMI was added to indicate the importance of guideline implementation and several quality indicators were proposed.

In 2019, the President and Executive Board of the TSOC decided to revise the 2012 Guidelines of the TSOC for the Management of STEMI and invited several members to form a writing group. The major topics in the guideline were assigned to the members of the writing group and the data from clinical trials as well as other publications in peer-reviewed journals related to the topics were reviewed. New or modified recommendations in this focused update reflect the latest progress in the diagnosis and treatment of STEMI. The readers may refer to the prior guideline about the clinical topics which were not addressed in this focused update.[2] In order to demonstrate the intensities of recommendations, the evidence-based classification system, including class of recommendation (COR) and level of evidence (LOE), was adopted in the guideline. The definitions of COR I to III and LOE A to C were the same as those in the 2018 Guidelines of the TSOC for the management of non ST-segment elevation acute coronary syndrome (ACS).[3]

EPIDEMIOLOGY OF STEMI

Recent epidemiological studies in Taiwan using the Taiwan National Health Insurance Research Database showed that the overall adjusted incidence of acute myocardial infarction (MI) increased progressively from 1999 to 2008.[1,4,5] The age- and sex-adjusted incidence rates (per 100,000 population) of acute MI increased from 30 in 1997 to 49.8 in 2009, which was mainly driven by the increase of non ST-segment elevation myocardial infarction (NSTEMI) and the increasing tendency was noted in both genders.[1,5] However, the adjusted incidence of acute MI remained constant after 2008 and estimated to be 49.8 in 2009 to 50.7 in 2015.[1] The adjusted incidence of STEMI decreased from 16.8 in 2009 to 14.4 in 2015, whereas NSTEMI continuously increased from 32.5 in 2009 to 35.7 in 2015 (Figure 1). The ratio of NSTEMI to STEMI incidence increased from 1.93 in 2009 to 2.47 in 2015.[1] For STEMI, the incidence decreased across all age group except in the young population (< 55 years).[1] There was a 7.7% increase of STEMI from 2009 to 2015 in young men and no sign of decreasing trend in young female.[1] In Taiwan, individuals hospitalized for STEMI were more likely to be younger and were
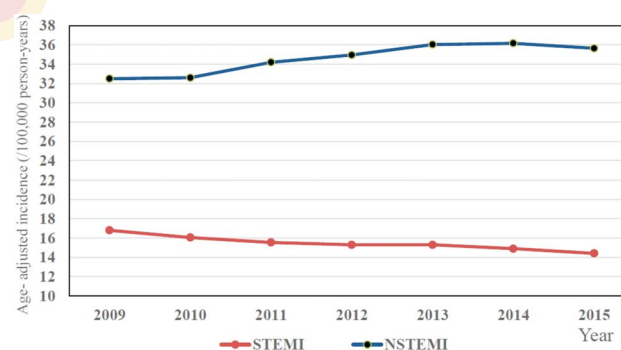
Figure 1. *The recent trends of decreasing incidence of STEMI and increasing incidence of NSTEMI in Taiwan. NSTEMI, non ST-segment elevation myocardial infarction; STEMI, ST-segment elevation myocardial infarction. Adapted from reference 1.*

less likely to have diabetes mellitus and hypertension in comparison with NSTEMI patients.[1] However, the incidence of dyslipidemia was higher in STEMI than NSTEMI patients.[1] For STEMI, the mean age was 1.3 years younger in 2015 compared with that in 2009 and there was a 19.8% increase of dyslipidemia during these years.[1] In Taiwan, most STEMI patients received primary PCI rather than fibrinolytic therapy.[1] Two nationwide ACS registries in Taiwan among different time periods (2008-2010 and 2012-2015) showed that the median door-to-balloon (D2B) time in primary PCI decreased from 96 minutes in the first registry to 71 minutes in the second registry.[6] One retrospective 10-year cohort study in a single medical center in Taiwan also showed that the median D2B time decreased from 142 minutes in 2005 to 69 minutes in 2014.[7] In secondary preventive pharmacological therapies, the in-hospital use of dual anti-platelet therapy (DAPT) (95.1% to 99.6%), angiotensin converting enzyme inhibitor (ACEI)/angiotensin receptor blocker (ARB) (63.8% to 77.5%), beta-blocker (48.8% to 71.4%), and statin (54.4% to 81.2%) all increased significantly between the two ACS registries.[6] The overall crude in-hospital mortality rate of STEMI decreased from 2009 (9.3%) to 2015 (7.6%) in Taiwan.[1] However, the mortality rate was persistently higher in female than male patients and there was no improving trend of mortality in STEMI for female patients.[1] The prescription rate of secondary preventive medications for STEMI in Taiwan was still relatively low compared with the data from Western country.[8]

Recommendation

- More actions should be taken to control the increasing incidence of STEMI in young population in Taiwan. (COR I, LOE C)
- To increase prescription rate of secondary preventive medications for STEMI in Taiwan is necessary. (COR I, LOE C)

DIAGNOSIS OF STEMI

Definition

Diagnosis of acute MI in this guideline is based on definition of the Fourth Universal Definition of MI 2018.[9] It defines acute MI as acute myocardial injury with clinical evidence of acute myocardial ischemia and with detection of a rise and/or fall of cardiac troponin values with at least one value above the 99th percentile upper reference limit with at least one of the following: symptoms of myocardial ischemia; new ischemic ECG changes; development of pathological Q waves; imaging evidence of new loss of viable myocardium or new regional wall motion abnormality in a pattern consistent with an ischemic etiology; identification of a coronary thrombus by angiography or autopsy.[9] Several types of acute MI were defined according to different pathophysiological mechanisms leading to ischemic myocardial injury. The typical STEMI is type 1 MI which is caused by coronary atherosclerosis with atherosclerotic plaque disruption, rupture or erosion and coronary thrombus formation. Most recommendations in this guideline can be applied to this type of MI. Some STEMIs fall into other types of MI which the managements are not included in this guideline.

ECG and biomarker

A 12-lead ECG is the most important diagnostic modality and determines the subsequent management pathways in patients presented with acute chest discomfort. No matter the patients are in an ambulance, local practitioner's clinic, or emergency department, an ECG should be performed immediately if it is available. The ECG should be interpreted as soon as possible to identify any possibility of STEMI or its equivalents by experienced physician, nurse or trained EMS personnel. A rapid transmission of the ECG through smartphone or other ways to emergency physicians or cardiologists not only speeds up the diagnosis of STEMI but also shortens the time for activation of primary PCI team.[10,11] Repeat ECG to follow up the ST-T changes is necessary if the first ECG is normal or equivocal when there are persistent symptoms of myocardial ischemia. Changes of biomarker confirm the presence of myocardial necrosis. Measurement of biomarker should not delay the process for primary PCI. High sensitivity cardiac troponin (hs-cTn) is the recommended biomarker because hs-cTn assays increase diagnostic accuracy for acute MI presenting early after chest pain and allow for a rapid rule-out of acute MI when there are doubts about the diagnosis.[12,13] The detailed recommendations of hs-cTn assays were described previously in the 2018 Guidelines of the TSOC for the management of non ST-segment elevation ACS (Figure 2).[3]
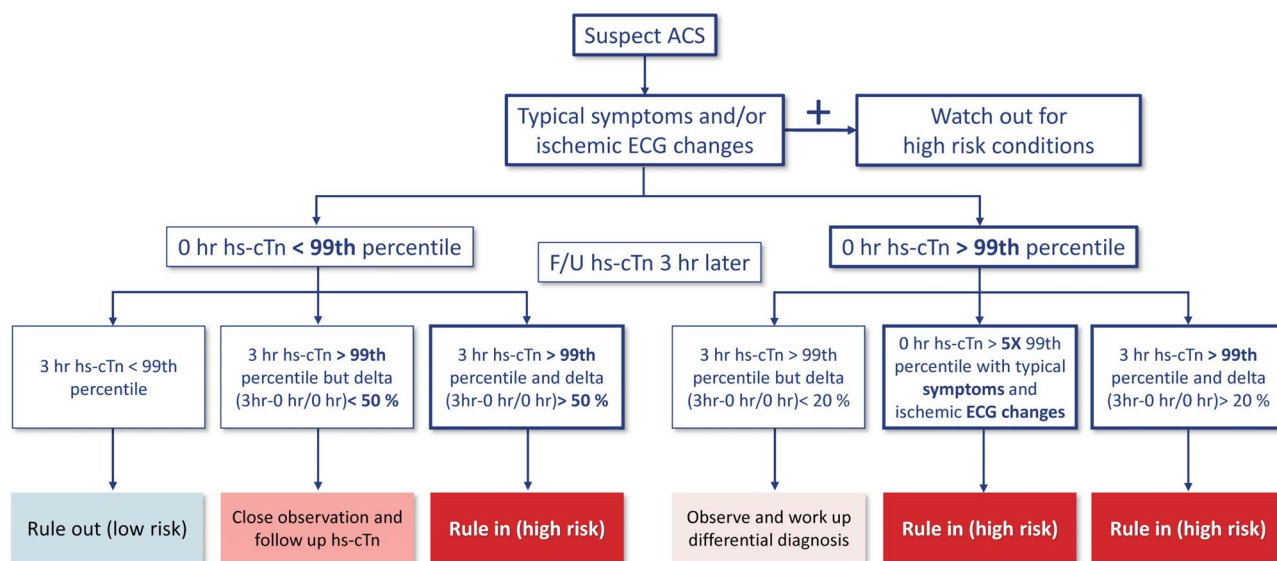
Figure 2. *The detailed recommendations of using high sensitivity cardiac troponin assay to diagnose and rule out acute myocardial infarction. ACS, acute coronary syndrome; ECG, electrocardiography; hs-cTn, high sensitivity cardiac troponin. Adapted from reference 3.*

Recommendation

- A 12-lead ECG should be performed immediately in patients presented with any symptom suggestive of STEMI. (COR I, LOE C)
- Rapid transmission of ECG by smartphone or other ways to emergency physicians or cardiologists for early diagnosis is recommended. (COR I, LOE B)
- Hs-cTn assay is recommended for rapid diagnosis and rule-out of acute MI. (COR I, LOE A)

STEMI equivalents

For rapid triage and primary PCI, this guideline adopts the conventional definition of STEMI as those with symptoms suggestive of myocardial ischemia and ST-segment elevation in at least two contiguous leads on ECG. However, there are several conditions that patients present without typical ST-segment elevation on a standard 12-lead ECG, but should be managed as STEMI equivalents. The first condition is posterior MI. The typical ECG changes of posterior MI include ST segment depression in precordial leads V1-V4 and a R/S ratio greater than 1 in leads V1 or V2.[14] If posterior MI is suspected, posterior leads V7 to V9 of ECG should be done to look for ST segment elevation in these leads.[14,15] Lead V7 is placed at the same level of V6 at the posterior axillary line; lead V8 is on the left side of the back at the tip of the scapula and V9 is placed at left paraspinal region at the same level as V6. The infarct related artery (IRA) in patients with typical ECG abnormalities of posterior MI is left circumflex artery. The second condition is left main MI. The typical ECG changes of left main MI include ST elevation in lead aVR with ST elevation in aVR ≥ V1 and extensive ST depression in leads I, II, and V4-6.[16,17] Patients presented clinical symptoms with these ECG changes require early coronary angiography to define the left main coronary artery anatomy. The third condition is STEMI in preexisting left bundle branch block (LBBB). The ST segment changes in LBBB make it difficult to diagnose STEMI directly. The Sgarbossa ECG criteria, including (1) concordant ST-segment elevation > 1 mm in at least one lead or (2) concordant ST-segment depression > 1 mm in any of the V1 to V3 leads or (3) discordant ST-segment elevation > 5 mm, are used to identify patients with STEMI in patients with preexisting LBBB.[18]

Recommendation

- Even without typical ST segment elevation on standard 12-lead ECG, STEMI equivalents should be managed as STEMI. (COR I, LOE C)

PREHOSPITAL MANAGEMENT

Public awareness of acute MI

STEMI is a time-sensitive disease because prompt treatment after symptoms onset improves patients'

prognosis. Mortality of STEMI could be reduced 1.5% for every 30-minute decrease in reperfusion time.[19] The key to successful treatment is early recognition of symptoms and rapid arrival at a hospital with PCI facility.[20] Patient delay is a critical factor. It commonly due to poor awareness of heart attack symptoms and not calling an ambulance even when acute MI is really occuring.[21] Previous study showed the awareness of acute MI symptoms in citizens ranged from 32.9% (arm or shoulder pain) to 70.2% (difficulty breathing) and 79.1% (chest pain and discomfort).[20] Overall, 67% citizens would call an ambulance if someone had signs of acute MI.[20] Currently, it is roughly estimated that only 10-20% STEMI patients were sent to hospitals by ambulance of EMS in Taiwan. Transportation of suspected STEMI patients by EMS ambulance is much safer because emergency medical technicians (EMT) received cardiopulmonary resuscitation (CPR) training and EMS ambulances are equipped with automated external defibrillator.[22-25] Since 2011, EMS in more than 90% of cities and counties in Taiwan started to set up ECG telemetry system in ambulances which may assist in early diagnosis of STEMI and directly transferring patients to PCI available hospitals. Therefore, ambulance transfer is highly recommended for patients suspected of acute MI with typical chest pain with or without dyspnea, cold sweating or nausea.

Recommendation

- Increased public awareness of the typical symptoms of acute MI is recommended. (COR I, LOE C)
- Ambulance transfer to PCI available hospitals is recommended for patients with typical symptoms of acute MI. (COR I, LOE C)

Transportation for primary PCI

Compared with fibrinolytic therapy, primary PCI is the preferred reperfusion strategy.[26] In Taiwan, primary PCI is the routine reperfusion therapy for STEMI, whereas fibrinolysis is used only in some special occasions, such as during severe pandemic infectious diseases or in adjacent small islands without PCI available hospitals.[6,27,28] Currently, with a population of 23 million in Taiwan, there are 103 PCI available hospitals. Approved by the national STEMI accreditation system from Taiwan Government, 58 hospitals provide 24-hour service of primary PCI, including 46 hospitals with high grade critical

care ability and 12 hospitals with moderate grade critical care ability (Figure 3). Through convenient highway system, ambulances usually could reach a PCI available hospital within 2 hours. However, pre-hospital delay is still a challenging issue in Taiwan due to multifactorial reasons. A well-organized STEMI network among different hospitals and EMS system is critical for optimization of STEMI care.[29-31] A city/county-based STEMI network should have a standard operating procedure to guide EMTs in the ambulance to transport STEMI patients directly to nearby PCI available hospitals and bypass non-PCI hospitals. EMTs could diagnose STEMI by ECG reading themselves or through on-line instruction from hospital staffs by ECG transmission via smartphone or telemetry ECG system in the field.[23-25,32] The network can activate primary PCI team in nearby hospital as soon as possible. EMS ambulance system should be equipped with ECG recorders, automated external defibrillators and auto CPR machines, which could diagnose STEMI in the field and provide critical life-saving treatment.[23,25,32]

STEMI patients can be diagnosed in a hospital without PCI facility or 24-hour PCI capability. Hospitals with 24-hour PCI capability should establish inter-hospital STEMI network with other hospitals in order to transport STEMI patients safely and rapidly. Inter-hospital STEMI network was reported to shorten D2B time, and
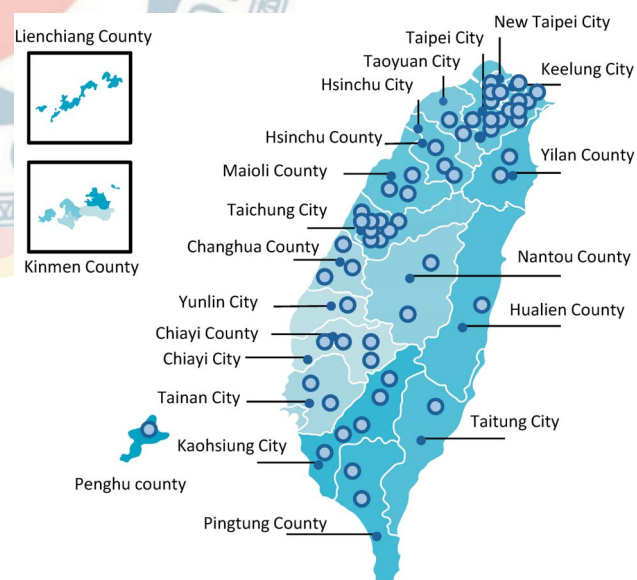
Figure 3. *Distribution of hospitals that provide 24-hour primary PCI service in Taiwan. Fibrinolysis is only suggested in special occasions, including special pandemic infection or islands without PCI available hospitals. PCI, percutaneous coronary intervention.*

hospitals with 24-hour PCI capability should take a "no-refusal" principle for all patients transferred for consideration of primary PCI.[33,34] The hospitals with 24-hour PCI capability should have a 24-hour hot line with other non-PCI hospitals. Inter-hospital transmission of ECG and/or laboratory data via smartphone or facsimile in order to early activation of PCI team is necessary. On arrival, the patients should be directly transferred to catheterization laboratory as soon as possible. There should be a feedback system inside the network between non-PCI and PCI hospitals. Figure 4 summarizes the transportation pathways for primary PCI from different places of patient presentation.

Recommendation

- Regional STEMI network should be established to guide direct transportation of STEMI patients to PCI available hospitals. (COR I, LOE B)
- The EMS ambulances should be equipped with ECG recorders, automated external defibrillators and auto CPR machines. (COR I, LOE C)
- The EMTs in ambulance should receive training for ECG recording, interpretation and transmission for early identification of STEMI. (COR I, LOE C)
- Inter-hospital network is recommended to facilitate transfer for primary PCI among non-PCI and PCI available hospitals. (COR I, LOE B)

Pre-hospital medication

Early observational studies showed that upstream clopidogrel treatment before arriving PCI hospitals was associated with a reduction of death or recurrent MI in patients with STEMI treated with primary PCI.[35,36] A later small randomized trial found that clopidogrel 600 mg loading in prehospital phase could not increase the patency rate of IRA before primary PCI, but was associated with a trend toward less adverse clinical event.[37] The ATALANTIC trial randomized STEMI patients to receive ticagrelor either during transfer to a primary PCI hospital or immediately before angiography. The study found
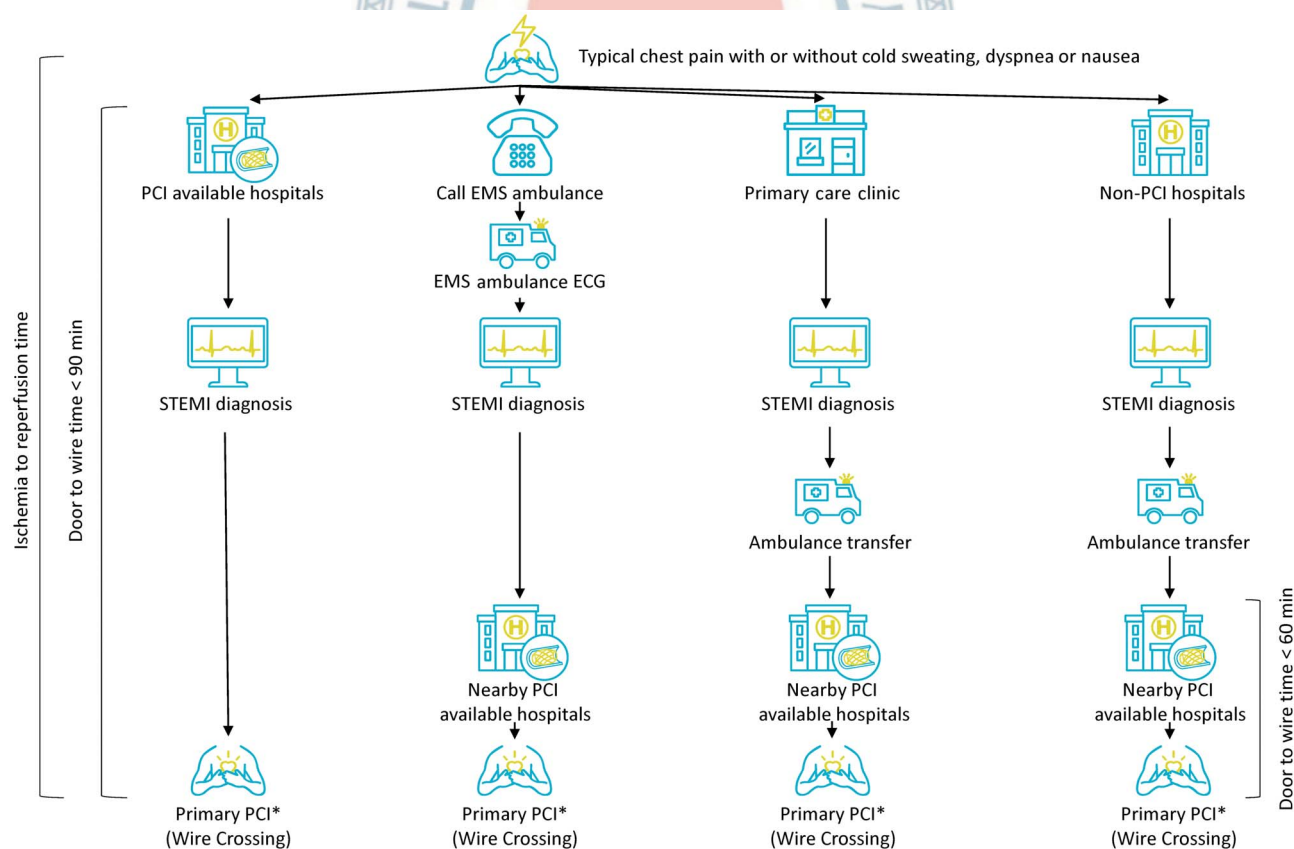
Figure 4. *Recommended transportation pathways and door-to-wire time for primary PCI from different places of patient presentation. PCI, percutaneous coronary intervention; STEMI, ST-segment elevation myocardial infarction. ECG, electrocardiography; EMS, emergency medical service.*

early ticagrelor treatment could not increase ST-segment elevation resolution or Thrombolysis in Myocardial Infarction (TIMI) blood flow in the IRA at initial angiography. But the rates of definite stent thrombosis were lower in 24 hour and 30 days in the prehospital group.[38] Currently, EMTs in 3 cities of Taiwan could administer DAPT in ambulance after on-line instruction by physicians in hospitals after reading ECG from telemetry transmission.

Recommendation

- Early use of DAPT (aspirin and P2Y12 inhibitor) in ambulance may be considered after on-line instruction by physicians in hospitals if no contraindication. (COR IIb, LOE C)

Out-of-hospital cardiac arrest

STEMI can be presented with out-of-hospital cardiac arrest (OHCA). After CPR and return of spontaneous circulation, emergency coronary angiography and PCI should be performed in awake or comatose patients with OHCA with suspected STEMI. Therapeutic hypothermia with targeted temperature management (TTM) should be considered because TTM after return of spontaneous circulation in cardiac arrest patients leads to improvements in mortality and neurological outcomes.[39,40] Previous study showed, after cardiac catheterization and TTM, there was a survival rate of 56% of the OHCA patients and most of the survivors had good neurological outcome.[41] However, previous studies using prehospital cold intravenous fluid resulted in worse outcomes including decreased rate of return of spontaneous circulation, increased chance of pulmonary edema, and increased incidence of diuretic use.[42,43]

Recommendation

- Primary PCI is recommended in STEMI patients with cardiac arrest post return of spontaneous circulation. (COR I, LOE B)
- TTM is recommended in comatose STEMI patients with cardiac arrest after return of spontaneous circulation. (COR I, LOE B)
- Prehospital cooling in ambulance with rapid infusion with cold saline is not recommended in STEMI patients with cardiac arrest post return of spontaneous circulation. (COR III, LOE B)

ANTIPLATELET THERAPY

DAPT with aspirin and P2Y12 inhibitor is the cornerstone therapy for STEMI. Clopidogrel was used in STEMI patients for many years and was the only P2Y12 inhibitor recommended in the 2012 Taiwan STEMI Guidelines.[2] New generation P2Y12 inhibitors, prasugrel and ticagrelor, showed superior efficacy compared with clopidogrel in improving clinical outcomes but at the expense of bleeding. Choosing either clopidogrel or potent P2Y12 inhibitors needs more consideration of the balance between clinical benefit and bleeding risk.

Clopidogrel

In large randomized studies, combination of clopidogrel with aspirin was associated with reduced ischemic event and mortality rate for STEMI, regardless of reperfusion strategies.[44,45] Four observational studies in Taiwan showed DAPT with aspirin and clopidogrel for more than 9 to 12 months significantly reduced ischemic risk and mortality rate in patients with ACS with or without PCI.[46-49] In patients receiving elective PCI, clopidogrel 600 mg loading dose was associated with more rapid and higher platelet inhibition than 300 mg dose.[50,51] But in the CURRENT−OASIS 7 trial, clopidogrel 600 mg loading dose did not reduce ischemic events but lead to higher major bleeding risk comparing with 300 mg loading dose in patients with ACS. However, in the subgroup analysis for patients receiving PCI, higher clopidogrel loading dose significantly reduced the rates of 30 days primary outcomes and stent thrombosis.[52] A meta-analysis demonstrated that higher clopidogrel loading dose with 600 mg was associated with reduced ischemic events and similar bleeding risk comparing with standard clopidogrel 300 mg loading dose in patients undergoing PCI.[53] In Taiwan, a loading dose of 300 mg to 600 mg clopidogrel is recommended for STEMI depending on patients' clinical conditions. There are some drawbacks of clopidogrel including slower onset time and drug response variability. Clopidogrel is an inactive prodrug and requires a 2-step metabolism to become an active metabolite,[54] which may be responsible to its slower drug onset and may lead to increased ischemic events in ACS patients with coronary thrombus formation. Furthermore, the prevalence of cytochrome P450 2C19 polymorphism with clopidogrel resistance is not uncom-

mon and may increase CV risk in ACS patients.[55,56] The percentage of CYP2C19 reduced function alleles carrier in Asian population is much higher than that in Caucasian population.[57,58] Therefore, newer P2Y12 inhibitors such as prasugrel or ticagrelor have been developed to overcome these unmet clinical needs of clopidogrel.

Prasugrel

Comparing with clopidogrel, prasugrel (60 mg loading and 10 mg daily dose) provides faster and greater platelet inhibitory effects in patients undergoing PCI.[59] The TRITON–TIMI 38 trial randomized 13608 ACS patients to receive either prasugrel or clopidogrel. The study found prasugrel reduced more ischemic events compared with clopidogrel [hazard ratio (HR) 0.82, 95% confidence interval (CI) 0.73-0.93], but also increased the risk of major bleeding (HR 1.40, 95% CI 1.05-1.88).[60] In the subgroup analysis for STEMI patients, the efficacy of prasugrel was consistent (HR 0.79, 95% CI 0.65-0.97) irrespective of the PCI timing.[61] It is worth of noticing that the post-hoc analysis of the TRITON-TIMI 38 study demonstrated that prasugrel was associated with net clinical harm due to a trend toward more major bleeding (p = 0.06) in patients with a history of ischemic stroke or transient ischemic attack (TIA). Patients aged 75 years or older and who were weighing less than 60 kg also had no clinical benefit from prasugrel.[60] Therefore, prasugrel is contraindicated in patients with prior history of stroke/TIA and should be used cautiously in patients with old age or low body weight.

In Taiwan and Japan, reduced-dose prasugrel (20 mg loading and 3.75 mg daily dose) is available due to the concern of bleeding risk in Asians. The reduced-dose regimen was studied in the PRASFIT-ACS trial which was conducted in Japan with the similar study design as the TRITON-TIMI 38 study. In the PRASFIT-ACS trial, about 50% of the study population was STEMI and those with prior ischemic stroke/TIA were excluded. After randomizing 1363 ACS patients undergoing PCI, the reduced-dose prasugrel was associated with a trend of 23% risk reduction (HR 0.77, 95% CI 0.56-1.07) of adverse CV events and similar risk of non-coronary artery bypass graft (CABG) major bleeding compared with clopidogrel.[62] A post-marketing observational study (PRASFIT-Practice I) enrolled 732 Japanese ACS patients receiving both PCI and reduced-dose prasugrel from 2014 to 2015

and 60% of the patients were STEMI. The rates of TIMI major bleeding and major adverse CV events were 1.6% and 3.1%, respectively during the observational period indicating the safety and efficacy of this regimen.[63] There was another larger nationwide registry study in Japan including 62737 ACS patients undergoing PCI in 2016. After propensity score matching, there were 12016 patients in the clopidogrel or prasugrel group, respectively. STEMI patients accounted for 30.7% in clopidogrel and 32.6% in prasugrel group. Compared with clopidogrel, reduced-dose prasugrel was associated with higher bleeding risk [odds ratio (OR) 1.65, 95% CI 1.10-2.51], similar rates of mortality (OR 1.11, 95% CI 0.89-1.38), and similar risk of stent thrombosis (OR 1.29, 95% CI 0.73-2.30). In subgroup analysis for STEMI patients, reduced-dose prasugrel was associated with numerically higher rate of bleeding than clopidogrel (0.67% vs. 0.47%; OR 1.44, 95% CI 0.76-2.78).[64] Therefore, larger randomized controlled trials are needed in the future to confirm the efficacy and safety of reduced-dose prasugrel in ACS or STEMI patients.

Ticagrelor

Another newer P2Y12 inhibitor, ticagrelor (180 mg loading and 90 mg twice daily dose), is an active drug that does not require hepatic metabolism for activation. The platelet inhibitory ability of ticagrelor is greater and faster than clopidogrel. In addition, ticagrelor binds to P2Y12 inhibitors reversibly, which lead to faster onset after platelet binding and offset after discontinuing the drug.[65] In the PLATO study, ticagrelor was associated with reduced combined risk of CV death, MI, or stroke compared with clopidogrel (HR 0.84, 95% CI 0.77-0.92) in 18,624 ACS patients. However, ticagrelor also increased the rate of non-CABG major bleeding (4.5% vs. 3.8%, p = 0.03).[66] The benefits of ticagrelor over clopidogrel in STEMI subgroup were consistent with those from the overall PLATO results. In STEMI patients receiving primary PCI, ticagrelor also reduced risks of MI, total mortality and definite stent thrombosis without increasing major bleeding risk.[67] In the TREAT study, STEMI patients receiving fibrinolysis were randomized to ticagrelor or clopidogrel with a median of 11.4 hours after fibrinolytic therapy. Ticagrelor was non-inferior to clopidogrel for TIMI major bleeding at 30 days in this study.[68] After 12 months follow-up, ticagrelor was associated with similar ischemic and bleeding events compared with

clopidogrel.[69] The largest real world data comes from SWEDEHEART registry which included 45073 ACS patients in Sweden from 2010 to 2013. In this study, ticagrelor versus clopidogrel was associated with a lower composite ischemic risk (HR 0.85, 95% CI 0.78-0.93) and a higher risk for re-admission with bleeding (HR 1.20, 95% CI 1.04-1.40) which was similar to the results in the PLATO study.[70] However, in Asia, data from small randomized control trials and observational studies comparing ticagrelor with clopidogrel in STEMI or ACS patients demonstrated conflicting results.[71-76] In Taiwan, three observational studies comparing ticagrelor with clopidogrel in ACS patients showed reduced ischemic risk without increasing major bleeding risk in patients receiving ticagrelor.[77-79]

Comparisons between P2Y12 inhibitors

When comparing the efficacy and safety between newer P2Y12 inhibitors (prasugrel/ticagrelor) and clopidogrel in STEMI patients undergoing PCI, a meta-analysis demonstrated that newer P2Y12 inhibitors versus clopidogrel significantly reduced all-cause death, major adverse CV events and stent thrombosis with similar risk in bleeding.[80] Another meta-analysis showed that both prasugrel and ticagrelor were associated with better clinical outcomes than clopidogrel, and prasugrel was even superior to ticagrelor in STEMI patients undergoing primary PCI.[81] In addition, there was a retrospective analysis from Korea using claim data from the Health Insurance Review and Assessment Service with 40706 acute MI patients undergoing PCI between 2010 to 2015 and 35% of the study population were STEMI. In this study, newer P2Y12 inhibitors including prasugrel and ticagrelor both had favorable effect on reducing 30-day mortality.[82] Furthermore, according to the data from KAMIR-NIH registry, treatment with both prasugrel and ticagrelor in ACS patients were shown to improve major adverse CV events-free survival rate compared to clopidogrel. The difference of major adverse CV events rate between prasugrel and ticagrelor in overall population and STEMI subgroups were not significant.[83] For head to head comparison of the efficacy and safety between the two newer P2Y12 inhibitors in ACS patients, a retrospective cohort analysis from claims database showed that patients received ticagrelor had both reduced ischemic and bleeding events compared with patients treated

with prasugrel.[84] However, in a large randomized control trial, the ISAR-REACT 5 study, which recruited 4018 ACS subjects and 41% of whom were STEMI patients, prasugrel was associated with significantly reduced ischemic composite risks including death, MI, or stroke than ticagrelor, and the incidence of bleeding was statistically insignificant between the two groups.[85]

Based on current available evidences, standard-dose ticagrelor and prasugrel should be the preferred P2Y12 inhibitor in STEMI patients. However, if concerns about bleeding prevail over ischemia, it is reasonable to choose clopidogrel rather than newer P2Y12 inhibitors. High bleeding risk features include old age, chronic kidney disease, anemia, low body weight, combination therapy with oral anticoagulant, prior intracranial hemorrhage, or history of previous major bleeding. Furthermore, based on Asians' data, reduced-dose prasugrel (20 mg loading and 3.75 mg daily maintenance dose) may also be considered in STEMI patients undergoing primary PCI in Taiwan. The selection of different P2Y12 inhibitors, different dose regimens, and the trade-off between ischemic and bleeding risk should be individualized to acquire the maximal net clinical benefit for STEMI patients.

Recommendation

- Ticagrelor (180 mg loading dose, 90 mg twice daily), prasugrel (60 mg loading dose, 10 mg daily dose), or clopidogrel (300-600 mg loading dose, 75 mg daily dose) is recommended in STEMI patients undergoing primary PCI unless contraindicated and ticagrelor or prasugrel is preferred to clopidogrel. (COR I, LOE B)
- Clopidogrel rather than ticagrelor or prasugrel may be considered in patients with increased bleeding risk features. (COR IIa, LOE C)
- Reduced dose of prasugrel (20 mg loading dose, 3.75 mg daily dose) may be considered in STEMI patients undergoing PCI based on Asian data. (COR IIa, LOE B)

PCI STRATEGY

Door-to-wire time

D2B time of primary PCI has been regarded as an important metric for STEMI patients because it could influence the clinical outcomes of the patients.[86-88] Previous international guidelines as well as 2012 Taiwan

STEMI guidelines have focused on the importance of D2B time.[2] However, later studies found that the total ischemia time, including the time from symptom onset to STEMI diagnosis and the time from STEMI diagnosis to primary PCI, is a more important determinant of clinical outcomes.[89-91] That is why much more effort now is devoted to shorten the total ischemia time by pre-hospital diagnosis of STEMI and early activation of PCI team. Due to the progress of PCI technique, balloon dilation is not always the first intervention step performed during primary PCI, therefore, the term has further evolved to medical contact-to-device time. Wire crossing the lesion in IRA is always necessary before any intracoronary procedure, therefore, the wire time instead of device time is preferred in our guideline. In Taiwan, if STEMI has already been diagnosed in primary care clinic, non-PCI hospital or in ambulance and transferred for primary PCI, a door-to-wire time ≤ 60 minutes is suggested in the transferred PCI available hospitals. In fresh cases that need time to diagnose STEMI, a door-to-wire time ≤ 90 minutes is suggested in PCI available hospitals.

Recommendation

- For patients with already diagnosed STEMI that are transferred for primary PCI, a door-to-wire time ≤ 60 minutes in PCI available hospitals is recommended. (COR I, LOE C)
- In fresh cases that need time to diagnose STEMI, a door-to-wire time ≤ 90 minutes in PCI available hospitals is recommended. (COR I, LOE B)

PCI procedures

The RIVAL trial was a large scale clinical trial that randomly allocated 7021 ACS patients including 1958 STEMI patients to radial or femoral artery access during PCI. The composite primary outcome of death, MI, stroke or non-CABG major bleeding at 30 days occurred significantly fewer in the radial group compared with the femoral group in patients with STEMI (HR 0.60, 95% CI 0.38-0.94) and in high volume radial centers (HR 0.49, 95% CI 0.28-0.87).[92] The radial procedural volume was important and independently associated with the primary outcome.[93] The MATRIX trial included a total of 8404 ACS patients (4008 STEMI) undergoing PCI and randomized to radial or femoral access. The 30-day co-primary outcomes were major adverse CV events (MACE),

defined as all-cause mortality, MI and stroke. The net adverse clinical events were defined as MACE or non-CABG major bleeding. The radial access group was associated with reduced MACE [risk ratio (RR) 0.85, 95% CI 0.74-0.99] and net adverse clinical events (RR 0.83, 95% CI 0.73-0.96). The difference was mainly driven by fewer non-CABG major bleeding and reduction of all-cause death.[94] Therefore, the radial access has become the favorable choice during primary PCI and is especially recommended to be performed by an experienced operator at high volume center.

The EXAMINATION study randomly assigned 1504 patients with STEMI to receive everolimus-eluting stent (EES) or bare-metal stent (BMS). The results showed both rates of target lesion revascularization and stent thrombosis were reduced in recipients of EES at 1 year.[95] Similarly, the COMFORTABLE AMI trial randomly assigned 1161 STEMI patients to receive biolimus-eluting stents or BMS in primary PCI. The group of biolimus-eluting stents with a biodegradable polymer was associated with reduced composite of cardiac death, target vessel-related reinfarction, and ischemia-driven target-lesion revascularization in STEMI patients at 1 year.[96] Based on these evidences, new generation drug-eluting stent (DES) is recommended during primary PCI for STEMI. The TASTE trial randomly assigned 7244 STEMI patients undergoing PCI to manual thrombus aspiration followed by PCI or to PCI only. The results revealed routine thrombus aspiration before PCI as compared with PCI alone did not reduce 30-day and 1-year mortality. In addition, this strategy did not reduce total mortality or the composite of death from any cause, rehospitalization for MI, or stent thrombosis up to 1 year.[97,98] A later and larger scale TOTAL study with 10732 STEMI patients also reported routine manual thrombectomy did not reduce the risk of CV death, recurrent MI, cardiogenic shock, or class IV heart failure within 180 days. In addition, this strategy in TOTAL trial was associated with an increased rate of stroke within 30 days, which was not observed in TASTE trial.[99-101] In summary, with compared to PCI alone, recent clinical trials have not shown any clinical benefit with routine thrombectomy during primary PCI.

Recommendation

- Radial access is recommended over femoral access in

experienced operators and high volume centers for primary PCI. (COR I, LOE A)

- New generation DESs are recommended for primary PCI. (COR I, LOE A)
- Thrombus aspiration during primary PCI is an optional but not a routine procedure during primary PCI. (COR I, LOE A)

Complete revascularization

About 40% of patients with acute MI carried multiple complex coronary lesions in multiple coronary arteries on angiography and these patients had poorer left ventricular function and increased risk for recurrent ischemia.[102] Whether to completely revascularize these non-culprit lesions or only treat culprit lesion during the index procedure of primary PCI is a common dilemma.[103,104] In addition, the optimal timing of complete revascularization also remains uncertain. Previous randomized trials have compared routine non-culprit lesion PCI with optimal medical therapy alone in patients with multivessel disease (MVD) who underwent primary PCI for STEMI, regardless of whether revascularization was performed during index or staged procedure. Although the results almost consistently revealed significant reduction in repeat revascularizations in the group of complete revascularization, none of which were powered for the hard end points of death or MI.[105-109] In a meta-analysis, compared to culprit lesion-only PCI, complete revascularization significantly reduced the combined end points of death or MI (OR 0.71, 95% CI 0.52-0.96). In addition, the benefit of routine non-culprit lesion PCI was only observed among patients who performed during the index primary PCI but not staged procedure.[110] Recently, the COMPLETE trial randomized 4041 STEMI patients with MVD but without cardiogenic shock who had undergone successful culprit-lesion primary PCI to a strategy of either complete revascularization with PCI of angiographically significant non-culprit lesions or no further revascularization. At a median follow-up of 3 years, the first co-primary outcome of CV death or MI was significantly lower in the complete-revascularization group than culprit-lesion-only PCI group (HR 0.74, 95% CI 0.60-0.91). In this study, all non-culprit lesion PCIs were staged procedures either during the index hospitalization or within 45 days after discharge. This study was statistically powered to concluded that routine staged

complete revascularization was superior to culprit lesion only PCI in reducing the risk of CV death, new MI, or ischemia driven revascularization in STEMI patients with MVD and without cardiogenic shock.[111]

In STEMI patients with MVD and cardiogenic shock (CS), the CULPRIT-SHOCK trial randomized 706 patients to either PCI of the culprit lesion only or multivessel PCI. At 30 days, the end points of death or renal replacement therapy were significantly lower in the culprit lesion only group and these benefits were maintained at 1 year.[112,113] In addition, a large-scale observational study also showed that culprit lesion only PCI in STEMI patients with CS had lower mortality rate than multivessel PCI at 30 days and at 1 year.[114] Figure 5 summarizes the current recommendations for PCI strategy for STEMI in Taiwan.

Recommendation

- In hemodynamically stable STEMI patients with MVD, immediate or staged PCI (< 45 days) for complete revascularization is recommended. (COR I, LOE A)
- In STEMI patients with CS and MVD, routine non-culprit lesion revascularization during primary PCI is not recommended. (COR III, LOE B)

CARDIOGENIC SHOCK

Definition and classification

Although there were some variations of the definition, CS complicating acute MI is generally defined as systolic blood pressure (BP) < 90 mmHg for $\geq$ 30 minutes with end-organ hypoperfusion $\pm$ hemodynamic criteria (cardiac index $\leq$ 2.2 L/min/m^2 and wedge pressure $\geq$ 15 mmHg) based on largest randomized controlled trials.[112,115,116] Recently, the Society of Cardiovascular Angiography and Interventions unified CS definition and recommended a classification system with 5 stages: A: at risk for CS development (e.g., anterior wall MI), B: beginning or preshock (clinical evidence of relative hypotension or tachycardia without hypoperfusion), C: classical CS (hypoperfusion requiring pharmacological or mechanical intervention), D: doom (worse with failing to respond to initial interventions), and E: extremis [cardiac arrest with ongoing CPR and/or extracorporeal membrane oxygenation (ECMO)].[117] The classification system not only

PCI strategy for STEMI
Radial access in experienced operators
New generation DES
Avoid routine thrombus aspiration

| Multivessel disease | Single vessel disease |

| **Stable hemodynamic status** Immediate or staged complete revascularization | **Cardiogenic shock** Avoid routine non-culprit lesion revascularization in index procedure | **Finish procedure after successful IRA revascularization** |

Figure 5. *Recommended PCI strategy for STEMI in Taiwan. DES, drug-eluting stent; IRA, infarct-related artery; PCI, percutaneous coronary intervention; STEMI, ST-segment elevation myocardial infarction.*

makes different CS trials more comparable but also emphasizes the effectiveness of early intervention on the phase of pre-shock or early shock.[118,119]

Pathophysiology

The incidence of CS with acute MI ranges from 3% to 13%.[120,121] Ventricular myocardial dysfunction following acute MI accounts for the majority of CS, comprising around 80% and 7% for left and right ventricular failure, respectively. The remaining 13% of CS victims result from mechanical complications, including acute mitral regurgitation (~7%), ventricular septal defect (~4%) and free wall rupture (~2%).[122] Impaired myocardial systolic and diastolic function subsequent to acute MI induce hypoperfusion and lung congestion leading to tissue ischemia and hypoxia.[123] It also chemically or biologically elicits a serial release of inflammatory cytokines or inducible nitric oxide synthase resulting in vasodilation which further decreases systemic and coronary perfusions and aggravates pre-existing pumping impairment.[124] The catastrophic vicious cycle results in 40-50% mortality rate of CS even in the era of early revascularization and mechanical circulatory support (MCS).[124,125]

Management

Management should be initiated at pre-shock phase when hypotension appears as the first sign of CS. Echocardiography should be performed immediately to exclude mechanical complications of acute MI as the po-

tential causes of CS. Intra-aortic balloon pumping (IABP) can be considered as a strategy to unload left ventricle and increase coronary perfusion if there is unstable hemodynamics due to mechanical complications. However, IABP should not be performed routinely in patients with CS complicating acute MI.[116] Emergent coronary angiography is strongly recommended and revascularization strategy should be determined after heart team evaluation. PCI to open the occluded culprit vessel can be performed but routine non-culprit lesions revascularization during the initial PCI is not recommended.[112,113] In patients with CS after initial treatment, complete revascularization during the index hospitalization maybe beneficial.[126]

Patients with CS should be treated with fluids, vasopressors, and inotropes to prevent or rescue multiple organ dysfunction syndrome (MODS).[127] If hemodynamic instability remains after fluid resuscitation with saline or Ringer's lactate > 200 mL in 15-30 minutes, pharmacological circulatory support with vasopressor (e.g., norepinephrine) and/or ventricular support with inodilator (e.g., dobutamine or levosimendan) should be considered.[128] The patients are closely monitored in intensive care units. Pulmonary artery catheter for diagnostic evaluation and therapeutic guidance may be considered if necessary.[129] Ultrafiltration may be considered for organ decongestion in acute cardiorenal syndrome with fluid overload and poor response to forceful diuretic therapy.[130] Although those resuscitated from cardiac ar-

rest or lethal arrhythmia are generally treated with hypothermia for neuroprotection, the effects of therapeutic hypothermia on hemodynamic or clinical outcomes in CS are still controversial.[131,132] For those with refractory shock or deteriorating organ dysfunctions, growing evidences have shown appropriate use of MCS could reduce catecholamine dosage, improve hemodynamics, and serve as bridge to recovery, destination, transplantation, or family's decision.[133-135] Nevertheless, there are still limited data from randomized clinical trials on when and how to use MCS devices properly in CS during acute MI. The survival outcome of CS with acute MI might be affected by different study designs, indications, and limitations of the MSC devices.[136]

Several reviews have concluded that a successful management of CS with acute MI depends on the following important components including early reperfusion therapy, early hemodynamic support, adequate left ventricular unload, and good quality of post-MI care.[137-139] A meta-analysis of 1,866 CS patients supported with ECMO has shown the MCS-associated complication rates were up to 50%, 40%, 30% and 15% for acute kidney injury, major bleeding, infection, and limb ischemia/neurologic deficit, respectively, implicating ECMO can result in survival to discharge but may be as-

sociated with considerable morbidity.[140] Prevention or prompt management of MCS-associated complications probably increases the chance of survival of CS. Although recent systematic review and meta-analysis have found MODS following CS could be prevented by short-term MCS if it is used at optimal timing at stages B or C of CS, with sufficient blood flow support with 2-7 L/min and without MCS-related complications, the overall survival rate was similar compared with control group.[137,141] Therefore, routine use of MCS in unselected patients with CS complicating acute MI is still not suggested. The MCS should be applied after heart team evaluation and according to operator's experience and patient's conditions. Figure 6 summarizes the recommendations of evaluation and management of CS complicating acute MI.

Recommendation
- Early heart team approach is recommended for treatment of mechanical complications as well as revascularization strategy in acute MI with CS. (COR I, LOE C)
- Emergency coronary angiography is recommended for acute MI patients with CS, followed by PCI of culprit vessel if coronary lesion is suitable, otherwise, emergency CABG is an alternative. (COR I, LOE B)
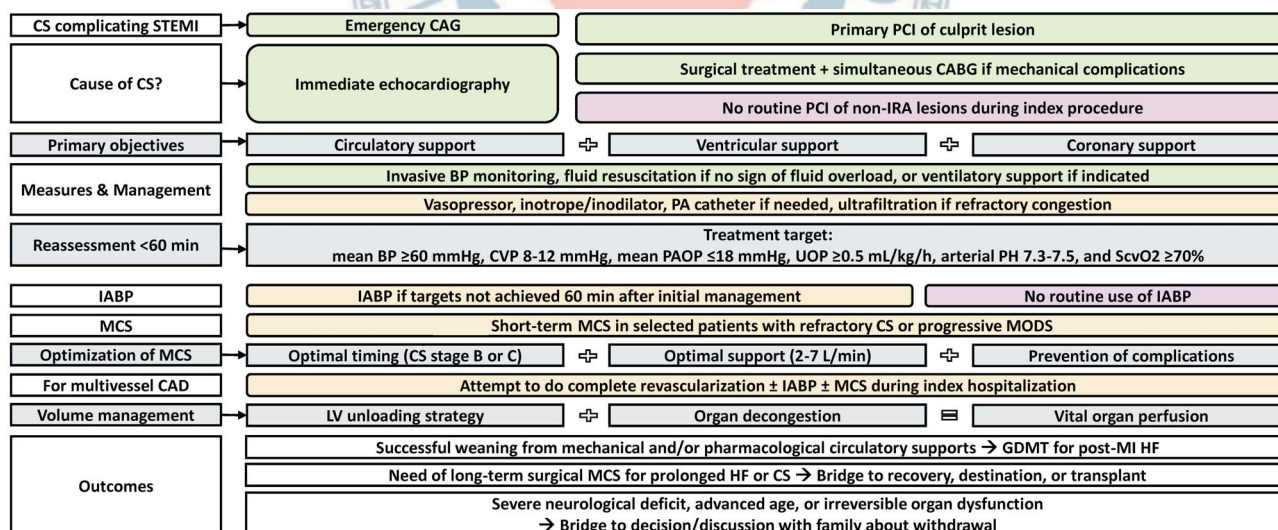
Figure 6. *Evidence-based algorithm for evaluation and management of cardiogenic shock complicating AMI. The recommendations were mainly based on the latest reviews and international guidelines. Class I, II, III recommendations were depicted with light green, light yellow, and pink colors, respectively. AMI, acute myocardial infarction; BP, blood pressure; CABG, coronary artery bypass grafting surgery; CAD, coronary artery disease; CAG, coronary angiography; CS, cardiogenic shock; CVP, central venous pressure; GDMT, guideline-directed medical therapy; HF, heart failure; IABP, intra-aortic balloon pumping; IRA, infarct-related artery; LV, left ventricular; MCS, mechanical circulatory support; MODS, multiple organ dysfunction syndrome; PAOP, pulmonary artery obstructive pressure; PCI, percutaneous coronary intervention; ScvO2, central venous oxygen saturation; STEMI, ST-segment elevation myocardial infarction; UOP, urine output.*

- For MI patients with CS and MVD, attempt of complete revascularization during index hospitalization is reasonable. (COR IIa, LOE B)
- Short-term mechanical support device (e.g., percutaneous cardiopulmonary support, ECMO, or ventricular assist device) with/without IABP may be considered as a rescue therapy in patients with refractory CS. (COR IIb, LOE C)

POST-MI MEDICAL THERAPIES

Aggressive control of risk factors with evidence-based medical therapies substantially improved prognosis of STEMI. Recent report from the TSOC ACS-Diabetes Mellitus Registry revealed a higher adherence rate of guideline-directed medical therapies could reduce about 40% CV events.[142] Repetitive and careful assessment of treatment goal achievement and medical adherence is crucial from acute to chronic stage of MI.[143] Additional efforts to enhance patients' drug adherence, such as using single-pill combination or participation of educational programs, are necessary.[144,145]

Hypertension

The Taiwan STEMI and hypertension guidelines both recommend a BP goal < 130/80 mmHg in STEMI patients.[2,146] Although more intensive treatment with systolic BP < 120 mmHg appeared to benefit high-risk individuals in the SPRINT study,[147] implementing this result to all STEMI patients in Taiwan might not be practical because of the method of BP measurement used in the SPRINT study and the concern of J-curve phenomenon of BP.[147-149] Effective medical regimens, including long-acting beta-blocker, ACEI/ARB and calcium channel blocker (CCB) are recommended to optimize BP control.[146] Beta-blocker, ACEI/ARB and/or mineralocorticoid receptor antagonist (MRA) are especially beneficial in STEMI patients with heart failure or depressed left ventricular ejection fraction.[146] MRA should not be used in those with creatinine clearance < 30 mL/min/1.73 m^2 or potassium level > 5 mEq/L. Routine administration of beta-blocker, ACEI or ARB in all STEMI patients was supported by international guidelines.[150,151] But baseline heart rate, comorbidity and beta receptor selectivity are likely to influence the efficacy of beta-blocker.[152-155]

Recommendation

- It is recommended to control BP < 130/80 mmHg in STEMI patients by long-acting beta-blocker, ACEI/ARB and/or CCB. (COR I, LOE B)
- Beta-blocker, ACEI/ARB and/or mineralocorticoid receptor antagonist are recommended for STEMI patients with heart failure and reduced ejection fraction if there is no contraindication. (COR I, LOE B)
- Routine use of ACEI/ARB for all STEMI patients is reasonable if no contraindication. (COR IIa, LOE A)
- Routine use of beta-blocker for all STEMI patients may be beneficial if no contraindication. (COR IIa, LOE B)

Diabetes

A treatment goal of HbA1c < 7% is recommended in patients with STEMI. However, clinicians can modify the HbA1c target based on patient's general condition and risk of hypoglycemia. A less stringent HbA1c target < 8% is reasonable if patients had hypoglycemic history, limited life expectancy, advanced micro- or macrovascular complications and extensive comorbid conditions. In contrast, individuals with least hypoglycemic risk are also eligible to have more stringent target of < 6.5%.[156] Metformin remains the usual first-line anti-diabetic agent.[157] Thiazolidinedione (TZD), sodium/glucose co-transporter 2 inhibitor (SGLT-2i) or glucagon-like peptide-1 receptor agonist (GLP-1 RA) are recommended as second-line therapies in coronary artery disease since favorable CV outcomes had been observed in relevant clinical studies.[157] Concerning the increased risk of development of post-MI heart failure, TZD is not generally recommended to all STEMI patients as a second-line agent and should be administered with caution. In patients with STEMI and heart failure, SGLT-2i can be considered as the first line therapy because the drug has been proved to improve the prognosis of heart failure with reduced ejection fraction in recent clinical trial.[158]

Recommendation

- It is recommended to control HbA1c < 7% in STEMI patients. The target of HbA1c could be individualized according to patient's condition (< 6.5% to < 8%). (COR I, LOE B)
- Metformin is recommended as the first-line therapy. (COR I, LOE B)
- The priority for add-on therapy includes SGLT-2i and

GLP-1 RA. (COR IIa, LOE A)

- SGLT-2i is recommended for STEMI patients with heart failure and reduced ejection fraction. (COR I, LOE B)

Hypercholesterolemia

Low-density lipoprotein cholesterol (LDL-C) remains the primary target for screening, diagnosis and management of dyslipidemia.[159,160] Current Taiwan lipid guidelines for high risk patients recommend a LDL-C goal < 70 mg/dl for patients with acute MI and < 55 mg/dl for acute MI in diabetic patients.[160] The major evidence-based lipid-lowering medications for ACS were limited to statin and ezetimibe in the past. Previous meta-analysis demonstrated that reduction of LDL-C with statin or nonstatin therapy was associated with similar risk reduction of major vascular events.[161] Due to its potency and scientific evidences, statin is the first-line therapy. In Taiwan, titration to high intensity statin (atorvastatin 40 mg/day or rosuvastatin 20 mg/day) or use statin plus ezetimibe combination therapy is suggested to treat to LDL-C goal in patients with acute MI.[160] A number of patients may develop adverse effects after taking high or any dose of statins.[162] This population has suboptimal LDL-C control and increased risk of CV events.[163] Recently published randomized controlled trials, FOURIER and ODYSSEY OUTCOMES studies, showed that add-on

proprotein convertase subtilisin/kexin type 9 inhibitors (PCSK9i) to statin therapy could further reduce 50-60% of LDL-C and obtain a 15% relative risk reduction of CV events in patients with stable ASCVD and recent ACS.[164,165] In the ODYSSEY OUTCOMES trial with recent ACS, the preset LDL-C target of PCSK9i group was 25 to 50 mg/dL and the mean achieved LDL-C level at 48-month follow-up was 53 mg/dL.[165] Intensification of LDL-C control by these potent agents could help STEMI patients to attain the current treatment LDL-C goal much more easier. However, due to the drugs are still very expensive, PCSK9i is usually suggested as the last resort after using maximally tolerated statin and ezetimibe.[166,167] Figure 7 summarizes the recommendations of the treatment target and drug of choice for long term post-MI medical therapies.

Recommendation

- It is recommended to control LDL-C < 70 mg/dL in STEMI patients. (COR I, LOE A)
- A lower target of LDL-C < 55 mg/dL can be considered in STEMI patients. (COR IIa, LOE B)
- LDL-C control should be intensified by statin plus nonstatin therapies, including ezetimibe and/or PCSK9i with full consideration of clinical efficacy, patient's preference as well as cost-effectiveness. (COR I, LOE A)
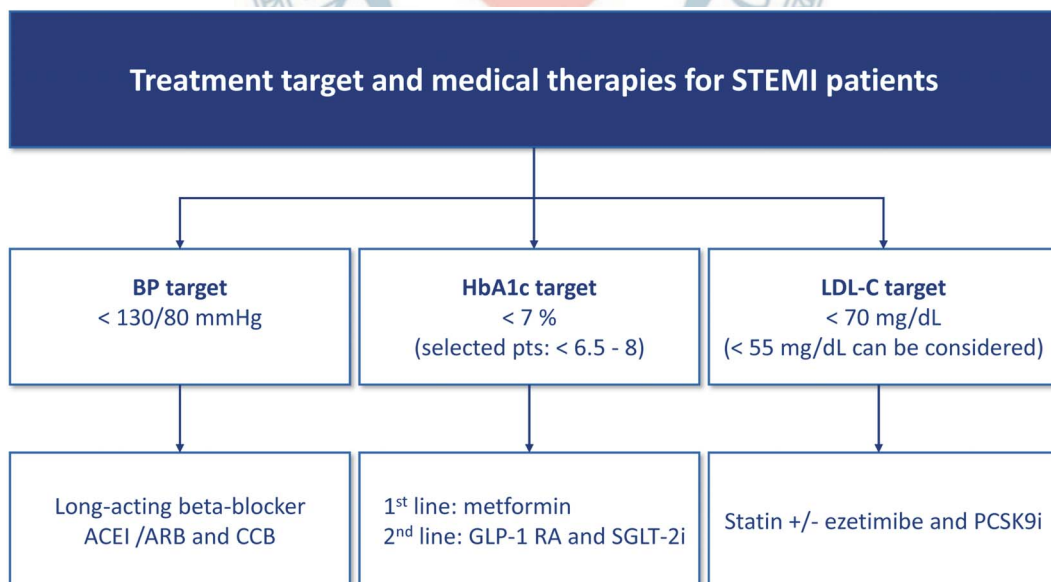
Figure 7. *Recommended treatment targets and medical therapies for STEMI patients. ACEI, angiotensin converting enzyme inhibitor; ARB, angiotensin receptor blocker; BP, blood pressure; CCB, calcium channel blocker; GLP-1 RA, glucagon-like peptide-1 receptor agonist; LDL-C, low-density lipoprotein cholesterol; PCSK9i, proprotein convertase subtilisin/kexin type 9 inhibitor; SGLT-2i, sodium/glucose co-transporter 2 inhibitor.*

QUALITY CARE OF STEMI

To reduce the gap between clinical practice and guideline recommendations in STEMI care, a quality evaluation system should be established.[168,169] The quality care of STEMI depends on regularly tracking time intervals of reperfusion therapy, monitoring measurable quality indicators and timely feedback to network stake-

holders. The major purpose is for continuous quality improvement of STEMI. The quality indicators, which can measure and compare the quality of health service provider, are divided into three dimensions, including structure, process and outcome indicators (Table 1).[170,171] The pre-hospital and hospital-based treatment delays or in-hospital medications can be monitored by routine audit meeting and updated STEMI management protocols. If the

Table 1. STEMI quality indicators

Dimension	Process	Setting	Indicators
Structure indicator	Diagnosis	Pre-hospital	• Ambulance equipped with telemetry pre-hospital ECG recorders • Ambulance equipped with automated external defibrillators • Ambulance equipped with auto CPR machines • City-based network system to record key factors and time to reperfusion
	Treatment	Hospital	• Single call to activate STEMI team • 24-hour service of catheterization laboratory
Process indicator	Diagnosis	Pre-hospital	• EMTs perform telemetry pre-hospital ECG for patients with typical symptoms of acute MI
	Diagnosis	Hospital	• Door to ECG time • Evaluation of LVEF before discharge
	Treatment	Emergent department	• Aspirin at arrival • P2Y12 receptor inhibitor at arrival
	Treatment	Catheterization laboratory	• Symptom onset to door time • Door to wire time
	Treatment	In-hospital	• Aspirin prescribed at discharge • P2Y12 receptor inhibitor prescribed at discharge • Beta blocker prescribed at discharge • Statin prescribed at discharge • ACEI or ARB or ARNI prescribed at discharge for LV systolic dysfunction (EF ≤ 40%) • Aldosterone antagonist prescribed at discharge for LV systolic dysfunction (EF ≤ 40%) • Cardiac rehabilitation referral from an inpatient setting • Immediate angiography for resuscitated OHCA in STEMI patients • Therapeutic hypothermia for comatose STEMI patients with OHCA • Smoking cessation advice or counseling before discharge
	Quality	Follow up	• Participation in ≥ 1 national STEMI accreditation system and/or other STEMI certification system
Outcome indicator	Quality	In-hospital	• In-hospital mortality
	Quality	Follow up	• 30-day mortality • 30-day readmission rate • 30-day re-infarction rate • 1-year mortality • 1-year readmission rate • 1-year re-infarction rate

ACEI, angiotensin converting enzyme inhibitor; ARB, angiotensin receptor blocker; ARNI, angiotensin receptor-neprilysin inhibitor; CPR, cardiopulmonary resuscitation; ECG, electrocardiography; EF, ejection fraction; EMT, emergency medical technicians; LV, left ventricle; MI, myocardial infarction; OHCA, out-of-hospital cardiac arrest; PCI, percutaneous coronary intervention; STEMI, ST-segment elevation myocardial infarction.

targets of quality indicators are not met, quality improvement program should be initiated to improve performance of the system and further maintain quality targets.

In Taiwan, a national STEMI accreditation system was developed by government to monitor the care quality of STEMI in hospitals that performs primary PCI every 3 years. The monitored items include door to ECG time, DAPT use, door to wire time in primary PCI, and other standard operation procedures of STEMI care. The hospitals with 24-hour PCI capability have to reach the following targets: (1) more than 80% of STEMI patients have door to ECG time < 10 minutes, (2) more than 80% of STEMI patients received DAPT, (3) more than 75% of STEMI patients have door to wire time in primary PCI < 90 minutes for those initially presented with ischemic symptoms and more than 70% of STEMI patients have door to wire time in primary PCI < 60 minutes for those diagnosed STEMI referred for primary PCI. The national STEMI accreditation system established the basic requirements for STEMI quality care in Taiwan.[27] The Joint Commission of Taiwan is a non-government organization with the missions of hospital accreditation, certification and healthcare quality inspection. The Joint Commission of Taiwan built up a Taiwan AMI Certification Hospitals system to help the hospitals to pursue a better quality of care for AMI. Taiwan AMI Certification Hospitals system has 3 categories and 27 detailed items. The three categories include STEMI teamwork and management, STEMI patients and family care and STEMI quality improvement. The ultimate purpose is to further improve the comprehensive care of AMI.

Recommendation

- Participation of national STEMI accreditation system and other certification system are recommended to audit the time delay and critical quality targets achievement for STEMI. (COR I, LOE C)
- STEMI quality control system, including monitoring quality indicators and regular quality care meetings, should be established in hospitals. (COR I, LOE C)

CONFLICTS OF INTEREST

REFERENCES

1. Lee CH, Fang CC, Tsai LM, et al. Patterns of acute myocardial infarction in Taiwan from 2009 to 2015. *Am J Cardiol* 2018;122: 1996-2004.
2. Li YH, Yeh HI, Tsai CT, et al. 2012 Guidelines of the Taiwan Society of Cardiology (TSOC) for the management of ST-segment elevation myocardial infarction. *Acta Cardiol Sin* 2012;28:63-89.
3. Li YH, Wang YC, Wang YC, et al. 2018 Guidelines of the Taiwan Society of Cardiology, Taiwan Society of Emergency Medicine and Taiwan Society of Cardiovascular Interventions for the management of non ST-segment elevation acute coronary syndrome. *J Formos Med Assoc* 2018;117:766-90.
4. Lee CH, Cheng CL, Kao Yang YH, et al. Trends in the incidence and management of acute myocardial infarction from 1999 to 2008: get with the guidelines performance measures in Taiwan. *J Am Heart Assoc* 2014;3:pii: e001066.
5. Yin WH, Lu TH, Chen KC, et al. The temporal trends of incidence, treatment, and in-hospital mortality of acute myocardial infarction over 15 years in a Taiwanese population. *Int J Cardiol* 2016; 209:103-13.
6. Li YH, Chiu YW, Cheng JJ, et al. Changing practice pattern of acute coronary syndromes in Taiwan from 2008 to 2015. *Acta Cardiol Sin* 2019;35:1-10.
7. Lee PT, Chao TH, Huang YL, et al. Analysis of the clinical characteristics, management, and causes of death in patients with ST-segment elevation myocardial infarction treated with primary percutaneous coronary intervention from 2005 to 2014. *Int Heart J* 2016;57:541-6.
8. Qian F, Ling FS, Deedwania P, et al. Care and outcomes of Asian-American acute myocardial infarction patients: findings from the American Heart Association Get With The Guidelines-Coronary Artery Disease program. *Circ Cardiovasc Qual Outcomes* 2012;5:126-33.
9. Thygesen K, Alpert JS, Jaffe AS, et al. Fourth universal definition of myocardial infarction (2018). *Eur Heart J* 2019;40:237-69.
10. Chao CC, Chen YC, Shih CM, et al. Smartphone transmission of electrocardiography images to reduce time of cardiac catheterization laboratory activation. *J Chin Med Assoc* 2018;81:505-10.
11. Chen KC, Yen DH, Chen CD, et al. Effect of emergency department in-hospital tele-electrocardiographic triage and interventional cardiologist activation of the infarct team on door-to-balloon times in ST-segment-elevation acute myocardial infarction. *Am J Cardiol* 2011;107:1430-5.
12. Lee CC, Huang SS, Yeo YH, et al. High-sensitivity-cardiac troponin for accelerated diagnosis of acute myocardial infarction: a systematic review and meta-analysis. *Am J Emerg Med* 2019; pii: S0735-6757(19)30774-0.
13. Tan WCJ, Inoue K, AbdelWareth L, et al. The Asia-Pacific Society of Cardiology (APSC) expert committee consensus recommendations for assessment of suspected acute coronary syndrome

using high-sensitivity cardiac troponin T in the emergency department. *Circ J* 2020;84:136-43.

14. Levis JT. ECG diagnosis: isolated posterior wall myocardial infarction. *Perm J* 2015;19:e143-4.

15. Briosa E Gala A, Rawlins J. Posterior-wall myocardial infarction. *N Engl J Med* 2019;381:e32.

16. Yamaji H, Iwasaki K, Kusachi S, et al. Prediction of acute left main coronary artery obstruction by 12-lead electrocardiography. ST segment elevation in lead aVR with less ST segment elevation in lead V(1). *J Am Coll Cardiol* 2001;38:1348-54.

17. Sen F, Ozeke O, Kirbas O, et al. Classical electrocardiographic clues for left main coronary artery disease. *Indian Heart J* 2016; 68 Suppl 2:S226-7.

18. Sgarbossa EB, Pinski SL, Barbagelata A, et al. Electrocardiographic diagnosis of evolving acute myocardial infarction in the presence of left bundle-branch block. GUSTO-1 (Global Utilization of Streptokinase and Tissue Plasminogen Activator for Occluded Coronary Arteries) Investigators. *N Engl J Med* 1996; 334:481-7.

19. McNamara RL, Wang Y, Herrin J, et al. Effect of door-to-balloon time on mortality in patients with ST-segment elevation myocardial infarction. *J Am Coll Cardiol* 2006;47:2180-6.

20. Kim HS, Lee H, Kim K, et al. The general public's awareness of early symptoms of and emergency responses to acute myocardial infarction and related factors in South Korea: a national public telephone survey. *J Epidemiol* 2016;26:233-41.

21. Finn JC, Bett JH, Shilton TR, et al. Patient delay in responding to symptoms of possible heart attack: can we reduce time to care? *Med J Aust* 2007;187:293-8.

22. Ryan D, Craig AM, Turner L, Verbeek PR. Clinical events and treatment in prehospital patients with ST-segment elevation myocardial infarction. *Prehosp Emerg Care* 2013;17:181-6.

23. Tanguay A, Brassard E, Lebon J, et al. Effectiveness of a prehospital wireless 12-lead electrocardiogram and cardiac catheterization laboratory activation for ST-elevation myocardial infarction. *Am J Cardiol* 2017;119:553-9.

24. Mercuri M, Welsford M, Schwalm JD, et al. Providing optimal regional care for ST-segment elevation myocardial infarction: a prospective cohort study of patients in the Hamilton Niagara Haldimand Brant Local Health Integration Network. *CMAJ Open* 2015;3:E1-7.

25. Ross G, Alsayed T, Turner L, et al. Assessment of the safety and effectiveness of emergency department STEMI bypass by defibrillation-only emergency medical technicians/primary care paramedics. *Prehosp Emerg Care* 2015;19:191-201.

26. Boden WE, Eagle K, Granger CB. Reperfusion strategies in acute ST-segment elevation myocardial infarction: a comprehensive review of contemporary management options. *J Am Coll Cardiol* 2007;50:917-29.

27. Wu CK, Juang JMJ, Chiang JY, et al. The Taiwan Heart Registries: its influence on cardiovascular patient care. *J Am Coll Cardiol* 2018;71:1273-83.

28. Chou LP, Zhao P, Kao C, et al. Women were noninferior to men in

cardiovascular outcomes among patients with ST-segment elevation myocardial infarction treated with primary percutaneous coronary intervention from Taiwan acute coronary syndrome full-spectrum registry. *Medicine (Baltimore)* 2018;97: e12998.

29. Holmes DR Jr, Bell MR, Gersh BJ, et al. Systems of care to improve timeliness of reperfusion therapy for ST-segment elevation myocardial infarction during off hours: the Mayo Clinic STEMI protocol. *JACC Cardiovasc Interv* 2008;1:88-96.

30. Fosbol EL, Granger CB, Jollis JG, et al. The impact of a statewide pre-hospital STEMI strategy to bypass hospitals without percutaneous coronary intervention capability on treatment times. *Circulation* 2013;127:604-12.

31. Le May MR, So DY, Dionne R, et al. A citywide protocol for primary PCI in ST-segment elevation myocardial infarction. *N Engl J Med* 2008;358:231-40.

32. Cantor WJ, Hoogeveen P, Robert A, et al. Prehospital diagnosis and triage of ST-elevation myocardial infarction by paramedics without advanced care training. *Am Heart J* 2012;164:201-6.

33. Kuo FY, Huang WC, Chiou KR, et al. The effect of failure mode and effect analysis on reducing percutaneous coronary intervention hospital door-to-balloon time and mortality in ST segment elevation myocardial infarction. *BMJ Qual Saf* 2013;22: 626-38.

34. Wong GC, Welsford M, Ainsworth C, et al. 2019 Canadian Cardiovascular Society/Canadian Association of Interventional Cardiology Guidelines on the acute management of ST-elevation myocardial infarction: focused update on regionalization and reperfusion. *Can J Cardiol* 2019;35:107-32.

35. Koul S, Smith JG, Scherstén F, et al. Effect of upstream clopidogrel treatment in patients with ST-segment elevation myocardial infarction undergoing primary percutaneous coronary intervention. *Eur Heart J* 2011;32:2989-97.

36. Dörler J, Edlinger M, Alber HF, et al. Clopidogrel pre-treatment is associated with reduced in-hospital mortality in primary percutaneous coronary intervention for acute ST-elevation myocardial infarction. *Eur Heart J* 2011;32:2954-61.

37. Zeymer U, Arntz HR, Mark B, et al. Efficacy and safety of a high loading dose of clopidogrel administered prehospitally to improve primary percutaneous coronary intervention in acute myocardial infarction: the randomized CIPAMI trial. *Clin Res Cardiol* 2012;101:305-12.

38. Montalescot G, van't Hof AW, Lapostolle F, et al. Prehospital ticagrelor in ST-segment elevation myocardial infarction. *N Engl J Med* 2014;371:1016-27.

39. Hypothermia after Cardiac Arrest Study Group. Mild therapeutic hypothermia to improve the neurologic outcome after cardiac arrest. *N Engl J Med* 2002;346:549-56.

40. Bernard SA, Gray TW, Buist MD, et al. Treatment of comatose survivors of out-of-hospital cardiac arrest with induced hypothermia. *N Engl J Med* 2002;346:557-63.

41. Mooney MR, Unger BT, Boland LL, et al. Therapeutic hypothermia after out-of-hospital cardiac arrest: evaluation of a regional

system to increase access to cooling. *Circulation* 2011;124:206-14.

42. Kim F, Nichol G, Maynard C, et al. Effect of prehospital induction of mild hypothermia on survival and neurological status among adults with cardiac arrest: a randomized clinical trial. *JAMA* 2014;311:45-52.

43. Yajnik V, Gomez H. Prehospital induction of mild hypothermia with cold normal saline for cardiac arrest: more harm than good? *Crit Care* 2014;18:559.

44. Chen ZM, Jiang LX, Chen YP, et al. Addition of clopidogrel to aspirin in 45,852 patients with acute myocardial infarction: randomised placebo controlled trial. *Lancet* 2005;366:1607-21.

45. Sabatine MS, Cannon CP, Gibson CM, et al. Addition of clopidogrel to aspirin and fibrinolytic therapy for myocardial infarction with ST-segment elevation. *N Engl J Med* 2005;352:1179-89.

46. Cheng CI, Chen CP, Kuan PL, et al. The causes and outcomes of inadequate implementation of existing guidelines for antiplatelet treatment in patients with acute coronary syndrome: the experience from Taiwan Acute Coronary Syndrome Descriptive Registry (T-ACCORD Registry). *Clin Cardiol* 2010;33:E40-8.

47. Chiang FT, Shyu KG, Wu CJ, et al. Predictors of 1-year outcomes in the Taiwan Acute Coronary Syndrome Full Spectrum Registry. *J Formos Med Assoc* 2014;113:794-802.

48. Chen SC, Hsiao FY, Lee CM, et al. Duration of dual antiplatelet therapy following percutaneous coronary intervention on rehospitalization for acute coronary syndrome. *BMC Cardiovasc Disord* 2014;14:21.

49. Li YH, Chiu YW, Cheng JJ, et al. Duration of clopidogrel-based dual antiplatelet therapy and clinical outcomes in patients with acute coronary syndrome undergoing percutaneous coronary intervention - a real-world observation in Taiwan from 2012 to 2015. *Circ J* 2019;83:1317-23.

50. Gurbel PA, Bliden KP, Zaman KA, et al. Clopidogrel loading with eptifibatide to arrest the reactivity of platelets: results of the Clopidogrel Loading With Eptifibatide to Arrest the Reactivity of Platelets (CLEAR PLATELETS) study. *Circulation* 2005;111:1153-9.

51. von Beckerath N, Taubert D, Pogatsa-Murray G, et al. Absorption, metabolization, and antiplatelet effects of 300-, 600-, and 900-mg loading doses of clopidogrel: results of the ISAR-CHOICE (Intracoronary Stenting and Antithrombotic Regimen: Choose Between 3 High Oral Doses for Immediate Clopidogrel Effect) trial. *Circulation* 2005;112:2946-50.

52. Mehta SR, Bassand JP, Chrolavicius S, et al. Dose comparisons of clopidogrel and aspirin in acute coronary syndromes. *N Engl J Med* 2010;363:930-42.

53. Siller-Matula JM, Huber K, Christ G, et al. Impact of clopidogrel loading dose on clinical outcome in patients undergoing percutaneous coronary intervention: a systematic review and meta-analysis. *Heart* 2011;97:98-105.

54. Schömig A. Ticagrelor--is there need for a new player in the antiplatelet-therapy field? *N Engl J Med* 2009;361:1108-11.

55. Matetzky S, Shenkman B, Guetta V, et al. Clopidogrel resistance is associated with increased risk of recurrent atherothrombotic events in patients with acute myocardial infarction. *Circulation* 2004;109:3171-5.

56. Collet JP, Hulot JS, Pena A, et al. Cytochrome P450 2C19 polymorphism in young patients treated with clopidogrel after myocardial infarction: a cohort study. *Lancet* 2009;373:309-17.

57. Hu XP, Xu JM, Hu YM, et al. Effects of CYP2C19 genetic polymorphism on the pharmacokinetics and pharmacodynamics of omeprazole in Chinese people. *J Clin Pharm Ther* 2007;32:517-24.

58. Veiga MI, Asimus S, Ferreira PE, et al. Pharmacogenomics of CYP2A6, CYP2B6, CYP2C19, CYP2D6, CYP3A4, CYP3A5 and MDR1 in Vietnam. *Eur J Clin Pharmacol* 2009;65:355-63.

59. Wiviott SD, Trenk D, Frelinger AL, et al. Prasugrel compared with high loading- and maintenance-dose clopidogrel in patients with planned percutaneous coronary intervention: the Prasugrel in Comparison to Clopidogrel for Inhibition of Platelet Activation and Aggregation-Thrombolysis in Myocardial Infarction 44 trial. *Circulation* 2007;116:2923-32.

60. Wiviott SD, Braunwald E, McCabe CH, et al. Prasugrel versus clopidogrel in patients with acute coronary syndromes. *N Engl J Med* 2007;357:2001-15.

61. Udell JA, Braunwald E, Antman EM, et al. Prasugrel versus clopidogrel in patients with ST-segment elevation myocardial infarction according to timing of percutaneous coronary intervention: a TRITON-TIMI 38 subgroup analysis (Trial to Assess Improvement in Therapeutic Outcomes by Optimizing Platelet Inhibition with Prasugrel-Thrombolysis In Myocardial Infarction 38). *JACC Cardiovasc Interv* 2014;7:604-12.

62. Saito S, Isshiki T, Kimura T, et al. Efficacy and safety of adjusted-dose prasugrel compared with clopidogrel in Japanese patients with acute coronary syndrome: the PRASFIT-ACS study. *Circ J* 2014;78:1684-92.

63. Nakamura M, Iizuka T, Sagawa K, et al. Prasugrel for Japanese patients with acute coronary syndrome in short-term clinical practice (PRASFIT-Practice I): a postmarketing observational study. *Cardiovasc Interv Ther* 2018;33:135-45.

64. Akita K, Inohara T, Yamaji K, et al. Impact of reduced-dose prasugrel vs. standard-dose clopidogrel on in-hospital outcomes of percutaneous coronary intervention in 62,737 patients with acute coronary syndromes: a nationwide registry study in Japan. *Eur Heart J Cardiovasc Pharmacother* 2019;pii: pvz056.

65. Gurbel PA, Bliden KP, Butler K, et al. Randomized double-blind assessment of the ONSET and OFFSET of the antiplatelet effects of ticagrelor versus clopidogrel in patients with stable coronary artery disease: the ONSET/OFFSET study. *Circulation* 2009;120:2577-85.

66. Wallentin L, Becker RC, Budaj A, et al. Ticagrelor versus clopidogrel in patients with acute coronary syndromes. *N Engl J Med* 2009;361:1045-57.

67. Steg PG, James S, Harrington RA, et al. Ticagrelor versus clopidogrel in patients with ST-elevation acute coronary syndromes

intended for reperfusion with primary percutaneous coronary intervention: A Platelet Inhibition and Patient Outcomes (PLATO) trial subgroup analysis. *Circulation* 2010;122:2131-41.

68. Berwanger O, Nicolau JC, Carvalho AC, et al. Ticagrelor vs clopidogrel after fibrinolytic therapy in patients with ST-elevation myocardial infarction: a randomized clinical trial. *JAMA Cardiol* 2018;3:391-9.

69. Berwanger O, Lopes RD, Moia DDF, et al. Ticagrelor versus clopidogrel in patients with STEMI treated with fibrinolysis: TREAT trial. *J Am Coll Cardiol* 2019;73:2819-28.

70. Sahlén A, Varenhorst C, Lagerqvist B, et al. Outcomes in patients treated with ticagrelor or clopidogrel after acute myocardial infarction: experiences from SWEDEHEART registry. *Eur Heart J* 2016;37:3335-42.

71. Goto S, Huang CH, Park SJ, et al. Ticagrelor vs. clopidogrel in Japanese, Korean and Taiwanese patients with acute coronary syndrome -- randomized, double-blind, phase III PHILO study. *Circ J* 2015;79:2452-60.

72. Park DW, Kwon O, Jang JS, et al. Clinically significant bleeding with ticagrelor versus clopidogrel in Korean patients with acute coronary syndromes intended for invasive management: a randomized clinical trial. *Circulation* 2019;140:1865-77.

73. Tang X, Li R, Jing Q, et al. Assessment of ticagrelor versus clopidogrel treatment in patients with ST-elevation myocardial infarction undergoing primary percutaneous coronary intervention. *J Cardiovasc Pharmacol* 2016;68:115-20.

74. Xin YG, Zhang HS, Li YZ, et al. Efficacy and safety of ticagrelor versus clopidogrel with different dosage in high-risk patients with acute coronary syndrome. *Int J Cardiol* 2017;228:275-9.

75. Park KH, Jeong MH, Ahn Y, et al. Comparison of short-term clinical outcomes between ticagrelor versus clopidogrel in patients with acute myocardial infarction undergoing successful revascularization; from Korea Acute Myocardial Infarction Registry-National Institute of Health. *Int J Cardiol* 2016;215:193-200.

76. Wang H, Wang X. Efficacy and safety outcomes of ticagrelor compared with clopidogrel in elderly Chinese patients with acute coronary syndrome. *Ther Clin Risk Manag* 2016;12:1101-5.

77. Chen IC, Lee CH, Fang CC, et al. Efficacy and safety of ticagrelor versus clopidogrel in acute coronary syndrome in Taiwan: a multicenter retrospective pilot study. *J Chin Med Assoc* 2016; 79:521-30.

78. Lee CH, Cheng CL, Yang KYH, et al. Cardiovascular and bleeding risks in acute myocardial infarction newly treated with ticagrelor vs. clopidogrel in Taiwan. *Circ J* 2018;82:747-56.

79. Lee CH, Tsai TH, Lin CJ, et al. Efficacy and safety of ticagrelor compared with clopidogrel in patients with end-stage renal disease with acute myocardial infarction. *Am J Cardiovasc Drugs* 2019;19:325-34.

80. Sun J, Xiang Q, Li C, et al. Efficacy and safety of novel oral P2Y12 receptor inhibitors in patients with ST-segment elevation myocardial infarction undergoing PCI: a systematic review and meta-analysis. *J Cardiovasc Pharmacol* 2017;69:215-27.

81. Rafique AM, Nayyar P, Wang TY, et al. Optimal P2Y12 inhibitor in

82. patients with ST-segment elevation myocardial infarction undergoing primary percutaneous coronary intervention: a network meta-analysis. *JACC Cardiovasc Interv* 2016;9:1036-46.

82. Kim C, Shin DH, Ahn CM, et al. The use pattern and clinical impact of new antiplatelet agents including prasugrel and ticagrelor on 30-day outcomes after acute myocardial infarction in Korea: Korean Health Insurance Review and Assessment Data. *Korean Circ J* 2017;47:888-97.

83. Choe JC, Cha KS, Ahn J, et al. Comparison of prescription rates and clinical outcomes in acute coronary syndrome patients who underwent percutaneous coronary intervention using different P2Y12 inhibitors in a large observational study. *Int J Cardiol* 2019;274:21-6.

84. Dawwas GK, Dietrich E, Winchester DE, et al. Comparative effectiveness and safety of ticagrelor versus prasugrel in patients with acute coronary syndrome: a retrospective cohort analysis. *Pharmacotherapy* 2019;39:912-20.

85. Schüpke S, Neumann FJ, Menichelli M, et al. Ticagrelor or prasugrel in patients with acute coronary syndromes. *N Engl J Med* 2019;381:1524-34.

86. Rathore SS, Curtis JP, Chen J, et al. Association of door-to-balloon time and mortality in patients admitted to hospital with ST elevation myocardial infarction: national cohort study. *BMJ* 2009;338:b1807.

87. McNamara RL, Wang Y, Herrin J, et al. Effect of door-to-balloon time on mortality in patients with ST-segment elevation myocardial infarction. *J Am Coll Cardiol* 2006;47:2180-6.

88. Nallamothu BK, Normand SL, Wang Y, et al. Relation between door-to-balloon times and mortality after primary percutaneous coronary intervention over time: a retrospective study. *Lancet* 2015;385:1114-22.

89. Brodie BR, Gersh BJ, Stuckey T, et al. When is door-to-balloon time critical? Analysis from the HORIZONS-AMI (Harmonizing Outcomes with Revascularization and Stents in Acute Myocardial Infarction) and CADILLAC (Controlled Abciximab and Device Investigation to Lower Late Angioplasty Complications) trials. *J Am Coll Cardiol* 2010;56:407-13.

90. Shiomi H, Nakagawa Y, Morimoto T, et al.; CREDO-Kyoto AMI investigators. Association of onset to balloon and door to balloon time with long term clinical outcome in patients with ST elevation acute myocardial infarction having primary percutaneous coronary intervention: observational study. *BMJ* 2012;344: e3257.

91. Lai CC, Chang KC, Liao PC, et al. Effects of door-to-balloon times on outcomes in Taiwanese patients receiving primary percutaneous coronary intervention: a report of Taiwan Acute Coronary Syndrome Full Spectrum Registry. *Acta Cardiol Sin* 2015; 31:215-25.

92. Jolly SS, Yusuf S, Cairns J, et al. Radial versus femoral access for coronary angiography and intervention in patients with acute coronary syndromes (RIVAL): a randomised, parallel group, multicentre trial. *Lancet* 2011;377:1409-20.

93. Jolly SS, Cairns J, Yusuf S, et al. Procedural volume and out-

comes with radial or femoral access for coronary angiography and intervention. *J Am Coll Cardiol* 2014;63:954-63.

94. Valgimigli M, Gagnor A, Calabró P, et al. Radial versus femoral access in patients with acute coronary syndromes undergoing invasive management: a randomised multicentre trial. *Lancet* 2015;385:2465-76.

95. Sabate M, Cequier A, Iñiguez A, et al. Everolimus-eluting stent versus bare-metal stent in ST-segment elevation myocardial infarction (EXAMINATION): 1 year results of a randomized controlled trial. *Lancet* 2012;380:1482-90.

96. Räber L, Kelbæk H, Ostojic M, et al. Effect of biolimus-eluting stents with biodegradable polymer vs bare-metal stents on cardiovascular events among patients with acute myocardial infarction: the COMFORTABLE AMI randomized trial. *JAMA* 2012; 308:777-87.

97. Frobert O, Lagerqvist B, Olivecrona GK, et al. Thrombus aspiration during ST-segment elevation myocardial infarction. *N Engl J Med* 2013;369:1587-97.

98. Lagerqvist B, Frobert O, Olivecrona GK, et al. Outcomes 1 year after thrombus aspiration for myocardial infarction. *N Engl J Med* 2014;371:1111-20.

99. Jolly SS, Cairns JA, Yusuf S, et al. Randomized trial of primary PCI with or without routine manual thrombectomy. *N Engl J Med* 2015;372:1389-98.

100. Jolly SS, Cairns JA, Yusuf S, et al. Outcomes after thrombus aspiration for ST elevation myocardial infarction: 1-year follow-up of the prospective randomized TOTAL trial. *Lancet* 2016; 387:127-35.

101. Jolly SS, Cairns JA, Yusuf S, et al. Stroke in the TOTAL trial: a randomized trial of routine thrombectomy vs. percutaneous coronary intervention alone in ST elevation myocardial infarction. *Eur Heart J* 2015;36:2364-72.

102. Goldstein JA, Demetriou D, Grines CL, et al. Multiple complex coronary plaques in patients with acute myocardial infarction. *N Engl J Med* 2000;343:915-22.

103. Bates ER, Tamis-Holland JE, Bittl JA, et al. PCI strategies in patients with ST-segment elevation myocardial infarction and multivessel coronary artery disease. *J Am Coll Cardiol* 2016;68: 1066-81.

104. Wood DA, Cairns JA, Mehta SR. Multivessel revascularization and ST segment-elevation myocardial infarction: do we have the complete answer? *Circ Cardiovasc Interv* 2017;10:pii: e005215.

105. Engstrom T, Kelbaek H, Helqvist S, et al. Complete revascularization versus treatment of the culprit lesion only in patients with ST-segment elevation myocardial infarction and multivessel disease (DANAMI-3-PRIMULTI): an open-label, randomized controlled trial. *Lancet* 2015;386:665-71.

106. Gershlick AH, Khan JN, Kelly DJ, et al. Randomized trial of complete versus lesion-only revascularization in patients undergoing primary percutaneous coronary intervention for STEMI and multivessel disease: the CvLPRIT trial. *J Am Coll Cardiol* 2015; 65:963-72.

107. Smits PC, Abdel-Wahab M, Neumann FJ, et al. Fractional flow reserve guided multivessel angioplasty in myocardial infarction. *N Engl J Med* 2017;376: 1234-44.

108. Wald DS, Morris JK, Wald NJ, et al. Randomized trial of preventive angioplasty in myocardial infarction. *N Engl J Med* 2013; 369:1115-23.

109. Lonborg J, Engstrom T, Kelbaek H, et al. Fractional flow reserve-guided complete revascularization improves the prognosis in patients with ST segment-elevation myocardial infarction and severe nonculprit disease: a DANAMI 3-PRIMULTI substudy (Primary PCI in Patients With ST Elevation Myocardial Infarction and Multivessel Disease: Treatment of Culprit Lesion Only or Complete evascularization). *Circ Cardiovasc Interv* 2017;10: e004460.

110. Bainey KR, Welsh RC, Toklu B, et al. Complete vs culprit-only percutaneous coronary intervention in STEMI with multivessel disease: a meta-analysis and trial sequential analysis of randomized trials. *Can J Cardiol* 2016;32:1542-51.

111. Mehta SR, Wood DA, Storey RF, et al. Complete revascularization with multivessel PCI for myocardial infarction. *N Engl J Med* 2019;381:1411-21.

112. Thiele H, Akin I, Sandri M, et al. PCI strategies in patients with acute myocardial infarction and cardiogenic shock. *N Engl J Med* 2017;377:2419-32.

113. Thiele H, Akin I, Sandri M, et al. One-year outcomes after PCI strategies in cardiogenic shock. *N Engl J Med* 2018;379:1699-710.

114. McNeice A, Nadra IJ, Robinson SD, et al. The prognostic impact of revascularization strategy in acute myocardial infarction and cardiogenic shock: insights from the British Columbia Cardiac Registry. *Catheter Cardiovasc Interv* 2018;92:E356-67.

115. Hochman JS, Sleeper LA, Webb JG, et al. Early revascularization in acute myocardial infarction complicated by cardiogenic shock. SHOCK Investigators. should we emergently revascularize occluded coronaries for cardiogenic shock. *N Engl J Med* 1999; 341:625-34.

116. Thiele H, Zeymer U, Neumann FJ, et al. Intraaortic balloon support for myocardial infarction with cardiogenic shock. *N Engl J Med* 2012;367:1287-96.

117. Baran DA, Grines CL, Bailey S, et al. SCAI clinical expert consensus statement on the classification of cardiogenic shock: this document was endorsed by the American College of Cardiology (ACC), the American Heart Association (AHA), the Society of Critical Care Medicine (SCCM), and the Society of Thoracic Surgeons (STS) in April 2019. *Catheter Cardiovasc Interv* 2019;94: 29-37.

118. Asleh R, Resar JR. Utilization of percutaneous mechanical circulatory support devices in cardiogenic shock complicating acute myocardial infarction and high-risk percutaneous coronary interventions. *J Clin Med* 2019;8:1209.

119. Vahdatpour C, Collins D, Goldberg S. Cardiogenic shock. *J Am Heart Assoc* 2019;8:e011991.

120. Aissaoui N, Puymirat E, Tabone X, et al. Improved outcome of cardiogenic shock at the acute stage of myocardial infarction: a

report from the USIK 1995, USIC 2000, and FAST-MI French nationwide registries. *Eur Heart J* 2012;33:2535-43.

121. Rathod KS, Koganti S, Iqbal MB, et al. Contemporary trends in cardiogenic shock: incidence, intra-aortic balloon pump utilisation and outcomes from the London Heart Attack Group. *Eur Heart J Acute Cardiovasc Care* 2018;7:16-27.

122. Hochman JS, Buller CE, Sleeper LA, et al. Cardiogenic shock complicating acute myocardial infarction--etiologies, management and outcome: a report from the SHOCK Trial Registry. SHould we emergently revascularize Occluded Coronaries for cardiogenic shocK? *J Am Coll Cardiol* 2000;36:1063-70.

123. van Diepen S, Katz JN, Albert NM, et al. Contemporary management of cardiogenic shock: a scientific statement from the American Heart Association. *Circulation* 2017;136:e232-68.

124. Werdan K, Gielen S, Ebelt H, Hochman JS. Mechanical circulatory support in cardiogenic shock. *Eur Heart J* 2014;35:156-67.

125. Thiele H, Ohman EM, de Waha-Thiele S, et al. Management of cardiogenic shock complicating myocardial infarction: an update 2019. *Eur Heart J* 2019;40:2671-83.

126. Lee JM, Rhee TM, Hahn JY, et al. Multivessel percutaneous coronary intervention in patients with ST-segment elevation myocardial infarction with cardiogenic shock. *J Am Coll Cardiol* 2018;71:844-56.

127. Vallabhajosyula S, Dunlay SM, Prasad A, et al. Acute noncardiac organ failure in acute myocardial infarction with cardiogenic shock. *J Am Coll Cardiol* 2019;73:1781-91.

128. Ponikowski P, Voors AA, Anker SD, et al. 2016 ESC Guidelines for the diagnosis and treatment of acute and chronic heart failure: the task force for the diagnosis and treatment of acute and chronic heart failure of the European Society of Cardiology (ESC) Developed with the special contribution of the Heart Failure Association (HFA) of the ESC. *Eur Heart J* 2016;37:2129-200.

129. Shah MR, Hasselblad V, Stevenson LW, et al. Impact of the pulmonary artery catheter in critically ill patients: meta-analysis of randomized clinical trials. *JAMA* 2005;294:1664-70.

130. Bart BA, Goldsmith SR, Lee KL, et al. Ultrafiltration in decompensated heart failure with cardiorenal syndrome. *N Engl J Med* 2012;367:2296-304.

131. Stegman BM, Newby LK, Hochman JS, Ohman EM. Post-myocardial infarction cardiogenic shock is a systemic illness in need of systemic treatment: is therapeutic hypothermia one possibility? *J Am Coll Cardiol* 2012;59:644-7.

132. Fuernau G, Beck J, Desch S, et al. Mild hypothermia in cardiogenic shock complicating myocardial infarction. *Circulation* 2019;139:448-57.

133. Starling RC, Naka Y, Boyle AJ, et al. Results of the post-U.S. Food and Drug Administration-approval study with a continuous flow left ventricular assist device as a bridge to heart transplantation: a prospective study using the INTERMACS (Interagency Registry for Mechanically Assisted Circulatory Support). *J Am Coll Cardiol* 2011;57:1890-8.

134. Sheu JJ, Tsai TH, Lee FY, et al. Early extracorporeal membrane oxygenator-assisted primary percutaneous coronary intervention improved 30-day clinical outcomes in patients with ST-segment elevation myocardial infarction complicated with profound cardiogenic shock. *Crit Care Med* 2010;38:1810-7.

135. Esposito ML, Zhang Y, Qiao X, et al. Left ventricular unloading before reperfusion promotes functional recovery after acute myocardial infarction. *J Am Coll Cardiol* 2018;72:501-14.

136. Hajjar LA, Teboul JL. Mechanical circulatory support devices for cardiogenic shock: state of the art. *Crit Care* 2019;23:76.

137. Thiele H, Jobs A, Ouweneel DM, et al. Percutaneous short-term active mechanical support devices in cardiogenic shock: a systematic review and collaborative meta-analysis of randomized trials. *Eur Heart J* 2017;38:3523-31.

138. Esposito M, Bader Y, Pedicini R, et al. The role of acute circulatory support in ST-segment elevation myocardial infarction complicated by cardiogenic shock. *Indian Heart J* 2017;69:668-74.

139. Tehrani BN, Truesdell AG, Sherwood MW, et al. Standardized team-based care for cardiogenic shock. *J Am Coll Cardiol* 2019;73:1659-69.

140. Cheng R, Hachamovitch R, Kittleson M, et al. Complications of extracorporeal membrane oxygenation for treatment of cardiogenic shock and cardiac arrest: a meta-analysis of 1,866 adult patients. *Ann Thorac Surg* 2014;97:610-6.

141. Potapov EV, Antonides C, Crespo-Leiro MG, et al. 2019 EACTS expert consensus on long-term mechanical circulatory support. *Eur J Cardiothorac Surg* 2019;56:230-270.

142. Chen KC, Yin WH, Wu CC, et al. In-hospital implementation of evidence-based medications is associated with improved survival in diabetic patients with acute coronary syndrome - data from TSOC ACS-DM Registry. *Acta Cardiol Sin* 2018;34:211-23.

143. Chowdhury R, Khan H, Heydon E, et al. Adherence to cardiovascular therapy: a meta-analysis of prevalence and clinical consequences. *Eur Heart J* 2013;34:2940-8.

144. Castellano JM, Sanz G, Peñalvo JL, et al. A polypill strategy to improve adherence: results from the FOCUS project. *J Am Coll Cardiol* 2014;64:2071-82.

145. Lee CK, Lai CL, Lee MH, et al. Reinforcement of patient education improved physicians' adherence to guideline-recommended medical therapy after acute coronary syndrome. *PLoS One* 2019;14:e0217444-e44.

146. Chiang CE, Wang TD, Ueng KC, et al. 2015 guidelines of the Taiwan Society of Cardiology and the Taiwan Hypertension Society for the management of hypertension. *J Chin Med Assoc* 2015;78:1-47.

147. Group SR, Wright JT Jr, Williamson JD, et al. A randomized trial of intensive versus standard blood pressure control. *N Engl J Med* 2015;373:2103-16.

148. Lip S, Tan LE, Jeemon P, et al. Diastolic blood pressure J-curve phenomenon in a tertiary-care hypertension clinic. *Hypertension* 2019;74:767-75.

149. Flint AC, Conell C, Ren X, et al. Effect of systolic and diastolic blood pressure on cardiovascular outcomes. *N Engl J Med* 2019;381:243-51.

150. Williams B, Mancia G, Spiering W, et al. 2018 ESC/ESH guidelines for the management of arterial hypertension: the task force for the management of arterial hypertension of the European Society of Cardiology (ESC) and the European Society of Hypertension (ESH). *Eur Heart J* 2018;39:3021-104.

151. Whelton PK, Carey RM, Aronow WS, et al. 2017 ACC/AHA/AAPA/ABC/ACPM/AGS/APhA/ASH/ASPC/NMA/PCNA Guideline for the prevention, detection, evaluation, and management of high blood pressure in adults: a report of the American College of Cardiology/American Heart Association Task Force on Clinical Practice Guidelines. *Hypertension* 2018;71:e13-115.

152. Park JJ, Kim SH, Kang SH, et al. Differential effect of β-blockers according to heart rate in acute myocardial infarction without heart failure or left ventricular systolic dysfunction: a cohort study. *Mayo Clin Proc* 2019;94:2476-87.

153. Wu VC, Chen SW, Ting PC, et al. Selection of β-blocker in patients with cirrhosis and acute myocardial infarction: a 13-year nationwide population-based study in Asia. *J Am Heart Assoc* 2018;7:e008982.

154. Su TH, Chang SH, Kuo CF, et al. β-blockers after acute myocardial infarction in patients with chronic obstructive pulmonary disease: a nationwide population-based observational study. *PLoS One* 2019;14:e0213187

155. Wang CC, Wu CK, Tsai ML, et al. 2019 focused update of the guidelines of the Taiwan Society of Cardiology for the diagnosis and treatment of heart failure. *Acta Cardiol Sin* 2019;35:244-83.

156. American Diabetes Association. Glycemic targets: standards of medical care in diabetes-2020. *Diabetes Care* 2020;43(Suppl 1):S66-76.

157. Chiang CE, Lin SY, Lin TH, et al. 2018 consensus of the Taiwan Society of Cardiology and the Diabetes Association of Republic of China (Taiwan) on the pharmacological management of patients with type 2 diabetes and cardiovascular diseases. *J Chin Med Assoc* 2018;81:189-222.

158. McMurray JJV, Solomon SD, Inzucchi SE, et al. Dapagliflozin in patients with heart failure and reduced ejection fraction. *N Engl J Med* 2019;381:1995-2008.

159. Mach F, Baigent C, Catapano AL, et al. 2019 ESC/EAS Guidelines for the management of dyslipidaemias: lipid modification to reduce cardiovascular risk. *Eur Heart J* 2020;41:111-88.

160. Li YH, Ueng KC, Jeng JS, et al. 2017 Taiwan lipid guidelines for high risk patients. *J Formos Med Assoc* 2017;116:217-48.

161. Silverman MG, Ference BA, Im K, et al. Association between lowering LDL-C and cardiovascular risk reduction among different therapeutic interventions: a systematic review and meta-analysis. *JAMA* 2016;316:1289-97.

162. Chien SC, Chen PS, Huang YH, et al. 2019 Taiwan Society of Lipids and Atherosclerosis expert consensus statement on statin intolerance. *J Formos Med Assoc* 2019;118:1385-92.

163. Serban MC, Colantonio LD, Manthripragada AD, et al. Statin intolerance and risk of coronary heart events and all-cause mortality following myocardial infarction. *J Am Coll Cardiol* 2017;69:1386-95.

164. Sabatine MS, Giugliano RP, Keech AC, et al. Evolocumab and clinical outcomes in patients with cardiovascular disease. *New Engl J Med* 2017;376:1713-22.

165. Schwartz GG, Steg PG, Szarek M, et al. Alirocumab and cardiovascular outcomes after acute coronary syndrome. *New Engl J Med* 2018;379:2097-107.

166. Virani SS, Akeroyd JM, Nambi V, et al. Estimation of eligibility for proprotein convertase subtilisin/kexin type 9 inhibitors and associated costs based on the FOURIER Trial (Further Cardiovascular Outcomes Research With PCSK9 Inhibition in Subjects With Elevated Risk): insights from the department of veterans affairs. *Circulation* 2017;135:2572-74.

167. Cannon CP, Khan I, Klimchak AC, et al. Simulation of lipid-lowering therapy intensification in a population with atherosclerotic cardiovascular disease. *JAMA Cardiology* 2017;2:959-66.

168. Fox KA, Goodman SG, Klein W, et al. Management of acute coronary syndromes. Variations in practice and outcome; findings from the Global Registry of Acute Coronary Events (GRACE). *Eur Heart J* 2002;23:1177-89.

169. Lenfant C. Shattuck lecture--clinical research to clinical practice--lost in translation? *N Engl J Med* 2003;349:868-74.

170. Schiele F, Gale CP, Bonnefoy E, et al. Quality indicators for acute myocardial infarction: a position paper of the Acute Cardiovascular Care Association. *Eur Heart J Acute Cardiovasc Care* 2017;6:34-59.

171. Jneid H, Addison D, Bhatt DL, et al. 2017 AHA/ACC clinical performance and quality measures for adults with ST-elevation and non-ST-elevation myocardial infarction: a report of the American College of Cardiology/American Heart Association task force on performance measures. *J Am Coll Cardiol* 2017;70:2048-90.

ENVIRONMENTAL TOXICOLOGY WILEY

Rutin-protected BisGMA-induced cytotoxicity, genotoxicity, and apoptosis in macrophages through the reduction of the mitochondrial apoptotic pathway and induction of antioxidant enzymes

Fu-Mei Huang[1,2] | Yu-Chao Chang[1,2] | Chun-Hung Su[3,4] | Sheng-Wen Wu[3,5] | Shiuan-Shinn Lee[6] | Min-Wei Lee[7] | Kun-Lin Yeh[8] | Chen-Yu Chiang[8] | Dom-Gene Tu[9,10] | Yin-Che Lu[11,12] | Yu-Hsiang Kuan[13,14] [ID]

[1]Department of Dentistry, Chung Shan Medical University Hospital, Taichung, Taiwan

[2]School of Dentistry, Chung Shan Medical University, Taichung, Taiwan

[3]Department of Internal Medicine, School of Medicine, Chung Shan Medical University, Taichung, Taiwan

[4]Department of Internal Medicine, Chung Shan Medical University Hospital, Taichung, Taiwan

[5]Division of Nephrology, Chung Shan Medical University Hospital, Taichung, Taiwan

[6]School of Public Health, Chung Shan Medical University, Taichung, Taiwan

[7]A Graduate Institute of Microbiology and Public Health, National Chung Hsing University, Taichung, Taiwan

[8]Department of Veterinary Medicine, National Chung Hsing University, Taichung, Taiwan

[9]Department of Nuclear Medicine, Ditmanson Medical Foundation Chia-Yi Christian Hospital, Chiayi, Taiwan

[10]Department of Biomedical Science, National Chung Cheng University, Chiayi, Taiwan

[11]Min-Hwei Junior College of Health Care Management, Tainan, Taiwan

[12]Division of Hematology-Oncology, Ditmanson Medical Foundation Chia-Yi Christian Hospital, Chiayi, Taiwan

[13]Department of Pharmacology, School of Medicine, Chung Shan Medical University, Taichung, Taiwan

[14]Department of Pharmacy, Chung Shan Medical University Hospital, Taichung, Taiwan

Correspondence

Yu-Hsiang Kuan, Department of Pharmacology, School of Medicine, Chung Shan Medical University, No. 110, Sector 1, Jianguo N. Road, Taichung 402, Taiwan, ROC.
Email: kuanyh@csmu.edu.tw

Abstract

Bisphenol-A-glycidyldimethacrylate (BisGMA) is a resin monomer frequently used in dentin restorative treatments. The leakage of BisGMA monomer from BisGMA-based polymeric resins can lead to cytotoxicity in macrophages. Rutin has various beneficial bioeffects, including antioxidation and antiinflammation. In this study, we found that pretreatment of RAW264.7 macrophages with rutin-inhibited cytotoxicity induced by BisGMA in a concentration-dependent manner. BisGMA-induced apoptosis, which was detected by levels of phosphatidylserine from the internal to the external membrane and formation of sub-G1, and genotoxicity, which was detected by cytokinesis-blocked micronucleus and single-cell gel electrophoresis assays, were inhibited by rutin in a concentration-dependent manner. Rutin suppressed the BisGMA-induced activation of caspase-3 and -9 rather than caspase-8. Rutin inhibited the activation of the mitochondrial apoptotic pathway, including cyto-chrome C release and mitochondria disruption, after macrophages were treated with

BisGMA. Finally, BisGMA-induced reactive oxygen species (ROS) generation and antioxidant enzyme (AOE) deactivation could be reversed by rutin. Parallel trends were observed in the elevation of AOE activation and inhibition of ROS generation, caspase-3 activity, mitochondrial apoptotic pathway activation, and genotoxicity. These results suggested that rutin suppressed BisGMA-induced cytotoxicity through genotoxicity, the mitochondrial apoptotic pathway, and relatively upstream factors, including reduction of ROS generation and induction of AOE.

KEYWORDS

antioxidant enzymes, BisGMA, macrophage, mitochondrial apoptotic pathway, rutin, toxic effects

1 | INTRODUCTION

Rutin, the chemical named 3,3′,4′,5,7-pentahydroxyflavone-3-rhamnoglucoside, also called rutoside, sophorin, and phytomelin, is a flavonol compound found abundantly in *Passiflora*, buckwheat seeds, citrus fruits, vegetables, and tea. Rutin possesses numerous pharmacological and beneficial effects including antioxidative, cytoprotective, anti-inflammatory, neuroprotective, cardioprotective, and anticarcinogenic activities.[1-6] Bisphenol A-glycidyl-methacrylate (BisGMA), which synthesizes epoxy resin from methacrylic acid and diglycidyl ether of bisphenol-A, is widely used in dentin restoration and as a bonding agent, a denture base material, a fissure sealant, and as bone cement.[7,8] The characteristics of BisGMA-based polymeric resins include modulus, less shrinkage, lower diffusivity, and water insolubility.[9] However, BisGMA monomer can be leachable from polymeric resins under long-term incubation with lipophilic or hydrophilic solvents.[9,10] Leachable BisGMA monomer causes harmful effects, including cytotoxic, inflammatory, and gastrointestinal responses through the activation of innate immunity.[11,12]

Macrophages play a critical role in the innate immune system and participate in innate defense against invading foreign pathogens through the production of antibacterial materials, including reactive oxygen species (ROS) and protease.[13,14] Invading foreign pathogen-induced macrophage activation induces overproduction of antibacterial materials, which result in peripheral tissue damage and inflammation.[13] Additionally, excessive activation of macrophage leads to cell damage, including DNA damage, apoptosis, genotoxicity, and cytotoxicity. BisGMA is one type of invading foreign material that could be reduced survival rate in macrophages.[15,16] In the previous studies have proposed that BisGMA-induced ROS generation leads to DNA damage and mitochondria disruption, which then leads to apoptosis in macrophages.[17,18] Until now, no studies have demonstrated the ameliorative effects of rutin on BisGMA-induced cytotoxic, genotoxic, and apoptotic effects in macrophages. In this study, we explored the protective effects and mechanism of rutin on RAW264.7 macrophage damage induced by BisGMA.

2 | MATERIALS AND METHODS

2.1 | Materials

Dulbecco's modified Eagle medium (DMEM), fetal bovine serum (FBS), and penicillin/streptomycin/fungizone were obtained from Hyclone (Logan, UT). Caspases fluorometric assay kits, antioxidant enzymes (AOEs) activities assay kit were obtained from Cayman (Ann Arbor, MI). Annexin V-FITC, propidium iodide (PI), and tetraethylbenzimidazolylcarbocyanine iodide (JC-1) were purchased from BioVision (San Jose, CA). FlowCellect Cytochrome C kit was purchased from EMD Millipore (Billerica, MA). True-Nuclear Transcription Factor Buffer Set and FITC anti-cytochrome c antibody were from Biolegend (San Diego, CA). Rutin, 3-(4,5-dimethylthiazol-2-yl)-2,5-diphenyl tetrazolium bromide (MTT), and other reagents, unless specifically stated, were purchased from Sigma-Aldrich (St. Louis, MO).

2.2 | Cell culture and treatments

Cells of the murine macrophage cell line RAW264.7 were purchased from the Bioresource Collection and Research Center (BCRC, Hsinchu, Taiwan). RAW264.7 cells were maintained in DMEM supplemented with 1% penicillin/streptomycin/fungizone and 10% FBS in an incubator at 37°C with 5% CO_2.[19] Cells were grown at a density of 200 000-500 000 cells/mL in culture plates. After replacement, replacing the medium to phenol red- and serum-free DMEM, the cells were treated with rutin at the concentrations of 0, 3, 10, 30, or 100 μM for 30 minutes. The cells were treated with BisGMA at a concentration of 0.3 μM for 4 hours.

2.3 | Cytotoxicity assay

An MTT assay was used to analyze the cytotoxicity rate as described in the previous study.[16] After treatment and washing, the cells were incubated with 0.5 mg/mL MTT for 2 hours. After washing, the

—WILEY 47

intracellular blue formazan crystals were dissolved in 100 μL dimethyl sulfoxide. The optical density was measured using the Synergy HT Multi-Mode Microplate Reader (BioTek, Winooski, VT) at 550 nm.

2.4 | Annexin V-FITC and PI staining assay

Apoptosis and necrosis were evaluated using flowcytometry analysis of cells, which were stained with Annexin V-FITC and PI as described in the previous studies.[16] After cells reacted and stained, data acquisition and analyses were performed with Accuri C6 flowcytometry software (BD Biosciences, San Jose, CA). Annexin V-FITC and PI staining were detected as green and red fluorescence, respectively. Annexin V-FITC and PI negative (AnnexinV −/PI−), annexin V-FITC positive (including AnnexinV+/PI− and AnnexinV+/PI+), and annexin negative and PI positive (AnnexinV −/PI+) cells were regarded as survival, apoptotic, and necrotic cells, respectively.

2.5 | Sub-G1 formation analysis by PI staining

Apoptosis was evaluated through sub-G1 formation stained with PI as described in the previous research.[20] After treatment, the harvested cells were fixed in 70% ethanol at −20°C overnight. After being washed, the cells were incubated with RNase A and PI for 30 minutes at 37°C in the dark. The percentage of sub-G1 phase cells was analyzed using flowcytometry.

2.6 | Cytokinesis-block micronucleus assay

Chromosomal damage determined by the micronucleus (MN) assay was performed as described in the previous research.[16] After treatment, the cells were incubated with cytochalasin-B to block cytokinesis and then treated with 75 mM potassium chloride. After washing, the cells were cotreated with a cold fixative solution containing acetic acid and methanol (1:3). The cells were loaded onto the slides and stained with Giemsa solution. MN frequencies in 1000 binucleated cells were estimated using a light microscope.

2.7 | Single-cell gel electrophoresis (comet) assay

DNA strand break assessment by the comet assay was performed as described in the previous research.[16] After treatment, the cells were resuspended in low-melting-point agarose solution and placed on microscope slides precoated with normal-melting-point agarose. The cells were lysed with comet lysis solution (1% Triton X-100, 2.5 M NaCl, 0.1 M EDTA, 10 mM Tris, and pH 10) for 1 hour at 4°C in the dark. After electrophoresis was conducted, slides were neutralized and stained with ethidium bromide. A fluorescence microscope (Nikon, Tokyo, Japan) with comet v.3 software

(Kinetic Imaging Ltd., Liverpool, UK) was used to score at least 50 cells per sample. The results were expressed as % DNA in tail, which indicates relative fluorescence intensity of tail, and tail length, which indicate the distance from the head center to the end of the tail.

2.8 | Caspase-3, -8, and -9 activities assay

Caspase-3, -8, and -9 activities assessed by the commercial assay kits were performed as described in the previous research.[16] After treatment, the cells were lysed by lysis buffer for 1 hour at 4°C. After centrifugation, the protein concentration of supernatants was measured by the Bradford assay. The lysate was incubated with the fluorogenic substrate of caspase-3, -8, and -9, which is DEVD-AFC, IETD-AFC, and LEHD-AFC, respectively. After incubation, the sample fluorescence intensity was measured with the microplate reader, which has excitation and emission wavelengths at 400 and 505 nm.

2.9 | Mitochondrial membrane potential assay

Changes in mitochondrial membrane potential detected by the lipophilic cationic dye JC-1 were performed as described in the previous research.[21] After being subjected to treatment and centrifugation, the cells were resuspended in phosphate-buffered saline (PBS, pH = 7.4) and incubated with 10 mg/mL of JC-1 for 30 minutes at 37°C in the dark. Afterward, the cells' fluorescence intensities were detected by flowcytometry with excitation wavelengths at 488 nm and emission wavelengths at 525 and 585 nm for green and red fluorescence, respectively.

2.10 | Measurement of cytoC release

After being subjected to treatment and centrifugation, the cells were fixed and permeabilized using the True-Nuclear Transcription Factor Buffer Set. After being washed, the cells were stained with FITC anti-cytochrome C for 1 hour at room temperature. The fluorescence intensities were detected by flowcytometry with excitation and emission wavelengths at 488 and 525 nm, respectively.

2.11 | Measurement of intracellular ROS level

Intracellular ROS generation was determined by a semiquantitative DCFH-DA fluorescence assay as described in the previous research.[21] After being subjected to treatment and centrifugation, the cells were resuspended in PBS and incubated with 5 μM DCFH-DA for 30 minutes at 37°C in the dark. The fluorescence intensity of DCF fluorescence was assayed using a microplate reader with excitation and emission wavelengths at 488 and 525 nm, respectively.

2.12 | AOE activity assay

The activities of AOEs, including SOD, CAT, and GPx, were measured by commercial assay kits. The process for determining AOE activities was described in the previous research and performed in accordance with the manufacturer's instructions.[20]

2.13 | Statistical Analysis

Data were present as mean ± SD of three or more independent experiments. One-way analysis of variance followed by Bonferroni's post-hoc comparisons test was used for P-value calculations for multigroup comparison. Differences with a probability value of $P < .05$ were considered statistically significant for each test.

3 | RESULTS

3.1 | Effects of rutin on BisGMA-induced cytotoxicity in RAW264.7 macrophages

To study the effects of rutin on BisGMA-induced cytotoxicity in RAW264.7 macrophages, the cells were pretreated with various rutin concentrations for 30 minutes before the administration of BisGMA at a concentration of 50 μM for 24 hours. As shown in Figure 1, BisGMA-induced cytotoxicity was attenuated by rutin in a dose-dependent manner with a significant inhibitory effect beginning at 10 μM ($P < .05$).
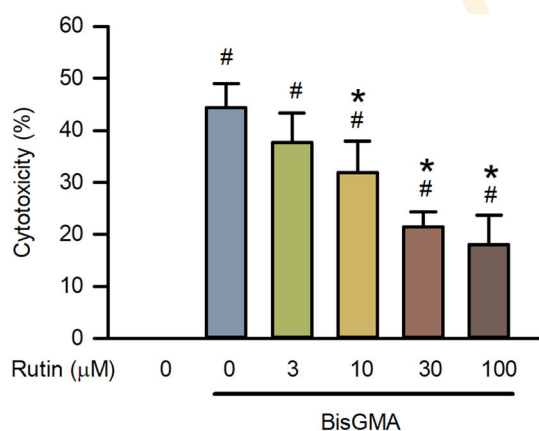
FIGURE 1 Effect of rutin on cytotoxicity in BisGMA-treated RAW264.7 macrophages. After macrophages were incubated with rutin at concentrations of 0-100 μM for 30 minutes, the cells were treated with or without BisGMA at 0.3 μM for 4 hours. Cytotoxicity was measured by an MTT colorimetric assay. Data were expressed as a percentage of the control group, which indicated treatment with BisGMA and rutin at a concentration of 0 μM. Results are expressed as means ±SD (n = 4). #$P < .05$ is considered statistically significant compared with the control group. *$P < .05$ is considered statistically significant compared with the BisGMA-treated group [Color figure can be viewed at wileyonlinelibrary.com]

3.2 | Effects of rutin on BisGMA-induced necrosis and apoptosis in RAW264.7 macrophages

After 24 hours of treatment, the partitions of necrosis and apoptosis were significantly considerably induced by BisGMA using annexin V-FITC and PI staining assay ($P < .05$). BisGMA-induced apoptosis was attenuated by rutin in a dose-dependent manner with a significant inhibitory effect beginning at 10 μM ($P < .05$). However, BisGMA-induced necrosis was not notably inhibited by rutin until the concentration at 30 μM (Figure 2A). Furthermore, we confirmed these results through sub-G1 formation analysis. As shown in Figure 2B, the formation of sub-G1 induced by BisGMA was inhibited by rutin in a dose-dependent manner with a significant inhibitory effect that began at 10 μM ($P < .05$).

3.3 | Effects of rutin on BisGMA-induced genotoxicity in RAW264.7 macrophages

MN and comet assay were used to study the protective effect of rutin on BisGMA-induced genotoxicity. MN formation was significantly induced by BisGMA as compared with the control group ($P < .05$). Pretreatment with rutin reduced BisGMA-induced MN formation in a dose-dependent manner with a significant inhibitory effect beginning at 10 μM ($P < .05$) (Figure 3A). Moreover, the tail length and %DNA in tail were significantly induced by BisGMA as compared with the control group ($P < .05$). Pretreatment with rutin reduced BisGMA-induced DNA damage in a dose-dependent manner and a significant inhibitory effect began at 10 μM ($P < .05$) (Figure 3B-D).

3.4 | Effects of rutin on BisGMA-induced caspase-3 and -9 activities in RAW264.7 macrophages

Caspase-3, -8, and -9 are key molecules in BisGMA-induced mitochondria-dependent apoptosis and genotoxicity in RAW264.7 cells.[17] Caspase-3, -8, and -9 activities were significantly induced by BisGMA as compared with the control group ($P < .05$). Pretreatment with rutin reduced BisGMA-induced caspase-3 and -9 activities in a dose-dependent manner with a significant inhibitory effect beginning at 10 μM ($P < .05$). However, BisGMA-induced caspase-8 activity was not significantly inhibited by rutin until it was at a concentration of 30 μM (Figure 4).

3.5 | Effects of rutin on BisGMA-induced cytoC release in RAW264.7 macrophages

Cytochrome C (cytoC) is released from mitochondria disruption and promotes caspase-9 activation.[22,23] CytoC liberation was significantly induced by BisGMA as compared with the control group ($P < .05$). Pretreatment with rutin reduced BisGMA-induced cytoC liberation in a dose-dependent manner with a significant inhibitory effect that began at 10 μM ($P < .05$; Figure 5).
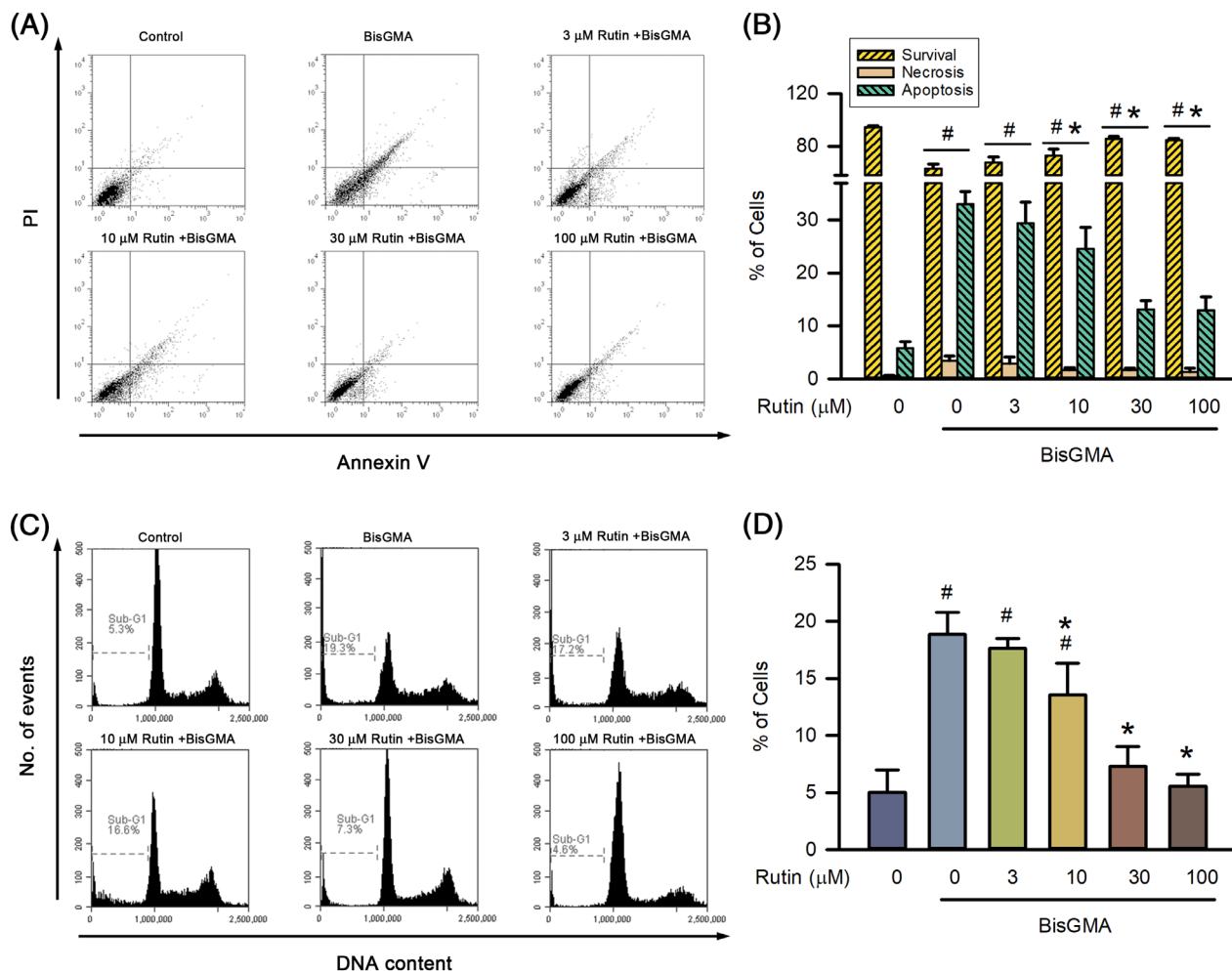
FIGURE 2 Effect of rutin on necrosis and apoptosis in BisGMA-treated RAW264.7 macrophages. After reaction and collection, the cells were stained with annexin V-FITC/PI and PI staining assay and analyzed by flowcytometry. A, The dot-plots of flowcytometry from the annexin V-FITC/PI staining assay are shown. B, After dot-plots quantitation was achieved, the percentage of necrosis, early apoptosis, late apoptosis, and viable cells was presented. C, The histograms of flow cytometry from a PI staining assay are shown. D, After histogram quantitation was conducted, the percentages of sub-G1 populations were presented. Results are expressed as means ±SD (n = 3). $^{\#}P < .05$ is considered statistically significant compared with the control group. $^{*}P < .05$ is considered statistically significant compared with the BisGMA-treated group [Color figure can be viewed at wileyonlinelibrary.com]

3.6 | Effects of rutin on BisGMA-induced mitochondrial dysfunction in RAW264.7 macrophages

As shown in Figure 6, mitochondrial dysfunction was significantly induced by BisGMA as compared with the control group ($P < .05$). Pretreatment with rutin reduced BisGMA-induced mitochondrial dysfunction in a dose-dependent manner with a significant inhibitory effect that began at 10 μM ($P < .05$; Figure 6).

3.7 | Effects of rutin on BisGMA-induced ROS generation in RAW264.7 macrophages

Generation of ROS participates in mitochondrial dysfunction in RAW264.7 macrophages treated with BisGMA. ROS generation was

significantly induced by BisGMA compared with the control group ($P < .05$). Pretreatment with rutin reduced BisGMA-induced ROS generation in a dose-dependent manner with a significant inhibitory effect that began at 10 μM ($P < .05$; Figure 7).

3.8 | Effects of rutin on BisGMA-inhibited AOE activities in RAW264.7 macrophages

For the protection of cell viability, the intracellular ROS is reduced by AOE, including GPx, SOD, and CAT. The AOE activities were significantly reduced by BisGMA as compared with the control group ($P < .05$). Pretreatment with rutin reversed BisGMA-reduced AOE activities in a dose-dependent manner with a significant reverse effect beginning at 10 μM ($P < .05$; Figure 8).

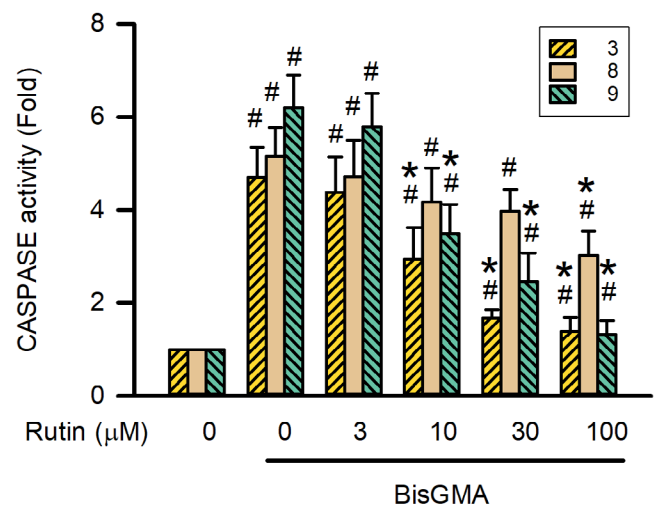**FIGURE 4** Effect of rutin on caspase activities in BisGMA-treated RAW264.7 macrophages. Results are expressed as means ±SD (n = 3). [#]$P < .05$ is considered statistically significant compared with the control group. *$P < .05$ is considered statistically significant compared with the BisGMA-treated group [Color figure can be viewed at wileyonlinelibrary.com]

FIGURE 3 Effect of rutin on genotoxicity in BisGMA-treated RAW264.7 macrophages. A, Effect of rutin on MN formation in BisGMA-treated RAW264.7 macrophages. B, After reactions and collections were achieved, the comet assay was conducted. DNA damages were quantified as tail moment (C) and tail length (D). Results are expressed as means ±SD (n = 3). [#]$P < .05$ is considered statistically significant compared with the control group. *$P < .05$ is considered statistically significant compared with the BisGMA-treated group [Color figure can be viewed at wileyonlinelibrary.com]

4 | DISCUSSION

Macrophages are effector cells of the nonspecific and innate immune system.[13,14] RAW264.7 cells are the murine macrophage cell line, which would not need the process of differentiation. The phenotype and functional characteristics of RAW 264.7 cell line remain stable through serial passages.[24] On the contrary, THP-1 cells and U937 cells, the human monocyte-like cell line, would be differentiated into macrophage-like cells by differentiators.[25] RAW264.7 cells are more characteristic of macrophages than THP-1 cells and U937 cells. Based on the previous studies, it has been proposed that the variability of RAW264.7 cells would be lower than the THP-1 cells and U937 cells due to the process of differentiation.[24,25] At present, we chose RAW264.7 cells for further study.

In clinical therapeutics, the polymer composite restorative materials are used in restoring the dental and bone cavities.[7,8] The most widely used monomer for the preparation of polymer composite restorative materials is BisGMA. The features of BisGMA contain high molecular weight and viscosity, low volatility, fast polymerization by organic light.[26] There is sufficient evidence to prove that BisGMA monomers dissociate from the polymer composite restorative materials after treatment with water- or organic-based solvents for 1-180 days.[9,10] Cytotoxicity could be induced by BisGMA in macrophages, dental pulp cells, and gingival fibroblasts, which can lead to oral inflammation.[11,12,17,27,28] In the previous study, it has been proposed that the treatment of RAW264.7 macrophages with 0.3 μM BisGMA for 4 hours can cause about 40% cytotoxicity.[17] At present, our results also showed that 44.37 ± 4.72% cytotoxicity induced by BisGMA at a concentration of 0.3 μM BisGMA for 4 hours in RAW264.7 macrophages. These findings were almost the same as

those reported earlier.[17] Rutin belongs to a group of plant bio-flavonoid glycoside compounds called vitamin P and has a capacity for cytoprotection, antiinflammation, neuroprotection, and cardio-protection.[1-6] Based on the previous study, it has been proposed that pretreatment of SH-SY5Y neurons with 1, 5, and 10 μM of rutin for 30 minutes significantly reverses the cytotoxic effect induced by rotenone.[29] In addition, pretreatment of RAW264.7 macrophages with 40 and 80 μM of rutin significantly reverse the nitric oxide production induced by LPS.[30] At present, pretreatment with 3-100 μM of rutin for 30 minutes significantly reverse the cytotoxic effect induced by BisGMA in RAW264.7 macrophages. Rutin considerably reduced BisGMA-induced cytotoxicity in a dose-dependent manner. According to these findings, we proposed that rutin could be a potential ameliorative reagent for BisGMA-induced macrophage cytotoxicity and proinflammatory response.

Apoptosis caused by BisGMA leads to cytotoxicity in several mammalian cells, including macrophages, dental pulp cells, and gingival fibroblasts.[17,25,31] Rutin inhibits apoptosis in the neuron of cadmium chloride ($CdCl_2$)-treated rat brain and pleural exudate cells of carrageenan-induced acute inflammation in rats.[32,33] In this study, we have demonstrated for the first time that RAW264.7 macrophages pretreated with rutin inhibit BisGMA-induced apoptosis in a dose-dependent manner through annexin V-FITC, PI staining assay, and sub-G1 formation analysis. Genotoxicity is another pathway in BisGMA-induced cytotoxicity in macrophages, gingival fibroblasts, and lymphocytes.[17,34,35] Genotoxicity and DNA damage are reduced by rutin in 2,5-hexanedione-treated rats and benzo(a)pyrene-treated mice.[36,37] Radiation-induced genotoxicity is reduced by rutin in lymphocytes.[38] Rutin administration in the present study significantly mitigated genotoxicity and DNA damage in BisGMA-incubated RAW264.7 macrophages through MN and comet assays, respectively. These results support the hypothesis that the reduction in BisGMA-induced cytotoxicity from rutin preincubation is associated with genotoxicity and apoptosis.

Under BisGMA stimulation of RAW264.7 macrophages, the caspase-dependent apoptotic pathway, which contains intrinsic and extrinsic pathways, activates caspase-3 leading to genotoxicity and apoptosis.[3,17] The proteolytic maturation of caspase-3, the
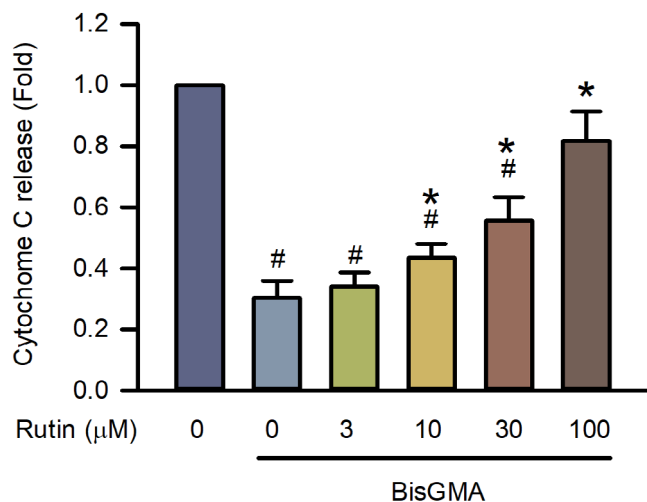
FIGURE 5 Effect of rutin on cytoC release in BisGMA-treated RAW264.7 macrophages. Results are expressed as means ±SD (n = 3). #$P < .05$ is considered statistically significant compared with the control group. *$P < .05$ is considered statistically significant compared with the BisGMA-treated group [Color figure can be viewed at wileyonlinelibrary.com]
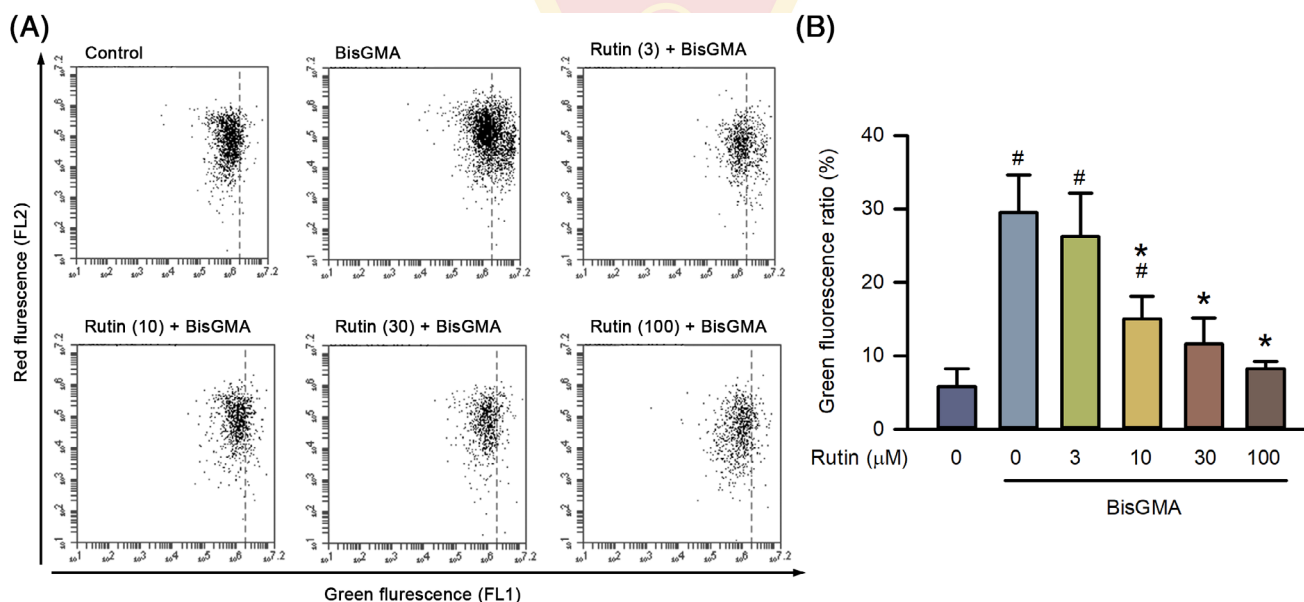
FIGURE 6 Effect of rutin on mitochondrial dysfunction in BisGMA-treated RAW264.7 macrophages. Results are expressed as means ±SD (n = 3). #$P < .05$ is considered statistically significant compared with the control group. *$P < .05$ is considered statistically significant compared with the BisGMA-treated group [Color figure can be viewed at wileyonlinelibrary.com]

executioner caspase, is induced by the activation of caspase-8 and -9.[22] Extrinsic apoptosis can be initiated through caspase-8 activation via the formation of death-inducing signaling complex recruited by death receptor activation.[39] The intrinsic apoptosis can be initiated through caspase-9 activation via apoptosome formation, which is generated by cytoC combined with Apaf-1 in the cytosol. CytoC releases into the cytosol due to mitochondria disruption induced by an apoptotic stimulator.[22,23] Rutin inhibits apoptosis through preserving mitochondrial integrity in the brain of $CdCl_2$-treated rats and mice with traumatic brain injury.[40,41] Mitochondrial apoptosis induced by hydrogen peroxide (H_2O_2) is inhibited by rutin in human umbilical vein endothelial cells.[42] The present study first revealed that a concentration of rutin under 30 μM could not significantly strongly inhibit BisGMA-induced caspase-8 activation. By contrast, rutin inhibited BisGMA-induced caspase-3 and -9 activation in a dose-dependent manner and started a significant concentration of

rutin at 10 μM. Moreover, pretreatment with rutin reduced cytoC release and mitochondria disruption in the BisGMA-treatment macrophages in a dose-dependent manner and started a significant concentration of rutin at 10 μM. Parallel trends were observed in the inhibition of caspase-3 and -9 activities, cytoC release, mitochondria disruption, apoptosis, and genotoxicity. Therefore, the reduction in BisGMA-induced apoptosis and genotoxicity from rutin pretreatment was associated with the activation of the mitochondrial apoptotic pathway.

The generation of intracellular ROS triggers the activation of the mitochondrial apoptotic pathway.[43] In H_2O_2-treated human umbilical vein endothelial cells, pretreatment rutin attenuates excessive ROS generation.[42] Rutin ameliorates carbon tetrachloride or vancomycin-induced kidney injury in mice models.[44,45] In the present study, levels of intracellular ROS could be reduced by rutin in BisGMA-treated macrophages. AOEs are capable of the deactivation and detoxification of ROS. Superoxide anion is rapidly converted by SOD into H_2O_2, which is transformed by CAT and GPx into H_2O.[46] Rutin significantly enhanced activities of SOD, CAT, and GPx in $CdCl_2$-treated rat brains, cobalt chloride-treated H9c2 myoblast cells, and endotoxin-treated injured kidneys and lungs.[6,40,47,48] We propose that pretreatment with rutin raised the activation level of SOD, CAT, and GPx in BisGMA-treated macrophages. These results indicated that rutin is able to reduce BisGMA-induced cytotoxicity and genotoxicity through the upregulation of AOE activation.

Flavonols are the most important member of secondary metabolite phytochemicals having the polyphenolic structure, which is the effective scavenger of free oxygen radicals both in vitro and in vivo.[49] The scavenging properties of oxidizing species have been found to exist on rutin, a type of flavonol.[50] Nicotinamide adenine dinucleotide phosphate oxidase (NOX)4, which is localized in mitochondria, is one of the intracellular ROS generating sources.[51] Excess ROS expression increases with NOX4 activation and results in DNA damage.[52] Rutin has been implemented in ROS-related dysfunction of the vascular endothelium and pulmonary arterial cells via NOX4 inhibition.[53,54] Based on these studies, we could hypothesize that BisGMA-induced toxic effects would be reduced by rutin via oxygen radical scavenging activity and NOX4 inhibition.

FIGURE 7 Effect of rutin on ROS generation in BisGMA-treated RAW264.7 macrophages. Results are expressed as means ±SD (n = 3). [#]$P < .05$ is considered statistically significant compared with the control group. [*]$P < .05$ is considered statistically significant compared with the BisGMA-treated group [Color figure can be viewed at wileyonlinelibrary.com]
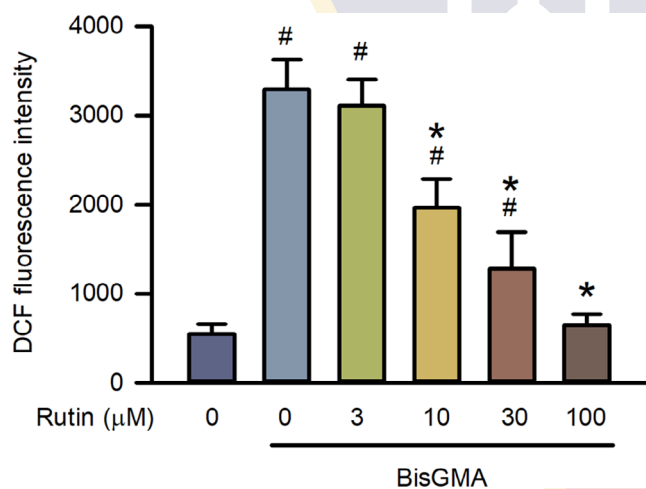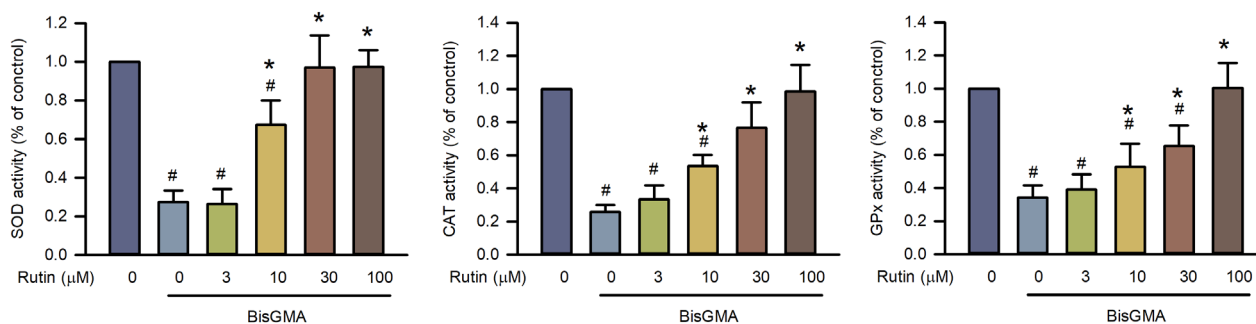

FIGURE 8 Effect of rutin on AOE activities in BisGMA-treated RAW264.7 macrophages. Results are expressed as means ±SD (n = 3). [#]$P < .05$ is considered statistically significant compared with the control group. [*]$P < .05$ is considered statistically significant compared with the BisGMA-treated group [Color figure can be viewed at wileyonlinelibrary.com]
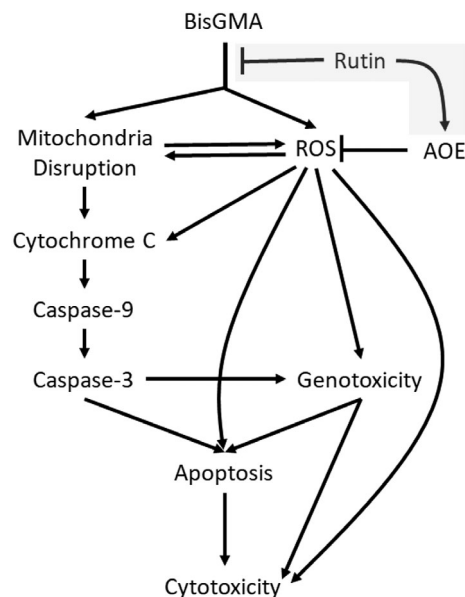
FIGURE 9 Schemes of the protective mechanisms of rutin on BisGMA-treated RAW264.7 macrophages

In conclusion, we demonstrated that macrophage cytotoxicity could be inhibited by rutin in BisGMA-treated RAW264.7 macrophages through apoptosis (Figure 9). The reduction of apoptosis was due to the inhibition of genotoxicity through reduced caspase-3 activation after treatment with rutin before BisGMA administration. BisGMA-induced caspase-3 activation was inhibited by rutin through the inhibition of caspase-8 rather than caspase-9. Moreover, rutin inhibited caspase-8 activity by downregulating the activation of mitochondrial apoptotic pathways, including cytoC release and mitochondria disruption. Finally, the protective mechanism of rutin on the BisGMA-induced activation of the mitochondrial apoptotic pathway included the diminution of ROS generation and the elevation of AOE activation. These findings show the capacity of rutin used for the reagent for the prevention of BisGMA-induced cytotoxicity, mitochondrial apoptosis, and genotoxicity in macrophages.

ACKNOWLEDGMENTS

CONFLICT OF INTEREST

The authors declare no potential conflict of interest.

ORCID

Yu-Hsiang Kuan https://orcid.org/0000-0002-8991-6394

REFERENCES

1. Nkpaa KW, Onyeso GI, Kponee KZ. Rutin abrogates manganese-induced striatal and hippocampal toxicity via inhibition of iron depletion, oxidative stress, inflammation and suppressing the NF-κB signaling pathway. *J Trace Elem Med Biol.* 2019;53:8-15.
2. Gęgotek A, Ambrożewicz E, Jastrząb A, Jarocka-Karpowicz I, Skrzydlewska E. Rutin and ascorbic acid cooperation in antioxidant and antiapoptotic effect on human skin keratinocytes and fibroblasts exposed to UVA and UVB radiation. *Arch Dermatol Res.* 2019;311:203-219.
3. Huang YC, Horng CT, Chen ST, et al. Rutin improves endotoxin-induced acute lung injury via inhibition of iNOS and VCAM-1 expression. *Environ Toxicol.* 2016;31:185-191.
4. Xianchu L, Lan Z, Ming L, Yanzhi M. Protective effects of rutin on lipopolysaccharide-induced heart injury in mice. *J Toxicol Sci.* 2018; 43:329-337.
5. Deepika MS, Thangam R, Sheena TS, et al. A novel rutin-fucoidan complex based phytotherapy for cervical cancer through achieving enhanced bioavailability and cancer cell apoptosis. *Biomed Pharmacother.* 2019;109:1181-1195.
6. Yeh CH, Yang JJ, Yang ML, Li YC, Kuan YH. Rutin decreases lipopolysaccharide-induced acute lung injury via inhibition of oxidative stress and the MAPK-NF-κB pathway. *Free Radic Biol Med.* 2014; 69:249-257.
7. Hamid A, Hume WR. A study of component release from resin pit and fissure sealants in vitro. *Dent Mater.* 1997;13:98-102.
8. Soderholm KJ, Mariotti A. BIS-GMA–based resins in dentistry: are they safe? *J Am Dent Assoc.* 1999;130:201-209.
9. Sideridou I, Tserki V, Papanastasiou G. Effect of chemical structure on degree of conversion in light-cured dimethacrylate-based dental resins. *Biomaterials.* 2002;2002:1819-1829.
10. Van Landuyt KL, Nawrot T, Geebelen B, et al. How much do resin-based dental materials release? A meta-analytical approach. *Dent Mater.* 2011;27:723-747.
11. Yap AU, Han VT, Soh MS, Siow KS. Elution of leachable components from composites after LED and halogen light irradiation. *Oper Dent.* 2004;29:448-453.
12. Bakopoulou A, Papadopoulos T, Garefis P. Molecular toxicology of substances released from resin-based dental restorative materials. *Int J Mol Sci.* 2009;10:3861-3899.
13. Weiss G, Schaible UE. Macrophage defense mechanisms against intracellular bacteria. *Immunol Rev.* 2015;264:182-203.
14. Wang Y, Smith W, Hao D, He B, Kong L. M1 and M2 macrophage polarization and potentially therapeutic naturally occurring compounds. *Int Immunopharmacol.* 2019;70:459-466.
15. Mytych J, Romerowicz-Misielak M, Koziorowski M. Long-term culture with lipopolysaccharide induces dose-dependent cytostatic and cytotoxic effects in THP-1 monocytes. *Toxicol In Vitro.* 2017;42:1-9.
16. Huang FM, Chang YC, Lee SS, et al. Bisphenol A exhibits cytotoxic or genotoxic potential via oxidative stress-associated mitochondrial apoptotic pathway in murine macrophages. *Food Chem Toxicol.* 2018; 122:215-224.
17. Li YC, Kuan YH, Huang FM, Chang YC. The role of DNA damage and caspase activation in cytotoxicity and genotoxicity of macrophages induced by bisphenol-A-glycidyl-dimethacrylate. *Int Endod J.* 2012; 45:499-507.
18. Kuan YH, Li YC, Huang FM, Chang YC. The upregulation of tumour necrosis factor-A and surface antigens expression on macrophages by bisphenol A-glycidyl-methacrylate. *Int Endod J.* 2012;45:619-626.
19. Huang FM, Chang YC, Lee SS, Yang ML, Kuan YH. Expression of pro-inflammatory cytokines and mediators induced by bisphenol A via ERK-NFκB and JAK1/2-STAT3 pathways in macrophages. *Environ Toxicol.* 2019;34:486-494.
20. Chien KJ, Yang ML, Tsai PK, et al. Safrole induced cytotoxicity, DNA damage, and apoptosis in macrophages via reactive oxygen species

generation and Akt phosphorylation. *Environ Toxicol Pharmacol*. 2018; 64:94-100.

21. Lee CY, Su CH, Tsai PK, et al. Cadmium nitrate-induced neuronal apoptosis is protected by N-acetyl-l-cysteine via reducing reactive oxygen species generation and mitochondria dysfunction. *Biomed Pharmacother*. 2018;108:448-456.

22. Tait SW, Green DR. Mitochondria and cell death: outer membrane permeabilization and beyond. *Nat Rev Mol Cell Biol*. 2010;11:621-632.

23. Raychaudhuri S, Skommer J, Henty K, Birch N, Brittain T. Neuroglobin protects nerve cells from apoptosis by inhibiting the intrinsic pathway of cell death. *Apoptosis*. 2010;15:401-411.

24. Taciak B, Białasek M, Braniewska A, et al. Evaluation of phenotypic and functional stability of RAW 264.7 cell line through serial passages. *PLoS One*. 2018;13:e0198943.

25. Madhvi A, Mishra H, Leisching GR, Mahlobo PZ, Baker B. Comparison of human monocyte derived macrophages and THP1-like macrophages as in vitro models for M. tuberculosis infection. *Comp Immunol Microbiol Infect Dis*. 2019;67:101355.

26. Srivastava R, Liu J, He C, et al. BisGMA analogues as monomers and diluents for dental restorative composite materials. *Mater Sci Eng C Mater Biol Appl*. 2018;88:25-31.

27. Chang MC, Chen LI, Chan CP, et al. The role of reactive oxygen species and hemeoxygenase-1 expression in the cytotoxicity, cell cycle alteration and apoptosis of dental pulp cells induced by BisGMA. *Biomaterials*. 2010;31:8164-8171.

28. Urcan E, Haertel U, Styllou M, Hickel R, Scherthan H, Reichl FX. Real-time xCELLigence impedance analysis of the cytotoxicity of dental composite components on human gingival fibroblasts. *Dent Mater*. 2010;26:51-58.

29. Park SE, Sapkota K, Choi JH, et al. Rutin from Dendropanax morbifera Leveille protects human dopaminergic cells against rotenone induced cell injury through inhibiting JNK and p38 MAPK signaling. *Neurochem Res*. 2014;39:707-718.

30. Su KY, Yu CY, Chen YP, Hua KF, Chen YLS. 3,4-Dihydroxytoluene, a metabolite of rutin, inhibits inflammatory responses in lipopolysaccharide-activated macrophages by reducing the activation of NF-κB signaling. *BMC Complement Altern Med*. 2014;14:21.

31. Engelmann J, Janke V, Volk J, et al. Effects of BisGMA on glutathione metabolism and apoptosis in human gingival fibroblasts in vitro. *Biomaterials*. 2004;25:4573-4580.

32. Abdel-Aleem GA, Khaleel EF. Rutin hydrate ameliorates cadmium chloride-induced spatial memory loss and neural apoptosis in rats by enhancing levels of acetylcholine, inhibiting JNK and ERK1/2 activation and activating mTOR signalling. *Arch Physiol Biochem*. 2018;124:367-377.

33. Adefegha SA, Leal DBR, de Oliveira JS, Manzoni AG, Bremm JM. Modulation of reactive oxygen species production, apoptosis and cell cycle in pleural exudate cells of carrageenan-induced acute inflammation in rats by rutin. *Food Funct*. 2017;8:4459-4468.

34. Lottner S, Shehata M, Hickel R, Reichl FX, Durner J. Effects of antioxidants on DNA-double strand breaks in human gingival fibroblasts exposed to methacrylate based monomers. *Dent Mater*. 2013;29:991-998.

35. Drozdz K, Wysokinski D, Krupa R, Wozniak K. Bisphenol A-glycidyl methacrylate induces a broad spectrum of DNA damage in human lymphocytes. *Arch Toxicol*. 2011;85:1453-1461.

36. Muhammad A, Arthur DE, Babangida S, et al. Modulatory role of rutin on 2,5-hexanedione-induced chromosomal and DNA damage in rats: validation of computational predictions. *Drug Chem Toxicol*. 2020;43 (2):113-126.

37. Shahid A, Ali R, Ali N, et al. Attenuation of genotoxicity, oxidative stress, apoptosis and inflammation by rutin in benzo(a)pyrene exposed lungs of mice: plausible role of NF-κB, TNF-α and Bcl-2. *J Complement Integr Med*. 2016;13:17-29.

38. Patil SL, Swaroop K, Kakde N, Somashekarappa HM. In vitro protective effect of rutin and quercetin against radiation-induced genetic damage in human lymphocytes. *Indian J Nucl Med*. 2017;32:289-295.

39. Stel AJ, Ten Cate B, Jacobs S, et al. Fas receptor clustering and involvement of the death receptor pathway in rituximab-mediated apoptosis with concomitant sensitization of lymphoma B cells to fas-induced apoptosis. *J Immunol*. 2007;178:2287-2295.

40. Mostafa DG, Khaleel EF, Badi RM, et al. Rutin hydrate inhibits apoptosis in the brains of cadmium chloride-treated rats via preserving the mitochondrial integrity and inhibiting endoplasmic reticulum stress. *Neurol Res*. 2019;41(7):594-608.

41. Zhai X, Ding Y, Wang Q, Zhang H, Li F. Rutin acid ameliorates neural apoptosis induced by traumatic brain injury via mitochondrial pathways in mice. *Neuroimmunomodulation*. 2016;23:179-187.

42. Gong G, Qin Y, Huang W, Zhou S, Yang X, Li D. Rutin inhibits hydrogen peroxide-induced apoptosis through regulating reactive oxygen species mediated mitochondrial dysfunction pathway in human umbilical vein endothelial cells. *Eur J Pharmacol*. 2010;628:27-35.

43. Wu Y, Zhao D, Zhuang J, Zhang F, Xu C. Caspase-8 and Caspase-9 functioned differently at different stages of the cyclic stretch-induced apoptosis in human periodontal ligament cells. *PLoS One*. 2016;11: e0168268.

44. Ma JQ, Liu CM, Yang W. Protective effect of rutin against carbon tetrachloride-induced oxidative stress, inflammation and apoptosis in mouse kidney associated with the ceramide, MAPKs, p53 and calpain activities. *Chem Biol Interact*. 2018;286:26-33.

45. Qu S, Dai C, Lang F, et al. Rutin attenuates vancomycin-induced nephrotoxicity by ameliorating oxidative stress, apoptosis, and inflammation in rats. *Antimicrob Agents Chemother*. 2018;63:e01545-18.

46. Schieber M, Chandel NS. ROS function in redox signaling and oxidative stress. *Curr Biol*. 2014;24:R453-R462.

47. Sundaram RL, Sali VK, Vasanthi HR. Protective effect of rutin isolated from Spermococe hispida against cobalt chloride-induced hypoxic injury in H9c2 cells by inhibiting oxidative stress and inducing apoptosis. *Phytomedicine*. 2018;51:196-204.

48. Khajevand-Khazaei MR, Mohseni-Moghaddam P, Hosseini M, et al. Rutin, a quercetin glycoside, alleviates acute endotoxemic kidney injury in C57BL/6 mice via suppression of inflammation and up-regulation of antioxidants and SIRT1. *Eur J Pharmacol*. 2018;833:307-313.

49. Garg SK, Shukla A, Choudhury S. Polyphenols and flavonoids. In: Gupta R, Srivastava A, Lall R, eds. *Nutraceuticals in Veterinary Medicine*. Cham: Springer; 2019:187-204.

50. Kamalakkannan N, Prince PS. Antihyperglycaemic and antioxidant effect of rutin, a polyphenolic flavonoid, in streptozotocin-induced diabetic wistar rats. *Basic Clin Pharmacol Toxicol*. 2006;98:97-103.

51. Vendrov AE, Vendrov KC, Smith A, et al. NOX4 NADPH oxidase-dependent mitochondrial oxidative stress in aging-associated cardiovascular disease. *Antioxid Redox Signal*. 2015;23:1389-1409.

52. Canugovi C, Stevenson MD, Vendrov AE, et al. Increased mitochondrial NADPH oxidase 4 (NOX4) expression in aging is a causative factor in aortic stiffening. *Redox Biol*. 2019;26:101288.

53. Wang W, Wu QH, Sui Y, Wang Y, Qiu X. Rutin protects endothelial dysfunction by disturbing Nox4 and ROS-sensitive NLRP3 inflammasome. *Biomed Pharmacother*. 2017;86:32-40.

54. Li Q, Qiu Y, Mao M, et al. Antioxidant mechanism of Rutin on hypoxia-induced pulmonary arterial cell proliferation. *Molecules*. 2014;19:19036-19049.

The Association Between Pleural Empyema and Peripheral Arterial Disease in Younger Patients: A Retrospective National Population-Based Cohort Study

Tzu-Yuan Wang [1,2†], Hsin-Hung Chen [3,4,5†], Chun-Hung Su [6,7], Sheng-Pang Hsu [8], Chun-Wei Ho [9], Ming-Chia Hsieh [9,10,11], Cheng-Li Lin [12,13] and Chia-Hung Kao [14,15,16,17]*

[1] Department of Internal Medicine, College of Medicine, China Medical University, Taichung, Taiwan, [2] Division of Endocrinology and Metabolism, China Medical University Hospital, Taichung, Taiwan, [3] Division of Endocrinology and Metabolism, Department of Internal Medicine, Asia University Hospital, Taichung, Taiwan, [4] School of Medicine, Institute of Medicine and Public Health, Chung Shan Medical University, Taichung, Taiwan, [5] Chung Sheng Clinic, Nantou, Taiwan, [6] Institute of Medicine, School of Medicine, Chung Shan Medical University, Taichung, Taiwan, [7] Division of Cardiology, Department of Internal Medicine, Chung Shan Medical University Hospital, Taichung, Taiwan, [8] Division of Endocrinology and Metabolism, Department of Medicine, Everan Hospital, Taichung, Taiwan, [9] Intelligent Diabetes Metabolism and Exercise Center, China Medical University Hospital, Taichung, Taiwan, [10] Graduate Institute of Integrative Medicine, China Medical University, Taichung, Taiwan, [11] Division of Clinical Nutrition, China Medical University Hospital, Taichung, Taiwan, [12] Management Office for Health Data, China Medical University Hospital, Taichung, Taiwan, [13] College of Medicine, China Medical University, Taichung, Taiwan, [14] Graduate Institute of Biomedical Sciences Science, College of Medicine, China Medical University, Taichung, Taiwan, [15] Department of Nuclear Medicine and PET Center, China Medical University Hospital, Taichung, Taiwan, [16] Department of Bioinformatics and Medical Engineering, Asia University, Taichung, Taiwan, [17] Center of Augmented Intelligence in Healthcare, China Medical University Hospital, Taichung, Taiwan

Background: To investigate the relationship between pleural empyema (PE) and peripheral arterial disease (PAD).

Methods: We conducted a retrospective cohort study using data from the National Health Institute Research Database. Univariable and multivariable Cox's proportional hazard regressions were performed to investigate the association between PE and the risk of PAD. Kaplan–Meier method and the differences were assessed using a log-rank test.

Results: The overall incidence of PAD was higher in the PE cohort than in the non-PE cohort (2.76 vs. 1.72 per 1,000 person-years) with a crude hazard ratio (HR) of 1.61 [95% confidence interval (CI) = 1.41–1.83]. After adjustment for age, gender, and comorbidities, patients with PE were noted to be associated with an increased risk of PAD compared with those without PE [adjusted HR (aHR) = 1.18, 95% CI = 1.03–1.35]. Regarding the age-specific comparison between the PE and non-PE cohorts, PAD was noted to be significantly high in the ≤49 years age group (aHR = 5.34, 95% CI = 2.34–10.1). The incidence of PAD was higher in the first 2 years, with an aHR of 1.35 (95% CI = 1.09–1.68) for patients with PE compared with those without PE.

Conclusion: The risk of PAD was higher if patients with PE were younger than 49 years and within the 2-year diagnosis of PE.

Keywords: pleural empyema, peripheral arterial disease, retrospective cohort study, NHIRD, National Health Insurance Research Database, Cox regression hazard model

WHAT IS ALREADY KNOWN ABOUT THIS TOPIC?

1. A previous report mentioned the association between PE and vascular diseases.
2. However, the association between PE and PAD is unknown.

WHAT DOES THIS ARTICLE ADD?

1. Our analysis determined that patients with PE had an increased risk of PAD.
2. Especially, they were younger than 49 years, of the female sex, and within the 2-year diagnosis of PE.

INTRODUCTION

In the United States, pleural empyema (PE) affects up to 65,000 patients annually, resulting in an estimated cost of 500 million dollars and a 15% mortality rate (1, 2). The etiology of PE varies from benign inflammatory disease to malignancy (3). PE could occur with pneumonia or secondary to thoracic surgery or chest injury and might cause the collection of purulent fluid in the pleural space. One study revealed that more than half of patients with bacterial pneumonia had PE (4–6). PE has various stages, such as exudative, fibrinopurulent, and organized phases, with its entire course lasting approximately 3–6 weeks. Notably, PE treatment included medicines such as antibiotics or surgical interventions for complete drainage of the infected fluid. Over the years, the incidence of PE has increased worldwide despite the availability of efficient therapies. One report mentioned that the rate of PE in adults caused by pneumococcal pneumonia increased from 7.6 to 14.9% (7, 8).

Peripheral arterial disease (PAD) is a lethal systemic disease caused by atherosclerosis resulting in a two- to six-fold increase in both cardiovascular and cerebrovascular diseases. The annual mortality rate of PAD was 4–6% (9, 10). The overall prevalence of PAD in adults was reported to be 12% in America. Notably, an estimated 8–10 million Americans were diagnosed as having PAD (11). Risk factors of PAD included old age, male sex in the younger age group, smoking, diabetes, hypertension, and dyslipidemia. PAD is characterized by an increased risk of coronary and cerebrovascular events, with a 15%—25% rate of carotid artery stenosis and a 30–50% incidence of coronary artery disease (CAD) (12, 13).

A previous report mentioned the association between PE and vascular diseases, such as stroke and aortic aneurysm, or systemic diseases, such as diabetes and kidney disease (14–17). However, the association between PE and PAD is unknown, and our study used the national claims data to investigate the probability of PAD development in patients with PE.

METHODS

Data Source

We conducted a retrospective cohort study by using data from the Taiwan National Health Institute Research Database (NHIRD), which was released by the Taiwan National Health Research Institutes. The National Health Insurance program is a mandatory universal health insurance program that offers comprehensive medical care coverage to all Taiwan residents (approximately more than 25 million) (18). Nevertheless, to protect the confidentiality of patients, the data on medical claims have been cryptographically scrambled. For this cohort study, we used a subset of the NHIRD, including files of inpatient claims and registry of beneficiaries. Diagnoses were coded based on the International Classification of Diseases, 9th Edition Clinical Modification (ICD-9-CM). This study was approved by the Institutional Review Board of China Medical University (CMUH104-REC2-115-AR4).

Sampled Participants

This study collected the complete medical information of patients aged > 20 years who were hospitalized for PE (ICD-9-CM codes 510, 510.0, 510.9) between January 1, 2000, and December 31, 2010, but had no previous medical history of PAD (ICD-9-CM codes 440.0, 440.2, 440.3, 440.8, 440.9, 443, 444.0, 444.22, 444.8, 447.8, and 447.9). The dates of the first health care admission for PE were defined as the index dates. We also excluded a history of empyema that was due to cancer. Overall, the PE cohort comprised 31,051 patients. Four non-PE control subjects for each PE case were frequency-matched based on gender, age group (5-year span), and the calendar year of the index date. Control individuals with a history of PAD before the index date, who had a history of empyema that was due to cancer, and who had incomplete medical records were excluded and replaced with another qualified control subject. Finally, 122,669 non-PE control subjects were included in this study.

Outcome and Comorbidities

Both PE and non-PE cohorts were followed up until PAD development, being censored due to loss to follow-up, or the end of 2011. Baseline comorbidities including diabetes (ICD-9-CM code 250), hypertension (ICD-9-CM codes 401–405), hyperlipidemia (ICD-9-CM code 272), chronic obstructive pulmonary disease (COPD) (ICD-9-CM codes 491, 492, 496), heart failure (ICD-9-CM codes 428), stroke (ICD-9-CM codes 430–438), and CAD (ICD-9-CM codes 410–414) were considered crucial factors affecting PAD occurrence.

TABLE 1 | Comparisons in demographic characteristics and comorbidities in patients with and without pleural empyema.

	Pleural empyema		P-value
	No	**Yes**	
	(N =122,669)	**(N =31,051)**	
Gender			0.91
Women	27,990(22.8)	7,076(22.8)	
Men	94,679(77.2)	23,975(77.2)	
Age stratified			0.69
≤49	31,854(26.0)	7,982(25.7)	
50–64	31,641(25.8)	7,986(25.7)	
65–74	40,121(32.7)	10,199(32.9)	
75+	19,053(15.5)	4,884(15.7)	
Age, mean ± SD[a]	61.5±16.9	62.3±16.8	<0.001
Comorbidity			
Diabetes	9,181(7.48)	9,440(30.4)	<0.001
Hypertension	18,594(15.2)	11,935(38.4)	<0.001
Hyperlipidemia	4,204(3.43)	2,246(7.23)	<0.001
COPD	5,698(4.65)	6,385(20.6)	<0.001
Heart failure	3,052(2.49)	3,259(10.5)	<0.001
CAD	9,220(7.52)	4,857(15.6)	<0.001
Stroke	8,527 (6.95)	6,847(22.1)	<0.001

Chi-square test, [a]t-test.

FIGURE 1 | Cumulative incidence of peripheral arterial disease in patients with pleural empyema and comparison patients.

Statistical Analysis

We presented the mean and standard deviation for age and number and percentage for gender, age group, and comorbidities. The t-test and chi-square test were used to examine the distribution differences for continuous and categorical variables, respectively. We calculated the follow-up time in person-years to assess the incident density rates until the PAD was either identified or censored. We used univariable and multivariable Cox's proportional hazard regressions to investigate the association between PE and the risk of PAD over time, indicated by the hazard ratio (HR) with a 95% confidence interval (CI). The multivariable model was simultaneously adjusted for age, gender, and comorbidities of diabetes, hypertension, hyperlipidemia, COPD, heart failure, CAD, and stroke. In addition, after stratification based on gender, age, and follow-up time, the relative risk of PAD development in patients with PE was compared with that of the non-PE cohort. The comparative cumulative incidence of PAD between the PE and non-PE cohorts was assessed using the Kaplan–Meier method, and the differences were assessed using a log-rank test. All statistical analyses were performed using the SAS package (version 9.3 for Windows; SAS Institute, Inc., Cary, NC, USA). We adopted a two-tailed P-value of <0.05 as statistically significant.

RESULTS

Table 1 presents the demographic characteristics and comorbidities of the study sample. This study had more male patients (77.2%), and 48.6% of the patients were of age more than 65 years (mean age 62.3 ± 16.8 years in the PE cohort and 61.5 ± 16.9 years in the non-PE cohort). Patients in the PE cohort exhibited a higher prevalence of comorbidities than those in the non-PE cohort (all P < 0.001). The average follow-up period was 3.49 years for the subjects with PE and 5.40 years for the non-PE cohort. The Kaplan–Meier analysis revealed that patients with PE had a significantly higher cumulative incidence of PAD than the non-PE controls (log-rank test, P < 0.001; **Figure 1**). The overall incidence of PAD was 61% higher in the PE cohort than in the non-PE cohort (2.76 vs. 1.72 per 1,000 person-years) with a crude HR of 1.61 (95% CI = 1.41–1.83) in the following 12 years (**Table 2**). After adjustment for age, gender, and comorbidities of diabetes, hypertension, hyperlipidemia, COPD, heart failure, CAD, and stroke, patients with PE were observed to be associated with an increased risk of PAD compared with those without PE [adjusted HR (aHR) = 1.18, 95% CI = 1.03–1.35]. The PAD incidence was higher with increased age and in those with comorbidities. Notably, compared with young adults (≤49 years of age), the aHR was 13.8 (95% CI = 10.5–18.2) for patients older than 75 years, 7.78 (95% CI = 5.98–10.1) for those aged 65–74 years, and 3.29 (95% CI 2.48–4.37) for those aged 50–64 years. Multivariate models revealed that PAD was independently associated with diabetes (aHR = 2.96, 95% CI = 2.61–3.35), hypertension (aHR = 1.49, 95% CI = 1.30–1.70), hyperlipidemia (aHR = 1.20, 95% CI = 1.00–1.44), heart failure (aHR = 1.82, 95% CI = 1.52–2.18), CAD (aHR = 1.39, 95% CI = 1.20–1.60), and stroke (aHR = 1.42, 95% CI = 1.24–1.64). The incidence of PAD was slightly higher in women than in men and increased with age in both cohorts (**Table 3**). A comparison between age-specific PE and non-PE cohorts revealed that the aHR

TABLE 2 | Incidence and hazard ratio for peripheral arterial disease and peripheral arterial disease-associated risk factor.

Variable	Event	PY	Rate[#]	Crude HR (95% CI)	Adjusted HR[†] (95% CI)
Pleural empyema					
No	1,140	662,279	1.72	1.00	1.00
Yes	299	108,518	2.76	1.61(1.41, 1.83)***	1.18(1.03, 1.35)*
Age, year					
≤49	62	233,569	0.27	1.00	1.00
50–64	224	213,823	1.05	3.99(3.01, 5.29)***	3.29(2.48, 4.37)***
65–74	725	244,851	2.96	11.4(8.83, 14.8)***	7.78(5.98, 10.1)***
75+	428	78,554	5.45	22.2(17.0, 29.1)***	13.8(10.5, 18.2)***
Gender					
Women	391	175,676	2.23	1.26(1.13, 1.42)***	1.04(0.92,1.17)
Men	1,048	595,121	1.76	1.00	1.00
Comorbidity					
Diabetes					
No	946	705,843	1.34	1.00	1.00
Yes	493	64,954	7.59	5.85(5.24, 6.52)***	2.96(2.61, 3.35)***
Hypertension					
No	815	663,572	1.23	1.00	1.00
Yes	624	107,225	5.82	4.96(4.46, 5.51)***	1.49(1.30, 1.70)***
Hyperlipidemia					
No	1,288	746,851	1.72	1.00	1.00
Yes	151	23,946	6.31	3.73(3.15, 4.41)***	1.20(1.00, 1.44)*
COPD					
No	1232	734,981	1.68	1.00	1.00
Yes	207	35,815	5.78	3.54(3.05, 4.11)***	1.11(0.95, 1.31)
Heart failure					
No	1,268	754,791	1.68	1.00	1.00
Yes	171	16,006	10.7	6.58(5.60, 7.73)***	1.82(1.52, 2.18)***
CAD					
No	1,096	721,861	1.52	1.00	1.00
Yes	343	48,936	7.01	4.74(4.19, 5.35)***	1.39(1.20, 1.60)***
Stroke					
No	1,120	724,096	1.55	1.00	1.00
Yes	319	46,701	6.83	4.59(4.04, 5.20)***	1.42(1.24, 1.64)***

[#] Rate, incidence rate, per 1,000 person-years.
Crude HR, relative hazard ratio; [†] adjusted HR: multiple analysis including age, gender, and comorbidities of diabetes, hypertension, hyperlipidemia, COPD, heart failure, CAD, and stroke; *$p < 0.05$, ***$p < 0.001$.

of PAD was significantly higher in the ≤49 years age group (aHR = 5.34, 95% CI = 2.82–10.1). The incidence density rate of PAD was higher in the first 2 years, with an aHR of 1.35 (95% CI = 1.09–1.68) for patients with PE compared with those without PE.

DISCUSSION

To the best of our knowledge, this is the first nationwide retrospective cohort study to evaluate the PAD risk associated with PE. Notably, patients with PE had a 1.18-fold higher risk of PAD than those without PE. The PAD incidence increased with increasing age, when there are comorbidities, and when there

was no gender difference. Compared with previous studies, PAD exhibited female sex preponderance (19). Our study revealed notable results that were different from those of previous studies on PE or PAD. Our study observed an increased risk of PAD if patients with PE were younger than 49 years and within the 2-year period of PE. Some possible mechanisms might explain our results. Ethnicity or genetics could have played a crucial role because PAD was more common in African Americans from the report of the National Health and Nutrition Examination Survey (19). Comorbidities were observed in both PE and PAD. Diabetes could cause the risk of not only *Klebsiella pneumoniae*–related PE but also atherosclerosis (20). A 5-year study indicated that the most common pathogens of PE were *K. pneumoniae*, followed by *Escherichia coli*, *Proteus mirabilis*, and others (21). A report

TABLE 3 | Comparison of incidence densities of peripheral arterial disease hazard ratio between with and without pleural empyema by gender, age, and follow-up time.

	Pleural empyema							
	No			Yes				
	Event	PY	Rate[#]	Event	PY	Rate[#]	Crude HR* (95% CI)	Adjusted HR[†] (95% CI)
Gender								
Women	304	151,837	2.00	87	23,838	3.65	1.83(1.44, 2.33)***	1.23(0.95, 1.59)
Men	836	510,442	1.64	212	84,679	2.50	1.53(1.32, 1.78)***	1.15(0.98, 1.35)
Stratify age								
≤49	17	193,683	0.09	45	39,885	1.13	12.9(7.37, 22.5)***	5.34(2.82, 10.1)***
50–64	146	181,956	0.80	78	31,867	2.45	3.17(2.41, 4.17)***	1.04(0.76, 1.43)
65–74	596	215,454	2.77	129	29,397	4.39	1.65(1.36, 2.00)***	0.89(0.73, 1.09)
75+	381	71,186	5.35	47	7,368	6.38	1.20(0.89, 1.63)	0.88(0.64, 1.21)
Follow-up time, years								
≤2	357	231,384	1.54	137	43,486	3.15	2.02(1.66, 2.46)***	1.35(1.09, 1.68)**
>2	783	430,894	1.82	162	65,032	2.49	1.38(1.17, 1.63)***	1.07(0.89, 1.28)

[#]Rate, incidence rate, per 1,000 person-years; *Crude HR, relative hazard ratio; [†] adjusted HR: multiple analysis including age, gender, and comorbidities of diabetes, hypertension, hyperlipidemia, COPD, heart failure, CAD, and stroke; **$p < 0.01$, ***$p < 0.001$.

regarding chest infections in Japan revealed that the percentages of lung abscesses and empyema were higher in patients infected with *Klebsiella* species and having diabetes and a smoking history (22). Furthermore, another common pathogen causing PE was indicated to be *Streptococcus pneumoniae* and was reported to intensify atherosclerosis and contribute to PAD in patients with PE (23). Smoking caused deleterious effects on cardiovascular and pulmonary systems, impeding the functional examinations, such as forced vital capacity, forced expiratory volume in 1 s, intima-media thickness, and ankle-brachial pressure index (ABI) (24), and lower ABI helps diagnose PAD (19). Due to data restriction and limitation, our study could not collect the smoking habit for the analysis of smoking, PE, and PAD, but we used COPD to represent smoking-related diseases and to reduce the confounding bias. Moreover, a Korean study indicated that the young age of diabetes onset was a distinctive feature of Asians (25). This finding supports our result that young people with PE might develop PAD. In addition, previous studies have reported the association between other comorbidities and PE (14, 15). Notably, patients with CVD, stroke, hyperlipidemia, and diabetes had an identically higher risk of generalized atherosclerosis with PAD. Moreover, age, hypertension, and hyperlipidemia were considered risk factors for PAD. Pleural effusion was most often caused by heart failure, cancer, and pneumonia and could be a potential risk factor for PE (26). Patients with heart failure and reduced ejection fraction had a higher prevalence of PAD (27). PAD can manifest in various ways, such as having no signs and symptoms or having intermittent claudication, ischemic ulcers, and gangrene. Limb loss with amputation was more prevalent in patients with ABI <0.5 (28). Moreover, PE could be associated with infection susceptibility and prolonged hospitalization. Of course, we just emphasized the association between PAD and PE. Through our big data analysis, we found the result. Further basic research should be done in the future such as gene analysis. In

our personal opinion, inflammation whether caused by infection or other chronic disease is one of the possible explanations.

Notably, being the first cohort study focusing on PAD incidence in patients with PE and using a large sample size for meaningful analyses were our study's strengths. Nonetheless, our study had several limitations. First, we could not entirely avoid the confounding effects of the preexisting comorbidities of PAD such as all cancers and inflammatory diseases, and any deaths from PAD must have been excluded. Second, NHIRD data on environmental risk factors influencing PAD and PE, such as cigarette smoking, alcohol consumption, nutritional status indicators such as body mass index, and family history, could not be obtained. Third, the laboratory data, such as ABI, chest X-ray images, bacterial species culture such as *Streptococcus* or *Klebsiella* species or Gram stain, and blood glucose level could not be obtained. Finally, even though our study revealed the possible role of PE in increasing the risk of PAD, further research is warranted to unravel the pathogenicity mechanisms involved in the development of PAD in patients with PE.

CONCLUSION

Our analysis determined that patients with PE had an increased risk of PAD, especially if they were younger than 49 years and within the 2-year diagnosis of PE.

DATA AVAILABILITY STATEMENT

The datasets presented in this article are not readily available because the dataset used in this study is held by the Taiwan Ministry of Health and Welfare (MOHW). The Ministry of Health and Welfare must approve our application to

access this data. Any researcher interested in accessing this dataset can submit an application form to the Ministry of Health and Welfare requesting access. Please contact the staff of MOHW (Email: stcarolwu@mohw.gov.tw) for further assistance. Taiwan Ministry of Health and Welfare Address: No.488, Sec. 6, Zhongxiao E. Rd., Nangang Dist., Taipei City 115, Taiwan (R.O.C.). Phone: +886-2-8590-6848. All relevant data are within the paper. Requests to access the datasets should be directed to stcarolwu@mohw.gov.tw.

ETHICS STATEMENT

The studies involving human participants were reviewed and approved by This study was approved by the Institutional Review Board of China Medical University (CMUH104-REC2-115-AR4). Written informed consent for participation was not required for this study in accordance with the national legislation and the institutional requirements.

AUTHOR CONTRIBUTIONS

H-HC and C-HK: conception and design. C-HK: provision of study materials. All authors: collection and/or assembly of data, data analysis and interpretation, manuscript writing, and final approval of the manuscript. All authors have contributed significantly and agree with the manuscript content.

FUNDING

REFERENCES

1. Semenkovich TR, Olsen MA, Puri V, Meyers BF, Kozower BD. Current state of empyema management. *Ann Thorac Surg.* (2018) 105:1589–96. doi: 10.1016/j.athoracsur.2018.02.027

2. Shen KR, Bribriesco A, Crabtree T, Denlinger C, Eby J, Eiken P, et al. The American Association for thoracic surgery consensus guidelines for the management of empyema. *J Thorac Cardiovasc Surg.* (2017) 153:e129–46. doi: 10.1016/j.jtcvs.2017.01.030

3. Porcel JM, Esquerda A, Vives M, Bielsa S. Etiology of pleural effusions: analysis of more than 3,000 consecutive thoracenteses. *Arch Bronconeumol.* (2014) 50:161–5. doi: 10.1016/j.arbr.2014.03.012

4. Ahmed AEH, Yacoub TE. Empyema thoracis. *Clin Med Insights Circ Respir Pulm Med.* (2010) 4:1–8. doi: 10.4137/CCRPM.S5066

5. Davies CW, Kearney SE, Gleeson FV, Davies RJ. Predictors of outcome and long-term survival in patients with pleural infection. *Am J Respir Crit Care Med.* (1999) 160:1682–7. doi: 10.1164/ajrccm.160.5.9903002

6. Ferguson AD, Prescott RJ, Selkon JB, Watson D, Swinburn CR. The clinical course and management of thoracic empyema. *QJM.* (1996) 89:285–9. doi: 10.1093/qjmed/89.4.285

7. Finley C, Clifton J, Fitzgerald JM, Yee J. Empyema: an increasing concern in Canada. *Can Respir J.* (2008) 15:85–9. doi: 10.1155/2008/975312

8. Burgos J, Falco V, Pahissa A. The increasing incidence of empyema. *Curr Opin Pulm Med.* (2013) 19:350–6. doi: 10.1097/MCP.0b013e3283606ab5

9. Malyar NM, Freisinger E, Meyborg M, Lüders F, Fürstenberg T, Kröger K, et al. Low rates of revascularization and high in-hospital mortality in patients with ischemic lower limb amputation: morbidity and mortality of ischemic amputation. *Angiology.* (2016) 67:860–9. doi: 10.1177/0003319715626849

10. Norgren L, Hiatt WR, Dormandy JA, Nehler MR, Harris KA, Fowkes FGR, et al. Inter-society consensus for the management of peripheral arterial disease (TASC II). *J Vasc Surg.* (2007) 45 Suppl S:S5–67. doi: 10.1016/j.jvs.2006.12.037

11. Kinlay S. Management of critical limb ischemia. *Circ Cardiovasc Interv.* (2016) 9:e001946. doi: 10.1161/CIRCINTERVENTIONS.115.001946

12. Haring R, Travison TG, Bhasin S, Vasan RS, Wallaschofski H, Davda MN, et al. Relation between sex hormone concentrations, peripheral arterial disease, and change in ankle-brachial index: findings from the framingham heart study. *J Clin Endocrinol Metab.* (2011) 96:3724–32. doi: 10.1210/jc.2011-1068

13. Dhaliwal G, Mukherjee D. Peripheral arterial disease: Epidemiology, natural history, diagnosis and treatment. *Int J Angiol.* (2007) 16:36–44. doi: 10.1055/s-0031-1278244

14. Wu CY, Su TW, Huang KY, Ko P-J, Yu S-Y, Kao T-C, et al. Pleural empyema and aortic aneurysm: a retrospective national population-based cohort study. *Medicine.* (2015) 94:e2142. doi: 10.1097/MD.0000000000002142

15. Shen TC, Lin CY, Lin CL, Chen C-H, Tu C-Y, Hsia T-C, et al. Risk of developing pleural empyema in patients with stroke: a propensity-matched cohort study. *Intern Emerg Med.* (2017) 12:1131–8. doi: 10.1007/s11739-017-1707-8

16. Shen TC, Chen CH, Wang IK, Lin C-L, Tu C-Y, Hsia T-C, et al. Risk of empyema in patients with end-stage renal disease: a nationwide propensity-matched cohort study. *QJM.* (2017) 110:425–30. doi: 10.1093/qjmed/hcx004

17. Lai SW, Lin CL, Liao KF. Population-based cohort study investigating the correlation of diabetes mellitus with pleural empyema in adults in Taiwan. *Medicine.* (2017) 96:e7763. doi: 10.1097/MD.0000000000007763

18. Database NHIR. Taiwan. Available online at: https://nhird.nhri.org.tw/en/index.htm (cited in 2015).

19. Dua A, Lee CJ. Epidemiology of peripheral arterial disease and critical limb ischemia. *Tech Vasc Interv Radiol.* (2016) 19:91–5. doi: 10.1053/j.tvir.2016.04.001

20. Chen KY, Hsueh PR, Liaw YS, Yang PC, Luh KT. A 10-year experience with bacteriology of acute thoracic empyema: emphasis on Klebsiella pneumoniae in patients with diabetes mellitus. *Chest.* (2000) 117:1685–9. doi: 10.1378/chest.117.6.1685

21. Chen W, Lin YC, Liang SJ, Tu C-Y, Chen H-J, Hang L-W, et al. Hospital-acquired thoracic empyema in adults: A 5-year study. *South Med J.* (2009) 102:909–14. doi: 10.1097/SMJ.0b013e3181b22c52

22. Ishiguro T, Uozumi R, Yoshioka H, Nishida T, Takayanagi N. Comparison Between Patients With Chest Infection Due to Klebsiella Spp. And Streptococcus Pneumoniae. *Intern Med.* (2020) 59:611–8. doi: 10.2169/internalmedicine.3531-19

23. De'nes A', Pradillo JM, Drake C, Sharp A, Warn P, Murray KN, et al. Streptococcus pneumonia worsens cerebral ischemia via interleukin 1 and platelet glycoprotein Iba. *Ann Neurol.* (2014) 75:670–83. doi: 10.1002/ana.24146

24. Sugiura T, Dohi Y, Takagi Y, Yokochi T, Yoshikane N, Suzuki K, et al. Close Association Between Subclinical Atherosclerosis and Pulmonary Function in Middle-Aged Male Smokers. *J Atheroscler Thromb.* (2020) 27:1230–42. doi: 10.5551/jat.55996

25. Rhee EJ. Diabetes in Asians. *Endocrinol Metab.* (2015) 30:263–9. doi: 10.3803/EnM.2015.30.3.263

26. Jany B, Welte T. Pleural effusion in adults-etiology, diagnosis, and treatment. *Dtsch Arztebl Int.* (2019) 116:377–86. doi: 10.3238/arztebl.2019.0377

27. Ullah W, Sattar Y, Darmoch F, Al-KhadraY, MirT, Ajmal R, et al. The impact of peripheral arterial disease on patients with mechanical circulatory support. *Int J Cardiol Heart Vasc.* (2020) 28:100509. doi: 10.1016/j.ijcha.2020.100509

28. Marston WA, Davies SW, Armstrong B, Farber MA, Mendes RC, Fulton JJ, et al. Natural history of limbs with arterial insufficiency and chronic ulceration treated without revascularization. *J Vasc Surg.* (2006) 44:108–14. doi: 10.1016/j.jvs.2006.03.026

An Examination System to Detect Deep Vein Thrombosis of a Lower Limb Using Light Reflection Rheography

Shing-Hong Liu [1]![ORCID]**, Jia-Jung Wang** [2,*]**, Wenxi Chen** [3] ![ORCID]**, Kuo-Li Pan** [4,5,*]![ORCID] **and Chun-Hung Su** [6,7]

1   Department of Computer Science and Information Engineering, Chaoyang University of Technology, Taichung 413310, Taiwan; shliu@cyut.edu.tw
2   Department of Biomedical Engineering, I-Shou University, Kaohsiung 84001, Taiwan
3   Biomedical Information Engineering Laboratory, The University of Aizu, Aizu-Wakamatsu City 965-8580, Fukushima, Japan; wenxi@u-aizu.ac.jp
4   Division of Cardiology, Chiayi Chang Gung Memorial Hospital, Chiayi City 61363, Taiwan
5   Department of Traditional Chinese Medicine, College of Medicine, Chang Gung University, Taoyuan City 33305, Taiwan
6   Institute of Medicine, School of Medicine, Chung-Shan Medical University, Taichung 40201, Taiwan; such197408@gmail.com
7   Department of Internal Medicine, Chung-Shan Medical University Hospital, Taichung 40201, Taiwan
*   Correspondence: wangjj@isu.edu.tw (J.-J.W.); pankuoli64@gmail.com (K.-L.P.); Tel.: +886-7-6151100-7464 (J.-J.W.); +886-5-362-1000-2854 (K.-L.P.)

Abstract: Deep vein thrombosis (DVT) of lower limbs can easily arise from prolonged sitting or standing. Elders and pregnant women are most likely to have this disease. When the embolus of DVT comes to pass the lung, it will become a life-threatening disease. Thus, for DVT disease, early detection and the early treatment are needed. The goal of this study was to develop an examination system to be used at non-medical places to detect the DVT of lower limbs with light reflection rheography (LRR). Consisting of a wearable device and a mobile application (APP), the system is operated in a wireless manner to control the actions of sensors and display and store the LRR signals on the APP. Then, the recorded LRR signals are processed to find the parameters of DVT examination. Twenty subjects were recruited to perform experiments. The veins of lower limbs were occluded by pressuring the cuff up to 100 mmHg and 150 mmHg to simulate the slight and serious DVT scenarios, respectively. Six characteristic parameters were defined to classify whether there was positive or negative DVT using the receiver operating characteristic curves, including the slopes of emptying and refilling curves in the LRR signal, and the changes of venous pump volume. Under the slight DVT scenario (0 mmHg vs. 100 mmHg), the first three parameters, m_{10}, m_{40}, and m_{50}, had accuracies of 72%, 69%, and 69%, respectively. Under the serious DVT scenario (0 mmHg vs. 150 mmHg), m_{10}, m_{40}, and m_{50} achieved accuracies of 73%, 76%, and 73%, respectively. The experimental results show that this proposed examination system may be practical as an auxiliary tool to screen DVT in homecare settings.

Keywords: deep vein thrombosis; light reflection rheography; wearable device; photoplethysmography

1. Introduction

Deep vein thrombosis (DVT) occurs when a blood clot forms in one or more of the deep veins in the human body, which will change the blood flow of veins and result in poor blood circulation. Detection of DVT is usually a clinical challenge for doctors of all medical specialties, and deterioration of such disease may make the treatment process more complicated. Moreover, DVT can happen even in the absence of serious disorders. As investigated, thrombosis can occur in any part of the venous system, but it appears most frequently at the deep veins of the legs [1]. Post-thrombotic syndromes arising from long-term morbidity can be common and substantial. Embolization of thrombus occurring in the lung due to DVT can be fatal. Furthermore, DVT is highly prevalent in Taiwan, and

its treatment consumes a lot of health insurance funds [2]. Thus, both early screening and proper treatment of DVT are important to prevent it from worsening and happening again.

Traveler's thrombosis is caused by sitting still in a transport vehicle for a long time, and blood clots are formed and deposited inside the deep veins of lower limbs, which constitutes DVT [3]. Scurr et al. have indicated incidences of 10% of asymptomatic calf vein thrombosis in air travelers above 50 years of age and traveling for more than 8 h [4]. Hence, the main risk factors of DVT include prolonged sitting or standing, family history of thrombus, pregnancy, diabetes, hyperlipidemia, and hypertension. The venous thrombus could flow to the pulmonary vein to cause the pulmonary embolism. Therefore, the early diagnosis and treatment of DVT can prevent the pulmonary embolism.

Clinical examinations of DVT are currently performed using ultrasound or venography, and they all need to be carried out by professional technicians or physicians in a hospital [5,6]. Moreover, these examinations are not performed in general clinics. In 1976, Hull et al. proposed impedance plethysmography [7,8] to detect DVT. Sandler et al. have examined DVT with Doppler ultrasound, impedance plethysmography, and venoscan, and the accuracy rates were 65%, 80%, and 82%, respectively, by comparison with the X-ray venography as the standard [9]. Thus, these techniques all have some limitations for the diagnoses of DVT, except for venography. Ginsberg et al. have applied D-dimer testing and impedance plethysmography to examine 98 patients with DVT symptoms. Their results showed that, when both methods were tested as "negative" after detailed examination, the accuracy rate was as high as 98% [10]. This is enough to show that the vein plethysmography could be an auxiliary tool to examine DVT.

Although the impedance plethysmography has good sensitivity in detecting venous thrombosis in the hip, thigh, and popliteal area, it is not very sensitive to calf vein thrombosis [8,11]. The study by Goodacre et al. found that the most common location for venous thrombosis is in about 50% of the lower limbs [12]. In 1984, Shepard et al. published a technique using light reflection rheography (LRR) to examine DVT in the calf [13]. Some studies for the applications of LRR were published in 1992 [14] and 1993 [15]. The LRR uses reflective photoplethysmography (PPG) to detect the blood volume changes in the superficial vein. According to the studies of Thomas et al. [16], LRR has a sensitivity of 92% and a specificity of 84% in detecting acute thrombosis of the calf. This technique has a negative predictive value of 92% in selecting those patients with no thrombosis. Thus, LRR can be employed to develop a wearable device to prevent the varicose veins of lower limbs.

In recent years, people have been fond of using wearable devices to monitor their bodies' condition in daily life. In various wearable devices, an exercise watch or band can be utilized to measure the heart rate and the number of steps [17,18], an electrocardiogram (ECG) patch can be used to record a long-term ECG signal [19], and an electromyogram (EMG) patch can be applied to detect muscle fatigue in real time [20]. The major differences between the wearable devices and medical apparatus include the size, weight, and usability. Thus, it is now possible for users to make use of these wearable devices to take care of their health conditions in daily life. These physiological data can be further utilized by artificial intelligent technologies to predict or diagnose diseases [21,22]. However, how to design wearable devices having the same functions as an apparatus with medical grade is a challenge to engineers, because such medical apparatus is usually large and heavy. Now, the advantages of advanced sensor chips are leading to lower power consumption, smaller size, and digitization in devices such as ECG sensors [23], PPG sensors [24], and accelerometers [25]. With those advanced sensor chips, it becomes more possible to develop a medical-grade wearable device.

LRR, a noninvasive and non-ionizing radiation measurement technique, can be applied to observe whether a lower limb has DVT by means of reflective PPG sensors. In the examination procedure, the physician has to look for an appropriate position for placing the PPG sensor to obtain a reliable PPG signal, and guides the patient to perform the dorsiflexion at the ankle to push the blood in the vein of the calf back to the heart. However, it is hard for users, at home, to check the vein condition by such medical grade apparatus.

The aim of this study is to develop an examination system, available for use in non-medical places, to detect the DVT of a lower limb. The system included a wearable device with commercial reflective PPG sensors and an accelerometer to measure LRR signals, and a mobile application (APP) to control the works of sensors, guide the rhythm of foot action, and display and store the LRR signals in real time. An array sensor embedded with three reflective PPG sensors was designed to detect the change of venous blood flow during the calf pumping. An accelerometer was placed at the foot to simultaneously monitor the dorsiflexion action at the ankle. In order to verify this prototype, twenty healthy subjects were included to participate in this study. The veins of a lower limb were partially or totally occluded by inflating the cuff up to 100 mmHg or 150 mmHg to simulate the stenosis phenomenon in slight or serious DVT scenarios, respectively. The identifiable rules for determining the quality of the LRR signals from the different PPG sensors were studied. Thus, the LRR signal with the best quality and sensitivity was chosen. Six characteristic parameters regarding the LRR signal were defined as the slopes of emptying and refilling curves in the LRR signal and the change of venous pump volume. Those parameters were used to classify whether the DVT occurrence was positive or negative by a receiver operating characteristic (ROC) curve. The results showed that the prototype of the examination system has the potential for screening for DVT in non-medical environments.

2. Materials and Methods

Figure 1 shows the architecture of the DVT examination system. The purple block is the APP that can display and store the LRR signals in real time, show the rhythm of dorsiflexion, and control the wearable device. The green block represents the wearable device that uses Bluetooth communication to receive APP comments and send the LRR data to the APP. The reflective PPG sensors and accelerometer are utilized to measure the LRR and the foot action signals, respectively. The orange block denotes the recorded LRR signals and the *x*-axis signal of the accelerometer that are uploaded to a personal computer for further smoothing of the LRR signals and for acquiring the characteristic parameters from the LRR signals with Matlab R2015a version.
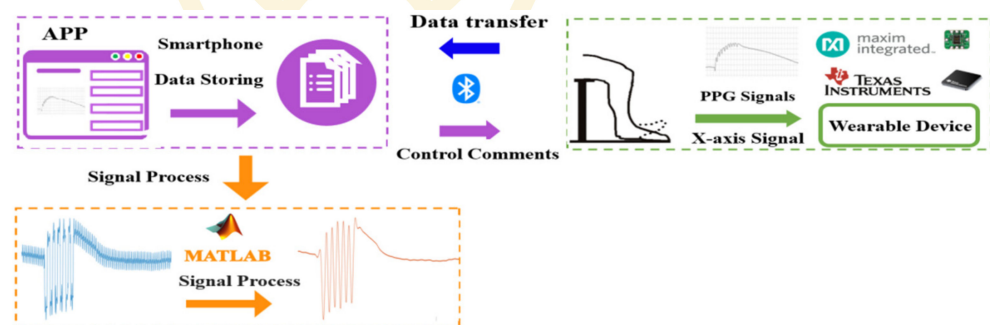
Figure 1. Architecture of the deep vein thrombosis (DVT) examination system. APP is the mobile application and PPG is the photoplethysmography.

2.1. LRR Wearable Device

Figure 2 shows the block diagram of the LRR wearable device that includes an array-type probe, accelerometer, and main board. The array-type probe consists of three MAX30102 PPG sensors (Maxim Integrated TM, San Jose, CA, USA), whose size is 16 mm × 45 mm, as shown in Figure 3a. Each MAX30102 PPG sensor contains two light-emitting diodes (LEDs), with wavelengths of 660 nm (red light) and 880 nm (infrared light). Moreover, a photo diode, an 18-bit analog-to-digital converter, and low-noise electronics with ambient light rejection are also included in this PPG sensor. Communication between the sensors and a microcontroller unit (MCU) is accomplished via a standard I2C-compatible interface. The sampling rate is set to 100 Hz. The *x*-axis signal of the accelerometer (ADXL325, Analog Devices, Norwood, MA, USA) is sampled by the MCU with a 12-bit analog-to-digital converter. The MCU of the main board is a 16-bit microcontroller (MSP430F5438A,

Texas Instruments TM, Dallas, TX, USA), which reconciles the workflow of the MAX30102 and ADXL325, performs the signal processing to obtain the DVT-related parameters, and transmits the data to the APP by a Bluetooth module (HC-05, Itead, Shenzhen, China). The power circuit includes a Li battery (150 mAh), a charging integrated circuit (IC) (TIBQ24072), and a regulator IC (XC62FP, 3.3 V). The size of the main board is 54 mm × 70 mm. Figure 3b shows the real picture of the LRR wearable device.
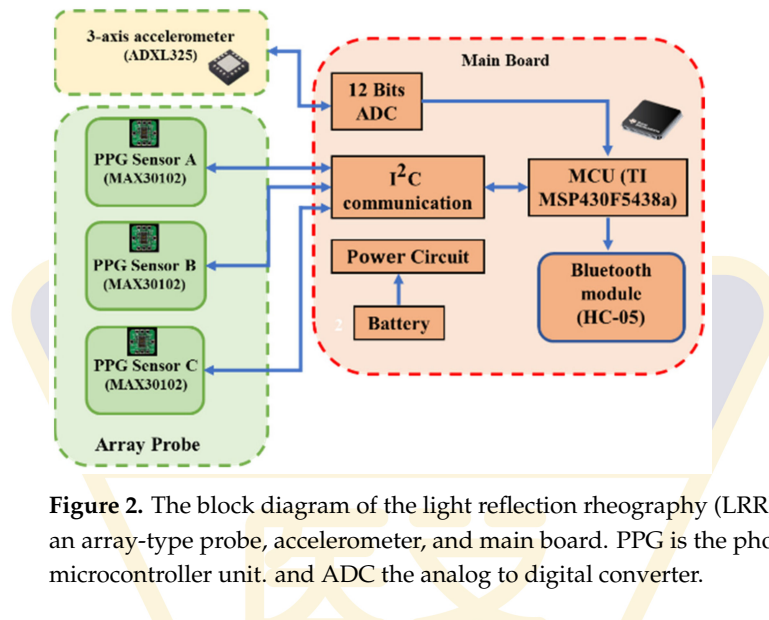
Figure 2. The block diagram of the light reflection rheography (LRR) wearable device consisting of an array-type probe, accelerometer, and main board. PPG is the photoplethysmography, MCU the microcontroller unit. and ADC the analog to digital converter.

(**a**)   (**b**)
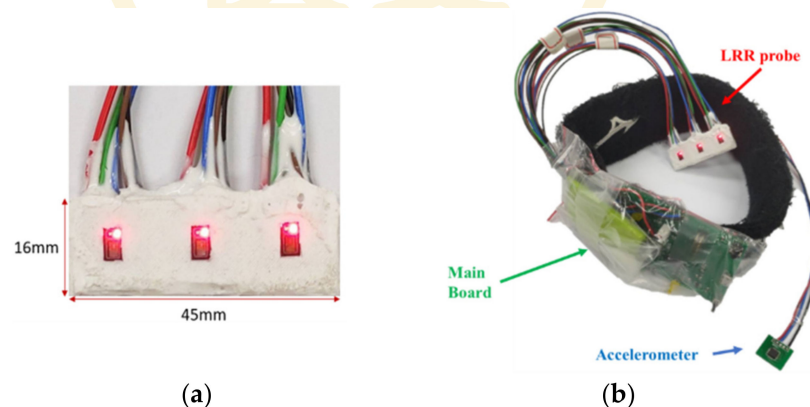
Figure 3. (**a**) Real photo of the array-type probe, (**b**) the real photo of the LRR wearable device.

2.2. Signal Processing

The LRR signal measured by PPG sensors is a direct current (DC) component of the PPG signal, representing the change of venous blood flow. However, The PPG signal not only contains the venous flow, but also contains the pulses of arterial blood flow. Thus, the proposed system applied a fourth-order Butterworth low-pass filter with a cut-off frequency of 0.5 Hz to filter out high-frequency noise and used a three-point interpolation technique to smooth the LRR signal. The zero-crossing points of the differential filtered signal were used to find the peaks and valleys of the LRR signal. Then, the median point between the neighbor peak and valley was found in the LRR signal. The continuous three median points were used to build the LRR interpolation signal by a second-order polynomial function for approximating the smooth LRR signal. Figure 4 shows the LRR signal at different steps in the digital signal processing. Figure 4a is the original LRR signal that couples with the arterial pulses and the change of venous blood flow. Figure 4b shows the output of this filter. The next process after filtering is to find the peaks and valleys of the filtered LRR signal (red line) marked by the inverse triangle symbols, followed by

differentiation, as shown in Figure 4c. The median points are marked by the circle symbols for building the smooth signal (blue line). Additionally, the synchronous *x*-axis signal is shown in Figure 4d.
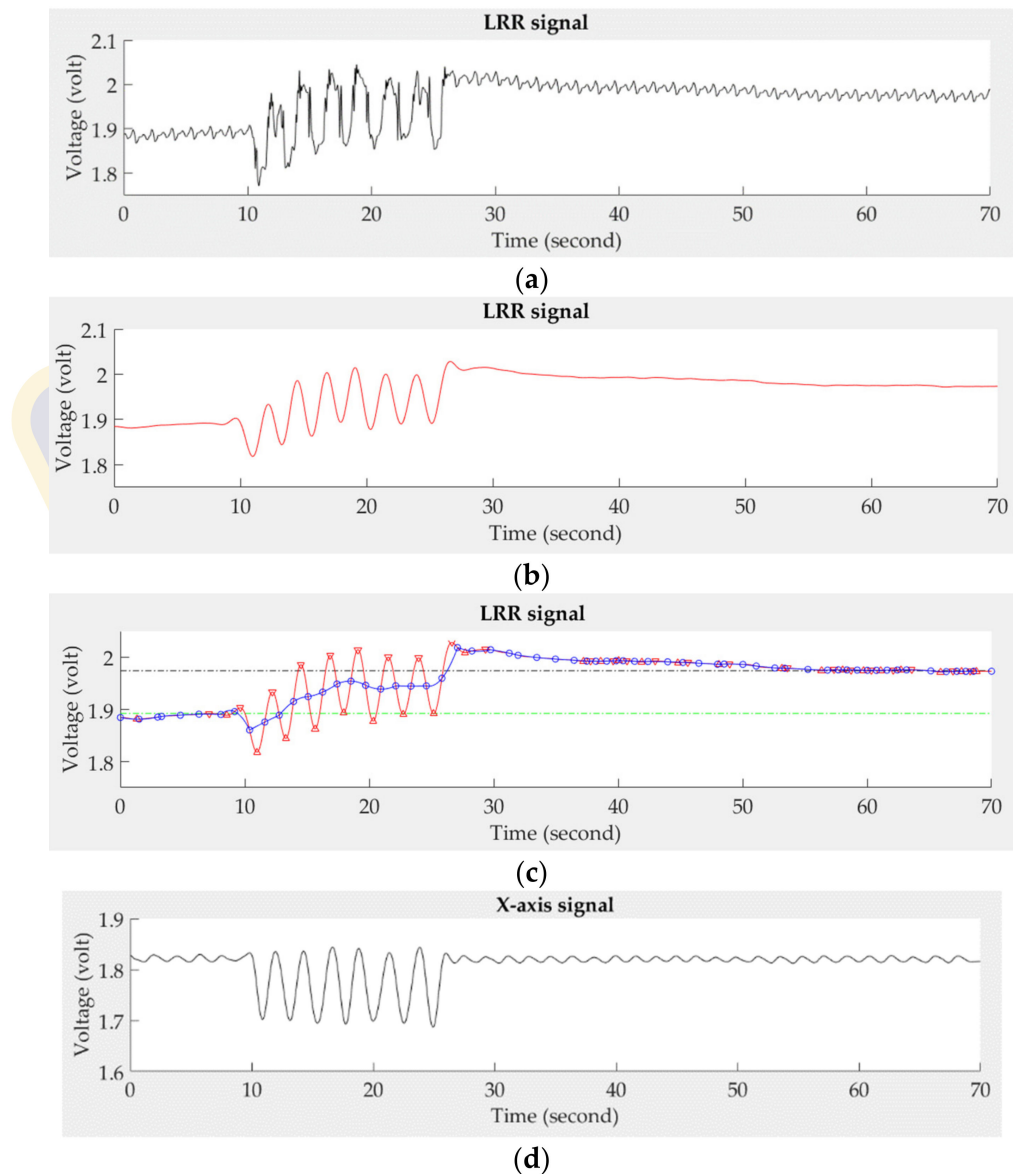
Figure 4. The signal processing steps for a normal LRR signal, (**a**) original signal, (**b**) the filtered signal, (**c**) the smooth (blue line) and filtered (red line) signals, (**d**) the synchronous *x*-axis signal.

2.3. Characteristic Parameters of the LRR Signal

Figure 5a shows four characteristics in the smooth LRR signal (blue line), the start (red circle symbol), and the end (black circle symbol) points in the emptying phase, and the two baselines (short green dash line and long blue dash line) in the resting and refilling phase. The filtered LRR signal is represented by the red line. In Figure 5b, we find that the *x*-axis signal has larger alternating amplitudes in the emptying phase than those in the resting and refilling phases. Thus, the first maximum negative and last positive changed points of the *x*-axis signal is used to define the start and end points, X_{start} and X_{end} (red and black star symbols), in the emptying phase. Then, the start maximum point of the smooth LRR signal, LRR_{start} (red circle symbol), is found between before and after 50 points of X_{start}, and the end maximum point of the smooth LRR signal, LRR_{end} (black circle symbol), is found between before and after 50 points of X_{end}, as shown in Figure 5a.
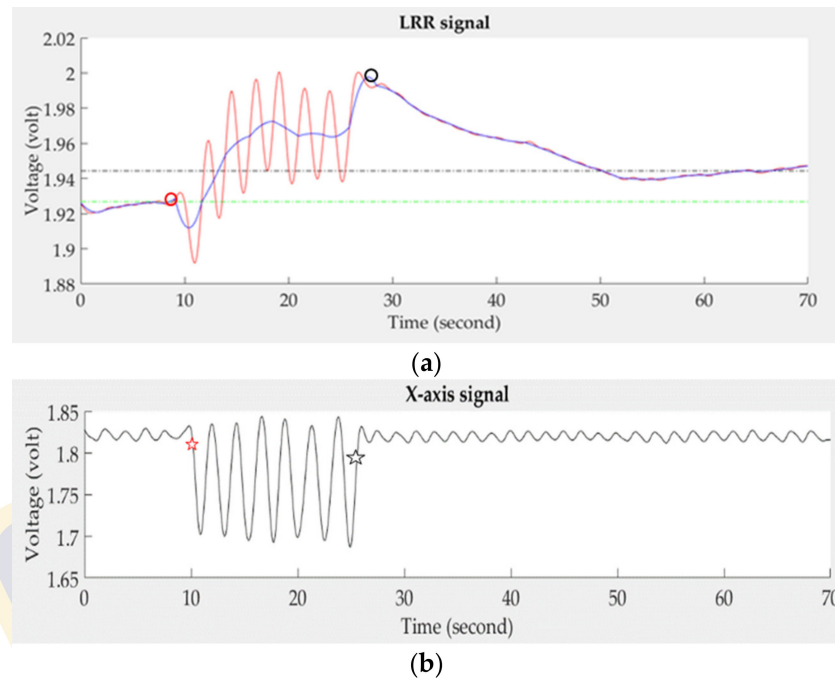
Figure 5. (**a**) Four characteristics of the smooth LRR signal (blue line), LRR$_{start}$ (red circle symbol), LRR$_{end}$ (black circle symbol), resting baseline (short green dash line), and refilling baseline (long blue dash line), (**b**) two characteristics of the accelerometer signal, X$_{start}$ and X$_{end}$ (red and black star symbols).

The average of the LRR signal within five seconds before LRR$_{start}$ corresponds to the resting baseline (short green dash line), and the average within the five seconds before the ending measurement represents the refilling baseline (long blue dash line). In the study, six characteristic parameters from the LRR signal were defined to identify the DVT, as follows. VP$_1$ is defined as the change of venous pump volume between the LRR$_{end}$ and resting baseline, VP$_2$ is the change of venous pump volume between the LRR$_{end}$ and refilling baseline, m_{10} is the slope of the empty curve from the LRR$_{end}$ to LRR$_{start}$, m_{40} is the slope of the refilling curve from the LRR$_{end}$ to the point at 40 s, m_{50} is the slope of the refilling curve from the LRR$_{end}$ to the point at 50 s, and m_{60} is the slope of the refilling curve from the LRR$_{end}$ to the point at 60 s.

2.4. Quality of LRR Signals

Two fundamental rules for determining the quality of LRR signals on the different PPG sensors were formulated. The first rule states that, according to LRR, the PPG sensor should detect the downstream of venous blood flow in the emptying phase. If the PPG sensor detects the upstream of venous blood flow, the sensor may have been placed at a wrong position. Thus, when the phase angle between the filtered LRR signal (red line) and *x*-axis signal is larger than 90°, such an LRR signal is considered of low quality, as show in Figure 6a. The second rule states that, when the foot is moving to empty the deep venous blood, the PPG sensor may move to a different place. The baseline of the LRR signal has a drift phenomenon. Thus, when VP$_1$ or VP$_2$ is negative, the LRR signal is determined to be of low quality, as show in Figure 6b.

2.5. APP Program

In the study, an APP program is designed to control the functions of the wearable device (Figure 7a), to instruct the rhythm of foot action (Figure 7b), and to display the results of the LRR signal in real time (Figure 7c). In the beginning, the APP program searches for the Bluetooth (BT) module of the wearable device and automatically connects

with it. Users can adjust the LED current to shift the baseline of the LRR curve, as shown in Figure 7d. Then, the APP starts the DVT measurements, as shown in Figure 7a.
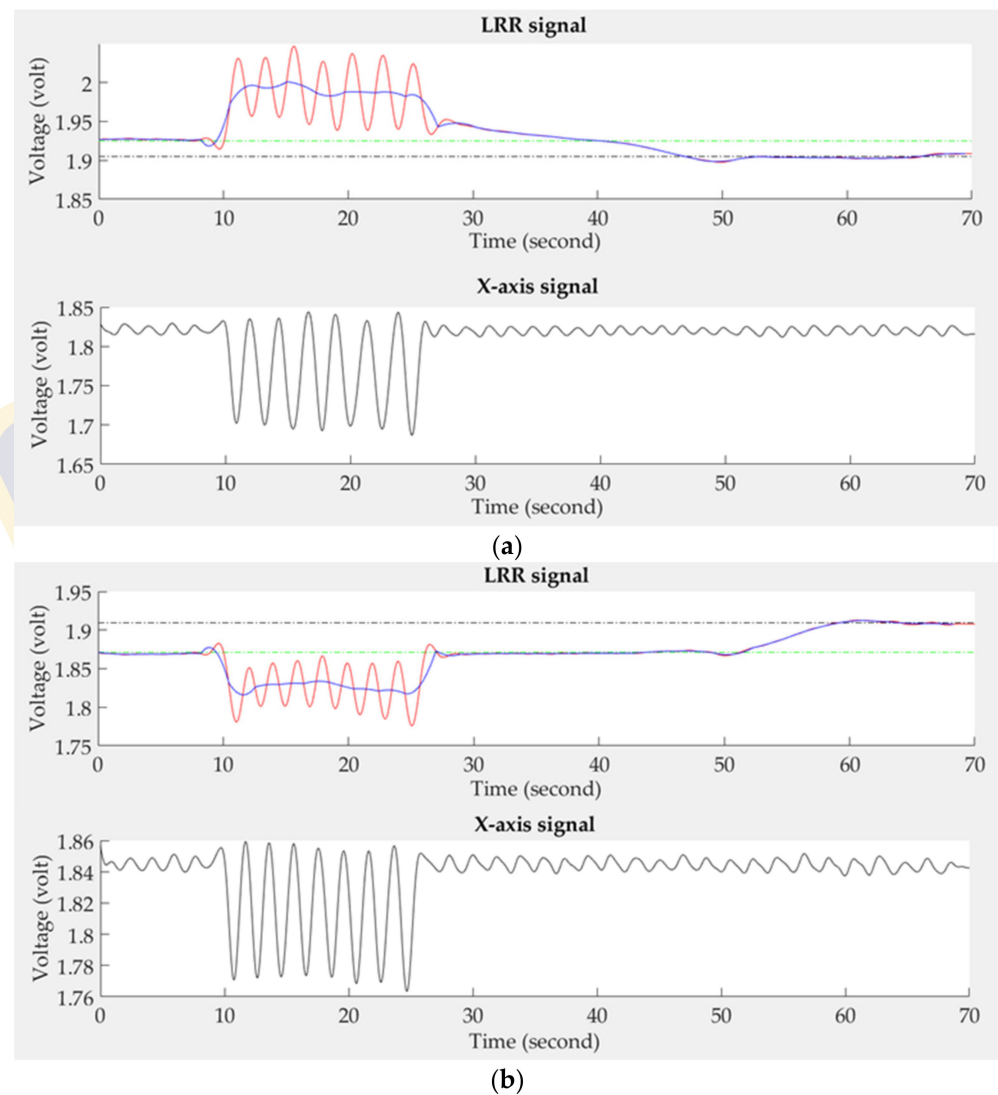
Figure 6. (**a**) The phase angle between the LRR signal and the *x*-axis signal is 180° because the PPG sensor detects the upstream of venous blood flow, (**b**) The LRR signal has the drift phenomenon.
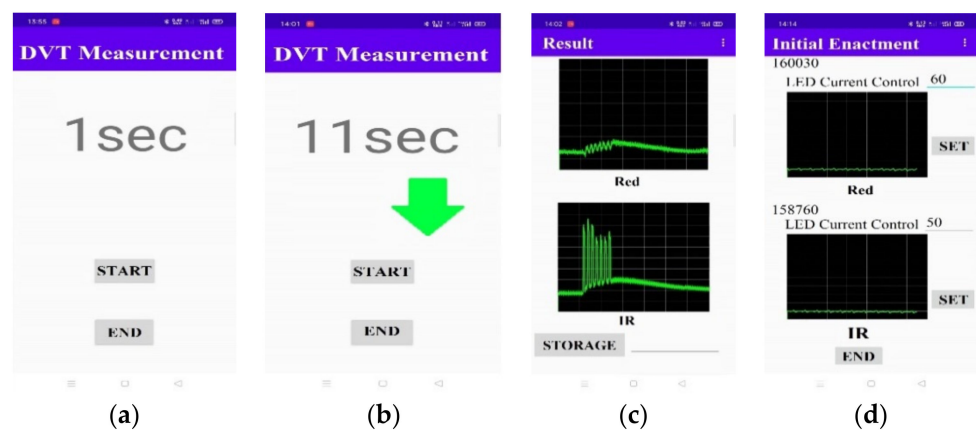
Figure 7. The screen displays of the APP program: (**a**) starting or ending the measurement, (**b**) the rhythm of foot action, (**c**) measured LRR signals, (**d**) adjustment of LED currents.

2.6. Protocol of Experiment

This study recruited twenty healthy subjects (10 male and 10 female) without cardio-vascular disease or injured limbs. Their age was between 20 and 24 years (21.8 $\pm$ 1.2 years, mean $\pm$ standard deviation), weight between 38 and 80 Kg (60.9 $\pm$ 10 Kg), and height between 150 and 180 cm (164.4 $\pm$ 9.2 cm). The vein of one lower limb was occluded by pressuring the cuff up to 100 mmHg and 150 mmHg to simulate the slight and serious DVT scenarios. This experiment was approved by the Research Ethics Committee of China Medical University & Hospital (No. CMUH107-REC3-061), Taichung, Taiwan.

Subjects were requested to comfortably sit on a chair with the foot resting flat on the floor, and the angle between calf and thigh was about 110°, as show in Figure 8a. A LRR probe was placed at the distal end of the calf muscle, which was fixed by transparent tape. An accelerometer was placed at the front end of the foot and an air cuff was wrapped around the thigh. The APP algorithm connected with the LRR device via Bluetooth. The APP displayed the LRR signal in real time. The light lumen of LED in the reflective PPG sensors affect the signal to noise ratios (SNRs) of the red-light and IR-light photo diodes, and skin color, skin thickness, and soft tissue also affect transmissible light lumen of the LED. To standardize the SNRs of the red-light and IR-light LRR signals for every subject, the baselines of the IR-light LRR signals for three PPG sensors were adjusted to 1.9 volts before measurement. Subjects were requested to move their feet. If the LRR signals had an emptying curve, it meant the LRR probe was placed at the right position. If not, the LRR probe was repositioned until an emptying curve appeared. Subjects were measured three times in the first experiment on the first day. The following week, they were asked to perform the second experiment. In the first measurement, the thigh was not occluded in the negative group. However, in the positive group, the thigh was partially or totally occluded by inflating the cuff up to 100 mmHg or 150 mmHg, respectively, to simulate the stenosis occurrence in mild or severe DVT. Subjects were requested to take a 10-min rest between the two measurements. They could move their feet to augment the venous blood flow. During the first measurement, the resting phase lasted for 10 s, the emptying phase 15 s, and the refilling phase 45 s. When the LRR probe was placed at the right position, users could push the start icon of the APP to record the displayed LRR signals in real time. In the emptying phase, the APP showed the rhythm of the foot action, as shown in Figure 8b. Subjects were requested to move their feet following a rhythm of 0.5 Hz.
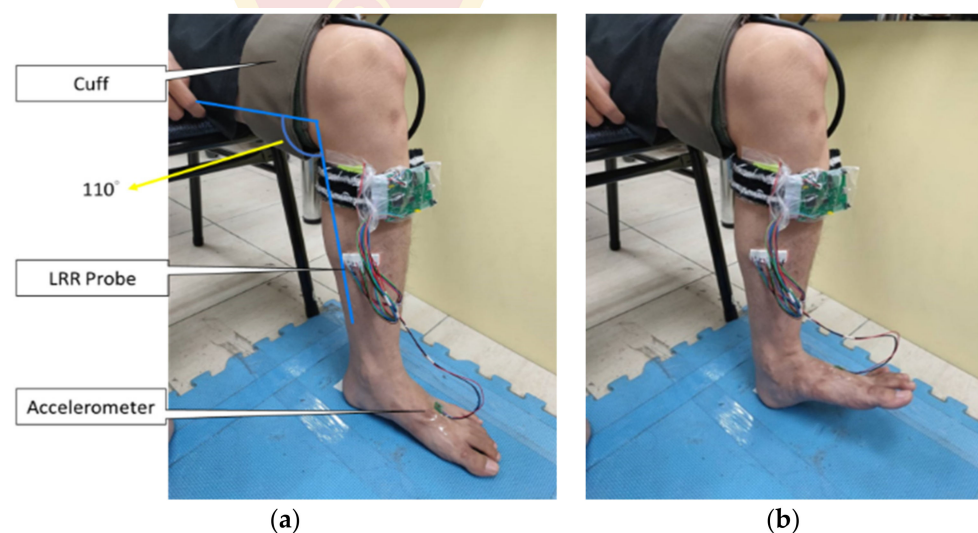
Figure 8. Real photo of LRR measurement: (**a**) placement of the cuff, LRR probe, and accelerometer, (**b**) the foot action.

In the study, the terms, true positive (TP), false positive (FP), true negative (TN) and false negative (FN), refer to the result of our experiments and the correctness of

the classification. TP means that a subject was correctly diagnosed as DVT, FP means "incorrectly diagnosed as DVT", TN means "correctly diagnosed as non DVT", and FN means "incorrectly diagnosed as non DVT". Here, the performance of the proposed method was evaluated using accuracy, (TP+TN)/(TP+FP+FN+TN); precision, TP/(TP+FP); sensitivity, TP/(TP+FN); and specificity, TN/(FN+TN).

3. Results

Table 1 shows the numbers of LRR signals with good quality for each subject. In the first experiment, there are no good-quality LRR signals in the red-light measurement under the venous non-occluded and occluded scenarios for Subject 9. For Subjects 8 and 15, there are no good-quality LRR signals under only one scenario. In the second experiment, for Subjects 3, 4, 9, and 11, some LRR signals with good quality are missing under the different venous occluded scenarios. Consequently, the total numbers of LRR signals with good quality in the red-light and IR-light measurements both are 224.

Table 1. The numbers of LRR signals with good quality for each subject.

| Subject No. | First Experiment | | | | | | Second Experiment | | | | | | Total | |
| | R-Light | | | IR-Light | | | R-Light | | | IR-Light | | | R-Light | IR-Light |
	0	100	150	0	100	150	0	100	150	0	100	150		
1	2	3	3	2	2	2	2	1	3	1	1	2	14	10
2	2	0	2	2	1	1	2	2	1	1	1	1	9	7
3	2	2	2	2	2	2	1	1	2	0	1	0	10	7
4	1	2	1	2	2	2	1	0	0	1	1	0	5	8
5	1	2	3	2	2	2	2	2	2	2	2	2	12	12
6	1	2	2	1	1	2	3	3	3	3	3	3	14	13
7	1	1	2	2	1	1	1	1	2	1	2	2	8	9
8	2	2	2	2	0	2	1	1	1	1	1	1	9	7
9	0	0	0	2	1	1	1	0	0	1	1	0	1	6
10	2	2	3	2	3	1	2	1	2	2	2	2	12	12
11	1	3	3	2	2	3	1	1	0	2	2	1	9	12
12	3	3	3	3	3	3	2	2	2	2	1	2	15	14
13	2	3	3	2	2	2	3	3	3	3	3	2	17	14
14	1	1	1	1	2	1	2	2	2	2	2	2	9	10
15	3	1	2	3	2	0	1	1	1	2	2	2	9	11
16	3	3	3	3	3	3	3	3	3	3	3	2	18	17
17	3	3	3	3	3	3	2	2	2	1	1	2	15	13
18	1	2	2	1	1	3	2	2	1	3	3	2	10	13
19	3	1	1	3	2	2	3	3	3	3	3	3	14	16
20	3	3	2	3	2	2	2	2	2	2	2	2	14	13
Sum	37	39	43	43	37	38	37	33	35	36	37	33	224	224

Table 2 shows the statistical analyses of six characteristic parameters under the different venous occluded scenarios in the red-light and IR-light measurements. We used the *t*-test to assess the performances of six parameters for the sensitivity of DVT detection. A *p*-value of 0.05 or lower is considered statistically significant (represented in red) between the negative (0 mmHg) and positive (100 and 150 mmHg) groups. We find that all parameters have significant differences between the negative and positive groups. However, under the same scenario comparison (0 mmHg vs. 150 mmHg), *p*-values of the six parameters in the IR-light measurement are lower than those in the red-light measurement. Moreover, the absolute mean values of six parameters all decrease as the colluded pressure increases. To select the best sensitivity value of each parameter from three LRR signals, we analyzed the maximum, median, and minimum values of parameters under the different venous occluded scenarios in the red-light and IR-light measurements, as shown in Table 3. If there were two LRR signals with good quality, the median value was the arithmetic average. If there was one LRR signal with good quality, maximum, median, and minimum values

were the same values. One of three values for each parameter had the lowest *p*-value, which was the optimal value to detect DVT. We find that m_{10}, VP_1, and VP_2 should select the maximum values; m_{50} and m_{60} should select the minimum values; and m_{40} should select the median values. An ROC curve was used to evaluate the performances of six parameters in the IR-light measurement in the various DVT scenarios. Table 4 shows the fusion matrix and performances of the six parameters. The first three parameters with better accuracy are m_{10}, m_{40}, and m_{50} in the slight DVT scenario (0 mmHg vs. 100 mmHg), having accuracies of 72%, 69%, and 69%, respectively. The first three parameters in the serious DVT scenario (0 mmHg vs. 150 mmHg) are m_{40}, m_{50}, and m_{10}, with accuracies of 76%, 73%, and 73%, respectively. The first three parameters with a larger ROC area in the slight DVT scenario are m_{40}, m_{10}, and VP_2, with areas of 0.82, 0.79, and 0.78, respectively. The first three parameters with larger ROC area in the serious DVT scenario are m_{40}, VP_2, and m_{50}, with areas of 0.86, 0.81, and 0.81, respectively. Therefore, m_{40} and m_{10} have the best performances to detect the DVT conditions in the serious DVT scenario, meaning that the cut points are -1.79 mV/s and 3.05 mV/s. Figure 9a shows the ROC curve of m_{40} in the slight DVT scenarios, and Figure 9b shows the ROC curve in the serious DVT scenario. When its sensitivity is 100% in the serious DVT scenario, its corresponding specificity is 20.2%.

Table 2. Statistical analyses of six parameters between the negative group (0 mmHg) and positive groups (100 mmHg and 150 mmHg) by *t*-test. A *p*-value of less than 0.05 is highlighted in red.

	R-Light			IR-Light		
	0 mmHg (N = 74)	100 mmHg (N = 72)	150 mmHg (N = 78)	0 mmHg (N = 79)	100 mmHg (N = 74)	150 mmHg (N = 71)
m_{10} (mV/s)	4.76 ± 2.47	3.86 ± 2.53 (0.0325)	3.74 ± 2.40 (0.0108)	3.41 ± 1.96	2.54 ± 1.84 (0.0056)	2.11 ± 1.48 (1.2×10^{-5})
m_{50} (mV/s)	-1.99 ± 1.26	-1.28 ± 0.89 (0.0002)	-1.21 ± 0.81 (1.1×10^{-5})	-1.86 ± 1.20	-1.28 ± 0.92 (0.0010)	-0.89 ± 0.58 (4.1×10^{-9})
VP_1 (mV)	73.7 ± 37.7	60.2 ± 39.2 (0.0365)	58.7 ± 38.0 (0.0158)	54.3 ± 31.4	39.8 ± 29.0 (0.0037)	33.2 ± 23.5 (7.6×10^{-6})
VP_2 (mV)	53.0 ± 30.8	38.0 ± 24.1 (0.0013)	40.0 ± 23.0 (0.0035)	47.2 ± 29.0	33.4 ± 23.8 (0.0017)	24.5 ± 14.8 (1.7×10^{-8})
m_{40} (mV/s)	-2.67 ± 2.06	-1.67 ± 1.25 (0.0007)	-1.30 ± 1.07 (8.0×10^{-7})	-2.74 ± 1.86	-1.96 ± 1.31 (0.0032)	-1.30 ± 0.91 (1.6×10^{-8})
m_{60} (mV/s)	-1.55 ± 0.92	-1.07 ± 0.70 (0.0006)	-1.12 ± 0.67 (0.001)	-1.41 ± 0.88	-0.98 ± 0.70 (0.0012)	-0.70 ± 0.44 (8.2×10^{-9})

Table 3. Statistical analyses of six parameters, being maximum, median, and minimum values between the negative group (0 mmHg) and positive groups (100 mmHg and 150 mmHg) by *t*-test. A *p*-value of less than 0.05 is highlighted in red.

		R-Light			IR-Light		
		0 mmHg	100 mmHg	150 mmHg	0 mmHg	100 mmHg	150 mmHg
VP_1 (mV)	Maxi.	87.4 ± 39.8	74.5 ± 46.2 (0.1969)	71.5 ± 43.1 (0.0997)	65.5 ± 32.6	48.5 ± 34.9 (0.0284)	40.6 ± 25.7 (0.0005)
	Med.	74.9 ± 35.0	65.0 ± 43.6 (0.2819)	58.8 ± 36.3 (0.0556)	54.7 ± 26.8	42.5 ± 34.1 (0.0840)	34.3 ± 23.0 (0.0007)
	Min.	62.0 ± 35.4	55.8 ± 44.5 (0.5029)	46.4 ± 32.0 (0.0501)	43.1 ± 26.1	36.7 ± 34.6 (0.3618)	28.2 ± 22.6 (0.0104)
VP_2 (mV)	Maxi.	65.4 ± 33.4	48.7 ± 26.0 (0.0192)	47.7 ± 25.5 (0.0125)	58.4 ± 31.6	39.4 ± 26.0 (0.0049)	30.4 ± 15.2 (7.2×10^{-6})
	Med.	54.7 ± 29.2	40.6 ± 23.2 (0.0244)	40.3 ± 21.2 (0.0182)	48.4 ± 26.6	34.1 ± 23.8 (0.0145)	25.2 ± 12.9 (1.0×10^{-5})
	Min.	44.2 ± 30.4	33.0 ± 24.0 (0.0839)	33.7 ± 19.3 (0.0820)	38.1 ± 26.3	28.8 ± 24.0 (0.1056)	20.7 ± 13.2 (0.0006)

Table 3. *Cont.*

		R-Light			IR-Light		
		0 mmHg	100 mmHg	150 mmHg	0 mmHg	100 mmHg	150 mmHg
m_{10} (mV/s)	Maxi.	5.65 ± 2.60	4.83 ± 2.97 (0.2098)	4.64 ± 2.64 (0.1019)	4.15 ± 2.03	3.07 ± 2.19 (0.0263)	2.59 ± 1.57 (0.0004)
	Med.	4.84 ± 2.24	4.21 ± 2.76 (0.2800)	3.79 ± 2.25 (0.0466)	3.42 ± 1.64	2.72 ± 2.16 (0.1119)	2.19 ± 1.42 (0.0192)
	Min.	3.99 ± 2.23	3.59 ± 2.81 (0.4841)	2.98 ± 2.04 (0.0452)	2.64 ± 1.59	2.37 ± 2.23 (0.5433)	1.80 ± 1.42 (0.0192)
m_{40} (mV/s)	Maxi.	-2.10 ± 2.00	-1.21 ± 1.01 (0.0196)	-0.93 ± 0.91 (0.0021)	-2.11 ± 1.66	-1.53 ± 1.08 (0.0723)	-1.02 ± 0.69 (0.0004)
	Med.	-2.83 ± 1.99	-1.74 ± 0.96 (0.0036)	-1.36 ± 0.91 (0.0001)	-2.83 ± 1.72	-1.90 ± 1.14 (0.0069)	-1.33 ± 0.77 (8.6×10^{-6})
	Min.	-3.48 ± 2.29	-2.30 ± 1.32 (0.0079)	-1.85 ± 1.12 (0.0002)	-3.46 ± 2.08	-2.30 ± 1.41 (0.0051)	-1.66 ± 0.98 (1.1×10^{-5})
m_{50} (mV/s)	Maxi.	-1.62 ± 1.22	-1.07 ± 0.86 (0.0254)	-0.97 ± 0.64 (0.0048)	-1.47 ± 1.04	-1.06 ± 0.86 (0.0597)	-0.72 ± 0.48 (0.0002)
	Med.	-2.06 ± 1.17	-1.37 ± 0.82 (0.0044)	-1.23 ± 0.70 (0.0005)	-1.91 ± 1.11	-1.28 ± 0.87 (0.0074)	-0.92 ± 0.49 (4.1×10^{-6})
	Min.	-2.48 ± 1.35	-1.69 ± 0.96 (0.0047)	-1.56 ± 0.89 (0.0009)	-1.06 ± 1.33	-1.52 ± 1.01 (0.0041)	-1.13 ± 0.60 (5.2×10^{-6})
m_{60} (mV/s)	Maxi.	-1.30 ± 0.91	-0.92 ± 0.70 (0.0536)	-0.94 ± 0.55 (0.048)	-1.13 ± 0.81	-0.83 ± 0.70 (0.084)	-0.59 ± 0.38 (0.0005)
	Med.	-1.61 ± 0.87	-1.14 ± 0.68 (0.0132)	-1.13 ± 0.60 (0.0083)	-1.43 ± 0.82	-0.99 ± 0.70 (0.0108)	-0.73 ± 0.38 (7.9×10^{-6})
	Min.	-1.92 ± 0.99	-1.40 ± 0.77 (0.0112)	-1.35 ± 0.74 (0.0061)	-1.74 ± 0.96	-1.16 ± 0.78 (0.0039)	-0.88 ± 0.45 (5.5×10^{-6})

Table 4. The fusion matrix, performances, cut points, and receiver operating characteristic (ROC) areas of six parameters. TP is the true positive, TN the true negative, FP the false positive, and FN the false negative.

Parameter	DVT Scenario	TP	TN	FP	FN	Acc. (%)	Pre. (%)	Sen. (%)	Spe. (%)	Cut Point	ROC Area(%)
VP_1 (mV)	100 mmHg	26	27	12	13	0.68	0.68	0.67	0.69	45	0.76
	150 mmHg	20	35	4	16	0.73	0.83	0.56	0.9	31	0.76
VP_2 (mV)	100 mmHg	29	23	16	10	0.67	0.64	0.74	0.59	41	0.78
	150 mmHg	19	35	4	17	0.72	0.83	0.53	0.9	26	0.81
m_{10} (mV/s)	100 mmHg	29	27	12	10	0.72	0.71	0.74	0.69	3.15	0.79
	150 mmHg	28	27	12	8	0.73	0.7	0.78	0.69	3.05	0.78
m_{40} (mV/s)	100 mmHg	32	22	17	7	0.69	0.65	0.82	0.56	-2.31	0.82
	150 mmHg	28	29	10	8	0.76	0.74	0.78	0.74	-1.79	0.86
m_{50} (mV/s)	100 mmHg	31	23	16	8	0.69	0.66	0.79	0.59	-1.76	0.76
	150 mmHg	26	29	10	10	0.73	0.72	0.72	0.74	-1.35	0.81
m_{60} (mV/s)	100 mHg	30	23	16	9	0.68	0.65	0.77	0.59	-1.33	0.76
	150 mmHg	22	32	7	14	0.72	0.76	0.61	0.82	-0.88	0.80

Note: Acc., Pre., Sen., and Spe. are abbreviations for accuracy, precision, sensitivity, and specificity, respectively.
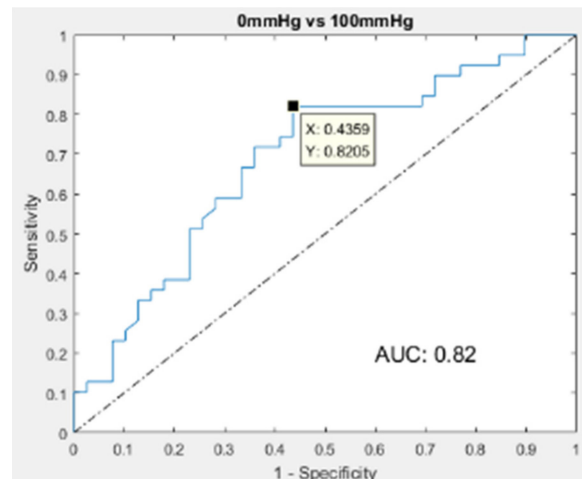
(**a**)
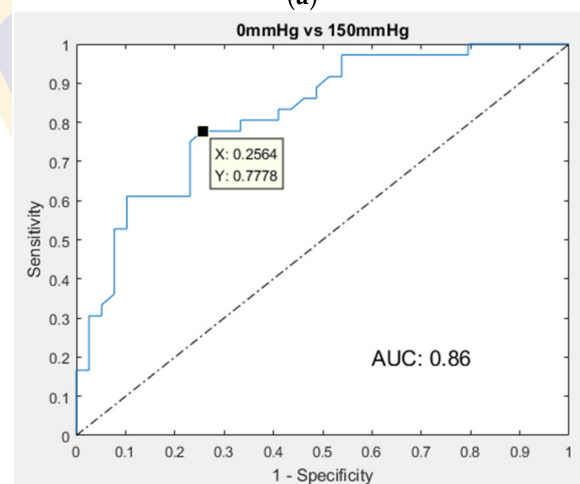
(**b**)

Figure 9. ROC curves of m_{40}: (**a**) the area under the curve is 0.82 in the slight DVT scenario, (**b**) the area under the curve is 0.86 in the serious DVT scenario.

4. Discussion

DVT is a prevalent disease with an occurrence of between 2.5% to 5% in the total population, and about $30-40\%$ of DVT patients will finally suffer from pulmonary embolism [26]. The diagnosis of DVT in the clinic is notoriously unreliable because only about 30% of patients have been shown to be positive on objective testing [6,27]. Therefore, suspected DVT in clinical diagnosis could lead to the unnecessary hospitalization of patients, and inappropriate anticoagulation therapy with potentially dangerous consequences.

The LRR technique has been used in several studies for the noninvasive examination of patients with suspected lower limb DVT [28,29]. The technique uses the parameters of the LRR curve, such as the amplitude and rate of venous emptying [30], the time of venous refilling [28], and the shape of the LRR curve [16]. Tan et al. proposed using the amplitude of venous emptying and time of venous refilling to test DVT diagnosis and found that the two parameters achieved an optimal sensitivity of 100% and 100%, and specificities of 35% and 47%, respectively. Additionally, the areas under the ROC curves for the two parameters are 0.74 and 0.75, respectively [29]. In the present study, one of our findings is that the performance of the IR-light measurement is better than that of the R-light measurement (Tables 2 and 3). The reason for this is partially due to deeper penetrating tissue by the IR light than by the red light [31]. Thus, the LRR signal with the IR-light measurement has a higher sensitivity for the positive DVT group. The accuracies and ROC areas of m_{40} and m_{10} in the serious DVT scenario are 76% and 73%, and 0.86 and 0.78, respectively. Moreover, for various venous occluded scenarios, the performance of

m_{40} is significantly lower using the occluded pressure of 100 mmHg than the occluded pressure of 150 mmHg, with sensitivity and specificity of 100% and 10% vs. sensitivity and specificity of 100% and 20.2%, respectively. The present results seem no better than previous ones [14–16]. The main reason for this could be that our study does not examine real DVT patients. In the present study, embolization due to thrombus is simulated by directly occluding veins through a high pressure (100 mmHg or 150 mmHg) cuff wrapping around the thigh. The cuffs inflated up to 100 and 150 mmHg are employed to simulate the mild or serious stenosis in deep veins. The deep veins of lower limbs in the 20 subjects may not effectively respond to the phenomenon of embolization in real time. It is found that the results for DVT detection are always better under the 150 mmHg compared with the 100 mmHg. Thus, such finding may, in part, explain this problem.

The study has successfully developed a DVT examination system that may be available in non-medical places and help to examine whether users have DVT of lower limbs. To do so, an obvious challenge is how to obtain an optimal position for the LRR probe in order to apply the system. In the first rule proposed in the study, both the accelerometer and the LRR signals in the emptying phase are used to determine if the PPG sensor detects the upstream or downstream venous blood flow. Once the LRR curve is obtained from the downstream of the venous blood flow, it can be further utilized to find two characteristic parameters, m_{40} and m_{10}. In the second rule, the values of both VP_1 and VP_2 parameters should be greater than zero. If the value of either the VP_1 or the VP_2 parameter is negative, the baseline drift phenomenon must exist in the LRR curve operation.

This study aimed to develop the prototype of an examination system used at non-medical places for detecting DVT in lower limbs using LRR. The prototype of this DVT examination system shows that the commercial reflective PPG sensors and accelerometer could be used for deep vein thrombosis (DVT) detection in lower limbs at a non-medical place. Moreover, based on a wireless technique, this measurement system can be operated to control the actions of sensors and display and store the LRR signals on the APP of a smartphone. To comply with the Subject Consent Form in the approved Institutional Review Board (IRB) project, the authors were only allowed to recruit healthy subject to do the related clinical trials. The DVT with stenosis phenomenon in unhealthy participants was reasonably simulated by inflating the cuff up to 100 mmHg or 150 mmHg. Although two characteristic parameters, m40 and m10, in the PPG signals measured with the prototype are available for distinguishing the negative from the positive group, we did not prove that these two parameters would become standard parameters for the DVT examination. The reason for this is that the recruited subjects were all healthy adults. In the next study, the authors will again apply the IRB for clinical trials including healthy and unhealthy subjects based on the current findings in applying the prototype.

In the system, an array of optical sensors and a motion sensor were designed. Users are asked to only put the two kinds of sensors at the proper places, and then operate the APP. The APP will automatically connect the wearable device to a smartphone and test the LRR signals, and the users should follow the instruction of the APP to move their foot. Finally, the examination reports will be promptly displayed by means of the APP. Moreover, the approved IRB only allows us to perform the clinical trial on healthy subjects. Thus, the included subjects all were the healthy young subjects (50% male and 50% female). However, based on the current results in this study for DVT detection, the authors will apply the IRB for the clinical trial on patients with DVT in the next study.

5. Conclusions

The wearable device must be user-friendly and easy to operate, and it must be usable at non-medical institutes. Based on the LRR, the examination system has been developed for screening tests in subjects with lower limb DVT and holds several advantages over previous LRR instruments. The proposed system includes a wearable device and APP program. The wearable device not only has an array probe with three reflective PPG sensors, but also has an accelerometer to detect the foot action conditions. The wearable

device can compensate blood displacement for different cutaneous optical densities because of skin color, skin thickness, and soft tissue, and it permits quantitative evaluation of vein position by the quality of the LRR signal. The APP program can control the functions of the wearable device, instruct the rhythm of the foot action, and display and store the LRR signals. Twenty healthy subjects were recruited to perform experiments to verify the performance of this prototype. One important finding is that the two characteristic parameters, m40 and m10, both can be applied to detect the DVT of loer limbs without missing any positive cases. This suggests that the prototype of the examination system has the potential for screening for DVT in non-medical environments.

Author Contributions: Conceptualization, S.-H.L.; methodology, J.-J.W. and S.-H.L.; software, S.-H.L.; validation, C.-H.S. and K.-L.P.; writing—original draft preparation, S.-H.L.; writing—review and editing, J.-J.W. and W.C. All authors have read and agreed to the published version of the manuscript.

References

1. Jaff, M.R.; McMurtry, M.S.; Archer, S.L.; Cushman, M.; Goldenberg, N.; Goldhaber, S.Z.; Jenkins, J.S.; Kline, J.A.; Michaels, A.D.; Thistlethwaite, P.; et al. Management of massive and submassive pulmonary embolism, iliofemoral deep vein thrombosis, and chronic thromboembolic pulmonary hypertension. *Circulation* **2011**, *123*, 1788–1830. [CrossRef]
2. Lee, C.H.; Lin, L.J.; Cheng, C.L.; Kao Yang, Y.H.; Chen, J.Y.; Tsai, L.M. Incidence and cumulative recurrence rates of venous thromboembolism in the Taiwanese population. *J. Thromb. Haemost.* **2010**, *8*, 1515–1523. [CrossRef] [PubMed]
3. Ansari, M.T.; Cheung, B.M.; Qing Huang, J.; Eklof, B.; Karlberg, J.P. Traveler's thrombosis: A systematic review. *J. Travel Med.* **2005**, *12*, 142–154. [CrossRef] [PubMed]
4. Scurr, J.H.; Machin, S.J.; Bailey-King, S.; Mackie, I.J.; McDonald, S.; Smith, P.D. Frequency and prevention of symptomless deep-vein thrombosis in long-haul flights: A randomised trial. *Lancet* **2001**, *357*, 1485–1489. [CrossRef]
5. White, R.H.; McGahan, J.P.; Daschbach, M.M.; Hartling, R.P. Diagnosis of deep-vein thrombosis using duplex ultrasound. *Ann. Intern. Med.* **1989**, *111*, 297–304. [CrossRef] [PubMed]
6. Lensing, A.W.; Büller, H.; Prandoni, P.; Batchelor, D.; Molenaar, A.H.; Cogo, A.; Vigo, M.; Huisman, P.M.; ten Cate, J.W. Contrast venography, the gold standard for the diagnosis of deep-vein thrombosis: Improvement in observer agreement. *Thromb. Haemost.* **1992**, *67*, 08–12.
7. Hull, R.; Aken, W.G.; Hirsh, J.; Gallus, A.; Hoicka, G.; Turpie, A.G.; Walker, I.; Gent, M. Impedance plethysmography using the occlusive cuff technique in the diagnostic of venous thrombosis. *Circulation* **1976**, *53*, 696–700. [CrossRef]
8. Hull, R.; Taylor, D.W.; Hirsh, J.; Sackett, D.L.; Powers, P.; Turpie, A.G.G.; Walker, I. Impedance plethysmography: The relationship between venous filling and sensitivity and specificity for proximal vein thrombosis. *Circulation* **1978**, *58*, 898–902. [CrossRef]
9. Sandler, D.A.; Duncan, J.S.; Ward, P. Diagnosis of deep-vein thrombosis: Comparison of clinical evaluation, ultrasound, plethysmography, and venoscan with X-ray venogram. *Lancet* **1984**, *324*, 716–719. [CrossRef]
10. Ginsberg, J.S.; Kearon, C.; Douketis, J.; Turpie, A.G.; Brill-Edwards, P.; Stevens, P.; Panju, A.; Patel, A.; Crowther, M.; Andrew, M.; et al. The use of D-Dimer testing and impedance plethysmographic examination in patients with clinical indications of deep vein thrombosis. *Arch. Intern. Med.* **1997**, *157*, 1077–1081. [CrossRef] [PubMed]
11. Lensing, A.W.A.; Prandoni, P.; Brandjes, D. Detection of deep-vein thrombosis by real-time B-mode ultrasonography. *N. Engl. J. Med.* **1989**, *320*, 342–345. [CrossRef] [PubMed]
12. Goodacre, S.; Sampson, F.; Stevenson, M.; Wailoo, A.; Sutton, A.; Thomas, S.; Locker, T.; Ryan, A. Measurement of the clinical and cost-effectiveness of non-invasive diagnostic testing strategies for deep vein thrombosis. *Health Technol. Assess.* **2006**, *10*, 1–168. [CrossRef] [PubMed]
13. Shepard, A.D.; Mackey, W.C.; O'Donnell, T.F.; Heggerick, P.A. Light reflection rheography: A new non-invasive test of venous function. *Bruit* **1984**, *8*, 266–270.

14. Neumann, H.A.; Boersma, I.D.S. Light reflection rheography: A non-Invasive diagnostic tool for screening for venous disease. *J. Dermatol. Surg. Oncol.* **1992**, *18*, 425–430. [CrossRef] [PubMed]

15. Arora, S.; Lam, D.; Kennedy, C.; Meier, G.H.; Gusberg, R.J.; Negus, D. Light reflection rheography: A simple noninvasive screening test for deep vein thrombosis. *J. Vasc. Surg.* **1993**, *18*, 767–772. [CrossRef]

16. Thomas, P.R.S.; Butler, C.M.; Bowman, J.; Bowman, J.; Grieve, N.W.T.; Bennett, C.E.; Taylor, R.S.; Thomas, M.H. Light reflection rheography: An effective non-invasive technique for screening patients with suspected deep venous thrombosis. *Br. J. Surg.* **1991**, *78*, 207–209. [CrossRef] [PubMed]

17. Prawiro, A.P.J.; Chou, N.-K.; Lee, M.-W.; Lin, Y.-H. A wearable system that detects posture and heart rate: Designing an integrated device with multi-parameter measurements for better health care. *IEEE Consum. Electron. Mag.* **2019**, *8*, 78–83. [CrossRef]

18. Yu, L.; Chan, W.; Zhao, Y.; Tsui, K.-L. Personalized health monitoring system of elderly wellness at the community level in Hong Kong. *IEEE Access* **2018**, *6*, 35558–35567. [CrossRef]

19. Liu, S.-H.; Wang, J.-J.; Su, C.-H.; Tan, T.-H. Development of a patch-type electrocardiographic monitor for real time heartbeat detection and heart rate variability analysis. *J. Med. Biol. Eng.* **2018**, *38*, 411–423. [CrossRef]

20. Liu, S.-H.; Lin, C.-B.; Chen, Y.; Chen, W.; Huang, T.-S.; Hsu, C.-Y. An EMG patch for the real-time monitoring of muscle-fatigue conditions during exercise. *Sensors* **2019**, *19*, 3108. [CrossRef]

21. Ijaz, M.F.; Attique, M.; Son, Y. Data-driven cervical cancer prediction model with outlier detection and over-sampling methods. *Sensors* **2020**, *20*, 2809. [CrossRef] [PubMed]

22. Alia, F.; El-Sappagh, S.; Islamd, S.M.R.; Kwake, D.; Alif, A.; Imrang, M.; Kwakh, K.-S. A smart healthcare monitoring system for heart disease prediction based on ensemble deep learning and feature fusion. *Inf. Fusion* **2020**, *63*, 208–222. [CrossRef]

23. Analog Devices. AD8232. Available online: http://www.analog.com/en/products/amplifiers/instrumentation-amplifiers/ad8232.html#product-overview (accessed on 31 March 2021).

24. MAX30101 Datasheet and Product Info Maxim Integrated. Available online: https://www.maximintegrated.com/en/products/sensors/MAX30101.html (accessed on 31 March 2021).

25. Analog Devices. ADXL325. Available online: http://www.analog.com/en/products/sensors-mems/accelerometers/adxl325.html (accessed on 31 March 2021).

26. Geerts, W.H.; Heit, J.A.; Clagett, G.P.; Pineo, G.F.; Colwell, C.W.; Anderson, F.A.; Wheeler, H.B. Prevention of venous thromboembolism. *Chest* **2001**, *119*, 132S–175S. [CrossRef] [PubMed]

27. Salcuni, M.; Fiorentino, P.; Pedicelli, A.; Di Stasi, C. Diagnostic imaging in deep vein thrombosis of the limbs. *Rays* **1996**, *21*, 328–339.

28. Abbott, G.T.; Diggory, R.T.; Harris, I. Comparison of light reflection rheography with ascending venography in the diagnosis of lower limb deep vein thrombosis. *Br. J. Radiol.* **1995**, *68*, 593–595. [CrossRef] [PubMed]

29. Tan, Y.K.; da Silva, A.F. Digital photoplethysmography in the diagnosis of suspected lower limb DVT: Is it useful? *Eur. J. Vasc. Endovasc. Surg.* **1999**, *18*, 71–79. [CrossRef]

30. Mitrani, A.A.; Gonzalez, M.L.; O'Connell, M.T.; Guerra, J.; Harwood, R.B.; Gardner, L.B. Detection of clinically suspected deep vein thrombosis using light reflection rheography. *Am. J. Surg.* **1991**, *161*, 646–650. [CrossRef]

31. Liu, J.; Yan, B.P.; Zhang, Y.T.; Ding, X.R.; Su, P.; Zhao, N. Multi-wavelength photoplethysmography enabling continuous blood pressure measurement with compact wearable electronics. *IEEE Trans. Biomed. Eng.* **2019**, *66*, 1514–1525. [CrossRef]

frontiers
in Neurology

Bilateral Vertebral Artery Hypoplasia and Fetal-Type Variants of the Posterior Cerebral Artery in Acute Ischemic Stroke

Chung-Fu Hsu [1,2], Kuan-Wen Chen [1,2], Chun-Hung Su [3,4], Chao-Yu Shen [3,5] and Hsin-Yi Chi [1,2,6*]

[1] Department of Neurology, Chung Shan Medical University Hospital, Taichung, Taiwan, [2] Department of Neurology, Chung Shan Medical University, Taichung, Taiwan, [3] Institute of Medicine, School of Medicine, Chung Shan Medical University, Taichung, Taiwan, [4] Division of Cardiology, Department of Internal Medicine, Chung Shan Medical University Hospital, Taichung, Taiwan, [5] Department of Medical Imaging, Chung Shan Medical University Hospital, Taichung, Taiwan, [6] College of Medicine, Pharmacological Institute, National Taiwan University, Taipei, Taiwan

Aim: Unilateral vertebral artery hypoplasia is considered a risk factor for posterior circulation infarction. Despite the increasing attention on unilateral vertebral artery hypoplasia, few studies have discussed bilateral vertebral artery hypoplasia, its influence on stroke, or its collateral supply from the circle of Willis. We aimed to identify its characteristics, stroke pattern, and unique ultrasonographic and brain imaging findings.

Materials and Methods: Of the 1,301 consecutive in-patients diagnosed with acute ischemic stroke from January 2013 to December 2015, medical and laboratory data and stroke or transient ischemic attack history were recorded. We enrolled patients who underwent both brain magnetic resonance imaging and sonography examinations. Vertebral artery and posterior cerebral artery analyses were conducted in accordance with clinical criteria.

Results: Adequate imaging data were available for 467 patients. Of these, eight patients met the criteria for bilateral vertebral artery hypoplasia. The mean age was 62.9 $\pm$ 12.1 years. There were six male (75.0%) and two female patients (25.0%). A high prevalence of hypertension (7/8, 87.5%) was noted.

Sonograms displayed a very low net flow volume in the vertebral arteries, with the average net flow volume being 28.9 $\pm$ 9.7 mL/min. A high frequency (6/8; 75.0%) of the fetal variant posterior cerebral artery from the carotids was found. The infarction patterns in these patients were all bilateral, scattered, and in multiple vascular territories.

Conclusion: Patients with bilateral vertebral hypoplasia displayed a unique collateral supply, special stroke pattern, and younger stroke onset. Early recognition and stroke prevention should be considered critical in clinical practice.

Keywords: posterior circulation infarction, vertebral artery hypoplasia, posterior cerebral artery, vertebrobasilar insufficiency, ultrasonagraphy

INTRODUCTION

Posterior circulation is comprised of two vertebral arteries that join to form a single basilar artery at the level of the pons. The basilar artery divides into two posterior cerebral arteries at the level of the midbrain (1–3). Conventionally, the major hemodynamics of this area is supplied by the net flow of the vertebral arteries and partially by the collateral flow from the spinal arteries or the fetal-type posterior cerebral artery (1, 4).

Case series studies suggest that vertebral artery hypoplasia (VAH) may contribute to posterior ischemic events, especially in patients with other cerebrovascular risk factors (5, 6). The concept of regional hypoperfusion is associated with unilateral VAH and posterior circulation stroke (7). The risk of posterior ischemia is related to an increasing degree of VAH (5, 6, 8), regardless of the net flow (7). Although an increasing number of studies highlight the importance of unilateral VAH on ischemic stroke (5, 6, 8, 9), literature discussing the influence of bilateral VAH on ischemic stroke is limited (10, 11).

With regard to bilateral VAH, low flow volume in a single vertebral artery as well as inadequate net flow volume in the basilar artery ensues. Because of the chronic nature of congenital hypoplasia, the clinical symptoms and stroke patterns of this vascular disorder would differ from unilateral VAH. Chronic inadequate posterior circulation leads to the development of intracranial and extracranial collateral flow (10, 12). Recently, a case series paper correlated the fetal-type posterior circle of Willis with vertebrobasilar hypoplasia (12, 13).

In order to identify obscure clinical features, we reviewed the characteristics of patients with bilateral VAH by analyzing their clinical presentations, stroke patterns, risk factors, and the hemodynamics of collateral flow using ultrasonography and brain magnetic resonance imaging (MRI).

MATERIALS AND METHODS

Patients

This is a retrospective, observational cross-sectional study. We reviewed 1,301 consecutive in-patients diagnosed with acute ischemic stroke at the Chung Shan Medical University Hospital from January 2013 to December 2015.

Upon admission, the series examination included an MRI, sonography exam, and a stroke risk factor survey. Patients who did not receive a brain MRI or sonography exam were excluded.

Patient medical and laboratory data were recorded; this included the age, sex, presence of systemic diseases, renal function, lipid profile, drug use, electrocardiogram, and history of previous stroke or transient ischemic attacks and related clinical manifestations.

This study was approved by the Institutional Review Board of Chung Shan Medical University Hospital, Taichung, Republic of China.

MRI

The infarction lesions were identified and classified by vascular territory according to MRI and three-dimensional time of flight (3D TOF) magnetic resonance angiography (MRA)

examinations. A 3-T MRI system (Siemens, Germany) with the following settings was used T2-weightedimages, TR/TE 6000/100 ms, diffusion-weighted images TR/TE 5100/60 ms, and 3D TOF TR/TE20/4 ms. The locations of ischemic stroke were categorized as proximal (medulla and posterior inferior cerebellum), middle (pons and anterior inferior cerebellum), and distal (rostral brainstem, superior cerebellum, and occipital and temporal lobes) intracranial posterior circulation territories (14, 15).

A fetal type posterior cerebral artery (PCA) was classified as complete or partial according to MRA (12, 13). A complete fetal-type PCA is considered if the P1 segment is not visualized, and a partial fetal-type PCA is considered if the P1 segment is smaller than the posterior communicating artery on brain MRI.

The basilar artery hypoplasia (BAH) was defined as a basilar artery (BA) diameter <2 mm. The BA diameter was calculated on TOF source images at the mid-pons level. Vascular dissection was diagnosed if intramural hematoma, intimal flap, the pearl-and-string, or the double lumen signs were visualized on MRI.

Brain images were reviewed by neuroradiologists and neurologists, with the former interpreting the fetal-type PCA.

Sonography

Color-coded carotid duplex and transcranial color-coded duplex examinations were reviewed for all enrolled patients. Intracranial and extracranial vessels conducted by experienced technicians using an IE-33 system (Philips Medical System, USA), equipped with a 2.0-MHz transducer. Routine measurements included thorough examinations of the bilateral neck carotid and transforaminal windows. The angle between the ultrasound beam and the direction of blood flow was adjusted manually. Blood flow examinations were targeted at the V2 and V4 segments of the vertebral artery as well as the region proximal to the distal basilar artery. The diameter and flow volume of each extracranial vertebral artery, as well as the mean velocity, and pulsatility index of the intracranial vertebrobasilar arteries were recorded and analyzed. VAH was defined according to sonographic criteria (4, 16, 17), including a ≤2.2 mm diameter over the V2 segment or a decreased vertebral flow volume of ≤30 mm/s. Bilateral VAH was defined as both vertebral arteries meeting the sonographic criteria of VAH and there was no evidence of dissection findings on MRI.

Statistics

All statistical analyses were performed using SPSS software (version 22.0; SPSS Inc., Chicago, IL, USA). Continuous data is expressed as mean±SD.

RESULTS

Of the 1,301 patients diagnosed with acute ischemic stroke, 467 (149 pateints with posterior circulation infarction) underwent both MRI and sonographic examinations and were enrolled in the present study. In patients with posterior circulation, 80 of them met the criteria of unilateral VAH. Eight of the enrolled patients met the diagnostic criteria for bilateral VAH. The mean BA diameter was 2.68 ± 0.20 mm (range from 2.29 to 3.08 mm).

In our study, the frequency of bilateral VAH was 1.7% (8/467), which is similar to that found in previous studies (11, 18). The characteristics of patients with bilateral VAH are listed in **Table 1**.

TABLE 1 | Demographic and clinical characteristics of eight patients with bilateral vertebral artery hypoplasia.

	Bilateral hypoplasia (n = 8)	Range
Age on stroke, years, mean ±SD	62.9 ± 12.1	46–87
Gender(male), n (%)	6 (75%)	
Hypertension, n (%)	7 (87.5%)	
Diabetes, n (%)	2 (25%)	
Hyperlipidemia, n (%)	1 (12.5%)	
Smoking, n (%)	2 (25%)	
Alcohol, n (%)	2 (25%)	
Renal function, eGFR(mg/dL)	77.3 ± 25.8	29–119
Atrial fibrillation or heart disease, n (%)	0 (0%)	

SD, standard deviation; Egfr, estimated glomerular filtration rate.

TABLE 2 | Total VA flow volume, onset age and stroke location analysis in bilateral, unilateral, or non-vertebral artery hypoplasia groups.

	Non-VAH (61 cases)	Unilateral-VAH (80 cases)	Bilateral-VAH (8 cases)
Total VA flow volume	132.9 ± 31.8 mL/min	71.4 ± 21.1 mL/min	28.9 ± 9.7 mL/min
Stroke onset age	66.6 ± 11.5	72.4 ± 10.2	62.9 ± 12.9
Multiple vascular territory infarctions	9/61 (14.7%)	17/80 (21.2%)	5/8 (62.5%)

VAH, vertebral artery hypoplasia; VA, vertebral artery.

There were six male (75.0%) and two female patients (25.0%). The average age was 62.9 years (range, 46–87). None of these patients had atrial fibrillation or heart disease. A high prevalence of hypertension (7/8, 87.5%) was noted. The prevalence of other stroke risk factors, including diabetes mellitus, dyslipidemia, smoking, and alcohol consumption ranged from 12.5 to 25.0%. We compared net flow volume, onset age, and stroke location analysis in bilateral VAH, unilateral VAH, and non-VAH groups, listed in **Table 2**. The mean net flow volume was 28.9 ± 9.7 mL/min, which is below the criteria of vertebrobasilar insufficiency (<100 mL/min) (7), and the defined value of unilateral VAH (30 mL/min) (16). In the bilateral VAH group, we found their onset age was younger and with more multiple vascular territory lesions.

The distribution of stroke and individual PCA types is listed in **Table 3**. Most of the infarctions were bilateral and multiple (5/8, 62.5%). A fetal-type PCA was recognized in six patients (6/8, 75.0 %), two with a complete bilateral, two with a partial bilateral, and two with a complete unilateral fetal-type PCA.

DISCUSSION

The prevalence of VAH ranges from 4 to 7% in the normal population (6, 7, 17). In posterior circulation stroke, the prevalence is increased to more than 40% according to different clinical studies (5, 18). Bilateral VAH is recognized in 1.6 to 3.4 % of patients with ischemic stroke (9, 18).

In our previous study, compared to anterior circulation infarction, there was a significantly higher frequency of VAH in posterior circulation infarction (22.38 vs. 44.75%, $p < 0.0001$) (7). Literature has demonstrated that VAH plays an important role in posterior circulation stroke (5–7, 9).

TABLE 3 | Infarction region and clinical manifestation of stroke in patient population.

Age	Gender	Infarction territory	Brain territory locations	PCA type	Initial manifestation at stroke
41–50	Male (Patient 1)	Pons, midbrain and bilateral cerebellum hemisphere	*P+M+D	Bilateral fetal type	Dizziness and unsteady gait
	Male (Patient 2)	Left PICA territory (lateral medulla)	P	Bilateral partial fetal type	Right limb paresthesia
51–60	Male (Patient 3)	Right medulla, pons, and cerebellum	P+M	Right fetal type	Dizziness, diplopia and left facial paresthesia
	Female (Patient 4)	Left pons and bilateral cerebellum hemisphere	P+M+D	Bilateral partial fetal type	Dizziness and unsteady gait
61–70	Male (Patient 5)	Left pons and left anterior medulla and right vermis	P+M+D	Non-fetal type	Right hemiparesis and unsteady gait, lethargy
	Male (Patient 6)	Left thalamus and left occipital lobe	D	Right fetal type	Blurred vision and right hemiparesis and right paresthesia
71–80	Male (Patient 7)	Bilateral pons (right>left), midbrain, and bilateral cerebellar hemisphere	P+M+D	Non-fetal type	Severe dysarthria and left hemiplegia
81–90	Female (Patient 8)	Bilateral pons and cerebellar hemisphere	M+D	Bilateral fetal type	Dysarthria, dysphagia, and unsteady gait

*P, proximal; M, middle; D, distal posterior circulation territory.

In this study, we found that patients with bilateral VAH developed stroke at a younger age (six patients <66 years) than the mean age of ischemic stroke, which ranges from 66 to 70 years [19], and other groups with posterior circulation infarctions (**Table 2**). The prevalence of hypertension in this group was significantly higher than the general stroke population [20]. Cerebral autoregulation for chronic vertebrobasilar insufficiency may explain the blood pressure response [21].

Table 3 displays the initial manifestation of the patient population, which included dizziness, severe dysarthria, hemiplegia, and ataxia. In unilateral VAH-related stroke, the location of the infarct is usually limited to the territory of the ipsilateral artery, particularly in lateral medullar infarction and posterior inferior cerebellar artery infarction [2, 22, 23]. In bilateral VAH, the infarction territory was mostly bilateral, involving multiple vascular territories, despite receiving collateral blood supply from the fetal-type PCA (**Table 3** and **Figure 1**). The clinical presentation of these patients illustrates the high variability and burden of posterior circulation infarction. Most cases of multiple infarctions resulted in severe handicap or coma; therefore, it is important to detect at-risk patients.

Scattered brain infarction is usually related to cardioembolic stroke or artery-to-artery embolism [24]; however, no patients in our population had atrial fibrillation, other heart disease, or significant atherosclerosis across the major arteries, suggesting the effect of hypoperfusion in bilateral VAH-related stroke. Several studies reported unilateral VAH to be associated with relative hypoperfusion in the dependent vascular territory [5, 7]. According to the extracranial ultrasonography of our patient group, the mean (±SD) of the total vertebral flow volume was low (28.9 ± 9.7 mL/min, **Table 2**), compared with the non-VAH or unilateral VAH group (**Table 2**), which suggest severe hypoperfusion of the vertebrobasilar system, and as a consequence, development of an earlier and more severe posterior circulation infarction (**Table 2**).

In this study, bilateral VAH evolving into a smaller basilar artery (mean BA diameter 2.68 ± 0.20 mm, range from 2.29 to 3.08 mm) was recognized. Artery to artery embolism from vertebrobasilar hypoplasia would also contribute to scattered infarctions. Literature has demonstrated [25] BAH was associated with pontine infarction and VAH was associated with the medulla and inferior cerebellum. Emboli were known to preferentially reach the distal posterior circulation arteries [14]. However, it is difficult to recognize the true origin of embolism since the artery to artery embolism and large artery hemodynamic should be one of concern.

For the treatment of bilateral VAH, early preventive drugs for ischemic insults, including antiplatelet or anticoagulant drugs, could be considered in symptomatic patients. Reconstruction of the blood supply, such as bypass surgery, would be another option [26].

Conventionally, a fetal-type PCA was thought to be a normal variant and common in the general population; however, in some reports this vascular type was associated with a higher risk for ischemic stroke, both in the anterior and posterior circulation [3, 4, 27, 28]. Until now, its significance has been under debate.

In the literature, the incidence of a unilateral and bilateral fetal-type PCA ranged from 4 to 26% and 2 to 4%, respectively [13, 27, 28]. Studies state commonly reported symptoms in patients with a fetal-type PCA to be dizziness, headache, and focal neurological deficits [3, 28]. In our population, 75% of patients with bilateral VAH also displayed a fetal-type PCA, illustrating a sizable co-existence (75%) of bilateral VAH and a unilateral or bilateral fetal-type PCA. This finding corresponds to findings from previous studies that suggest the simultaneous occurrence of a hypoplastic vertebrobasilar system and fetal-type circle of Willis, and the increased development of ischemic events in the posterior circulation [3, 12].

From an embryological perspective, due to the delayed development of the P1 segment, the PCAs are supplied by the internal carotid arteries via the posterior communicating arteries temporally.

Typically, an adult PCA is complete at 6–7 weeks of embryological development [29]. Inadequate flow of the basilar PCA system may interrupt the normal development of the PCA. Nevertheless, it is not clear how a fetal-type circle of Willis responds to unilateral VAH [30] or significantly inadequate basilar flow (in this study), or how it evolves to the adult configuration, which leads to a higher risk for both anterior and post-ischemic strokes [12, 27]. However, the significance and pathophysiology of a fetal-type PCA in stroke remains unclear. Further comprehensive research is necessary.

In this study, most patients with bilateral VAH displayed a fetal variant of the PCA, supplied from the anterior circulation via the posterior communicating artery segment. However, with such hemodynamic compensation, supplementation via the fetal-type PCA still failed to support the vertebrobasilar system, resulting in a multifocal scattered infarction in the posterior circulation.

There were several limitations in this study. First, the case number of bilateral VAH is small, and we enrolled our samples from in-patients and not in healthy subjects. Overestimated frequencies and symptoms of bilateral VAH would be suspected. Because we applied the duplex ultrasonographic criteria of VAH, stenosis over the VA orifice or decreased VA flow volume due to atherosclerosis stenosis is a possible trap as applying the sonographic criteria of VAH diagnosis. Compared evaluation of the contrast-enhanced MRA images at the same time would result in a more reliable diagnosis.

CONCLUSION

We evaluated the clinical and vascular characteristics of patients with stroke and bilateral VAH. We found a younger age at stroke onset, obvious hypertension, bilateral and multiple vertebrobasilar infarcts, and a high prevalence of the fetal PCA in our enrolled patients.

Clinically, bilateral VAH may pose a significant risk to the posterior circulation; therefore, early detection and prevention are crucial in this patient group.
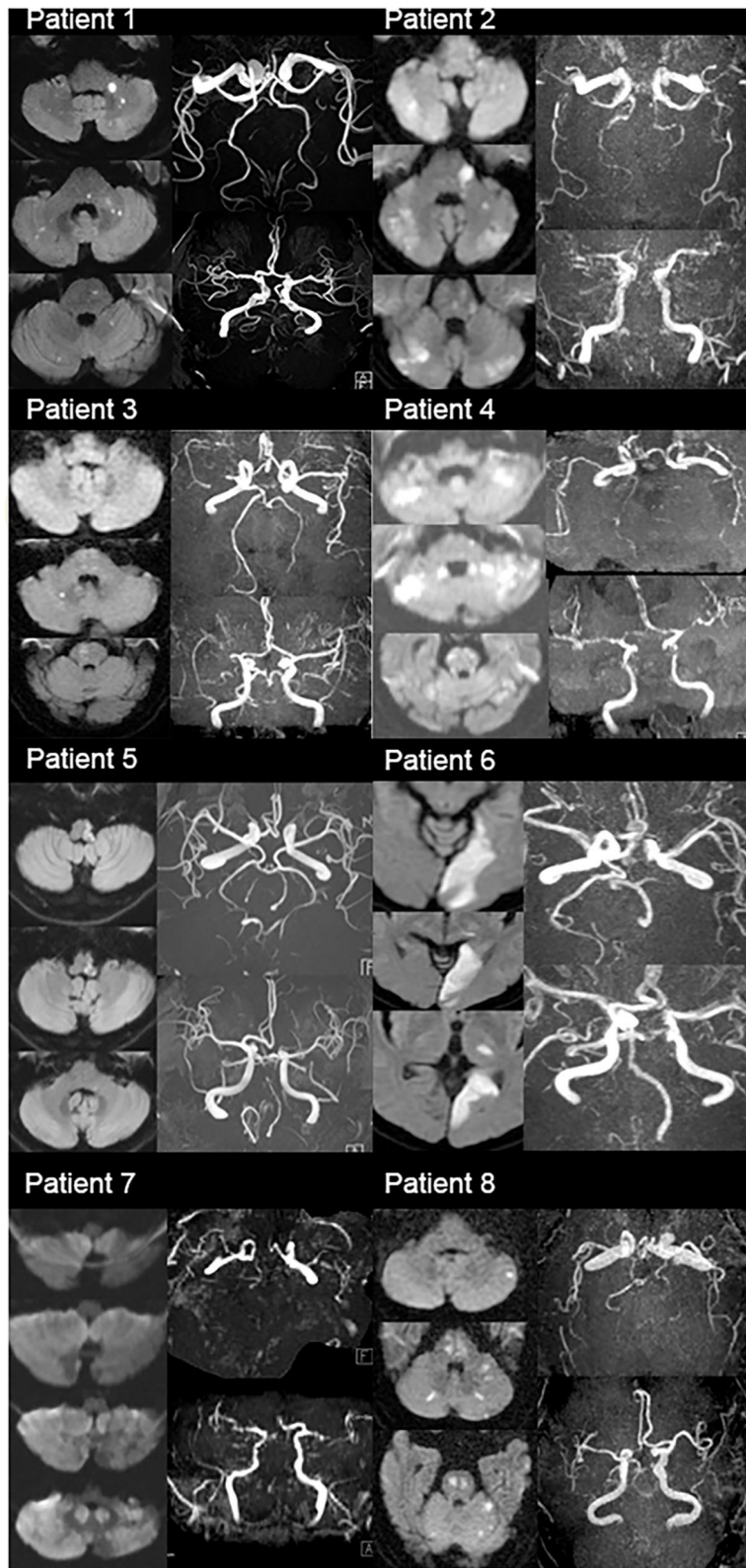
FIGURE 1 | MRI diffusion-weighted images (DMI) and MRA images of total eight patients (MRI DWI showed multiple infarctions in these patients; MRA showed fetal type PCA, vertebral hypoplasia, small caliber of basilar artery, or invisible vertebrobasilar arteries).

DATA AVAILABILITY STATEMENT

The raw data supporting the conclusions of this article will be made available by the authors, without undue reservation.

ETHICS STATEMENT

The studies involving human participants were reviewed and approved by Institutional Review Board of Chung Shan Medial University Hospital, Taichung, Republic of China. The patients/participants provided their written informed consent to participate in this study.

AUTHOR CONTRIBUTIONS

H-YC designed the study. C-FH, K-WC, C-HS, and C-YS collected and organized data. C-FH and H-YC analyzed and interpreted the data. All authors read and approved the final manuscript.

ACKNOWLEDGMENTS

The authors would like to thank the neurologists, radiographers, and radiologists at Chung Shan Medical University Hospital.

REFERENCES

1. Scheel P, Ruge C, Schoning M. Flow velocity and flow volume measurements in the extracranial carotid and vertebral arteries in healthy adults: reference data and the effects of age. *Ultrasound Med Biol*. (2000) 26:1261–6. doi: 10.1016/S0301-5629(00)00293-3

2. Nouh A, Remke J, Ruland S. Ischemic posterior circulation stroke: a review of anatomy, clinical presentations, diagnosis, and current management. *Front Neurol*. (2014) 5:30. doi: 10.3389/fneur.2014.00030

3. Arjal RK, Zhu T, Zhou Y. The study of fetal-type posterior cerebral circulation on multislice CT angiography and its influence on cerebral ischemic strokes. *Clin Imaging*. (2014) 38:221–5. doi: 10.1016/j.clinimag.2014.01.007

4. Schoning M, Walter J, Scheel P. Estimation of cerebral blood flow through color duplex sonography of the carotid and vertebral arteries in healthy adults. *Stroke*. (1994) 25:17–22. doi: 10.1161/01.STR.25.1.17

5. Thierfelder KM, Baumann AB, Sommer WH, Armbruster M, Opherk C, Janssen H, et al. Vertebral artery hypoplasia: frequency and effect on cerebellar blood flow characteristics. *Stroke*. (2014) 45:1363–8. doi: 10.1161/STROKEAHA.113.004188

6. Zhang DP, Lu GF, Zhang JW, Zhang SL, Ma QK, Yin S. Vertebral artery hypoplasia and posterior circulation infarction in patients with isolated vertigo with stroke risk factors. *J Stroke Cerebrovasc Dis*. (2017) 26:295–300. doi: 10.1016/j.jstrokecerebrovasdis.2016.09.020

7. Chi HY, Hsu CF, Chen AC, Su CH, Hu HH, Fu WM. Extracranial and intracranial ultrasonographic findings in posterior circulation infarction. *J Ultrasound Med*. (2018) 37:1605–10. doi: 10.1002/jum.14501

8. Sauer T, Wolf ME, Ebert AD, Szabo K, Chatzikonstantinou A. Vertebral artery hypoplasia does not influence lesion size and clinical severity in acute ischemic stroke. *J Stroke Cerebrovasc Dis*. (2016) 25:1770–5. doi: 10.1016/j.jstrokecerebrovasdis.2016.03.050

9. Mitsumura H, Miyagawa S, Komatsu T, Hirai T, Kono Y, Iguchi Y. Relationship between vertebral artery hypoplasia and posterior circulation ischemia. *J Stroke Cerebrovasc Dis*. (2016) 25:266–9. doi: 10.1016/j.jstrokecerebrovasdis.2015.09.027

10. Janzen A, Steinhuber CR, Bogdahn UR, Schuierer GR, Schlachetzki F. Ultrasound findings of bilateral hypoplasia of the vertebral arteries associated with a persistent carotid-hypoglossal artery. *BMJ Case Rep*. (2009) 2009:bcr07.2008.0486. doi: 10.1136/bcr.07.2008.0486

11. Mestan MA. Posterior fossa ischemia and bilateral vertebral artery hypoplasia. *J Manipulative Physiol Ther*. (1999) 22:245–9. doi: 10.1016/S0161-4754(99)70051-5

12. Lochner P, Golaszewski S, Caleri F, Ladurner G, Tezzon F, Zuccoli G, et al. Posterior circulation ischemia in patients with fetal-type circle of Willis and hypoplastic vertebrobasilar system. *Neurol Sci*. (2011) 32:1143–6. doi: 10.1007/s10072-011-0763-5

13. Shaban A, Albright KC, Boehme AK, Martin-Schild S. Circle of willis variants: fetal PCA. *Stroke Res Treat*. (2013) 2013:105937. doi: 10.1155/2013/105937

14. Caplan L, Chung CS, Wityk R, Glass T, Tapia J, Pazdera L, et al. New England medical center posterior circulation stroke registry: I. Methods, data base, distribution of brain lesions, stroke mechanisms, and outcomes. *J Clin Neurol*. (2005) 1:14–30. doi: 10.3988/jcn.2005.1.1.14

15. Caplan L, Wityk R, Pazdera L, Chang HM, Pessin M, Dewitt L. New England medical center posterior circulation stroke registry II. Vascular lesions. *J Clin Neurol*. (2005) 1:31–49. doi: 10.3988/jcn.2005.1.1.31

16. Jeng JS, Yip PK. Evaluation of vertebral artery hypoplasia and asymmetry by color-coded duplex ultrasonography. *Ultrasound Med Biol*. (2004) 30:605–9. doi: 10.1016/j.ultrasmedbio.2004.03.004

17. Chen YY, Chao AC, Hsu HY, Chung CP, Hu HH. Vertebral artery hypoplasia is associated with a decrease in net vertebral flow volume. *Ultrasound Med Biol*. (2010) 36:38–43. doi: 10.1016/j.ultrasmedbio.2009.08.012

18. Park JH, Kim JM, Roh JK. Hypoplastic vertebral artery: frequency and associations with ischaemic stroke territory. *J Neurol Neurosurg Psychiatry*. (2007) 78:954–8. doi: 10.1136/jnnp.2006.105767

19. Tsai CF, Thomas B, Sudlow CL. Epidemiology of stroke and its subtypes in Chinese vs white populations: a systematic review. *Neurology*. (2013) 81:264–72. doi: 10.1212/WNL.0b013e31829bfde3

20. Moreno-Rojas AJ, Gonzalez-Marcos JR, Gil-Peralta A, Serrano-Castro V. Vascular risk factors in patients with infratentorial vertebrobasilar ischemia. *Revista de neurologia*. (1998) 26:113–7. doi: 10.33588/rn.26149.981096

21. Gong X, Liu J, Dong P, Zhang P, Li N, Zhao X, et al. Assessment of dynamic cerebral autoregulation in patients with basilar artery stenosis. *PLoS ONE*. (2013) 8:e77802. doi: 10.1371/journal.pone.0077802

22. Tao WD, Liu M, Fisher M, Wang DR, Li J, Furie KL, et al. Posterior versus anterior circulation infarction: how different are the neurological deficits? *Stroke*. (2012) 43:2060–5. doi: 10.1161/STROKEAHA.112.652420

23. Searls DE, Pazdera L, Korbel E, Vysata O, Caplan LR. Symptoms and signs of posterior circulation ischemia in the new England medical center posterior circulation registry. *Arch Neurol*. (2012) 69:346–51. doi: 10.1001/archneurol.2011.2083

24. Koennecke HC, Bernarding J, Braun J, Faulstich A, Hofmeister C, Nohr R, et al. Scattered brain infarct pattern on diffusion-weighted magnetic resonance imaging in patients with acute ischemic stroke. *Cerebrovasc Dis*. (2001) 11:157–63. doi: 10.1159/000047632

25. Olindo S, Khaddam S, Bocquet J, Chausson N, Aveillan M, Cabre P, et al. Association between basilar artery hypoplasia and undetermined or lacunar posterior circulation ischemic stroke. *Stroke*. (2010) 41:2371–4. doi: 10.1161/STROKEAHA.110.593145

26. Raheja A, Taussky P, Kumpati GS, Couldwell WT. Subclavian-to-Extracranial vertebral artery bypass in a patient with vertebrobasilar insufficiency: 3-dimensional operative video. *Oper Neurosurg (Hagerstown)*. (2018) 14:312. doi: 10.1093/ons/opx130

27. Lambert SL, Williams FJ, Oganisyan ZZ, Branch LA, Mader EC Jr. Fetal-type variants of the posterior cerebral artery and concurrent infarction in the major arterial territories of the cerebral hemisphere. *J Investig Med High Impact Case Rep*. (2016) 4(3):2324709616665409. doi: 10.1177/2324709616665409

28. Wu HM, Chuang YM. The clinical relevance of fetal variant of the circle of Willis and its influence on the cerebral collateral circulation. *Acta Neurol Taiwan*. (2011) 20:232–42. doi: 10.29819/ANT.201112.0002

29. Menshawi K, Mohr JP, Gutierrez J. A Functional perspective on the embryology and anatomy of the cerebral blood supply. *J Stroke*. (2015) 17:144–58. doi: 10.5853/jos.2015.17.2.144

30. Chaturvedi S, Lukovits TG, Chen W, Gorelick PB. Ischemia in the territory of a hypoplastic vertebrobasilar system. *Neurology*. (1999) 52:980–3. doi: 10.1212/WNL.52.5.980

Conflict of Interest: The authors declare that the research was conducted in the absence of any commercial or financial relationships that could be construed as a potential conflict of interest.

PLOS ONE

Effect of aspirin treatment duration on clinical outcomes in acute coronary syndrome patients with early aspirin discontinuation and received P2Y12 inhibitor monotherapy

Ming-Yun Ho[1]●, Po-Wei Chen[2]●, Wen-Han Feng[3], Chun-Hung Su[4], Sheng-Wei Huang[4], Chung-Wei Cheng[5], Hung-I Yeh[5], Ching-Pei Chen[6], Wei-Chun Huang[7], Ching-Chang Fang[8], Hui-Wen Lin[2], Sheng-Hsiang Lin[9,10,11], I-Chang Hsieh[1‡]*, Yi-Heng Li[2‡]*
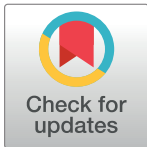
1 Chang Gung Memorial Hospital, Chang Gung University College of Medicine, Taoyuan, Taiwan, 2 National Cheng Kung University Hospital, College of Medicine, National Cheng Kung University, Tainan, Taiwan, 3 Kaohsiung Municipal Ta-Tung Hospital and Kaohsiung Medical University Hospital, Kaohsiung, Taiwan, 4 Chung Shan Medical University Hospital and Chung Shan Medical University, Taichung, Taiwan, 5 MacKay Memorial Hospital, Taipei, Taiwan, 6 Changhua Christian Hospital, Changhua, Taiwan, 7 Kaohsiung Veterans General Hospital, Fooyin University, Kaohsiung and National Yang Ming University, Taipei, Taiwan, 8 Tainan Municipal Hospital, Tainan, Taiwan, 9 Institute of Clinical Medicine, College of Medicine, National Cheng Kung University, Tainan, Taiwan, 10 Department of Public Health, College of Medicine, National Cheng Kung University, Tainan, Taiwan, 11 Biostatistics Consulting Center, National Cheng Kung University Hospital, College of Medicine, National Cheng Kung University, Tainan, Taiwan

● These authors contributed equally to this work.
‡ These authors also contributed equally to this work.
* heng@mail.ncku.edu.tw (YHL); hsiehic@ms28.hinet.net (ICH)

Abstract

Recent clinical trials showed that short aspirin duration (1 or 3 months) in dual antiplatelet therapy (DAPT) followed by P2Y12 inhibitor monotherapy reduced the risk of bleeding and did not increase the ischemic risk compared to 12-month DAPT in acute coronary syndrome (ACS) patients undergoing percutaneous coronary intervention (PCI). However, it is unclear about the optimal duration of aspirin in P2Y12 inhibitor monotherapy. The purpose of this study was to evaluate the influence of aspirin treatment duration on clinical outcomes in a cohort of ACS patients with early aspirin interruption and received P2Y12 inhibitor mono-therapy. From January 1, 2014 to December 31, 2018, we included 498 ACS patients (age 70.18 ± 12.84 years, 71.3% men) with aspirin stopped for various reasons before 6 months after PCI and received P2Y12 inhibitor monotherapy. The clinical outcomes between those with aspirin treatment ≤ 1 month and > 1 month were compared in 12-month follow up after PCI. Inverse probability of treatment weighting was used to balance the covariates between groups. The mean duration of aspirin treatment was 7.52 ± 8.10 days vs. 98.05 ± 56.70 days in the 2 groups (p<0.001). The primary composite endpoint of all-cause mortality, recurrent ACS or unplanned revascularization and stroke occurred in 12.6% and 14.4% in the 2 groups (adjusted HR 1.19, 95% CI 0.85–1.68). The safety outcome of BARC 3 or 5 bleeding was also similar (adjusted HR 0.69, 95% CI 0.34–1.40) between the 2 groups. In conclusion, patients with ≤ 1 month aspirin treatment had similar clinical outcomes to those

National Cheng-Kung University Hospital,
Professor Ting-Tsung Chang. Professor Ting-
Tsung Chang may be contacted at: ttchang@mail.
ncku.edu.tw.

with treatment > 1 month. Our results indicated that ≤ 1-month aspirin may be enough in
P2Y12 inhibitor monotherapy strategy for ACS patients undergoing PCI.

Introduction

Current guidelines recommend 12-month dual antiplatelet therapy (DAPT) with aspirin and a
P2Y12 inhibitor for patients with acute coronary syndromes (ACS) undergoing percutaneous
coronary intervention (PCI) [1, 2]. However, the optimal duration of DAPT is still controver-
sial because the DAPT-associated bleeding is a major clinical challenge. Multiple lines of evi-
dence have shown that major bleeding is a significant risk factor for cardiac morbidity and
mortality in patients with ACS or after coronary stenting [3, 4]. The platelet inhibitory effects
are greater with P2Y12 inhibitors than aspirin. Aspirin provides little additional antiplatelet
effects under P2Y12 inhibitor treatment [5, 6]. Therefore, one of the ways to decrease bleeding
risk while preserving antithrombotic efficacy is to abandon aspirin early after PCI and use
P2Y12 inhibitor monotherapy [5, 6]. Recently, this strategy of short-term DAPT (aspirin 1 or
3 months) followed by P2Y12 inhibitor monotherapy was evaluated in a number of clinical tri-
als. These studies demonstrated that P2Y12 inhibitor monotherapy could be an effective and
safe antiplatelet strategy in patients undergoing PCI [7–11]. A meta-analysis, involving these 5
clinical trials (GLOBAL-LEADERS, TWILIGHT, SMART-CHOICE, STOPDAPT-2, and
TICO) with 32,361 patients, provided strong evidence that P2Y12 inhibitor monotherapy
results in significantly lower rate of bleeding compared with conventional 12-month DAPT
with no signal of increased ischemic risk [12]. In the TWILIGHT, SMART-CHOICE and
TICO trials, the DAPT duration was 3 months; while the length of DAPT was only 1 month in
GLOBAL-LEADERS and STOPDAPT-2 trials. When P2Y12 inhibitor monotherapy is consid-
ered as an alternative antiplatelet strategy for ACS patients at bleeding risk, it is still unclear
about the optimal duration of aspirin. We designed this study to include ACS patients who
underwent PCI but only received short duration of aspirin for various reasons and received
P2Y12 inhibitor monotherapy. The clinical outcomes were compared between those with aspi-
rin treatment duration ≤ 1 month and > 1 month after PCI and switching to P2Y12 inhibitor
monotherapy.

Methods

Study population

The design of this multicenter, retrospective, observational study was published previously
[13]. In brief, ACS patients who received PCI during admission and were treated with P2Y12
inhibitor monotherapy were enrolled from January 2014 to December 2018 from 8 major
teaching hospitals in Taiwan. Patients were eligible if they were ≥ 18 years, admitted with a
major diagnosis of ACS, received PCI with bare metal stent (BMS) and/or contemporary drug
eluting stent (DES) implantation during hospitalization, survived to discharge, and regularly
followed up in outpatient clinic for at least 1 year after discharge. A patient could receive more
than one stent during PCI. Aspirin was stopped within 6 months after PCI in all included
patients due to various reasons. P2Y12 inhibitor monotherapy with either clopidogrel 75 mg
daily or ticagrelor 90 mg twice daily was used. The exclusion criteria were patients with (1)
life-threatening malignancy with life expectancy less than 1 year, (2) hematological disease
with bleeding tendency, (3) treatment with immunosuppressive agents, and (4) need of oral
anticoagulation therapy. The demographic data, coronary risk factors, major disease history,

PCI procedures and medications were collected from the patients' medical records according to a pre-determined study protocol. The timing and reasons for aspirin discontinuation after PCI were recorded. Enrolled patients were divided into 2 groups by the timing of aspirin withdrawal: ≤ 1 month or > 1 month after PCI. The study was conducted according to the principles expressed in the Declaration of Helsinki and was approved by the Institutional Review Boards of the 8 participating hospitals. All data from the medical records were fully anonymized. The study protocol was approved by the Medical Ethics Committee of National Cheng Kung University Hospital (IRB: A-ER-107-375) and granted a waiver of informed consent due to its study nature.

Follow-up

All patients were followed up for at least 12 months after discharge or until one of the primary composite endpoints occurred. The primary composite endpoints included all-cause mortality, recurrent ACS or unplanned revascularization, and stroke within 12 months after the index PCI. The secondary endpoint was the breakdown incidence of the primary composite endpoints. Recurrent ACS was defined as readmission to a hospital for a primary diagnosis of new onset ST-segment elevation myocardial infarction (STEMI), non-ST segment elevation myocardial infarction (NSTEMI) or unstable angina. Unplanned revascularization was defined as the first unexpected revascularization after discharge, including redo PCI or coronary artery bypass graft (CABG) after the index PCI due to new onset ischemic symptoms. Stroke, including ischemic or hemorrhagic stroke, was diagnosed by the occurrence of new-onset neurological symptoms and signs with neuroimaging studies. All clinical events of the primary composite endpoints were documented in the medical records and reported by the physicians that followed up the patients. The safety endpoint was the occurrence of major bleeding, which was defined as the Bleeding Academic Research Consortium (BARC) type 3 and 5 bleedings [14].

Statistical analysis

Continuous variables were expressed as mean ± standard deviation and categorical variables were expressed as numbers and percentages. Unpaired Student's t test for continuous variables and chi-square test for categorical variables were used for comparison between groups. The level of statistical significance was set at p < 0.05 (2-tailed). To adjust for potential confounding due to baseline imbalances in study covariates while preserving sample size, we used the inverse probability of treatment weights (IPTW) method based on the propensity score. The propensity score is the probability conditional on baseline covariates, including age, sex, STEMI status, diabetes mellitus, hypertension, hyperlipidemia, smoker, previous MI, previous PCI, previous CABG, previous ischemic stroke, previous hemorrhagic stroke, chronic kidney disease without dialysis, end stage renal disease with dialysis, heart failure, atrial fibrillation, peripheral artery disease, left ventricular ejection fraction, coronary angiography finding, PCI procedure, location of lesion treated, stent, and medications. With IPTW method, the propensity score was used to generate patient specific stabilized weights that control for covariate imbalances [15, 16]. The propensity-score weight was calculated as the inverse of the propensity score for each client. Both the absolute standardized mean difference (ASMD) and p value were used to assess the balance between groups before and after weighting. The Cox proportional-hazards models were then adjusted for differences in the treatment groups using IPTW derived from the propensity score which was designated as IPTW model. In the IPTW model after matching, the clinical factors with ASMD > 0.1 were put into the multivariate Cox proportional-hazards models for further adjustment. Adjusted hazard ratios (HRs) and 95%

confidence intervals (CIs) were calculated. We used the same Cox proportional hazards model to estimate p values for interaction in the subgroup analysis. SAS statistical package (version 9.4 for Windows; SAS Institute, Cary, NC, USA) was used for all analyses.

Results

Overall, a total 498 patients (mean age 70.18 ± 12.84 years, men 71.3%) that fulfilled the inclusion and exclusion criteria were included in this study. The mean duration of aspirin treatment was 40.25 ± 55.63 days. There were 318 patients (63.9%) whose aspirin was stopped before 1 month after PCI. The mean time of aspirin treatment was 7.52 ± 8.10 days in those with aspirin treatment duration $\leq$ 1 month and 98.05 ± 56.70 days in those with > 1 month (p < 0.001). Table 1 shows the comparisons of baseline characteristics of patients between the 2 groups. Among all patients, 28.3% had STEMI, 54.4% had diabetes, and 49.8% had chronic kidney disease, including 13.7% receiving dialysis. For PCI procedure, 44.2% were intervention of multiple lesions and 57% received DES. The percentage of P2Y12 inhibitors, including 54.4% clopidogrel and 45.6% ticagrelor, were similar between the 2 groups. After propensity score matching, the 2 groups were almost balanced in clinical characteristics and intervention procedures (Table 1). Table 2 illustrates the reasons for premature discontinuation of aspirin. The most common reason to stop aspirin was gastrointestinal bleeding (46.59%) with a similar percentage in both groups. Aspirin allergy or intolerance and gastrointestinal upset were also common reasons to stop aspirin. Aspirin allergy or intolerance was more common in those with aspirin treatment duration $\leq$ 1 month; while gastrointestinal upset and discomfort were higher in those with > 1 month. There were 23.49% patients that had other or unknown causes.

The mean follow-up time was 336.75 ± 81.87 and 332.61 ± 75.75 days in each group (p = 0.578). The clinical outcomes during the 12-month follow-up were shown in Table 3. For primary composite endpoints, there were 40 events (12.6%) in those with aspirin treatment duration $\leq$ 1 month and 26 events (14.4%) in those with > 1 month. No significant difference was found between the groups after multivariate adjustment (adjusted HR 1.19, 95% CI 0.85–1.68). In the secondary endpoint, there were also no significant differences of recurrent ACS or unplanned revascularization and all-cause death between the groups. The risk of stroke was low with only 1 event. For safety outcome, there was one bleeding event of intracerebral hemorrhage and defined as BARC 5 bleeding. All other BARC 3 bleeding was gastrointestinal bleeding. Overall, the BARC 3 or 5 bleeding was 3.8% in those with aspirin treatment duration $\leq$ 1 month and 3.3% in those with > 1 month and there was no significant difference (adjusted HR 0.69, 95% CI 0.34–1.40) between the 2 groups. Fig 1 shows the main findings of this study. Subgroup analysis showed that aspirin treatment duration $\leq$ 1 month had a consistent effect on the primary outcome across subgroups of age, sex, STEMI, clopidogrel or ticagrelor, diabetes mellitus, hypertension, chronic kidney disease, single or multiple-lesion intervention, and DES except in the subset of patients with multi-vessel PCI (Fig 2).

Discussion

This study analyzed the impact of different aspirin treatment duration on 12-month clinical outcomes in ACS patients received P2Y12 inhibitor monotherapy. Our results indicated that aspirin treatment > 1 month did not gain more ischemic risk reduction than those with aspirin treatment $\leq$ 1 month. The current recommendation of 12-month DAPT after ACS was mainly based on the previous clinical trials showing that, compared to aspirin monotherapy, DAPT reduced recurrent major adverse cardiovascular event (MACE) [17, 18]. The benefits of 12-month DAPT maybe no longer valid in the context of the recent progress in newer

Table 1. Baseline characteristics of patients with different duration of aspirin use.

										Inverse probability of treatment weighting			
			Before							After			
	All		**≤ 1 month**		**> 1 months**		**p value**	**ASMD**		**≤ 1 month**	**> 1 months**	**p value**	**ASMD**
	N = 498	**(%)**	**N = 318**	**(%)**	**N = 180**	**(%)**				**(pseudo data)**	**(pseudo data)**		
Age	70.18 ± 12.84		71.00 ± 12.57		68.74 ± 13.20		0.059	0.175		70.24 ± 16.05	71.45 ± 22.22	0.319	0.063
Male	355	71.29	237	74.53	118	65.56	0.043	0.197		71.53	70.9	0.904	0.014
STEMI	141	28.31	89	27.99	52	28.89	0.912	0.020		28.21	23.99	0.364	0.096
Diabetes mellitus	271	54.42	173	54.40	98	54.44	1.000	0.001		54.80	59.78	0.400	0.101
Hypertension	376	75.50	233	73.27	143	79.44	0.153	0.146		75.27	76.39	0.821	0.026
Hyperlipidemia	273	54.82	170	53.46	103	57.22	0.473	0.076		54.36	51.75	0.683	0.052
Smoker	146	29.32	101	31.76	45	25.00	0.136	0.150		28.98	25.05	0.415	0.089
Previous MI	78	15.66	50	15.72	28	15.56	1.000	0.005		14.98	13.99	0.786	0.028
Previous PCI	140	28.11	103	32.39	37	20.56	0.007	0.271		27.00	32.78	0.424	0.127
Previous CABG	16	3.21	11	3.46	5	2.78	0.881	0.039		2.94	3.07	0.946	0.008
Previous ischemic stroke	76	15.26	49	15.41	27	15.00	1.000	0.011		16.22	14.99	0.753	0.034
Previous hemorrhagic stroke	3	0.60	2	0.63	1	0.56	1.000	0.010		0.57	0.46	0.857	0.015
CKD without dialysis	180	36.14	120	37.74	60	33.33	0.376	0.092		36.06	37.15	0.866	0.023
ESRD with dialysis	68	13.65	39	12.26	29	16.11	0.287	0.110		13.32	15.65	0.652	0.066
Heart failure	168	33.73	93	29.25	75	41.67	0.007	0.262		33.48	32.26	0.818	0.026
Atrial fibrillation	66	13.25	47	14.78	19	10.56	0.231	0.127		12.93	10.87	0.538	0.064
Peripheral artery disease	32	6.43	21	6.60	11	6.11	0.980	0.020		6.86	9.85	0.550	0.108
LVEF	57.17 ± 14.53		56.43 ± 14.01		58.48 ± 15.35		0.130	0.140		57.29 ± 17.89	58.12 ± 25.14	0.140	0.040
CAG finding							0.702	0.061				0.897	0.055
1-vessel disease	123	24.70	80	25.16	43	23.89	0.836	0.030		25.19	23.16	0.661	0.048
2-vessel disease	141	28.31	93	29.25	48	26.67	0.610	0.058		28.30	30.43	0.744	0.047
3-vessel disease	234	46.99	145	45.60	89	49.44	0.464	0.077		46.51	46.42	0.988	0.002
PCI procedure							0.258	0.115				0.644	0.061
Single lesion intervention	278	55.82	171	53.77	107	59.44				56.03	53.02		
Multiple lesions intervention	220	44.18	147	46.23	73	40.56				43.97	46.98		
Single-vessel PCI	331	66.47	209	65.72	122	67.78	0.713	0.044		67.80	66.08	0.771	0.036
Multi-vessel PCI	167	33.53	109	34.28	58	32.22				32.20	33.92		
Location of lesion treated													
LM	38	7.63	29	9.12	9	5.00	0.137	0.161		7.56	8.64	0.824	0.040
LAD	319	64.06	207	65.09	112	62.22	0.586	0.060		63.61	65.11	0.788	0.031
LCX	194	38.96	131	41.19	63	35.00	0.205	0.128		38.13	35.7	0.686	0.050
RCA	234	46.99	153	48.11	81	45.00	0.565	0.062		46.82	41.49	0.377	0.108
SVG	2	0.40	0	0.00	2	1.11	0.130	0.150		.	0.39	.	
Stent													
Bare metal stent	214	42.97	141	44.34	73	40.56	0.468	0.077		42.59	38.06	0.433	0.093
Everolimus-eluting stent	93	18.67	63	19.81	30	16.67	0.456	0.082		18.70	22.5	0.563	0.094
Zotarolimus-eluting stent	99	19.88	58	18.24	41	22.78	0.270	0.113		20.09	17.31	0.483	0.071
Biolimus-eluting stent	26	5.22	16	5.03	10	5.56	0.966	0.023		5.17	4.22	0.624	0.045
Siroliums-eluting stent	65	13.05	36	11.32	29	16.11	0.166	0.140		13.54	12.5	0.761	0.031
Medications													
Clopidogrel	271	54.42	175	55.03	96	53.33	0.786	0.034		54.05	59.41	0.369	0.108
Ticagrelor	227	45.58	143	44.97	84	46.67	0.786	0.034		45.95	40.59	0.369	0.108
Beta blocker	367	73.69	228	71.70	139	77.22	0.215	0.127		73.28	69.82	0.589	0.079
RAS inhibitor	283	56.83	170	53.46	113	62.78	0.055	0.190		56.15	54.57	0.807	0.032

(Continued)

Table 1. (Continued)

			Inverse probability of treatment weighting								
			Before					After			
	All		≤ 1 month		> 1 months		p value	ASMD	≤ 1 month	> 1 months	p value	ASMD
	N = 498	(%)	N = 318	(%)	N = 180	(%)			(pseudo data)	(pseudo data)		
Statin	405	81.33	246	77.36	159	88.33	0.004	0.294	81.26	73.38	0.297	0.189
PPI use	203	40.76	127	39.94	76	42.22	0.687	0.047	39.62	39.12	0.934	0.010

ASMD, absolute standardized mean difference; CABG, coronary artery bypass graft; CAG, coronary angiography; CKD, chronic kidney disease; ESRD, end stage renal disease; LAD, left anterior descending artery, LCX, left circumflex artery; LM, left main artery; LVEF, left ventricular ejection fraction; MI, myocardial infarction; PCI, percutaneous coronary intervention; PPI, proton pump inhibitor; RAS, renin angiotensin system; RCA, right coronary artery; STEMI, ST-segment elevation myocardial infarction. Everolimus-eluting stent: Xience, Promus/Synergy, Zotarolimus-eluting stent: Resolute integrity/Onyx, Biolimus-eluting stent: BioMatrix, Siroliums-eluting stent: Nobori/Ultimaster, Orsiro.

https://doi.org/10.1371/journal.pone.0251109.t001

generation coronary stents, intracoronary imaging-guided optimal stent implantation and appearance of more potent P2Y12 inhibitors. Aspirin has been long considered to be the cornerstone of antiplatelet therapy. However, previous studies found aspirin added little additional inhibition of platelet aggregation under the treatment of potent P2Y12 inhibitors [19, 20]. Therefore, short-duration aspirin followed by P2Y12 inhibitor monotherapy become an alternative antiplatelet strategy in patients received PCI. The recent 5 clinical trials to test P2Y12 monotherapy strategy all designed to give aspirin in the first 1 or 3 months, traditionally regarded as the most vulnerable phase after PCI [7–11]. In our study, we found aspirin treatment ≤ 1 month (mean duration 7.52 ± 8.10 days) had similar ischemic outcomes to those having aspirin > 1 month (mean duration 98.05 ± 56.70 days). In patients with atrial fibrillation (AF) and PCI, recent meta-analysis studies indicated that omission of aspirin after PCI and use P2Y12 inhibitor plus oral anticoagulant not only reduced the risk of bleeding, but also carried no significant increase of MACE [21, 22]. In the post hoc analysis of the AUGUSTUS study for AF and PCI, use of aspirin up to 30 days resulted in more bleeding events but fewer ischemic events than placebo. However, prolonged use of aspirin over 30 days only increased bleeding risk, but without any significant benefit of reducing ischemic events [23]. Recently, a pioneer clinical trial in which patients with low-risk stable coronary artery disease were treated with prasugrel monotherapy without aspirin after elective PCI. No stent thrombosis was found after 3 months follow up in this study indicating aspirin-free strategy with P2Y12 inhibitor monotherapy may be feasible and safe in selected stable patients undergoing PCI [24]. Recent meta-analyses studies comparing P2Y12 inhibitor monotherapy vs. DAPT demonstrated that early aspirin discontinuation (1–3 months) with P2Y12 inhibitor monotherapy decreased bleeding risk and did not increase the risk of MACE, even in ACS patients

Table 2. Reasons for premature discontinuation of aspirin.

	All	≤ 1 month	> 1 month	p value
	N = 498 (%)	N = 318 (%)	N = 180 (%)	
Gastrointestinal bleeding	232 (46.59)	147 (46.23)	85 (47.22)	0.904
Other sites bleeding	35 (7.03)	17 (5.35)	18 (10.00)	0.077
Aspirin allergy or intolerance	53 (10.64)	42 (13.21)	11 (6.11)	0.021
Gastrointestinal upset or discomfort	48 (9.64)	18 (5.66)	30 (16.67)	<0.001
Need surgery or thrombocytopenia	13 (2.61)	8 (2.52)	5 (2.78)	1.000
Other or unknown causes	117 (23.49)	86 (27.04)	31 (17.22)	0.018

https://doi.org/10.1371/journal.pone.0251109.t002

Table 3. Clinical outcomes at 12-month follow up.

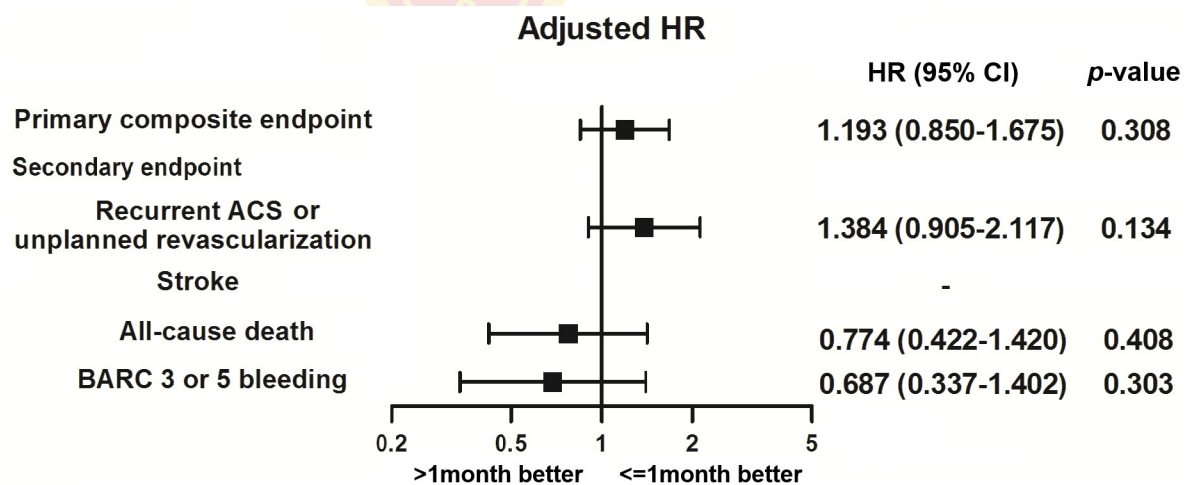|	All	1≤ month	> 1 month	Crude HR	p value	Adjusted HR	p value
	N = 498	N = 318 (Ref)	N = 180	(95% CI)		(95% CI)	
Primary composite endpoint	66 (13.25)	40 (12.58)	26 (14.44)	1.304 (0.934–1.820)	0.119	1.193 (0.850–1.675)	0.308
Secondary endpoint							
Recurrent ACS or unplanned revascularization	41 (8.23)	24 (7.55)	17 (9.44)	1.625 (1.074–2.457)	0.022	1.384 (0.905–2.117)	0.134
Stroke	1 (0.20)	0	1 (0.56)	-		-	
All-cause death	24 (4.82)	16 (5.03)	8 (4.44)	0.722 (0.395–1.321)	0.291	0.774 (0.422–1.420)	0.408
BARC 3 or 5 bleeding	18 (3.61)	12 (3.77)	6 (3.33)	0.684 (0.337–1.387)	0.292	0.687 (0.337–1.402)	0.303

ACS, acute coronary syndrome; BARC, Bleeding Academic Research Consortium.

Adjusted variables included diabetes mellitus, previous PCI, peripheral artery disease, P2Y12 inhibitor, and statin.

https://doi.org/10.1371/journal.pone.0251109.t003

[25, 26]. The remaining question is the optimal choice of P2Y12 inhibitor in patients prescribed monotherapy. It is well known that clopidogrel has a significant interpatient variability of antiplatelet activity [27]. In ACS patients under the background aspirin therapy, prasugrel and ticagrelor have better cardiovascular outcomes than clopidogrel [28, 29]. In ACS patients who received P2Y12 inhibitor monotherapy, our previous observation study showed that ticagrelor had a lower risk of ischemic outcome compared with clopidogrel during the 12-month follow up after PCI [13]. It seems that, if P2Y12 inhibitor monotherapy is adopted, a more potent P2Y12 inhibitor is a better choice than clopidogrel. Further randomized clinical trials are necessary to compare the efficacy and safety between ticagrelor vs. clopidogrel in P2Y12 inhibitor monotherapy.

One of the major limitations of our study is its non-randomized, observational study design and the study was not registered in a clinical trials database, such as ClinicalTrials.gov. Although the statistical method, IPTW, was used to balance the differences between the groups, some unmeasured or unidentified confounding factors still potentially may bias the clinical outcomes. For example, the duration of aspirin was not predefined in each group. The time to develop the reasons for stopping aspirin was variable. In about 23.5% patients, the true reasons for early aspirin discontinuation were unclear due to limited information recorded in the charts. Furthermore, only patients with available one-year follow-up data were included is

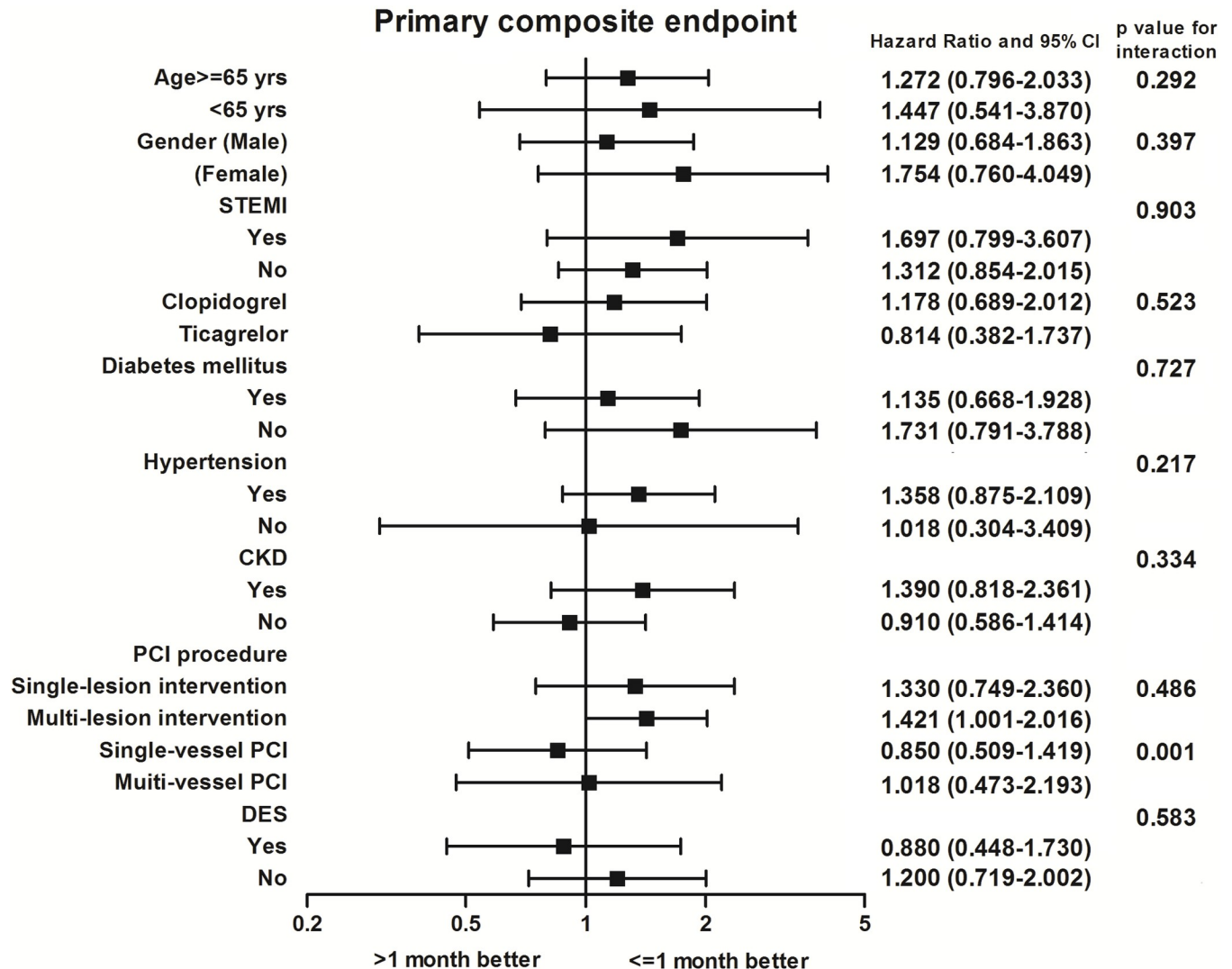**Fig 1. Clinical outcomes at 12-month follow up.**

https://doi.org/10.1371/journal.pone.0251109.g001

Primary composite endpoint

	Hazard Ratio and 95% CI	p value for interaction
Age>=65 yrs	1.272 (0.796-2.033)	0.292
<65 yrs	1.447 (0.541-3.870)	
Gender (Male)	1.129 (0.684-1.863)	0.397
(Female)	1.754 (0.760-4.049)	
STEMI		0.903
Yes	1.697 (0.799-3.607)	
No	1.312 (0.854-2.015)	
Clopidogrel	1.178 (0.689-2.012)	0.523
Ticagrelor	0.814 (0.382-1.737)	
Diabetes mellitus		0.727
Yes	1.135 (0.668-1.928)	
No	1.731 (0.791-3.788)	
Hypertension		0.217
Yes	1.358 (0.875-2.109)	
No	1.018 (0.304-3.409)	
CKD		0.334
Yes	1.390 (0.818-2.361)	
No	0.910 (0.586-1.414)	
PCI procedure		
Single-lesion intervention	1.330 (0.749-2.360)	0.486
Multi-lesion intervention	1.421 (1.001-2.016)	
Single-vessel PCI	0.850 (0.509-1.419)	0.001
Muiti-vessel PCI	1.018 (0.473-2.193)	
DES		0.583
Yes	0.880 (0.448-1.730)	
No	1.200 (0.719-2.002)	

>1 month better   <=1 month better

Fig 2. Subgroup analysis of the effect of different aspirin duration on primary composite endpoints.

https://doi.org/10.1371/journal.pone.0251109.g002

another limitation because this cohort potentially could not represent the whole patient group with early aspirin interruption and selection bias could occur. Second, the small patient number is another major limitation of our study. It may cause a problem of underpower to evaluate the clinical events. Third, we found there was no significant difference in the risk of major bleeding (BARC type 3 to 5) between patients with longer or shorter aspirin treatment duration. In our study, all clinical events were investigator-reported, but not adjudicated by a clinical events committee. Recently, the Academic Research Consortium (ARC) for High Bleeding Risk (HBR) criteria were proposed and validated to identify patients with bleeding risk [30–32]. The rate of BARC 3 or 5 bleeding at 1 year was 3.6% in our cohort which can be defined as borderline HBR according to the 4% cut-off proposed by the ARC-HBR to identify HBR patients [31, 32]. Among the studies of P2Y12 inhibitor monotherapy, the SMART-CHOICE, STOPDAPT-2 and TICO trials were performed in East Asian countries. In the SMART-CHOICE study that compared aspirin plus a P2Y12 inhibitor for 3 months and followed by P2Y12 inhibitor monotherapy vs. DAPT for 12 months, the major bleeding risk defined as

BARC type 3 to 5 bleeding was also similar between the groups (HR 0.87, 95% CI 0.40 to 1.88) [10]. In the STOPDAPT-2 compared 1-month DAPT followed by P2Y12 inhibitor monotherapy versus 12-month DAPT. The BARC type 3 or 5 bleeding was lower in the monotherapy group (HR 0.30, 95% CI 0.13–0.65), but the severe bleeding defined by GUSTO criteria was similar (HR 0.37, 95% CI 0.12–1.15) between the groups [9]. Only the TICO study exclusively included ACS patients [11]. The TICO study showed ACS patients received ticagrelor monotherapy after 3-month DAPT had a significantly lower risk of major bleeding (HR, 0.56, 95% CI 0.34–0.91). Overall, it is difficult to compare the results between these clinical trials and our study because of differences in P2Y12 inhibitor used and aspirin treatment duration. Fourth, 43% patients in this study received BMS and 54% patients still received clopidogrel. The data reflected current treatment status of ACS in Taiwan [33, 34]. The use of BMS is due to the restriction of the Taiwan National Health Insurance which only reimburses the price of BMS. Patients have to pay $1,500 to $2,000 US dollars for using one DES. For fear of bleeding, clopidogrel instead of ticagrelor, is still commonly used in most East Asian countries, including Taiwan. The ischemic outcome could be different if more ticagrelor and DES were used in our patients. Finally, we did not have the data about the percentage of patients that received complex PCI or complete revascularization. These factors cannot be analyzed in the subgroup analysis. There was a significant interaction in the subgroup analysis between single and multi-vessel PCI. Aspirin > 1 month was more favored in the subset of the patients with single vessel PCI. In the initial study protocol, we only recorded single lesion or multiple lesions intervention. The data of single or multi-vessel PCI was not recorded. We used the original CAG findings (1-vessel, 2-vessel, 3-vesssel disease), location of lesion treated, and PCI procedure (single or multiple lesions intervention) to roughly estimate the percentage of single or multivessel PCI. The influence of aspirin duration on clinical outcomes in these specific patient groups with different PCI procedures needs further investigation. We also did not know the effects of prasugrel monotherapy. Prasugrel was introduced into Taiwan in the end of 2018. There were only few patients received prasugrel during the study period, so no case of prasugrel monotherapy was included in this study.

Conclusions

In conclusion, the risk of ischemic events was similar between those with aspirin treatment > 1 month versus ≤ 1 month in ACS patients undergoing PCI and received P2Y12 inhibitor monotherapy. Under P2Y12 inhibitor therapy, early discontinuation of aspirin ≤ 1 month after PCI may be feasible and safe. Due to the study's limitations, further randomized clinical trials are needed to reconfirm our study results.

Author Contributions

Investigation: Ming-Yun Ho, Po-Wei Chen, Wen-Han Feng, Chun-Hung Su, Hui-Wen Lin, Yi-Heng Li.

Methodology: Po-Wei Chen, Wen-Han Feng, Hui-Wen Lin, Sheng-Hsiang Lin.

Project administration: Po-Wei Chen, Wen-Han Feng, Yi-Heng Li.

Software: Hui-Wen Lin, Sheng-Hsiang Lin.

Supervision: Sheng-Hsiang Lin, I-Chang Hsieh, Yi-Heng Li.

Validation: Hui-Wen Lin, Sheng-Hsiang Lin, I-Chang Hsieh.

Visualization: Sheng-Hsiang Lin, I-Chang Hsieh.

Writing – original draft: Ming-Yun Ho, Po-Wei Chen, Yi-Heng Li.

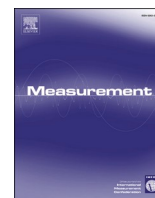**Writing – review & editing:** Po-Wei Chen, Yi-Heng Li.

References

1. Levine GN, Bates ER, Bittl JA, Brindis RG, Fihn SD, Fleisher LA, et al. 2016 ACC/AHA guideline focused update on duration of dual antiplatelet therapy in patients with coronary artery disease: a report of the American College of Cardiology/American Heart Association Task Force on Clinical Practice Guidelines. J Am Coll Cardiol 2016; 68:1082–1115. https://doi.org/10.1016/j.jacc.2016.03.513 PMID: 27036918

2. Valgimigli M, Bueno H, Byrne RA, Collet JP, Costa F, Jeppsson A, et al. 2017 ESC focused update on dual antiplatelet therapy in coronary artery disease developed in collaboration with EACTS: The Task Force for dual antiplatelet therapy in coronary artery disease of the European Society of Cardiology (ESC) and of the European Association for Cardio-Thoracic Surgery (EACTS). Eur Heart J 2018; 39:213–260. https://doi.org/10.1093/eurheartj/ehx419 PMID: 28886622

3. Valgimigli M, Costa F, Lokhnygina Y, Clare RM, Wallentin L, Moliterno DJ, et al. Trade-off of myocardial infarction vs. bleeding types on mortality after acute coronary syndrome: lessons from the Thrombin Receptor Antagonist for Clinical Event Reduction in Acute Coronary Syndrome (TRACER) randomized trial. Eur Heart J 2017; 38:804–810. https://doi.org/10.1093/eurheartj/ehw525 PMID: 28363222

4. Costa F, Van Klaveren D, Feres F, James S, Räber L, Pilgrim T, et al. Dual antiplatelet therapy duration based on ischemic and bleeding risks after coronary stenting. J Am Coll Cardiol 2019; 73:741–754. https://doi.org/10.1016/j.jacc.2018.11.048 PMID: 30784667

5. Gargiulo G, Windecker S, Vranckx P, Gibson CM, Mehran R, Valgimigli M. A critical appraisal of aspirin in secondary prevention: is less more? Circulation 2016; 134:1881–1906. https://doi.org/10.1161/CIRCULATIONAHA.116.023952 PMID: 27920074

6. Feng WH, Hsieh IC, Li YH. P2Y12 inhibitor monotherapy after percutaneous coronary intervention: is it safe to abandon aspirin? Acta Cardiol Sin 2021; 37:1–8. https://doi.org/10.6515/ACS.202101_37(1).20200806A PMID: 33488022

7. Vranckx P, Valgimigli M, Jüni P, Hamm C, Steg PG, Heg D, et al; GLOBAL LEADERS Investigators. Ticagrelor plus aspirin for 1 month, followed by ticagrelor monotherapy for 23 months vs aspirin plus clopidogrel or ticagrelor for 12 months, followed by aspirin monotherapy for 12 months after implantation of a drug-eluting stent: a multicentre, open-label, randomised superiority trial. Lancet 2018; 392:940–949. https://doi.org/10.1016/S0140-6736(18)31858-0 PMID: 30166073

8. Mehran R, Baber U, Sharma SK, Cohen DJ, Angiolillo DJ, Briguori C, et al. Ticagrelor with or without aspirin in high-risk patients after PCI. N Engl J Med 2019; 381:2032–2042. https://doi.org/10.1056/NEJMoa1908419 PMID: 31556978

9. Watanabe H, Domei T, Morimoto T, Natsuaki M, Shiomi H, Toyota T, et al.; STOPDAPT-2 Investigators. Effect of 1-month dual antiplatelet therapy followed by clopidogrel vs 12-month dual antiplatelet therapy on cardiovascular and bleeding events in patients receiving PCI: the STOPDAPT-2 randomized clinical trial. JAMA 2019; 321:2414–2427. https://doi.org/10.1001/jama.2019.8145 PMID: 31237644

10. Hahn JY, Song YB, Oh JH, Chun WJ, Park YH, Jang WJ, et al.; SMART-CHOICE Investigators. Effect of P2Y12 inhibitor monotherapy vs dual antiplatelet therapy on cardiovascular events in patients undergoing percutaneous coronary intervention: the SMART-CHOICE randomized clinical trial. JAMA 2019; 321:2428–2437. https://doi.org/10.1001/jama.2019.8146 PMID: 31237645

11. Kim BK, Hong SJ, Cho YH, Yun KH, Kim YH, Suh Y, et al. Effect of ticagrelor monotherapy vs ticagrelor with aspirin on major bleeding and cardiovascular events in patients with acute coronary syndrome. JAMA 2020; 323:2407–2416. https://doi.org/10.1001/jama.2020.7580 PMID: 32543684

12. McClure JD, Ramsay JC, Berry C. Pooled analysis of bleeding, major adverse cardiovascular events, and all-cause mortality in clinical trials of time-constrained dual-antiplatelet therapy after percutaneous coronary intervention. J Am Heart Assoc 2020; 9:e017109. https://doi.org/10.1161/JAHA.120.017109 PMID: 32779497

13. Chen PW, Feng WH, Ho MY, Su CH, Huang SW, Cheng CW, et al. P2Y12 inhibitor monotherapy with clopidogrel versus ticagrelor in patients with acute coronary syndrome undergoing percutaneous coronary intervention. J Clin Med 2020; 9:1657. https://doi.org/10.3390/jcm9061657 PMID: 32492818

14. Mehran R, Rao SV, Bhatt DL, Gibson CM, Caixeta A, Eikelboom J, et al. Standardized bleeding definitions for cardiovascular clinical trials: a consensus report from the Bleeding Academic Research Consortium. Circulation 2011; 123:2736–2747. https://doi.org/10.1161/CIRCULATIONAHA.110.009449 PMID: 21670242

15. Austin PC. An introduction to propensity score methods for reducing the effects of confounding in observational studies. Multivariate Behav Res 2011; 46:399–424. https://doi.org/10.1080/00273171.2011.568786 PMID: 21818162

16. Burden A, Roche N, Miglio C, Hillyer EV, Postma DS, Herings RM, et al. An evaluation of exact matching and propensity score methods as applied in a comparative effectiveness study of inhaled corticosteroids in asthma. Pragmat Obs Res 2017; 8:15–30. https://doi.org/10.2147/POR.S122563 PMID: 28356782

17. Yusuf S, Zhao F, Mehta SR, Chrolavicius S, Tognoni G, Fox KK. Effects of clopidogrel in addition to aspirin in patients with acute coronary syndromes without ST-segment elevation. N Engl J Med 2001; 345:494–502. https://doi.org/10.1056/NEJMoa010746 PMID: 11519503

18. Mehta SR, Yusuf S, Peters RJ, Bertrand ME, Lewis BS, Natarajan MK, et al. Effects of pretreatment with clopidogrel and aspirin followed by long-term therapy in patients undergoing percutaneous coronary intervention: the PCI-CURE study. Lancet 2001; 358:527–533. https://doi.org/10.1016/s0140-6736(01)05701-4 PMID: 11520521

19. Armstrong PC, Leadbeater PD, Chan MV, Kirkby NS, Jakubowski JA, Mitchell JA, et al. In the presence of strong P2Y12 receptor blockade, aspirin provides little additional inhibition of platelet aggregation. J Thromb Haemost 2011; 9:552–561. https://doi.org/10.1111/j.1538-7836.2010.04160.x PMID: 21143373

20. Traby L, Kollars M, Kaider A, Eichinger S, Wolzt M, Kyrle PA. Effects of P2Y12 receptor inhibition with or without aspirin on hemostatic system activation: a randomized trial in healthy subjects. J Thromb Haemost 2016; 14:273–281. https://doi.org/10.1111/jth.13216 PMID: 26663880

21. Lopes RD, Hong H, Harskamp RE, Bhatt DL, Mehran R, Cannon CP, et al. Optimal antithrombotic regimens for patients with atrial fibrillation undergoing percutaneous coronary intervention: an updated network meta-analysis. JAMA Cardiol 2020; 5:582–589. https://doi.org/10.1001/jamacardio.2019.6175 PMID: 32101251

22. Gargiulo G, Goette A, Tijssen J, Eckardt L, Lewalter T, Vranckx P, et al. Safety and efficacy outcomes of double vs. triple antithrombotic therapy in patients with atrial fibrillation following percutaneous coronary intervention: a systematic review and meta-analysis of non-vitamin K antagonist oral anticoagulant-based randomized clinical trials. Eur Heart J. 2019; 40:3757–3767. https://doi.org/10.1093/eurheartj/ehz732 PMID: 31651946

23. Alexander JH, Wojdyla D, Vora AN, Thomas L, Granger CB, Goodman SG, et al. Risk/benefit tradeoff of antithrombotic therapy in patients with atrial fibrillation early and late after an acute coronary syndrome or percutaneous coronary intervention: insights from AUGUSTUS. Circulation 2020; 141:1618–1627. https://doi.org/10.1161/CIRCULATIONAHA.120.046534 PMID: 32223444

24. Kogame N, Guimarães PO, Modolo R, De Martino F, Tinoco J, Ribeiro EE, et al. Aspirin-free prasugrel monotherapy following coronary artery stenting in patients with stable CAD: The ASET Pilot Study. JACC Cardiovasc Interv 2020; 13:2251–2262. https://doi.org/10.1016/j.jcin.2020.06.023 PMID: 32950419

25. O'Donoghue ML, Murphy SA, Sabatine MS. The safety and efficacy of aspirin discontinuation on a background of a P2Y12 inhibitor in patients after percutaneous coronary intervention: a systematic review and meta-analysis. Circulation 2020; 142:538–545. https://doi.org/10.1161/CIRCULATIONAHA.120.046251 PMID: 32551860

26. Giacoppo D, Matsuda Y, Fovino LN, D'Amico G, Gargiulo G, Byrne RA, et al. Short dual antiplatelet therapy followed by P2Y12 inhibitor monotherapy vs. prolonged dual antiplatelet therapy after percutaneous coronary intervention with second-generation drug-eluting stents: a systematic review and meta-analysis of randomized clinical trials. Eur Heart J 2021; 42:308–319. https://doi.org/10.1093/eurheartj/ehaa739 PMID: 33284979

27. O'Donoghue M, Wiviott SD. Clopidogrel response variability and future therapies: clopidogrel: does one size fit all? Circulation 2006; 114:e600–e606. https://doi.org/10.1161/CIRCULATIONAHA.106.643171 PMID: 17130347

28. Wiviott SD, Braunwald E, McCabe CH, Montalescot G, Ruzyllo W, Gottlieb S, et al. Prasugrel versus clopidogrel in patients with acute coronary syndromes. N Engl J Med 2007; 357:2001–2015. https://doi.org/10.1056/NEJMoa0706482 PMID: 17982182

29. Wallentin L, Becker RC, Budaj A, Cannon CP, Emanuelsson H, Held C, et al. Ticagrelor versus clopidogrel in patients with acute coronary syndromes. N Engl J Med 2009; 361:1045–1057. https://doi.org/10.1056/NEJMoa0904327 PMID: 19717846

30. Urban P, Mehran R, Colleran R, Angiolillo DJ, Byrne RA, Capodanno D, et al. Defining high bleeding risk in patients undergoing percutaneous coronary intervention: a consensus document from the Academic Research Consortium for High Bleeding Risk. Eur Heart J 2019; 40:2632–2653. https://doi.org/10.1093/eurheartj/ehz372 PMID: 31116395

31. Corpataux N, Spirito A, Gragnano F, Vaisnora L, Galea R, Svab S, et al. Validation of high bleeding risk criteria and definition as proposed by the academic research consortium for high bleeding risk. Eur Heart J 2020; 41:3743–3749. https://doi.org/10.1093/eurheartj/ehaa671 PMID: 33029615

32. Ueki Y, Bär S, Losdat S, Otsuka T, Zanchin C, Zanchin T, et al. Validation of the Academic Research Consortium for High Bleeding Risk (ARC-HBR) criteria in patients undergoing percutaneous coronary intervention and comparison with contemporary bleeding risk scores. EuroIntervention 2020; 16:371–379. https://doi.org/10.4244/EIJ-D-20-00052 PMID: 32065586

33. Lee CH, Fan CC, Tsai LM, Gan ST, Lin SH, Li YH. Patterns of acute myocardial infarction in Taiwan from 2009 to 2015. Am J Cardiol 2018; 122:1996–2004. https://doi.org/10.1016/j.amjcard.2018.08.047 PMID: 30301543

34. Wu CK, Juang JJ, Chiang JY, Li YH, Tsai CT, Chiang FT. The Taiwan Heart Registries: its influence on cardiovascular patient care. J Am Coll Cardiol 2018; 71:1273–1283. https://doi.org/10.1016/j.jacc.2018.02.006 PMID: 29544612

Contents lists available at ScienceDirect

Measurement

journal homepage: www.elsevier.com/locate/measurement

Convolutional neural Network-based detection of deep vein thrombosis in a low limb with light reflection rheography

Shing-Hong Liu [a], Wenxi Chen [b], Chun-Hung Su [c,d], Kuo-Li Pan [e,f,*]

[a] Department of Computer Science and Information Engineering, Chaoyang University of Technology, Taichung 413310, Taiwan, ROC
[b] Biomedical Information Engineering Laboratory, The University of Aizu, Aizu-Wakamatsu City, Fukushima 965-8580, Japan
[c] Institute of Medicine, School of Medicine, Chung-Shan Medical University, Taichung 402, Taiwan, ROC
[d] Department of Internal Medicine, Chung-Shan Medical University Hospital, Taichung 402, Taiwan, ROC
[e] Division of Cardiology, Chiayi Chang Gung Memorial Hospital, Chiayi City 61363, Taiwan, ROC
[f] School of Medicine, College of Medicine, Chang Gung University, Taoyuan City 33305, Taiwan, ROC

ARTICLE INFO

ABSTRACT

Artificial intelligence has been widely used in the biomedical engineering field, which can assist the clinicians in disease diagnoses, help the engineers in physiological signal processing, or serve the people with chronic diseases in the homecare management. Blood clots in the deep veins of human body is called the deep vein thromboses (DVT). If the embolus passes through the lung, patient will have a life-threatening risk. Therefore, how to use the artificial intelligence to serve daily monitoring of the DVT condition is a valuable exploration. The light reflection rheography (LRR) has been used to detect the DVT of low limbs. In the previous study, the wearable device using LRR technique has been developed. But, this examination system could not be used by non-physician because the signal-quality evaluation of LRR and the classification of positive or negative DVT using the LRR signal all need the manual process. The goal of this study is to use a two-dimension convolutional neural network (2D CNN) to evaluate the qualities of LRR signals and classify the positive or negative DVT from the LRR signal with high reliability. The LRR signal and the smoothed signal were combined together to form a 450x450 image as the input pattern. In this study, twenty subjects were recruited to perform four-time experiments. A cuff pressured to 100 mmHg and 150 mmHg occluded the veins of low limbs to simulate the slight and serious DVT scenarios, and which was placed at the top and bottom of the knee of left leg to simulate the distal and proximal embolization. In the signal-quality evaluation, there were 700 samples including 476 high qualities and 224 low qualities, which were marked by the experts according to the vein emptying phenomenon. In the DVT classification, there were 476 samples including 167 negative samples, 158 slight positive samples, and 151 serious positive samples. A 19-layer CNN model proposed by Visual Geometry Group (VGG-19) was used in the two experiments. We performed the inter-group and intra-group analysis. Both results were better than the previous study. The accuracies of signal-quality evaluation and DVT classification were 0.92 and 0.75, respectively. Thus, the proposed method could support people with the high risk for DVT examination at non-medical settings.

Fig. 1. A normal LRR signal has resting, emptying and refilling phases, red line is the filtered signal, the blue line is the smoothed signal, the green dash line is the baseline in resting phase, and the black dash dot line is the baseline in refilling phase. (For interpretation of the references to color in this figure legend, the reader is referred to the web version of this article.)

1. Introduction

Today, deep learning (DL) techniques have helped doctors diagnose disease in clinics more quickly and accurately [1,2]. Some researchers are developing computer-aided diagnosis systems to diagnose the diseases in health care environment [3–5]. These studies with the DL methods almost focused on the diagnosis of medical images [6–8]. However, diagnoses of physiological signals, i.e. electrocardiogram (ECG) or electroencephalogram (EEG) usually use the machine learning (ML) methods [9,10]. However, these signals before the classification have to be preprocessed to remove the artifact noise, and extract their features. These ML methods may include, e.g., the support vector machine [11], K-nearest neighbor [12], fuzzy neural network [13], and Adaboost [14]. In fact, data can be processed more quickly when using ML algorithms. But the performance of ML is closely related to the signal processing methods and characteristics of extracted features.

In recent years, some DL algorithms can process the time series signals, like as accelerometers and gyroscopes [15,16] sensing body activities, ECG for classification of arrhythmia beats [17], or EEG for detection of brain wave [18]. Among many DL methods, long short-term memory (LSTM) as a sequential DL model and variation of recurrent neural network (RNN) have the well performances for temporal information processing. Some studies transfer the pattern of signal as an image and use two-dimension convolutional neural network (2D CNN) to perform the classification, like as the classification of arrhythmia of ECG signals [19,20], and the signal quality of pulse waveform measured by photoplethysmography (PPG) [21,22] In a *meta*-analysis, the transient response of physiological parameters can be used to evaluate the functional variation of some organs. Wei et al. used the spectral harmonic energy of pulse signal ratio to evaluate the elasticity of radial arterial. They found the spectral energy in the fourth to sixth harmonics overly decreased in palpitation patients [23]. Many studies found that the heart rate recovers immediately after exercise is closely relation with the risk of mortality [24,25]. How to use DL algorithms to evaluate or predict the risks of some diseases is an exciting challenge requiring novel approaches.

When a blood clot forms in one or more of the deep veins in the human body, it will change the blood flow of veins and lead to poor circulation, which is called deep vein thromboses (DVT). How to immediately detect DVT is usually a clinical challenge for doctors. Deterioration of DVT would make the treatment process more complicated. Now, many reports show that vaccine of COVID-19 also has the risk to induce the embolus [26]. The thrombosis can occur in any part of the venous system, but it appears most frequently at deep veins of legs [27]. Patients could have the life threatening when the thrombus occurs

in the lung. DVT is highly prevalent in Taiwan and its treatment costs a lot of health insurance funds [28]. Thus, if DVT can be early screened and properly treated, it will be prevented worsening and happening again.

Travelers have the thrombosis when they are sitting at a vehicle for a long time. The embolus may be produced and pass along the deep veins of low limbs [29]. Scurr *et al.* reported when travelers' ages are above 50 years and sitting time is more than 8 h in an air cabin, they have an incidence 10% of asymptomatic calf vein thrombosis [30]. Hence, the happening risk factors of DVT include sitting or standing for a long time, family history of thrombus, pregnancy, diabetes, hyperlipidemia, and hypertension.

The ultrasound or venography is frequently used to examine the DVT, which has to be carried out by professional technicians or physicians in a hospital [31,32]. The general clinics do not perform these examinations. The light reflection rheography (LRR), which uses the optical technique to detect the blood flow of veins, has been used to examine the DVT in calf [33,34]. According to the studies of Thomas et al. [35], LRR has a sensitivity of 92% and a specificity of 84% in detecting the acute thrombosis of calf. LRR uses the reflective PPG sensors to detect the blood volume changes in the calf vein. According to the measuring method of LRR, Liu et al. developed a wearable examination system, available for non-medical settings, to detect the DVT at the low limbs [36]. The system included a wearable device using the commercial reflective PPG sensors and accelerometer to measure LRR signals, and a mobile application (APP) to control the works of sensors, guide the rhythm of foot action, display and store the LRR signals in real time. Six characteristic parameters were defined to classify whether there was positive or negative DVT using the receiver operating characteristic (ROC) curves, including the slopes of emptying and refilling curves in the LRR signal, and the changes of venous pump volume. Under the slight and serious DVT scenarios, the best accuracies were 72% and 76%, respectively. However, this study has some limitations. First, the LRR signals with the low qualities were deleted by the manual processing. Second, the parameters of LRR signal were chosen from the statistical analysis, which all belonged to the local changes of LRR signal. Therefore, the accuracies of these parameters would have some changes in the different experiment [33–35]

The goal of this study is to use a 19-layer CNN model (VGG-19) proposed by Visual Geometry Group to evaluate the qualities of LRR signals and classify the positive or negative DVT from the LRR signal. Because the LRR signal depends on the placement position of the sensor, the sensor must be placed directly above the vein. If it is not placed at the right position, the LRR signal has the distortion. Under the examination of DVT using the LRR, the key for diagnosis is to find the LRR changes in
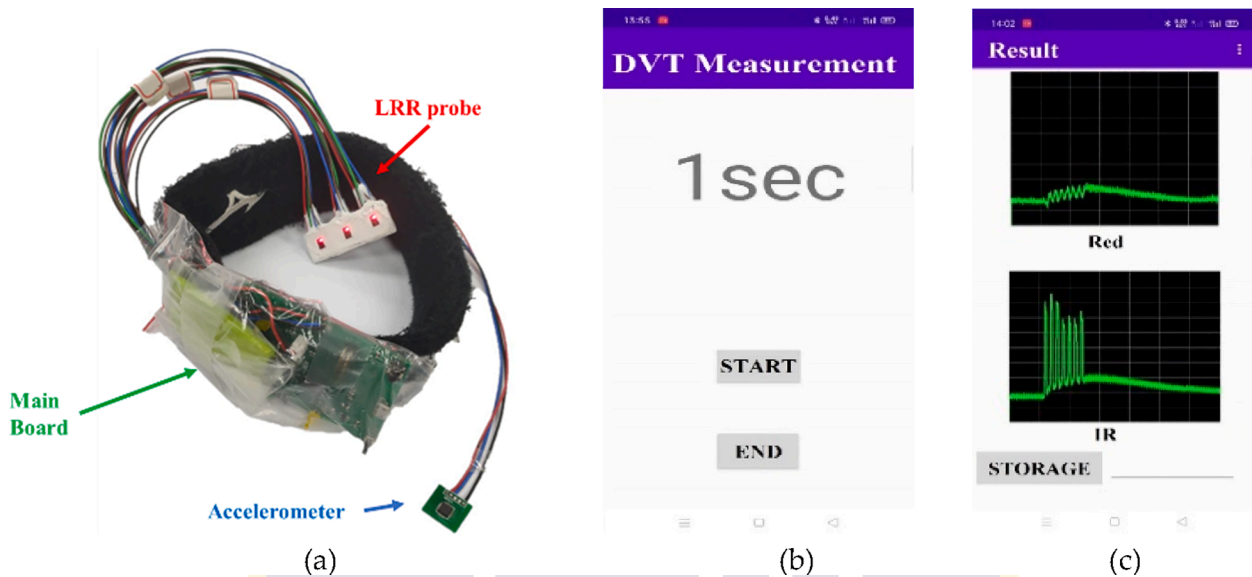
Fig. 2. The LRR measurement system, (a) the LRR wearable device, (b) the measuring screen of APP, (c) the displaying screen of APP.

emptying and refilling phases comparing with in the resting phase. The morphology of LRR signal belongs to macro-pattern. In the previous study [36], a wearable device using LRR technique has been developed. But, this examination system could not be used by non-physician because the signal-quality evaluation of LRR and the classification of positive or negative DVT using the LRR signal all need the manual process. In this study, the LRR patterns were the input to train and test two VGG-19 models. Then, we compared the performance of VGG-19 model with the ROC curve for the DVT classification. The assumptions of the experiment were that the veins of a low limb were partially or wholly occluded by inflating the cuff up to 100 mmHg or 150 mmHg to simulate the stenosis phenomenon in slight and serious DVT scenarios, respectively. The cuff was placed at the top and bottom of the knee of left leg to simulate the distal and proximal embolization. The results showed that the performance of VGG-19 model was better than the ROC curve for the serious scenario. Moreover, the quality of LRR signal could be successfully classified, which accuracy reaching to 92% was better than previous studies [21,22].

2. Light reflection rheography measurement

PPG using a light-emitting diode (LED) and a photoelectric diode (PD) can detect changes of blood flow of superficial arteries and veins. The LED and PD are placed at the same side and detect the venous blood flow. We call this technique LRR measurement. During exercise, the amount of blood in the skin of the lower limb decreases as a result of venous emptying by the calf muscle pump. The elimination of blood volume relates primarily to the effectiveness of the pump mechanism. The time taken for the skin to refill with blood after the pump mechanism is known as the refilling time. In the presence of venous disease, the refilling time is affected by the occurrence and severity of deep and superficial low limb venous thrombosis. When PPG sensor is placed on the skin of the lower limb, it can detect the LRR signal. Fig. 1 shows a normal LRR signal in resting, emptying and refilling phases. The red line is the original signal, the blue line is the smoothing signal, the green dash line is the baseline in resting phase, and the black dash dot line is the baseline in refilling phase.

2.1. DVT examination system

Liu *et al.* designed a LRR measurement system including a LRR wearable device (Fig. 2(a)) and the measuring screen and displaying

Table 1
The specifications of chips used in the wearable device.

Chips	Number	Company
MCU	MSP430 F5438A	Texas Instruments TM
Accelerometer	ADXL 325	Analog Devices
PPG sensor	MAX 30,102	Maxim Integrated TM
Bluetooth module	HC-05	Itead
Charging Chip	TIBQ 24,072	Texas Instruments TM
Regulator Chip	XC62FP	Torex Semiconductor

screen of APP in a smart phone (Fig. 2(b) and (c)) [36]. The LRR wearable device includes an array-type probe, accelerometer, and main board. The array-type probe consists of three MAX30102 PPG sensors (Maxim Integrated TM, San Jose, CA, USA). We only used infrared LED to get LRR signal. An APP program is designed to control the functions of the wearable device, to instruct the rhythm of foot action, to display the results of the LRR signal in real time, and to adjust the IR LED driving current. The sampling frequency is 100 Hz. Communication between the sensors and a microcontroller unit (MCU) is accomplished via a standard I2C-compatible interface. The x-axis signal of the accelerometer (ADXL325, Analog Devices, Norwood, MA, USA) is sampled by the MCU with a 12-bit analog-to-digital converter. The MCU of main board is a 16-bit microcontroller (MSP430F5438A, Texas Instruments TM, Dallas, TX, USA), which reconciles the workflow of the MAX30102 and ADXL325, and transmits the data to the APP by a Bluetooth module (HC-05, Itead, China). The power circuit includes a Lithium battery (150 mAh), a charging IC (TIBQ24072, Texas Instruments TM, Dallas, TX, USA), and a regulator IC (XC62FP, 3.3 V, Torex Semiconductor, Japan). The size of main board is 54 mm × 70 mm. Table 1 summarizes the specifications of chips used in the wearable device.

2.2. LRR signal processing

The measured LRR signal was filtered by a fifty-order finite impulse response (FIR) low-pass filter with a cut-off frequency of 3.4 Hz to remove high-frequency noise. The median point between the neighbor peak and valley was found in the filtered LRR signal. A second-order polynomial function was used to fit the curve of continuous three median points for smoothing the filtered LRR signal. In Fig. 3(a), the red line is the filtered LRR signal, blue line is the smoothed LRR signal. The average of the filtered LRR signal within five seconds before the
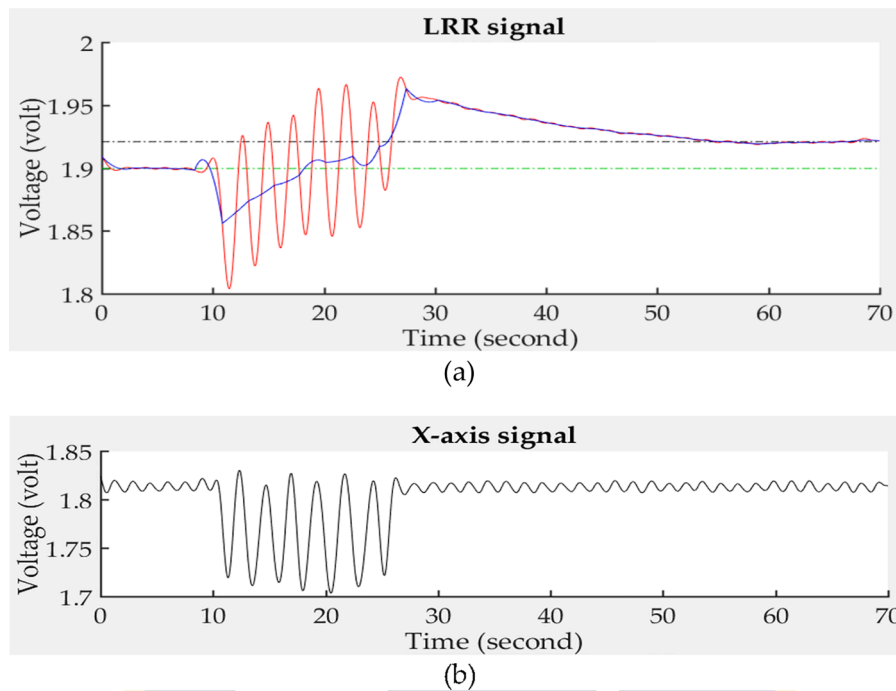
Fig. 3. (a) the filtered (red) and smoothed (blue) LRR signals, and the baselines in resting (green dash line) and refilling (black dash dot line) phases, (b) the x-axis signal. (For interpretation of the references to color in this figure legend, the reader is referred to the web version of this article.)
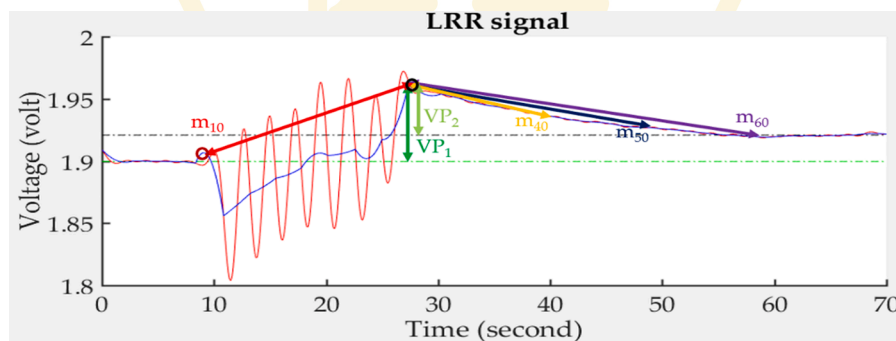

Fig. 4. Illustrative definition of six parameters, VP_1 (green), VP_2 (light green), m_{10} (red), m_{40} (original), m_{50} (black), and m_{60} (purple). (For interpretation of the references to color in this figure legend, the reader is referred to the web version of this article.)

emptying phase corresponds to the resting baseline (green dash line), and the average within the five seconds before the ending measurement represents the refilling baseline (black dash dot line). Fig. 3(b) shows the synchronous x-axis signal of accelerometer.

2.3. Six parameters of LRR signal

According to previous study [36], there were six parameters defined from the smoothed LRR signal to classify the DVT. Fig. 4 shows the six parameters. The start point of emptying action is defined as the LRR_{start} (red circle symbol), and the ending point of emptying action is defined as the LRR_{end} (black circle symbol). VP_1 is defined as the change of venous pump volume between the LRR_{end} and resting baseline (green dash line), VP_2 the change of venous pump volume between the LRR_{end} and refilling baseline (black dash dot line), m_{10} the slope of the emptying curve from the LRR_{end} to LRR_{start} (red double arrow line), m_{40} is the slope of the refilling curve from the LRR_{end} to the point at 40 s (original double arrow line), m_{50} is the slope of the refilling curve from the LRR_{end} to the point at 50 s (black double arrow line), and m_{60} is the slope of the refilling curve from the LRR_{end} to the point at 60 s (purple double arrow line).

2.4. Determination of LRR signal quality

If the LRR sensor is not placed directly above the vein, the LRR signal will have distortion because PPG sensor detecting the upstream of venous flow in the emptying phase. Thus, when the phase angle between the filtered LRR signal and x-axis signal is larger than 90°, this LRR signal is considered of low quality. Another distortion reason is the sensor motion during the emptying action. The baseline of LRR signal has a drift phenomenon. Thus, when VP_1 or VP_2 is negative, the LRR signal is considered of low quality.

2.5. Protocol of experiment

The assumptions of the experiment were that the veins of a low limb were partially or wholly occluded by inflating the cuff up to 100 mmHg or 150 mmHg to simulate the stenosis phenomenon in slight and serious DVT scenarios, respectively. Twenty healthy subjects (10 males and 10 females) without cardiovascular disease or injured limbs were recruited. Their age was between 20 and 24 years (21.8 ± 1.2 years, mean $\pm$ standard deviation), weight between 38 and 80 Kg (60.9 ± 10 Kg), and height between 150 and 180 cm (164.4 ± 9.2 cm). This experiment was
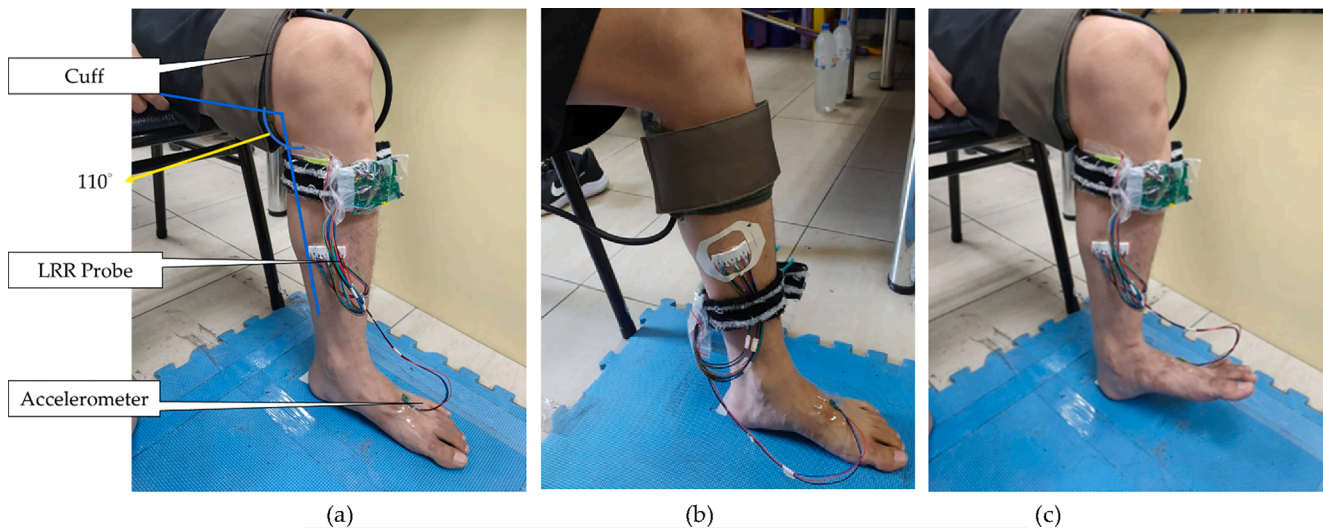
Fig. 5. The experimental photos, (a) the places of the air cuff, PPG probe and accelerometer, (b) another place of the air cuff, (c) the foot action following the rhythm of 0.5 Hz.

Table 2
Fundamental information about the VGG-19 model and associated parameters of the network architecture.

Type	Filter Size (pixel × pixel)	Channel Number	Input Size (pixel × pixel × channel)
Conv1	3 × 3	64	450 × 450 × 3
	3 × 3	64	450 × 450 × 64
Max pool	3 × 3	–	450 × 450 × 64
Conv2	3 × 3	128	225 × 225 × 64
	3 × 3	128	225 × 225 × 128
Max pool	3 × 3	–	225 × 225 × 128
Conv3	3 × 3	256	112 × 112 × 128
	3 × 3	256	112 × 112 × 256
	3 × 3	256	112 × 112 × 256
	3 × 3	256	112 × 112 × 256
Max pool	3 × 3	–	112 × 112 × 256
Conv4	3 × 3	512	56 × 56 × 256
	3 × 3	512	56 × 56 × 512
	3 × 3	512	56 × 56 × 512
	3 × 3	512	56 × 56 × 512
Max pool	3 × 3	–	56 × 56 × 512
Conv5	3 × 3	512	28 × 28 × 512
	3 × 3	512	28 × 28 × 512
	3 × 3	512	28 × 28 × 512
	3 × 3	512	28 × 28 × 512
Max pool	3 × 3	–	28 × 28 × 512
Flatten	–	1	14 × 14 × 512
Fc	–	1	100,352
Out	–	2	512

approved by the Research Ethics Committee of China Medical University & Hospital (No. CMUH107-REC1-167), Taichung, Taiwan.

Subjects were requested to comfortably sit on a chair with the foot resting flat on the floor, and the angle between calf and thigh is about 110°. The LRR probe was placed at the distal end of the calf muscle, which was fixed by a transparent tape. An accelerometer was placed at the front end of foot and an air cuff is wrapped around the thigh, as show in Fig. 5(a). The baselines of LRR signals for three PPG sensors were adjusted to 1.9 V. A cuff pressured to 100 mmHg and 150 mmHg occluded the veins of low limbs to simulate the slight and serious DVT scenarios, and was placed at the top and bottom of the knee of left leg to simulate the distal and proximal embolization. Fig. 5(b) shows that the air cuff is wrapped around the calf. For each experiment, subjects would perform two times. The interval days of each experiment must be more than one week. In one experiment, subjects would be measured three times in the non-occluded condition, and the occluded conditions with

100 mmHg or 150 mmHg, respectively. The interval time of each measurement is 10 min. In the measurement, the resting phase lasts 10 s, the emptying phase is 15 s, and the refilling phase is 45 s. In emptying phase, subjects were requested to move their feet following a rhythm of 0.5 Hz, as shown in Fig. 5(c).

3. Method

We proposed two models to process the problems of LRR signal in the evaluation of signal quality and the classification of DVT. Since the number of samples was not large enough and there were not many differences in the characteristics of patterns, a VGG-19 model was chosen to perform the evaluation task in the study [37]. In the output layer, we replaced the 1000 fully-connection with the softmax activation by a 2 or 3 fully-connection according to the number of categories. VGG-19 model was pretrained for object detection task on the ImageNet dataset [38]. The detailed description of VGG-19 model is shown in Table 2. All of the filters in VGG-19 are of 3x3 in size. The down-sampling is performed directly by maximum pooling layers that have a stride of 2, batch size is 16, learning rate is 0.00001, and batch normalization is performed right after each convolution and before ReLU activation. Two fully connected layers have an identical size of 512.

The number of samples for the signal-quality evaluation are 700. The scales of twenty LRR signals are out of the range. Thus, they are not included in the study. In the DVT classification, only LRR signals with the high quality are used. Table 3 shows the number of LRR signal for each subject in the four experiments. The experiments 1 and 2 are the cuff placed on the top of knee, while experiments 3 and 4 are on the bottom of knee. The number samples are 476.

We used the inter-group and intra-group analysis to evaluate their performances. The fusion matrix includes true positive (TP) as it is classified positive and labeled positive, false positive (FP) as it is classified positive while labeled negative, true negative (TN) as it is classified negative and labeled negative, and false negative (FN) as it is classified negative while labeled positive. Here, the performance of the proposed method was evaluated using accuracy = (TP + TN)/(TP + FP + FN + TN), precision = TP/(TP + FP), sensitivity = TP/(TP + FN), and specificity = TN/(FP + TN).

3.1. Signal-Quality evaluation

According to Section 2.4, the evaluation for the quality of LRR signal

Table 3

The number of LRR signal for each subject in the four experiments. The experiments 1 and 2 are the cuff placed on the top of knee, while experiments 3 and 4 are on the bottom of knee.

Experiment	1			2			3			4			
Subject	0	100	150	0	100	150	0	100	150	0	100	150	Sum
1	2	2	2	1	1	2	3	1	3	3	3	3	26
2	2	0	1	1	1	1	2	2	3	1	1	1	16
3	2	2	2	0	0	1	3	3	3	2	2	3	23
4	1	2	2	1	1	0	1	2	3	2	1	0	16
5	2	2	2	2	2	2	2	2	1	2	2	2	23
6	1	1	2	3	3	3	3	3	3	3	3	3	31
7	1	1	1	1	2	2	3	3	2	2	2	1	21
8	2	0	2	1	1	1	2	3	1	3	3	3	22
9	1	0	1	1	1	0	1	1	0	3	1	2	12
10	2	3	1	2	2	2	3	3	2	2	2	2	26
11	2	2	3	2	2	2	2	1	1	2	1	1	21
12	3	3	3	2	1	2	3	3	2	2	2	0	26
13	2	2	2	3	3	3	3	3	3	2	2	0	28
14	1	2	1	3	2	2	3	3	3	3	2	0	25
15	0	1	0	2	2	2	1	1	1	3	3	2	18
16	3	3	3	3	3	2	3	3	3	3	2	3	34
17	3	3	3	1	1	2	3	3	2	3	3	3	30
18	1	2	3	3	3	2	3	3	1	1	0	1	23
19	3	2	2	3	3	3	2	2	2	2	2	2	28
20	3	2	2	2	2	1	3	2	3	3	2	2	27
Sum	37	35	38	37	36	35	49	47	42	47	39	34	476
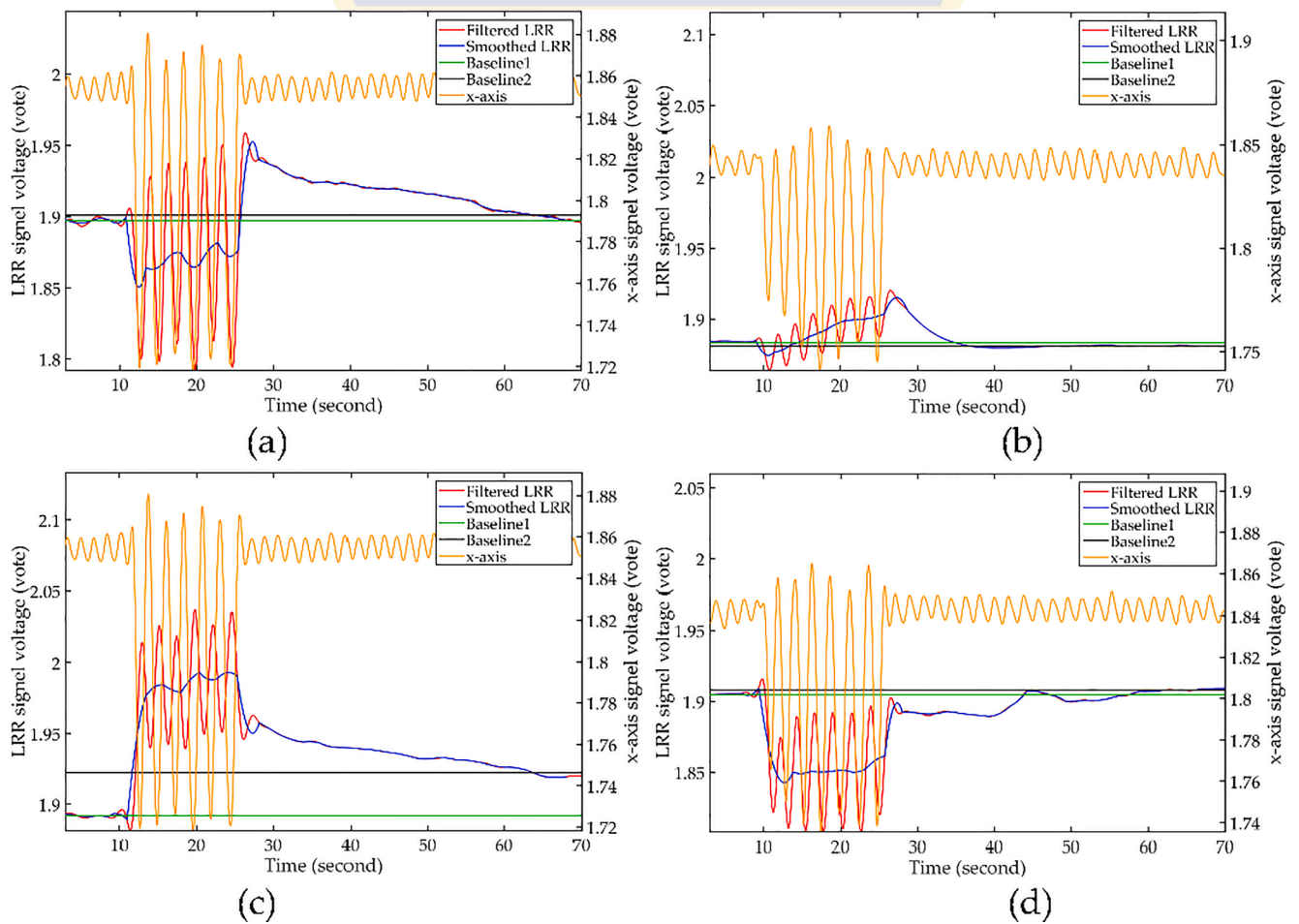
Fig. 6. Four examples of signal-quality pattern, (a) high quality with larger amplitude, (b) high quality with smaller amplitude, (c) low quality with a phase difference about 180° between the LRR signal and x-axis signal, (d) low quality with the negative values of VP_1 and VP_2.
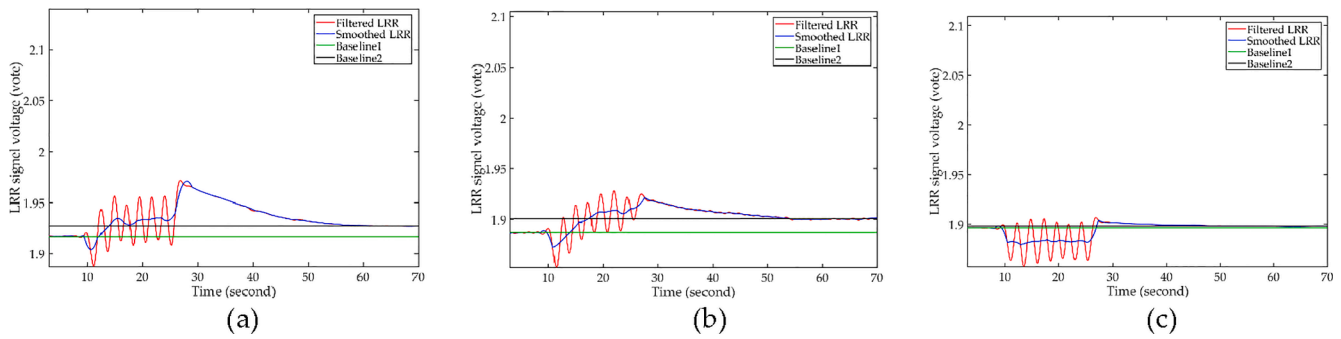
Fig. 7. Three different LRR patterns, (a) no occlusion, (b) occlusion with 100 mmHg, (c) occlusion with 150 mmHg.

not only considers the VP_1 and VP_2, but also the phase difference between the x-axis signal of accelerometer and LRR signal in the emptying phase. Therefore, the input pattern includes the filtered LRR signal (red line), smoothed LRR signal (blue line), x-axis signal (original line), resting baseline (green line), and refilling baseline (black line), as shown in Fig. 6. Fig. 6(a) and (b) show the patterns belonging to the high quality. The pattern in Fig. 6(c) is the low quality because there is a phase difference about 180°between the LRR signal and x-axis signal in the emptying phase. The pattern in Fig. 6(d) is the low quality because VP_1 and VP_2 are the negative values.

The quality of LRR signal was evaluated as two categories of high and low. Then, in order to test the generalization of the model, the inter-group and intra-group analyses were used to evaluate the performance of VGG-19. In the inter-group analysis, the samples in the experiments 1 and 3 were used as the training data. Thus, the numbers of high-quality and low-quality samples were 248 and 96, respectively. The testing data used the samples of experiments 2 and 4. The numbers of high-quality and low-quality samples were 228 and 128, respectively. In the intra-group analysis, the samples of subjects 1 to 10 were used as the training data, thus, the number of high-quality and low-quality samples were 216 and 131, respectively. The testing data used the samples of subjects 11 to 20. The numbers of high-quality and low-quality samples were 260 and 93, respectively.

3.2. DVT classification

According to Section 2.5, the vein of low limb was occluded by cuff pressure of 100 mmHg or 150 mmHg to simulate the slight and serious scenarios of DVT. The changes of LRR signal in the emptying phase and refilling phase have the significant difference [36]. Therefore, the input pattern includes the filtered LRR signal (red line), smoothed LRR signal (blue line), resting baseline (green line), and refilling baseline (black line), as shown in Fig. 7. Fig. 7(a) shows the pattern belonging to the low limb without occlusion, which is considered as the negative group. The patterns in Fig. 7(b) and (c) are the low limb with occlusion under 100 mmHg and 150 mmHg, which are considered as the positive group.

The DVT was classified as two categories, positive and negative. Then, in order to test the generalization of the model, the inter-group and intra-group analyses were used to evaluate the performance of VGG-19. In order to compare our method with the ROC curve method, the samples were separated three categories, Non-DVT (N-DVT), Slight-DVT (L-DVT), and Serious-DVT (S-DVT), and performed the cross-classification, N-DVT vs. L-DVT, and N-DVT vs. S-DVT. In inter-group analysis, the samples in the experiments 1 and 3 were used as the training data. Thus, the numbers of N-DVT, L-DVT, and S-DVT samples were 86, 80 and 82, respectively. The testing data used the samples of experiments 2 and 4. The numbers of N-DVT, L-DVT, and S-DVT samples were 81, 78 and 69, respectively. In intra-group analysis, the samples of Subjects No. 1 to 10 were used as the training data. Thus, the numbers of N-DVT, L-DVT, and S-DVT samples were 72, 71 and 73, respectively. The testing data used the samples of Subjects No. 11 to 20. The numbers of N-

Table 4
The fusion matrices and performances of the VGG-19 for the signal-quality evaluation in the inter-group and intra-group analyses.

	TP	TN	FP	FN	Acc.	Pre.	Sen.	Spe.
Inter-group	206	119	9	22	0.91	0.96	0.90	0.93
Intra-group	241	79	14	19	0.91	0.95	0.93	0.85

Note: Acc. is the abbreviation of accuracy, Pre. is the abbreviation of precision, Sen. is the abbreviation of sensitivity, Spe. is the abbreviation of specificity. Acc. = (TP + TN)/(TP + FP + FN + TN), Pre. = TP/(TP + FP), Sen. = TP/(TP + FN), and Spe. = TN/(FP + TN).

Table 5
The statistical analyses of six parameters for the negative group (0 mmHg) and positive groups (100 mmHg and 150 mmHg) by t-test. The p-value by red color is lower than 0.05.

	0 mmHg (N = 79)	100 mmHg (N = 77)	150 mmHg (N = 73)
VP_1 (mV)	39.6 ± 25	33.2 ± 30.4 $p = 0.153$	24.1 ± 20.9 $p = 6.30E-05$
VP_2 (mV)	34.8 ± 23.9	26.7 ± 20.9 $p = 0.026$	18.8 ± 12.5 $p = 1.14E-06$
m_{10} (mV/s)	2.55 ± 1.55	2.15 ± 1.99 $p = 0.163$	1.6 ± 1.33 $p = 8.57E-05$
m_{40} (mV/s)	-3.03 ± 1.8	-2.21 ± 1.27 $p = 0.001$	-1.55 ± 0.97 $p = 4.80E-09$
m_{50} (mV/s)	-2.08 ± 1.17	-1.51 ± 0.93 $p = 0.001$	-1.04 ± 0.62 $p = 3.96E-10$
m_{60} (mV/s)	-1.59 ± 0.86	-1.16 ± 0.73 $p = 0.001$	-0.81 ± 0.47 $p = 2.12E-10$

DVT, L-DVT, and S-DVT samples were 95, 87 and 78, respectively.

4. Results

4.1. Performance of Signal-Quality evaluation

Table 4 shows the fusion matrices and performances of the VGG-19 for the signal-quality evaluation in the inter-group and intra-group analyses. The number of epochs was 70 in the training process. The accuracies for the two analyses are all 0.91. But the sensitivity (0.93) for the intra-group analysis is better than that (0.90) for the inter-group analysis, and the specificity (0.85) for the intra-group analysis is worse than that (0.93) for the inter-group analysis. The sensitivities for inter-group vs. intra-group analyses are 0.90 vs. 0.93, and the specificities for inter-group vs. intra-group analyses are 0.93 vs. 0.85. Thus, the generalization of proposed model is well for the signal-quality evaluation.

Table 6

The fusion matrix and performances of six parameters.

Parameter	DVT Scenario (mmHg)	TP	TN	FP	FN	Acc.	Pre.	Sen.	Spe.	Cut Point	AUC
VP_1 (mV)	100	28	64	14	50	0.59	0.67	0.36	0.82	20.2	0.61
	150	57	46	32	15	0.69	0.64	0.79	0.59	29.2	0.72
VP_2 (mV)	100	41	57	21	37	0.63	0.66	0.53	0.73	20.9	0.63
	150	44	62	16	28	0.71	0.73	0.61	0.79	18.1	0.76
m_{10} (mV/s)	100	28	66	12	50	0.60	0.7	0.36	0.85	1.28	0.62
	150	51	53	25	21	0.69	0.67	0.71	0.68	1.67	0.72
m_{40} (mV/s)	100	63	34	44	15	0.62	0.59	0.81	0.44	−3.04	0.64
	150	52	56	22	20	**0.72**	0.7	0.72	0.72	−1.92	0.78
m_{50} (mV/s)	100	58	42	36	20	0.64	0.62	0.74	0.54	−1.76	0.65
	150	53	55	23	19	**0.72**	0.7	0.74	0.71	−1.35	0.79
m_{60} (mV/s)	100	57	42	36	21	0.63	0.61	0.73	0.54	−1.31	0.66
	150	47	63	15	25	**0.73**	0.76	0.65	0.81	−0.85	0.8

Note: Acc, Pre, Sen, Spe and AUC are the abbreviations of accuracy, precision, sensitivity, specificity, and area under the curve, respectively.

Fig. 8. The ROC curves and their AUC in serious DVT scenario, (a) m_{40}, (b) m_{50}, (c) m_{60}. Sensitivity is defined as TP/(TP + FN), and Specificity is defined as TN/(FP + TN).

Table 7

The fusion matrices and performances of the VGG-19 for the DVT classification in the inter-group and intra-group analyses.

Parameter	DVT Scenario(mmHg)	TP	TN	FP	FN	Acc.	Pre.	Sen.	Spe.
Inter-group	100	43	49	32	35	0.58	0.57	0.55	0.60
	150	42	70	11	27	**0.75**	0.69	0.61	0.86
Intra-group	100	73	24	71	14	0.53	0.51	0.84	0.25
	150	52	77	18	26	**0.75**	0.74	0.67	0.81

Note: Acc, Pre, Sen, and Spe are the abbreviations of accuracy, precision, sensitivity, and specificity, respectively.

4.2. Performance of DVT classification

Table 5 shows the statistical analyses of six parameters for the negative group (0 mmHg) and positive groups (100 mmHg and 150 mmHg) by *t*-test. When the *p*-value is lower than 0.05, it is represented by red number. Because LRR signals of three sensors for some subjects are all missing, as shown in Table 3, the numbers of total subjects in the 0 mmHg, 100 mmHg, and 150 mmHg experiments are 79, 77, and 73, respectively. We find that the six parameters under 0 mmHg vs. 150 mmHg all have the significant differences. But, only three parameters, m_{40}, m_{50}, and m_{60}, under 0 mmHg vs. 100 mmHg have the significant differences. Table 6 shows the fusion matrix and performances of six parameters. The first three parameters with better accuracy are m_{50}, m_{60} and VP_2 in the L-DVT scenario (0 mmHg vs 100 mmHg), having accuracies of 0.64, 0.63 and 0.63, and area under the curve (AUC) of 0.65,

0.66, and 0.63, respectively. The first three parameters in the S-DVT scenario (0 mmHg vs 150 mmHg) are m_{60}, m_{50} and m_{40} with accuracies of 0.73, 0.72 and 0.72, and AUC of 0.80, 0.79, and 0.78, respectively. We find that the accuracy for the S-DVT classification is higher than that for the L-DVT classification. Fig. 8 shows the ROC curve of m_{60}, m_{50} and m_{40} for the S-DVT scenario.
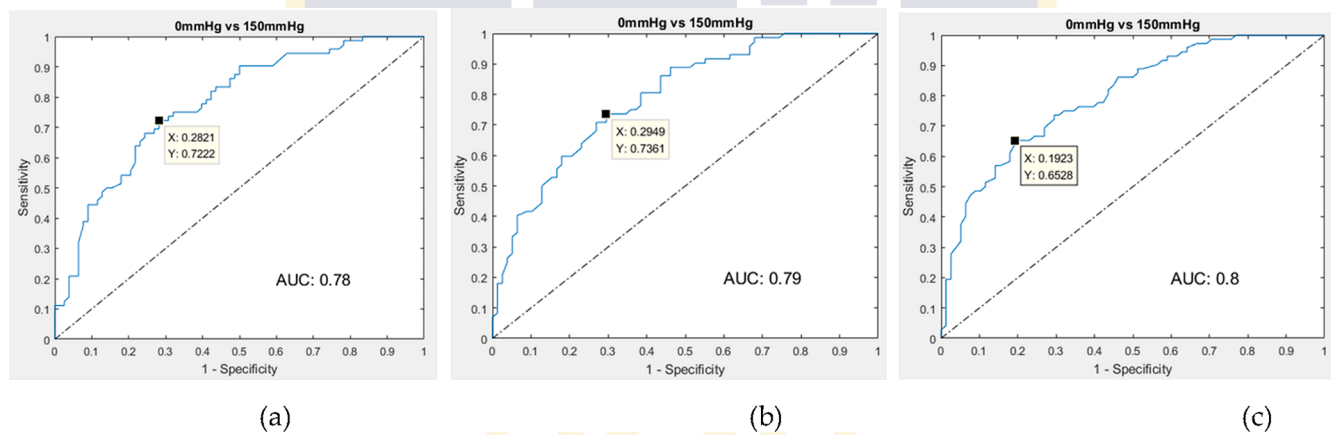
Table 7 shows the fusion matrices and performances of the VGG-19 for the DVT classification in the inter-group and intra-group analyses. The number of epochs was 35 in the training process. The accuracies for two analyses are all 0.75 in the S-DVT scenario (0 mmHg vs 150 mmHg). The sensitivities for inter-group vs. intra-group analyses are 0.61 vs. 0.67, and the specificities for inter-group vs. intra-group analyses are 0.86 vs. 0.81. Thus, the generalization of proposed model is well for the S-DVT scenario. However, for the L-DVT scenario (0 mmHg vs 100 mmHg), although the accuracies for inter-group vs. intra group analyses
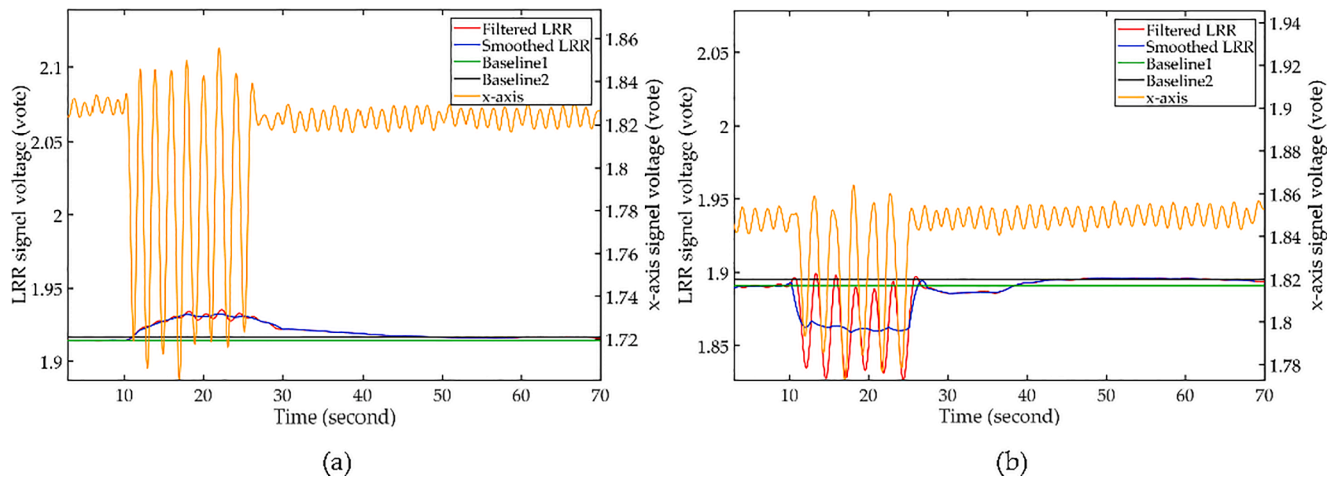
Fig. 9. Two examples for the false positive patterns, (a) the amplitude of alternating signal in the emptying phase is very small, (b) VP$_1$ and VP$_2$ are very small.

are 0.58 vs. 0.53, the sensitivities and specificities for two analyses are 0.55 vs. 0.84, and 0.6 vs. 0.25, respectively. Thus, the generalization of proposed model is bad for the L-DVT scenario.

5. Discussions

Two and a half to five percent of total population have the DVT which is considered as a prevalent disease. There are 30% to 40% DVT patients undergoing the pulmonary embolism [39]. Moreover, there are only about 30% of patients diagnosed as the positive whom have the DVT symptoms [32,40]. Therefore, if DVT can be detected and treated early, it can greatly reduce the mortality caused by pulmonary embolism. Although, the Doppler ultrasound and venoscan with X-ray are the standard inspection method for DVT [31,32], LRR technique can be used as an initial diagnosis tool for patients with the suspected low limb DVT [41]. Thus, subjects without DVT can avoid unnecessary hospitalization and inappropriate anticoagulation therapy. However, how to place the probe of LRR at the right position and determine severity of the DVT are the reasons that the LRR examination has to be carried out at hospitals. Liu et al, developed a wearable LRR system carried out by non-physicians [36]. But, their system is hard to develop an automatic system because the signal-quality evaluation and parameters of DVT decision all need using the manual process. In order to develop an automatic system, the patterns of LRR signals were directly used to classify the quality of LRR signals and the positive or negative DVT with a 2D CNN model in this study.

The rule-based evaluation for signal qualities of PPG pulses is to extract the finite characteristics in time or frequency domains [42,43]. The quality of pulse belongs to a micro-pattern. For the different PPG applications, the optimal filtered conditions are the differences, like as the heart rate and cuffless blood pressure measurements needing the good main peak [44,45], left ventricular ejection time measurement needing the clear foot and dicrotic notch [46], and pulse oximeter needing the stable baseline and amplitude [22]. Thus, the performances of such rule-based approaches depended on the kind and number of characteristics. Some studies used the hierarchical decision rules [47], fuzzy logic [48], supervised machine learning [49–51], and deep learning [21]. But, the quality of PPG segment belongs to a macro-pattern. According to the study of Liu et al., the performance of deep learning was worse than machine learning [22]. The reason was that a PPG segment including many pulses. If waveforms of these pulses do not have the consistency, this segment will be hard to pertain to a generalized decision by the 2D CNN.

This study is the first research focusing on the quality classification of LRR signal using the VGG-19 model. For the performance of signal-quality classification, 0.92 of accuracy by our method was better than 0.90 [21] and 0.86 [22] in previous studies. Although the quality classification of LRR also belongs to a macro-pattern decision, the quality of LRR could be determined by the other signals, like as the x-axis of accelerometer and baselines in the resting and refilling phases. Thus, when the input pattern included the x-axis signal, resting and refilling baselines. The 5 convolutional blocks of VGG-19 could extract these features. Fig. 9(a) shows the false positive patterns that the amplitude of alternating signal in emptying phase is very small. Thus, these patterns
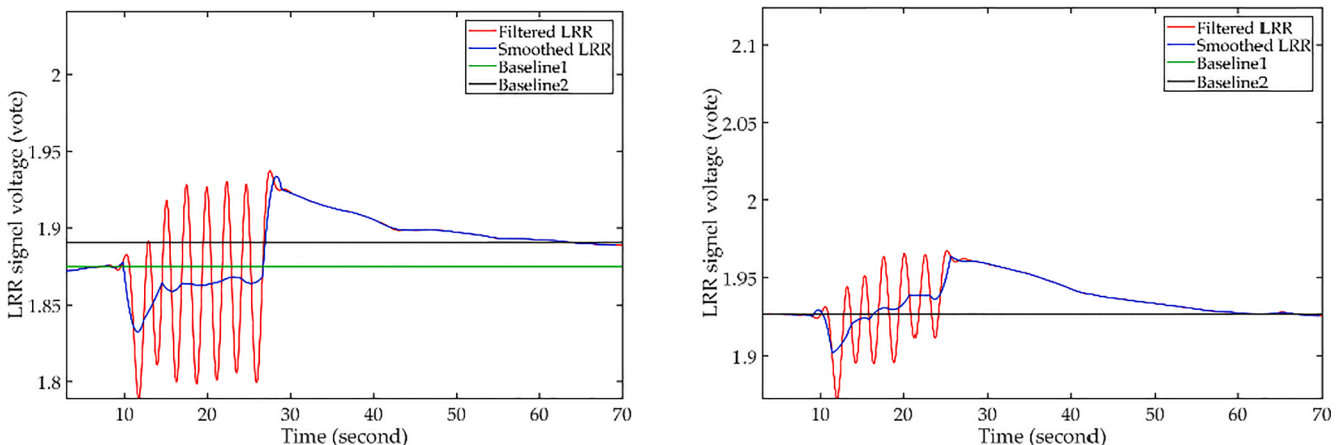

Fig. 10. The two examples for the false negative patterns under 100 mmHg.
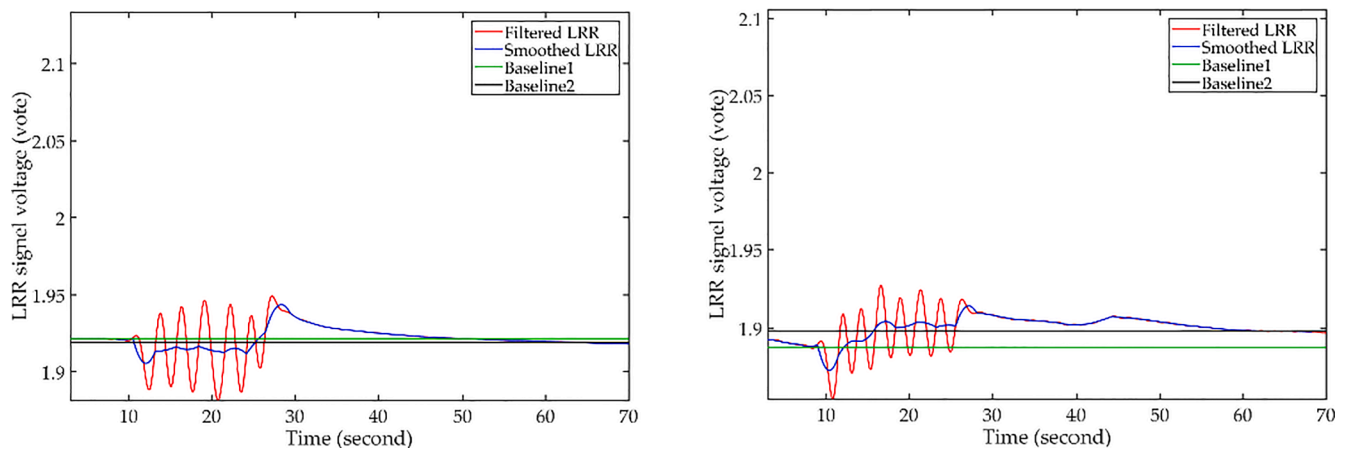
Fig. 11. The two examples for the patterns under 150 mmHg classified as the patterns under 100 mmHg.

are easily misidentified. Fig. 8(b) shows the pattern that VP_1 and VP_2 are very small. Thus, these patterns also are identified as the high quality.

This study is the first research focusing on the DVT classification by the LRR signal using the VGG-19 model to detect the morphologic changes of LRR signal. 0.75 of its accuracy is better than the accuracies of traditional parameters. The previous studies for the DVT diagnosis by the LRR technique all used the analysis of ROC curve for the different parameters, like as the amplitude and rate of venous emptying [52], the time of venous refilling [53], and the shape of LRR curve [36]. Tan et al. have proposed the amplitude of venous emptying and time of venous refilling to test DVT diagnosis and found that the method using two parameters achieved the optimal sensitivity of 100% and 100%. But, their specificities were only 35% and 47%, and AUCs were 0.74 and 0.75, respectively [41]. In Table 6, the AUCs of optimal parameters, m_{50} and m_{60}, are 0.80 and 0.79, which accuracies are 0.73 and 0.72, respectively. According to the above understandings, we found that these studies all explored the optimal parameters extracted from the LRR signal to determine the DVT conditions. The different instruments will have the different optimal parameter set. Just as the LRR technique for DVT examination, these parameters described the morphologic changes of LRR signal in emptying and refilling phases. The advantage of our proposed method is unnecessary to search the optimal parameters of LRR signal. If the LRR signal is scaled to a definite range, the different LRR signal measured by the different instrument will be available to build the model for DVT classification.

The cuffs inflated up to 100 and 150 mmHg are employed to simulate the slight and serious stenosis in deep veins. In Table 7, the accuracies under 150 mmHg are better than those under 100 mmHg in the inter-group and intra-group analyses, 0.75 vs. 0. 58 and 0.75 vs. 0.53. Moreover, in Table 5, only the three parameters have the significant differences in the L-DVT scenario. But, the six parameters have the significant differences in S-DVT scenario. The reason could be that 20 subjects may not effectively respond to the phenomenon of embolization under the 100 mmHg because their systolic blood pressure was higher than the occluding pressure. Moreover, the morphology of LRR signal under 100 mmHg is very close to the morphology under 0 mmHg. Fig. 10 shows two examples for the false negative patterns under 100 mmHg. They are very similar to the pattern in Fig. 6(c). Of course, some morphology of LRR signals under 150 mmHg is very close to the morphology under 100 mmHg. Fig. 11 shows two examples for the patterns under 150 mmHg classified as the patterns under 100 mmHg, which are very similar to the pattern in Fig. 6(b).

The limitation of LRR method is the inabilities of patients to move their foots for emptying the blood of venous in the calf. Therefore, the image techniques, like as ultrasound and x-ray, are the general methods for examining the DVT of low limbs because patients just lie on a table or bed in the clinical practice. Thus, LRR method is suitable developed as a portable apparatus used for the people with the mobility and at a non-medical environment.

The boundary conditions of this research were the results just only fitting the healthy young subjects under the slight and serious DVT scenarios because the ethics approval only allowed us to perform the clinical trial on healthy subjects. Moreover, there were only 700 samples in this study. For a deep learning algorithm (VGG-19 model), the number of samples is too few. Thus, if there are the more data got from the patients with the DVT, we will train the proposed model again to improve the results of this study. Therefore, in the future, authors will apply the ethics approval for the clinical trial on patients with DVT to verify the proposed method that could be used for the DVT examination.

6. Conclusions

DVT is a prevalent disease. Moreover, adults have a chance of thrombosis a few days after vaccine of COVID-19. Development of a wearable device used at a non-medical environment could support people with the hidden risk in the DVT to examine their embolus condition every day. In the previous study, the wearable device using LRR technique has been developed. This examination system could not be used by non-physician because the signal-quality evaluation and the classification of positive or negative DVT using the LRR signals all need the manual process. In this study, the contribution is to utilize the VGG-19 model to resolve the above two problems. The input patterns are the LRR signals and x-axis signal that are scaled in definite ranges. The accuracy for determining the quality of LRR signal was higher than the previous studies. The ROC method with the parameters extracted from LRR signal was the benchmark in the DVT classification. The proposed method has the better performance. Thus, it has the potential for screening the DVT in non-medical environments in the future.

Funding

CRediT authorship contribution statement

Shing-Hong Liu: Conceptualization, Methodology, Software, Validation, Writing – review & editing. **Wenxi Chen:** Writing – review & editing. **Chun-Hung Su:** Writing – original draft. **Kuo-Li Pan:** Writing – original draft.

Declaration of Competing Interest

The authors declare that they have no known competing financial interests or personal relationships that could have appeared to influence the work reported in this paper.

References

[1] D.-C. Cheng, C.-C. Liu, T.-C. Hsieh, K.-Y. Yen, C.-H. Kao, Bone metastasis detection in the chest and pelvis from a whole-body bone scan using deep learning and a small dataset, Electronics 10 (2021), 1201, https://doi.org/10.3390/electronics10101201.

[2] S.M. Hassan, A.K. Maji, M. Jasinski, Z. Leonowicz, E. Jasinska, Identification of plant-leaf diseases using CNN and transfer-learning approach, Electronics 10 (2021), 1388, https://doi.org/10.3390/electronics10121388.

[3] R. Miotto, F. Wang, S. Wang, X. Jiang, J.T. Dudley, Deep learning for healthcare: review, opportunities and challenges, Brief Bioinform 19 (2018) 1236–1246, https://doi.org/10.1093/bib/bbx044.

[4] K.-H. Yu, A.L. Beam, I.S. Kohane, Artificial intelligence in healthcare, Nat. Biomed. Eng. 2 (10) (2018) 719–731, https://doi.org/10.1038/s41551-018-0305-z.

[5] O. Asan, A.E. Bayrak, A. Choudhury, Artificial intelligence and human trust in healthcare: focus on clinicians, Journal of medical Internet research 22 (6) (2020) e15154, https://doi.org/10.2196/15154.

[6] S. Soffer, A. Ben-Cohen, O. Shimon, M.M. Amitai, H. Greenspan, E. Klang, Convolutional neural networks for radiologic images: a radiologist's guide, Radiology 290 (3) (2019) 590–606, https://doi.org/10.1148/radiol.2018180547.

[7] R. Yamashita, M. Nishio, R.K.G. Do, K. Togashi, Convolutional neural networks: an overview and application in radiology, Insights into Imaging 9 (4) (2018) 611–629, https://doi.org/10.1007/s13244-018-0639-9.

[8] D.R. Sarvamangala, R.V. Kulkarni, Convolutional neural networks in medical image understanding: a survey, in: *Evolutionary Intelligence* **publish on line 3 Jan**, 2021, https://doi.org/10.1007/s12065-020-00540-3.

[9] S.-H. Liu, D.-C. Cheng, C.-M. Lin, Arrhythmia identification with two-lead electrocardiograms using artificial neural networks and support vector machines for a portable ECG monitor system, Sensors 13 (2013) 813–828, https://doi.org/10.3390/s130100813.

[10] G. Biagetti, P. Crippa, L. Falaschetti, G. Tanoni, C. Turchetti, A comparative study of machine learning algorithms for physiological signal classification, Procedia Comput. Sci. 126 (2018) 1977–1984, https://doi.org/10.1016/j.procs.2018.07.255.

[11] C. Cortes, V. Vapnik, Support-vector networks, Machine Learning 20 (3) (1995) 273–297, https://doi.org/10.1007/BF00994018.

[12] K.Q. Weinberger, L.K. Saul, Distance metric learning for large margin nearest neighbor classification, Journal of Machine Learning Research 10 (2009) 207–244.

[13] C.-F. Jung, C.-T. Lin, An on-line self-constructing neural fuzzy inference network and its application, IEEE Trans Fuzzy Syst 6 (1998) 12–32, https://doi.org/10.1109/91.660805.

[14] B. Kégl, The return of AdaBoost.MH: multi-class Hamming trees. arXiv:1312.6086 **20 Dec. 2013**.

[15] D. Garcia-Gonzalez, D. Rivero, E. Fernandez-Blanco, R. Luaces, A public domain dataset for real-life human activity recognition using smartphone sensors, Sensors 20 (2020), 2200, https://doi.org/10.3390/s20082200.

[16] I.K. Ihianle, A.O. Nwajana, S.H. Ebenuwa, R.I. Otuka, K. Owa, M.O. Orisatoki, A deep learning approach for human activities recognition from multimodal sensing devices, IEEE Access 8 (2020) 179028–179038, https://doi.org/10.1109/Access.628763910.1109/ACCESS.2020.3027979.

[17] S. Saadatnejad, M. Oveisi, M. Hashemi, LSTM-based ECG classification for continuous monitoring on personal wearable devices, IEEE J. Biomed. Health. Inf. 24 (2) (2020) 515–523, https://doi.org/10.1109/JBHI.622102010.1109/JBHI.2019.2911367.

[18] S. Kumar, A. Sharma, T. Tsunoda, Brain wave classification using long short-term memory network based OPTICAL predictor, Sci. Rep. 9 (2019), 9153, https://doi.org/10.1038/s41598-019-45605-1.

[19] E. Ramirez, P. Melin, G. Prado-Arechig, Hybrid model based on neural networks, type-1 and type-2 fuzzy systems for 2-lead cardiac arrhythmia classification, Expert Syst. Appl. 126 (2019) 295–307, https://doi.org/10.1016/j.eswa.2019.02.035.

[20] Y. Poma, P. Melin, C.I. González, G.E. Martínez, Optimization of convolutional neural networks using the fuzzy gravitational search algorithm, Journal of Automation, Mobile Robotics and Intelligent Systems (2020) 109–120, https://doi.org/10.14313/JAMRIS/1-202010.14313/JAMRIS/1-2020/12.

[21] S.-H. Liu, R.-X. Li, J.-J. Wang, W. Chen, C.-H. Su, Classification of photoplethysmographic signal quality with deep convolution neural networks for accurate Measurement of cardiac stroke volume, Appl. Sci. 10 (2020), 4612, https://doi.org/10.3390/app10134612.

[22] S.-H. Liu, H.-C. Liu, W. Chen, T.-H. Tan, Evaluating quality of photoplethymographic signal on wearable forehead pulse oximeter with supervised classification approaches, IEEE Access 8 (2020) 185121–185135, https://doi.org/10.1109/Access.628763910.1109/ACCESS.2020.3029842.

[23] C.-M. Huang, C.-C. Wei, Y.-T. Liao, H.-C. Chang, S.-T. Kao, T.-C. Li, Developing the effective method of spectral harmonic energy ratio to analyze the arterial pulse spectrum. *Evidence-based Complementary and Alternative Medicine* **2011**, 2011, article ID 342462. doi: 10.1093/ecam/neq054.

[24] S. Qiu, X. Cai, Z. Sun, L. Li, M. Zuegel, J.M. Steinacker, U. Schumann, Heart rate recovery and risk of cardiovascular events and all-cause mortality: a meta-analysis of prospective cohort studies, J Am Heart Assoc 6 (2017), e005505, https://doi.org/10.1161/JAHA.117.005505.

[25] C.R. Cole, E.H. Blackstone, F.J. Pashkow, C.E. Snader, M.S. Lauer, Heart-rate recovery immediately after exercise as a predictor of mortality, N Engl J Med 341 (18) (1999) 1351–1357, https://doi.org/10.1056/NEJM199910283411804.

[26] Pharmacovigilance risk assessment committee (PRAC) signal assessment report on embolic and thrombotic events (SMQ) with COVID-19 Vaccine. European Medicines Agency, **24 March 2021**.

[27] M.R. Jaff, M.S. McMurtry, S.L. Archer, M. Cushman, N. Goldenberg, S.Z. Goldhaber, J.S. Jenkins, J.A. Kline, A.D. Michaels, P. Thistlethwaite, S. Vedantham, R.J. White, B.K. Zierler, Management of massive and submassive pulmonary embolism, ili-ofemoral deep vein thrombosis, and chronic thromboembolic pulmonary hypertension, Circulation 123 (16) (2011) 1788–1830, https://doi.org/10.1161/CIR.0b013e318214914f.

[28] C.H. Lee, L.J. Lin, C.L. Cheng, Y.H. Kao-Yang, J.Y. Chen, L.M. Tsai, Incidence and cumulative recurrence rates of venous thromboembolism in the Taiwanese population. *J Thromb Haemost* **2010**, 8, 1515-1523.doi: 10.1111/j.1538-7836.2010.03873.x.

[29] M.T. Ansari, B.M. Cheung, J. Qing-Huang, B. Eklof, J.P. Karlberg, Traveler's thrombosis: a systematic review, J Travel Med 12 (2005) 142–154, https://doi.org/10.2310/7060.2005.12303.

[30] J.H. Scurr, S.J. Machin, S. Bailey-King, I.J. Mackie, S. McDonald, P.D.C. Smith, Frequency and prevention of symptomless deep-vein thrombosis in long-haul flights: a randomised trial, Lancet 357 (9267) (2001) 1485–1489, https://doi.org/10.1016/S0140-6736(00)04645-6.

[31] R.H. White, J.P. McGahan, M.M. Daschbach, R.P. Hartling, Diagnosis of deep-vein thrombosis using duplex ultrasound, Ann Intern Med 111 (1989) 297–304, https://doi.org/10.7326/0003-4819-111-4-297.

[32] A.W. Lensing, H. Büller, P. Prandoni, D. Batchelor, A.H. Molenaar, A. Cogo, M. Vigo, P.M. Huisman, J.W. ten Cate, Contrast venography, the gold standard for the diagnosis of deep-vein thrombosis: improvement in observer agreement, J Thromb Haemost 67 (1992) 8–12, https://doi.org/10.1055/s-0038-1648130.

[33] A.D. Shepard, W.C. Mackey, T.F. O'Donnell, P.A. Heggerick, Light reflection rheography: a new non-invasive test of venous function, Bruit 8 (1984) 266–270.

[34] H.A. Neumann, I.D.S. Boersma, Light reflection rheography: A non-invasive diagnostic tool for screening for venous disease, J Dermatol Surg Oncol 18 (1992) 425–430, https://doi.org/10.1111/j.1524-4725.1992.tb03696.x.

[35] P.R.S. Thomas, C.M. Butler, J. Bowman, J. Bowman, N.W.T. Grieve, C.E. Bennett, R.S. Taylor, M.H. Thomas, Light reflection rheography: An effective non-invasive technique for screening patients with suspected deep venous thrombosis, Br J Surg 78 (1991) 207–209, https://doi.org/10.1002/bjs.1800780225.

[36] S.-H. Liu, J.-J. Wang, W. Chen, K.-L. Pan, C.-H. Su, An examination system to detect deep vein thrombosis of a lower limb using light reflection rheography, Sensors 21 (2021), 2446, https://doi.org/10.3390/s21072446.

[37] K. Simonyan, A. Zisserman, Very deep convolutional networks for large-scale image recognition. arXiv **2014**, 1556, article ID 1409.

[38] Keras Applications. Available online: https://keras.io/applications/ (accessed on **14 May 2020**).

[39] J.P. Fletcher, D. Mclellan, J. Cade, C. Fisher, H. Gibbs, M. Stacey, A. Vedig, Prevention of venous thrombo-embolism, Chest 69 (1) (1999) 4–5, https://doi.org/10.1046/j.1440-1622.1999.01487.x.

[40] M. Salcuni, P. Fiorentino, A. Pedicelli, C. DiStasi, Diagnostic imaging in deep vein thrombosis of the limbs, Rays 21 (1996) 328–339.

[41] Y.K Tan, A.F da Silva, Digital photoplethysmography in the diagnosis of suspected lower limb DVT: is it useful? Eur J Vasc Endovasc Surg 18 (1) (1999) 71–79, https://doi.org/10.1053/ejvs.1999.0886.

[42] S.-H. Liu, J.-J. Wang, W. Chen, K.-L. Pan, C.-H. Su, Classification of photoplethysmographic signal quality with fuzzy neural network for improvement of stroke volume measurement, Appl. Sci. 10 (2020), 1476, https://doi.org/10.3390/app10041476.

[43] Kejia Li, S. Warren, B. Natarajan, Onboard tagging for real-time quality assessment of photoplethysmograms acquired by a wireless reflectance pulse oximeter, IEEE Trans Biomed Circuits Syst 6 (1) (2012) 54–63, https://doi.org/10.1109/TBCAS.2011.2157822.

[44] J.-J. Huang, H.-Y. Syu, Z.-L. Cai, A.R. See, Development of a long term dynamic blood pressure monitoring system using cuff-less method and pulse transit time, Measurement 124 (2018) 309–317, https://doi.org/10.1016/j.measurement.2018.04.047.

[45] Andrew M. Carek, Hewon Jung, Omer T. Inan, A reflective photoplethysmogram array and channel selection algorithm for weighing scale based blood pressure measurement, IEEE Sensors J. 20 (7) (2020) 3849–3858, https://doi.org/10.1109/JSEN.736110.1109/JSEN.2019.2960063.

[46] S.-H. Liu, J.-J. Wang, C.-H. Su, D.-C. Cheng, Improvement of left ventricular ejection time measurement in the impedance cardiography combined with the reflection photoplethysmography, Sensors 18 (2018), 3036, https://doi.org/10.3390/s18093036.

[47] Simhadri Vadrevu, M. Sabarimalai Manikandan, Real-time PPG signal quality assessment system for improving battery life and false alarms, IEEE Transactions on Circuits and Systems 66 (11) (2019) 1910–1914, https://doi.org/10.1109/TCSII.892010.1109/TCSII.2019.2891636.

[48] S.K. Prabhakar, H. Rajaguru, S.H. Kim, Fuzzy-inspired photoplethysmography signal classification with bio-inspired optimization for analyzing cardiovascular disorders, Diagnostics 10 (2020), 763, https://doi.org/10.3390/diagnostics10100763.

[49] E. Sabeti, N. Reamaroon, M. Mathise, J. Gryak, M. Sjoding, K. Najarian, Signal quality measure for pulsatile physiological signals using morphological features: Applications in reliability measure for pulse oximetry. Informatics in Medicine Unlocked, 2019, 16, 2019, article ID:100222 doi: 10.1016/j.imu.2019.100222.

[50] Tania Pereira, Kais Gadhoumi, Mitchell Ma, Xiuyun Liu, Ran Xiao, Rene A. Colorado, Kevin J. Keenan, Karl Meisel, Xiao Hu, A supervised approach to robust photoplethysmography quality assessment, IEEE J. Biomed. Health. Inf. 24 (3) (2020) 649–657, https://doi.org/10.1109/JBHI.622102010.1109/JBHI.2019.2909065.

[51] C. El-Hajj, P.A. Kyriacou, A review of machine learning techniques in photoplethysmography for the non-invasive cuff-less measurement of blood pressure. Biomedical Signal Processing and Control, 2020, 58, article ID: 101870. doi: 10.1016/j.bspc.2020.101870.

[52] Alberto A. Mitrani, Marco L. Gonzalez, Mark T. O'Connell, Jorge Guerra, Ronna B. Harwood, Laurence B. Gardner, Detection of clinically suspected deep vein thrombosis using light reflection rheography, Am J Surg 161 (6) (1991) 646–650, https://doi.org/10.1016/0002-9610(91)91248-H.

[53] G.T. Abbott, R.T. Diggory, I. Harris, Comparison of light reflection rheography with ascending venography in the diagnosis of lower limb deep vein thrombosis, Br J Radiol 68 (1995) 593–595, https://doi.org/10.1259/0007-1285-68-810-593.
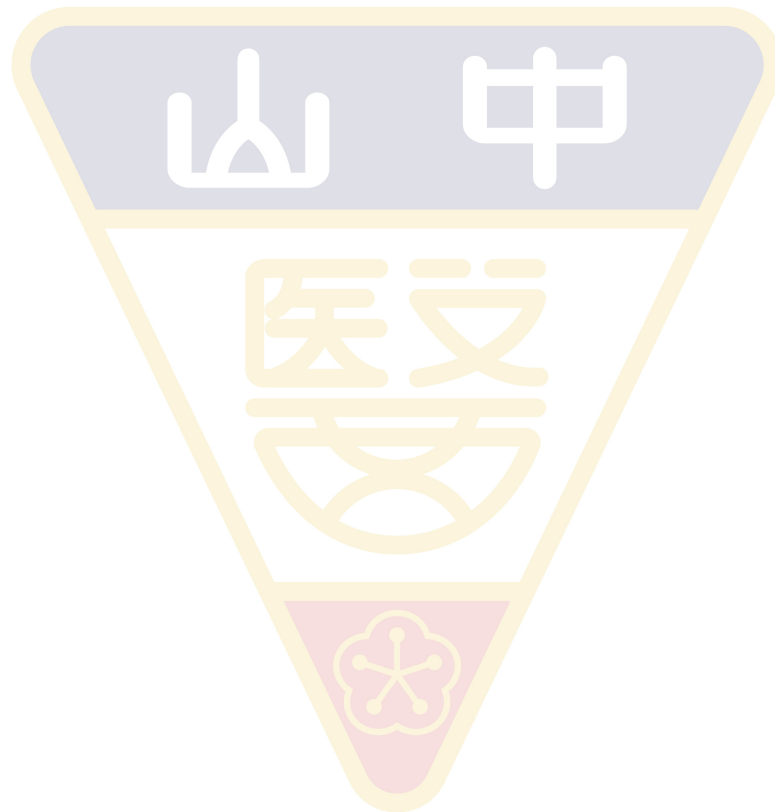
Case Report

Nutcracker syndrome treated by intravascular ultrasound-guided endovascular stenting

Kuan-Chieh Tu [1], Po-Yu Lai [1], Chun-Hung Su [3,4†], Shao-Fan Huang [3], Kai-Wei Chang [3†*]

[1] Department of Internal Medicine, YongKong Chi-Mei hospital, Tainan city, Taiwan

[2] Division of Cardiology, Family medicine, Changhua Christian Hospital, Changhua City, Taiwan

[3] Division of Cardiology, Department of Internal Medicine, Chung Shan Medical University Hospital, Taichung City, Taiwan

[4] School of Medicine, Chung Shan Medical University, Taichung City, Taiwan

[†] *These authors contributed equally to this work.*

Nutcracker syndrome is an uncommon disease and should be easily overlooked. It is characterized by left renal vein entrapment between the abdominal aorta and the superior mesenteric artery. Hematuria and abdominal or flank pain are the most common symptoms. We present a 36-year-old female with chronic lower abdominal pain for 2 months. Computed tomography revealed extrinsic compression of the left renal vein by the aorta and superior mesenteric artery. Venography with pressure measurement showed a 6-mmHg pressure gradient between the left renal vein and the inferior vena cava. Nutcracker syndrome was confirmed. Endovascular stenting was performed under intravascular ultrasound guidance. After procedure, the pressure gradient between the left renal vein and inferior vena cava fell to 0-mmHg and her symptoms resolved. Endovascular stenting is becoming popular among intervention therapies as it is less invasive with a satisfactory result. Intravascular ultrasound can provide more precise lesion information and is helpful in stent sizing and identifying appropriate landing zone.

Keywords: Nutcracker syndrome; endovascular stenting; intravascular ultrasound

1. Introduction

Nutcracker syndrome (NCS) is a rare clinical condition referring to the compression of the left renal vein (LRV) between the superior mesenteric artery (SMA) and the aorta.[1] The extrinsic compression of the LRV causes a variety of symptoms, ranging from microscopic hematuria to macroscopic hematuria, proteinuria, abdominal or flank pain, dyspareunia, dysmenorrhea, and severe pelvic congestion.[1, 2] NCS is an easily missed diagnosis due to its rarity and wide variability of symptomatic presentations.[3] Consequently, its true prevalence is unknown.[1] Diagnosis is generally made after the exclusion of other more common causes, and is confirmed by imaging results, including Doppler ultrasonography (DUS), computed tomography (CT), magnetic resonance imaging (MRI) and venography.[1] The standard treatment of NCS is controversial. Options range from conservative treatment to nephrectomy, with many open survey techniques and endovascular procedures in between, depending on the severity of the clinical symptoms.[1, 4] We present herein the case of a 36-year-old female treated with intravascular ultrasound-guided endovascular stenting with satisfactory results and no reoccurrence of symptoms during a five-year follow-up period.

---

* Correspondence Author: Kai-Wei Chang
  Address: No. 110, Sec. 1, Jianguo N. Rd., Taichung City, 40201, Taiwan
  Tel: +886-4-24739595 ext. 32527
  E-mail: ckwnemo@gmail.com
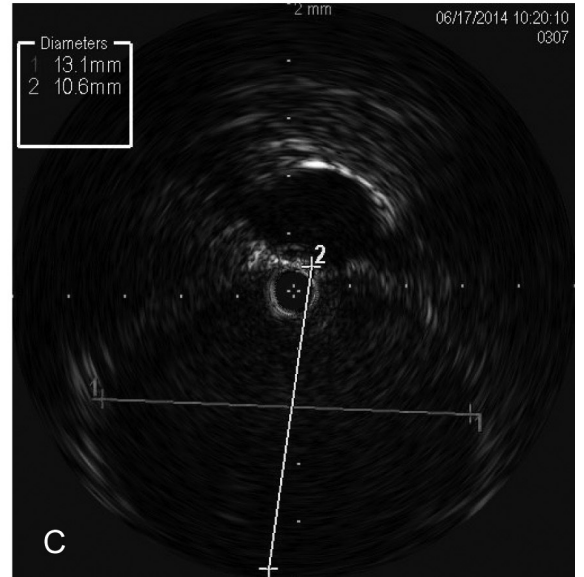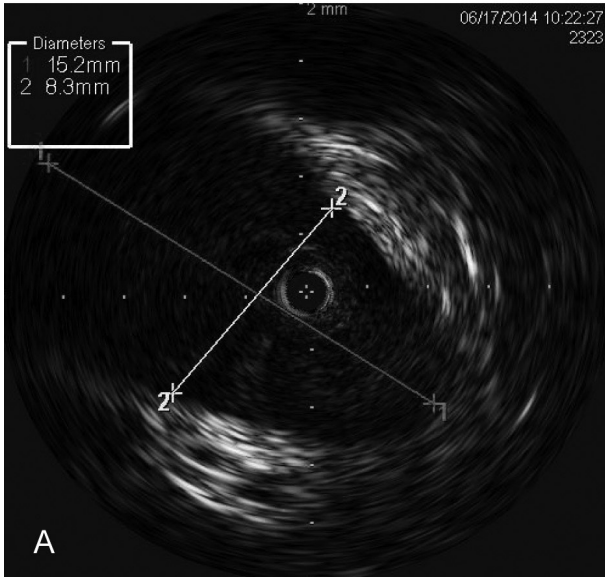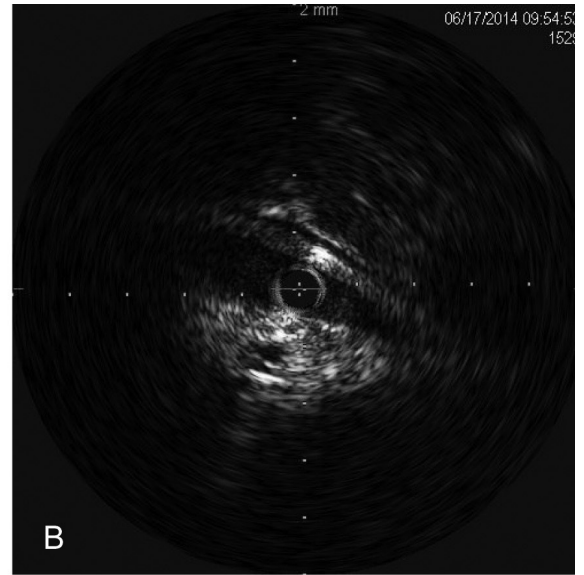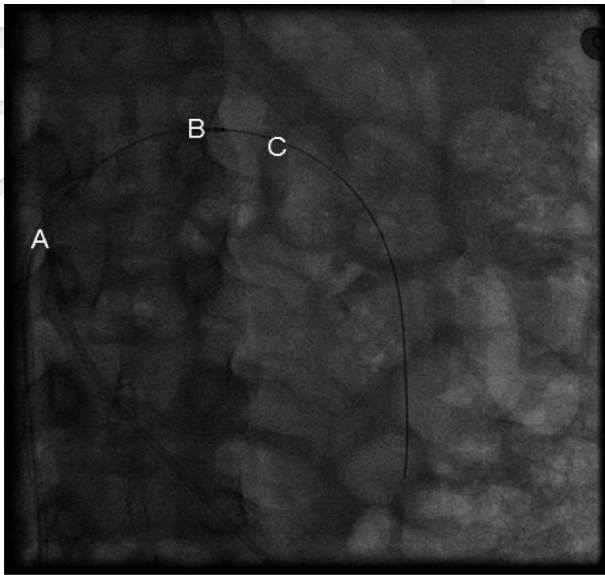
Fig. 1. Accurate IVUS detection of LRV diameter at different sites (A, B, C). (A) Proximal renal vein. (B) Narrowest site of renal vein. (C) Distal renal vein.

2. Case Report

A 36-year-old female with no remarkable history presented with lower abdominal fullness and intermittent cramping pain for 2 months. She had visited a local medical clinic for an initial evaluation, and upper gastrointestinal endoscopy had revealed a shallow peptic ulcer. Her abdominal pain persisted after medical therapy and hence she sought further assessment in the colorectal clinic of the hospital outpatient department. Other than intermittent

abdominal pain, she reported no other gastrointestinal symptoms. A physical examination found no abdominal tenderness or flank knocking pain. Furthermore, her blood biochemistry data were all within normal limits and a urine analysis showed no hematuria or pyuria.

Abdomen and pelvic contrast-enhanced CT revealed no gastrointestinal abnormalities. However, extrinsic compression of the LRV by the aorta and SMA was noted, with proximal venous dilatation and an engorged ipsilateral gonadal vein. The diameter of
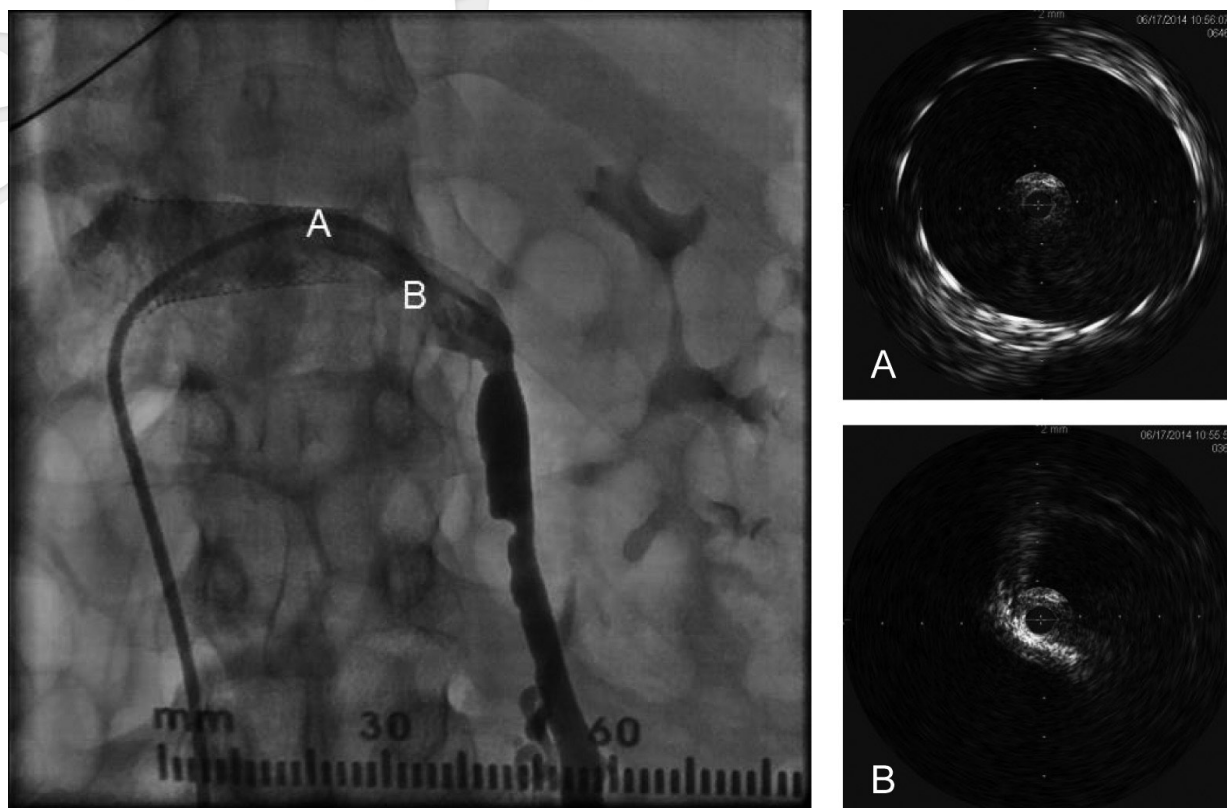
Fig. 2. Successful expansion of compression site following stent placement. IVUS images show increased vessel diameter with final pressure gradient of 0 mmHg. (A) Stent full expansion. (B) Enlarged diameter of narrowest segment.

the LRV at its most compressed level was 4.34 × 4.09 mm, while that at its most dilated level was 20.9 × 15.35 mm. In addition, the diameter of the ipsilateral proximal gonadal vein was 12 mm. NCS was thus highly suspected. The patient's abdominal pain persisted after 2 months of conservative treatment. Therefore, renal venography was performed and showed significant eccentric stenosis of the LRV with a 6-mmHg pressure gradient between the LRV and the inferior vena cava (IVC). NCS was confirmed. Following thorough consideration of the risks and benefits of different procedures, the patient chose endovascular treatment.

During the procedure, the LRV was cannulated with a 7F renal double curve (RDC) guiding catheter. A V-18™ guidewire (Boston Scientific Corp.) was advanced into the left gonadal vein and intravascular ultrasound (IVUS) (Volcano, Visions PV .018) was used to identify and size the stenotic segment of the LRV (Fig. 1). An Amplatz Super Stiff™ guidewire (Boston Scientific Corp.)

was deployed for better support and a 14 × 40-mm Wallstent™ (Boston Scientific Corp.) was then deployed under IVUS guidance. The stent shortened after expansion and the stenotic segment was not fully covered. However, IVUS showed that the diameter of the LRV increased in the narrowest segment (Fig. 2). Furthermore, the pressure gradient between the LRV and the IVC fell to 0 mmHg after stent deployment. Therefore, an additional stent was not used.

After the procedure, the patient's abdominal pain resolved. Antithrombotic agents with warfarin were given for 2 months, followed by aspirin (100 mg/day) alone. Follow-up CT imaging 2 months later showed that there was no stent migration (Fig. 3) and the engorged left gonadal vein was the normal size (Fig. 4). Furthermore, at 5-year follow-up, the patient was still symptom free and chest X-rays showed no stent migration.

3. Discussion
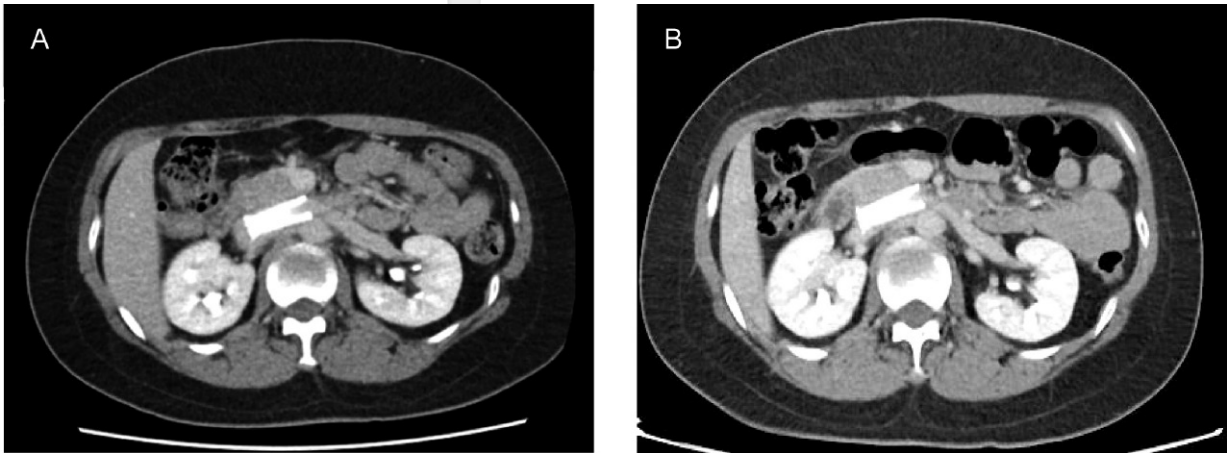
Fig. 3. CT images following stent placement (transverse view). (A) 1 day after stent placement. (B) 2 months after stent placement (no stent migration).
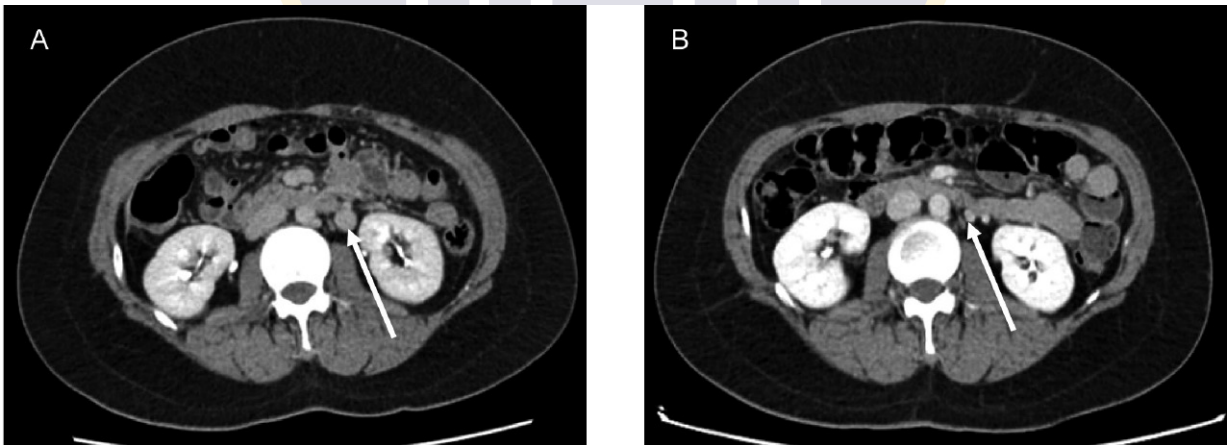
Fig. 4. CT image of left gonadal vein (arrowed). (A) Before stent placement. (B) 2 months after stent placement. The engorged gonadal vein returned to normal size after stent placement.

As described above, NCS is associated with a variety of symptoms. However, not all of these symptoms are specific to the disease. There is no consensus regarding the diagnostic criteria for NCS. Hence, diagnosis is generally made after the exclusion of other more common causes.[1] Real-time DUS is generally recommended as the first diagnostic test in patients with suspected NCS due to its high sensitivity (~78%) and specificity (as much as 100%). [5, 6] However, other studies have suggested that the renocaval pressure gradient cannot be properly predicted by the Doppler flow velocity since the flow rate depends on the degree of compensatory collateral vein formation.[3] According to a previous review article, the diagnostic criteria for NCS include:

a) A venous pressure gradient between the LRV and the IVC $\geq$ 3 mmHg;

b) A five-times increase in the maximum flow velocity in the LRV as it passes the SMA relative to that in the renal hilum;

c) Computed tomography angiography or magnetic resonance angiography showing an angle between the aorta and the SMA of less than 45o.[1]

The treatment options for NCS range from simple observation to nephrectomy, depending on the severity of the clinical symptoms.[3, 4] However, interventions should only be considered when the symptoms are severe or persistent, including severe, unrelenting pain, severe hematuria, renal insufficiency, and failure to respond to conservative treatment after 24 months. [3] In a recent study, Hangge et al.[7] reported that a higher compression of the LRV is correlated

to more hematuria, abdominal pain and more proteinuria. In the case of the patient considered herein, the abdominal pain persisted after 2 months of conservative treatment and CT imaging revealed a high degree of LRV compression with an engorged ipsilateral gonadal vein. Consequently, invasive diagnostic venography was performed.

Intervention therapies for NCS include open surgery and endovascular stenting. Open surgery, specifically LRV transposition, is the mainstay of treatment. However, it has several key disadvantages, including a prolonged period of renal congestion, the need for additional anastomosis, and extensive dissection.[1] By contrast, endovascular stenting is less invasive and generally achieves satisfactory results. For example, a previous study compared 15 patients treated using endovascular stenting with 5 patients treated using open surgery, and found that all of the patients treated with stents were asymptomatic during the follow-up period with the exception of a single case, in which the stent migrated to the right atrium and required surgical intervention to effect its removal.[8] Another study on a cohort of 61 patients with a mean follow-up period of 64 months also showed that endovascular stenting for LRV was safe and effective. [9] However, a later study of the same cohort reported a 6.7% stent migration rate attributed to inappropriate LRV diameter measurement or stent sizing during the original intervention.[10] Therefore, stent migration may not in fact be as rare as originally thought. The authors thus suggested that the preoperative anatomic parameters of the LRV must be more accurately measured. IVUS is beneficial in this regard due to the ability it provides to identify the true compressed lesion and vessel size. For example, in a recent published cohort of 18 patients, IVUS was used in 11 patients (61%), and no stent migration occurred.

In the present case, endovascular stenting was chosen as the intervention therapy after extensive discussions between the patient and the surgeon. In performing the intervention, difficulties were encountered in accurately identifying the stenotic segment by venography since the stenosis was eccentric. Accordingly, IVUS was used to recognize the accurate lesion location and vessel size. Based on the IVUS observations, a 14 x 40 mm Wallstent® was chosen for implantation. The stent shortened after expansion and did not position ideally. Thus, the implantation of a second stent was considered. However, the pressure gradient between the LRV and the IVC resolved and IVUS showed a reduced extrinsic compression of the LRV. Consequently, the second stent was considered to be unnecessary and was therefore not implanted. CT imaging performed 2 months after the procedure revealed that no stent migration occurred, and the engorgement of the left gonadal vein was significantly reduced. In other words, the stent functioned well despite its shortening in the implantation procedure. Furthermore, the patient was still symptom-free 5 years after the procedure. According to a previous study, WallStent™ is the most frequently used stent, but may exhibit more than 30% shrinkage in length on implantation.[9] Consequently, Wang et al recommended that stents with a length of 6 or 8 centimeters should be employed.[12] In addition, to avoid migration of the stent, its diameter should be specified around 20% larger than the venous diameter at the renal hilum. Thus, the basic size is considered to be 14 mm in diameter for patients of the Eastern population.[9]

After stent placement, antithrombotic agents are necessary for preventing thrombosis. However, no standard antithrombotic therapy exists. Thus, the use of anticoagulant for 3 days to 3 months, followed by dual antiplatelet therapy (aspirin and clopidogrel) for 1 to 3 months, and then aspirin alone indefinitely is often suggested.[1, 3, 11]

In conclusion, endovascular stenting is a safe and effective therapy for NCS, and is gaining popularity among intervention therapies. However, to achieve proper stent apposition and avoid stent migration, the preoperative anatomic parameters of the LRV must be accurately measured and venography with corresponding IVUS performed to obtain more precise lesion information. Furthermore, a longer stent (6 to 8 centimeters) is recommended to compensate for stent shortening during implantation.

References

1. de Macedo, G.L., M.A. Dos Santos, A.B. Sarris, and R.Z. Gomes, *Diagnosis and treatment of the Nutcracker syndrome: a review of the last 10 years.*

J Vasc Bras, 2018. **17**(3): p. 220-228.

2. Nickavar, A., *Nutcracker syndrome; a rare cause of hematuria.* J Nephropathol, 2016. **5**(4): p. 144-145.

3. Kurklinsky, A.K. and T.W. Rooke, *Nutcracker phenomenon and nutcracker syndrome.* Mayo Clin Proc, 2010. **85**(6): p. 552-9.

4. He, Y., Z. Wu, S. Chen, L. Tian, D. Li, M. Li, W. Jin, and H. Zhang, *Nutcracker syndrome--how well do we know it?* Urology, 2014. **83**(1): p. 12-7.

5. Quevedo, H.C., S.A. Arain, and N. Abi Rafeh, *Systematic review of endovascular therapy for nutcracker syndrome and case presentation.* Cardiovasc Revasc Med, 2014. **15**(5): p. 305-7.

6. Takebayashi, S., T. Ueki, N. Ikeda, and A. Fujikawa, *Diagnosis of the nutcracker syndrome with color Doppler sonography: correlation with flow patterns on retrograde left renal venography.* AJR Am J Roentgenol, 1999. **172**: p. 39-43.

7. Hangge, P.T., N. Gupta, A. Khurana, K.B. Quencer, H. Albadawi, S.J. Alzubaidi, M.G. Knuttinen, S.G. Naidu, and R. Oklu, *Degree of Left Renal Vein Compression Predicts Nutcracker Syndrome.* J Clin Med, 2018. **7**(5).

8. Zhang, H., M. Li, W. Jin, P. San, P. Xu, and S. Pan, *The left renal entrapment syndrome: diagnosis and treatment.* Ann Vasc Surg, 2007. **21**(2): p. 198-203.

9. Chen, S., H. Zhang, H. Shi, L. Tian, W. Jin, and M. Li, *Endovascular Stenting for Treatment of Nutcracker Syndrome: Report of 61 Cases With Long-Term Followup.* Journal of Urology, 2011. **186**(2): p. 570-575.

10. Wu, Z., X. Zheng, Y. He, X. Fang, D. Li, L. Tian, and H. Zhang, *Stent migration after endovascular stenting in patients with nutcracker syndrome.* J Vasc Surg Venous Lymphat Disord, 2016. **4**(2): p. 193-9.

11. Avgerinos, E.D., Z. Saadeddin, R. Humar, K. Salem, M. Singh, E. Hager, M. Makaroun, and R.A. Chaer, *Outcomes of left renal vein stenting in patients with nutcracker syndrome.* Journal of Vascular Surgery: Venous and Lymphatic Disorders, 2019. **7**(6): p. 853-859.

12. Wang, X., Y. Zhang, C. Li, and H. Zhang, *Results of endovascular treatment for patients with nutcracker syndrome.* J Vasc Surg, 2012. **56**(1): p. 142-8.

Article

Cuffless and Touchless Measurement of Blood Pressure from Ballistocardiogram Based on a Body Weight Scale

Shing-Hong Liu [1], Bing-Hao Zhang [1], Wenxi Chen [2], Chun-Hung Su [3,4] and Chiun-Li Chin [5,*]

1 Department of Computer Science and Information Engineering, Chaoyang University of Technology, Taichung City 41349, Taiwan; shliu@cyut.edu.tw (S.-H.L.); s11027608@gm.cyut.edu.tw (B.-H.Z.)
2 Biomedical Information Engineering Laboratory, The University of Aizu, Aizu-Wakamatsu City 965-8580, Fukushima, Japan; wenxi@u-aizu.ac.jp
3 Institute of Medicine, School of Medicine, Chung-Shan Medical University, Taichung City 40201, Taiwan; such197408@gmail.com
4 Department of Internal Medicine, Chung-Shan Medical University Hospital, Taichung City 40201, Taiwan
5 Department of Medical Informatics, Chung-Shan Medical University, Taichung City 40201, Taiwan
* Correspondence: ernestli@csmu.edu.tw; Tel.: +886-911865102

Abstract: Currently, in terms of reducing the infection risk of the COVID-19 virus spreading all over the world, the development of touchless blood pressure (BP) measurement has potential benefits. The pulse transit time (PTT) has a high relation with BP, which can be measured by electrocardiogram (ECG) and photoplethysmogram (PPG). The ballistocardiogram (BCG) reflects the mechanical vibration (or displacement) caused by the heart contraction/relaxation (or heart beating), which can be measured from multiple degrees of the body. The goal of this study is to develop a cuffless and touchless BP-measurement method based on a commercial weight scale combined with a PPG sensor when measuring body weight. The proposed method was that the $PTT_{BCG-PPGT}$ was extracted from the BCG signal measured by a weight scale, and the PPG signal was measured from the PPG probe placed at the toe. Four PTT models were used to estimate BP. The reference method was the $PTT_{ECG-PPGF}$ extracted from the ECG signal and PPG signal measured from the PPG probe placed at the finger. The standard BP was measured by an electronic blood pressure monitor. Twenty subjects were recruited in this study. By the proposed method, the root-mean-square error (E_{RMS}) of estimated systolic blood pressure (SBP) and diastolic blood pressure (DBP) are 6.7 ± 1.60 mmHg and 4.8 ± 1.47 mmHg, respectively. The correlation coefficients, r^2, of the proposed model for the SBP and DBP are 0.606 ± 0.142 and 0.284 ± 0.166, respectively. The results show that the proposed method can serve for cuffless and touchless BP measurement.

Keywords: ballistocardiogram; photoplethysmogram; pulse transit time (PTT); weight scale; blood pressure

1. Introduction

The COVID-19 virus has been spreading all over the world for more than two years and has led to a large population being isolated at home or quarantined in specified spaces. Thus, physical activity of these isolated people is restricted. According to a previous study, physical inactivity causes more than 5 million deaths worldwide, which does great harm to the finances of public health systems [1]. During physical inactivity, body weight increased, and the weekly energy expenditure and quality of life were reduced [2]. Moreover, the main route of COVID-19 virus infection is the spitting infection. Most people accidentally touch the spit of patients and can very easily become infected. Thus, the World Health Organization suggests that people must wash their hands frequently. The other method is to avoid touching public goods. When the physical activities of people are limited, their dietary assessment will be an important issue to control weight. Moreover, a diet rich in fruits, vegetables, low-fat dairy products, fiber and minerals, would produce a potent anti-hypertensive effect [3,4]. Many studies show that there is a positive relationship between

being overweight or obese and blood pressure (BP) with the risk of hypertension [5,6]. Thus, daily measurements of weight and blood pressure could monitor the effectiveness of dietary management by the individual. However, for BP measurement, people must touch the cuff bladder, for which it is very hard to perform sterilization. How to improve the convenience and accuracy of touchless measurements of body weight and BP will be a challenge during this pandemic era.

A pulse wave in the aorta caused by the heart contraction will transmit to the peripheral arterioles. The pulse transit time (PTT) is defined and calculated as the time interval between the R wave of electrocardiogram (ECG) as the starting time and the foot point of photoplethysmogram (PPG) as the ending time [7–9]. Some studies used the bioimpedance plethysmogram to replace ECG [10,11], or PPG [12,13]. Moreover, the standard definition of PTT is that the blood pressure pulse wave passes from one position to another position. Weltman et al. derived the pulse wave velocity (PWV) utilizing PTT over a known arterial length [14]. The relationship between PWV and BP was quantitatively evaluated by the well-known Bramwell and Hill equation [15]. The cuffless BP measurement based on the PTT has been studied extensively in the past decades. In 2005, Ahlstrom proposed the use of PTT to estimate the continuous systolic BP that compared with the invasive BP. Its results showed that their correlation could be as high as 0.8. Moreover, when the BP has an instantaneous drop, this method could effectively monitor the rapid change in BP [16]. We all know that the BP measured by the oscillometric method [17] represents an average BP in a short period of time. Thus, it is not suitable for continuous BP measurement. In order to develop a wearable BP measurement with the PTT continuously, some studies only measured the time interval from the wrist to finger [11,18,19]. However, their methods were hard to approach the goal of wearable and touchless measurement.

The ballistocardiography (BCG) converts the pulse pressure in the aorta caused by the heart contraction into mechanical vibration that is transmitted to the body by multiple degrees of freedom [20,21]. A mass-damper-spring model was built to represent the vibration transmission in the body, and to predict the BCG waveforms at upper and lower limb locations. A BCG signal can be measured by a MEMS accelerometer placed at the wrist or foot [22], or by a strain gauge sensor placed at a weight scale [23]. Shin et al. used BCG measured by a MEMS accelerometer placed at the wrist to replace ECG for the BP measurement [20]. Martin et al. used a force sensor placed at the foot to acquire the BCG signal to estimate the BP [23]. However, according to the mass-damper-spring model, the damping and stiffness parameters of a weight scale would affect the pattern and phase of the BCG signal.

The pulse wave measured by PPG is easily affected by some factors, such as the subject's skin, tissue, and light density of LED. The PTT values derived from PPG and ECG depend largely on the placement of PPG sensors [24]. Moreover, the ECG is an electrical signal, but the BCG is a mechanical signal. Therefore, when the BCG was measured from the weight scale, and the PPG was measured from the PPG probe placed at the toe when a subject was standing on a commercial weight scale, the reliability and reproducibility of BP measurement with the PTT measured by BCG and PPG signals need to be explored. Thus, the goal of this study is to develop a cuffless and touchless BP measurement method based on a commercial weight scale combined with a PPG sensor when a person is measuring body weight. The BCG signal was extracted from the strain gauge of a commercial weight scale, and a PPG probe placed at a toe was used to measure the pulse signal. The PTT measured by the ECG and PPG of the finger as the reference method was compared with the PTT by the proposed method. Four PPT models for estimating BP were used to explore the reliability and reproducibility of the proposed method. Twenty subjects were recruited in this study, and were asked to exercise to raise their blood pressures. The results showed that the BP measured by the proposed method was close to the BP measured by the reference method.

2. Materials and Methods

In order to use a commercial weight scale to measure BP in real time, we designed a measurement system including a portable acquisition device, ECG, PPG and BCG driving circuits, and a graphic user interface (GUI) on a notebook PC. The portable acquisition device has eight measuring channels, a 3.0 Bluetooth module, and independent dual power supplies from a battery [25]. Figure 1 shows the structure diagram of the measurement system. The four strain gauges (SGs) of a commercial weight scale (HBF-371, Omron, Osaka City, Japan) were used to sense the body weight and BCG signal. Two PPG probes (DS-100A, Nellcor Puritan Bennett, Pleasanton, CA, USA) were placed on the middle finger of the left hand and a toe of the left foot, respectively, which sensed the PPG signals, PPG_F and PPG_T. The Lead I ECG was measured. Four signals, ECG, BCG, PPG_F and PPG_T, were synchronously acquired and transferred via Bluetooth connection to a notebook PC for data visualization and recording. $PTT_{ECG+PPGF}$ values were extracted from ECG and PPG_F signals, and $PTT_{BCG+PPGT}$ values were extracted from BCG and PPG_T signals. Then, four PTT models were built to estimate BP.
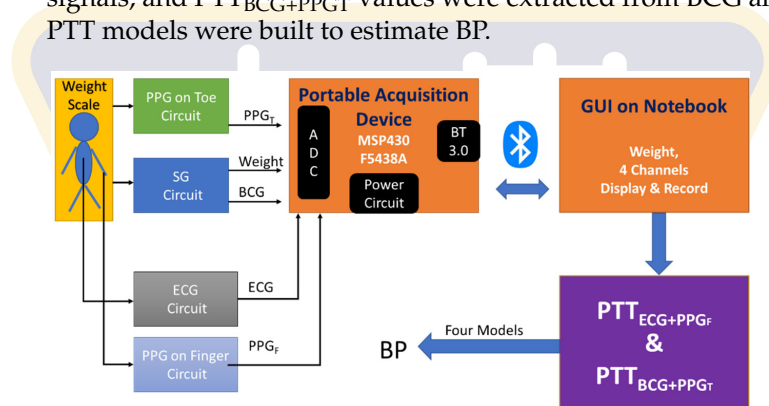
Figure 1. The structure diagram of measurement system including the sensor circuits, portable acquisition device and a graphic user interface (GUI) on the notebook. The PTTECG + PPGF and PTTBCG + PPGT are used to estimate BP with four models. PPG: point of photoplethysmogram; SG: strain gauges; ECG: electrocardiogram; BCG: ballistocardiogram; PTT: pulse transit time; BP: blood pressure.

2.1. Portable Acquisition Device

The portable acquisition device is a modified version used in the previous study of Liu et al. [25]. The main part of this portable acquisition device was a 16-bit microcontroller (MCU), TI MSP430 F5438A, of which sampling rate was 500 Hz and resolution of analog to digital conversion (ADC) was 12 bits. The main clock rate of MCU was 24 MHz. The BT 3.0 module (BTM-204B) was used and connected with the MCU by a UART port. A 12-byte transmission package included the first two bytes, 066 as the header of a transmission package, and the remaining ten bytes for ADC values from each channel consisting of high byte and low byte. In the power circuit, a chip (BQ24072, Texas Instruments, Dallas City, TX, USA) for charging the battery was employed, a regulator chip (TPS78233, Texas Instruments, Dallas City, TX, USA) provided a regulated DC voltage of 3.3 V and current of 400 mA, and another regulator chip (TPS60400, Texas Instruments, Dallas City, TX, USA) provided a negative DC voltage of −3.3 V and current of 60 mA. The dual power supplies offered the power not only for the portable acquisition device, but also for the related external ECG, PPG, and BCG circuits.

2.2. Ballistocardiograph Circuit

The BCG signal is the alternating signal of SGs produced by the pulse pressure. Its energy and signal-noise ratio (SNR) are very low. Figure 2 shows the BCG circuit that includes an instrumentation amplifier (U1), a highpass filter (U2A and U4B), a noninverting amplifier (U2B and U5A), a lowpass filter (U3 and U4A) and a baseline shifter (U5B). The instrumentation amplifier is AD620 (Analog Device, Norwood City, OH, USA), and the

operational amplifier is AD082 (Analog Device, Norwood City, OH, USA). Their working voltages are ±3.3 V. All filters are implemented by the Butterworth structure. The cutoff frequencies of the highpass filter and lowpass filter are 0.3 Hz and 10 Hz, respectively. The total gain is 2000. Finally, the baseline of the BCG signal is shifted to 1.5 V.
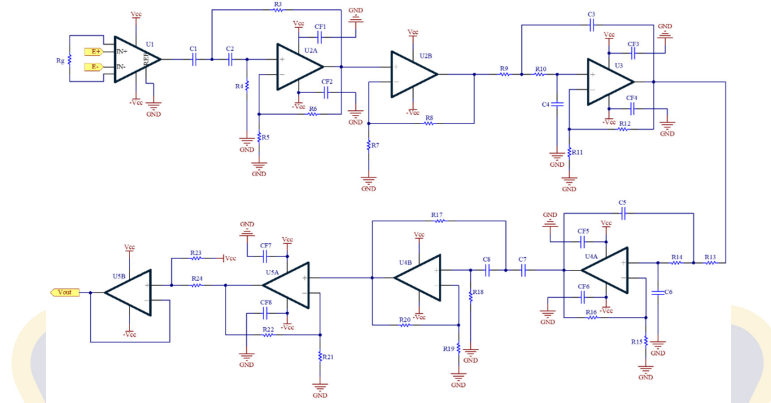
Figure 2. The circuit schematic for BCG measurement.

2.3. Photoplethysmograph Circuit

The PPG circuit detects the alternating component in PPG signal produced by the pulsatile blood flow. Figure 3 shows the PPG circuit that includes a highpass filter (U1A), a noninverting amplifier (U1B), a lowpass filter (U2A and U2B) and a baseline shifter (U3). R1 is a pull-up resistor to convert the current signal to the voltage signal. The operational amplifier is AD082 (Analog Device, Norwood City, OH, USA). Their working voltages are also ±3.3 V. All filters are implemented by the Butterworth structure. The cutoff frequencies of highpass filter and lowpass filter are 0.3 Hz and 40 Hz, respectively. The total gain is 100. Finally, the baseline of PPG signal is shifted to 1.5 V.
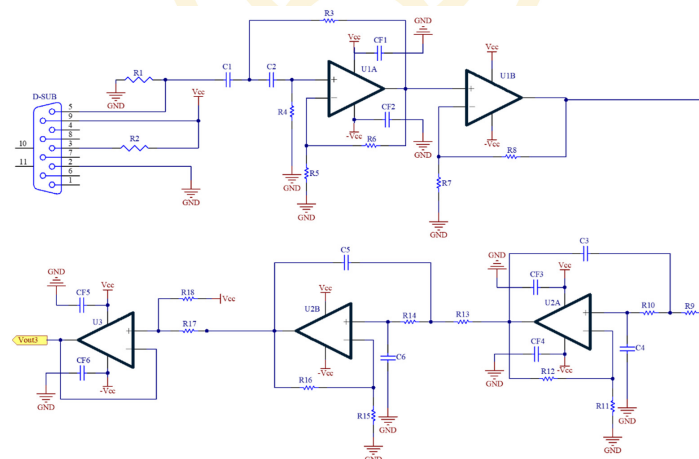
Figure 3. The circuit schematic for PPG measurement.

2.4. Electrocardiograph Module

The chip, AD 8232 (Analog Device, Norwood City, OH, USA) was used to measure Lead I ECG, of which working voltage was 3.3 V, and bandwidth and gain were 0.5 to 40 Hz and 1100, respectively. The baseline is set to 1.5 V.

2.5. Digital Signal Processing

All measured signals were filtered to remove the wandering noise in baseline and the high frequency noise using a 4th-order Butterworth bandpass filter in which the lower and upper cutoff frequencies were 0.5 Hz and 10 Hz, respectively. In order to reduce to the differences of phase lag among different signals, an 8th-order all-pass filter was designed to

equalize the group delay within the passband. Figure 4 shows the ECG (blue), PPG$_F$ (red), PPG$_T$ (green), BCG (black), differential PPG$_F$ (DPPG$_F$, pink) and differential PPG$_T$ (DPPG$_T$, purple). The PTT based on ECG and PPG signals was derived from the R wave of ECG to the foot point of PPG as PTT1 and from the R wave of ECG to main peak of differential PPG as PTT2 [26]. The PTT measured by BCG and PPG signals was defined as an interval between the J wave of BCG and the foot point of PPG for PTT1, and an interval between the J wave of BCG and main peak of differential PPG as PTT2 [27]. In Figure 4, the R wave of ECG, J wave of BCG, and main peak of differential PPG all have the largest point in one heart-beat cycle (marked by black dots). The foot point of PPG (marked by black dots) is the first zero crossing point of differential PPG [20,28].
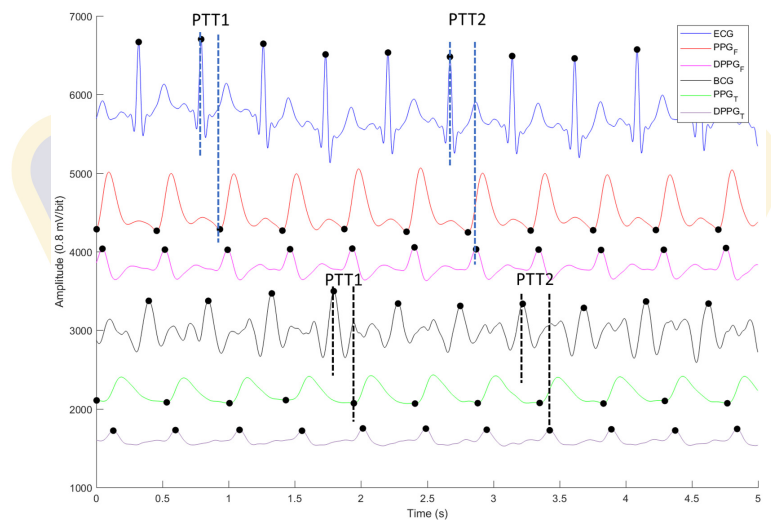
Figure 4. The four signals and their differential signals, ECG (blue), PPGF (red), PPGT (green), BCG (black), differential PPGF (DPPGF, pink) and PPGT (DPPGT, purple). The R wave of ECG, J wave of BCG, main peak of differential PPG, and foot point of PPG are marked by black dots.

2.6. PTT Models for Blood Pressure Estimation

PTT is the time interval between the R wave of ECG and a characteristic point of PPG [29]. The commonly used time stamps on the pulse wave are the foot [30,31], peak [32,33] and middle-point of the rising edge [34,35]. In this study, we defined PTT1 as the time interval between the R wave of ECG and foot point of PPG$_F$, or the J wave of BCG and foot point of PPG$_T$, and PTT2 as the time interval between the R wave of ECG and main peak of differential PPG$_F$ (DPGG$_F$), or the J wave of BCG and main peak of differential PPG$_T$ (DPPG$_T$), as shown in Figure 4.

In order to compare the performance of *BP* estimated by reference and the proposed methods, we utilized three *PTT* models to estimate *BP* that had been published previously [36–38].

$$BP = a * PTT1 + b, \tag{1}$$

$$BP = a * \ln(PTT1) + b, \tag{2}$$

$$BP = a * PTT1 + b * HR + c, \tag{3}$$

where *HR* is the heart rate. Moreover, Heard et al. [39] have simplified the pressure–volume distensibility given by Bramwell and Hill equation to propose an inverse square model. Thus, we proposed an inverse model that included *PTT1*, *PTT2* and *HR*,

$$BP = \frac{a}{PTT1} + \frac{b}{PTT2} + c * HR + d. \tag{4}$$

The linear multi-dimension regression model was used to explore the correlation between the independent variable (*x*) and the dependent variable (*y*), and the estimated

variable ($\hat{y}$) [40]. The independent variables include *PPT1*, *PPT2*, and *HR* measured by reference and proposed methods, the dependent variable is the standard blood pressure measured by an electronic blood pressure monitor, and the estimated variable is the output of the model using reference and proposed methods. The regression model is

$$y = B_0 + B_1 x_{i1} + B_2 x_{i2} + \cdots + B_k x_{ik} + e_i, \tag{5}$$

where e_i is the error, and $B = [B_0, B_1, \ldots, B_k]$ is the parameter vector of the model. The loss function (root-mean-square error), $E_{RMS}(B)$, is used to evaluate the performance of this method,

$$E_{RMS}(B) = \left(\frac{1}{n} \sum_{i=1}^{n} (y_i - \hat{y}_i)^2\right)^{0.5}, \tag{6}$$

where n is the number of data. An optimal estimate of parameter vector was determined from the measurement data by minimizing the loss function [41].

2.7. Statistic Analysis

The quantitative data is expressed as the mean $\pm$ standard deviation (SD). A two-tailed paired *t*-test is used to compare the average of delay time ($DT_{ECG\text{-}BCG}$) between the ECG and BCG, and the delay time ($DT_{PPGF\text{-}PPGT}$) between the PPG_F and PPG_T. A *p*-value of 0.05 or less was considered statistically significant. The degree of linear regression between the PTT parameters (x variable) by the reference or proposed method and the standard BP (y variable) is expressed with a Pearson correlation coefficient, r^2,

$$r^2 = \left(\frac{n(\sum xy) - (\sum x)(\sum y)}{\sqrt{[n \sum x^2 - (\sum x)^2][n \sum y^2 - (\sum y)^2]}}\right)^2, \tag{7}$$

where n is the number of data. Furthermore, the precision and agreement between the standard BP and estimated BP by reference and proposed methods are compared using a Bland–Altman plot.

2.8. Experiment Protocol

Twenty subjects were recruited whose ages were 20.3 ± 1.03 years (eight males and twelve females ranged from 23 to 19 years of age), weights were 55.8 ± 8.86 Kg (from 44 to 75 Kg), and heights were 164.4 ± 7.66 cm (from 152 to 181 cm). This experiment was approved by the Research Ethics Committee of Chung Shan University Hospital (No. CS2-21194), Taichung city, Taiwan.

Subjects were asked to rest for five minutes and fill out an informed consent form before the measurement. The subjects' information, including age, weight, height, medical treatment of illness, and health condition, was recorded. The subjects suffered from arrhythmia and asthma were excluded from the experiment. An electronic blood pressure monitor (HM-7210, Omron, Osaka City, Japan) was used to measure the blood pressure as the standard in this experiment. The cuff of the blood pressure monitor was wrapped on the left upper arm, the probes of PPG were placed on the first finger of right hand and toes of right foot, separately, and the electrodes of ECG were placed on the chest to measure the Lead I equivalent signal. The subject ran on a treadmill to raise their BP. The experiment procedure is described below:

1. Subjects stood on the weight scale to measure ECG, PPG_F, PPG_T, and BCG signals for five minutes, as shown in Figure 5. This measurement was used as the baseline of this experiment. At the same time, the blood pressure was measured once; and its finish-time was marked at the PPG signal.
2. Subjects ran on the treadmill at a speed of about 6 km/h firstly for at least three minutes, and 8 km/h for the last four minutes.

3. Subjects were requested to stand on the weight scale again, to measure ECG, PPG_F, PPG_T, and BCG signal for six minutes. The blood pressures of subjects were measured repeatedly once a minute within standing on the weight scale.
4. One measurement would take about 18 min. Each subject was measured four times. The interval between two measurements was at least one week.

Figure 5. A subject stands on the commercial weight scale. The finger of right hand and toe of right foot wears the PPG probes. The cuff of blood pressure monitor is wrapped on the left hand. Lead I ECG is measured.

Table 1 shows the maximum and minimum standard blood pressures of subjects in the four measurements. Four signals were cut into segments every minute. The qualities of four signals were determined by the manual selection in each segment. If any one of the four signals measured did not have good quality for at least 10 s, the signals within this segment would be ignored. The PTT1 values and PTT2 values were extracted from each heartbeat of four signals, which would be ranked. The average of inter-quartile range of PTT1 values and PTT2 values represented the PTT1 and PTT2 within this one minute. Therefore, the maximum and minimum sample numbers for all subjects were 24 and 12. Table 1 also shows the sample number (N) of each subject.

Table 1. The maximum and minimum standard blood pressures of subjects in the four measurements.

Subject (N)	SBP Max.~Min. mmHg	DBP Max.~Min. mmHg	Subject (N)	SBP Max.~Min. mmHg	DBP Max.~Min. mmHg
01 (N = 21)	142~111	102~74	11 (N = 23)	150~116	106~85
02 (N = 17)	121~84	81~66	12 (N = 24)	154~116	88~58
03 (N = 24)	172~124	121~85	13 (N = 16)	153~126	103~89
04 (N = 24)	156~116	88~68	14 (N = 12)	146~114	77~100
05 (N = 24)	154~106	83~59	15 (N = 12)	132~100	90~76
06 (N = 19)	173~134	104~85	16 (N = 17)	137~104	90~80
07 (N = 23)	152~123	99~83	17 (N = 23)	148~98	90~75
08 (N = 23)	154~118	114~76	18 (N = 16)	113~91	95~67
09 (N = 12)	133~108	85~74	19 (N = 23)	144~112	92~76
10 (N = 24)	132~103	103~74	20 (N = 19)	141~96	74~54

ps: min. is the abbreviation of minimum, max. is the abbreviation of maximum.

3. Results

In this study, we used four models, Equations (1)–(4), to verify the performance of the proposed method based on the BCG and PPG_T signals that was compared with the previous studies as the reference method based on the ECG and PPG_F signals [29]. We used E_{RMS} and correlation coefficient (r^2) to describe the performances of two methods. Table 2 shows the results of estimated systolic and diastolic blood pressures (SBP and DBP) with Equation (1). The E_{RMS} of estimated SBP and DBP by the reference method are 6.6 ± 2.40 mmHg and 5.1 ± 1.67 mmHg, and E_{RMS} of estimated SBP and DBP by the proposed method are 9.1 ± 2.14 mmHg and 5.2 ± 1.61 mmHg. The r^2 of reference method for the SBP and DBP are 0.572 ± 0.204 and 0.157 ± 0.128, and r^2 of proposed method for the SBP and DBP are 0.204 ± 0.181 and 0.087 ± 0.111.

Table 2. The results of estimated systolic and diastolic blood pressures with Equation (1).

| Subjects | Reference Method | | | | Proposed Method | | | |
| | SBP | | DBP | | SBP | | DBP | |
	E_{RMS} (mmHg)	r^2	E_{RMS} (mmHg)	r^2	E_{RMS} (mmHg)	r^2	E_{RMS} (mmHg)	r^2
01	5.0	0.740	5.2	0.193	9.672	0.031	5.7	0.019
02	6.8	0.472	4.4	0.001	7.598	0.348	4.1	0.145
03	8.2	0.641	7.0	0.062	13.760	0.000	5.7	0.376
04	8.7	0.445	4.9	0.014	11.675	0.005	4.9	0.004
05	4.7	0.831	5.2	0.330	7.608	0.570	5.6	0.234
06	9.6	0.296	4.9	0.098	8.772	0.424	5.1	0.034
07	6.9	0.359	3.8	0.276	8.665	0.012	4.4	0.014
08	7.8	0.476	8.0	0.059	9.609	0.218	8.1	0.030
09	4.6	0.609	2.7	0.023	5.702	0.408	2.7	0.000
10	4.7	0.714	5.8	0.066	6.646	0.443	5.3	0.227
11	5.7	0.583	6.8	0.026	7.624	0.278	6.8	0.000
12	4.8	0.783	6.6	0.159	10.218	0.047	6.4	0.221
13	5.8	0.501	3.5	0.371	8.210	0.003	4.4	0.004
14	5.8	0.685	5.8	0.273	9.523	0.164	6.8	0.003
15	4.1	0.839	3.9	0.155	7.300	0.499	3.7	0.233
16	7.2	0.350	1.9	0.432	8.185	0.175	2.5	0.001
17	13.6	0.063	3.5	0.003	12.846	0.171	3.5	0.008
18	5.1	0.583	7.5	0.143	7.655	0.078	8.1	0.001
19	3.0	0.902	2.7	0.235	9.445	0.039	3.0	0.029
20	9.4	0.565	6.2	0.228	13.079	0.161	6.5	0.155
Mean $\pm$ SD	6.6 ± 2.40	0.572 ± 0.204	5.0 ± 1.67	0.157 ± 0.128	9.2 ± 2.14	0.204 ± 0.181	5.2 ± 1.61	0.087 ± 0.111

ps: SD, SBP, DBP are the abbreviations for standard deviation, systolic blood pressure, diastolic blood pressure, respectively.

Table 3 shows the results of estimated SBP and DBP with Equation (2). The E_{RMS} of estimated SBP and DBP by the reference method are 6.2 ± 1.74 mmHg and 5.0 ± 1.65 mmHg, and E_{RMS} of estimated SBP and DBP by the proposed method are 8.6 ± 2.12 mmHg and 5.0 ± 1.48 mmHg. The r^2 of reference method for the SBP and DBP are 0.611 ± 0.157 and 0.167 ± 0.135, and r^2 of proposed method for the SBP and DBP are 0.272 ± 0.241 and 0.119 ± 0.134.

Table 4 shows the results of estimated SBP and DBP with Equation (3). The E_{RMS} of estimated SBP and DBP by the reference method are 5.7 ± 1.76 mmHg and 4.9 ± 1.72 mmHg, and E_{RMS} of estimated SBP and DBP by the proposed method are 7.0 ± 1.59 mmHg and 4.8 ± 1.48 mmHg. The r^2 of reference method for the SBP and DBP are 0.699 ± 0.138 and 0.241 ± 0.162, and r^2 of proposed method for the SBP and DBP are 0.548 ± 0.157 and 0.246 ± 0.167.

Table 3. The results of estimated systolic and diastolic blood pressures with Equation (2).

Subjects	Reference Method				Proposed Method			
	SBP		DBP		SBP		DBP	
	E_{RMS} (mmHg)	r^2	E_{RMS} (mmHg)	r^2	E_{RMS} (mmHg)	r^2	E_{RMS} (mmHg)	r^2
01	4.8	0.761	5.2	0.178	9.6	0.026	5.8	0.001
02	6.7	0.486	4.4	0.001	6.9	0.458	3.8	0.229
03	8.1	0.650	7.1	0.039	13.2	0.070	6.2	0.256
04	7.9	0.534	4.8	0.029	10.8	0.149	4.8	0.045
05	4.4	0.851	5.0	0.382	6.5	0.684	5.5	0.270
06	9.2	0.354	4.9	0.108	10.8	0.114	5.1	0.016
07	6.9	0.369	3.8	0.276	8.4	0.059	4.3	0.041
08	8.0	0.446	7.7	0.120	8.9	0.326	7.5	0.165
09	5.1	0.511	2.7	0.019	5.1	0.508	2.7	0.025
10	4.9	0.690	5.8	0.067	7.0	0.369	5.5	0.159
11	4.7	0.715	6.6	0.055	8.8	0.034	6.8	0.002
12	6.1	0.659	6.9	0.089	7.1	0.527	5.6	0.393
13	5.5	0.542	3.5	0.382	8.2	0.000	4.4	0.023
14	6.5	0.607	5.7	0.292	9.2	0.207	5.1	0.430
15	3.7	0.870	3.8	0.184	10.2	0.007	4.2	0.026
16	7.0	0.397	1.9	0.439	4.5	0.744	2.5	0.030
17	8.2	0.655	3.5	0.003	8.1	0.666	3.5	0.000
18	5.1	0.590	7.5	0.146	7.5	0.102	8.0	0.039
19	2.8	0.910	2.7	0.205	9.0	0.115	3.0	0.011
20	8.8	0.614	5.8	0.319	12.1	0.274	6.2	0.224
Mean ± SD	6.2 ± 1.74	0.611 ± 0.157	5.0 ± 1.65	0.167 ± 0.135	8.6 ± 2.12	0.272 ± 0.241	5.0 ± 1.48	0.119 ± 0.134

ps: SD, SBP, DBP are the abbreviations for standard deviation, systolic blood pressure, diastolic blood pressure, respectively.

Table 4. The results of estimated systolic and diastolic blood pressures with Equation (3).

Subjects	Reference Method				Proposed Method			
	SBP		DBP		SBP		DBP	
	E_{RMS} (mmHg)	r^2	E_{RMS} (mmHg)	r^2	E_{RMS} (mmHg)	r^2	E_{RMS} (mmHg)	r^2
01	4.8	0.766	5.4	0.179	7.3	0.477	5.6	0.112
02	4.3	0.798	3.0	0.553	5.3	0.703	3.4	0.441
03	8.3	0.650	7.2	0.052	11.0	0.384	6.4	0.256
04	7.5	0.608	4.8	0.098	9.0	0.436	4.5	0.210
05	4.5	0.853	4.6	0.505	6.1	0.734	4.1	0.597
06	5.9	0.749	5.0	0.122	6.8	0.673	5.0	0.120
07	7.0	0.378	3.8	0.283	7.6	0.276	4.3	0.102
08	8.0	0.478	7.9	0.121	7.5	0.546	7.6	0.188
09	2.4	0.905	2.7	0.105	4.8	0.607	2.7	0.069
10	5.0	0.693	5.8	0.121	6.9	0.413	5.5	0.197
11	4.3	0.772	6.1	0.243	7.9	0.255	7.0	0.012
12	6.2	0.659	7.0	0.091	6.9	0.579	5.5	0.434
13	5.5	0.570	3.4	0.449	6.3	0.444	3.5	0.407
14	6.8	0.613	6.0	0.294	8.0	0.463	5.4	0.433
15	3.0	0.920	3.7	0.299	6.3	0.662	3.7	0.304
16	5.7	0.618	2.0	0.444	3.5	0.857	2.4	0.158
17	8.3	0.665	3.6	0.013	8.2	0.671	3.6	0.003
18	4.8	0.651	7.8	0.148	4.9	0.644	7.3	0.243
19	2.9	0.911	2.8	0.209	7.4	0.435	2.9	0.126
20	7.8	0.718	5.3	0.482	7.9	0.710	5.2	0.501
Mean ± SD	5.7 ± 1.76	0.699 ± 0.138	4.9 ± 1.72	0.241 ± 0.162	7.0 ± 1.59	0.548 ± 0.157	4.8 ± 1.48	0.246 ± 0.167

ps: SD, SBP, DBP are the abbreviations for standard deviation, systolic blood pressure, diastolic blood pressure, respectively.

Table 5 shows the results of estimated SBP and DBP with Equation (4). The E_{RMS} of estimated SBP and DBP by the reference method are 5.4 ± 1.71 mmHg and 4.9 ± 1.68 mmHg, and E_{RMS} of estimated SBP and DBP by the proposed method are 6.7 ± 1.60 mmHg and 4.8 ± 1.47 mmHg. The r^2 of reference method for the SBP and DBP are 0.742 ± 0.131 and

0.293 ± 0.169, and r^2 of proposed method for the SBP and DBP are 0.606 ± 0.142 and 0.284 ± 0.166. Figure 6a shows the Bland–Altman plot of estimated SBPs by reference (black) and proposed (red) methods with Equation (4), and the standard SBP. The limits of agreement for the proposed method are larger than the reference method. The SBP differences of proposed method within 100 mmHg to 150 mmHg are larger than the reference method. Figure 6b shows the Bland–Altman plot of estimated DBPs by reference (black) and proposed (red) methods with Equation (4), and the standard DBP. The limits of agreement for the proposed method are smaller than the reference method. The DBP differences of proposed method within the 80 mmHg to 120 mmHg are also smaller than the reference method.

Table 5. The results of estimated systolic and diastolic blood pressures with Equation (4).

| Subjects | Reference Method | | | | Proposed Method | | | |
| | SBP | | DBP | | SBP | | DBP | |
	E_{RMS} (mmHg)	r^2	E_{RMS} (mmHg)	r^2	E_{RMS} (mmHg)	r^2	E_{RMS} (mmHg)	r^2
01	4.9	0.770	5.4	0.203	5.8	0.684	5.5	0.192
02	4.4	0.807	2.8	0.639	5.2	0.734	3.5	0.447
03	8.3	0.664	6.7	0.219	10.7	0.446	5.7	0.435
04	7.2	0.654	4.8	0.138	8.8	0.483	4.5	0.231
05	4.3	0.871	4.7	0.505	5.8	0.767	4.2	0.615
06	5.9	0.770	5.2	0.121	6.7	0.702	5.2	0.123
07	7.3	0.365	4.0	0.277	7.6	0.305	4.4	0.112
08	7.8	0.534	7.7	0.213	7.6	0.548	7.5	0.255
09	2.6	0.897	2.8	0.107	4.7	0.670	2.9	0.098
10	4.8	0.730	5.9	0.139	6.6	0.491	5.4	0.264
11	4.5	0.772	6.2	0.259	7.3	0.390	7.1	0.014
12	4.8	0.802	6.6	0.247	5.9	0.704	5.8	0.417
13	5.0	0.679	3.4	0.493	5.9	0.548	3.6	0.449
14	4.8	0.830	6.2	0.327	7.8	0.544	5.6	0.449
15	3.1	0.926	3.7	0.386	5.6	0.761	3.9	0.327
16	5.9	0.621	1.9	0.515	3.7	0.851	2.5	0.166
17	7.8	0.722	3.7	0.018	8.4	0.679	3.7	0.008
18	4.1	0.766	8.0	0.173	5.0	0.663	7.5	0.268
19	2.7	0.925	2.7	0.301	7.5	0.441	2.7	0.309
20	7.7	0.738	4.9	0.579	8.0	0.716	5.3	0.508
Mean ± SD	5.4 ± 1.71	0.742 ± 0.131	4.9 ± 1.68	0.293 ± 0.169	6.7 ± 1.60	0.606 ± 0.142	4.8 ± 1.47	0.284 ± 0.166

ps: SD, SBP, DBP are the abbreviations for standard deviation, systolic blood pressure, diastolic blood pressure, respectively.
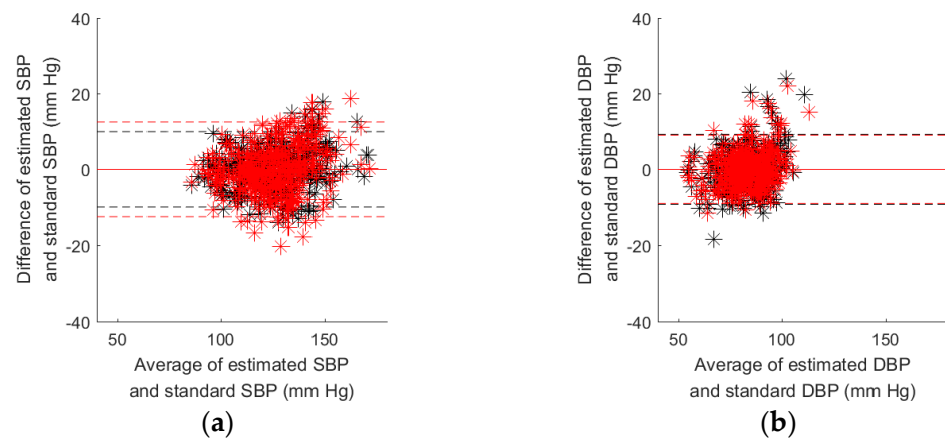
Figure 6. (**a**) Bland–Altman plot of estimated SBPs by reference (black) and proposed (red) methods with Equation (4), and the standard SBP; (**b**) Bland–Altman plot of estimated DBPs by the reference (black) and proposed (red) methods with Equation (4), and the standard SBP.

We found that the reference method to estimate BP has better performance than the proposed method. In order to explore this problem, we analyzed the differences of PTT1 and PTT2 measured by reference and proposed methods. Table 6 shows the statistic of total PTT1 and PTT2 that were measured by reference and proposed methods. The number of PTT1 or PTT2 is 396. $PTT1_{ECG}$ is extracted from the ECG and PPG_F signals, and $PTT1_{BCG}$ is extracted from the BCG and PPG_T signals. $PTT2_{ECG}$ is extracted from the ECG and DPPG signals, and $PTT2_{BCG}$ is extracted from the BCG and DPGG signals. We used the paired *t*-test to compare the differences of PTT1 and PTT2 data between reference and proposed methods. We found that not only is $PTT1_{ECG}$ (164.8 $\pm$ 21.46 ms) significantly greater than $PTT1_{BCG}$ (142.2 $\pm$ 17.57 ms), but also $PTT2_{ECG}$ (227.4 $\pm$ 24.29 ms) is significantly greater than $PTT2_{BCG}$ (212.0 $\pm$ 18.81 ms).

Table 6. The statistic of total PTT1 and PTT2 measured by reference and proposed methods.

	$PTT1_{ECG}$ (ms)	$PTT1_{BCG}$ (ms)	$PTT2_{ECG}$ (ms)	$PTT2_{BCG}$ (ms)
Mean	164.8	142.2	227.4	212.0
SD	21.46	17.57	24.29	18.81
p-value	2.76×10^{-51}		5.23×10^{-22}	

ps: SD is the abbreviation of standard deviation.

The ECG is an electric signal, while BCG is a mechanical signal. Moreover, although PPG_F and PPG_T are all PPG signals, their transit distances are not the same. Thus, we explored the delay time ($DT_{ECG-BCG}$) between the ECG and BCG, and the delay time ($DT_{PPGF-PPGT}$) between the PPG_F and PPG_T in Table 7. The number of all pulses used to get the PTT1 and PTT2 is 4364. $DT_{ECG-BCG}$ (82.8 $\pm$ 22.73 ms) is significantly greater than $DT_{PPGF-PPGT}$ (61.6 $\pm$ 17.47 ms).

Table 7. The statistic of delay time ($DT_{ECG-BCG}$) between the ECG and BCG, and the delay time ($DT_{PPGF-PPGT}$) between the PPG_F and PPG_T.

	$DT_{ECG-BCG}$ (ms)	$DT_{PPGF-PPGT}$ (ms)
Mean	82.8	61.6
SD	22.73	17.47
p-value	0.000	

ps: SD is the abbreviation of standard deviation.

4. Discussion

The BP is adjusted by the autonomic nervous system and central nervous system. However, in the clinical diagnosis, BP is measured when people have rested for five minutes, which represents the rest BP. Therefore, some studies used the beat-to-beat BP measured by the invasive method to calibrate the BP measured by the cuffless methods [42,43]. Thus, the accuracies of these studies were higher. However, when the blood pressure changes under spinal anesthesia [44] or exercise [12], the accuracy of blood pressure measured by the PTT would become fairly poor. In the pilot study of Sharwood-Smith, the correlation coefficient between the mean blood pressure and PTT was only r^2 = 0.55 [44]. The result for the exercise experiment was only r^2 = 0.49 [12]. In this study, the BP of subjects was raised by the exercise, and measured by the commercial electronic BP monitor. The best r^2 and E_{RMS} of estimated SBP with the proposed method was 0.606 $\pm$ 0.142 and 6.7 $\pm$ 1.60 mmHg, respectively. These results were very close to the previous studies.

There are many studies investigating the relations between the PTT and BP [24,26]. The PTT could be defined as the interval between the R wave of ECG and the specific point of PPG because the PTT contains the intra-cardiac (pre-ejection period, PEP) and the vascular transit time [45]. The PET is a time delay that is affected by stress, physical activity, age, and emotion [9]. Thus, the foot point of PPG wave is usually used as the characteristic point to reduce influence of the PEP, which represents the ending time of the

cardiac diastolic cycle. Some studies proposed the PTT using the middle-point of the rising edge as the characteristic point of the PPG signal because the rest BP is also controlled by the autonomic nervous system. Therefore, we proposed a new relation between the inverse PTT and BP, as in Equation (4). The PTT includes the PTT1 (interval between the R wave of ECG and the foot point of PPG) and PTT2 (interval between the R wave of ECG and the middle-point of the rising edge of PPG). We found that the proposed model, Equation (4), has the best performance among the other three models, Equations (1)–(3), in terms of E_{RMS} of estimated SBP: 5.4 ± 1.71 mmHg vs. 6.6 ± 2.40 mmHg, 6.2 ± 1.74 mmHg, and 5.7 ± 1.76 mmHg.

In Table 5, the performance of the proposed method seems not to be better than the reference method in terms of E_{RMS} of estimated SBP: 6.7 ± 1.60 mmHg vs. 5.4 ± 1.71 mmHg, and r^2 for the SBP with Equation (4): 0.606 ± 0.142 vs. 0.742 ± 0.131. The PTT1 and PTT2 measured by the proposed method are significantly smaller than the reference method in Table 6. Then, we analyzed the delay time between the ECG and BCG, and between the PPGF and PPGT in Table 7. $DT_{ECG\text{-}BCG}$ (82.8 ± 22.73 ms) is significantly greater than $DT_{PPGF\text{-}PPGT}$ (61.6 ± 17.47 ms). Thus, the accuracy of PTT measured by the BCG is lower than the ECG. Shin et al. used the BCG measured from the wrist and the PPG measured from the finger to estimate the SBP. The correlation coefficient, r^2, approaches 0.64, which is better than 0.606 ± 0.142 in our study [20]. Martin et al. used the BCG and PPG measured from the foot to estimate the SBP [23]. E_{RMS} was only 11.8 ± 1.6 mm, which was worse than 5.4 ± 1.71 mmHg in our study. Thus, the farther away from the heart the PTT is measured, the less accurate the estimate is.

BCG could be measured when a person is standing on a weight scale [46], lying on a bed [47], or sitting in a chair [48]. The SNR of BCG is affected by the posture of a person [22]. Moreover, the SNR of BCG measured by the weight scale is the lowest among the other two. Inan et al. studied the relation between SNR of BCG and the electromyogram power of feet during movement, and the correlation coefficient, r, was 0.89 [46]. Thus, the main limitation of the proposed method is that subjects must stand stably. In this study, subjects were all young people whose leg muscles were normal. That is, the SNR of BCG would be high. If the muscles of users' legs are abnormal, such as in sarcopenia or handicapped legs, they are not suitable to use this method to measure BP. Moreover, PPG is to measure the change of blood volume in the capillary [49], for which morphologies are different at the different body sites. In Figure 4, the power of PPG measured from the finger is larger than the toe. If users have poor circulation in the lower extremities, the PPG waveform will be indistinct. Thus, the performance of cuffless BP measurement using the weight scale must be worse. However, its advantage is that this method could approach to develop cuffless and touchless BP measurement in the future, when the PPG sensor is embedded in the weight scale.

5. Conclusions

Cuffless and touchless BP measurement has the potential benefit of reducing infection risk during the COVID-19 epidemic. In this study, we used the commercial weight scale to sense the BCG signal that replaced the ECG. Four PTT models were used to estimate BP. The PTT of the reference method was detected by the ECG and PPG$_F$. The proposed method used the BCG and PPG$_T$ to extract the PTT. In terms of the performance of the proposed method, the expected result was worse than that of the reference method. However, E_{RMS} of estimated SBP by the proposed method is 6.7 ± 1.60 mmHg, which is within the range of agreement. Therefore, this method could be implemented in a cuffless and touchless system to measure the continuous beat-to-beat blood pressure. In the future, we will use deep learning techniques to estimate the BP for increasing the accuracy of blood pressure measurements.

Author Contributions: Conceptualization, S.-H.L.; methodology, S.-H.L.; software, B.-H.Z.; validation, B.-H.Z. and S.-H.L.; writing—original draft preparation, S.-H.L. and C.-L.C.; writing—review

References

1. Lee, I.-M.; Shiroma, E.J.; Lobelo, F.; Puska, P.; Blair, S.N.; Katzmarzyk, P.T. Effect of physical inactivity on major non-communicable diseases worldwide: An analysis of burden of disease and life expectancy. *Lancet* **2012**, *380*, 219–229. [CrossRef]
2. De Matos, D.G.; Aidar, F.J.; de Almeida-Neto, P.F.; Moreira, O.S.; de Souza, R.F.; Marcal, A.C.; Marcucci-Barbosa, L.S.; Martins Júnior, F.D.A.; Lobo, L.F.; dos Santos, J.L.; et al. The impact of measures recommended by the government to limit the spread of coronavirus (COVID-19) on physical activity levels, quality of life, and mental health of Brazilians. *Sustainability* **2020**, *12*, 9072. [CrossRef]
3. Röhling, M.; Kempf, K.; Banzer, W.; Braumann, K.M.; Führer-Sakel, D.; Halle, M.; McCarthy, D.; Martin, S.; Scholze, J.; Toplak, H.; et al. A High-Protein and Low-Glycemic formula diet improves blood pressure and other hemodynamic parameters in High-Risk individuals. *Nutrients* **2022**, *14*, 1443. [CrossRef] [PubMed]
4. Hermansen, K. Diet, blood pressure and hypertension. *Br. J. Nutr.* **2000**, *83*, 113–119. [CrossRef]
5. Harsha, D.W.; Bray, G.A. Weight loss and blood pressure control (Pro). *Hypertension* **2008**, *51*, 1420–1425. [CrossRef]
6. Neter, J.E.; Stam, B.E.; Kok, F.J.; Grobbee, D.E.; Geleijnse, J.M. Influence of weight reduction on blood pressure: A meta-analysis of randomized controlled trials. *Hypertension* **2003**, *42*, 878–884. [CrossRef]
7. Mukkamala, R.; Hahn, J.O.; Inan, O.T.; Mestha, L.K.; Kim, C.S.; Töreyin, H.; Kyal, S. Toward ubiquitous blood pressure monitoring via pulse transit time: Theory and practice. *IEEE Trans. Bio-Med. Eng.* **2015**, *62*, 1879–1901. [CrossRef]
8. Buxi, D.; Redouté, J.-M.; Yuce, M.R. A survey on signals and systems in ambulatory blood pressure monitoring using pulse transit time. *Physiol. Meas.* **2015**, *36*, R1-26. [CrossRef]
9. Peter, L.; Noury, N.; Cerny, M. A review of methods for non-invasive and continuous blood pressure monitoring: Pulse transit time method is promising? *IRBM* **2014**, *35*, 271–282. [CrossRef]
10. Ding, X.; Liu, J.; Dai, W.; Carvalho, P.; Magjarevic, R.; Zhang, Y.-T. An attempt to define the pulse transit time. In Proceedings of the International Conference on Biomedical and Health Informatics, Singapore, 9 October 2015.
11. Huynh, T.H.; Jafari, R.; Chung, W.Y. Noninvasive cuffless blood pressure estimation using pulse transit time and impedance plethysmography. *IEEE Trans. Bio-Med. Eng.* **2019**, *66*, 967–976. [CrossRef]
12. Liu, S.-H.; Cheng, D.-C.; Su, C.-H. A cuffless blood pressure measurement based on the impedance plethysmography technique. *Sensors* **2017**, *17*, 1176. [CrossRef] [PubMed]
13. Buxi, D.; Redout, J.M.; Yuce, M.R. Blood pressure estimation using pulse transit time from bioimpedance and continuous wave radar. *IEEE Trans. Bio-Med. Eng.* **2017**, *64*, 917–927. [CrossRef] [PubMed]
14. Weltman, G.; Sullivan, G.; Bredon, D. The continuous measurement of arterial pulse wave velocity. *Med. Electron. Biol. Eng.* **1964**, *2*, 145–154. [CrossRef] [PubMed]
15. Bramwell, J.C.; Hill, A.V. The velocity of the pulse wave in man. *Proc. R. Soc. B Biol. Sci.* **1922**, *93*, 298–306.
16. Ahlstrom, C.; Johansson, A.; Uhlin, F.; Länne, T.; Ask, P. Noninvasive investigation of blood pressure changes using the pulse wave transit time: A novel approach in the monitoring of hemodialysis patients. *J. Artif. Organs* **2005**, *8*, 192–197. [CrossRef]
17. Liu, S.-H.; Wang, J.-J.; Huang, K.-S. A new Oscillometry-Based Method for estimating the dynamic brachial artery compliance under loaded conditions. *IEEE Trans. Biomed. Eng.* **2008**, *55*, 2463–2470. [CrossRef]
18. Rachim, V.P.; Chung, W.-Y. Multimodal wrist biosensor for wearable Cuff-less blood pressure monitoring system. *Sci. Rep.* **2019**, *9*, 7947. [CrossRef]
19. Ibrahim, B.; Jafari, R. Cuffless blood pressure monitoring from an array of wrist Bio-Impedance sensors using Subject-Specific regression models: Proof of concept. *IEEE Trans. Biomed. Circuits Syst.* **2019**, *13*, 1723–1735. [CrossRef]
20. Shin, S.; Yousefian, P.; Mousavi, A.S.; Kim, C.S.; Mukkamala, R.; Jang, D.G.; Ko, B.H.; Lee, J.; Kwon, U.K.; Kim, Y.H.; et al. A unified approach to wearable Ballistocardiogram gating and wave localization. *IEEE Trans. Biomed. Eng.* **2021**, *68*, 1115–1122. [CrossRef]

21. Yousefian, P.; Shin, S.; Mousavi, A.S.; Kim, C.S.; Finegan, B.; McMurtry, M.S.; Mukkamala, R.; Jang, D.G.; Kwon, U.; Kim, Y.H.; et al. Physiological association between limb ballistocardiogram and arterial blood pressure waveforms: A mathematical model-based analysis. *Sci. Rep.* **2019**, *9*, 5146. [CrossRef]

22. Inan, O.T.; Migeotte, P.F.; Park, K.S.; Etemadi, M.; Tavakolian, K.; Casanella, R.; Zanetti, J.; Tank, J.; Funtova, I.; Prisk, G.K.; et al. Ballistocardiography and seismocardiography: A review of recent advances. *IEEE J. Biomed. Health Inform.* **2015**, *19*, 1414–1427. [CrossRef]

23. Martin, S.L.O.; Carek, A.M.; Kim, C.S.; Ashouri, H.; Inan, O.T.; Hahn, J.O.; Mukkamala, R. Weighing scale-based pulse transit time is a superior marker of blood pressure than conventional pulse arrival time. *Sci. Rep.* **2016**, *6*, 39273. [CrossRef] [PubMed]

24. Ding, X.; Zhang, Y.-T. Pulse transit time technique for cuffless unobtrusive blood pressure measurement: From theory to algorithm. *Biomed. Eng. Lett.* **2019**, *9*, 37–52. [CrossRef]

25. Liu, S.-H.; Wang, J.-J.; Tan, T.-H. A portable and wireless multi-channel acquisition system for physiological signal measurements. *Sensors* **2019**, *19*, 5314. [CrossRef] [PubMed]

26. Sharma, M.; Barbosa, K.; Ho, V.; Griggs, D.; Ghirmai, T.; Krishnan, S.K.; Hsiai, T.K.; Chiao, J.C.; Cao, H. Cuff-Less and Continuous Blood Pressure Monitoring: A Methodological Review. *Technologies* **2017**, *5*, 21. [CrossRef]

27. Liu, S.-H.; Wang, J.-J.; Su, C.-H.; Cheng, D.-C. Improvement of left ventricular ejection time measurement in the impedance cardiography combined with the reflection photoplethysmography. *Sensors* **2018**, *18*, 3036. [CrossRef] [PubMed]

28. Liu, S.-H.; Wang, J.-J.; Chen, W.; Pan, K.-L.; Su, C.-H. Classification of photoplethysmographic signal quality with fuzzy neural network for improvement of stroke volume measurement. *Appl. Sci.* **2020**, *10*, 1476. [CrossRef]

29. Geddes, L.A.; Voelz, M.H.; Babbs, C.F.; Bourland, J.D.; Tacker, W.A. Pulse transit time as an indicator of arterial blood pressure. *Psychophysiology* **1981**, *18*, 71–74. [CrossRef]

30. Chen, W.; Kobayashi, T.; Ichikawa, S.; Takeuchi, Y.; Togawa, T. Continuous estimation of systolic blood pressure using the pulse arrival time and intermittent calibration. *Med. Biol. Eng. Comput.* **2000**, *38*, 569–574. [CrossRef]

31. Zheng, Y.; Poon, C.C.Y.; Zhang, Y.-T. Investigation of temporal relationship between cardiovascular variables for cuffless blood pressure estimation. In Proceedings of the 2012 IEEE-EMBS International Conference on Biomedical and Health Informatics, Hong Kong, China, 5–7 January 2012.

32. Allen, R.A.; Schneider, J.A.; Davidson, D.M.; Winchester, M.A.; Taylor, C.B. The covariation of blood pressure and pulse transit time in hypertensive patients. *Psychophysiology* **1981**, *18*, 301–306. [CrossRef]

33. Ma, H.T. A blood pressure monitoring method for stroke management. *Biomed Res. Int.* **2014**, *2014*, 571623. [CrossRef] [PubMed]

34. García, M.T.G.; Acevedo, M.F.T.; Guzmán, M.R.; de Montaner, R.A.; Fernández, B.F.; del Río Camacho, G.; González-Mangado, N. Puede ser el tiempo de tránsito de pulso útil para detectar hipertensión arterial en pacientes remitidos a la unidad de sueño? *Arch. Bronconeumol.* **2014**, *50*, 278–284. [CrossRef] [PubMed]

35. Forouzanfar, M.; Ahmad, S.; Batkin, I.; Dajani, H.R.; Groza, V.Z.; Bolic, M. Model-based mean arterial pressure estimation using simultaneous electrocardiogram and oscillometric blood pressure measurements. *IEEE Trans. Instrum. Meas.* **2015**, *64*, 2443–2452. [CrossRef]

36. Wong, M.-Y.; Poon, C.-C.; Zhang, Y.-T. An evaluation of the cuffless blood pressure estimation based on pulse transit time technique: A half year study on normotensive subjects. *Cardiovasc. Eng.* **2009**, *9*, 32–38. [CrossRef]

37. Proença, J.; Muehlsteff, J.; Aubert, X.; Carvalho, P. Is pulse transit time a good indicator of blood pressure changes during short physical exercise in a young population? In Proceedings of the 2010 Annual International Conference of the IEEE Engineering in Medicine and Biology (EMBC), Buenos Aires, Argentina, 31 August–4 September 2010.

38. Cattivelli, F.S.; Garudadri, H. Noninvasive cuffless estimation of blood pressure from pulse arrival time and heart rate with adaptive calibration. In Proceedings of the 2009 Sixth International Workshop on Wearable and Implantable Body Sensor Networks, Berkeley, CA, USA, 3–5 June 2009.

39. Heard, S.O.; Lisbon, A.; Toth, I.; Ramasubramanian, R. An evaluation of a new continuous blood pressure monitoring system in critically ill patients. *J. Clin. Anesth.* **2000**, *12*, 509–518. [CrossRef]

40. Liu, S.-H.; Liu, L.-J.; Pan, K.-L.; Chen, W.; Tan, T.-H. Using the characteristics of pulse waveform to enhance the accuracy of blood pressure measurement by a multi-dimension regression model. *Appl. Sci.* **2019**, *9*, 2922. [CrossRef]

41. Lin, C.-T.; Liu, S.-H.; Wang, J.-J.; Wen, Z.-C. Reduction of interference in oscillometric arterial blood pressure measurement using fuzzy logic. *IEEE Trans. Bio-Med. Eng.* **2003**, *50*, 432–441.

42. Young, C.C.; Mark, J.B.; White, W.; DeBree, A.; Vender, J.S.; Fleming, A. Clinical evaluation of continuous noninvasive blood pressure monitoring: Accuracy and tracking capabilities. *J. Clin. Monit.* **1995**, *11*, 245–252. [CrossRef]

43. Zong, W.; Moody, G.B.; Mark, R.G. Effects of vasoactive drugs on the relationship between ECG-pulse wave delay time and arterial blood pressure in ICU patients. *Comput. Cardiol.* **1998**, *25*, 673–676.

44. Sharwood-Smith, G.; Bruce, J.; Drummond, G. Assessment of pulse transit time to indicate cardiovascular changes during obstetric spinal anaesthesia. *Br. J. Anesth.* **2006**, *96*, 100–105. [CrossRef]

45. Obrist, P.A.; Light, K.C.; McCubbin, J.A.; Hutcheson, J.; Hoffer, J.L. Pulse transit time: Relationship to blood pressure. *Behav. Res. Methods Instrum.* **1978**, *10*, 623–626. [CrossRef]

46. Inan, O.T.; Park, D.; Giovangrandi, L.; Kovacs, G.T.A. Noninvasive Measurement of Physiological Signals on a Modified Home Bathroom Scale. *IEEE Trans. Bio-Med. Eng.* **2012**, *59*, 2137–2143. [CrossRef] [PubMed]

47. Su, B.Y.; Enayati, M.; Ho, K.C.; Skubic, M.; Despins, L.; Keller, J.; Popescu, M.; Guidoboni, G.; Rantz, M. Monitoring the Relative Blood Pressure Using a Hydraulic Bed Sensor System. *IEEE Trans. Bio-Med. Eng.* **2019**, *66*, 740–748. [CrossRef] [PubMed]
48. Koivistoinen, T.; Junnila, S.; Värri, A.; Kööbi, T. A new method for measuring the ballistocardiogram using EMFi sensors in a normal chair. In Proceedings of the 2004 Annual International Conference of the IEEE Engineering in Medicine and Biology (EMBC), San Francisco, CA, USA, 1–5 September 2004.
49. Allen, J.; Murray, A. Similarity in bilateral photoplethysmographic peripheral pulse wave characteristics at the ears, thumbs and toes. *Physiol. Meas* **2000**, *21*, 369–377. [CrossRef] [PubMed]